



**HAL**  
open science

## Calix[n]arenes in nano bio-systems

Yannick Tauran

► **To cite this version:**

Yannick Tauran. Calix[n]arenes in nano bio-systems. Medicinal Chemistry. Université Claude Bernard - Lyon I, 2014. English. NNT : 2014LYO10245 . tel-01127416

**HAL Id: tel-01127416**

**<https://theses.hal.science/tel-01127416>**

Submitted on 7 Mar 2015

**HAL** is a multi-disciplinary open access archive for the deposit and dissemination of scientific research documents, whether they are published or not. The documents may come from teaching and research institutions in France or abroad, or from public or private research centers.

L'archive ouverte pluridisciplinaire **HAL**, est destinée au dépôt et à la diffusion de documents scientifiques de niveau recherche, publiés ou non, émanant des établissements d'enseignement et de recherche français ou étrangers, des laboratoires publics ou privés.

**THESE**

délivrée

par l'**UNIVERSITE CLAUDE BERNARD - LYON I**

pour l'obtention

du **DIPLÔME DE DOCTORAT**

(arrêté du 7 août 2006)

présentée et soutenue publiquement le 26 Novembre 2014

à l'**UNIVERSITE DE TOKYO**

par

**Mr. Yannick TAURAN**

## **CALIX[n]ARENES IN NANO BIO-SYSTEMS**

Directeur de Thèse : Dr. Anthony W. Coleman FRSC

Jury :

**A. Brioude**

Professeur de  
l'Université Claude Bernard Lyon I, Lyon

**Y. Rondelez**

Directeur de Recherche CNRS,  
LIMMS, Tokyo

**Rapporteur**

**D. Kim**

Professeur de l'Université des sciences  
et technologies de Pohang, Pohang

**Rapporteur**

**H. Fujita**

Professeur de l'Université de Tokyo, Tokyo

**D. Collard**

Directeur de Recherche CNRS, LIMMS, Tokyo

**B. Kim**

Professeur de l'Université de Tokyo, Tokyo

**A.W. Coleman**

Directeur de Recherche CNRS, LMI, Lyon



# UNIVERSITE CLAUDE BERNARD - LYON 1

## Président de l'Université

Vice-président du Conseil d'Administration

Vice-président du Conseil des Etudes et de la Vie Universitaire

Vice-président du Conseil Scientifique

Directeur Général des Services

**M. François-Noël GILLY**

M. le Professeur Hamda BEN HADID

M. le Professeur Philippe LALLE

M. le Professeur Germain GILLET

M. Alain HELLEU

## ***COMPOSANTES SANTE***

Faculté de Médecine Lyon Est – Claude Bernard

Faculté de Médecine et de Maïeutique Lyon Sud – Charles  
Mérieux

Faculté d'Odontologie

Institut des Sciences Pharmaceutiques et Biologiques

Institut des Sciences et Techniques de la Réadaptation

Département de formation et Centre de Recherche en Biologie  
Humaine

Directeur : M. le Professeur J. ETIENNE

Directeur : Mme la Professeure C. BURILLON

Directeur : M. le Professeur D. BOURGEOIS

Directeur : Mme la Professeure C. VINCIGUERRA

Directeur : M. le Professeur Y. MATILLON

Directeur : Mme. la Professeure A-M. SCHOTT

## ***COMPOSANTES ET DEPARTEMENTS DE SCIENCES ET TECHNOLOGIE***

Faculté des Sciences et Technologies

Département Biologie

Département Chimie Biochimie

Département GEP

Département Informatique

Département Mathématiques

Département Mécanique

Département Physique

UFR Sciences et Techniques des Activités Physiques et Sportives

Observatoire des Sciences de l'Univers de Lyon

Polytech Lyon

Ecole Supérieure de Chimie Physique Electronique

Institut Universitaire de Technologie de Lyon 1

Ecole Supérieure du Professorat et de l'Education

Institut de Science Financière et d'Assurances

Directeur : M. F. DE MARCHI

Directeur : M. le Professeur F. FLEURY

Directeur : Mme Caroline FELIX

Directeur : M. Hassan HAMMOURI

Directeur : M. le Professeur S. AKKOUCHE

Directeur : M. le Professeur Georges TOMANOV

Directeur : M. le Professeur H. BEN HADID

Directeur : M. Jean-Claude PLENET

Directeur : M. Y. VANPOULLE

Directeur : M. B. GUIDERDONI

Directeur : M. P. FOURNIER

Directeur : M. G. PIGNAULT

Directeur : M. le Professeur C. VITON

Directeur : M. le Professeur A. MOUGNIOTTE

Directeur : M. N. LEBOISNE



# Acknowledgment

This thesis has been conducted in collaboration between two laboratories located in two different countries France and Japan. Each country has taught me something different for improving my research work, in the way to plan and to perform experiments, to realize original works and to share knowledge. During these three last years, I had the opportunity to meet and to learn from a lot of great people who has contributed in this work at various levels scientifically, technically, administratively, culturally and friendly. Without them, this work wouldn't have been achieved.

First I would like to express my sincere gratitude to Dr. A.W. Coleman for giving me the opportunity to realize this thesis in an international context, for supervising me and for providing me guidance and precious advices during all along these years. I would like also to thank Prof. B. Kim for welcoming me and supervising my work in Japan, giving me strong support, opportunity for giving lectures and also inspiring advices.

I would like to thank the others referees of my thesis defence, Prof. D. Kim, Prof. H. Fujita, Dr. Y. Rondelez, Dr. D. Collard and Prof. A. Brioude for their constructive advices and corrections and for attending the defence.

Regarding the University of Lyon, my thanks go to Prof. H. Parrot who made this thesis possible, and for her help and support. Thanks to Prof. C. Brylinsky and Prof. A. Brioude who welcomed me respectively in LMI research unit and in Nanostructured Functional Material MFN research team in Lyon (France). I would like to thank also all the MFN research members in Lyon for their productive comments and their warm welcoming when I arrived four years ago (Laurence, Fernand, Cédric, Catherine, Mathieu, Vincent, François and Bérangère). I'm also indebted to the administrative and technical staff of LMI (Patricia, Fabienne, Nicolas and Laurent). Prof. C. Goutedier was also really helpful in administrative advices for obtaining grants in order to support my expenses in Japan.

Turning to Japan, I thank also Dr. D. Collard, Prof. T. Fuji and more recently Prof. H. Kawakatsu for welcoming me in LIMMS/IIS. It was a fantastic experience to research in such high scientific and cultural environment. LIMMS/IIS staff (Yumi, Masayo, Eiko, Sachie, Chikako and Nathalie) was also really helpful for all the different administrative processes required during my stay in Japan. Thanks also to all the LIMMS members that become more than simple co-workers (sorry the list is too long).

I would like to thank all the members of the Kim Laboratory that hosted me so many times during these 3 years. Thanks particularly to Tomita and Takama San for their continuous help and of course all the students and ex-students (Ueno, Tokunaga, Yamada, Makino, Oya, Yukawa, Amano, Mizuno, Kawano, Yuhki, Simon, Dominik, Samuel, Dr Byun and Dr. Park).

I would like to express my sincere thanks to all the others researchers that have collaborated with me in the different studies included in that thesis (Dr. F. Perret, Dr. M. Rhimi, Prof. C. Anjard, Dr. A.N. Lazar, Dr. S. Jebors, Dr. M. Tarhan, Prof. K. Suwinska, Prof. M. Fitzgerald, Dr. C. Collard and Prof. H. Fujita).

Finally, I would like to thanks my previous professors or supervisors who gave me the taste of learning, being curious, and performing a research work as well as possible (Dr. F. Dumas, Dr. C. Bergaud, Dr. N. Liviu, Dr. C. Pannetier, Dr. Y. Morel and Dr. A. Chaboud)

## Remerciements

Sur une note plus personnelle, je souhaiterai également remercier en français mes amis et ma famille française qui m'ont apporté leurs soutiens au cours de ces trois années de thèse. Sans eux ce travail n'aurait sans doute pas pu être réalisé.

Je souhaiterai d'abord remercier les amis que j'ai pu rencontrer au Japon et qui ont facilité mon intégration dans ce pays si différent (Yasuko B., Elliot M., Marie P., Louis G., Gregoire P., Adrien P., Alexandre B., Mehult, Raphael R., Denis D., Bertrand S., Floriant L, Nathalie F., Christian P., Ueno, Tokunaga et tous les autres.)

Merci aussi à tous les amis 'scientifiques' français qui ont partagés les joies et les difficultés de la vie de laboratoire et de la recherche en général. Leurs écoutes et conseils accompagnés de quelques verres, ont pu me permettre de passer les différentes épreuves de ce travail (Saïd J., Tomas F., Steven R., Moez R., Jean-Baptiste G., Vincent G., Jean-Phillipe R., Isabelle G.).

Enfin les amis de toujours qui m'ont apporté leurs soutiens sans failles, et qui m'ont permis de décompresser et de me ressourcer (Eric L. et toute sa bande, Yann M., Caroline R., Cédric et Fanny, Stéphanie L., Amélie D., Fabien, Mapi et Pascal, Lado, Georges, Nidya Z.).

Et pour finir, je souhaiterai remercier ma famille qui a toujours été une source d'inspiration et de force dans ma vie. J'ai une pensée plus particulière pour ma sœur et mes parents qui m'ont appris à ne jamais renoncer.

# Copyright

A part of this thesis is reproduced by permission of

The Royal Society of Chemistry from references [1-5] ;

Baishideng Publishing Group from reference [6] ;

MDPI from reference [7] ;

Springer from references [8, 9] ;

Hindawi Publishing Corporation from reference [10].

## References :

- 1- **Y. Tauran**, M. Grosso, A. Brioude, R. Kassab and A. W. Coleman, Colourimetric and spectroscopic discrimination between nucleotides and nucleosides using para-sulfonato-calix[4]arene capped silver nanoparticles. *Chem. Commun.*, 2011, 47, 10013-10015;
- 2- **Y. Tauran**, M. Kumemura, N. Lafitte, U. Ryohei, L. Jalabert, Y. Takayama, D. Collard, H. Fujita, A. W. Coleman and B. Kim. Mechanical effect of calix[n]arene capped silver nanoparticles on DNA measures with Silicon Nano Tweezers. MicroTAS, Okinawa, JAPAN, 2012. 1882-1885.
- 3- **Y. Tauran**, A. Brioude, P. Shahgaldian, Alessandro Cumbo, B. Kim, F. Perret, A. W. Coleman and I. Montasser. Calixarene silver nanoparticles interactions with surfactants are charge, size and critical micellar concentration dependent. *Chem. Commun.*, 2012, 48, 9483-9485;
- 4- S. Boudebbouze, A.W. Coleman, **Y. Tauran**, H. Mkaouar, F. Perret, A. Garnier, A. Brioude, B. Kim, E. Maguin, M. Rhimi. Discriminatory antibacterial effects of calix[n] arene capped silver nanoparticles with regard to Gram positive and Gram negative bacteria. *Chem. Commun.*, 2013, 49 (64), 7150-7152;
- 5- **Y. Tauran**, C. Anjard, B. Kim, M. Rhimi and A. W. Coleman. Large supramolecular organic macrocycles as inhibitors of endonuclease enzymes. *Chem. Commun.*, 2014, 50, 11404-11406;
- 6- **Y. Tauran**, A. Brioude, A. W. Coleman, M. Rhimi, B. Kim. Review: Molecular recognition by gold, silver and copper nanoparticles. *World Journal of Biological Chemistry*. 2013, 4(3), 35-63;
- 7- **Y. Tauran**, A. Brioude, B. Kim, F. Perret, A. W. Coleman. Anionic Calixarene-Capped Silver Nanoparticles Show Species-Dependent Binding to Serum Albumins. *Molecules*, 2013, 18 (5) 5993-6007.
- 8- K. Suwinska, E. Janneau, **Y. Tauran**, A. W. Coleman. The solid-state structures of the ethanol solvated complexes of para-sulphonato-calix[4]arene with magnesium and calcium ions. *J Incl Phenom Macrocycl Chem*, 2013, DOI 10.1007/s10847-013-0342-x
- 9- **Y. Tauran**, M. Rhimi, R. Ueno, M. Grosso, A. Brioude, E. Janneau, K. Suwinska, R. Kassab, P. Shahgaldian, A. Cumbo, B. Kim, A. W. Coleman. Cytosine: para-sulphonato-calix[4]arene assemblies: in solution, in the solid-state and on the surface of hybrid silver nanoparticles. *J Incl Phenom Macrocycl Chem*, 2013, 77, 213-221
- 10- F. Perret, **Y. Tauran**, K. Suwinska, B. J. Kim, C. Chassain-Nely, M. Boulet, A. W. Coleman. Molecular Recognition and Transport of Active Pharmaceutical Ingredients on Anionic Calix[4]arene-Capped Silver Nanoparticles. *J. Chem.*, 2013, DOI: 10.1155/2013/191828



# Summary

Supramolecular assemblies are among the basic biochemical reactions in the cellular functions (e.g. DNA replication, immune response). Calix[n]arenes are macrocyclic molecules that have been reported for interacting with a wide range of biomolecules. As a consequence, they can be found in many biological applications from diagnosis to therapeutic treatment. Their functionalization on silver nanoparticles have produced new nano hybrid compounds with unique optical, electrical and biochemical properties. This thesis has been dedicated to the study of these nano-systems for bio-sensing and for their potent biomedical applications.

Cost effective, portable and ultra-sensitive analytical tools are one of the major expectations of the applications of silver nanoparticles capped with calix[n]arenes. Calix[n]arenes nanoparticles have been reported here for following the micellisation process of mixed surfactants or for discriminating a type of molecule such nucleic acid or a serum albumin specie.

In a second part, these hybrid nanoparticles have been evaluated for series of biological activities. They've been shown to possess anti-oxidant and antibacterial activities, to transport Active Pharmaceutical Ingredient and to reach antiviral and anti-cancer targets.

**Key words:** Calix[n]arene, Silver nanoparticles, Biomolecules, Optical biosensors, API transporter, Antibacterial, Antiviral, Silicon Nano Tweezers.

# Résumé

Les assemblages supramoléculaires font parties des réactions biochimiques de base dans les fonctions cellulaires (ex: réplication de l'ADN ou réponse immunitaire). Les calix[n]arènes ont été décrit pour interagir avec une large gamme de biomolécules. En conséquence, ils peuvent être trouvés dans de nombreuses applications biologiques tel qu'en diagnostic ou en traitement thérapeutique. Leurs fonctionnalisations sur des nanoparticules d'argent ont produit de nouveaux nano-composés hybrides ayant des propriétés optique, électrique et biologique uniques. Cette thèse a été dédiée à l'étude de ces nano systèmes pour la bio-détection et leurs potentielles applications biomédicales.

Le développement de capteur analytique à bas coût, portable et ultra-sensible représente une des attentes majeures dans les applications des calix[n]arènes sur nanoparticules d'argent. Dans cette thèse, ces nano-composés ont été étudiés selon leurs capacités à suivre la micellisation de surfactant mixtes, et pour discriminer un type moléculaire tel qu'une famille d'acide nucléique ou une espèce d'albumine sérique.

Dans une deuxième partie, ces nanoparticules hybrides ont été évaluées pour une série d'activités biologiques. Ils ont montré des facultés antibiotiques et anti-oxydantes, de transporter des Ingrédients Pharmaceutiques Actifs, et d'atteindre des cibles antivirales et anticancéreuses.

**Mot clés:** Calix[n]arènes, Nanoparticules d'argent, Biomolécules, Biocapteurs optiques, Transporteurs d'API, Antibactériens, Antiviraux, Silicon Nano Tweezers.

# Table of Contents

<b>ACKNOWLEDGMENT</b> .....	<b>I</b>
<b>REMERCIEMENTS</b> .....	<b>II</b>
<b>COPYRIGHTS</b> .....	<b>III</b>
<b>SUMMARY</b> .....	<b>V</b>
<b>RESUME</b> .....	<b>VI</b>
<b>TABLE OF CONTENTS</b> .....	<b>VII</b>
<b>GENERAL INTRODUCTION</b> .....	<b>1</b>
<b>PART A – STATE OF THE ART</b> .....	<b>5</b>
<b>I. Biological activities of calix[n]arenes</b> .....	<b>7</b>
1. Introduction .....	10
2. Hemotoxicity.....	14
3. Detoxifying agents .....	14
4. Anti-coagulant behaviour .....	17
5. Activity against membrane proteins.....	19
6. Fluorescent probes .....	21
7. Antibacterial activity .....	22
8. Antiviral activity .....	27
9. Antifungal activity .....	31
10. Anti-cancer activity .....	32
11. DNA delivery .....	38
12. Other types of drug delivery .....	40
12. General mechanistic guidance of calix[n]arene design for biological function...	41
14. Conclusion and the future .....	43
<b>II. Localized Surface Plasmon Resonance</b> .....	<b>55</b>
1. LSPR principle.....	57
2. Parameters affecting plasmonic properties of nanoparticles .....	59

<b>III. Molecular recognition by gold, silver and copper nanoparticles ...</b>	<b>69</b>
1. Introduction .....	71
2. Preparation and modification of nanoparticles.....	72
3. Properties.....	72
4. Coating and molecular recognition.....	74
5. Toxicity concern .....	91
6. Conclusion.....	92
<b>IV. Bio-applications of calix[n]arene capped silver nanoparticles .....</b>	<b>101</b>
1. Introduction .....	103
2. Synthesis .....	107
3. Bio-detection.....	109
4. Therapeutical applications.....	125
5. Conclusion and future perspective .....	130
<b>PART B – RESULTS.....</b>	<b>139</b>
<b>I. Biosensing by calix[n]arene capped silver nanoparticles .....</b>	<b>141</b>
1. Colourimetric and spectroscopic discrimination between nucleotides and nucleoside using para-sulphonato-calix[4]arene capped silver nanoparticles .....	143
2. Cytosine : para-sulphonato-calix[4]arene assemblies : in solution, in the solid-state and on the surface of hybrid silver nanoparticles .....	147
3. Anionic calixarene capped silver nanoparticles show species-dependent bind to serum albumins.....	157
4. Calix-arene silver nanoparticles interactions with surfactants are charge, size and critical micellar concentration dependent .....	173
<b>II. Biological activities of calix[n]arene nanoparticles.....</b>	<b>177</b>
1. Discriminatory antibacterial effects of calix[n]arene capped silver nanoparticles with regard to Gram positive and Gram negative bacteria.....	179
2. Molecular recognition and transport of Active Pharmaceutical Ingredients on anionic calix[4]arene capped silver nanoparticles.....	183
3. Large negatively charged organic host molecules as inhibitors of endonuclease enzymes .....	193

4. Multifunctional curcumin-nanocarriers based on host-guest interaction, for Alzheimer disease .....	197
<b>DISCUSSION .....</b>	<b>209</b>
<b>I. Biosensing by calix[n]arene capped silver nanoparticles .....</b>	<b>209</b>
<b>II. Biological activities of calix[n]arene nanoparticles.....</b>	<b>214</b>
<b>III. Toxicity concerns.....</b>	<b>216</b>
<b>GENERAL CONCLUSION .....</b>	<b>221</b>
<b>ANNEX .....</b>	<b>223</b>
1. Supporting information: Colourimetric and spectroscopic discrimination between nucleotides and nucleoside using para-sulphonato-calix[4]arene capped silver nanoparticles .....	225
2. Supporting information: Calix-arene silver nanoparticles interactions with surfactants are charge, size and critical micellar concentration dependent.....	233
3. Supporting information: Discriminatory antibacterial effects of calix[n]arene capped silver nanoparticles with regard to Gram positive and Gram negative bacteria.....	268
4. Supporting information: Large negatively charged organic host molecules as inhibitors of endonuclease enzymes.....	273
5. The solid structures of the ethanol complexes of para-sulphonato-calix[4]arene with magnesium and calcium ions.....	279
6. Mechanical effect of calix[n]arene capped silver nanoparticles on DNA measured with Silicon Nano Tweezer.....	287



# General introduction

The biologic functions of living organisms are governed by complex chemical processes including the interactions of various macro-molecules such as DNA, proteins, carbohydrates or lipids. These chemicals are involved in a wide range of biochemical reactions inside the cell and can structure the cellular shape, maintain intra-cellular physical constants (pH, redox potential, osmotic pressure and ionic strength), transcript and translate the genetic information encoded in DNA and ensure cellular duplication. All these functions are related to the reversible assembly of these macromolecules by non-covalent weak energy bonds.

Supramolecular chemistry has been defined as the study of non-covalent bonds, how molecules can recognize, assemble and function between each other or between themselves. These assembly forces include hydrogen bonding, metal coordination, hydrophobic forces, van der Waals forces,  $\pi$ - $\pi$  and electrostatic interactions. Biology has inspired the development of new classes of synthetic macrocyclic molecule hosts able to be bioactive. These synthetic molecules include crown ethers, cyclodextrins, calix[n]arenes or cucurbit[n]urils. However, the area of supramolecular chemistry study is not limited to biology and can be extended to material science with regard to the understanding and manipulation of the molecular assembly.

In this thesis, the assembly of anionic calix[n]arenes has been particularly investigated for their general advantages over other macrocyclic systems, such advantages include their high solubility, their low toxicities and their abilities to interact with positively charged amine groups carried by various biomolecules (protein, DNA, surfactants).

The ability of calix[n]arene to organize themselves in nano-systems by auto assembling in nanoparticles or by being capped over metal nanoparticles has shown new physical, chemical and biological properties and need to be understood.

Noble metal nanoparticles have recently attracted a great interest in academic and industrial fields because of their unique optical and biological properties. Silver metal

nanoparticles have particularly shown promising applications like molecular colorimetric sensors or antibacterial agents.

The study of the combination of silver nanoparticles and macrocyclic molecular hosts has been one of the main purposes in that thesis. An important part of this work has been to characterize and to understand the molecular assembly occurring when calix[n]arene capped silver nanoparticles selectively recognize a biomolecule.

This thesis will be divided in two parts. The first part (A) will be dedicated to the bibliographic description of the molecular recognition of noble metal nanoparticles, the biological activities of calix[n]arenes and calix[n]arene capped on silver nanoparticles. These three sections will be presented under a scientific review format. The review about the bio-applications of calix[n]arene capped silver nanoparticles presents particularly the contribution of this thesis work in that research field. Another additional section on the Localized Plasmon Resonance (LSPR) has been included in order to describe and to understand the unique optical properties of silver nanoparticles.

The second part (B) presents the results obtained during this thesis. These results are also presented under a published scientific article format. They are sub-divided in two chapters according to their different scopes: bio-sensing and biological activities.

The first chapter describes bio-sensing applications of calix[n]arene capped silver nanoparticles along four different articles. Calix[n]arene derivatives used for capping nanoparticles in those studies were calix[4]arene diphosphonate and calix[4,6,8]arenes bearing sulphonate groups at the *para* and/or phenolic faces. These calix[n]arenes have been selected both for their hydrophilic and argentophilic nature. They've been also characterized for interacting with a wide range of biomolecules by solid state structure (amino acid, nucleic acid, protein, etc.). The calix[n]arene capped silver nanoparticles have been shown to discriminate optically different class of biomolecules such as purine or pyrimidine nucleic acids, serum albumin species (pork, human, sheep and goat) and charged surfactants. In the last case, the optical behaviour of the hybrid nanoparticles has been shown to be dependant of the Critical Micellar Concentration and to be extended to mixed ionic micelles. A fourth article describes extensively the interaction and aggregation of the hybrid particle by various physicochemical analytical methods (DOSY NMR, fluorescence spectroscopy, Dynamic Light Scattering (DLS), Single Crystal Solid State Diffraction, Visible Spectroscopy and

Electron Microscopy). The results demonstrate how cytosine initiates the aggregation of the hybrid silver / *para*-sulphonato-calix[4]arene hybrid nanoparticles.

The second chapter presents the biological activities of calix[n]arene nanoparticles through four different articles. Calix[n]arene capped silver nanoparticles have been demonstrated to possess a high antibiotic activity (at a lowest concentration of 100 nM) compared to the classical antibiotic hexamidine and chlorhexidine which have antibacterial effect above 1  $\mu$ M. Their effects have also been shown to be discriminatory according to the Gram type of bacteria. In a second study, the complexation and transportation of antibiotic by calix[n]arene capped silver nanoparticles have been investigated. These two studies demonstrate the promising use of these hybrid compounds associated or not with antibiotics for treating or preventing the proliferation of pathogenic multi resistant bacteria. A third study has evaluated the role of calix[n]arenes as inhibitors of endonuclease enzymes. These proteins are new pharmaceutical targets against cancer cells or some viruses (e.g. influenza or Epstein Bar virus). For the first time, it has been demonstrated that large macrocyclic negatively charged molecule such as *para*-sulphonato-calix[6,8]arene can inhibit eukaryotic endonucleases. The inhibitory activity is not significantly changed when a macrocyclic sulphated cyclodextrin is combined onto silver nanoparticles. Finally, a last article shows how *para*-sulphonato-calix[6,8]arenes complexed with curcumin can form nano-carriers and can be used for diagnosis and a subsequent treatment of Alzheimer Disease.



## Part A

# State of The Art



# Part A

## Section 1

Biological activities of calix[n]arenes  
at the cellular level and *in vivo*



**Review article:****BIOLOGICAL ACTIVITIES OF CALIX[n]ARENES AT THE CELLULAR LEVEL AND *IN VIVO*****Yannick Tauran<sup>\*1,2</sup>, Beomjoon Kim<sup>2,3</sup> and Anthony W. Coleman FRSC<sup>\*1</sup>**

1 LMI CNRS UMR 5615, Université Lyon 1

2 LIMMS/CNRS-IIS (UMI 2820), The University of Tokyo

3 CIRMM, Institute of Industrial Science, The University of Tokyo

\* Corresponding authors: Yannick Tauran and Anthony W. Coleman

Address : LMI CNRS UMR 5615, Université Lyon 1, Villeurbanne, F69622, FRANCE;

Ph : +33 4 4243 1027 ;

E-mail: [yannick.tauran@univ-lyon1.fr](mailto:yannick.tauran@univ-lyon1.fr); [anthony.coleman@univ-lyon1.fr](mailto:anthony.coleman@univ-lyon1.fr).**ABSTRACT**

The biological activities of the calix[n]arenes have been extensively reported on various forms of life from virus, bacteria, fungi and mammalian cells to human beings. This article reviews more than one hundred different calix[n]arenes classified according to the biological effects directly observed on living species. These basket shaped molecules have been reported as detoxifying agents, antibacterial, antiviral, anticoagulant, anticancer, antifungal, membrane protein modulator / extractor, drug transporters and fluorescent probes. Special *in vivo* sections, **highlighted**, have been inserted when it was possible for each biological effect in order to show the impact of the calix[n]arenes on whole living system such as animals or humans.

**Keywords: Calix[n]arenes, *In vivo*, Cells, Biological applications, Active Pharmaceutical Ingredients.**

## 1. Introduction

Calix[n]arenes are macrocyclic molecules consisting of repeated phenolic unit, generally, linked to each other by methylene bridges. Because of the similarity of shape between this molecule and a vase, Gutsche *et al.* have named them calix[n]arenes, derived from the Greek calix meaning “vase” or “chalice” and arene which indicates the presence of aryl residues in the macrocyclic array (Gutsche, 2008).

In 1872, Von Baeyer has first reported the synthesis of these chemicals as a resinous product coming from the condensation of aldehydes and phenols. Later in the 1940's, Zinke and Ziegler have simplified the chemical process by mixing a *para*-substitued phenol with formaldehyde giving cyclic tetramer (Zinke *et al.*, 1952). In 1955, Cornforth, an Australian–British chemist (Nobel Prize in Chemistry, 1975), first reported the biological properties of calix[n]arene (called macrocylclon at that time), finding that certain calix[n]arenes possessed anti-tuberculosis properties (Cornforth *et al.*, 1955). After that, no biological studies of calix[n]arenes in cellular bioassays or *in vivo* were described during almost 30 years. At the end of 1980's, calix[n]arenes became one of the most popular macrocyclic polymers among molecules of supramolecular chemistry for bio-applications (Schrader, 2012). The parent calix[n]arenes are poorly soluble in water. Since biological reactions occur in aqueous media, hydro-soluble calix[n]arenes were required and have been reported around that time (Casnati *et al.*, 2001). First, Ungaro *et al.* made sparingly hydrosoluble derivatives (ca 1 mM) by functionalizing them with carboxylate functions (Ungaro *et al.*, 1984). The breakthrough came from Shinkai who introduced the synthesis of *para*-sulphonated calix[n]arene exhibiting the molar solubility (Shinkai *et al.*, 1984). Kalchenko *et al.* have contributed by the synthesis of hydro-soluble calix[n]arene phosphonate (Lipkowski *et al.*, 1998). Amino-calix[n]arene derivatives have been also described as water soluble (Nagasaki *et al.*, 1992). Nowadays a wide range of highly hydrosoluble or dispersible calix[n]arenes are available to the biologist (Perret *et al.*, 2013).

Comparing with the other two classical water soluble macrocycles, cyclodextrins and cucurbiturils, calix[n]arenes possess different cavity structure, much lower framework rigidity particularly for the higher oligomers, and complexation driving forces are far more readily modified by substitution at the *para* face, further more selective hydrophobic substitution at the phenolic face is relatively simple and which afford unique recognition and assembly features in building responsive host–guest systems. Generally the chemistry of the calix[n]arenes is trivial if compared to the other wto host systems (Guo *et al.*, 2014).

The chemistry of calix[n]arenes is versatile, the repeating unit of the calix[n]arene can be phenol, resorcinol or pyrogallol and their easily differentiated functionalization either at upper rim or/and at lower offers a wide variety of different compounds (Figure 1) (Gutsche, 2008). A major point here is the lack of contaminants in the products, none of the toxic reagents used in their synthesis are found in the products (Parker, 1996). As a consequence, calix[n]arenes can assemble, according to their nature and their molecular environment, in many different ways in liquids, at the liquid-air interface or at the liquid-solid interface (Coleman *et al.*, 2008a). They can be found in liquid media from a simple monomer to various assembly structures such as dimeric nanocapsules (Maerz *et al.*, 2010), specific

geometrical structures like snub cubes (MacGillivray *et al.*, 2000), micelle and unimolecular micelle (Shinkai *et al.*, 1989) or Solid Lipid Nanoparticle (Montasser *et al.*, 2013). At the liquid-air interface, they can form Langmuir monolayer (Jebors *et al.*, 2010). Finally, at liquid-solid interface it has been shown that they can assemble in barrels into membrane lipidic bilayer in order to create artificial pores (Gorteau *et al.*, 2004 and 2005). The assembly properties of calix[n]arenes present considerable interest as bio-active molecules or for drug transport in medical applications.

Since the 1990's, the biochemistry of calix[n]arenes has been widely investigated for in the context of their interaction with numerous bio-molecules (Perret *et al.*, 2011). Calix[n]arenes have been reported to interact with hormone and steroids, drugs, nucleic acids, amino acids, DNA, peptides and proteins (Perret *et al.*, 2006). The association of calix[n]arenes with biomolecules induces a large potential for biomedical applications, for example, calix[n]arenes can modulate protein folding and protein / ligand interactions (Perret *et al.*, 2007). *In vitro* experiments have shown that calix[n]arenes can activate, inhibit or modulate the activity of a wide range of proteins (membrane proteins, enzymes, ion channels, etc.) (Perret *et al.*, 2013). Supramolecular association of *para*-sulphonato-calix[n]arenes with a specific peptide sequence has been reported for use in the detection of the pathogenic prion protein (Coleman *et al.*, 2007).

In the 2000's, Coleman *et al.* have investigated the toxicity of calix[n]arenes on normal cells with haemolysis tests (Da Silva *et al.*, 2004) and *in vivo* experiments on mice (Coleman *et al.*, 2008b). An absence of non-specific immune response has been also demonstrated for calix[n]arenes (Paquet *et al.*, 2006).

A large number of reviews have now been published concerning the biological activities of the calix[n]arenes and these may be exemplified as follows: detoxifying agents, antibacterials, antivirals, anticoagulant, anticancer APIs, antifungals, membrane protein modulators / extractors, drug transporters and fluorescent probes. Rodick *et al.* have presented biomedical applications of calix[n]arene including *in vitro* studies (Rodick *et al.*, 2009). In 2009, De Fátima *et al.* provided an overview of biological activity of the calix[n]arenes and discussed the possibility of drug development using calix[n]arenes (De Fátima *et al.*, 2009). Dondoni and Sansone have reported the biological activities of calix[n]arene glycosides (Dondoni *et al.*, 2010) (Sansone *et al.*, 2013). Ukhatskaya *et al.* have reviewed the encapsulation of drug molecules by cationic amino-calix[n]arenes for biopharmaceutical applications (Ukhatskaya *et al.*, 2013). Coleman and Perret have published a series of Featured Articles in Chemical Communications, *para*-sulphonato-calix[n]arene biochemistry (Perret *et al.*, 2006) the biochemistry anionic calix[n]arenes (Perret *et al.*, 2011), with third article updating the behavior of anionic calix[n]arenes to appear in 2014 or 2015. A recent review on certain aspects of the biological properties of *para*-sulphonato-calix[n]arenes has been published by Guo in 2014 (Guo *et al.*, 2014). In 2011, Mokhtari and Pourabdollah have summarized biochemical and structural studies of a wide range of calix[n]arene for pharmacological applications (Mokhtari *et al.*, 2012). The biological applications of calix[n]arene capped silver nanoparticles is due in 2015 (Tauran *et al.*, 2015).

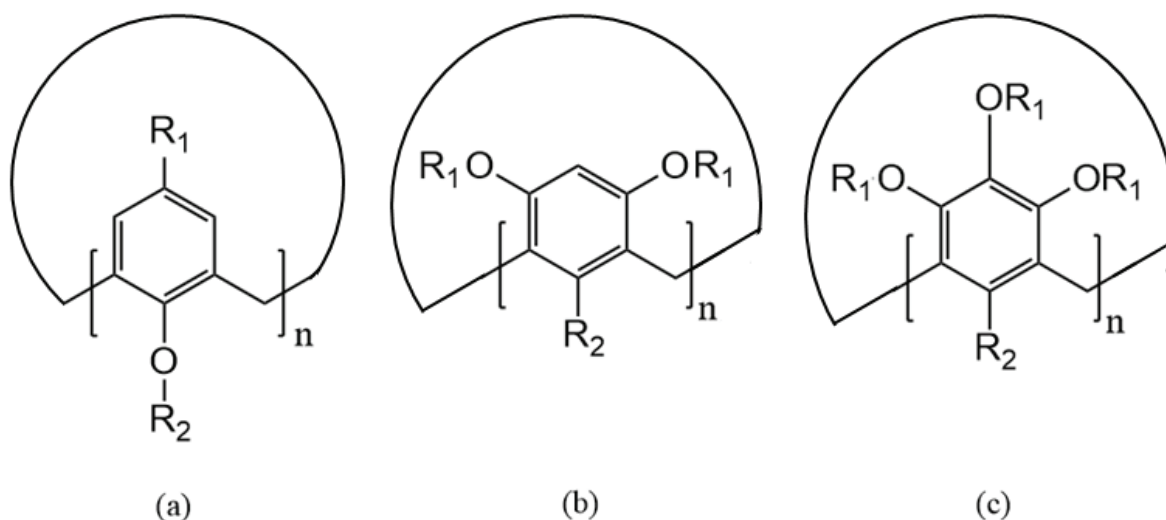


**Figure 1-** General structures of calix[n]arene (a), calix[n]resorcinarene (b) and calix[n]pyrogallol (c).

Previous reviews have either tended to concentrate on the authors particular interests or cover a chronological period, with probably the exception of the Perret and Coleman chapter on protein complexation (Perret *et al.*, 2013). Here, we have chosen to review the effects of the calix[n]arenes on various living organisms ranging from viruses, through bacteria and fungi to animals. Over 100 different calix[n]arene molecules are described for their biological properties. A special *in vivo* subsection (highlighted as pale blue insets) has been added for each biological activity in order to provide another type of biological data (e.g. effect on biological system more complex, way of administration, dose evaluation) and to establish where the subject lies with regard to future medicinal use of calix[n]arenes. Thus the aim of the review is to show the reader where the calix[n]arenes are situated in terms of living organisms in 2014.

Table 1- List of calix[n]arene presented in this review

- 1:  $R_1 = \text{SO}_3\text{H}$  (tetra);  $R_2 = \text{H}$  (no);  $n=4$   
2:  $R_1 = \text{SO}_3\text{H}$  (hexa);  $R_2 = \text{H}$  (no);  $n=6$   
3:  $R_1 = \text{SO}_3\text{H}$  (octa);  $R_2 = \text{H}$  (no);  $n=8$   
4:  $R_1 = \text{SO}_3\text{H}$  (tetra);  $R_2 = -\text{CH}_2-\text{COOH}$  (mono);  $n=4$   
5:  $R_1 = \text{SO}_3\text{H}$  (hexa);  $R_2 = -\text{CH}_2-\text{COOH}$  (mono);  $n=6$   
6:  $R_1 = \text{SO}_3\text{H}$  (octa);  $R_2 = -\text{CH}_2-\text{COOH}$  (mono);  $n=8$   
7:  $R_1 = \text{SO}_3\text{H}$  (tetra);  $R_2 = -(\text{CH}_2)_2-\text{NH}_2$  (mono);  $n=4$   
8:  $R_1 = \text{SO}_3\text{H}$  (hexa);  $R_2 = -(\text{CH}_2)_2-\text{NH}_2$  (mono);  $n=6$   
9:  $R_1 = \text{SO}_3\text{H}$  (octa);  $R_2 = -(\text{CH}_2)_2-\text{NH}_2$  (mono);  $n=8$   
10:  $R_1 = -(\text{CH}_2)_4-\text{CH}_3$  (tetra);  $R_2 = \text{H}$ (no);  $n=4$   
11:  $R_1 = -(\text{CH}_2)_6-\text{CH}_3$  (tetra);  $R_2 = \text{H}$ (no);  $n=4$   
12:  $R_1 = -(\text{CH}_2)_8-\text{CH}_3$  (tetra);  $R_2 = \text{H}$ (no);  $n=4$   
13:  $R_1 = -(\text{CH}_2)_{10}-\text{CH}_3$  (tetra);  $R_2 = \text{H}$ (no);  $n=4$   
14:  $R_1 = -(\text{CH}_2)_{10}-\text{CH}_3$  (tetra);  $R_2 = -\text{PO}(\text{OC}_2\text{H}_5)_2$  (di);  $n=4$   
15:  $R_1 = -(\text{CH}_2)_{10}-\text{CH}_3$  (tetra);  $R_2 = -\text{PO}(\text{OH})_2$  (di);  $n=4$   
16:  $R_1 = \text{H}$  (no);  $R_2 = -\text{Amphotericin B}$  (tetra);  $n=4$   
17:  $R_1 = -\text{C}(\text{CH}_3)_3$  (no);  $R_2 = -\text{Amphotericin B}$  (tetra);  $n=4$   
18:  $R_1 = -\text{CH}_2-\text{NH}-\text{CH}_3$  (tetra);  $R_2 = -(\text{CH}_2)_2-\text{CH}_3$  (tetra);  $n=4$   
19:  $R_1 = -\text{CH}_2-\text{NH}(\text{CH}_2)_2-\text{OH}$  (tetra);  $R_2 = -(\text{CH}_2)_2-\text{CH}_3$  (tetra);  $n=4$   
20:  $R_1 = -\text{CH}_2-\text{NH}(\text{CH}_2)_2-\text{OH}$  (tetra);  $R_2 = -(\text{CH}_2)_7-\text{CH}_3$  (tetra);  $n=4$   
21:  $R_1 = -\text{C}(\text{CH}_3)_3$  (no);  $R_2 = -\text{CH}_2-\text{COOH}$  (tri);  $n=6$   
25:  $R_1 = -\text{PO}(\text{OH})_2$  (tetra);  $R_2 = \text{H}$  (no);  $n=4$   
26:  $R_1 = -\text{NH}-\text{Lysine}$  (tetra);  $R_2 = -\text{CH}_2-\text{CH}_3$  (octa);  $n=8$   
27:  $R_1 = -\text{PO}(\text{OH})_2$  (di);  $R_2 = -\text{CH}_2-\text{CH}_3$  (di);  $n=4$   
28:  $R_1 = -\text{C}(\text{CH}_3)_3$  (no);  $R_2 = -\text{CH}_2-\text{CO}-\text{NH}-\text{Chacolneamide}$  (ono);  $n=6$   
29:  $R_1 = \text{NH}-\text{C}(\text{CF}_3)_2-\text{NH}-\text{SO}_2-\text{Ph}$  (tetra);  $R_2 = -(\text{CH}_2)_2-\text{CH}_3$  (mono);  $n=4$   
30:  $R_1 = \text{CH}_2-\text{O}(\text{CH}_2)_3-\text{CH}_3$  (tetra);  $R_2 = -\text{CH}_2-\text{CO}-\text{NH}(\text{CH}_2)_3-\text{NH}(\text{CH}_2)_4-\text{NH}_3$  (tetra);  $n=4$   
31:  $R_1 = -\text{CH}_2-\text{COOH}$  (tri);  $R_2 = -\text{CH}_3$  (mono);  $n=4$   
32:  $R_1 = -\text{CH}_2-\text{COOH}$  (tri);  $R_2 = -(\text{CH}_2)_2-\text{CH}_3$  (mono);  $n=4$   
33:  $R_1 = -\text{CH}_2-\text{COOH}$  (tri);  $R_2 = -(\text{CH}_2)_6-\text{CH}_3$  (mono);  $n=4$   
34:  $R_1 = -\text{CH}_2-\text{COOH}$  (tri);  $R_2 = -(\text{CH}_2)_9-\text{CH}_3$  (mono);  $n=4$   
35:  $R_1 = -\text{CH}_2-\text{COOH}$  (tri);  $R_2 = -(\text{CH}_2)_{11}-\text{CH}_3$  (mono);  $n=4$   
37:  $R_1 = -\text{CH}_2-\text{COONa}$  (tetra);  $R_2 = -\text{CH}_2-(\text{C}_5\text{H}_3\text{N})_2-\text{CH}_3$  (di);  $n=4$   
38:  $R_1 = -\text{CH}_2-\text{COONa}$  (tetra);  $R_2 = -\text{CH}_2-(\text{C}_5\text{HNS})_2-\text{CH}_3$  (di);  $n=4$   
39:  $R_1 = -\text{CH}_2-\text{COONa}$  (tetra);  $R_2 = -\text{CH}_2-((\text{C}_5\text{H}_2\text{N})-\text{COONa})_2-\text{CH}_3$  (di);  $n=4$   
40:  $R_1 = -\text{CH}_2-\text{COONa}$  (tetra);  $R_2 = -\text{CH}_2-((\text{C}_5\text{HNS})-\text{COONa})_2-\text{CH}_3$  (di);  $n=4$   
41:  $R_1 = -\text{CH}_2-\text{COONa}$  (tetra);  $R_2 = -\text{H}$  (no);  $n=4$   
43:  $R_1 = -\text{CH}_2-\text{NH}-\text{C}(\text{NH}_2)_2$  (tetra);  $R_2 = -\text{CH}_2-(\text{C}_5\text{H}_3\text{N})_2-\alpha\text{CH}_3$  (di);  $n=4$   
44:  $R_1 = -\text{CH}_2-\text{NH}-\text{C}(\text{NH}_2)_2$  (tetra);  $R_2 = -\text{CH}_2-(\text{C}_5\text{HNS})_2-\text{CH}_3$  (di);  $n=4$   
45:  $R_1 = -\text{CH}_2-\text{NH}-\text{C}(\text{NH}_2)_2$  (tetra);  $R_2 = -\text{CH}_2-(\text{C}_5\text{H}_3\text{N})_2-\beta\text{CH}_3$  (di);  $n=4$   
46:  $R_1 = -(\text{CH}_2)_2-\text{NH}_2$  (tetra);  $R_2 = -(\text{CH}_2)_3-\text{O}-\text{quinolone}$  (mono);  $n=4$   
47:  $R_1 = -(\text{CH}_2)_2-\text{NH}_2$  (tetra);  $R_2 = -(\text{CH}_2)_3-\text{OH}$  (mono);  $n=4$   
48:  $R_1 = -\text{C}(\text{CH}_3)_3$  (no);  $R_2 = -\text{O}-\text{CO}-\text{S}(\text{C}_2\text{N}_2\text{O})-\text{C}_5\text{H}_4\text{N}$  (di);  $n=4$   
49:  $R_1 = -\text{C}(\text{CH}_3)_3$  (no);  $R_2 = -\text{O}-\text{CO}-\text{NH}(\text{C}_2\text{N}_2\text{S})-\text{C}_5\text{H}_4\text{N}$  (di);  $n=4$   
50:  $R_1 = -\text{C}(\text{CH}_3)_3$  (no);  $R_2 = -\text{O}-\text{CO}-\text{NH}(\text{C}_2\text{N}_2\text{O})-\text{C}_5\text{H}_4\text{N}$  (di);  $n=4$   
51:  $R_1 = -\text{C}(\text{CH}_3)_3$  (no);  $R_2 = -\text{O}-\text{CO}-\text{S}(\text{C}_2\text{N}_2\text{O})-\text{C}_5\text{H}_4\text{N}$  (di);  $n=4$   
52:  $R_1 = -\text{C}(\text{CH}_3)_3$  (no);  $R_2 = -\text{O}-\text{CO}-\text{NH}(\text{C}_2\text{N}_2\text{S})-\text{C}_5\text{H}_4\text{N}$  (di);  $n=4$   
53:  $R_1 = -\text{C}(\text{CH}_3)_3$  (no);  $R_2 = -\text{O}-\text{CO}-\text{S}(\text{C}_2\text{N}_2\text{O})-\text{Ph}$  (di);  $n=4$   
54:  $R_1 = -\text{C}(\text{CH}_3)_3$  (no);  $R_2 = -\text{O}-\text{CO}-\text{NH}(\text{C}_2\text{N}_2\text{S})-\text{Ph}$  (di);  $n=4$   
55:  $R_1 = -\text{C}(\text{CH}_3)_3$  (no);  $R_2 = -\text{O}-\text{CO}-\text{S}(\text{C}_2\text{N}_2\text{O})-(\text{CH}_2)_2-\text{Ph}$  (di);  $n=4$   
56:  $R_1 = -\text{C}(\text{CH}_3)_3$  (no);  $R_2 = -\text{O}-\text{CO}-\text{NH}(\text{C}_2\text{N}_2\text{S})-(\text{CH}_2)_2-\text{Ph}$  (di);  $n=4$   
57:  $R_1 = -(\text{NH}-\text{CO}-\text{CH}_2)_2-\text{Fucose}$  (tetra);  $R_2 = -(\text{CH}_2)_2-\text{CH}_3$  (tetra);  $n=4$   
58:  $R_1 = \text{H}$  (no);  $R_2 = -(\text{CH}_2)_3-\text{SO}_3\text{H}$  (tetra);  $n=4$   
59:  $R_1 = \text{H}$  (no);  $R_2 = -(\text{CH}_2)_3-\text{SO}_3\text{H}$  (hexa);  $n=6$   
60:  $R_1 = \text{H}$  (no);  $R_2 = -(\text{CH}_2)_3-\text{SO}_3\text{H}$  (octo);  $n=8$   
61:  $R_1 = \text{SO}_3\text{H}$  (tetra);  $R_2 = -(\text{CH}_2)_3-\text{SO}_3\text{H}$  (tetra);  $n=4$   
62:  $R_1 = \text{SO}_3\text{H}$  (tetra);  $R_2 = -(\text{CH}_2)_3-\text{SO}_3\text{H}$  (hexa);  $n=6$   
63:  $R_1 = \text{SO}_3\text{H}$  (tetra);  $R_2 = -(\text{CH}_2)_3-\text{SO}_3\text{H}$  (octo);  $n=8$   
64:  $R_1 = -\text{C}(\text{CH}_3)_3$  (no);  $R_2 = -\text{H}$  (no);  $n=8$   
65:  $R_1 = -\text{Ph}$  (octa);  $R_2 = -\text{H}$  (no);  $n=8$   
66:  $R_1 = \text{SO}_3\text{H}$  (octa);  $R_2 = -(\text{CH}_2)_{11}-\text{CH}_3$  (octa);  $n=8$   
69:  $R_1 = -\text{PO}(\text{OH})_2$  (tetra);  $R_2 = -\text{H}$  (no);  $n=4$   
70:  $R_1 = -\text{PO}(\text{OH})_2$  (tetra);  $R_2 = -\text{CH}_2-(\text{C}_3\text{HNS})_2-\text{CH}_3$  (di);  $n=4$   
71:  $R_1 = -\text{CO}-\text{NH}-\text{C}_6\text{H}_3-(\text{COOH})_2$  (tetra);  $R_2 = -(\text{CH}_2)_3-\text{CH}_3$  (tetra);  $n=4$   
72:  $R_1 = \text{Amantadine}$  (tetra);  $R_2 = -\text{H}_3$  (no);  $n=4$   
73:  $R_1 = \text{Amantadine}$  (tetra);  $R_2 = -(\text{CH}_2)_3-\text{CH}_3$  (tetra);  $n=4$   
75:  $R_1 = -\text{SO}_3\text{Na}$  (tetra);  $R_2 = -\text{CH}_2-(\text{C}_3\text{HNS})_2-\text{CH}_3$  (di);  $n=4$   
77:  $R_1 = -\text{N}=\text{N}-\text{Ph}-\text{SO}_3\text{H}$  (tetra);  $R_2 = \text{H}$  (no);  $n=4$   
78:  $R_1 = -\text{H}$  (no);  $R_2 = \text{H}$  (no);  $n=4$   
79:  $R_1 = -\text{H}$  (no);  $R_2 = \text{H}$  (no);  $n=6$   
80:  $R_1 = -\text{H}$  (no);  $R_2 = \text{H}$  (no);  $n=8$   
81:  $R_1 = -\text{C}(\text{CH}_3)_3$  (no);  $R_2 = \text{H}$  (no);  $n=4$   
82:  $R_1 = -\text{C}(\text{CH}_3)_3$  (no);  $R_2 = \text{H}$  (no);  $n=6$   
83:  $R_1 = -\text{C}(\text{CH}_3)_3$  (no);  $R_2 = \text{H}$  (no);  $n=8$   
86:  $R_1 = -\text{H}$  (no);  $R_2 = -\text{CH}_2-\text{N}(\text{CH}_3)_2$  (tetra);  $n=4$   
90:  $R_1 = -\text{H}$  (no);  $R_2 = -\text{CH}_2-\text{CO}(\text{COO})_2-\text{Pt}(\text{NH}_3)_2$  (tetra);  $n=4$   
91:  $R_1 = -\text{PO}(\text{OH})_2$  (tetra);  $R_2 = -\text{H}$  (no);  $n=4$   
92:  $R_1 = -\text{PO}(\text{OH})_2$  (tetra);  $R_2 = -(\text{CH}_2)_5-\text{CH}_3$  (tetra);  $n=4$   
93:  $R_1 = -\text{PO}(\text{OH})_2$  (tetra);  $R_2 = -(\text{CH}_2)_7-\text{CH}_3$  (tetra);  $n=4$   
94:  $R_1 = -\text{PO}(\text{OH})_2$  (tetra);  $R_2 = -(\text{CH}_2)_9-\text{CH}_3$  (tetra);  $n=4$   
95:  $R_1 = -\text{PO}(\text{OH})_2$  (tetra);  $R_2 = -(\text{CH}_2)_{11}-\text{CH}_3$  (tetra);  $n=4$   
96:  $R_1 = -\text{PO}(\text{OH})_2$  (tetra);  $R_2 = -(\text{CH}_2)_{13}-\text{CH}_3$  (tetra);  $n=4$   
97:  $R_1 = -\text{PO}(\text{OH})_2$  (tetra);  $R_2 = -\text{H}$  (no);  $n=5$   
98:  $R_1 = -\text{NH}-\text{CO}-\text{TA}$  antigen (tetra);  $R_2 = -\text{P3CS}$  (mono);  $n=4$   
99:  $R_1 = -\text{NH}-\text{CO}-\text{TA}$  antigen (tetra);  $R_2 = -\text{P3CS}$  (mono);  $n=8$   
100:  $R_1 = -\text{NH}_2$  (tetra);  $R_2 = -(\text{CH}_2)_{11}-\text{CH}_3$  (tetra);  $n=4$   
101:  $R_1 = \text{CH}_2\text{OH}-\text{N}(\text{CH}_3)_2$  (tetra);  $R_2 = -(\text{CH}_2)_7-\text{CH}_3$  (tetra);  $n=4$   
102:  $R_1 = -\text{NH}-\text{C}(\text{NH}_2)_2$  (tetra);  $R_2 = -(\text{CH}_2)_5-\text{CH}_3$  (tetra);  $n=4$   
103:  $R_1 = -\text{NH}-\text{C}(\text{NH}_2)_2$  (tetra);  $R_2 = -(\text{CH}_2)_7-\text{CH}_3$  (tetra);  $n=4$   
104:  $R_1 = -\text{C}(\text{CH}_3)_3$  (no);  $R_2 = -(\text{CH}_2)_3-\text{NH}-\text{CH}(\text{NH}_2)_2$  (tetra);  $n=4$   
105:  $R_1 = -\text{H}$  (no);  $R_2 = -(\text{CH}_2)_3-\text{NH}-\text{CH}(\text{NH}_2)_2$  (tetra);  $n=4$   
106:  $R_1 = -\text{CH}_2-\text{CH}_3$  (tetra);  $R_2 = -(\text{CH}_2)_3-\text{NH}-\text{CH}(\text{NH}_2)_2$  (tetra);  $n=4$   
107:  $R_1 = -\text{H}$  (no);  $R_2 = -\text{PO}(\text{OH})_2$  (di);  $n=4$   
117:  $R_1 = -\text{NH}-\text{CO}-\text{CH}_2-\text{NH}_3$  (tetra);  $R_2 = -(\text{CH}_2)_2-\text{CH}_3$  (tetra);  $n=4$   
118:  $R_1 = -\text{C}(\text{CH}_3)_3$  (no);  $R_2 = -\text{CH}_2-\text{COOH}$  (tetra);  $n=4$

## 2. Hemotoxicity (also Haemotoxicity)

In the development process of new therapeutical compounds, analysis of haemolytic effects is clearly the first and easiest step, initial work by Coleman *et al.* concerned the series of calix[n]arenes derivatives **1** to **9** (Table 1) (Da Silva *et al.*, 2004).

*Para*-sulphonato-calix[n]arene derivatives show no or little haemolytic effect. In the worst case, a maximum haemolysis of 30% for *para*-sulphonato-calix[8]arene **3** has been observed at a concentration of 200mM (equivalent to 300g per liter of human blood). The hemotoxicity of a series of amphiphilic calix[n]arenes, **10** to **15**, assembled as Solid Lipid Nanoparticle has been also reported by the same group (Shahgaldian *et al.*, 2003). Neither variation in chain length of the hydrophobic moiety (with variation from 4, 6, 8 and 10 carbons in alkyl chain) nor variation in the nature of polar head (hydroxide, ethyl phosphate or phosphate) led to haemolysis in human erythrocytes. The hemotoxicity of amphiphilic calix[n]arenes **16** and **17** conjugated to the antifungal drug Amphotericin B has been evaluated. The index  $EH_{50}$  is conventionally used for determining the haemotoxicity of a compound, it corresponds to the concentration of one molecule for releasing 50% of total haemoglobin from dead erythrocytes.  $EH_{50}$  of the conjugated calix[n]arene **16** has been determined to be 50  $\mu$ M. Even if the hemotoxicity of the compound is much higher than the previous calix[n]arenes **1**, **2** and **3**, this is still 10 times lower than the drug itself where the  $EH_{50}$  is 4  $\mu$ M (Paquet *et al.*, 2006).

A few examples of hemotoxicity of cationic calix[n]arene have been reported in the literature. Compared to the anionic calix[n]arene described above, cationic calix[n]arenes are expected to possess higher hemotoxicity because of their ability to interact with negatively charged membrane. Loftsson *et al.* investigated three different amino-calix[4]arene derivatives. **19** and **20** have showed significant haemolytic properties with an  $EH_{50}$  around 50  $\mu$ M. Despite its structural similarity **18** has surprisingly shown less than 1.4% of haemolysis at 100  $\mu$ M (Ukhatskaya *et al.*, 2013).

## 3. Detoxifying agents

### *Ex vivo* experiments

Calix[n]arenes have been evaluated for treating skin contamination by Uranium. The high risk on human health of this element is well known but no efficient treatment is available yet. Fattal *et al.* have proposed a *para-tert*-butyl-calix[6]arene **21** for complexing uranium by chelation. Under the form of a nano-emulsion, calix[n]arene has been able to extract 80% of uranium in solution. The *in vitro* skin diffusion bioassays were performed on Franz Cell chambers, which consist of 2 primary chambers separated by a pig ear skin. When the calix[n]arene has been applied topically, the decrease of uranium diffusion through the skin has been reported to be 98 % (Spagnul *et al.*, 2010). Later, complementary results were given with the diffusion of same compounds through skin pig excoriated in order to mimic contamination on wounds (Spagnul *et al.*, 2011a). The application of the calix[n]arene

nanoemulsion immediately after the contamination step induced a decrease of 97.5% diffusion (Spagnul *et al.*, 2011b).

### ***In vivo* experiments**

The pioneering work of Coleman *et al.* reported the non-toxicities of *para*-sulphonato-calix[4]arene **1** in mice, with injections up to 200mg/Kg (extrapolated from the known mouse weight), within a rapid clearance from the body in urine (Coleman *et al.*, 2008). No accumulation in the liver was observed here. Since that point, *para*-sulphonato-calix[n]arenes have been investigated *in vivo* as detoxifying agents for the treatment of diverse contaminations or poisonings. Liu and Qi groups respectively evaluated *para*-sulphonato-calix[n]arene for preventing and detoxifying paraquat and viologen poisoning. The co-injection of complex **3** / paraquat decreased significantly the mouse mortality compared to the paraquat injection (Wang *et al.*, 2009). Later, the detoxification of contaminated mice has been assessed with injection of paraquat in rats, 30 minutes before receiving a calix[n]arene injection. A survival rate of 100% was achieved with a molar ratio paraquat / calix[n]arene **3** of 1:1, while the untreated poisoned mice have shown 50% of mortality after 7 days (Wang *et al.*, 2011). A dosage method of paraquat in blood by HPLC has been developed in order to understand that the complex is excreted by clearance on gastrointestinal tract while paraquat alone is absorbed by the blood vessels of the mouse leading to death.

Recently, another study has pointed out the detoxification ability of *para*-sulphonato-calix[8]arene **3** for a leukotoxin called Panton-Valentine Leucocidin PVL (Laventie *et al.*, 2013). These virulent proteins are one of the most common bacterial toxins which cause necrosis of human cells by forming holes in the host cell membrane. *Para*-sulphonato-calix[8]arene **3** has been demonstrated as interacting with this toxin by mass spectrometry and inhibiting its insertion in the membrane using flow cytometry (by monitoring the penetration of a fluorophore molecule through the pores formed by the toxin). These effects were also observed *in vivo* on New Zealand rabbit by injecting in the eyes a saline solution containing a leukotoxin and/or **3** at 30 or 300 µg. The inflammation response induced by the toxin is considerably reduced by **3** (Figure 2).

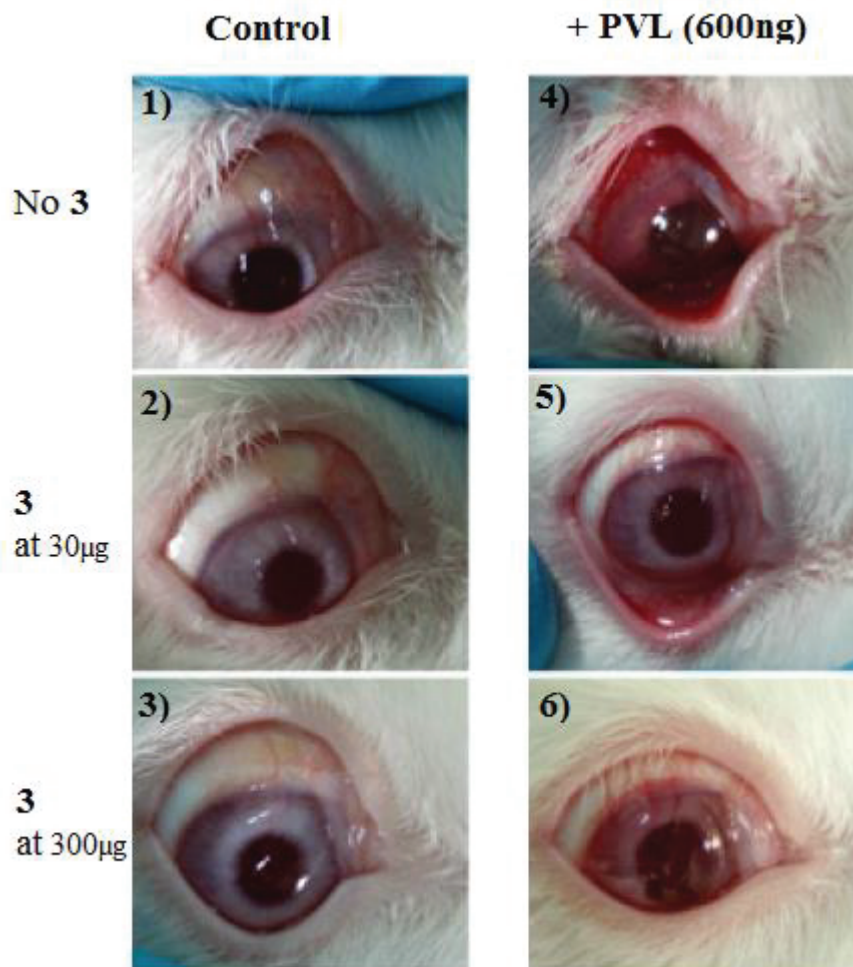
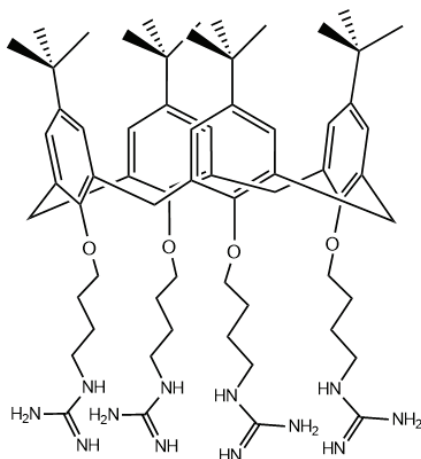


**Figure 2-** Rabbit eye *in vivo* toxicity assays (Laventie *et al.*, 2013). Pictures represent the injection of 1) Blank, 2) **3** at 30µg, 3) **3** at 300µg, 4) PVL at 600ng, 5) PVL at 600ng + **3** at 30µg, 6) PVL at 600ng + **3** at 300µg. With permission from Biochemical Society.

Mayo *et al.* have also reported the neutralization of another bacterial protein toxin, Lipo Poly Saccharide LPS endotoxin which can trigger macrophages to produce high level of cytokines and to induce septic shock. One amino calix[n]arene derivative **22** (Figure 3) has shown particularly good results with 100 % survival in a mice group when it was co-injected with a lethal dose of endotoxin. 0 % survival has been found for the control group. (Chen *et al.*, 2006)



22

**Figure 3-** Structure of amino-calix[n]arene derivative **22** studied by Mayo (Chen *et al.*, 2006).

#### 4. Anti-coagulant Behaviour

Blood coagulation is a result of a complex cascade of biochemical reactions that lead to the gelification of blood. Thus it prevents blood loss and allows damaged blood vessels to be repaired. This process is vital and its disorder can lead to severe diseases such as haemophilia (no or low coagulation rate) or thromboembolism which can happen after a surgery (induced by an excessive coagulation and causing the complete obstruction of the blood vessels). Hwang *et al.* have first highlighted, in a patent, the action of anionic calix[n]arenes as anticoagulant agents (Hwang *et al.*, 1995). Here the experiments were undertaken on blood plasma, platelet suspensions and *in vivo*. The decrease of coagulation rate has been observed in all case for one sulphonate-calix[n]arene **23** (Figure 4). More details are given in the '*In vivo*' section below.

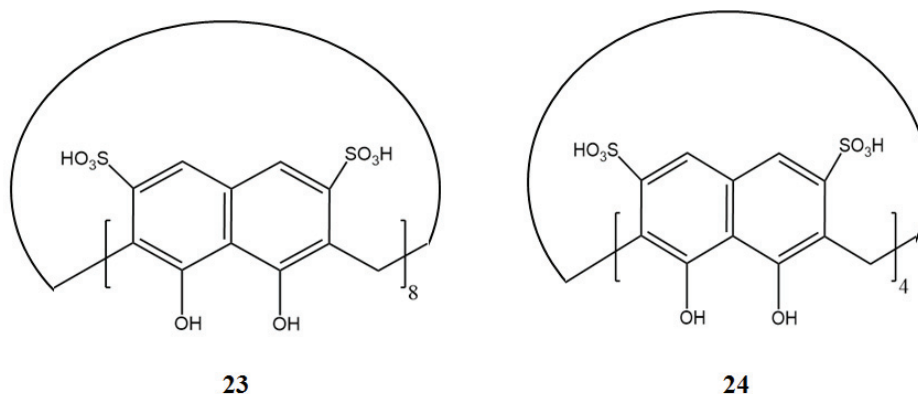


**Figure 4-** Structure of sulphonato-calix[n]arene derivatives **23** and **24** studied by Hwang (Hwang *et al.*, 1995)

Later, Coleman *et al* have investigated the anti-thrombotic activity on others sulphonate-calix[n]arene derivatives **1** to **9** (Da Silva *et al.*, 2005). Thrombin is a serine protease involved in several reactions of the coagulation reactions pathway. An important example of his action results in the conversion of soluble fibrinogen into insoluble strands of fibrin by thrombin, which ultimately results in the coating of the damaged vessel. It can be inhibited by Anti-Thrombin (AT) and Heparin Cofactor II (HC-II). For evaluating this anticoagulant activity on fresh blood plasma, an Activated Partial Thromboplastin Time (APTT) has been used. This bioassay consists by adding  $\text{CaCl}_2$  in order to trigger blood cascade coagulation and to monitor the time of coagulation by spectroscopy. Without calix[n]arene the coagulation time is 70s while after adding 13  $\mu\text{M}$  of calix[6,8]arene **2**, **3**, **5**, **6**, **8** and **9** the time of coagulation have been increased respectively to 250, 325, 220, 400, 240 and 260 s. The calix[4]arene **1**, **4**, **7** have not increased the initial coagulation time (70s). Here it has been found that sulphonate-calix[n]arene derivatives inhibit preferentially HC-II and a large sized calix[n]arene cavity (8 phenolic units) is shown to be more efficient for decreasing coagulation time. Calix[8]arene **3** and **6** increase respectively the coagulation time by 5.7 and 4.6 at 13  $\mu\text{M}$ .

Kalchenko *et al.* have investigated the effects of calix[n]arene phosphonic acid derivatives as a matter of fibrin polymerisation. Calix[n]arene **25** has been shown to be a specific inhibitor of fibrin polymerisation with an  $\text{IC}_{50}$  of 1.26  $\mu\text{M}$  and also double blood coagulation time at 11  $\mu\text{M}$  (Lugovskoy *et al.*, 2011).

On the other hand, cationic calix[n]arenes have been studied by Cunsolo *et al.* as antagonists of heparin A (isolated from porcine intestinal mucosa) for their coagulating properties (Cunsolo *et al.*, 2007). Heparin, a sulphonated polysaccharide belonging to the glycosaminoglycans family, is a compound having anticoagulant activity due to its ability to enhance specifically Anti-Thrombin and subsequently inhibit thrombin and other enzymatic factors involved in the coagulation cascade reaction. A polycationic calix[8]arene derivative, **26**, bearing lysine groups at *para* face has been demonstrated to neutralize heparin faster and more efficiently than classical heparin antagonists (protamine and polylysine) in blood (Mecca *et al.*, 2006). Later, this cationic calix[n]arene has been grafted on PVC surface in order to develop a new filter or membrane material enable to remove heparin (treatment required after a surgery). The treated material has been estimated to remove 0.7mg of Heparin for 10mg of resin by titrating the anticoagulant activity before and after filtration. There is a loss of 30% compared to heparin in aqueous solution, probably due to the attachment of non-specific proteins present in the blood (Mecca *et al.*, 2010).

### ***In vivo* experiments**

To our knowledge, Hwang *et al.* are the only one who have investigated the effect of calix[n]arenes *in vivo* as anti-coagulant agents. The main routes of drug delivery are intravenous and oral, with the preferred route being oral. Both **23** and **24** have been administrated using both routes to rats and have been shown to be active (with a higher effect for **23**, which has showed additional anti-platelet activity). Peak effects after oral administration were dose dependent and were observed between about 0.5 and 4 hours

following oral administration of 450 mg/kg **23**, as assessed by *in vitro* coagulation experiment. Sulphonato calix[n]arene derivative **23** produces significant anticoagulant activity for 4 or more hours when it has been injected by intravenous administration, the duration of effect being dependent on the dose administered. When administered orally, the bleeding (or anticoagulation time) has been increased by compound **23** almost 2 times compared to blank.

## 5. Activity against membrane proteins

Membrane proteins accomplish various vital functions in human cells, such as cell signalling transduction, ions / molecules transport, cellular adhesion and other enzymatic functions. Therefore, they represent a target of choice for pharmaceutical companies. In cell culture experiments, various calix[n]arenes have been investigated as extracting agents and as activity modulators of membrane proteins.

Kalchenko *et al.* have studied in depth the action of various calix[n]arenes on ATPases. These membrane proteins are essential for importing many of the metabolites from outside medium to the cellular metabolism and in return exporting toxins, wastes, and solutes that can hinder cellular processes.  $\text{Na}^+/\text{K}^+$  ATPases maintain the cell membrane potential while  $\text{Ca}^{2+}/\text{Mg}^{2+}$  ATPases control intracellular calcium concentration for muscular contraction function. Calix[n]arene phosphonic acids have been demonstrated to inhibit  $\text{Na}^+/\text{K}^+$  ATPase more efficiently than Ouabain (cardiac drug). A specific effect with **27** has been shown on myocytes (muscle cells) with 84-88% of activity decrease compared to spermatozoid control cells where a 15-20% of activity decrease was observed (Kalchenko *et al.*, 2013). A later study has shown the enhancement of  $\text{Ca}^{2+}$  transportation by ATPase in mitochondria (20%) and sarcoplasmic reticulum (40%) with calix[4]arene N-chalconeamide **28**. The experiment was performed with various calix[n]arenes on myocytes from rat uterus and the  $\text{Ca}^{2+}$  accumulation has been followed by radioactive tracer (Klyachina *et al.*, 2008). More recently, the Kiev group has found that calix[4]arene **29** with four trifluoromethylphenyl sulfonylimine groups at the *para* face inhibits selectively  $\text{Ca}^{2+}/\text{Mg}^{2+}$  ATPase compared to  $\text{Na}^+/\text{K}^+$  ATPase. In a preliminary study, the increase of intracellular calcium concentration upon the addition of calix[n]arene **29** in myocyte rat cells was measured by use of a  $\text{Ca}^{2+}$  sensitive fluorescent probe (Veklich *et al.*, 2014). This calix[n]arene derivative could be a promising drug for some uterine pathologies related to contraction disorder such as uterine inertia, uterine bleeding, etc.

*In vitro* experiments have shown that calix[n]arenes inhibit chloride channel membrane protein by *para*-sulfonato-calix[4,6,8]arenes **1**, **2**, **3** (Atwood *et al.*, 1996) and p64 membran protein by *para*-tetra(sulfonato)-tetra(methoxy)calix[4]arene (Edwards *et al.*, 1998). However their effect on cell lines is varied. In cellular experiments, calix[n]arenes have shown little effect on chloride channel protein expressed in cultured rat Sertoli cells (Auzanneau *et al.*, 2006) and has been more often used as negative control of Cystic Fibrosis Transmembrane conductance Regulator protein (CFTR) which is also a chloride channel

membrane protein (Li *et al.*, 2004) (Bertrand *et al.*, 2010). However, Izzo *et al.* have used with success an 1,3-Alternate amino calix[4]arene **30**. The inhibition of the anionic transport has been characterized *in vitro* and an anti-proliferative effect on cancer cell lines was demonstrated (with a concentration of 47  $\mu\text{M}$  for inhibiting 50% of the proliferation (Izzo *et al.*, 2008).

One of the big challenges in biochemical research is to determine the solid-structure of membrane proteins in order to design more efficient new drugs. Coleman *et al.*, have proposed an elegant method using micelle forming calix[n]arenes (**31**, **32**, **33**, **34** and **35**) in order to extract the membrane protein (BmrA, YheI/YheH, ABCG2, AcrB or SR  $\text{Ca}^{2+}$ -ATPase membrane proteins) from cell membranes while retaining its activity (Matar-Merheb *et al.*, 2011). Amphiphilic calix[n]arene derivatives have been synthesized and used for extracting different membrane proteins from prokaryote (*E. coli*) to higher eukaryote cell lines (*Spodoptera frugiperda* insect cells and Human Embryonic Kidney cells). In particular, a Bacillus Multidrug-transporting Resistance ATP protein (BMRA) has been successfully extracted by calix[n]arenes **31** and **32** compared to the commercially available detergents DDM and FC12. The protein extracted with calix[n]arene is still fully functional and has been crystallized in order to determine its structure (Figure 5). A patent relating a method for selectively extracting membrane proteins using calix[n]arenes has been obtained and the product is now commercialised (Coleman *et al.*, 2011).

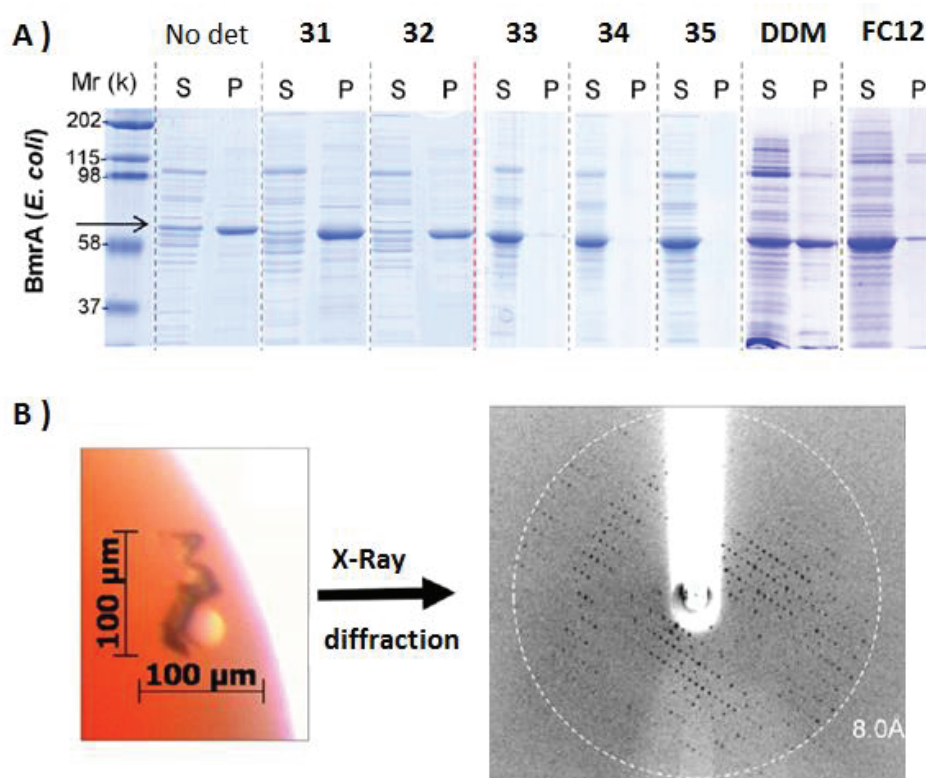


**Figure 5-** A) SDS Page electrophoresis gel showing protein before and after purification and/or calix[n]arene. From left to right, the extraction was performed without any compound (No det), with Calix[n]arene **31**, **32**, **33**, **34** and **35** and then DDM and FC12. B) Protein extracted by calix[n]arene is crystallized on left and the X-Ray diffraction pattern on right (Matar-Merheb *et al.*, 2011).

## 6. Fluorescent probes

Matthews and Mueller have reported the use of different calix[n]arene derivatives as fluorescent probes for cytoplasm or lysosome markers. First, an amino-calix[4]arene derivative **36** conjugated to the fluorescent marker NBD has demonstrated interesting properties: stability, low toxicity, cytoplasmic localization (Figure 6) (Lalor *et al.*, 2008). The toxicity of this calix[n]arene has been reported in a preliminary study for two cell lines Chinese Hamster Ovarian (CHO) and Human promyelocytic leukemia (HL-60) cell lines with respective  $IC_{50}$  value of 82 mM and 8 mM. Moreover, uptake of the calix[n]arene has been demonstrated to be a non-specific process, not based on main endocytic pathways such as caveolae-linked endocytosis.

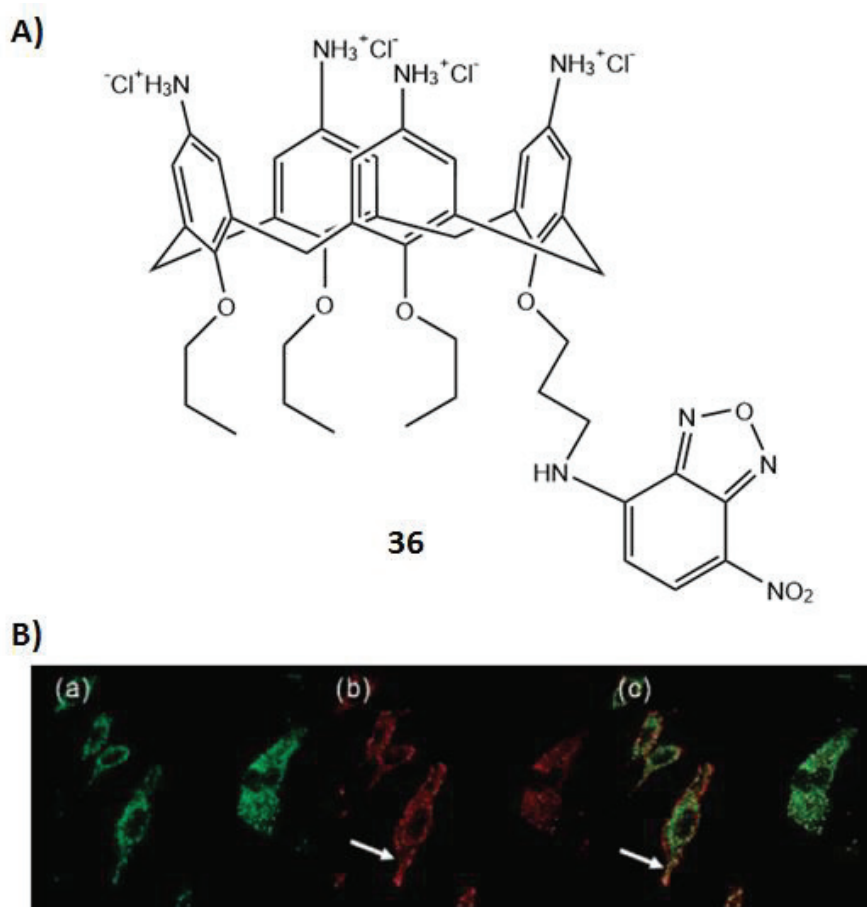


**Figure 6-** A) Structure of amino-calix[4]arene derivative **36** investigated by Matthews (Lalor *et al.*, 2008) B) Fluorescence images of colocalization studies showing cytoplasmic localization of **36**. In green: **36** (a) In red: an antibody anti-CCR5 receptor (b) In green and red: **36** + antibody anti-CCR5 (c) With permission from American Chemical Society.

Later, the localization of this calix[n]arene has been demonstrated to be specific to lysosome and to possess advantages over some commercial available marker. Compared to LysoTracker® Red, the calix[n]arene does not need special dye cell medium after staining (Mueller *et al.*, 2011). A vanadyl sulfonylcalix[4]arene has been selected as a potent fluorescent probe, among 6 vanadyl calix[4]arene derivatives. It has shown some interesting

capacity such as its cellular uptake and its non-toxicity. After its uptake inside the cell, it exhibits a blue fluorescence (475 nm) and no toxicity over the range 0.0001-1mM for CHO, HL-60, HeLa (cervical cancer cells) and THP1 (human monocytic cells) cell lines. However, the uptake kinetic of the calix[n]arene is too slow (no uptake is visible after 15 minutes) for further study as a useful fluorescent probe (Redshaw *et al.*, 2012).

To our knowledge, no *in vivo* studies have as yet cited the use of calix[n]arenes as fluorescent probes.

## 7. Antibacterial Activity

Calix[n]arenes has been reported by Cornforth *et al.* as early as 1955 to be antibiotic agent (Cornforth *et al.*, 1955). However, because of the efficiency of classical antibiotics, these molecules were not further investigated until recently. Nowadays, the emergence of multi-resistant drug pathogenic bacteria is requiring the development of new drugs for efficient antibiotic treatment and the calix[n]arenes have once more attracted attention in this area.

In this research field, the group of Regnouf-de-Vains has undertaken a large body of work. The antimicrobial activity of calix[n]arenes reported in the literature is summarized in Table 2. The bacterial species have been selected for covering Gram + and Gram – strains that grow aerobically, following the guidelines of the CLSI (Grare *et al.*, 2010). The antimicrobial activity has been mostly reported by Minimum Inhibition Concentrations method which is defined as the lowest concentration of an antimicrobial that will inhibit the visible growth of a microorganism after overnight incubation (Andrews, 2001).

With regard to the table 2, it is important to note that *para*-guanidoethyl-calix[4]arene **42** derivative has the lowest MIC values corresponding to the highest antibacterial effects for *E. coli* bacteria Gram -. A remarkable gain of antibacterial activity has been shown from integration of bi-thiazolyl-methyl subunits at the phenyl position of *para*-guanidoethyl-calix[4]arene derivative **44** (up to 6 times for Gram + for *E. faecalis*) (Grare *et al.*, 2007). This may be attributable to the new amphiphilic nature of the calix[n]arene. The lack of cytotoxicity makes these compounds as promising antibiotic or antiseptic candidates. Recently, the bactericide mechanism of action of this calix[n]arene **42** has been elucidated on *P. aeruginosa* by AFM experiments (Formosa *et al.*, 2012). The effect on bacterial cell wall nanoscale organization has been particularly studied using lectin functionalized AFM tips. Lectin possesses strong adhesion properties against peptidoglycans in contrast to the outer membrane of Gram - bacteria. Peptidoglycan layer becomes visible when the outer membrane is damaged by lectin functionalized AFM tips. First the cationic calix[n]arene interacts with the negatively charged ultrastructures of the bacterial surface (i.e. phospholipids and lipopolysaccharides) and then it has been clearly demonstrated that the calix[n]arene damages the outer membrane of negative bacteria strain by creating holes in it (Figure 7).

**Table 2-** Antibacterial effect of calix[n]arenes presented in this review

Article	Calixarene	Antibacterial effect expressed in MIC ( $\mu$ M)								
		Gram -				Gram +				
		<i>E. coli</i> (ATCC 25922)	<i>E. coli</i> (MTCC 443)	<i>P. aeruginosa</i> (ATCC 27853)	<i>P. aeruginosa</i> (MTCC 1688)	<i>E. faecalis</i> (ATCC 29212)	<i>S. aureus</i> (ATCC 25923)	<i>S. aureus</i> (ATCC 29213)	<i>S. aureus</i> (MTCC 96)	<i>S. pyogenes</i> (MTCC 442)
Mourer <i>et al.</i> , 2012	37	>194	ND*	>194	ND*	>194	>194	>194	ND*	ND*
	38	>197	ND*	>197	ND*	>197	>197	>197	ND*	ND*
	39	>105	ND*	>105	ND*	>105	>105	>105	ND*	ND*
	40	>141	ND*	>141	ND*	>141	70.5	>141	ND*	ND*
	41	>275	ND*	>275	ND*	>278	>276	>277	ND*	ND*
Grare <i>et al.</i> , 2007	42	3.2	ND*	26	ND*	26	6.5	6.5	ND*	ND*
Mourer <i>et al.</i> , 2009	43	8.6	ND*	8.6	ND*	8.6	8.6	8.6	ND*	ND*
	44	17	ND*	17	ND*	4.2	4.2	4.2	ND*	ND*
	45	9.5	ND*	9.5	ND*	4.7	4.7	9.5	ND*	ND*
Massimba Dibama <i>et al.</i> , 2009	46	25	ND*	100	ND*	100	50	50	ND*	ND*
	47	110	ND*	220	ND*	>220	220	220	ND*	ND*
Ukhatskaya <i>et al.</i> , 2013	18	15.6	ND*	ND*	ND*	ND*	ND*	15.6	ND*	ND*
	19	28	ND*	ND*	ND*	ND*	ND*	13.9	ND*	ND*
	20	22.4	ND*	ND*	ND*	ND*	ND*	11.2	ND*	ND*
Patel <i>et al.</i> , 2012	48	ND*	184	ND*	184	ND*	ND*	ND*	91.9	184
	49	ND*	92.1	ND*	184	ND*	ND*	ND*	184	184
	50	ND*	94.9	ND*	94.9	ND*	ND*	ND*	237	237
	51	ND*	184	ND*	184	ND*	ND*	ND*	91.9	230
	52	ND*	230	ND*	230	ND*	ND*	ND*	230	184
	53	ND*	184	ND*	184	ND*	ND*	ND*	92.1	184
	54	ND*	231	ND*	231	ND*	ND*	ND*	231	231
	55	ND*	87.9	ND*	87.9	ND*	ND*	ND*	87.9	176
	56	ND*	176	ND*	88	ND*	ND*	ND*	176	176
	Ampicillin	ND*	269	ND*	269	ND*	ND*	ND*	673	269
Grare <i>et al.</i> , 2010	Hexamidine	11.9	ND*	47.8	ND*	6	3	<1.5	ND*	ND*
	Chlorhexidine	<1.11	ND*	4.4	ND*	<1.1	<2.2	<1.1	ND*	ND*

ND\*: Not Determined

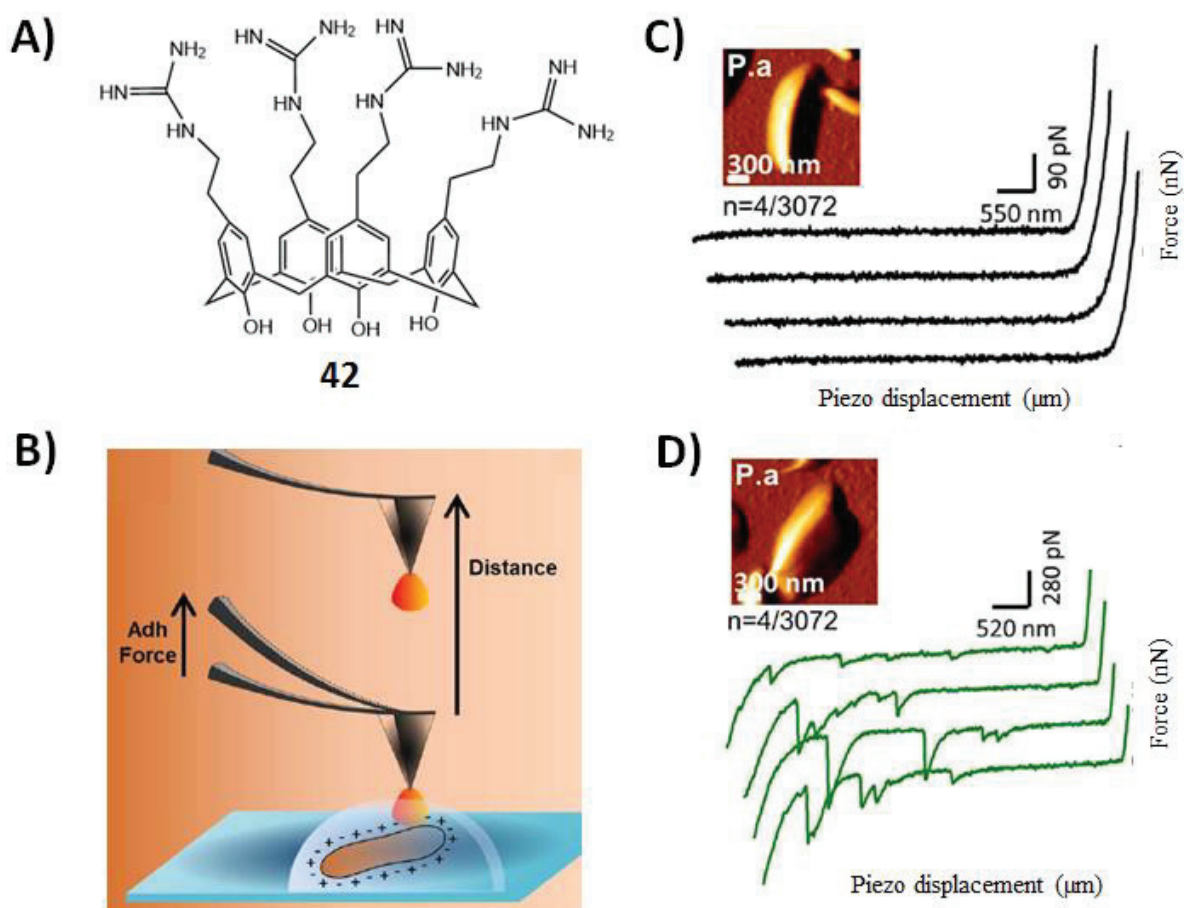


**Figure 7-** A) Structure of *para*-guadinoethyl-calix[4]arene **42** studied by Regnouf-de-Vains (Formosa *et al.*, 2012) B) Schematic representation of AFM experiment C) AFM force spectroscopy images of bacteria without treatment D) AFM force spectroscopy images of bacteria treated with **42**. With permission of Nature Publishing Group.

Consoli *et al.* have reported a new calix[n]arene-based C-fucosyl derivative **57** as a new *P. aeruginosa* biofilm inhibitor (Consoli *et al.*, 2011). The fucosyl group plays the role of a glycon mimic blocking the adhesion and colonization of the bacteria. In liquid medium, the calix[n]arene has not shown any antimicrobial activity at 200  $\mu\text{M}$ . However, when the calix[n]arenes are mixed with the bacterial culture, biofilm formation has been inhibited at a lowest concentration value of 12.5  $\mu\text{M}$ .

A series of 57 calix[n]arene derivatives has been evaluated by Lamartine *et al.* against another Gram + bacteria, *Corynebacterium*. Seven among them have shown antibacterial properties including *para*-sulphonato-calix[n]arene **1**, **2** and **3**. Sulphonate groups have been highlighted to be important in the antibacterial action. Here the synthetic route used causes the results for **1**, **2** and **3** to be treated with caution (Lamartine *et al.*, 2002).

Recently, Coleman and Rhimi have investigated sulphonato calix[n]arene derivatives (**1**, **2**, **3**, **58**, **59**, **60**, **61**, **62** and **63**) capped on silver nanoparticles as antibacterial agents. These hybrid nanoparticles have shown antibacterial properties at 100 nM of calix[n]arene, with discriminative effects according to the Gram type of bacteria. *Para*-sulphonato-calix[n]arenes **1**, **2** and **3** have been demonstrated to be effective against Gram + with

increasing effect as a matter of their large size. In contrast, with sulphonate groups present on both side of the calix[n]arene, **61** and **62**, affect only Gram – bacteria (Boudebouze *et al.*, 2012).

Anti-tuberculosis or anti-mycobacterial agents form a special class in antibacterial compounds. Tuberculosis (TB) is an infectious, often fatal, disease caused by the bacillus *Mycobacterium tuberculosis*, classified as acid-fast Gram + bacteria due to their lack of an outer cell membrane. In 2012, 8.6 million people fell ill with TB and 1.3 million died. The persistent resistance of these bacteria to antibiotic has required the development of new drugs. Calix[n]arenes are reported as one of new promising anti-tuberculosis evaluated with antibacterial experiment and tested *in vivo*. Fernandes *et al.* have complexed *para*-sulphonato-calix[n]arene with Isonicotinic hydrazide (INH), a classic commercial Active Pharmaceutical Ingredient (API). After having demonstrated the inclusion of INH in *para*-sulphonato-calix[n]arene by NMR, the MICs have been determined to be comparable between INH (1.5 mM) and the complex **1** / INH (2.6 mM) and **2** / INH (1.8 mM) (De Assis *et al.*, 2012). Therefore, the calix[n]arene derivatives keep available the active region of the API. This is a great interest for developing new formulations with better pharmaceutical paramounts such as higher solubility or better bio-availability.

### ***In vivo* experiments**

To our knowledge, the only *in vivo* study of the antibacterial effect of calix[n]arenes is for anti-tuberculosis action. In 1955, Cornforth *et al.* evaluated the effect of amphiphilic calix[n]arene derivatives *in vivo* (Cornforth *et al.*, 1955). The best chemotherapeutic results were achieved with a calix[n]arene **111** bearing on the lower rim a short aliphatic chain and were comparable to the effect of streptomycin. None of the calix[n]arene evaluated have anti-tuberculous effect *in vitro*. Thus, it has been suggested that these calix[n]arene derivatives act indirectly against the host rather than by direct antibacterial action. During this period, a number of anti-tuberculosis agents have been developed such as streptomycin, p-aminosalicylic acid, pyrazinamide, cycloserine and INH in 1952 as the first-line medication in prevention and treatment of tuberculosis. The commercialization of these drugs associated with the establishment of a wide vaccination program had almost eradicated tuberculosis, and subsequently stopped the research on calix[n]arene as anti-tuberculosis agent. Because of the recent re-emergence of tuberculosis and particularly highly resistant strains, Hailes *et al.* have re-investigated the antituberculous effect of the same active calix[n]arene used by Cornforth and other derivatives (See table 3) (Goodworth *et al.*, 2011). Therefore homogeneous calix[n]arene macrocylcon studied from Cornforth, a new series of amphiphilic and sulphonated calix[n]arene analogues have been synthesized and evaluated *in vivo* on mice. The homogenous pegylated calix[n]arene of Cornforth **111** has confirmed his high antituberculous activity. Moreover, the pegylation of *para*-tert-butylcalix[8]arene **64** has enhanced readily its antituberculosis activity. When they are not pegylated at the lower rim, *para*-tert-butylcalix[8]arene **64** and *para*-phenylcalix[8]arene **65** are more active than same calix[n]arenes with a smaller ring size **108**, **109** and **110**. Finally, *Para*-sulphonato-calix[8]arene alkylated **66** or not **3** have similar activity when injected in mice at 10-15 mg/mL (corresponding to 5mM of **3**). However the sulphonate calix[n]arene **3** is highly

soluble compared to the amphiphilic derivative and could be used at higher concentration in order to reach better therapeutic effect and better biodistribution. The anti-tuberculosis mechanism of action of the calix[n]arenes remains unclear.

**Table 3-** Anti-tuberculous activity of calixa[n]arene derivatives. All activities measured *M. tuberculosis* growth in mice spleens and lung. – is non-detectable activity; ± is 0-20% activity; + is 20-50% activity; ++ is 50-80% activity and +++ is 80-100% activity. From (Goodworth *et al.*, 2011).

Calixarene	Ring size (n)	R <sub>1</sub>	R <sub>2</sub>	Anti tuberculous activity	Reference
<b>111</b>	8	tC <sub>8</sub> H <sub>19</sub>	(CH <sub>2</sub> CH <sub>2</sub> O) <sub>n</sub> H (with n = avg 12.5)	+++	Cornforth <i>et al.</i> , 1955
	8	tC <sub>4</sub> H <sub>9</sub>	(CH <sub>2</sub> CH <sub>2</sub> O) <sub>6</sub> H	+++	Calston <i>et al.</i> , 2004
	8	tC <sub>4</sub> H <sub>9</sub>	(CH <sub>2</sub> CH <sub>2</sub> O) <sub>12</sub> H	+++	
	8	tC <sub>4</sub> H <sub>9</sub>	(CH <sub>2</sub> CH <sub>2</sub> O) <sub>3</sub> Me	+++	Goodworth <i>et al.</i> , 2011
<b>3</b>	8	SO <sub>3</sub> H	H	++	
<b>66</b>	8	SO <sub>3</sub> H	OC <sub>12</sub> H <sub>25</sub>	++	
	8	tC <sub>4</sub> H <sub>9</sub>	bi-substituted (CH <sub>2</sub> CH <sub>2</sub> O) <sub>12</sub> H	+	
	8	tC <sub>4</sub> H <sub>9</sub>	bi-substituted (CH <sub>2</sub> CH <sub>2</sub> O) <sub>6</sub> H	+	
	8	tC <sub>8</sub> H <sub>17</sub>	bi-substituted (CH <sub>2</sub> CH <sub>2</sub> O) <sub>6</sub> H	+	
<b>64</b>	8	tC <sub>4</sub> H <sub>9</sub>	H	+	
<b>65</b>	8	Ph	H	+	
	8	tC <sub>4</sub> H <sub>9</sub>	(CH <sub>3</sub> ) <sub>2</sub> CN	±	
	8	Ph	bi-substituted (CH <sub>2</sub> CH <sub>2</sub> O) <sub>6</sub> H	±	
	8	Ph	(CH <sub>2</sub> CH <sub>2</sub> O) <sub>6</sub> H	±	
	8	Ph	COCH <sub>3</sub>	Enhance tuberculosis activity	
	8	tC <sub>4</sub> H <sub>9</sub>	COCH <sub>3</sub>	Enhance tuberculosis activity	
	7	Ph	(CH <sub>2</sub> CH <sub>2</sub> O) <sub>12</sub> H	+++	
	7	Ph	(CH <sub>2</sub> CH <sub>2</sub> O) <sub>6</sub> H	+	
	7	Ph	(CH <sub>2</sub> CH <sub>2</sub> O) <sub>3</sub> Me	±	
<b>108</b>	7	Ph	H	±	
	6	tC <sub>4</sub> H <sub>9</sub>	(CH <sub>2</sub> CH <sub>2</sub> O) <sub>6</sub> H	+++	Calston <i>et al.</i> , 2004
	6	tC <sub>4</sub> H <sub>9</sub>	bi-substituted (CH <sub>2</sub> CH <sub>2</sub> O) <sub>6</sub> H	+	Goodworth <i>et al.</i> , 2011
	6	tC <sub>4</sub> H <sub>9</sub>	(CH <sub>3</sub> ) <sub>2</sub> CN	±	
<b>109</b>	6	tC <sub>4</sub> H <sub>9</sub>	H	None	Calston <i>et al.</i> , 2004
<b>110</b>	4	tC <sub>4</sub> H <sub>9</sub>	H	None	Goodworth <i>et al.</i> , 2011

## 8. Antiviral Activity

The study of the antiviral properties of calix[n]arenes has been sparse and was initially focused at first on patents concerning the therapeutical applications against few specific viruses (see Table 4). In 1986, Munson and Tankersley investigated the antiviral activity of calix[n]arene on HSV (Herpes Simplex Virus) (Munson *et al.*, 1986). Their inhibition activity has been determined by  $IC_{50}$  representing the concentration of drug required for reducing infection by 50%. The infection experiment assay has been carried out on HEP-2 cell line (isolated from Human Larynx carcinoma), infected with HSV-1 and HSV-2 strains. The most effective  $IC_{50}$  values were obtained with polymerized alkylnaphthalene sulfonic acid **112** for HSV-1 (1  $\mu\text{g/mL}$ ) and with condensed naphthalene sulfonic acid **113** for HSV-2 (1-10  $\mu\text{g/mL}$ ).

**Table 4** – Antiviral activity of calix[n]arene derivatives.

Calix[n]-arene and other drugs	Ring size (n)	Calix[n]-arene unit	R <sub>1</sub>	R <sub>2</sub>	methylene functionalization	Anti viral activity	Virus	Reference
<b>112</b>	NM**	naphthalene	-alkyl (NM**)	-SO <sub>3</sub> H	-H	$IC_{50} = 1 \mu\text{g/mL}$	HSV-1	Munson <i>et al.</i> , 1986
<b>113</b>	NM**	naphthalene	-H	-SO <sub>3</sub> H	-H	$IC_{50} = 1 - 10 \mu\text{g/mL}$	HSV-2	
<b>72</b>	4	phenol	-Amantadine	-H	-H	$IC_{100}^* = 10 \text{ mg/mL}$ (9.3 mM)	HSV-2	Motornaya <i>et al.</i> , 2006
<b>73</b>	4	phenol	-Amantadine	-(CH <sub>2</sub> ) <sub>3</sub> CH <sub>3</sub>	-H	None	HSV-2	
<b>Aciclovir</b>						$IC_{100}^* = 0.25 \text{ mg/mL}$ (1.1 mM)	HSV-2	
<b>3</b>	8	phenol	-H	-SO <sub>3</sub> H	-H	$IC_{50} = 7 \mu\text{g/mL}$ (4 $\mu\text{M}$ )	HSV-1 and HSV-2	Chen <i>et al.</i> , 1994
<b>3</b>	8	phenol	-H	-SO <sub>3</sub> H	-H	$IC_{50} = 16 \mu\text{g/mL}$ (9 $\mu\text{M}$ )	HIV-1	Chen <i>et al.</i> , 1995
<b>AZT</b>						$TC_{50} / EC_{50} = 62500$ (1000 $\mu\text{M}$ / 0.16 $\mu\text{M}$ )	HIV-1	Harris <i>et al.</i> , 1995
<b>67</b>	4	pyrogallol	-Br	-CH <sub>2</sub> COOK	-(CH <sub>2</sub> ) <sub>3</sub> C H <sub>3</sub>	$TC_{50} / EC_{50} = 6250$ (200 $\mu\text{M}$ / 0.032 $\mu\text{M}$ )	HIV-1	
<b>114</b>	4	pyrogallol	-Br	-CH <sub>2</sub> COON H <sub>4</sub>	-Ph-Br (para)	$TC_{50} / EC_{50} = 20000 \text{ to } 50000$ (1000 $\mu\text{M}$ / 0.02 to 0.05 $\mu\text{M}$ )	HIV-1	

115	4	pyrogallol	-Br	-CH <sub>2</sub> COOH	-naphtalene	TC <sub>50</sub> / EC <sub>50</sub> = 13332 to 40000 (800 μM / 0.02 to 0.06 μM)	HIV-1	
76	4	pyrogallol	-H	-CH <sub>2</sub> COOK	-Ph-F (para)	EC <sub>50</sub> = 4 μg/mL (2 μM)	HIV-1	Coveney <i>et al.</i> , 2005
116	4	resorcinol	-H	-CH <sub>2</sub> COOK	-Ph-F (para)	EC <sub>50</sub> = 20 μg/mL (12 μM)	HIV-1	
68	4	phenol	-NH-Ph- COOH(meta) - COO- Ph(meta)	-(CH <sub>2</sub> ) <sub>3</sub> CH <sub>3</sub>	-H	EC <sub>50</sub> = 0.33 μM	HIV-1	Tsou <i>et al.</i> , 2012
1	4	phenol	-SO <sub>3</sub> H	-H	-H	IC <sub>50</sub> = 38 μM	HIV-1	Mourrer <i>et al.</i> , 2010
75	4	phenol	-SO <sub>3</sub> H	-CH <sub>2</sub> - (C <sub>3</sub> HNS) <sub>2</sub> - CH <sub>3</sub> (di)	-H	IC <sub>50</sub> = 1.6 μM	HIV-1	
69	4	phenol	-PO <sub>3</sub> HNa	-H	-H	IC <sub>50</sub> > 100 μM	HIV-1	
70	4	phenol	-PO <sub>3</sub> HNa	-CH <sub>2</sub> - (C <sub>3</sub> HNS) <sub>2</sub> - CH <sub>3</sub> (di)	-H	IC <sub>50</sub> = 14 μM	HIV-1	
71	4	phenol	-CO-NH- C <sub>6</sub> H <sub>3</sub> -(COOH) <sub>2</sub>	-(CH <sub>2</sub> ) <sub>3</sub> CH <sub>3</sub>	-H	IC <sub>50</sub> = 0.36 μM	HIV-1	
71						IC <sub>50</sub> = 1.8 μM	HCV	
74	4	See Figure 8 for structure				IC* <sub>100</sub> = 110 μM	BKV	Marra <i>et al.</i> , 2008
74						IC* <sub>100</sub> = 300 μM	Influenza A (H <sub>3</sub> N <sub>2</sub> )	
75	4	phenol	-SO <sub>3</sub> H	-CH <sub>2</sub> - (C <sub>3</sub> HNS) <sub>2</sub> - CH <sub>3</sub> (di)	-H	IC <sub>50</sub> = 1.6 μM	Coronavir us 229E	Geller <i>et al.</i> , 2010
117	5	pillar	-CH <sub>2</sub> - COONa	-CH <sub>2</sub> - COONa	-H	IC <sub>50</sub> = 0.62 mM	HPV	Zheng <i>et al.</i> , 2014

IC\*<sub>100</sub>: Minimum concentration for complete inhibition

NM\*\*: Not Mentioned

Later, in 1994, Hwang *et al.* extended in another patent the anti-viral activity of calix[n]arene **3** with regard to different enveloped virus species: HIV, HSV and Influenza A (Chen *et al.*, 1994). Calix[n]arene derivatives (with a phenyl or naphtyl repeated unit) bearing anionic group such as sulphate, sulphonamide, phosphate and carboxylate, have shown inhibitory effect on virus infection. Anionic calix[n]arene *para*-sulphonato-calix[8]arene **3** has exhibited strong inhibition activity with IC<sub>50</sub> values of 7 μg/mL (4μM) against HSV-1 and HSV-2 strains, and IC<sub>50</sub> of 16 μg/mL (9μM) against HIV-1.

Then, Harris (Harris, 1995 and 2002) and later Coveney and Costello (Coveney *et al.*, 2005) evaluated these compounds for specific HIV targets. Other indices were added for better understanding of the antiviral effect such EC<sub>50</sub> and TC<sub>50</sub>. EC<sub>50</sub> corresponds to the half

of total number of cells protected from virus injection. The concentration of the drug which reduces cell growth by 50% is designated as  $TC_{50}$ . The lower the  $EC_{50}$  concentration the better the anti-viral effect but the real criterion of effectiveness *in vitro* testing on cell cultures is the therapeutic index corresponding to the  $TC_{50}/EC_{50}$  ratio. AZT, known as the referent drug for HIV infection, presents a therapeutic index superior to 62500. Calix[n]arene **67**, **114** and **115** developed by Harris presents in the best cases the respective values of 6250, 20000 - 50000, and 13333 - 40000 (see table 4).

The calix[n]arenes have been reported to inhibit the viral integrase and fusion enzymes (Harris, 2002). *In vivo* experiment has been also performed and will be more detailed in the section below. Later Coveney and Costello (Coveney *et al.*, 2005) have investigated the viral inhibition of calix[n]arene derivatives (with pyrogallol **76** or resorcinarene **116** sub-units) *in vitro* by carrying out 2 tests on infected blood and on Human T cell lymphoblast-like cell line (CEM cell line). It has been demonstrated on ELISA plates, that the calix[n]arene derivatives inhibit the interaction of the gp120 viral envelop protein with the cellular receptor protein CD4.

Elsewhere, Hamilton *et al.* have targeted the inhibition of a HIV entry in cells by blocking the gp120 protein. A carboxylate calix[n]arene derivative **68** has shown an  $EC_{50}$  as low as 0.33  $\mu\text{M}$ . A docking study of the calix[n]arene on a crystal structure of gp120 protein and CD4 has been realised in order to understand the inhibition mechanism of the calix[n]arene. Anionic functional groups of the calix[n]arene derivative are pointed toward the polar pocket of gp120 and hinder the interaction of CD4 (Figure 8). This mechanism is supported by the fact that the calix[n]arene does not interfere with an antibody which binds to another site of gp120 (Tsou *et al.*, 2012).

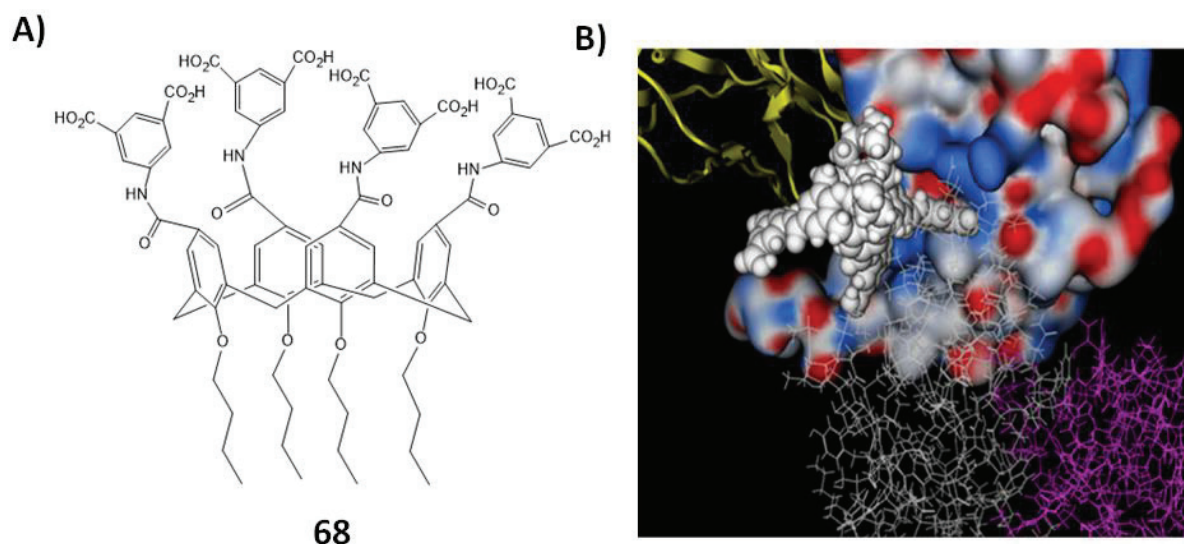


**Figure 8-** A) Structure of carboxylate calix[n]arene derivative **68** B) Docking study of calix[n]arene **68** binding to gp120. In yellow: CD4. In white: **68**, In globular shaped blue-white-red colour: gp120, In grey and Purple: Antibody anti-gp120. (Tsou *et al.*, 2012) With Permission from Elsevier.

Regnouf-de-Vains *et al.* have also investigated the anti-HIV efficiency of 9 anionic calix[4]arenes incorporating sulphonate, phosphate or carboxylate groups at upper rim and two 2,2'-bithiazole subunit at the lower rim. Most of the compounds have an activity in a 10-50  $\mu\text{M}$  range, excepted for phosphonate derivative **69** (see Table 4). The introduction of bithiazole subunits increases generally the inhibition activity. As an example, the introduction of bithiazole subunits on *para*-sulphonato-calix[4]arene **75** has improved the  $\text{IC}_{50}$  from 38 to 1.6  $\mu\text{molar}$  (Mourer *et al.*, 2010). Hamilton *et al.* have also demonstrated that calix[n]arene derivatives can both inhibit HIV and Hepatite C Virus (HCV). This could be useful in case of co-infection. A tetrabutoxy-calix[4]arene **71** has been reported to have an  $\text{IC}_{50}$  of 0.36  $\mu\text{M}$  for HIV and 1.8  $\mu\text{M}$  for HCV (Tsou *et al.*, 2010).

Anti-HSV properties of calix[n]arenes have been investigated in only one research article (Motornaya *et al.*, 2006). Two calix[n]arene derivatives **72** and **73** have been conjugated to the anti-HSV drug, amantadine. The infection inhibition tests have been undertaken by infecting HSV-2 into the monkey kidney cell line (Vero-B). Calix[n]arene **72** exhibited significant inhibition effect (50% of inhibition was observed at 5mg/mL in 48h).

Glycoside groups are present at the surface of mammalian cells and play an important role in the recognition and adhesion of virus and bacteria. Dondoni *et al.* have developed new calix[n]arene-based glycoside derivatives and have evaluated them as inhibitors for a polyomavirus BK and influenza A virus (H3N2 strain) (Marra *et al.*, 2008). Standard Hemagglutination Inhibition assay (HI) has been performed on Vero cells for BK virus and on MDKC cell line for influenza. Calix[n]arenes polysialosides derivatives either at upper or lower rim were able to inhibit the hemagglutination process at sub-milli molar concentration range, especially for **74** that inhibit completely (HI index) BKV at a minimum concentration of 110  $\mu\text{M}$ . Immuno fluorescence experiments have shown that when cells were pre-incubated with calix[n]arene inhibitor, no antigen was present in the nuclei of the cells (Figure 9).

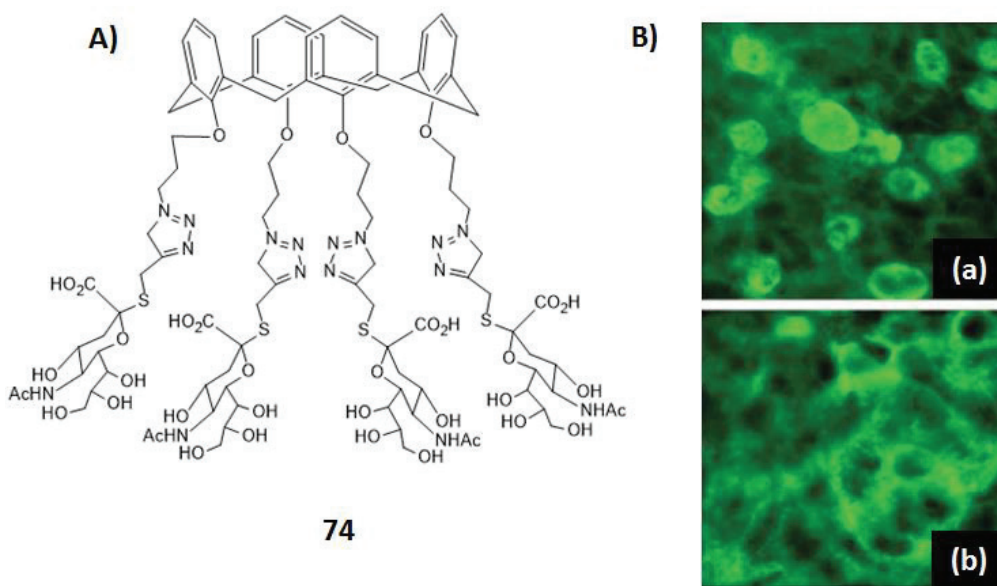


**Figure 9-** A) General structure of sialoside calix[n]arene derivative **74** B) Inhibition of the cytopathic effect in Vero cell cultures infected by BKV. The fluorescent nuclei indicate

the expression of viral proteins. In a) Cell infected with BKV, b) Cell infected with BKV + **74**. (Marra *et al.*, 2008) With Permission from The Royal Society of Chemistry.

So far, it is noteworthy that the most of the effort has been focused on their properties as anti-HIV, anti-HSV agents and some common strain of influenza virus. Only few recent biological studies have mentioned their promising inhibition effect on other virus such as coronavirus and papillomavirus. 1,3 bis(bithiazolyl)-*tetra-para*-sulphonato-calix[4]arene **75** has shown good inhibition against coronavirus, with a stronger activity than the classical chlorhexidine (Geller *et al.*, 2010). Finally, *para*-sulphonato-calix[4]arene **1** and carboxylate-pillar[5]arene were reported very recently as efficient inhibitors of human papillomavirus 16 L1. The viral capsid formation consisting of a pentamer of viral L1 protein rich in arginine / lysine has been slowed down by the calix[n]arene derivatives, especially the carboxylate-pillar[5]arene (Zheng *et al.*, 2014).

### ***In vivo* experiments**

Hwang *et al.* have evaluated the anti-HSV properties of calix[n]arenes on guinea pigs by topical (applied on body surface) and oral administrations (Chen *et al.*, 1994). Studies conducted have shown that the calix[n]arene were available in the plasma for a period from about 0.5 hours after oral administration with a peak at about 2-4 hours. The short half-life of the drugs could be bypassed with intravenous injections if needed. The effect of topical treatment after 6 or 24 hours post infection by HSV, resulted in reduced numbers of apparent lesions in comparison to placebo treatment. No sign of any skin irritation from any of the formulations was observed.

More interestingly, Harry *et al.* have extended their patent to a clinical trial with the oral administration of calix[n]arene to 3 human patients infected by HIV at a level of 500mg per day (three doses of 167mg each 8 hours) (Harris 2002). It is the only case to our knowledge where calix[n]arenes have been administrated to humans. The patients treated were all at an advanced stage of the disease. In particular, one female patient had, prior to treatment, 500,000 viral copies per ml of blood. After treatment with calix[n]arene **67** her viral loads were reduced by 99% and were maintained for at least a year and were found to be fairly constant during this time period. A man with 750,000 viral copies per ml of blood was found 3 months later after treatment with **67** to have 50,000 viral copies with great improvement in clinical condition. Patients being treated with the drugs of the present invention did not experience any side effects and their clinical condition dramatically improved in all cases. Furthermore, this therapeutical effect was associated with reduced incidence of opportunistic infections, which is an important issue to solve in HIV infection.

## **9. Antifungal Activity**

Fungi are classified as a kingdom in biology, distinct from animal, plant and bacteria. They consist of uni- (yeast) or pluri-cellular (mould or mushroom) eukaryotic organisms which possesses a unique membrane composed of chitin. Some species of yeast are involved in a number of diseases such as candidiasis, paracoccidioidomycosis or other opportunistic

diseases present in immuno-depressed patients. However, antifungal research is one of the most neglected therapeutic research fields and calix[n]arenes could be potent drug candidates in this domain.

Since the pioneering work of Harris in 1995 presenting the therapeutic properties of calix[n]arenes, only a few articles have investigated the anti-fungal activities of these molecules. The Harris patent presents in particular one calix[4]pyrogallol **76** which inhibits strongly *Candida albicans*, a causal agent of opportunistic oral and genital infections in humans (Harris, 1995). However, the study is preliminary and no numerical data was reported. Later, Lamartine *et al.*, have investigated calix[n]arenes as pesticide candidate for two fungi parasites of plant, *Rosellinia necatrix* and *Colletotricum dematium* (Lamartine *et al.*, 2002). A total antifungal activity was demonstrated for 4 calix[n]arenes, **1**, **2**, **3** and **77** bearing a sulphonate group at *para* position. In another approach, Amphoterin B (Amp B), a major anti-fungal drug, has been conjugated to calix[4]arene **16** and **17** (Paquet *et al.*, 2006). The antifungal activity has been evaluated against *Saccharomyces cerevisiae* as a model yeast. A MIC of 0.1  $\mu\text{M}$  was found for calix[n]arene **16** instead of 0.3  $\mu\text{M}$  for Amp B alone. The gain of antifungal activity is not so important (3 times) but correlated to a dramatic decrease of hemaetotoxicity (10 times lower for the conjugates), the work shows the interest of such complexes as anti-funga agents. Despite this promise, until recently, only De Fatima *et al.* have reported other calix[n]arene derivatives as anti-fungals against *Parracoccidioides*. (De Olievera *et al.*, 2012) This fungus is prevalent in a portion of South America, and causes blastomycosis (severe skin lesion). 6 calix[4,6,8]arenes *para-tert*-butylated (**81**, **82** and **83**) or not (**78**, **79** and **80**) dissolved in DMSO have been evaluated over 2 different *Parracoccidioides* species *lutzi* (one strain) and *brasiliensis* strains (six strains). Interestingly, *para-tert*-butyl-calix[n]arene has shown higher antifungal effects than the non *tert*-butylated one. In particular, **81** was the most promising compound with a MIC of 16  $\mu\text{g}/\text{mL}$  (20  $\mu\text{M}$ ) for *lutzi* specie and a MIC between 16 to 64  $\mu\text{g}/\text{mL}$  (20 to 80  $\mu\text{M}$ ) for *brasiliensis* specie. Beside, no strong toxicities have been reported for *tert*-butylated calix[n]arenes in cytotoxic assays. This study confirms the interest of calix[n]arenes as antifungi drug candidates.

## 10. Anti-cancer Activity

Among all their biological properties, the ability of calix[n]arenes to act against cancer cells represents one of the major therapeutic fields investigated in the literature. The reason comes probably because of the important financial investment and an easier access for chemists to cytotoxic screening assays, in the 15 last years. Several strategies have been employed for using calix[n]arenes as anti-cancer agents. The main lines have concerned calix[n]arenes as transporter of APIs for drug delivery, or as an API itself acting against targeted proteins present in the cancer cells. Other more recent researches have investigated them as adjuvants for cancer vaccines, as photosensitizers for photodynamic therapy, or as antioxidants for preventing cancer.

## Calix[n]arenes as direct anti-cancer agents

One of the major drawbacks in chemotherapy treatment against cancer is to find the good therapeutic window, treating a disease without unacceptable toxicity for the patient. In case of cancer, this concern is bigger because proliferative cancer cells possess the same metabolic requirement than proliferative normal cells (Vander Heiden *et al.*, 2011). The challenge for using calix[n]arene as anti-cancer is to reach the lowest  $IC_{50}$  value for cancer cells and the highest  $IC_{50}$  value for normal cells. However, most of the research articles presented here at the exception of Coleman (Coleman *et al.*, 2007) take only in account the  $IC_{50}$  against cancer cell line. *In vivo* experiments will also provide the potent efficiency of calix[n]arene as anti-cancer treatment (see *in vivo* section).

In a series of papers Hamilton and Sebti have demonstrated the anti-cancer properties of cyclohexapeptidomimetic calix[n]arene **87** derived from calix[n]arene **68** (Figure 10) (Sebti *et al.*, 2000). These calix[n]arene derivatives have been able to antagonize the growth factor hormones PDGF and VEGF overexpressed in some cancer cells with an  $IC_{50}$  value of 250 nM for PDGF (Blaskovich *et al.*, 2000) and 750 nM for VEGF (Sun *et al.*, 2004). Bioassays have been performed on NIH 3T3 cells for PDGF and on NIH 3T3 cells and human prostate tumour cells for VEGF. More recently, a calix[n]arene **88** more soluble and easier to synthesize was proposed and exhibit an  $IC_{50}$  value of 190 nM for PDGF (Zhou *et al.*, 2006). The complexation of calix[n]arenes to these growth hormones has led to the suppression of angiogenesis (generation of new blood vessels) and tumorigenesis. *In vivo* experiments will be more described in the section below.

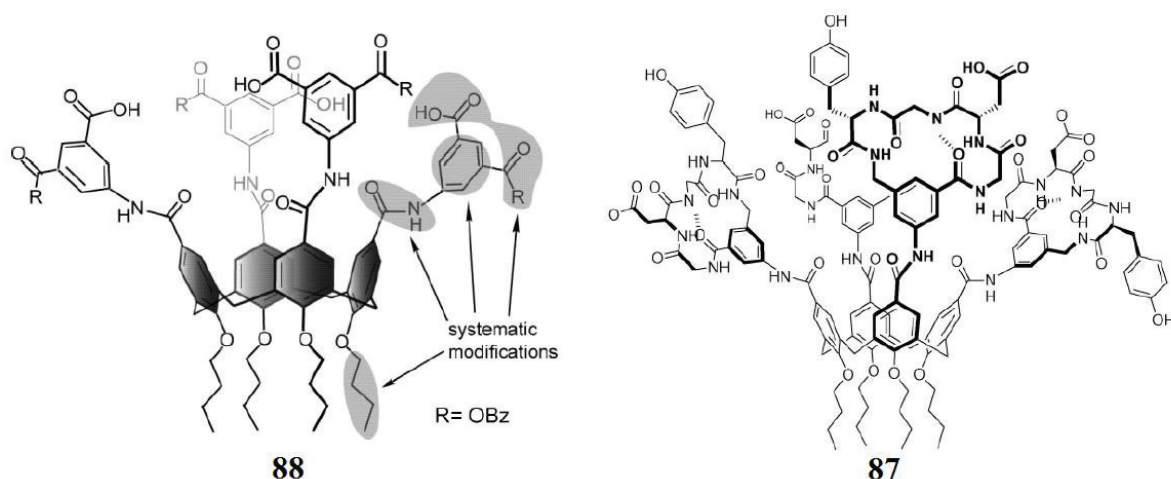


**Figure 10-** Structures of calix[n]arene **87** and **88** studied by Hamilton and Sebti for anti-cancer properties (Zhou *et al.*, 2006). With Permission from The Royal Society of Chemistry.

Mayo *et al.* have carried out a large body of work using calix[n]arenes themselves as anti-cancer APIs. First, two amphiphilic calix[n]arene derivatives **84** and **85** have been identified as inhibitors of endothelial cell line growth with respective  $IC_{50}$  values of 2 and 8

$\mu\text{M}$  (Figure 11) (Dings *et al.*, 2006). Calix[n]arene **84** has been characterized to be a specific inhibitor of Human Galectin-1. Galectin-1 is involved in pathological disorders such as the carcinogenesis and migration of endothelial cells. Flow cytometry experiments have been undertaken in order to demonstrate the interaction between the calix[n]arene and the carbohydrate sites of the lectin localized on the membrane of the cancer cell. (Dings *et al.*, 2012) Recently, new derivatives of **84** have been evaluated and one in particular **86** has shown new promising anti-cancer properties with very low  $\text{IC}_{50}$  ranging from 0.2 to 2  $\mu\text{M}$  as a function of cell line used. More interestingly, calix[n]arene **86** has shown inhibitory effect on the proliferation of human cancer cells exhibiting various drug resistances (Dings *et al.*, 2013).

Coleman *et al.* have shown that phosphonate calix[n]arene derivatives have anticancer activities (Coleman *et al.*, 2007). A series of phosphonate calix[n]arene derivatives have been evaluated over a wide range of normal and cancer cells. A dihydrophosphonic acid calix[4]arene derivative, **107** has in particular shown specific toxicity towards the cancer cell lines Hep-G2 (hepatocellular carcinoma) and Huh7 (human hepatoma) with respective  $\text{IC}_{50}$  of 27 and 36  $\mu\text{M}$  while  $\text{IC}_{50}$  value of 1 mM has been obtained for normal cell leukocyte, thus there is 50 fold therapeutic window. This is combined with activity against non-resistant and resistant cancer cells.

Calix[6]arene **79** has recently been identified over other calix[n]arene *tert*-butylated (**81**, **82** and **83**) or not (**78**, **79** and **80**), as an anti-cancer agent against human pancreatic cancer cells induced by reticulum stress and autophagy. The  $\text{IC}_{50}$  was determined to be 25  $\mu\text{M}$  after 24 hours. The autophagy induced by the calix[n]arenes was determined by the ultrastructural characteristics of autophagosome inside the cell (double membrane vacuole) observed by electronic and fluorescence microscopies. Also, calix[6]arene **79** has been shown to stop the cell cycle and also to stop the transduction signal of some specific tyrosine kinase receptor Mer and AXL (Pelizzaro-Rocha *et al.*, 2013).

### *In vivo* experiments

In studies undertaken by Mayo *et al.* (Dings *et al.*, 2006), the anti-angiogenesis effect has been determined using the chorioalloantoic membrane assay in fertilized chicken eggs. After daily application during 10 days, the angiogenesis was reduced compared to untreated control (Figure 12). The tumour growth inhibition assays were all assessed in the B16F10 tumour mouse model. The compounds were administrated by intraperitoneal injection for 8 days. Calix[n]arenes **84** and **86** have shown a tumour growth inhibition of 77 % at 10mg/Kg for PT008 and 50% at 0.2mg/Kg for PT0013 while the positive control Anginex (a commercial anti-angiogenesis drug) was 57% at 10mg/Kg. **84** is currently in a human Phase I clinical trial.

Hamilton and Sebti have evaluated the anti-cancer activity of the new compounds **87** and **88** *in vivo* by tumour growth inhibition studies in the nude mouse human xenograft model implanted with different tumours. The calix[n]arene **87** has shown inhibition on human brain tumour U87MG with 56, 81 and 88% after 32 days with daily injection of 50, 100 and 200 mg/Kg. This inhibition was also extended to Human Lung adenocarcinoma A-

549 with 62% effect at 50 mg/Kg after 30 days (Blaskovich *et al.*, 2000). The other calix[n]arene **88** inhibits 50% of tumour growth in 10 days at 10 mg/Kg daily (Zhou *et al.*, 2006).

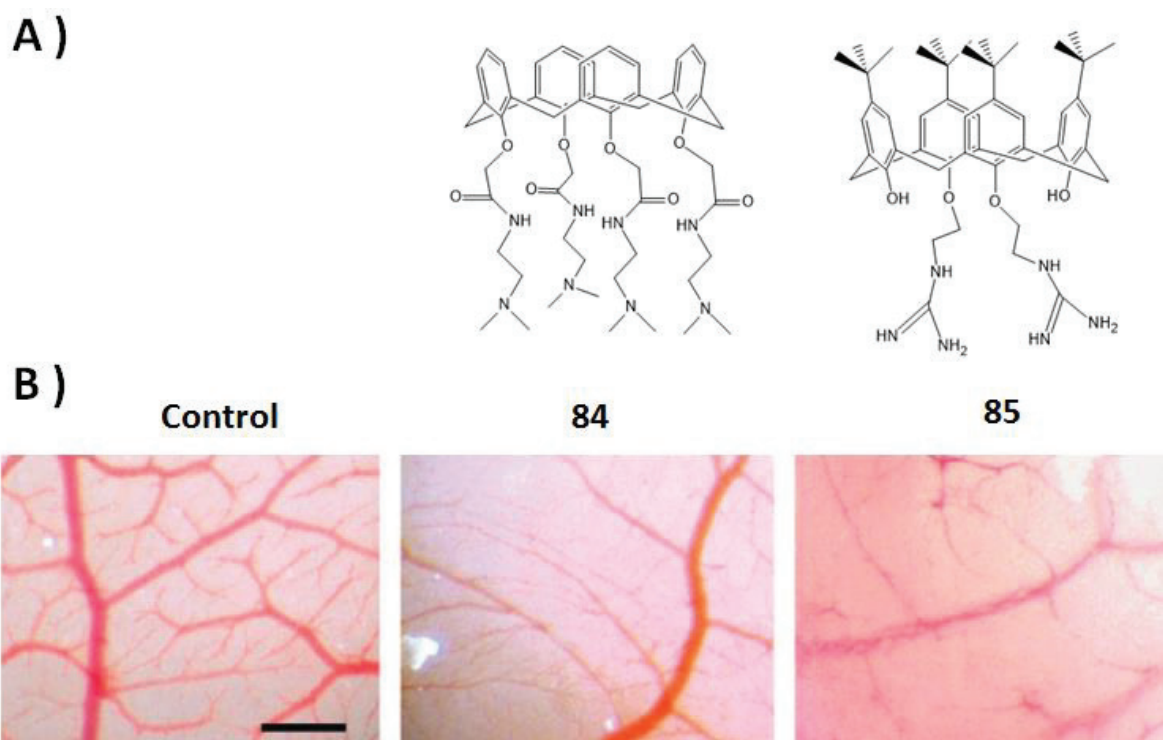


**Figure 11-** A) Structure of calix[n]arenes **84** and **85** studied by Mayo (Dings *et al.*, 2006). B) In vivo angiogenesis inhibition assay. Left picture corresponds to the blank, Picture in the middle corresponds to **84** injection, Right picture represents injection of **85**. Scale bar is 0.5 mm. With permission from Oxford University Press.

### Calix[n]arene drug conjugates

Sonnet *et al.* have developed a series of calix[4]arenes conjugated or not with a strong iron chelator ICL670 for targeting iron which plays an important role in cancer proliferation (Rouge *et al.*, 2010) (Latxague *et al.*, 2011). Their effects have been evaluated on hepatocarcinoma HepaRG cell line (Figure 12), which has the ability to store iron. The best antiproliferative effect was obtained with the calix[n]arene **89** mono-substituted by ICL670 and were stronger than ICL670 itself with an  $IC_{50}$  of 6  $\mu$ M (without iron added in the medium) and 37  $\mu$ M (with 20  $\mu$ M of iron added in the medium) (Rouge *et al.*, 2012).

Platinum-based chemotherapy drugs are among the most powerful and widely used against cancer, even in view of their considerable side effects. As an example, carboplatin is a common platinum chemotherapy drug, approved in 1980, and still used today against various type of cancer. Its conjugation with calix[n]arenes has been considered as promising for enhancing the effects and reducing the side effects. (Pur *et al.*, 2014) A complex composed of cis-diammineplatinum and 1,3 alternate carboxy calix[4] arenderivative **90** has shown  $IC_{50}$

values of 2.6  $\mu\text{M}$  for A549, 5.7  $\mu\text{M}$  (lung cell line) for HepG2 (liver cell line) and 4.9  $\mu\text{M}$  for MCF7 (breast cell line). This is 2 to 6 times better than the classical carboplatin. Another study has shown that calix[4]pyrrole conjugated with a monomer of cis-platin inhibited the proliferation of various cancer cell lines (breast, ovarian, ) with an  $\text{IC}_{50}$  ranging from 20 to 40  $\mu\text{M}$ . This is better than carboplatin (50 - 90  $\mu\text{M}$ ) but lower than cis-platin (5 - 20  $\mu\text{M}$ ) (Cafeo *et al.*, 2013).

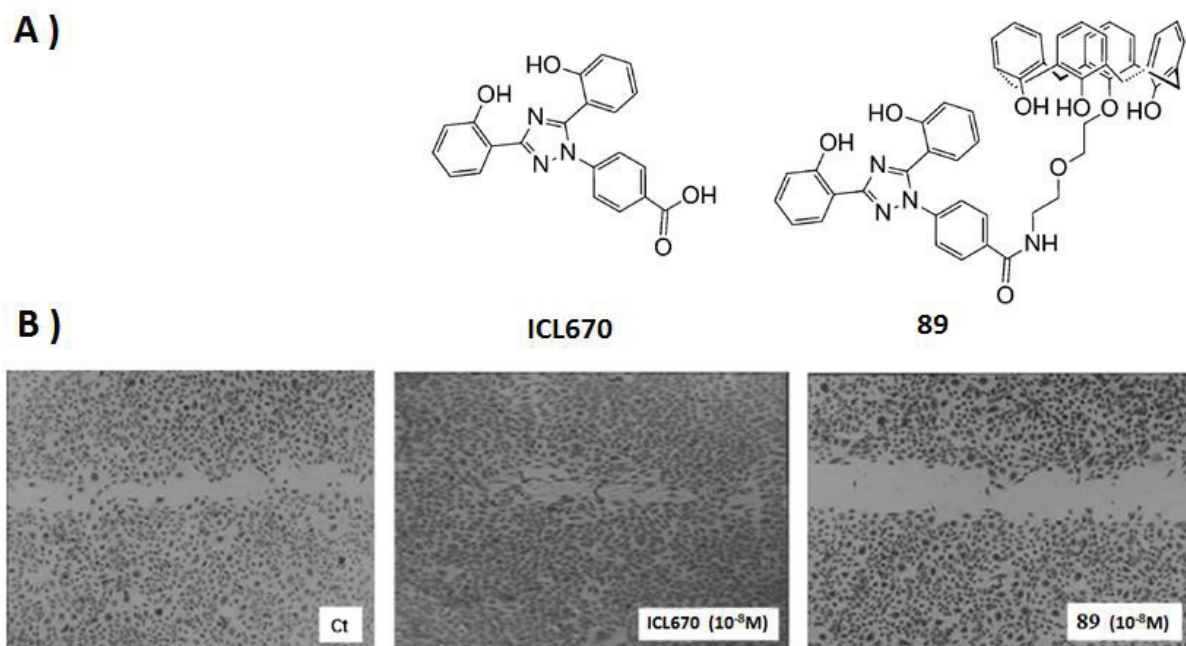


**Figure 12-** A) Structure of ICL670 and calix[4]arene **89** monosubstituted by ICL670. B) Effect of **89** and ICL670 on HUVEC cell migration. B) Pictures by optical microscopy of HUVEC after injection of Control (Left) ICL670 (Middle) **89** (Right). (Rouge *et al.*, 2012) With permission from John Wiley and Sons Publisher.

Platinum-based drugs have been complexed by *para*-sulphonato-calix[n]arene and have been reported for evaluating their transport (Krause-Heuer *et al.*, 2008). *Para*-sulphonato-calix[4]arene **1** complexed with dinuclear platinum compounds have been characterized by NMR and have shown no cytotoxicity when they are injected together on ovarian cell line A2780. This finding is interesting in order to avoid side effects of chemotherapy (Brown *et al.*, 2012). Liu *et al.* have proposed a controllable released of an anti-cancer Doxorubicin (DOX) previously encapsulated in a *para*-sulphonato-calix[4]arene **1** (Wang *et al.*, 2011). Vesicles formed by the complex of an average size of 360nm have been characterized and can respond to different stimuli such as temperature in order to release the anti-cancer drug. Cytotoxicity assays have shown that the loading of DOX in vesicle does not affect the therapeutic effect on cancer cells, whereas the damage to normal cells was reduced.

## Antioxidant Activity

Reactive Oxygen Species (ROS) have been identified as one of the important factors leading to carcinogenesis. Several years ago, Consoli and Geraci have described for the first time the antioxidant activities and the radical scavenging effects of two calix[4]arene derivatives (Consoli *et al.*, 2006). Raston *et al.* have synthesized a series of amphiphilic *para*-phosphonic acid calix[n]arene derivatives (compounds **91** to **97**) capable of forming micelles and to transport curcumin, as a model of antioxidant. These calix[n]arenes have increased solubility of curcumin and have decreased the cytotoxicity of the calix[n]arenes themselves (on rat PC12 cell line and primary cultures of mixed retinal cells) (James *et al.*, 2013). However, so far no cellular antioxidant assays have been reported in the literature. Very recently, Fitzgerald and Coleman have demonstrated the anti-oxidant effect of sulphonato-calix[n]arene derivatives **1**, **2**, **3**, **59**, **60**, **61**, **62** and **63** (functionalised at upper, lower and both faces) on neural cell lines PC12 by using 2'-7'-Dichlorodihydrofluorescein diacetate (DCFH-DA) as part of an intracellular ROS assay kit. Glutamate has been used for stressing cells and increasing their ROS levels. Then, antioxidant activities have been only observed when the calix[n]arene is capped on silver nanoparticles. The highest antioxidant effect was obtained with *para*-sulphonato-calix[4]arene **1** capped silver nanoparticles over the others hybrids nanoparticles, which decrease the ROS level by 59% as compared to blank (DI Water) when diluted at 1 µg/mL (1.3 µM).

## Photodynamic therapy

Photodynamic therapy is a form of phototherapy using nontoxic light-sensitive compounds that once exposed to light, release ROS and then destroy the targeted pathogenic cells. Neagu *et al.* have recently investigated the anticancer effect of *para*-sulphonato-calix[n]arenes **2** and **3** by this method (Neagu *et al.*, 2010). The cytotoxicity assays were assessed on human myelogenous leukaemia cell line K562. Surprisingly, **2** is much more photoactive than **3**. Post irradiation with a Hg lamp, compared to a control, the mortality of cells increases by 60% for *para*-sulphonato-calix[6]arene at 1 µg/mL and only 30% for *para*-sulphonato-calix[8]arene at 20 µg/mL.

## Cancer vaccine

Geraci and Spadaro have introduced the idea of using calix[n]arenes as a vaccine, constructed a platform exhibiting on one face, tumoral antigens and on the other face an adjuvant. Firstly, the concept have been demonstrated with a calix[4]arene **98** conjugated at the upper rim to 4 specific tumor-associated carbohydrate antigens (TAs) who are weak immunogens by themselves, and at the lower rim a tripalmitoyl-S-glycerylcysteinylserine (P<sub>3</sub>CS) to adjust the immune response (Geraci *et al.*, 2008). Very recently this work was extended to the calix[8]arene **99** bearing another antigen targeting MUC1 (Geraci *et al.*, 2013). MUC1 is a trans-membrane protein overexpressed in many cancer types. Here only the peptidic sequence PDTRP representing the immune part of the protein MUC1 has been conjugated to the calix[n]arene.

### *In vivo* experiments

In all cases, the general protocol for evaluating the efficiency of the vaccine has consisted of intraperitoneally injecting, 2 times at one week intervals, 300 $\mu$ L of the calix[n]arene at 0.030  $\mu$ M in saline solution with some stabilizers and solubility enhancers. After 21 days from the 1<sup>st</sup> immunization, sera were collected and evaluated on ELISA assay with the antigen coated on the surface. After washing, the coated antigen was recognised by a first mouse antibody and then revealed by a secondary anti-mouse antibody fluorescent. The tetravalent TAs calix[4]arene **98** has been detected in the sera at 16000 times dilution. The production of anti-Tas induced by **99** is 4 times stronger than the monovalent TAs calix[4]arene (Geraci *et al.*, 2008). In the case of MUC1 vaccine, the antibody octavalent anti-PDTRP calix[8]arene **99** has shown better immune stimulation than the tetravalent derivative. This can be explained by the higher flexibility calix[8]arene skeleton which offer better orientation in space for being recognized and processed by the immune system of the mouse. Moreover, the multivalency approach defined by Whitesides can also explain this effect (Krishnamurthy *et al.*, 2006). This concept is describes more precisely in the general mechanistic guidance of calix[n]arene design for biological function at the end of the review.

## 11. DNA delivery

The introduction of foreign DNA inside a host cell is a major challenge in biology. The applications are of considerable interest in the development of genetic engineering methods and in gene therapy. In contrast to non-viral methods, viral methods present serious drawbacks with the risk of random insertion, cytopathogenesis and mutagenesis of the DNA delivered. For non-viral methods, the process is termed transfection when the host cell is eukaryotic, and transformation when the host cell is bacterial. Schrader *et al.* have investigated the interaction of calix[n]arenes with DNA, these molecules showing them be serious candidates for transfection (Li *et al.*, 2012).

Aoyama *et al.* have reported the transfection of DNA by an amphiphilic resorcin[4]arene conjugated totally or partially to three glycoside functions (maltose, galactose or cellobiose). These calix[n]arene conjugates have produced self-assembled particles of 4 nm size, and their interaction with DNA generate larger complex (from 50 to 300 nm). The size of the complex has been determined to be critical for efficient transfection. Pinocytosis (non-specific and restricted to particle uptake under 100nm) has been deduced among endocytic processes (Nakai *et al.*, 2003).

Later, transfection of DNA with calix[n]arene has been reported with a multi-amino-calix[n]arene amphiphilic by Matthews (Lalor *et al.*, 2007), Shahgaldian with amino calix[n]arene **100** and chitosan (Figure 13) based solid lipid nanoparticles (Nault *et al.*, 2010) and Klymchenko with the amino calix[n]arene derivative **101** as a micellar suspension (Rodik *et al.*, 2011). The cationic amine groups interact with the negative phosphate groups of DNA and are supposed and to get closer on the globally positive charged cell membrane. The alkyl

chains are here for being inserted inside the cell membrane and initiate the uptake of the complex in the cell. In the last example **101** has shown excellent viability and transfection ratio on HeLa cells as detected by fluorescence imagery with a DNA marker. Table 5 summarizes these transfection efficiencies versus cellular viability.

**Table 5** – Transfection efficiency and cellular viability of calix[n]arene studied.

Calixarene	Transfection efficiency	Cellular viability	Reference
<b>100 + chitosan</b>	32 % at 90µg / mL on MDCK cell line (100 % for Lipofectamine™)	100 % at 90µg / mL on MDCK cell lines	(Nault et al., 2010)
<b>101 + lipid DOPE</b>	10 <sup>7</sup> RLU / mg at 10 µM on COS-7 cell line (4x10 <sup>8</sup> RLU / mg for jetPEI™)	80 % at 1.5-10 µM on COS-7 cell line	(Rodik et al., 2011)
<b>102</b>	Minimum observable concentration for transfection: 15-20µM	62-78 % at 10µM on RD-4 cell line	(Sansone et al., 2006)
<b>103</b>			
<b>104 + lipid DOPE</b>	3-4 % at 10 µM on RD-4 cell line (30 % for Lipofectamine™)	100 % at 10µM on RD-4 cell line	(Bagnacani et al., 2008)
<b>105 + lipid DOPE</b>	48 % at 10 µM on RD-4 cell line (30 % for Lipofectamine™)	100 % at 10µM on RD-4 cell line	
<b>106 + lipid DOPE</b>	6-7 % at 10 µM on RD-4 cell line (30 % for Lipofectamine™)	100 % at 10µM on RD-4 cell line	
<b>117</b>	10% on CHO at 500µM cell line (50% for FuGene™)	100 % at 1mM on CHO, HEK cell lines	(Lalor et al., 2007)

Finally, Sansone *et al.* have carried out a large body of work in the area of transfection. In a first study, the transfection efficiency has been examined as a matter of the condensation generated by the interaction of a calix[n]arene with DNA (Sansone *et al.*, 2006). Calix[n]arene derivatives bearing guanidinium groups at the upper rim **102**, **103** have promoted transfection but still at low efficiency and with high cytotoxicity. Later, calix[n]arenes bearing guanidinium groups at the lower rim **104**, **105** and **106** have shown higher transfection efficiency on RD-4 human cell and Vero cell lines (similar than commercial lipofectamine) (Bagnacani *et al.*, 2008). Very recently, new amphiphilic calix[n]arenes bearing basic amino acid groups at upper face (arginine or lysine) have been proposed as transfection agents. An arginine calix[n]arene conjugate has shown low cytotoxicity and general higher transfection than the corresponding lysine calix[n]arene conjugate and also commercial transfection agents, and functions with a variety of cell lines (Bagnacani *et al.*, 2013).

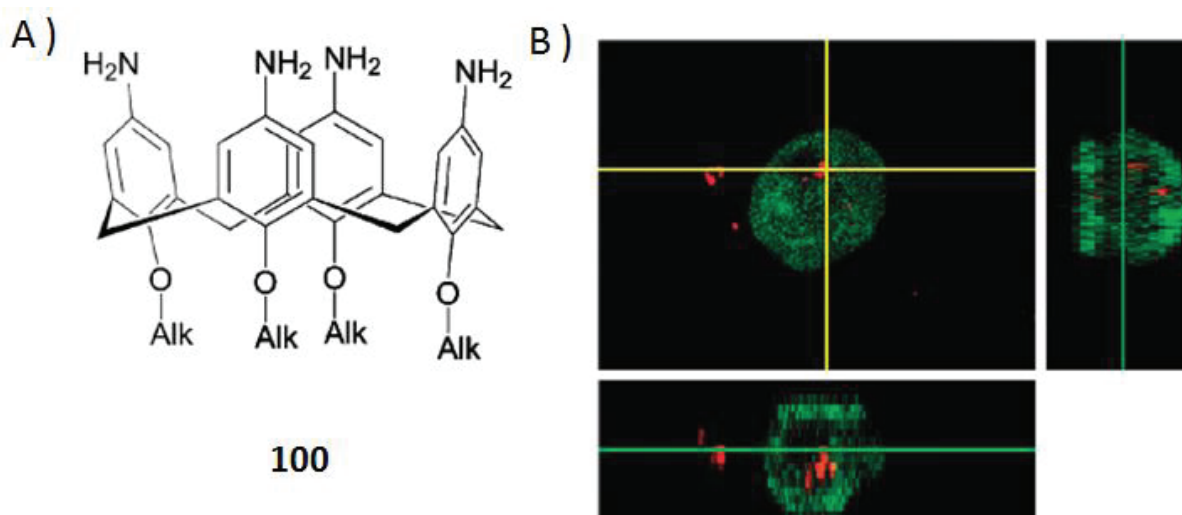


**Figure 13-** A) Structure of calix[n]arene **100** studied by Shahgaldian (Nault *et al.*, 2010) B) Confocal micrograph of a transfected cell that has expressed GFP (in green). The red colour representing the labeled-chitosan appeared to be in the cytoplasmic compartment of the cell. With permission from The Royal Society of Chemistry

## 12. Other types of drug delivery

Matile *et al.* have investigated the effect of a carboxylated calix[4]arene **118** among several other carboxylate molecules for transporting oligo-peptides rich in arginine into HeLa cells. It was found that the planar pyrene carboxylate was more efficient in arginine transport than the spherical carboxylate fullerene and the macrocyclic carboxylate calix[4]arene derivative. This effect has been also shown to be dependent on the membrane composition and fluidity. It has been suggested that this effect could be reversed for bacteria (Nishihara *et al.*, 2005).

Benzocaine is an anaesthetic drug (inhibitor of the nerve stimulation) presenting some toxic side effects which could be overcome by improving its bioavailability. Complexes between *para*-sulphonato-calix[n]arenes, **1** and **2** and benzocaine have been characterized by NMR and their cytotoxicity on mouse 3T3 fibroblast cells has been assessed (Arantes *et al.*, 2014). While the calix[n]arenes themselves do not show cytotoxicity, benzocaine and the calix[n]arene complexes have affected the cellular viability. The higher cytotoxicity of the complex compared to benzocaine alone, has been interpreted as due to the calix[n]arene improving the solubility of the drug and hence its bioavailability.

### *In vivo* experiments

Menon *et al.* have included *in vivo* tests in their studies concerning the biological effects of complexation between drugs and calix[n]arenes or calix[n]resorcinarenes bearing sulphonate groups at aromatic face. *Para*-sulphonato-calix[n]arenes **1** and **2** improved greatly

the solubility of carvediol by forming inclusion complexes. Carvediol is a non-selective  $\beta$ -blocker practically insoluble in aqueous solution. After characterization, the two complexes have been orally administrated to Swiss albino mice, in order to assess the toxicities of the compounds. Lethal dose indice  $LD_{50}$  corresponding to the amount of substance which causes the death of 50% of a tested group of animals.  $LD_{50}$  of Carvediol has been reported as 8 g/Kg while both complexes have shown no toxicities at over 12 g/Kg (at respective molar ratios 1 and 0.5 for the complex Carvediol : **1** and Carvediol : **2**) (Menon *et al.*, 2012). As a comparison, glucose has an  $LD_{50}$  on rats of 30g/Kg. In the same approach, *para*-sulphonatocalix[4]resorcinarene has been investigated and has been shown to increase the solubility and decrease the *in vivo* toxicity of 2 drugs, the immunosuppressant mycophenolate mofetil (MMF) (Menon *et al.*, 2011) and the anticonvulsant lamotrigine (LMN) (Patel *et al.*, 2013).  $LD_{50}$  of MMF and LMN have been respectively determined as 145 and 1000 mg/Kg in mice, while the *para*-sulphonato-calix[4]resorcinarene / drug complexes have respectively shown no mice mortality up to 450 and 2200 mg/Kg.

### 13. General mechanistic guidance of calix[n]arene design for biological function

The main biological functions in the cells are in part regulated through the reversible assembly of the intra cellular bio-macromolecules (DNA, protein, or lipids) by non-covalent or weak energy bonds. These assembly forces include hydrogen bonding, metal coordination, hydrophobic forces, Van der Waals forces,  $\pi$ - $\pi$  and electrostatic interactions. Calix[n]arene modulates the biological functions through its assembly with the biomolecules by the same type of forces (Gutsche, 2008). Two approaches have been done for studying the biological effect of calix[n]arene derivatives. They have been either screened over a large range of biomolecules (Goodworth *et al.*, 2011) or selected among several derivatives with similar structural characteristics in order to distinguish a molecular mechanism (Kalchenko *et al.*, 2013). The design of the calix[n]arene structure for the best biological action is expected to be tuned by the physicochemical properties of his type of functional groups, the combination of functional groups both at *para* or phenolic face, the size of the hydrophobic pocket, the flexibility due to its ring size, and the multivalence toward its ligand (Nimse *et al.*, 2013).

As mentioned in introduction, the versatile chemistry allows the derivation of calix[n]arene by at least two types of functional groups, at *para* or phenolic face. This is one of main advantage presented by calix[n]arene. The combination of the various functional groups drive the affinity of calix[n]arene toward biomolecules, and subsequently lead to different therapeutical strategies for blocking viral infection, increasing transfection efficiency, killing pathogenic micro-organism (Perret *et al.*, 2013)

Cationic amphiphilic molecules are considered as efficient transfection agents because of their micellar organization and their both interactions toward phosphate groups of DNA and phospholipids of the cellular membrane leading to the cellular uptake of the complex (Hafez *et al.*, 2001). Cationic amino calix[n]arene derivatives bearing alkyl chains increases particularly the transfection efficiency compared to other molecules with lower toxicity (table 5). The macrocyclic effect increases significantly the penetration of the DNA complex in the cells. This is particularly truth when the cationic groups are positioned on the upper rim suggesting that the conic geometry of calix[n]arene might also play a role in the membrane

fusion (Bagnacani *et al.*, 2013). Regnouf-de-Vain *et al.* have also used this ability for inserting cationic calix[n]arene amphiphilic derivative **42** inside the outer membrane of Gram – bacteria by creating holes in it and leading to the bacterial death (Formosa *et al.*, 2012).

On the other hand, the anionic calix[n]arene derivatives which are not supposed to destabilize the cellular membrane have shown generally lower haemotoxicity in particular for *para*-sulphonato-calix[n]arene **1**, **2** and **3** (Da Silva *et al.*, 2004). Anionic calix[n]arenes have been shown to interact with various protein considered as pharmaceutical targets through their cationic amino acids (Perret *et al.*, 2011). As an example, the inhibition of HIV virus entry by the anionic carboxylic calix[n]arene bearing alkyl chains **68** has been recently elucidated. It has been shown that the anionic calix[n]arene amphiphiles interact both with the amino acids present in the active site located in the hydrophobic pocket of the viral protein gp120. As a consequence, the interaction of the viral protein with the cellular receptor is inhibited and the cellular uptake of the virus becomes impossible (Tsou *et al.*, 2012). The enlargement of the ring size increases the flexibility of calix[n]arene. This appears to be a main paramount in the inhibition of protein endonuclease (Tauran *et al.*, 2014). This might be explained by an easier introduction in the viral protein active site with a better surface contact to the active site.

The ring size is also an important paramount in the inclusion of molecule guest (Menon *et al.*, 2012). This criterion is particularly interesting in the design of calix[n]arene for detoxifying strategy. In that case, the hydrophobic toxic molecule has to fit with the hydrophobic pocket of the calix[n]arene for being included inside by  $\pi$ - $\pi$  interactions. Then, the toxic molecule complexed in calix[n]arene is not available anymore for affecting the cells (Wang *et al.*, 2009).

Finally, the multivalence is one of the most important paramount for tuning the force of interaction between a molecule receptor to multi ligand linked to each other (in our case calix[n]arene exhibits several ligands). Multivalency approach defined by Whitesides explains how to convert an inhibitor with low affinity ( $K_d$  at mM -  $\mu$ M range) to high avidity ( $K_d$  at nM range) when two or more molecular recognition events occurs between two compounds (antibody and calixarene) at the same time (Krishnamurthy *et al.*, 2006). The affinity is defined by the dissociation constant of a monovalent interaction between 2 compounds while the avidity is defined by the dissociation constant of the multivalent interactions from the completely associated receptor-ligand complex to the completely dissociated form of the multivalent receptor and ligand. The key thermodynamic principle in multivalency is that, ideally, the enthalpy of binding of a multivalent system is more favorable than that of the monomers (Mammen *et al.*, 1998). Moreover since the ligands are connected to each other through a molecule, their local concentration is increased and the multivalent interactions of the receptor are favoured. As a representative example, calix[n]arene have been used as scaffold for exhibiting several antigens to an antibody. The octavalent anti-PDTRP calix[8]arene **99** has shown higher avidity and better immune stimulation than the tetravalent derivative (Geraci *et al.*, 2008).

The combination of all these characteristics makes these macrocyclic calix[n]arenes versatile and promising for various medical applications. However the design of calix[n]arene is still challenging because it is difficult to induce a specific molecular assembly over the

wide range of biomolecules present in a cell and in a larger extent to a living organism. This makes really complex to predict or to identify one main biochemical mechanism that will finally lead to an efficient biological effect.

#### 14. Conclusion and the Future

Most of papers described in the present review have been reported during the last 10 years, indicating a rise in the interest of academic researchers for the use of these molecules in biology. As an important example that characterizes the level of maturity of the field, calix[n]arenes have been recently administrated to human patients for curing cancer or HIV. We have shown here that over 100 calix[n]arene derivatives have been tested for at least some aspects of their biological behaviour and with an increasing range of cellular and other living models.

However, this review has also pointed out some missing research areas that should be addressed in applications such as the limited number of virus species evaluated for anti-viral activity. Research has been in majority focused on HIV, HSV and Influenza A.

Moreover, antifungal activity of calix[n]arenes has been reported, but only a small quantity of research has been carried out in that area. New bioassays should be performed on a larger set of calix[n]arenes and various fungi species in the future. The review also presents emerging works that are promising in anti-cancer research field using calix[n]arene as platform for vaccine or as antioxidants when calix[n]arenes are capped on silver nanoparticles.

Major areas where information is lacking include simple studies such determining complexation for a much wider range of biomolecules including amino-acids, nucleobases, nucleosides and nucleotides. Also much work is required in the structural study of calix[n]arene complexes with systems such as proteins, where, as of 2014 only one structure is known.

The paucity of knowledge of even such basic information as haemolytic effects needs to be addressed, as does systematic analysis of the cytotoxicity of the large number of calix[n]arenes tested in biology.

Finally and most evidently, we need to move to animal models as rapidly as the screening of cell toxicity advances, here there is a major drawback: cost! Substantial investment will be required and we will need strong industrial interest.

In the twenty years since I (AWC) came back to start the study of the biology of calix[n]arenes much has been achieved but it is nice to think that the field is still wide open for new research.

## REFERENCE

- Andrews JM. Determination of minimum inhibitory concentrations. *J Antimicrob Chemoth* 2001. 48: 5-16.
- Atwood JL, Bridges RJ, Juneja RK, Singh AK. Calix[n]arene chloride-channel blockers. Patent US 5489612 A, 1996.
- Arantes LM, Varejao EVV, Pelizzaro-Rocha KJ, Cereda CMS, De Paula E, Lourenco MP, *et al.* Benzocaine complexation with p-sulfonic acid calix[n]arene: experimental (<sup>1</sup>H-NMR) and theoretical approaches. *Chem Biol Drug Des* 2014. 83: 550–559.
- Auzanneau C, Norez C, Noel S, Jouglu C, Becq F, Vanderbruck C. Pharmacological profile of inhibition of the chloride channels activated by extracellular acid in cultured rat Sertoli cells. *Reprod Nutr Dev* 2006. 46: 241-255.
- Bagnacani V, Sansone F, Donofrio G, Baldini L, Casnati A, Ungaro R. Macrocyclic nonviral vectors: high cell transfection efficiency and low toxicity in a lower rim guanidinium calix[4]arene. *Org Lett* 2008. 10: 3953-3956.
- Bagnacani V, Franceschi V, Bassi M, Lomazzi M, Donofrio G, Sansone F, *et al.* *Nature Commun* 2013. 4: 1-7.
- Bertrand J, Boucherle B, Billet A, Melin-Heschel P, Dannhoffer L, Vandebrouck C, *et al.* Identification of a novel water-soluble activator of wild-type and F508del CFTR: GPact-11a. *Eur Respir J* 2010. 36: 311–322.
- Blaskovich MA, Lin Q, Delarue FL, Sun J, Soon Park H, Coppola D, *et al.* Design of GFB-111, a platelet-derived growth factor binding molecule with antiangiogenic and anticancer activity against human tumors in mice. *Nat Biotechnol* 2000. 18: 1065-1070.
- Boudebouze S, Coleman AW, Tauran Y, Mkaouar H, Perret F, Garnier A, *et al.* Discriminatory antibacterial effects of calix[n]arene capped silver nanoparticles with regard to Gram positive and Gram negative bacteria. *Chem Commun* 2013. 49: 7150-7152.
- Brown SD, Plumb JA, Johnston BF, Wheate NJ. Folding of dinuclear platinum anticancer complexes within the cavity of para-sulphonatocalix[4]arene. *Inorg Chim Acta* 2012. 393: 182–186.
- Cafeo G, Carbotti G, Cuzzola A, Fabbi M, Ferrini S, Kohnke FH, *et al.* Drug Delivery with a Calixpyrrole–trans-Pt(II) Complex. *J Am Chem Soc* 2013. 135: 2544-2551.
- Castani A, Sciotto D, Arena G. Water soluble calix[n]arenes. In *calix[n]arenes 2001*; Asfari Z, Bohmer V, Harrowfield J, Vicens J. Eds.; Kluwer Academic Publisher; Dordrecht, 2001. 2001: 440-456.

Chen J, Choy W, Hwang KM, Liu SY, Qi YM. Inhibition and treatment of infection by enveloped virus with calix(n)arene compounds. Patent WO1994003164 A1; 1994.

Chen X, Dings RPM, Nesmelova I, Debbert S, Haseman JR, Maxwell J, et al. Topomimetics of Amphipathic  $\alpha$ -Sheet and Helix-Forming Bactericidal Peptides Neutralize Lipopolysaccharide Endotoxins. *J Med Chem* 2006. 49: 7754-7765.

Coleman AW, Perret F, Cecillon S, Moussa A, Martin A, Dupin M, *et al.* Enhanced detection of the pathogenic prion protein by its supramolecular association with para-sulfonato-calix[n]arene derivatives. *New J Chem* 2007. 31: 711-717.

Coleman AW, Jebors S, Shahgaldian P, Ananchenko GS, Ripmeester JA. para-acylcalix[n]arenes: from molecular to macroscopic assemblies. *Chem Commun* 2008a. 2291-2303.

Coleman AW, Jebors S, Cecillon S, Perret P, Garin D, Marti-Battle D, Moulin M. Toxicity and biodistribution of para-sulphonato-calix[4]arene in mice. *New J Chem* 2008b. 32: 780-782.

Coleman AW, Baggetto LG, Lazar AN, Michaud MH, Magnard S. Calix[n]arene derivatives as anticancer agent. Patent WO2007119027 A1. 2007.

Coleman AW, Mbemba C, Falson P, Matar R, Huché F. Method for selectively extracting membrane proteins using calix[n]arenes. Patent US20110144314 A1, 2011.

Consoli GML, Galante E, Daquino C, Granata G, Cunsolo F, Geraci C. Hydroxycinnamic acid clustered by a calix[n]arene platform: radical scavenging and antioxidant activity. *Tetrahedron Lett* 2006. 47: 6611-6614.

Consoli GML, Granata G, Cafiso V, Stefani S, Geraci C. Multivalent calix[n]arene-based C-fucosyl derivative: a new *Pseudomonas aeruginosa* biofilm inhibitor. *Tetrahedron Lett* 2011. 52: 5831-5834.

Cornforth JW, D'arcy hart P, Nicholls GA, Rees RJW, Stock JA. Antituberculosis effects of certain surface active polyethylene ethers. *Brit J Pharmacol* 1955. 10: 73-86.

Coveney D, Costello B, Preparation of alkylated pyrogallol calix[n]arene type compounds as anti-viral compounds. Patent US 20050113454 A1; 2005.

Cunsolo F, Consoli G, Geraci C, Mecca T. Protamine-mimetic compounds; calix[n]arenes substituted with amino acids bearing salifiable amino groups; In post-surgical protocols to prevent thromboembolism, clotting and thrombi; to prevent clotting in dialysis circuits; side effects reduction; minimize the risk of hemorrhage in dialysed patients. Patent US 20070082951 A1; 2007.

Dalgarno SJ, Atwood JL, Raston CL. Sulfonatocalix[n]arenes: molecular capsule and 'Russian doll' arrays to structures mimicking viral geometry. *Chem Commun* 2006. 4567-4574

Da Silva E, Shahgaldian P, Coleman AW. Haemolytic properties of some water-soluble para-sulphonato-calix-[n]-arenes. *Int J Pharm* 2004. 273: 57-62.

Da Silva E, Ficheux D, Coleman AW. Anti-thrombotic activity of water-soluble calix[n]arenes. *J Incl Phenom Macrocycl Chem* 2005. 52:201–206.

De Assis JV, Teixeira MG, Soares CGP, Lopes JF, Carvalho GSL, Lourenço MCS, *et al.* Experimental and theoretical NMR determination of isoniazid and sodium p-sulfonatocalix[n]arenes inclusion complexes. *Eur J Pharm Sci* 2012. 47: 539–548.

De Fátima A, Fernandes SA, Sabino AA. Calix[n]arenes as New Platforms for Drug Design. *Current Drug Discovery Technologies*, 2009, 6:1-20.

De Oliveira MC, Souza Reis F, De Fátima A, Ferreira Magalhães TF, Da Silva DL, Rodrigues Porto R, *et al.* Synthesis and anti-paracoccidioides activity of calix[n]arenes. *Letters in Drug Design Discovery* 2012. 9: 30-36.

Dings RPM, Chen X, Hellebrekers DMEI, Van Eijk LI, Zhang Y, Hoye TR, *et al.* Design of nonpeptidic topomimetics of antiangiogenic proteins with antitumor activities. *Journal National Cancer Institute* 2006. 98: 932-936.

Dings RPM, Miller MC, Nesmelova I, Astorgues-Xerri L, Kumar N, Serova M, *et al.* Antitumor agent calix[n]arene 0118 targets human galectin-1 as an allosteric inhibitor of carbohydrate binding. *J Med Chem* 2012. 55: 5121–5129.

Dings RPM, Levine JI, Brown SG, Astorgues-Xerri L, MacDonald JR, Hoye TR, *et al.* Polycationic calix[n]arene PTX013, a potent cytotoxic agent against tumors and drug resistant cancer. *Invest New Drugs* 2013. 31: 1142–1150.

Dondoni A, Marra A. Calix[n]arene and calixresorcarene glycosides: Their synthesis and biological applications. *Chem Rev* 2010. 110: 4949–4977.

Edwards JC, Tulk B, Schlesinger PH. Functional expression of p64, an intracellular chloride channel protein. *J Membrane Biol* 1998. 163: 119-127.

Formosa C, Grare M, Jauvert E, Coutable A, Regnouf-de-Vains JB, Mourer M, *et al.* Nanoscale analysis of the effects of antibiotics and CX1 on a *Pseudomonas aeruginosa* multidrug-resistant strain. *Scientific reports* 2012. 2 : 575-583.

Geller C, Fontanay S, Mourer M, Massimba Dibama H, Regnouf-de-Vains JB, Finance C, *et al.* Antiseptic properties of two calix[4]arenes derivatives on the human coronavirus 229E. *Antivir Res* 2010. 88: 343–346.

Geraci C, Consoli GML, Galante E, Bousquet E, Pappalardo M, Spadaro A. Calix[4]arene decorated with four Tn antigen glycomimetic units and P3CS immunoadjuvant: synthesis, characterization, and anticancer immunological evaluation. *Bioconjugate Chem* 2008. 19: 751–758.

Geraci C, Consoli GML, Granata G, Galante E, Palmigiano A, Pappalardo M, *et al.* First self-adjuvant multicomponent potential vaccine candidates by tethering of four or eight MUC1 antigenic immunodominant PDTRP units on a calix[n]arene platform: synthesis and biological evaluation. *Bioconjugate Chem* 2013. 24: 1710–1720.

Goodworth KJ, Herve AC, Stavropoulos E, Herve G, Casades I, Hill AM, *et al.* Synthesis and in vivo biological activity of large-ringed calix[n]arenes against *Mycobacterium tuberculosis*. *Tetrahedron* 2011. 67: 373-382.

Gorteau V, Perret F, Bollot G, Mareda J, Lazar AN, Coleman AW, *et al.* Synthetic multifunctional pores with external and internal active sites for ligand gating and noncompetitive blockage. *J Am Chem Soc* 2004. 126: 13592-13593.

Gorteau V, Bollot G, Mareda J, Pasini D, Tran DH, Lazar AN, *et al.* Synthetic multifunctional pores that open and close in response to chemical stimulation. *Bioorg Med Chem* 2005. 13: 5171–5180.

Grare M, Massimba Dibama H, Lafosse S, Ribon A, Mourer M *et al.* Cationic compounds with activity against multidrug-resistant bacteria: interest of a new compound compared with two older antiseptics, hexamidine and chlorhexidine. *Clin Microbiol Infect* 2010. 16: 432-438.

Grare M, Mourer M, Fontanay S, Regnouf-de-Vains JB, Finance C, Duval RE. In vitro activity of para-guanidinoethylcalix[4]arene against susceptible and antibiotic-resistant Gram-negative and Gram-positive bacteria. *J Antimicrob Chem* 2007. 60: 575–581.

Guo DS, Liu Y. Supramolecular chemistry of p-sulfonatocalix[n]arenes and its biological applications. *Acc Chem Res* 2014. 47: 1925-1934.

Gutsche CD. *Calix[n]arenes an Introduction*, 2nd Edition. The Royal Society of Chemistry, Cambridge, UK. 2008.

Hafez IM, Maurer N, Cullis PR. On the mechanism whereby cationic lipids promote intracellular delivery of polynucleic acids. *Gene Therapy*. 2001. 8: 1188–1196.

Harris SJ, Calix[n]arene-based compounds having antibacterial, antifungal, anticancer-hiv activity. Patent WO1995019974 A2; 1995.

Harris SJ, Anti-viral compounds. Patent WO2002044121 A1; 2002.

Hwang KM, Qi YM, Liu SY, Lee TC, Choy W, Chen J. Antithrombotic treatment with calix(n)arene compounds. Patent US 5409959 A; 1995.

Izzo I, Licen S, Maulucci N, Autore G, Marzocco S, Tecilla P, *et al.* Cationic calix[4]arenes as anion-selective ionophores. *Chem Commun* 2008. 26: 2986–2988.

James E, Eggers PK, Harvey AR, Dunlop SA, Fitzgerald M, Stubbs KA, *et al.* Antioxidant phospholipid calix[4]arene mimics as micellar delivery systems. *Org Biomol Chem* 2013. 11: 6108-6112.

Jebors S, Lesniewska B, Shkurenko O, Suwinska K, Coleman AW. Para-acylcalix[6]arenes: their synthesis, per-O-functionalisation, solid-state structures and interfacial assembly properties. *J Incl Phenom Macrocycl Chem* 2010. 68: 207–217.

Kalchenko VI, Cherenok SO, Kosterin SO, Lugovskoy EV, Komisarenko SV, Vovk AI, *et al.* Calix[n]arene phosphonous acids: Synthesis and biological activity. *Phosphorus Sulfur and Silicon* 2013. 188:232–237.

Klyachina MA, Boyko VI, Yakovenko AV, Babich LG, Shlykov SG, Kosterin SO, *et al.* Calix[4]arene N-chalconeamides: synthesis and influence on Mg<sup>2+</sup>,ATP-dependent Ca<sup>2+</sup> accumulation in the smooth muscle subcellular structures. *J Incl Phenom Macrocycl Chem* 2008. 60:131–137.

Krause-Heuer AM, Wheate NJ, Tilby MJ, Graham Pearson D, Ottley CJ, Aldrich-Wright JR. Substituted b-cyclodextrin and calix[4]arene as encapsulatory vehicles for platinum(II)-based DNA intercalators. *Inorg Chem* 2008. 47: 6880-6888.

Krishnamurthy VM, Estroff LA, Whitesides GM. Multivalency in ligand design, in: *Fragment-based Approaches in Drug Discovery*. Eds: W. Jahnke and D.A. Erlanson. Wiley-VCH, Weinheim, Germany 2006. 34: 11-53.

Lalor R, Baillie-Johnson H, Redshaw C, Matthews SE, Mueller A. Cellular uptake of a fluorescent calix[4]arene derivative. *J Am Chem Soc* 2008. 130: 2892-2893.

Lalor R, DiGesso JL, Mueller A, Matthews SE. Efficient gene transfection with functionalised multicalix[n]arenes. *Chem Commun* 2007. 4907–4909.

Lamartine R, Tsukada M, Wilson D, Shirat A. Antimicrobial activity of calix[n]arenes. *C. R. Chimie* 2002. 5: 163–169.

Latxague L, Gaboriau F, Chassande O, Leger JM, Pires V, Rouge P, *et al.* Antiproliferative effect on HepaRG cell cultures of new calix[4]arenes. Part II. *J Enzym Inhib Med Ch* 2011. 26(2): 204–215.

Laventie BJ, Potrich C, Atmanene C, Saleh M, Joubert O, Viero G, *et al.* p-Sulfonato-calix[n]arenes inhibit staphylococcal bicomponent leukotoxins by supramolecular interactions. *Biochem J*. 2013. 450: 559-571.

Lehn JM. *Supramolecular Chemistry: Receptors, Catalysts, and Carrier*. *Science* 1985. 227: 849-856.

Li H, Findlay IA, Sheppard DN. The relationship between cell proliferation, Cl<sup>-</sup> secretion, and renal cyst growth: A study using CFTR inhibitors. *Kidney Int* 2004. 66: 1926–1938.

Li M, Peters MS, Schrader T. Interactions of calix[n]arenes with nucleic acids. *Nat Prod Commun* 2012. 7: 409-417.

Lipkowski J, Simonov Y, Kalchenko VI, Vystsky MA, Markovsky LN. Molecular and crystal structure of water soluble 25,57-bis(dihydroxyphosphoryloxy)calix[4]arene. *An Quim Int Ed* 1998. 94: 328-331.

Lugovskoy EV, Gritsenko PG, Koshel TA, Koliesnik IO, Cherenok SO, Kalchenko OI, *et al.* Calix[4]arene methylenebisphosphonic acids as inhibitors of fibrin polymerization. *FEBS Journal* 2011. 278: 1244-1251.

MacGillivray LR, Atwood JL. A chiral spherical molecular assembly held together by 60 hydrogen bonds. *Nature* 1997. 389: 469-472.

Maerz AK, Thomas HM, Power NP, Deakyne CA, Atwood JL. Dimeric nanocapsule induces conformational change. *Chem Commun* 2010. 46:1235–1237

Mammen M, Choi SK, Whitesides GM. Polyvalent interactions in biological systems: Implication for design and use of multivalent ligands and inhibitors. *Angew. Chem. Int. Ed. Engl.* 1998. 37: 2755-2794.

Matar-Merheb R, Rhimi M, Leydier A, Huche F, Galian C, Desuzinges-Mando E, *et al.* Structuring detergents for extracting and stabilizing functional membrane proteins. *Plos One* 2011. 6: 1-10.

Marra A, Moni L, Pazzi D, Corallini A, Bridib D, Dondoni A. Synthesis of sialoclusters appended to calix[4]arene platforms via multiple azide-alkyne cycloaddition. New inhibitors of hemagglutination and cytopathic effect mediated by BK and influenza A viruses. *Org Biomol Chem* 2008. 6: 1396–1409.

Massimba Dibama H, Clarot I, Fontanay S, Ben Salem A, Mourer M, Finance C, *et al.* Towards calix[n]arene-based prodrugs: Drug release and antibacterial behaviour of a water-soluble nalidixic acid/calix[4]arene ester adduct. *Bioorg Med Chem Lett* 2009. 19: 2679–2682.

Mecca T, Consoli GML, Geraci C, La Spina R, Cunsolo F. Polycationic calix[8]arenes able to recognize and neutralize heparin. *Org Biomol Chem*, 2006, 4: 3763-3768.

Mecca T, Cunsolo F. Polycationic calix[8]arene receptors grafted onto polymeric matrix: smart material for heparin neutralization. *Polym Adv Technol* 2010. 21: 752-757.

Menon SK, Modi NR, Mistry B, Joshi K. Improvement of some pharmaceutical properties of mycophenolate mofetil (MMF) by para-sulphonatocalix[4]resorcinarene inclusion complex. *J Incl Phenom Macrocycl Chem* 2011. 70:121–128.

Menon SK, Mistry BR, Joshi KV, Modi NR, Shashtri D. Evaluation and solubility improvement of Carvedilol: PSC[n]arene inclusion complexes with acute oral toxicity studies. *J Incl Phenom Macrocycl Chem* 2012. 73: 295–303.

Mokhtari B, Pourabdollah K. Applications of calix[n]arene nano-baskets in pharmacology. *J Incl Phenom Macrocycl Chem* 2012. 73:1–15.

Montasser I, Shahgaldian P, Perret F, Coleman AW. Solid Lipid Nanoparticle-based calix[n]arenes and calix-resorcinarenes as building blocks: synthesis, formulation and characterization. *Int J Mol Sci* 2013. 14: 21899-21942.

Motornaya AE, Alimbarova LM, Shokova EA, Kovalev VV. Synthesis and antiherpetic activity of N-(3-amino-1-adamantyl)calix[4]arenes. *Pharm Chem J* 2006. 40: 68-72.

Mourer M, Massimba Dibama H, Fontanay S, Grare M, Duval RE, Finance C, *et al.* p-Guanidinoethyl calix[n]arene and parent phenol derivatives exhibiting antibacterial activities. Synthesis and biological evaluation. *Bioorg Med Chem* 2009. 17: 5496–5509.

Mourer M, Psychogios N, Laumond G, Aubertin AM, Regnouf-de-Vains JB. Synthesis and anti-HIV evaluation of water-soluble calix[n]arene-based bithiazolyl podands. *Bioorg Med Chem* 2010. 18: 36–45.

Mourer M, Fontanay S, Duval RE, Regnouf-de-Vains JB. Synthesis, Characterization, and biological evaluation as antibacterial agents of water-soluble calix[4]arenes and phenol derivatives incorporating carboxylate groups. *Helv Chim Acta* 2012. 95: 1373-1386.

Mueller A, Lalor R, Moyano Cardaba C, Matthews SE. Stable and sensitive probes for lysosomes: cell-penetrating fluorescent calix[4]arenes accumulate in acidic vesicles *Cytom Part A* 2011. 79A: 126-136.

Munson HR, Tankersley RW. Antiviral sulfonated naphthalene formaldehyde condensation polymers. Patent US 4604404; 1986.

Naegu M, Ion RM, Manda G, Constantin C, Radu E, Cristu Z. Antitumoral effect of calix[n]arenes in experimental photodynamic therapy with K562 tumour cell line. *Rom J Biochem* 2010. 47: 17–35.

Nagasaki T, Sisido K, Arimura K, Shinkai S. Novel conformational isomerism of water-soluble calix4arenes. *Tetrahedron* 1992. 48: 797-804.

Nakai T, Kanamori T, Sando S, Aoyama Y. Remarkably Size-Regulated Cell Invasion by Artificial Viruses. Saccharide-Dependent Self-Aggregation of Glycoviruses and Its Consequences in Glycoviral Gene Delivery. *J Am Chem Soc* 2003. 125: 8465-8475.

Nault L, Cumbo A, Pretot RF, Sciotti MA, Shahgaldian P. Cell transfection using layer-by-layer (LbL) coated calix[n]arene-based solid lipid nanoparticles (SLNs). *Chem Commun* 2010. 46: 5581–5583.

Nishihara M, Perret F, Takeuchi T, Futaki S, Lazar AN, Coleman AW, *et al.* Arginine magic with new counterions up the sleeve. *Org Biomol Chem* 2005. 3:1659–1669.

Pacllet MH, Rousseau CF, Champion Y, Morel F, Coleman AW. An absence of non-specific immune response towards para-sulphonato-calix[n]arenes. *J Incl Phenom Macrocycl Chem* 2006. 55:353–357.

Paquet V, Zumbuehl A, Carreira EM. Biologically Active Amphotericin B-Calix[4]arene Conjugates. *Bioconjugate Chem* 2006. 17: 1460-1463.

Parker D. *Macrocyclic synthesis: a practical approach*, Oxford University Press, Oxford, 1996.

Patel MB, Modi NR, Raval JP, Menon SK. Calix[4]arene based 1,3,4-oxadiazole and thiadiazole derivatives: Design, synthesis, and biological evaluation. *Org Biomol Chem* 2012. 10: 1785–1794.

Patel MB, Valand NN, Modi NR, Joshi KV, Harikrishnan U, Kumar SP, *et al.* Effect of p-sulfonatocalix[4]resorcinarene (PSC[4]R) on the solubility and bioavailability of a poorly water soluble drug lamotrigine (LMN) and computational investigation. *RSC Advances* 2013. 3: 15971–15981.

Pelizzaro-Rocha KJ, Bispo de Jesus M, Ruela-de-Sousa RR, Vataru Nakamura C, Souza Reis F, De Fátima A, *et al.* Calix[6]arene bypasses human pancreatic cancer aggressiveness: Downregulation of receptor tyrosine kinases and induction of cell death by reticulum stress and autophagy. *Biochim Biophys Acta* 2013. 1833: 2856–2865.

Perret F, Coleman AW. Biochemistry of anionic calix[n]arenes. *Chem Commun* 2011. 47: 7303-7319.

Perret F, Coleman AW. Interactions of calix[n]arenes and other organic supramolecular systems with proteins (Chapter 6). In: *Supramolecular Systems in Biomedical Fields*. Schneider H-J (Ed.), The Royal Society of Chemistry, Cambridge, UK, 2013.

Perret F, Lazar AN, Coleman AW. Biochemistry of the para-sulfonato-calix[n]arenes. *Chem Commun* 2006. 23: 2425-2438.

Perret F, Peron H, Dupin M, Coleman AW. Calixarenes as protein sensors, in *Topic in current chemistry, Creative chemical sensor systems*, ed. T. Schrader, Springer, Berlin, 2007, 277: 31–88.

Pur FN, Dilmaghani KA. Calixplatin: novel potential anticancer agent based on the platinum complex with functionalized calix[n]arene. *J Coord Chem* 2014. 67: 440-448.

Redshaw C, Elsegood MRJ, Wright JA, Baillie-Johnson H, Yamato T, De Giovannie S, *et al.* Cellular uptake of a fluorescent vanadyl sulfonylcalix[4]arene. *Chem Commun* 2012. 48: 1129-1131.

Rodik RV, Klymchenko AS, Jain N, Miroshnichenko SI, Richert L, Kalchenko VI, *et al.* Virus-sized DNA nanoparticles for gene delivery based on micelles of cationic calix[n]arenes. *Chem Eur J* 2011. 17: 5526–5538.

Rodik RV, Boyko VI, Kalchenko VI. Calix[n]arenes in biomedical researches. *Curr Med Chem* 2009. 16: 1630–1655.

Rodik RV, Klymchenko AS, Jain N, Miroshnichenko SI, Richert L, Kalchenko VI, *et al.* Virus-sized DNA nanoparticles for gene delivery based on micelles of cationic calixarenes. *Chem. Eur. J.* 2011. 17: 5526 – 5538.

Rouge P, Silva Pires V, Gaboriau F, Dassonville-Klimpt A, Guillon J, Da Nascimento S, *et al.* Antiproliferative effect on HepaRG cell cultures of new calix[4]arenes. *J Enzym Inhib Med Chem* 2010. 25: 216–227.

Rouge P, Dassonville-Klimpt A, Cezard C, Boudesocque S, Ourouda R, Amant C, *et al.* Synthesis, physicochemical studies, molecular dynamics simulations, and metal-ion-dependent antiproliferative

and antiangiogenic properties of cone ICL670-substituted calix[4]arenes. *ChemPlusChem* 2012. 77: 1001-1016.

Sansone F, Casnati A. Multivalent glyco-calix[n]arenes for recognition of biological macromolecules: glyco-calix mimics capable of multitasking. *Chem Soc Rev.*, 2013. 42: 4623-4639.

Sansone F, Dudic M, Donofrio G, Rivetti C, Baldini L, Casnati A. DNA condensation and cell transfection properties of guanidinium calix[n]arenes: dependence on macrocycle lipophilicity, size, and conformation. *J Am Chem Soc* 2006. 128: 14528-14536.

Sebti M, Hamilton AD. Design of growth factor antagonists with antiangiogenic and antitumor properties. *Oncogene* 2000. 19: 6566-6573.

Shahgaldian P, Da Silva E, Coleman AW. A First Approach to the study of calix[n]arene Solid Lipid Nanoparticle (SLN) toxicity. *J Incl Phenom Macrocycl Chem* 2003. 46: 175-177.

Schrader T. Protein recognition: Calix[n]arene connection. *Nature Chemistry* 2012. 4: 519–520.

Shinkai S, Tsubaki T, Sone T, Manabe O. *Tetrahedron Lett* 1984. 25: 5315-5318.

Shinkai S, Arimura T, Araki K, Kawabata H, Satoh H, Tsubaki T, *et al.* Syntheses and aggregation properties of new water-soluble calix[n]arenes. *J Chem Soc Perkin Trans* 1989. 1: 2039-2045.

Spagnul A, Bouvier-Capely C, Phan G, Rebiere F, E. Fatta. A new formulation containing calix[n]arene molecules as an emergency treatment of Uranium skin contamination. *Health Physics* 2010. 99: 430-434.

Spagnul A, Bouvier-Capely C, Phan G, Landon G, Tessier C, Suhard D, *et al.* Ex vivo decrease in uranium diffusion through intact and excoriated pig ear skin by a calix[n]arene nanoemulsion. *Eur J Pharm Biopharm* 2011a. 79: 258–267.

Spagnul A, Rebiere F, Phan G, Bouvier-Capely C, Fattal E. Cosmetic and pharmaceutical formulations of calixarene molecules. US 20110281948 A1. 2011b.

Sun J, Blaskovich MA, Jain RK, Delarue F, Paris D, Brem S. Blocking angiogenesis and tumorigenesis with GFA-116, a synthetic molecule that inhibits binding of vascular Endothelial Growth Factor to its receptor. *Cancer Res* 2004. 64: 3586-3592.

Tauran Y, Anjard C, Kim B, Rhimi M, Coleman AW. Large supramolecular organic macrocycles as inhibitors of endonuclease enzymes. *Chem Commun* 2014. Under revision.

Tauran Y, Coleman AW. Bio-applications of calix[n]arene capped silver nanoparticles. *Nanomedicine* 2014. Under submission.

Tsou LK, Dutschman GE, Gullen EA, Telpoukhovskaia M, Cheng YC, Hamilton AD. Discovery of a synthetic dual inhibitor of HIV and HCV infection based on a tetrabutoxy-calix[4]arene scaffold. *Bioorg Med Chem Lett* 2010. 20: 2137–2139.

Tsou LK, Chen CH, Dutschman GE, Cheng YC, Hamilton AD. Blocking HIV-1 entry by a gp120 surface binding inhibitor. *Bioorg Med Chem Lett* 2012. 22: 3358-3361.

Ukhatskaya EV, Kurkov SV, Hjálmsdóttir MA, Karginovd VA, Matthews SE, Rodik RV, *et al.* *Int J Pharm* 2013. 458: 25-30.

Vander Heiden MG. Targeting cancer metabolism: a therapeutic window opens. *Nat. Rev. Drug Disc.* 2011. 10: 671-684.

Veklich TA, Shkrabak AA, Slinchenko NN, Mazur II, Rodik RV, Boyko VI. Calix[4]arene C 90 selectively inhibits Ca<sup>2+</sup>,Mg<sup>2+</sup> ATPase of myometrium cell plasma membrane. *Biochemistry (Moscow)* 2014. 79: 417-424.

Wang GF, Ren XL, Zhao M, Qiu XL, Qi AD. Paraquat detoxification with p-sulfonatocalix-[4]arene by a pharmacokinetic study. *J Agric Food Chem* 2011. 59: 4294–4299.

Wang K, Guo DS, Zhang HQ, Li D, Zheng XL, Liu Y. Highly effective binding of viologens by p-sulfonatocalix[n]arenes for the treatment of viologen poisoning. *J Med Chem* 2009. 52: 6402-6412.

Wang K, Guo DS, Wang X, Liu Y. Multistimuli responsive supramolecular vesicles based on the recognition of p-sulfonatocalix[n]arene and its controllable release of doxorubicin. *ACS Nano* 2011. 5: 2880–2894.

Zinke A, Kretz R, Leggewie E, Hössinger K, Hoffmann G, Weber v Ostwalden P, *et al.* Zur Kenntnis des Härtungsprozesses von Phenol-Formaldehyd-Harzen. *Monats Chem* 1952. 83: 1213-1227.

Zheng DD, Fu DY, Wu Y, Sun YL, Tan LL, Zhou T. Efficient inhibition of human papillomavirus 16 L1pentamer formation by a carboxylatopillarene and a p-sulfonatocalix[n]arene. *Chem Commun* 2014. 50: 3201-3203.

Zhou H, Wang D, Baldini L, Ennis E, Jain R, Carie A, *et al.* Structure–activity studies on a library of potent calix[4]arene-based PDGF antagonists that inhibit PDGF-stimulated PDGFR tyrosine phosphorylation. *Org Biomol Chem* 2006. 4: 2376–238.



Part A

Section 2

## Localized Surface Plasmon Resonance



## Localized Surface Plasmon Resonance

The collective excitation of conduction electrons (also called free electron) along a surface, triggered by the stimulation of light (at visible to NIR frequency) is described as a surface plasmon. Indeed, the electro-magnetic radiation of the incident light induces a polarization of the free electron on the surface, while the positive charges are assumed to be fixed ionic core. Therefore, the polarized electronic movement behaves as a dipolar oscillation along the surface (Figure 1). (Daghestani *et al.*, 2010)

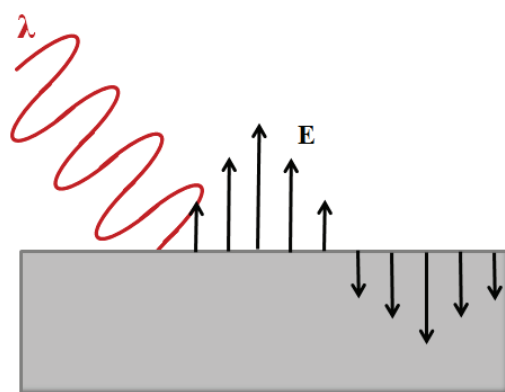


**Figure 1.** Interaction of light on a metallic surface. The incident the electrical wavelength of light (in red) induces an electronic collective oscillation. The black arrows represent the electronic field  $E$  generated at the surface.

This section will provide to the reader, an analytical explanation of the LSPR principle, followed by a description of the plasmonic and optical effects induced by the change of several parameters (material, molecular environment, size, shape) affecting the nanoparticle. The presentation of this plasmonic phenomenon is necessary for understanding the optical behaviour of metal nanoparticles described in the ‘Results’ chapter of this manuscript.

### 1. LSPR principle

In Surface Plasmon Resonance, surface plasmon waves (called polaritons) propagate along a smooth metal surface, while in Localized Surface Plasmon Resonance (LSPR), the surface plasmon is confined to a metallic particle size comparable to the wavelength of light. (Willets *et al.*, 2007) In LSPR, the particle’s optical extinction has a maximum at the plasmon resonance frequency. This happens at visible wavelength for noble metal nanoparticles. When nanoparticles exhibit such plasmonic phenomenon, two conditions should be filled: 1) the dielectric permittivity of the metal needs to be negative 2) the free-space wavelength should be large in comparison to the nanoparticle diameter (Jain *et al.*, 2008).

The dielectric permittivity  $\epsilon$  relates the ability of the material to transmit (or to permit) the electric field. This parameter is directly related to the electronic susceptibility  $\chi$  of a material, which corresponds to the polarizability induced by the electronic field.

$$\epsilon = \epsilon_r \epsilon_0 = (1 + \chi) \epsilon_0 \quad (1)$$

In SI units, permittivity  $\epsilon$  is measured in farads per meter (F/m); electric susceptibility  $\chi$  is dimensionless. Where  $\epsilon_r$  is permittivity of the material, and  $\epsilon_0$  is the vacuum permittivity. When the permittivity of a material is negative, such as for noble metal nanoparticles, the polarization vector  $P$  has the opposite direction of the incident electric field  $E_0$ . As a consequence, the surface electric charges create a depolarizing electric field  $E'$ , which has the same direction as  $E_0$  (Figure 2 A). Therefore the total electric field  $E = E' + E_0$  will be locally enhanced in the nanoparticle. On the contrary, nanoparticles with a positive dielectric permittivity will decrease the total electric field (Figure 2B). (Kelly *et al.*, 2003)

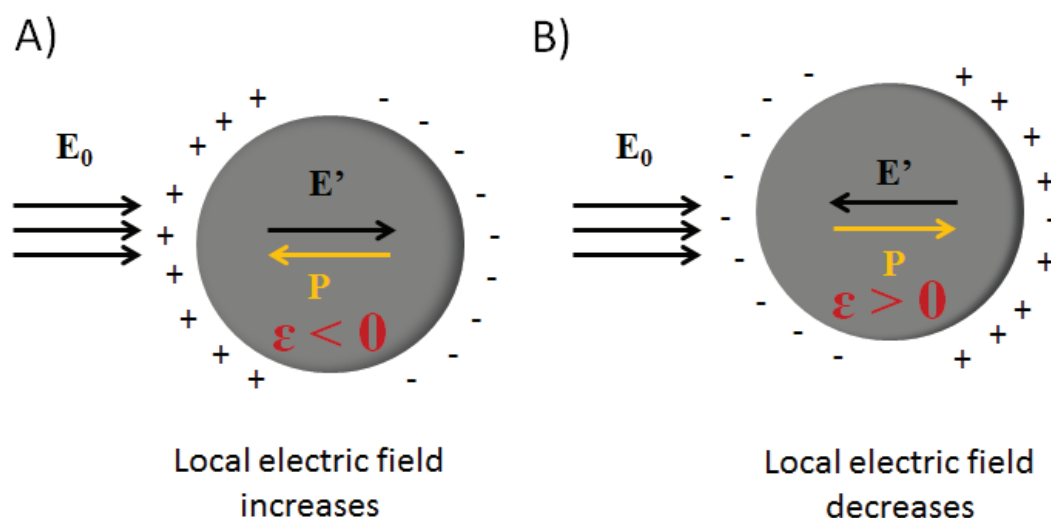


**Figure 2.** Effect of electric field on nanoparticles with a dielectric permittivity A) negative or B) positive.

When the wavelength is larger than the diameter of the nanoparticle, the electric field of light can be taken as constant over the nanoparticle. Thus, the effect is electrostatic instead of electrodynamic. In that case, the phenomenon is called quasistatic because the dielectric constant of the metal particle  $\epsilon$  (corresponding to dielectric permittivity ratio  $\epsilon / \epsilon_0$ ) and the surrounding medium  $\epsilon_m$  can be described by electrostatic theory. (Ghosh *et al.*, 2007)

The relation between the electric field applied  $E_0$  and the depolarizing electric field  $E'$  is given by the following equation:

$$E' = E_0 \frac{3\epsilon_m}{\epsilon + 2\epsilon_m} \quad (2)$$

It is possible to deduce the static polarizability  $\alpha$  of a spherical nanoparticle by using Laplace's equation. Then, the Clausius-Mosotti equation is given by :

$$\alpha = 4\pi\epsilon_0 R^3 \frac{\epsilon - \epsilon_m}{\epsilon + 2\epsilon_m} \quad (3)$$

in which  $R$  is the radius of the spherical nanoparticle.  $\epsilon$  is a complex function, described by:

$$\epsilon = \epsilon_1(\omega) + i\epsilon_2(\omega) = (n + ik)^2 \quad (4)$$

where  $n$  is the index of refraction and  $k$  related to light absorption.

Therefore, the wavelength of plasma resonance arising at the highest polarizability  $\alpha$ , occurs when the wavelength  $\omega$  dependant dielectric constants correspond to  $\epsilon_1(\omega) = -2\epsilon_m$  and  $\epsilon_2(\omega)$  is small and/or weakly dependant on the wavelength  $\omega$ .

In the early 1900's, Mie has developed an analytical solution based on Maxwell's equation. (Mie *et al.*, 1908) Then the size dependence of spherical nanoparticles has been described as a matter of their coefficient extinction  $\sigma_{ext}$ , absorption  $\sigma_{abs}$  and scattering  $\sigma_{sca}$ . The equation is given by

$$\sigma_{ext} = \sigma_{abs} + \sigma_{sca} \quad (5)$$

with

$$\sigma_{ext} = 9 \frac{\omega}{c} \epsilon_m^{3/2} V \frac{\epsilon_2(\omega)}{[\epsilon_1(\omega) + 2\epsilon_m(\omega)]^2 + [\epsilon_2(\omega)]^2} \quad (6)$$

where  $c$  is the speed of light,  $\omega$  is the angular frequency of the light and  $V$  is the particle volume.

The optical materials functions determine the position and the shape of the plasmonic resonance. While the real part of the dielectric constant  $\epsilon_1(\omega)$  determines the enhancement of the local electrical field, the imaginary part of the dielectric constant  $\epsilon_2(\omega)$  corresponds to the energy loss. The width and height of the resonance depends on the imaginary part of the dielectric constant of the nanoparticle  $\epsilon_2(\omega)$ . The width is also dependant of the dielectric constant of the surrounding medium  $\epsilon_m$ . (Hovel *et al.*, 1993) Subsequently, the resonance frequency and the optical response of metal nanoparticles are closely dependant of four parameters, which are the nature of material, the size, the shape and the molecular environment surrounding the nanoparticle.

## 2. Parameters affecting the plasmonic properties of nanoparticles

### 2.1 Nanoparticle material

The dispersion relation describes the dispersion of wave going through a specific medium. It relates the frequency of the wave to its wavelength. In ideal case, when there is no

energy loss (electrons collisions are negligible) the dispersion relation of  $\epsilon(\omega)$  of a metallic nanoparticle corresponds to:

$$\epsilon(\omega) = \epsilon_0 \left(1 - \frac{\omega_p^2}{\omega^2}\right) \quad (7)$$

with

$$\omega_p^2 = \frac{e^2 N}{\epsilon_0 m} \quad (8)$$

where  $\omega_p$  is the plasma frequency of the nanoparticle and  $N$  is the electron density. (Mayer *et al.*, 2011)

The electron density of gold and silver are respectively of  $5.9 \times 10^{22}$  and  $5.86 \times 10^{22}$   $\text{cm}^{-3}$ . The real part of the dielectric constant  $\epsilon_1(\omega)$  is then almost the same for gold than silver (Figure 3A). Figure 3 shows the complex dielectric functions of silver and gold from experimental data (Johnson *et al.*, 1972). On the other hand, the imaginary part of the dielectric constant  $\epsilon_2(\omega)$ , shows that the losses are much stronger for silver than gold (Figure 3 B). The ratio of dielectric constant real over imaginary corresponds to the quality of the plasmon resonance. This ratio is the higher for silver at any wavelength, making silver the reference as metal nanoparticle for optical sensing.

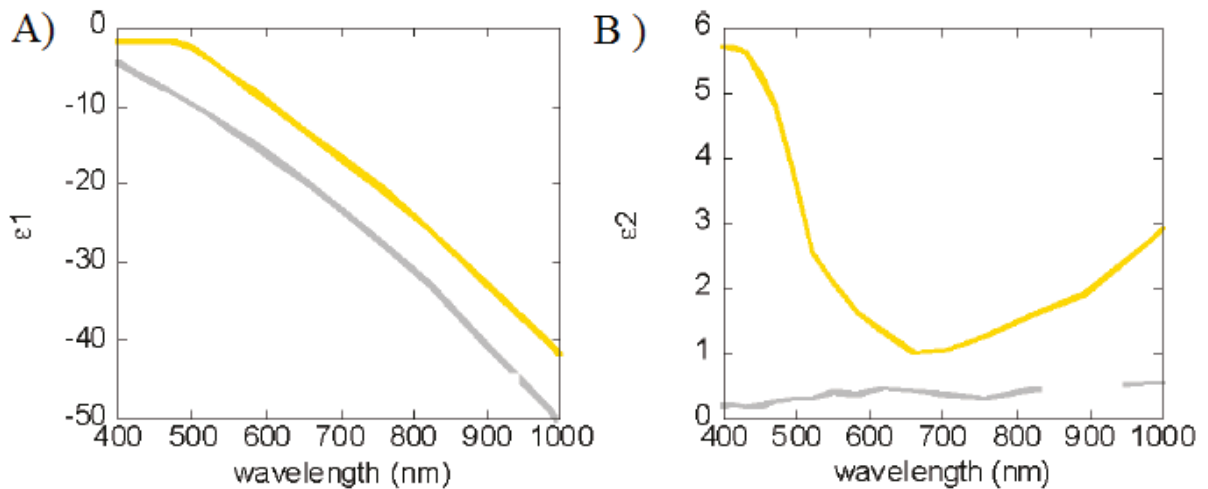


**Figure 3.** Complex dielectric functions of silver (in grey) and gold (in yellow). Graph A) represents their real part and graph B) represent their imaginary part as a matter of wavelength emitted. From (Mayer *et al.*, 2011)

The imaginary part of the dielectric constant  $\epsilon_2(\omega)$  can be calculated by introducing a friction term corresponding to the energy loss. Then, the dielectric permittivity  $\epsilon(\omega)$  can be deduced as:

$$\epsilon(\omega) = \epsilon_0 \left[1 - \frac{\omega_p^2}{\omega(\omega + j\gamma)}\right] \quad (9)$$

where  $\gamma$  is the plasma relaxation frequency. (Mayergoyz *et al.*, 2013)

This formula corresponds to the Drude model of the dielectric permittivity, which is one of the main component (Clausius-Mosotti equation and Mie theory) for understanding the plasmon resonance.

## 2.2 Molecular environment of the nanoparticle

The Drude model can be used for describing the dependence between the optical frequency of nanoparticle and refractive index surrounding the metal nanoparticle. In the case of visible and near infra-red frequency, the plasma relaxation frequency  $\gamma$  is largely inferior to the plasma frequency  $\omega_p$ . Then, the Drude model can be simplified to the equation 7. (Jensen *et al.*, 1999)

Moreover, it has been previously demonstrated that at the resonance conditions,  $\epsilon_1(\omega) = -2\epsilon_m$ . Then equation 7 can be written as:

$$\omega_{\max} = \frac{\omega_p}{\sqrt{2\epsilon_m + 1}} \quad (10)$$

If the plasmonic frequency is converted in wavelength, and the dielectric permittivity is changed into the index ( $\epsilon_m = n_m^2$ ) the expression becomes:

$$\lambda_{\max} = \lambda_p \sqrt{2n_m^2 + 1} \quad (11)$$

where  $\lambda_{\max}$  is the plasmonic wavelength and  $\lambda_p$  is the wavelength corresponding to the plasma frequency of the bulk metal.  $n_m$  is the index of the molecular environment surrounding the nanoparticle.

Figure 4 shows the effect of differing refractive index media on optical frequency of silver nanoparticles. It can be seen that the relation between the plasmonic frequency and the refractive index could be qualified as approximatively linear.

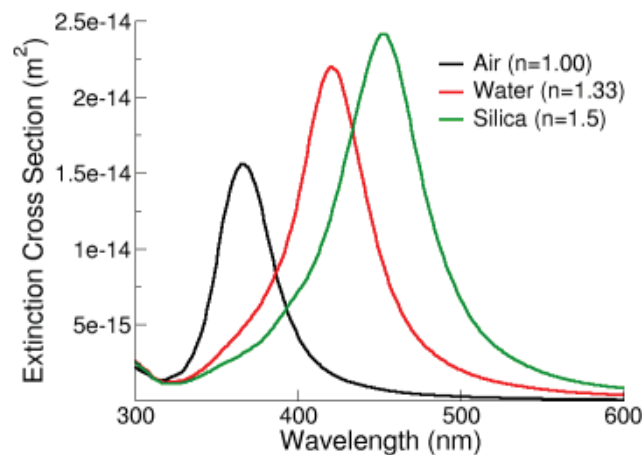


**Figure 4.** Extinction coefficient of silver nanoparticles in 3 different media. From (NanoComposix)

Then, the optical detection of molecules interacting along the metal nanoparticles will be based on the dependence of the plasmonic resonance to the refractive index of the molecular environment surrounding the nanoparticle. (Jain *et al.*, 2010) The LSPR shift response  $R$  (in nm), can be also expressed as:

$$R = m(n_{eff} - n_{ext}) \quad (12)$$

where  $m$  is the refractive index sensitivity of the hybrid nanoparticles,  $n_{eff}$  is the refractive index of the nanoparticles and  $n_{ext}$  is the refractive index of the molecular environment surrounding the nanoparticle. (Haes *et al.*, 2002)

Van Duyne's group have largely contributed in that field and have shown the dependence of length carbon chain attached on silver nanoparticle by using alkyl Self Assembled Monolayer. (Malinsky *et al.*, 2001)

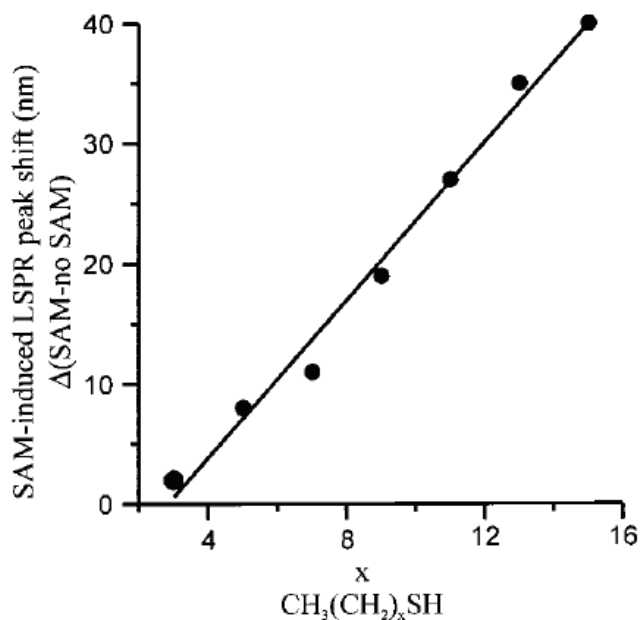


**Figure 5.** Alkanethiol chain length dependence on the LSPR spectral peak shift. From (Malinsky *et al.*, 2001)

Beside, the dependence of the light absorbance on plasmonic nanoparticles and the attachment of ligand to the surface has also been described as approximately linear (Figure 4). (Zhao *et al.*, 2009) The absorbance light corresponds to the amount of photon taken from light for producing exciton, which is an electron formed by a photon from its valence band to its conduction band. The refractive index of the molecular environment surrounding the nanoparticle is dependant to the dielectric complex function and the polarizability. As a consequence, the depolarization of nanoparticles will enhance the plasmonic resonance and the absorbance of light. (Niesen *et al.*, 2012)

The sensitivity to the medium refractive index could be improved by changing the size / shape of the nanoparticles. (Haes *et al.*, 2002)

### 2.3 Nanoparticle size

The surface of the nanoparticles plays an important role in the propagation of the electronic wave because it changes the conditions of polarizability of the metal and therefore shifts the plasmon frequency. (Derkachova *et al.*, 2013)

The Mie theory has been previously described in equation 6 for small metal nanoparticles with a diameter inferior to 20 nm. In that case, the plasmonic resonance mode is dipolar. However higher modes of resonance can be observed when the nanoparticle size increase. This is because the light cannot polarize the nanoparticles homogeneously anymore. The effects of energy losses are enhanced with higher resonance modes and cause huge shift and broadening of the plasmonic resonance. As a consequence, the plasmonic wavelength of nanoparticles will be red-shifted and the absorbance intensity will be decreased (Figure 6). (Kreibig *et al.*, 1995)

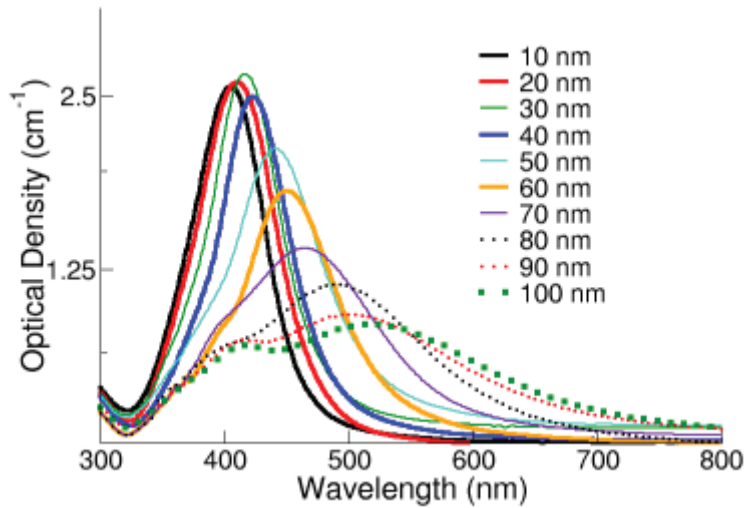


**Figure 6.** UV-visible spectra of silver nanoparticles of different sizes. From (NanoComposix)

This optical response is typical of the aggregation of metal nanoparticles in solution. The agglomeration of small nanoparticle into higher complex, leads to a red shift and a broader plasmonic absorption, as seen in Figure 6. (Amendola *et al.*, 2010)

### 2.4 Nanoparticle shape

In 1912, Gans has extended the Mie theory, which was initially confined to spherical nanoparticles, to spheroid nanoparticles with different dimensions ratio ( $A > B = C$ ). The absorption coefficient has been expressed as :

$$\sigma_{abs} = \frac{\omega}{3c} \epsilon_m^{\frac{3}{2}} V \sum_j \frac{\epsilon_2 \left( \frac{1}{P_j^2} \right)}{\left[ \epsilon_1 + \left[ \frac{1-P_j}{P_j} \right] \epsilon_m \right]^2 + \epsilon_2^2} \quad (13)$$

where  $j$  considers the three dimensions A, B, C of the particles.  $P_j$  correspond to the depolarization factor of each axis of the particle. (Gans *et al.*, 1912)

As a consequence, there are two different absorbance coefficients one for the dimension A and another one for the dimensions B and C (Figure 6). Experiment with polarized light microscopy has demonstrated the dependence of the orientation of nanorod and the plasmonic mode (transversal or longitudinal). (Orendorff *et al.*, 2006)

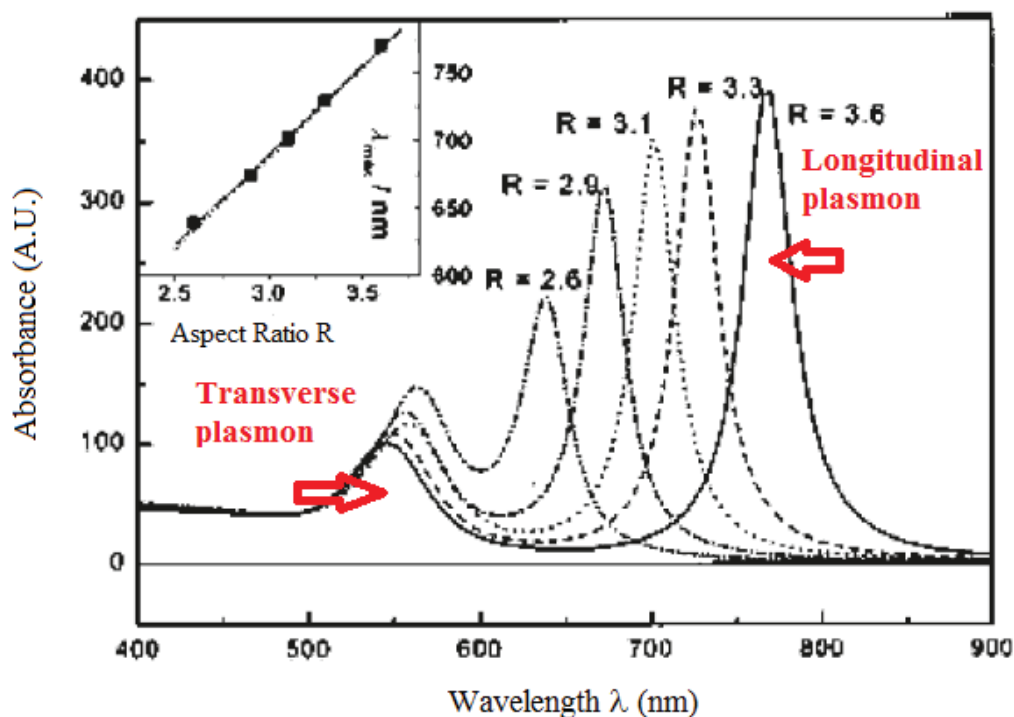


**Figure 7** – Calculation of optical absorbance of nanorod particle with different aspect ratio  $R$ . Transversal and longitudinal plasmonic absorbance are shown in red arrows for  $R=3.6$ . From (Mayer *et al.*, 2011)

Other geometries than spherical and spheroid nanoparticles require modern calculation and cannot be calculated by analytical methods. Numerical computations such discrete dipole approximation, finite difference time domain and finite element method have been developed to describe various plasmonic resonance modes of different shape of nanoparticles. (Mayergoyz *et al.*, 2013) Figure 8 shows how the geometry of nanoparticles influences the plasmonic resonance along the nanoparticle surface.

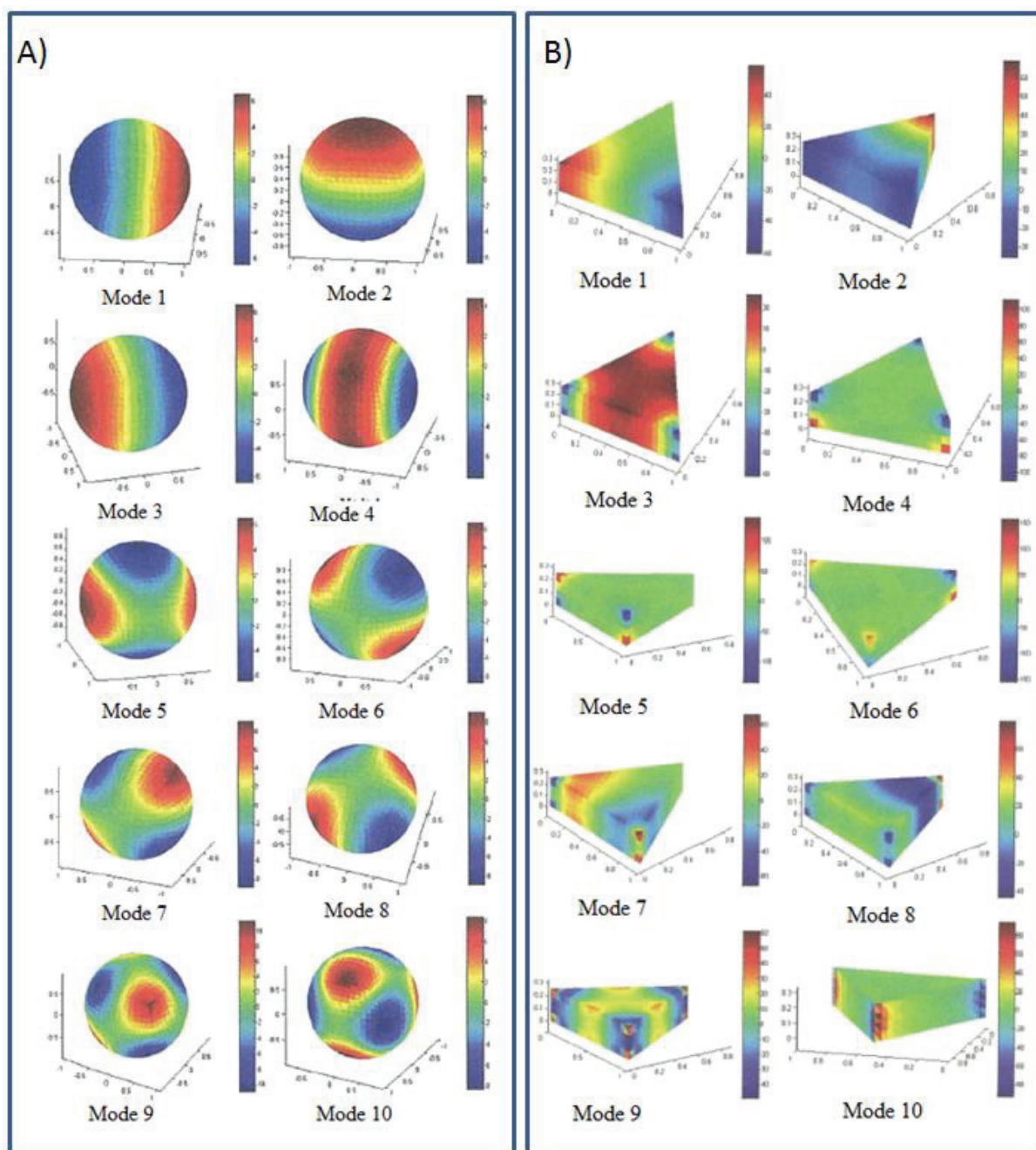


**Figure 8.** Numerical simulations of 10 different plasmonic modes of nanoparticle A) spherical and B) triangular. From (Mayergoyz *et al.*, 2013)

## Reference

Daghestani H.N., Day B.W. Theory and applications of surface plasmon resonance, resonant mirror, resonant waveguide grating, and dual polarization interferometry biosensors. *Sensors* 2010, 10, 9630-9646.

Willems K.A., Van Duyne R.P. Localized surface plasmon resonance spectroscopy and sensing. *Annu. Rev. Phys. Chem.* 2007, 58, 267–297.

Jain P.K., Huang X., El-Sayed I. El-Sayed M. Noble metals on the nanoscale: Optical and photothermal properties and some applications in imaging, sensing, biology, and medicine. *Acc. Chem. Res.* 2008, 41, 1578–1586.

Kelly K.L., Coronado E, Zhao L.L., Schatz G.C., The optical properties of metal nanoparticles: the influence of size, shape and dielectric environment. *J. Phys. Chem. B* 2003, 107, 668-677.

Ghosh S.K., Pal T. Interparticle coupling effect on the surface plasmon resonance of gold nanoparticles: From theory to application. *Chem. Rev.* 2007, 107, 4797-4862.

Mie G. Beitrage zur Optik truber Medien speziell kolloidaler Metallosungen. *Ann. Phys.* 1908, 25, 377-445.

Hovel H., Fritz S., Hilger A., Kreibig U., Vollmer M. Width of cluster plasmon resonances: bulk dielectric functions and chemical interface damping. *Phys. Rev. B.* 1993, 48, 18178-18188.

Johnson P.B., Christy R.W. Optical constants of the noble metals. *Phys. Rev. B.* 1972, 6, 4370-4379.

Mayer K.M., Hafner J.H. Localized surface plasmon resonance sensors. *Chem. Rev.* 2011, 111, 3828-3857.

Mayergoyz I.D.; Editor, World Scientific Publishing. Volume 6: Plasmon resonances in nanoparticles. 2013

Jensen T.R., Duval M.L., Kelly K.L., Lazarides A., Schatz G.C., Van Duyne R.P. Nanosphere lithography: Effect of the external dielectric medium on the surface plasmon resonance spectrum of a periodic array of silver nanoparticles. *J. Phys. Chem. B.* 1999, 103, 9846-9853.

Nano Composix ® compagny web site : <http://nanocomposix.com/pages/silver-nanoparticles-optical-properties>

Jain P.K., El-Sayed M.A. Plasmonic coupling in noble metal nanostructures. *Chem. Phys. Lett.* 2010, 487, 153–164.

Haes A.J., Van Duyne R.P. A nanoscale optical biosensor: sensitivity and Selectivity of an approach based on the localized surface plasmon resonance spectroscopy of triangular silver nanoparticles. *J. Am. Chem. Soc.* 2002, 124, 10596–10604.

Malinsky M.D., Kelly K.L., Schatz G.C., Van Duyne R.P. Chain length dependence and sensing capabilities of the localized surface plasmon resonance of silver nanoparticles chemically modified with alkanethiol self-assembled monolayers. *J. Am. Chem. Soc.* 2001, 123, 1471-1482.

Zhao W.B., Park J., Caminade A.M., Jeong S.J., Jang Y.H., Kim S.O., Majoral J.P., Cho J., Kim D.H. Localized surface plasmon resonance coupling in Au nanoparticles/phosphorus dendrimer multilayer thin films fabricated by layer-by-layer self-assembly method. *J. Mater. Chem.* 2009, 19, 2006–2012.

Niesen B., Rand B.P., Van Dorpe P., Cheyng D., Shen H., Maes B., Heremans P. Near-field interactions between metal nanoparticle surface plasmons and molecular excitons in thin-films. Part I: absorption. *J. Phys. Chem. C.* 2012, 116, 24206–24214.

Kreibig U., Vollmer M. Editor, Springer. *Optical properties of metal clusters.* 1995.

Derkachova A., Kolwas K., Simple analytical tool for spectral control of dipole plasmon resonance frequency for gold and silver nanoparticles. *Photonics Letters of Poland.* 2013, 5, 69-71.

Amendola V., Bakr O.M., Stellacci F. A study of the surface plasmon resonance of silver nanoparticles by the discrete dipole approximation method: Effect of shape, size, structure and assembly. *Plasmonic,* 2010, 5, 85-97.

R. Gans, The shape of ultramicroscopic gold particles, *Ann. Phys.,* 1912, 37, 881-900.

Orendorff C.J., Sau T.K., Murphy C.J. Shape-Dependent Plasmon-Resonant Gold Nanoparticles. *Small* 2006, 2, 636-639.

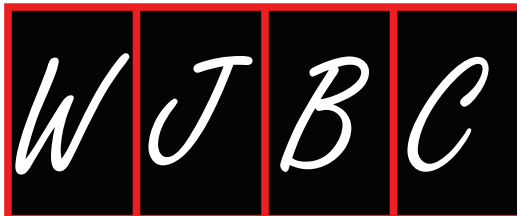


# Part A

## Section 3

### Molecular recognition by gold, silver and copper nanoparticles





## Molecular recognition by gold, silver and copper nanoparticles

Yannick Tauran, Arnaud Brioude, Anthony W Coleman, Moez Rhimi, Beonjoom Kim

Yannick Tauran, Arnaud Brioude, Anthony W Coleman, CNRS, LMI, University of Lyon 1, F69622 Villeurbanne, France  
Yannick Tauran, Anthony W Coleman, Beonjoom Kim, Institute of Industrial Science, University of Tokyo, Tokyo 153-0041, Japan

Moez Rhimi, IFE-Micalis, INRA-AgroPariTech, Jouy-en-Josas, F78352 domaine de Vilvert, France

Author contributions: Tauran Y, Coleman AW, Rhimi M and Kim BJ wrote the paper; Tauran Y, Coleman AW, Brioude A and Kim BJ contributed to the proof reading and literature data search; Tauran Y was responsible for verifying the originality of the text.

Correspondence to: Anthony W Coleman, FRSC, Research Director CNRS, LMI, University of Lyon 1, CNRS UMR 5615, F69622 Villeurbanne, France. [antony.coleman@adm.univ-lyon1.fr](mailto:antony.coleman@adm.univ-lyon1.fr)  
Telephone: +33-4-72431027 Fax: +33-4-72440618

Received: May 2, 2013 Revised: June 11, 2013

Accepted: June 18, 2013

Published online: August 26, 2013

### Abstract

The intrinsic physical properties of the noble metal nanoparticles, which are highly sensitive to the nature of their local molecular environment, make such systems ideal for the detection of molecular recognition events. The current review describes the state of the art concerning molecular recognition of Noble metal nanoparticles. In the first part the preparation of such nanoparticles is discussed along with methods of capping and stabilization. A brief discussion of the three common methods of functionalization: Electrostatic adsorption; Chemisorption; Affinity-based coordination is given. In the second section a discussion of the optical and electrical properties of nanoparticles is given to aid the reader in understanding the use of such properties in molecular recognition. In the main section the various types of capping agents for molecular recognition; nucleic acid coatings, protein coatings and molecules from the family of supramolecular chemistry are described along with their numerous applications.

Emphasis for the nucleic acids is on complementary oligonucleotide and aptamer recognition. For the proteins the recognition properties of antibodies form the core of the section. With respect to the supramolecular systems the cyclodextrins, calix[n]arenes, dendrimers, crown ethers and the cucurbitales are treated in depth. Finally a short section deals with the possible toxicity of the nanoparticles, a concern in public health.

© 2013 Baishideng. All rights reserved.

**Key words:** Hybrid nanoparticles; Gold; Silver; Copper; Metal; Molecular recognition; DNA; Protein; Supramolecular assembly; Toxicity

**Core tip:** The article is an in-depth review of the state of the art of molecular recognition processes involving hybrid nanoparticles and bio-molecular substrates. We describe the methods of preparation and physical characterization. The capping by proteins, DNA, peptides and supramolecular assemblies, including cyclodextrins, calix[n]arenes, cucurbitales, dendrimers and crown ethers is then discussed. There is a large analysis of the interactions of these systems with various substrates, such as complimentary oligo-nucleotides, antibodies, active pharmaceutical ingredients and pollutants. Finally we discuss the problem of possible toxicity.

Tauran Y, Brioude A, Coleman AW, Rhimi M, Kim B. Molecular recognition by gold, silver and copper nanoparticles. *World J Biol Chem* 2013; 4(3): 35-63 Available from: URL: <http://www.wjgnet.com/1949-8454/full/v4/i3/35.htm> DOI: <http://dx.doi.org/10.4331/wjbc.v4.i3.35>

### INTRODUCTION

Nanoparticle (NP) science and technology is considered to be a quintessential aspect of 20<sup>th</sup> and 21<sup>st</sup> century

science and research, however the use of Noble metal nanoparticles dates back to at least the Roman epoch<sup>[1]</sup>. At that time colloidal suspensions of gold were used to stain glass. Somewhat later, in ninth century Mesopotamia copper and silver nanoparticles were used to introduce a metallic luster into pottery glazes<sup>[2]</sup>. In parallel, in India noble metal nanoparticles were first applied in medicine. During the sixteenth and seventeenth centuries Cassius and Kunckel refined the process of glass staining although still without a fundamental understanding of the subject<sup>[3]</sup>. Similarly, Herschel developed a photographic process using colloidal gold<sup>[4]</sup>. It was in 1857 that Faraday first characterized the optical properties of nanoparticles<sup>[5]</sup>. Subsequent work has shown that the differing colours observed for various forms of noble metal nanoparticles are related to the particle size<sup>[6]</sup>. With the understanding of plasmon physics, a clear understanding of the behavior of nanoparticles has emerged<sup>[7]</sup>.

In fact, nanoparticles are based on small well defined aggregates of the Noble metals in the zero valent state. The preparation of Noble metal nanoparticles is generally based on a wet chemical reduction of a suitable metal salt in the presence of a capping or stabilizing agent to prevent both aggregation and oxidation away from the reduced state<sup>[8]</sup>. The size and more importantly the shape of the nanoparticles can be controlled by the reducing agent, the capping agent and the reaction conditions used in the preparation<sup>[9]</sup>. While spherical forms are most commonly prepared, rod-like shapes, cubes, hexagonal and even hollow forms are known<sup>[10]</sup>.

In this review we will concentrate on how the introduction of various capping agents allows the introduction of molecular recognition properties to the surface of the noble metal nanoparticles. The choice of the capping agent has opened up applications in biomedical science<sup>[11]</sup>, antibacterial systems<sup>[12]</sup>, drug carriers<sup>[13]</sup> and as sensing elements<sup>[14]</sup>. The last application, sensing *via* molecular recognition is greatly facilitated by the sensitivity of the wavelength and intensity of the Plasmon Resonance peak to the nature of the local environment around the nanoparticles<sup>[15]</sup> and also to the aggregation state of the colloidal system<sup>[16]</sup>. In a final section we will deal with some of the health concerns related to the use of such nanoparticles<sup>[17]</sup>.

---

## PREPARATION AND MODIFICATION OF NANOPARTICLES

---

### *Noble metal nanoparticle preparation*

Numerous techniques have been developed to synthesize Noble metal nanoparticles, including both chemical methods (*e.g.*, chemical reduction, photochemical reduction, coprecipitation, thermal decomposition, hydrolysis, *etc.*) and physical methods (*e.g.*, vapor deposition, laser ablation, grinding, *etc.*) The ultimate goal is to obtain nanoparticles with a high level of homogeneity and provide fine control over size, shape and surface properties<sup>[18]</sup>.

Table 1 presents the different strategies employed in

the literature for preparing and functionalizing metallic nanoparticles.

### **Nanoparticle functionalization methods**

Molecular functionalization on inorganic supports has been made through a variety of techniques that includes physical adsorption, electrostatic binding, specific recognition, and covalent coupling. Recently, these immobilization techniques have been applied to bring together biomolecules and nanoparticles. Willener has reviewed<sup>[19]</sup> these methods of functionalization and has identified three types: (1) Electrostatic adsorption; (2) Chemisorption; and (3) Affinity-based methods.

The electrostatic adsorption method involves the adsorption of positively charged molecules on nanoparticles that are stabilized by anionic ligands such as carboxylic acid derivatives (citrate, ascorbate). Protein and in particular, antibodies have been used in this way, to functionalize nanoparticles since the work of Faulk and Taylor in 1971<sup>[20]</sup>.

Chemisorption involves capping nanoparticles using the affinity of Noble metals for thiol-containing molecules or by covalent binding through bifunctional linkers. Nucleic acids can be prepared with pendant thiol groups using solid-phase synthesis, thus facilitating their attachment to the metal nanoparticle<sup>[21]</sup>. Otherwise, an anchor group can be used for covalent binding through bifunctional linkers. Such functionalization can be divided into a two-step process: in 1, the activation step, a chemical anchor layer is formed on the nanoparticle surface to provide active functional groups to which biological molecules (*i.e.*, antibodies) can be covalently attached; and in 2, the functionalization step, biomolecules are covalently linked to the anchor layer to yield systems for molecular recognition<sup>[22]</sup>. The affinity based method is defined as the functionalization of nanoparticles with groups that provide affinity sites for the binding of biomolecules, and has been used for the specific attachment of proteins and oligonucleotides. For example, streptavidin-functionalized gold nanoparticles have been used for the affinity binding of biotinylated proteins (*e.g.*, immunoglobulins and serum albumins) or biotinylated oligonucleotides<sup>[23]</sup>. Doria summarized the advantages and disadvantages of the three methods: the advantage of electrostatic adsorption is the ease of usage while chemisorption and affinity-based functionalisations are robust and allow an orientation of the capped molecules. The disadvantages of electrostatic adsorption include sensitivity to the external environment (pH, ionic strength) and the restricted choice of charged molecules for capping. Also, chemisorption and affinity-based functionalization usually require the modification of the capped molecules<sup>[24]</sup>.

---

## PROPERTIES

---

### *Optical properties*

The optical attributes of metal nanoparticles, as reflected in their bright intense colors, are due to their unique interaction with light. In the presence of the oscillating

**Table 1 Summary of various strategies for functionalizing and preparing different metal nanoparticles**

Metal	Molecule	Type of conjugation	Nanoparticle preparation	Ref
Gold	Oligonucleotide	Thiol labelled oligo	Citrate reduction	[35,41]
Gold	Aptamer	Thiol labelled oligo	Citrate reduction	[54,56]
Gold	Antisera	Electrostatic attraction	Reduction	[20]
Gold	Antibody : anti-epidermal growth factor receptor	Electrostatic attraction	Citrate reduction	[89]
Gold	Monoclonal antibody LCC (ALT04)	Electrostatic attraction	Citrate reduction	[204]
Gold	Antibody: anti-goat, antimouse, anti-sheep	Covalent bond (protein/MUA SAM)	Seed-mediated growth	[91,22]
Gold	Avidin	Succinimyl labelled avidin	Frens-Turkevich method	[71]
Gold	Peptide	Covalent bonds (peptide-NH <sub>2</sub> /COOH-PEG-NP)	seed-mediated growth and coated with thiolated-PEG-COOH	[75]
Gold	Cyclodextrin	Thiol labelled cyclodextrin	NaBH <sub>4</sub> reduction	[119,121]
Gold	Cyclodextrin	Hydrophobic	Laser-induced ablation	[205]
Gold	Calix[n]arene	Thiol labelled calix[n]arene	NaBH <sub>4</sub> reduction	[136]
Gold	Calix[n]arene	Thiol labelled calix[n]arene	Citrate reduction	[135]
Gold	Calix[n]arene	Chemisorbtion (sulphonate/gold)	NaBH <sub>4</sub> reduction	[138]
Gold	Dendron	Thiol labelled dendron	NaBH <sub>4</sub> reduction	[160]
Gold	Dendron	Thiol labelled dendron	Thiol-Ligand Substitution	[161]
Gold	Dendrimer	Electrostatic attraction	Acetic Acid reduction	[158]
Gold	Crown Ether	Thiol labelled crown ether	NaBH <sub>4</sub> reduction	[206]
Gold	Crown Ether	Thiol labelled crown ether	Citrate reduction	[178]
Silver	Oligonucleotide	Thiol labelled oligo	NaBH <sub>4</sub> reduction	[39]
Silver	Oligonucleotide	Physical adsorption	Photo-Induced	[48]
Silver	Aptamer	Thiol labelled oligo	NaBH <sub>4</sub> reduction	[159]
Silver	Antibody: IgG	Electrostatic attraction	Citrate reduction	[207]
Silver	Antibody: anti-ngn1	Electrostatic attraction	Citrate reduction and coated with DL-mercaptosuccinic acid (MSA)	[101]
Silver	Norvancomycin	Covalent bond (peptide-NH <sub>2</sub> /COOH-MA-NP)	NaBH <sub>4</sub> reduction stabilized with Mercaptoacetic Acid (MA)	[82]
Silver	Gluteraldehyde	Electrostatic attraction	NaBH <sub>4</sub> reduction	[104]
Silver	Peptide	Electrostatic attraction	Ascorbate sodium reduction	[76]
Silver	Peptide	Electrostatic attraction	trisodium citrate and hydroxylamine hydrochloride reduction	[77]
Silver	Peptide	Electrostatic attraction	NaOH added to silver nitrate and peptid	
Silver	Cyclodextrin	Host-guest by Electrostatic interaction	NaBH <sub>4</sub> reduction stabilized with Cetyl Trimethyl Ammonium (CTA)	[208]
Silver	Cyclodextrin	Thiol labelled cyclodextrin	NaBH <sub>4</sub> reduction	[127]
Silver	Cyclodextrin	Thiol labelled cyclodextrin	Citrate reduction	[126]
Silver	Cyclodextrin	Electrostatic attraction	NaBH <sub>4</sub> reduction	[124]
Silver	Calix[n]arene	Chemisorbtion (sulphonate/silver)	NaBH <sub>4</sub> reduction	[145,147]
Silver	Calix[n]arene	Electrostatic attraction	Hydrogen gaz reduction	[143]
Silver	Calix[n]arene	Electrostatic attraction	Photo-chemical reduction	[144]
Silver	Dendrimer	Electrostatic attraction	UV reduction	[164,168]
Silver	Dendrimer	Electrostatic attraction	NaBH <sub>4</sub> reduction	[166]
Silver	Crown Ether	Thiol labelled crown ether	NaBH <sub>4</sub> reduction	[177]
Silver	Cucurbit[n]uril	Chemisorbtion	NaBH <sub>4</sub> reduction	[179]
Silver	Cucurbit[n]uril	Chemisorbtion	NaOH induced	[180]
Copper	Oligonucleotide	Electrostatic attraction	Chemical reduction (ascorbic acid)	[53]
Copper	Antibody	Electrostatic attraction	Pyrometallurgically by heating copper metal (Sigma, China)	[109]
Copper	Peptide	Electrostatic attraction	NADH reduction by fungus <i>F. oxysporum</i>	[84]
Copper	Peptide/latex	Electrostatic attraction	Ascorbate sodium reduction	[83]
Copper	Cyclodextrin	Electrostatic attraction	ultrasound irradiation	[128]
Copper	Cyclodextrin	Electrostatic attraction	calcination	[129]
Copper	Calix[n]arene	Chemisorbtion (sulphonate/copper)	hydrazine reduction	[151]
Copper	Dendrimer	Electrostatic attraction	Ascorbic acid reduction	[171]
Copper	Dendrimer	Electrostatic attraction	Electrochemical reduction	[170]

electromagnetic field of light, the free electrons of the metal nanoparticle undergo a collective coherent oscillation (Figure 1). This motion is resonant at a particular light frequency and is termed the localized surface plasmon resonance (LSPR) oscillation<sup>[25]</sup>. The surface

plasmon oscillation either decays by radiating its energy, resulting in light scattering, or decays non-radiatively as a result of conversion of absorbed light to heat. The electric field intensity and the scattering and absorption characteristics of the nanoparticles are all strongly enhanced

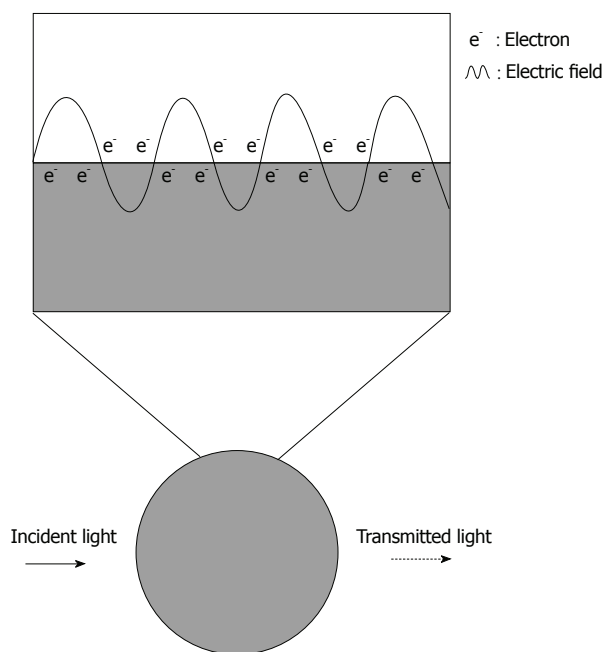


**Figure 1** Scheme representing the plasmonic effect induced by white light on the absorbance of a silver nanoparticle. The plasmon is represented above by the oscillation of an electron cloud along the surface of the nanoparticle. The silver nanoparticle absorbs light at 390 nm giving a dotted line.

at the LSPR frequency, which for gold, silver and copper lies in the visible region<sup>[26]</sup>.

The plasmonic resonance of metallic nanoparticles will depend on several parameters: (1) the size of the nanoparticles; (2) the geometry of the nanoparticles (spherical, triangle, rods, *etc.*); (3) the physical properties of the medium in which the nanoparticles are dispersed (air, liquid, solid); and (4) the nature of the metallic nanoparticles.

In water, the absorption of spherical nanoparticles, with sizes ranging from 3 nm to 80 nm and composed of copper (Cu), silver (Ag) or gold (Au), lies in the visible range and gives rise to a narrow peak<sup>[27]</sup>, respectively at 400, 520 and 570 nm. The metal plasmon absorption frequency for copper, silver and gold nanoparticles were 500-550 nm, 390-400 nm, 565-570 nm respectively.

### Electrical properties

The electrical properties of metal particles which have a size greater than 2 nm diameter, are similar to those of the corresponding bulk metals<sup>[28]</sup>. Electron transport is not confined to the discreet energy levels of several atoms but appears as a continuum energy level of a bulk metal. Hence, surface charging and electron transport processes in metal nanoparticles may be understood with relatively simple classical physical expressions, as for resistance/capacitor electronic circuit diagrams. In contrast to molecules and semiconductor nanoparticles whose electron transport properties require a quantum mechanical description, metal nanoparticles only require knowledge of their size and the dielectric properties of the surrounding medium to determine their properties<sup>[18]</sup>. The electronic properties of metallic nanoparticles have

been used for many applications, such as electrical sensors using metal nanoparticle as a tag for recognizing a specific target molecule<sup>[29]</sup>, and the development of new electronic chips<sup>[30]</sup>.

## COATING AND MOLECULAR RECOGNITION

### Nucleic acid coating

After proteins, the nucleic acids are the most studied biomolecules for capping Noble metal nanoparticles. Many reviews regarding gold nanoparticles, can be found in the literature<sup>[31-34]</sup>. Such hybrid systems have been extensively investigated since Mirkin, first used oligonucleotides as a capping agent to provide a basis for recognition<sup>[35]</sup>. Nucleic acid molecules consist of a sequence of nucleotides distinguished by which nucleobase they contain. In DNA, the four bases present are adenine (A), cytosine (C), guanine (G), and thymine (T), whereas RNA contains adenine (A), cytosine (C), guanine (G), and uracil (U). Nucleic acids have the property that two strands will only bind to each other to form a double helix if the two sequences are complementary, with A only binding to T in DNA A binds to U in RNA, and C only to G, linked by hydrogen bonds (Figure 2).

Moreover, the ability of nucleic acids to self assemble extends their molecular recognition properties from complementary sequences to various molecular targets such as small molecules, proteins, and even cells, tissues and organisms<sup>[36]</sup>. Aptamers (Apt), oligo-nucleic acids engineered to bind a specific ligand, have shown considerable potential to be used as a capping agent for nanoparticles<sup>[21]</sup>.

**Oligonucleotides:** As noted above, oligonucleotides bind, in a sequence-specific manner, to their respective complementary oligonucleotides, DNA, or RNA to form duplexes or, less often, hybrids of a higher order. This basic property serves as a foundation for the use of oligonucleotides as probes for detecting DNA or RNA. Many applications can be found in biology such as Polymerase Chain Reaction (PCR), DNA microarrays, Southern blots, fluorescent *in situ* hybridization (FISH)<sup>[37]</sup>. As an example, DNA microarrays use thousands of different oligonucleotides probes in order to measure the expression levels of large numbers of genes simultaneously or to genotype multiple regions of a genome. The fundamental idea behind most microarrays is to exploit complementary base pairing of the oligonucleotide probes to measure the amount of the different types of mRNA molecules in a cell, thus indirectly measuring the expression levels of the genes that are responsible for the synthesis of those particular mRNA molecules<sup>[38]</sup>.

**Gold:** Oligonucleotide Gold Nanoparticle (OGN) conjugates are powerful tools for the detection of target DNA sequences by the complementary assemblage of double stranded DNA. Practically all the research and applica-

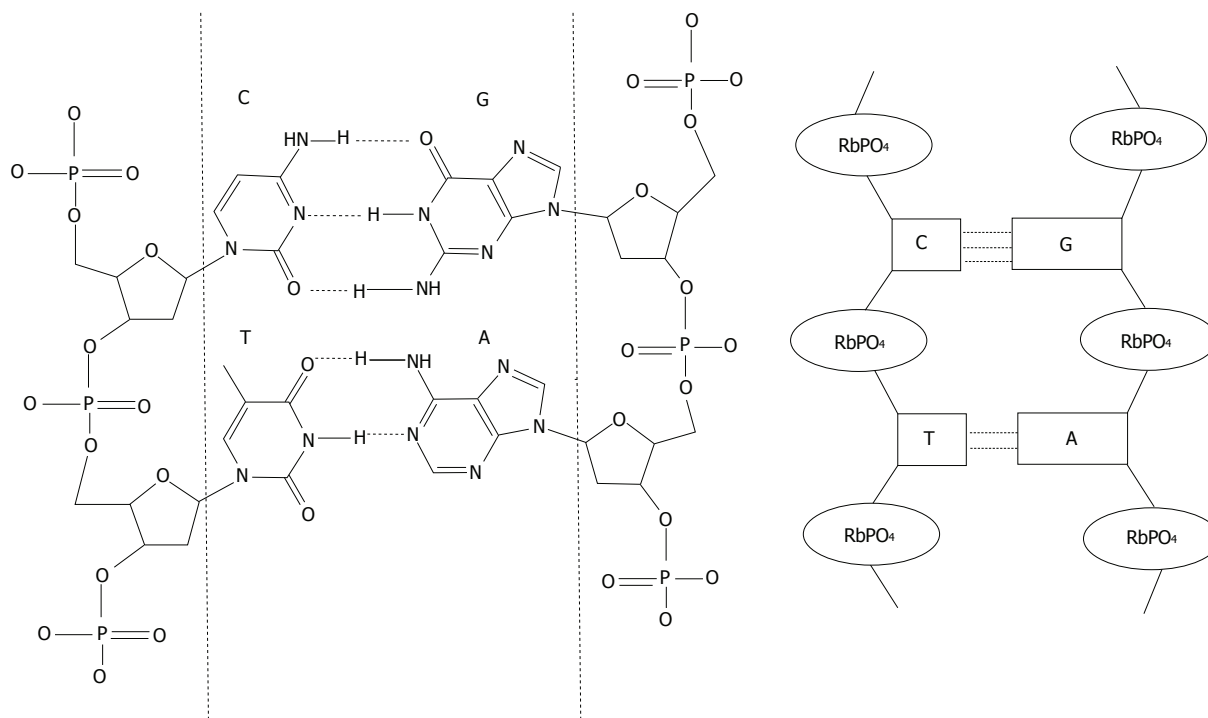


**Figure 2 Matching DNA base.** Nucleotides structures are represented between the dashed lines. A (adenine) match with T (thymine), C (cytosine) match with G (guanine). Ribose phosphate structures link the nucleotides. On the left, a scheme representing the double stranded DNA based on the sequence nucleotide recognition.  $\text{RbPO}_4$  is ribophosphate.

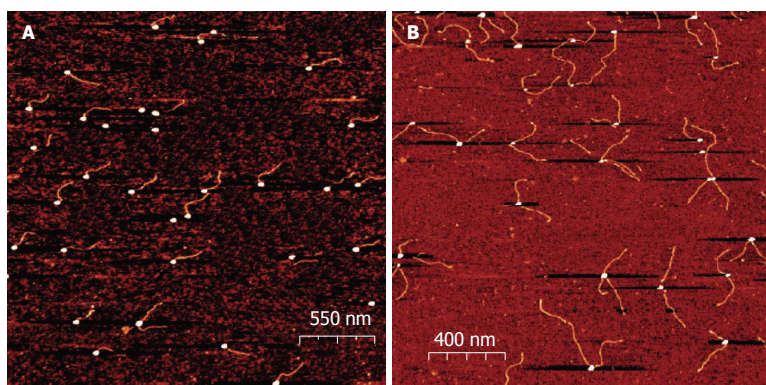


**Figure 3 Atomic Force Microscopy images of oligonucleotide Oligonucleotide Gold Nanoparticles conjugates.** The conjugates were deposited on a mica surface in 2 mmol/L  $\text{MgCl}_2$  and scanned in a semi contact mode as described. From Borovok *et al.*<sup>[46]</sup>, reproduced with permission from American Chemical Society Publications.

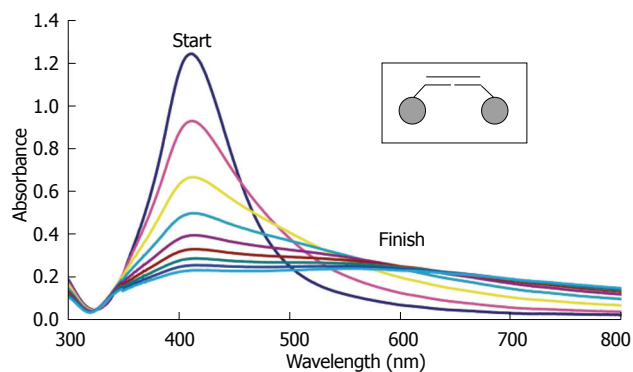
tions of these conjugates have used gold nanoparticles to the exclusion of other Noble metal nanoparticles<sup>[39]</sup>. Initially, Mirkin demonstrated the colorimetric detection of hybrid gold nanoparticles<sup>[35]</sup>. Subsequently Mirkin used non-complementary thiolated oligonucleotide probes attached by chemisorption on 13 nm gold nanoparticles<sup>[40]</sup>, addition of DNA containing the complementary sequence for both oligonucleotide probes led to aggregation of the nanoparticles.

Subsequent biological applications led to the development of an oligonucleotide gold nanoparticle set for the detection of mutation of a polynucleotide sequence<sup>[41]</sup>. With the development of DNA arrays, oligonucleotide capped gold nanoparticles have been shown to be alternative markers to classical fluorophores, bringing very high sensitivity (50 fM of targeted DNA)<sup>[42]</sup>.

Sun *et al.*<sup>[43]</sup> demonstrated the ability to use such a hybrid system for multiple DNA sequence detection by

the surface-enhanced raman scattering (SERS) technique. The assembly of nanoparticles provoked by molecule junctions, enhances strongly the Raman scattering<sup>[44]</sup>. This has been used for detecting and identifying each set of oligonucleotide capped gold nanoparticles which hybridize with the unknown DNA.

The emergence of DNA origami, first described by Rothmund<sup>[45]</sup>, offered new applications of nucleic acid capped gold nanoparticles. In electronic and plasmonic applications, the self assembly properties of DNA can be associated with metallic nanoparticles to construct a variety of metallized and nanostructured shapes. Borovok has developed a method for controlling a specific number of short (25 base) ssDNA molecules<sup>[46]</sup>. This method allows variation in the size of nanoparticles, the distance between them (by changing the length of a DNA linker), and the number of connections that each particle establishes (Figure 3). Such work opens up horizons for

Tauran Y *et al.* Nanoparticle molecular recognition

**Figure 4** UV-vis spectra taken every 5 min of Oligonucleotide Silver Nanoparticles conjugates (25 pmol/L) hybridizing to a fully complementary target oligonucleotide (2.5 nmol/L). Full spectrum scans were taken every 10 min for 80 min. The inset shows that the conjugates are hybridizing in the "tail-to-tail" juxtaponition. From Thompson *et al.*<sup>[39]</sup>, reproduced with permission from American Chemical Society Publications

nucleic acid capped gold nanoparticles to be used for developing new functional materials.

**Silver:** In 2008 Thompson reported the synthesis of oligonucleotide silver nanoparticle conjugates and demonstrated their use in a sandwich assay format<sup>[39]</sup> (Figure 4). These conjugates have practically identical properties to their gold analogues and due to their greater extinction coefficient, absorption analyses can occur at much lower concentrations.

Li *et al.*<sup>[47]</sup> showed that oligonucleotide silver nanoparticle conjugates could be developed for multiplexed DNA electrochemical detection. Although the emergence of DNA chip technology has accelerated this process, it is still a challenge to perform ultrasensitive DNA assays at attomol concentrations. With the use of oligonucleotide silver nanoparticles and a suitable device, it is possible to detect concentrations as low as 5 aMol/L of viral DNA.

Recently Zon *et al.*<sup>[48]</sup> reported the photo-induced nucleation and growth of silver nanoparticles in the presence of DNA oligomers. An organic dye (Cy5) was used as a photosensitizer to initiate nanoparticle growth. Irradiation of the precursor solutions with light at the Cy5 absorption maximum triggered the instantaneous formation of spherical particles with a metallic core of 15 nm in diameter.

The emergence of a new class of so-called Oligonucleotide Capped Silver Nano Clusters (OSNC), consisting of silver nanoparticles from 2 to 10 atoms of silver (2 nm maximum), has led to the observation of novel fluorescence properties, including tunable emission and high photostability. At these sizes, discrete atomic energy levels merge into highly polarizable, continuous, plasmon-supporting bands, thereby leading to very strong absorption and emission<sup>[49]</sup>. The preparation is very simple, requiring mixing of a suitable salt of silver with the desired oligonucleotide and addition of a reducing agent. Interestingly, the fluorescence properties depend on the sequence of the oligonucleotide. The main applications are sensors for genes, proteins, small molecules, or metal anions. For

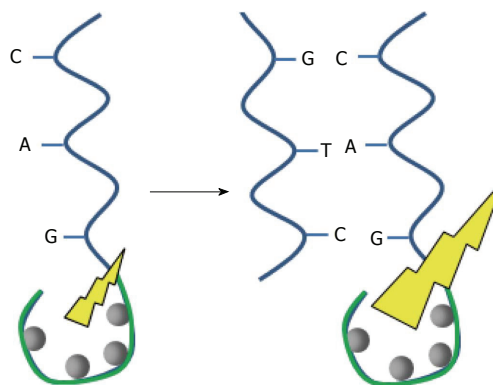


**Figure 5** Schematic representation of the DNA sequence detection by fluorescence enhancement of silver nanocluster. A: Adenine; T: Thymine; C: Cytosine; G: Guanine.

example, OSNC can be used instead of oligonucleotide probes tagged with a fluorophore to detect a targeted DNA sequence. Their hybridization with a targeted DNA sequence enhances the fluorescence (Figure 5). Chang has developed a system able to detect single point mutations in the gene involved in the hereditary disease tyrosinemia type I<sup>[50]</sup>. Additionally, these structures promise potential for labeling biomolecules for imaging purposes, as they can be prepared to yield fluorescence in the red or NIR. Antibodies have been conjugated for imaging NIH 3T3 cells<sup>[51]</sup>.

**Copper:** Because of their ease of back-oxidation, copper systems are still not widely used as nanoparticle cores. However, oligonucleotide capped copper nanoclusters have recently been developed and offer an excellent choice as functional biological probes. Rotaru showed that copper can selectively metallize a double stranded DNA on an oligonucleotide probe, allowing control of the size of the cluster<sup>[52]</sup>. Moreover, the fluorescence of DNA-hosted Cu nanoclusters is very sensitive to the base type located in the major groove. The advantages of this method over current fluorescence based assays employed for the detection of mismatches in DNA (as Real time quantitative PCR) are a simpler design of probes and the fact that no conjugation of fluorophore on the probes is required<sup>[53]</sup>.

**Apt:** In comparison to antibodies, Apt possess certain advantages, including their relatively simple and inexpensive synthesis, tolerance to internal labeling, and long storage times without losing their biological activity. The use of Apt as capping agents for metal nanoparticles started in 2004, when Pavlov used such nanoparticles to detect thrombin with a Quartz Crystal Microbalance (QCM)<sup>[54]</sup>. The resonance of the QCM is disturbed by small mass changes due to film deposition on the surface of the acoustic resonator. Here, the advantage of using metallic particles is to give a weight effect so as to increase the sensitivity of the targeted molecule (Figure 6).

Chang has used Apt gold nanoparticles as biosensors for detecting Platelet-Derived Growth Factor (PDGF)<sup>[55]</sup>, which is overexpressed in some cancer cells.

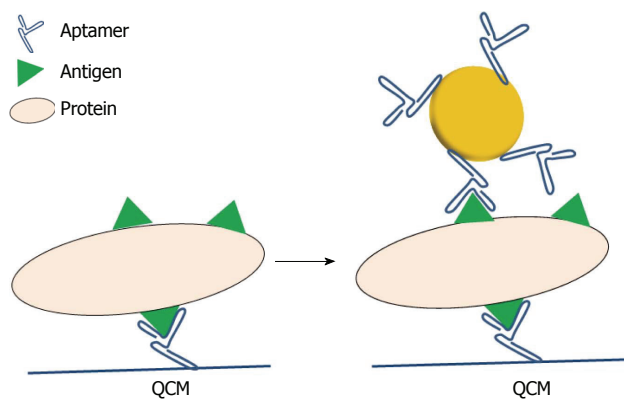


**Figure 6** Schematic representation of the detection of proteins on a Quartz Crystal Microbalance using aptamer capped gold nanoparticles.

They proposed an aggregation-based assay using Apt gold nanoparticles to detect PDGF at the nM level. By the same principle, other Apt gold nanoparticles were developed toward adenosine triphosphate and glutathione<sup>[56]</sup>.

The same group later used Apt gold nanoparticles as a contrast agent for detecting cancer cells over-expressing PDGF<sup>[57]</sup>. Nanoparticles enter the cell where PDGF induces aggregation, and produces a colour (Figure 7). When compared to immunostaining, this approach offers advantages of lower cost and minimum matrix interference. Similarly, Liu used Apt gold nanoparticles for recognizing cancer cells with a strip biosensor<sup>[58]</sup>.

Very recently, one study described the use of silver as a nanoparticle material<sup>[59]</sup>. In this case silver was chosen because of its excellent optical properties for metal enhanced fluorescence<sup>[60]</sup>. Based on the results, an aptamer based fluorescent switch has been constructed. In the “OFF” state, without the target molecule, there is a greater spacing distance between the dye and the silver nanoparticle giving comparatively lower fluorescence intensity. However in the “ON” state, in the presence of target molecules, the fluorescence signal is increased due to a shortened distance between the dye and the nanoparticle (Figure 8). This Apt-sensor linearly detects adenosine concentrations from 200 nmol/L to 200  $\mu$ mol/L with a detection limit of 48 nmol/L.

### Protein coatings

The structural versatility, biological importance and biomedical impact of proteins make them one of the most widely studied classes of molecules in bio-recognition. There has long been a major interest in the use of capping metallic nanoparticles with proteins<sup>[19,61]</sup>. Among proteins with molecular recognition abilities, antibodies, key elements of the immune response, are probably the most widely studied<sup>[62,63]</sup>. Enzymes have also been studied as capping agents for metallic nanoparticles. Willner *et al.*<sup>[64]</sup> reviewed recent advances in the development of enzyme-metallic nanoparticle conjugates and their specific applications for biosensing and the generation of nanostructure.

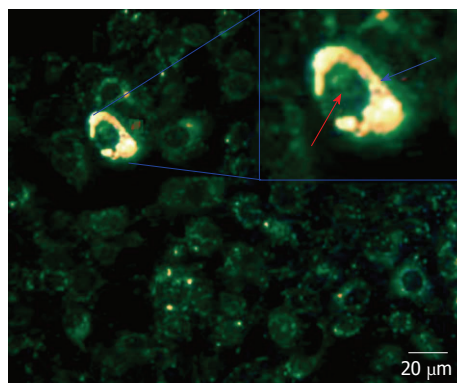


**Figure 7** Dark Field Microscopy images of mixtures of cancer MDA-MB-231 and normal 184B5F5/M10 cells at 1:100 ratio, after incubation for 3 h in a medium containing aptamer gold nanoparticles. Gold nanoparticles showing a high reflection are colored in yellow. The lower reflection corresponding to the cells are colored in green. In the inset, a magnification of a cell containing nanoparticles. The distribution of nanoparticles is highlighted by blue arrow corresponding to cytoplasm. Red arrow corresponds to the cell nucleus<sup>[57]</sup>.

**Peptides:** Peptides which are distinguished from proteins on the basis of size (typically containing fewer than 50 monomer units), and their folding, are well known to be involved in molecular recognition events. Peptide-capped metal nanoparticles combine several advantages. Peptide chemistry is versatile and provides the possibility to utilize functional groups found in the 20 naturally occurring amino acids plus the possibility to introduce non-natural amino acids<sup>[65]</sup>. Peptides and peptide conjugates are readily commercially available. The preparation of peptide-capped nanoparticles is rapid, simple, and amenable to high-throughput approaches. This allows, in a single step, the production of stable and functional nanoparticles. Peptide-capped gold nanoparticles and, more generally, peptide-capped nanomaterials have immediate applications as bioanalytical sensors and cell imaging, but, perhaps more importantly, they offer an almost unlimited range of possibilities for the design and preparation of the advanced functional nanomaterials of the future<sup>[66]</sup>.

**Gold:** The use of peptide-capped gold nanoparticles as enzyme mimics, also called nanozymes has been previously reviewed<sup>[67,68]</sup>. The fundamental idea is to engineer a micro environment, within a self assembled monolayer, that resembles the catalytic site of natural enzyme. Pengo developed a functional artificial protein by grafting a thiol functionalized dodecapeptide onto the surface of gold nanoparticles. This system was able to catalyze the hydrolysis of carboxylate esters. It was found that certain substrates affected the structure of the catalytic site by altering its hydration, demonstrating that the nanozyme can regulate its own activity just as proteins do<sup>[69]</sup>.

Brust used peptide-capped gold nanoparticles as artificial substrates for kinases to develop a colorimetric protocol for the evaluation of kinase activity and inhibition<sup>[70]</sup>. Sun reported the use of these hybrid particles in a microarray format<sup>[71]</sup>. The method is based on labeling peptide phosphorylation events on a microarray with

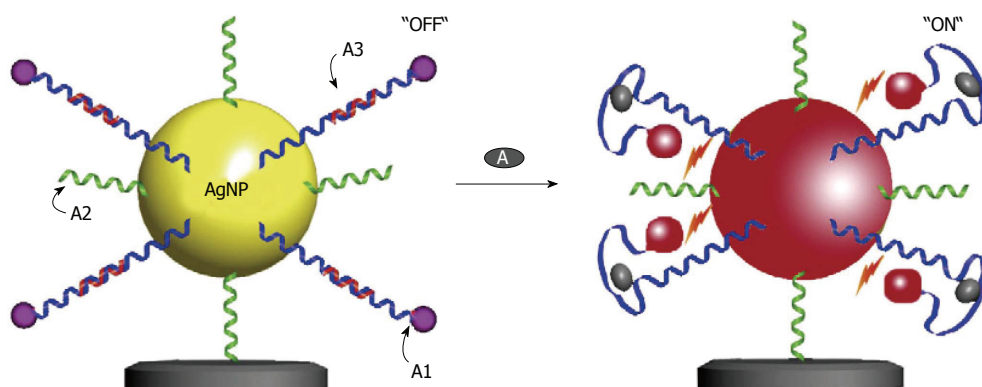


Figure 8 Schematic diagrams of the aptamer-based silver nanoparticles nanosensor showing the “OFF” (a) and “ON” (b) state based on the spacing distance between the Cyanine 3 and the silver nanoparticle surface in the detection of adenine. From Wang *et al.*<sup>[50]</sup>, reproduced with permission from Elsevier.

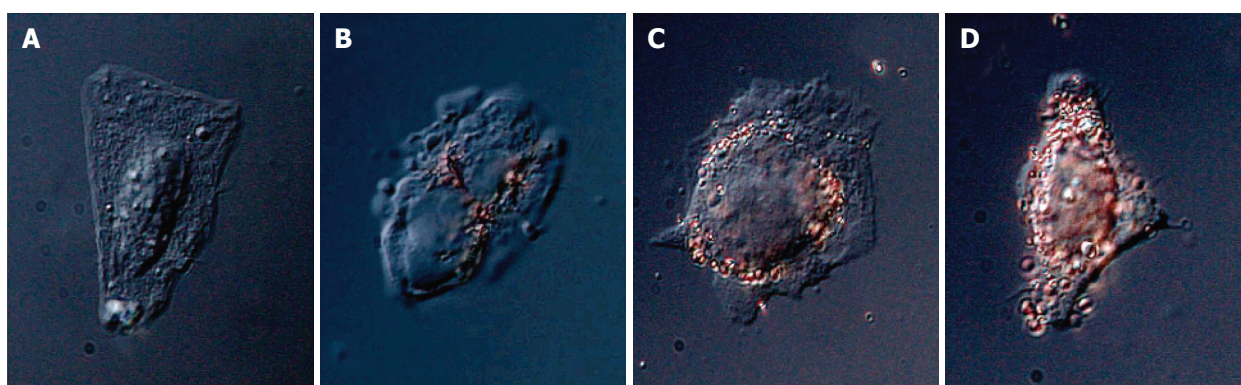


Figure 9 Nanoparticle-peptide complexes incubated with HepG2 cells for 2 h: displaying 4 different sequences in A, B, C and D. From Tkachenko *et al.*<sup>[74]</sup>, reproduced with permission from American Chemical Society Publications.

gold nano-particles and using resonance light scattering (RLS) detection<sup>[72]</sup>. They demonstrated that it is possible to screen kinases with single or multiple inhibitors simultaneously on the same microarray<sup>[73]</sup>.

Targeting transmembrane transport is another field of application in which peptide-capped gold nanoparticles have been used. Franzen reported a method for assessing the efficiency of various combinations of targeting peptides using nanoparticle complexes for nuclear targeting. VEC-DIC combination microscopy permits observation of the localization of the peptide-capped gold nanoparticles according to the peptide sequence<sup>[74]</sup> (Figure 9). Recently El Sayed investigated the quantitative tumor uptake of a class of elongated gold nanoparticles (nanorods) that were covalently conjugated to tumor-targeting peptides<sup>[75]</sup>. The results suggest that for photothermal cancer therapy, the preferred route of gold nanorod administration is intratumoral injection. With direct tumor injection, the peptide-capped gold nanoparticles were mainly found in the tumor cells while peptide-capped gold nanoparticles injected with intravenous injection are mainly localized around blood vessels, in the tumor stromal matrix.

**Silver:** To date, few articles describe the use of peptide capped silver nanoparticle for colorimetric sensing. Most studies focus on the nature of the peptide/silver interaction

and the effect of the peptide on the formation of the silver nanoparticles<sup>[76,77]</sup>. Recently, Cui has demonstrated that at basic pH the peptide secondary structure was modified, and could affect the size of the silver nanoparticles<sup>[78]</sup>.

Qu reported a homogenous assay for colorimetric and quantitative detection of a cancer marker and the promising antitumor target, cyclin A2, using the aggregation of unmodified gold nanoparticles and/or silver nanoparticles<sup>[79]</sup>. They used the difference in coagulating ability of a cationic peptide probe (P1) and its binding form toward unmodified nanoparticles, in order to detect cyclin A2. In the absence of cyclin A2, P1 aggregates particles immediately, whereas cyclin A2 binding prevents the interaction of P1 with the surface, significantly reducing the aggregation. The extent of aggregation is dependent on the concentration of the target protein cyclin A2 and the difference in color can readily be distinguished by spectrometer (Figure 10).

Generally, peptide capped silver nanoparticles are used for their anti-microbial activity. Taglietti studied the mechanism of action of glutathione (GSH) capped nanoparticles. GSH peptide displays a thiol function, capable of being anchored to silver surfaces, and three pH-dependent, charged functional groups (carboxylates and amines), that promote water solubility and interactions with complex biostructures<sup>[80]</sup>. GSH capped nanoparticles have shown a bacteriocidal effect related to their penetra-

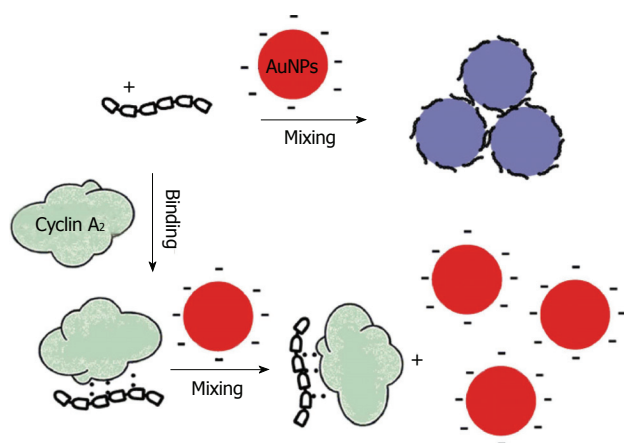


**Figure 10** Schematic illustration of colorimetric detection of cyclin A2 based on noncross linking aggregation of unmodified Gold nanoparticles induced by preferential adsorption of unbound P1. From Wang *et al.*<sup>[79]</sup>, reproduced with permission from Elsevier.

tion of bacterial cells. They show a stronger bacteriocidal effect on *Escherichia coli* (*E. coli*) (Gram negative strain) than on *Staphylococcus aureus* (gram positive strain). Moreover GSH capped Ag nanoparticles showed lower antibacterial activity when grafted onto functionalized glass surfaces, which prevent the nanoparticle from penetrating the bacterial cell<sup>[81]</sup>. Wei *et al.*<sup>[82]</sup> investigated another mechanism of the antibacterial effect using the peptide norvancomycin, a treatment of choice for antibiotic resistant bacteria. The silver nanoparticles decrease the stability of the lipopolysaccharide (LPS) present in the outer membrane of gram negative strains. Using the molecular recognition ability of norvancomycin, the hybrid nanoparticles bind to the peptidoglycan inner membrane and improve the destruction of the bacteria by increasing access of norvancomycin.

**Copper:** Peptide capped copper nanoparticles have received less interest. Recently, Thakore produced peptide-capped copper nanoparticles of 12-16 nm by chemical reduction<sup>[83]</sup>. The synthesis was carried out using stem latex of the medicinal plant, *Euphorbia nivulia*. The nanoparticles were stabilized and subsequently capped by peptides and terpenoids present within the latex. The study demonstrated that peptide capped copper nanoparticles are toxic to A549 cells in a dose dependent manner. Cell viability assay (MTT) determined an LD<sub>50</sub> concentration of 20 µg/mL. The dose dependent cytotoxicity (biocompatible below 1 µg/mL) suggests that these nanoparticles could be used in the future to induce apoptotic destruction of cancer cells. Hossieni reported a promising method for producing such hybrid compounds<sup>[84]</sup>. The group reported the bio-production of copper sulfide nanoparticles from CuSO<sub>4</sub> solution by the reduction of NADH released from the fungus *Fusarium oxysporum*. transmission electron microscopy (TEM) images demonstrated that spherical particles of 2-5 nm, were enclosed in spherical peptide shells of about 20 nm in diameter.

**Antibodies:** Antibodies constitute one of the most important specific defense mechanisms in vertebrate

animals. All of them are bifunctional molecules in a Y-form with two identical domains for antigen recognition (Fab fragment), and two identical domains with effector functions (Fc fragment). The antigen-binding region is highly specific to individual antibodies and large numbers of different antibodies are available<sup>[85]</sup>. Antibodies act as neutralizers of pathogens or toxins, as well as in the recruitment of immune elements (complement, phagocytosis, antibody dependent cytotoxicity by natural killer cells, *etc.*). In addition they may transport molecules including toxins, drugs, fluorophores, and be used in diagnostic procedures, or in therapy to destroy a specific target. The conjugation of antibodies to nanoparticles generates a versatile product that combines, the small size and their thermal, electrical, or optical characteristics of nanoparticles with the abilities of antibodies for specific and selective recognition<sup>[61,86]</sup>.

**Gold:** So far, antibody capped gold particles are the most popular hybrid systems for the exploitation of the molecular recognition properties of the capping agent. In 1971, Faulk reported their use as a specific marker for Salmonella surface antigens using TEM because of their high electron-dense metal density<sup>[20]</sup>. Later Horisberger demonstrated their use for Scanning Electron Microscopy<sup>[87]</sup>. Subsequently, Sokolov showed that when 12 nm gold nanoparticles were conjugated to anti-epidermal growth factor receptor (anti-EGFR) antibodies, they specifically bound to EGFR proteins overexpressed on the surfaces of cervical cancer cells<sup>[88]</sup>. Illumination of nanoparticle-labeled cells with laser light lit up the gold nanoparticles, and thus, the associated cancer cells. Later, El-Sayed used simple dark field optical microscopy to detect gold nanoparticle-labeled cancer cells. Anti-EGFR antibody conjugated gold nanoparticles were incubated with a nonmalignant epithelial cell line (HaCaT) and two malignant oral epithelial cell lines. The hybrid nanoparticles bound to the surface of the cancer type cells with 600% greater affinity than to the noncancerous cells<sup>[88]</sup>.

Within the last decade, there has been substantial interest in antibody capped gold based contrast agents for *in vivo* X-ray imaging<sup>[89,90]</sup>. They are a promising candidate for next generation X-ray contrast materials, and their use in combined radiotherapy is under evaluation<sup>[91]</sup>.

One of the most promising aspects of gold nanoparticle use in medicine, is targeted drug delivery. The most popular objects for targeted delivery are antitumor drugs<sup>[33]</sup>. Combination with antibody capping has been demonstrated to increase the intracellular uptake of gold nanoparticle carriers as compared to non-functionalized conjugates<sup>[92]</sup>. Chan investigated the cellular uptake of antibody-functionalized gold nanoparticles of different sizes, 2-100 nm<sup>[93]</sup>. It was found that nanoparticles with diameter of 40-50 nm enter cells more efficiently than either smaller and larger sized gold nanoparticles. At this size the antibody-capped gold nanoparticles maximize interactions with cell surface receptors and thus enter *via* receptor-mediated endocytosis (Figure 11)<sup>[94]</sup>.

Another promising therapeutic application of antibody

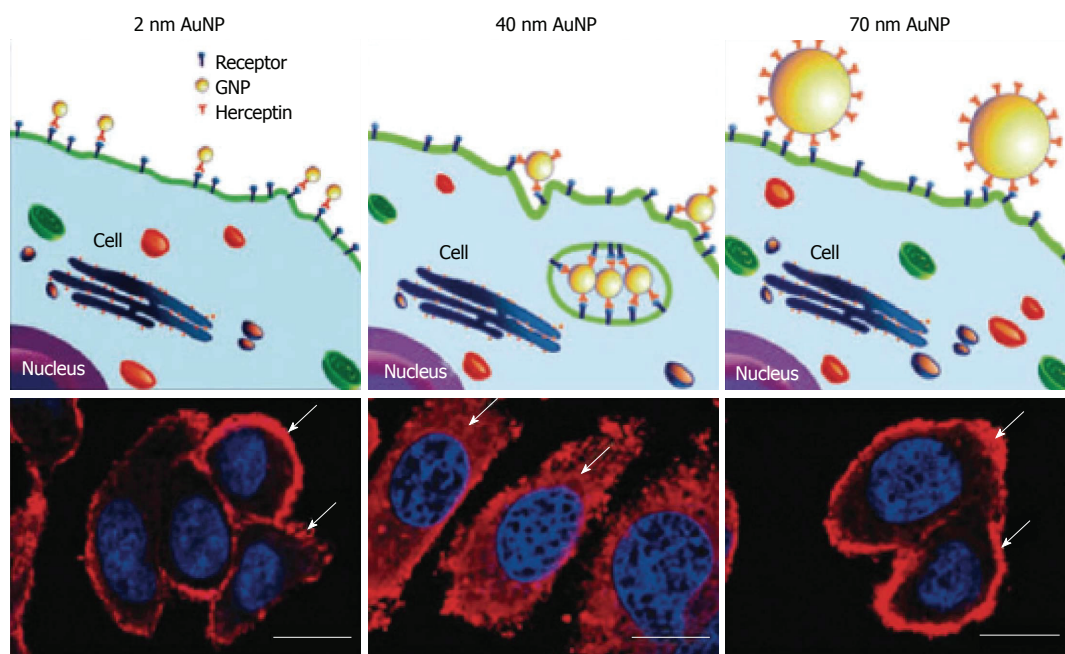


**Figure 11** Illustration demonstrating binding of gold nanoparticles (G2, G40, G70 for 2, 40, 70 nm diameter) functionalized with Herceptin antibodies, which recognize receptors on the cell surface. Arrows indicate ErbB2 receptors, and the nucleus is counterstained in blue with 4,6-Diamidino-2-phenylindole, scale bar = 10  $\mu\text{m}$ . From Jiang *et al.*<sup>[94]</sup>, reproduced with permission from Nature Publishing Group. AuNP: gold nanoparticles.

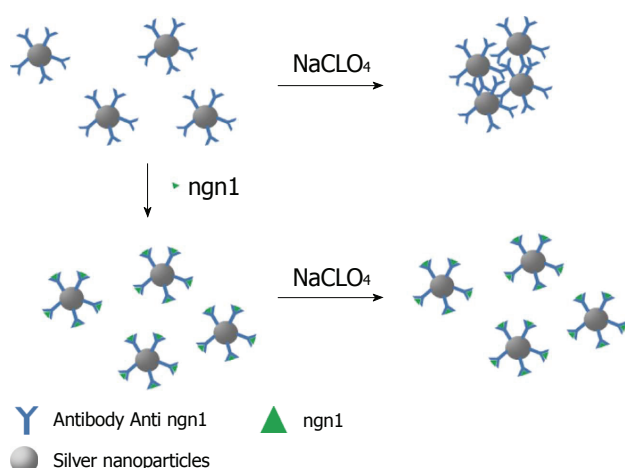


**Figure 12** Schematic illustration of ngn1 detection using the anti-ngn1 antibody conjugated silver nanoparticle mediated by  $\text{NaClO}_4$  salt.

capped gold nanoparticles concerns photothermal damage to cells. Current research is focused on the treatment of cancer and infectious diseases<sup>[95]</sup>. Gold nanoparticles have an absorption maximum in the visible or near infrared region and become very hot when irradiated at the resonant frequency. If the gold nanoparticles are located inside or at the surface of target cells, these cells will overheat and die. Such work has been reviewed in depth<sup>[96,97]</sup>.

Finally, gold nanoparticle-antibody conjugates have been used for as biosensors for their complementary antigens. A wide variety of such antibody-antigen interactions been reviewed<sup>[19,24,33]</sup>. As an illustrative example, the aggregation of gold nanoparticles by antigen-antibody interactions in solution was applied to develop immunoassay procedures with optical detection of the associa-

tion process<sup>[98,99]</sup>. A laser based double-beam absorption detection system for aggregation immunoassays has been developed. The assay is based on the aggregation of antigen capped gold nanoparticles, in the presence of the corresponding antibodies. The aggregation of the gold nanoparticles resulted in a change in the absorption bands with a detection limit for an antibody of  $3 \times 10^{-8} \text{M}$ .

**Silver:** A range of highly sensitive biosensing methods using antibodies have been developed by exploring different physicochemical properties of the Noble metal nanoparticles, such as LSPR, metal fluorescence enhancement/quenching, SERS, electrochemical activity, *etc.*<sup>[24]</sup>. To date, a number of colorimetric sensors using silver nanoparticles as probes have been developed<sup>[100]</sup>. In an effort to overcome the lower stability of silver nanoparticles Yuan reported a colorimetric sensing scaffold for neurogenin 1 (ngn1), a peptide expressed in neuronal precursor cells with the function of controlling the differentiation of neurons<sup>[101]</sup>. The detection procedure is based on an anti-aggregation mechanism, by which ngn1 inhibits the aggregation of the probe in the presence of  $\text{NaClO}_4$ . The anti-ngn1 antibody conjugated silver nanoparticles (AgNP-Ab) is negatively charged, and binding of the negatively charged ngn1 to the probe enhances interparticle electrostatic repulsion. Accompanying the increase of ngn1 concentration, the color of the solution varies from red to yellow, presenting an approach for the detection of ngn1. This assay exhibits a linear response range over nearly two orders of magnitude, from 50 to 800 ng/mL, and a detection limit of 30 ng/mL (Figure 12).

In the area of micro- and nanotechnology-derived biosensors the use of antibody capped silver nanoparticles

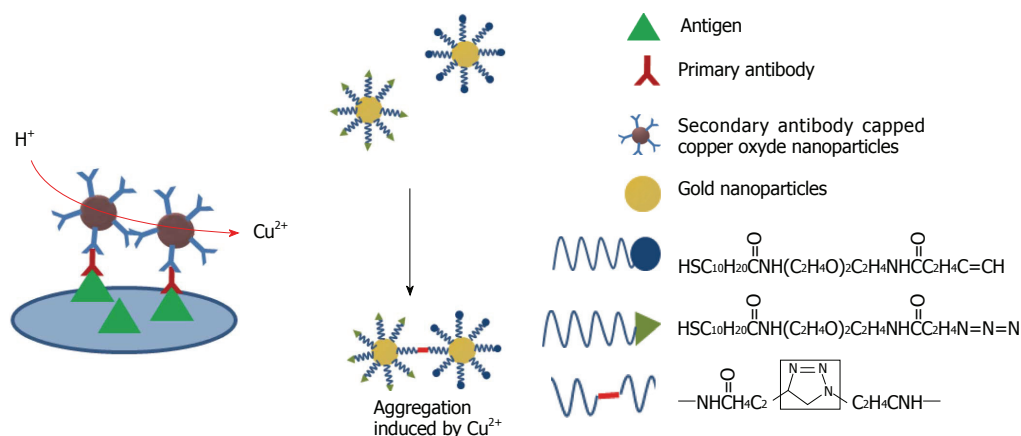


Figure 13 Schematic representation of immunoassay based on CuO-labeled antibody.

has received attention<sup>[102]</sup>. Silver nanoparticles are promising as the detection agent for electrochemical sensors. Porter highlighted the fact that although the number of assays reported with gold nanoparticles is much higher than those with silver, it is the silver nanoparticles that exhibit the better electrochemical properties<sup>[103]</sup>. Chen has developed the most sensitive electrochemical immunoassaying method with a dynamic concentration range of 1-1000 ng/mL and a detection limit of 0.4 ng/mL<sup>[104]</sup>.

The anti-microbial properties of silver are well documented<sup>[105]</sup>, and the antimicrobial activity of silver nanoparticles dominates research in this area<sup>[106]</sup>. Recently, Singh reported the use of these hybrid compounds as anti-viral agents. The addition of silver nanoparticles to antibodies significantly increased the neutralizing potency in prevention of cell-associated human immunodeficiency virus (HIV)-1 transmission/infection (from 10% of inhibition for antibodies alone to 60%-71% for antibody capped silver nanoparticles)<sup>[107]</sup>.

**Copper:** Since copper is easily oxidized, gold and silver nanostructures are more attractive for optical applications. In an effort to overcome this issue, research has been undertaken using different strategies. Zhang *et al.*<sup>[108]</sup> proposed to cover the surface of copper nanoparticles with gold in order to combine the voltammetric activity of copper and the stability and biocompatibility of gold. The functionalization with antibody permits the detection of *E. coli* with a detection limit of 30 CFU/mL. More recently, Wang developed a method using antibody capped copper nanoparticles<sup>[109]</sup>. When  $\text{Cu}^{2+}$  is released into solution by HCl treatment, it can be assayed (Figure 13). The limit of detection for the GP41 glycoprotein of HIV was about 150 ng/mL.

#### Molecules from the family of supramolecular chemistry

Supramolecular chemistry concerns the domain of chemistry beyond that of the covalent bond and focuses on chemical systems made up of a discrete number of non-covalently assembled molecular subunits or components. The forces responsible for the spatial organization may vary from weak (intermolecular forces, van der Waals),

through medium (aromatic-aromatic stacking or dipole-dipole) to strong (electrostatic, coordination bonds or hydrogen bonding)<sup>[110]</sup>. The assembly of the molecules will depend on molecular recognition events. Because of their recognition capability, molecules such as cyclodextrins (CDs), calix[n]arenes, dendrimers, crown ethers or cucurbiturils have attracted interests as capping agents on metallic nanoparticles<sup>[111]</sup> (Figure 14).

**Cyclodextrins:** The CDs are a family of soluble molecules generally consisting of 6, 7 or 8 D-glucopyranosyl residues (denoted as  $\alpha$ -CD,  $\beta$ -CD and  $\gamma$ -CD, respectively) linked in a cyclic structure by  $\alpha$ -1,4 glycosidic bonds. They can form inclusion complexes incorporating various molecular guests within their hollow, truncated cone shaped cavity structures, enabling them to be used as drug carriers. The host-guest interactions involved have been attributed to a combination of weak interactions such as van der Waals forces, and hydrophobic interactions and stronger interactions including hydrogen bonds<sup>[112,113]</sup>. Their combination with metal nanoparticles was the first reported among the supramolecular family<sup>[114]</sup>.

**Gold:** CD capped gold nanoparticles were initially investigated by Kaifer, in 1998, with the development of a new method based on the aqueous solubilization of aliphatic thiols by  $\alpha$ -CD (Figure 15), which effectively binds to the aliphatic chains and carries the hydrophobic thiol molecules to the surface of the gold particles, where they undergo chemisorption<sup>[115]</sup>. This method can be used to prepare gold colloidal particles (diameter > 10 nm) modified with long chain alkanethiols. If the alkanethiol contains a bulky terminal group, such as ferrocene, the  $\alpha$ -CD host is trapped after surface attachment, yielding CD-based rotaxanes supported on the gold nanoparticles. With the use of thiolated CDs, Liu *et al.*<sup>[116]</sup> functionalized gold nanospheres (2-7 nanometers). The resulting monolayer-protected nanoparticles behave as multisite hosts in aqueous media, engaging in host-guest interactions with conventional guest molecules for CDs. Similarly, the group of Liu used the recognition ability of  $\gamma$ -CD for C60 fullerene, in order to create  $\gamma$ -CD

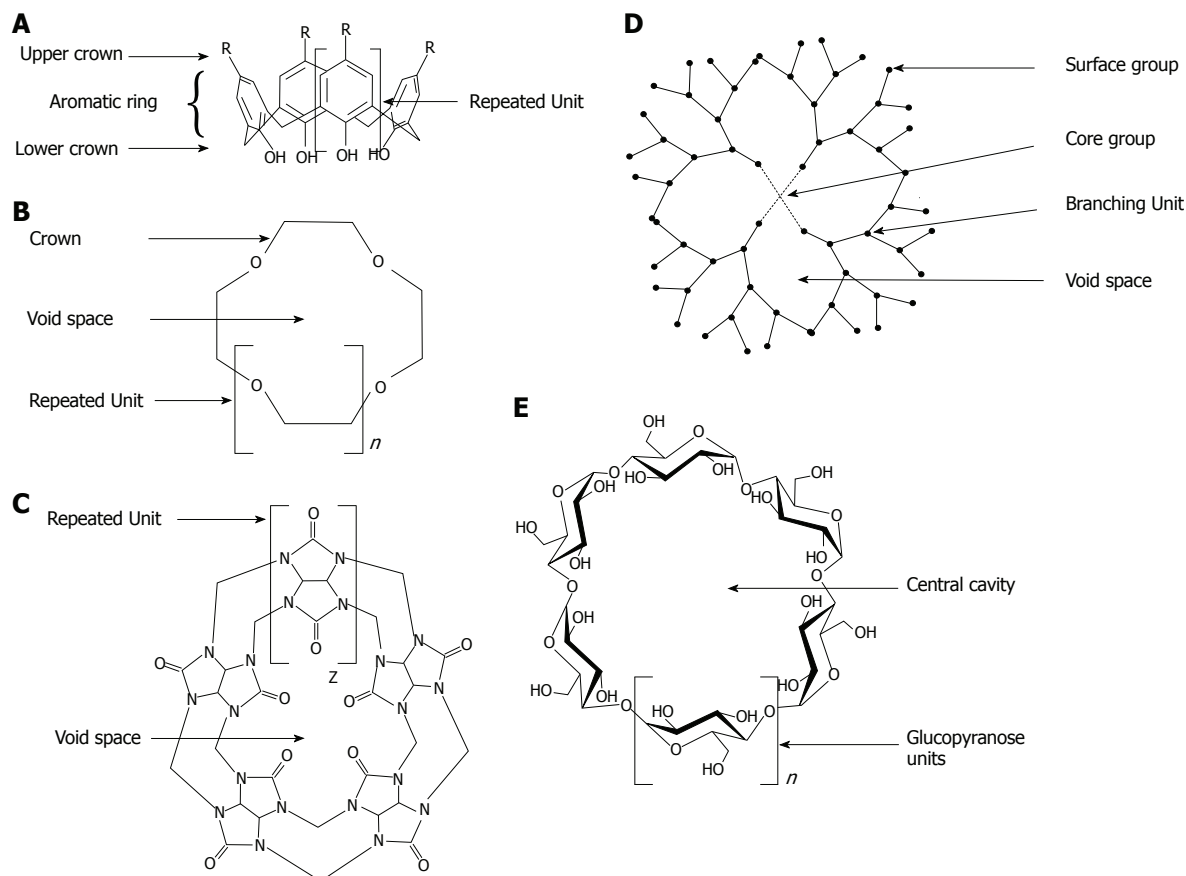


Figure 14 General structure of molecules from supramolecular family. A: Calixarene; B: Crown ether; C: Cucurbituril; D: Dendrimer; E: cyclodextrin.

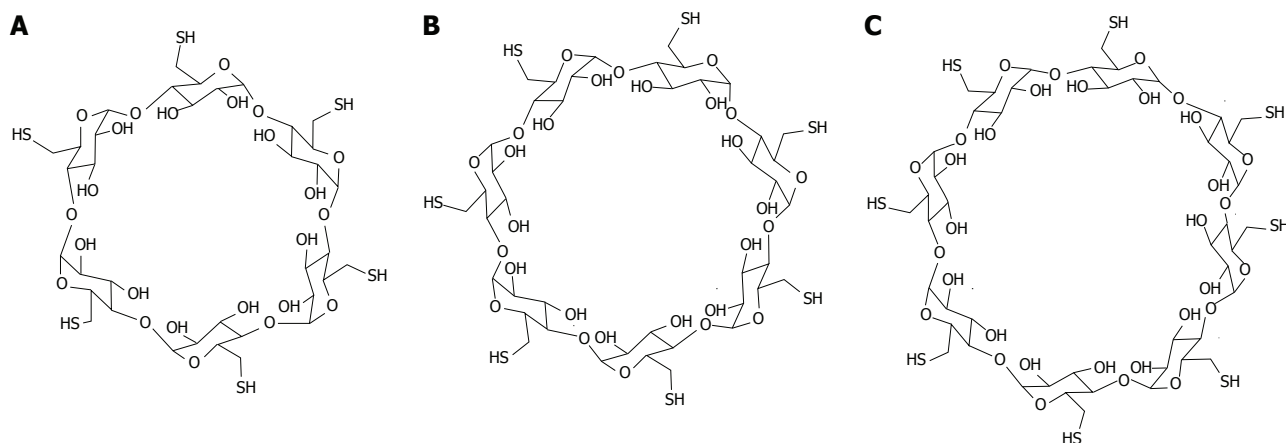
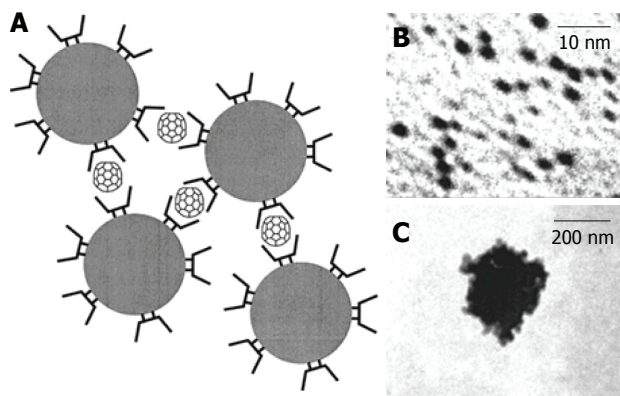


Figure 15 Structure of thiolated cyclodextrins. A: Per-6-thio- $\alpha$ -cyclodextrin; B: Per-6-thio- $\beta$ -cyclodextrin; C: Per-6-thio- $\gamma$ -cyclodextrin.

-capped gold nanoparticles as a C60 extracting agent. Even though C60 is extremely insoluble, an aqueous suspension containing  $\gamma$ -CD-capped gold nanoparticles (3.2 nm diameter) can partially solubilize C60<sup>[117]</sup>. This solubilization involves the formation of complexes between one molecule of C60 and two  $\gamma$ -CD hosts attached to different nanoparticles (Figure 16). Therefore, the fullerenes act as a sort of “molecular glue”, leading to the formation of soluble nanoparticle aggregates with sizes around 290 nm.

A number of studies describe the use of CDs as cap-

ping agents for gold nanoparticles in order to construct nanoparticulate superstructures in a reversible way<sup>[118,119]</sup>. In this area, Chen and Jiang have developed a reversible self-assembly of  $\alpha$ -CD capped gold nanoparticles to vesicles, mediated by a guest (azobenzene) conjugated to the double hydrophilic block copolymers Poly-Isopropylacrylamide (PNIPAM) and poly dimethyl acrylamide<sup>[120]</sup>. This assembly mechanism occurs in pure water under the stimulus of temperature. A possible mechanism is *via* the thermal responsive coil-to-globule transition of the PNIPAM block (Figure 17).



**Figure 16** In A is represented a scheme of fullerene-induced network with cyclodextrin capped gold nanoparticles in aqueous solution, in B is shown Transmission Electronic Microscope image of dispersed cyclodextrin capped gold nanoparticles and in C is shown a Transmission Electronic Microscope image of fullerene-induced aggregate. From Liu *et al.*<sup>[117]</sup>, reproduced with permission from American Chemical Society Publications.

Recently, CD-capped gold nanoparticles have been used as nanozymes<sup>[121]</sup>. They were utilized as a backbone to install metal catalytic centers by supramolecular assembly of the copper complex of triethylnetetramine-adamantane and 6-thio- $\beta$ -CD 15.2 receptors immobilized on the gold surface by thiol groups. The catalytic behaviour of  $\beta$ -CD-15.2-modified gold nanoparticles with adjacent multi-metal catalytic centers were investigated as an esterase mimic. Strong hydrolase activity for cleavage of an active ester 4,4'-dinitrodiphenyl carbonate (DND-PC) was observed. The rate acceleration is approximately 2600-fold with CD-capped gold nanoparticles compared to the reaction rate for the non-catalyzed hydrolysis of DNDPC in the same buffer solution.

**Silver:** CD capped silver nanoparticles were developed more recently than CD capped gold nanoparticles, being first demonstrated by Fan<sup>[122]</sup>. The method is simple, addition of  $\text{NaBH}_4$  to an aqueous solution of silver nitrate and  $\alpha$ -CD. The authors explain the stabilization of the silver nanoparticles by hydrophobic interactions of  $\alpha$ -CD primary faces. Then, hydrogen-bonding interactions between the exposed secondary -OH groups facilitates the threading of neighboring CDs, leading to the self-assembly of the silver nanoparticles into 1-D "pearl necklace" arrays.

Other studies have focused on the use of such hybrid systems to develop new antibacterial agents<sup>[123,124]</sup>. Wang developed silver nanoparticle-embedded one-dimensional  $\beta$ -CD-Poly-Vinyl-Pyrrolidone composite nanofibers using a one-step electrospinning technique. This composite exhibited good antibacterial properties against *E. coli* and *Staphylococcus aureus*<sup>[125]</sup>.

CD capped silver nanoparticle have also been used as biosensors by using SERS<sup>[126]</sup> or visual inspection<sup>[127]</sup>. In the latter case, Chen described the development of a robust, colorimetric detection method, sensitive to different isomers of aromatic compounds. 6-thio- $\beta$ -CD-15.2 was capped by chemisorption of the thiol function on

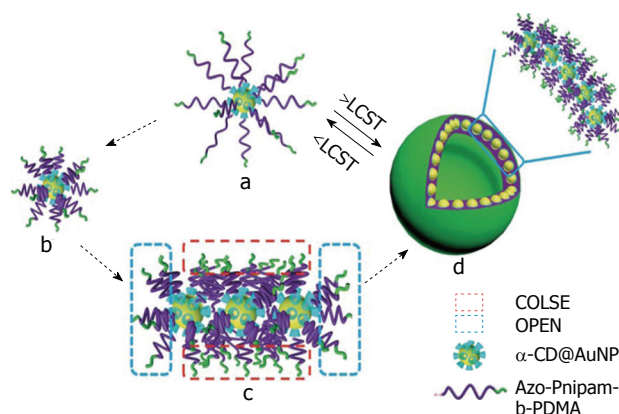


**Figure 17** Schematic representation of a possible mechanism of Hybrid Inclusion Complex-vesicle formation. From Wei *et al.*<sup>[120]</sup>, reproduced with permission from Royal Society of Chemistry. CD: Cyclodextrin; PDMA: Poly dimethyl acrylamide; AuNP: Gold nanoparticle; LCST: Lower critical solution temperature.

10 nm sized silver nanoparticles. The assay relies on the distance-dependent optical properties of silver nanoparticles and the different inclusion binding strength of the aromatic guests to CD. In the presence of different isomers of aromatic compounds, silver nanoparticles could be rapidly induced to aggregate, thereby resulting in an apricot to red colour change. With a spectrophotometer, this method is quantitative for monitoring the behaviour of the CD-modified silver nanoparticles as a function of the aromatic (Figure 18). The cited detection limit for different isomers of aromatic compounds is  $5 \times 10^{-5}$  mol/L.

**Copper:** CD based copper nanoparticles have been developed according to various methods. Zhu used 2-Hydroxypropyl- $\beta$ -CD 4 (Figure 19) as a template to fabricate hollow spherical copper sulfide nanoparticle assemblies using sonication. The average size of the prepared copper sulfide nanoparticles was estimated to be 10 nm<sup>[128]</sup>. Geckeler reported the preparation of uniform copper oxide (tenorite) nanoparticles *via* a green pathway by thermal decomposition, using a novel supramolecular complex, in which  $\beta$ -CD is selected to encapsulate the precursor copper(II) acetate<sup>[129]</sup>.

**Calix[n]arenes:** The calix[n]arenes are one the most widely studied classes of organic supramolecular hosts<sup>[111]</sup>. This popularity arises from their ease of synthesis and the fact that they contain two very different chemistries, one at the phenolic functions and a second at the *para*-position on the aromatic ring. This is coupled with the possibility to region-selectively modify them with varying degrees of controlled substitution at either face (Figure 20). Finally, their molecular recognition abilities added to their lack of toxicities<sup>[130]</sup> have given calix[n]arenes many applications in biology from protein sensors, stabilizers, enzyme inhibitors to active pharmaceutical ingredient (API) solubilizers<sup>[131]</sup>. A secondary property that has proved highly advantageous is the propensity of the calix[n]arenes to crystallize, allowing solid-state studies of a wide range of their complexes with bio-active

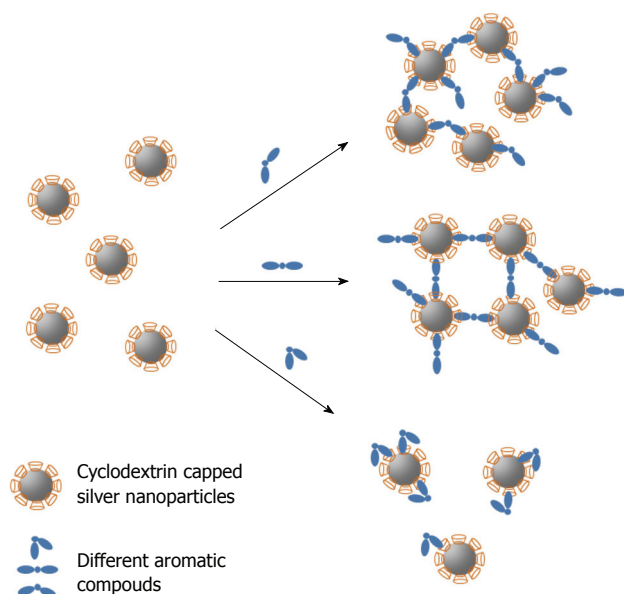


**Figure 18** Schematic of host-guest recognition for Cyclodextrin capped silver nanoparticles with different aromatic compounds.

molecules<sup>[132]</sup>. Combined with the electronic and optical properties of metal nanoparticles, calixarene capped nanoparticles have already started to show new applications, as recently described<sup>[133,134]</sup>.

**Gold:** So far, calixarene based gold nanoparticles have been mainly applied as colorimetric sensors. Pochini has carried out a large body of work in the use of thiolated derivatives of calix[4]arene for capping gold nanoparticles (Figure 21). The recognition of immobilized cationic pyridinium moieties with 5\_GNP<sup>[135]</sup>, or quaternary ammonium salts with 5\_GNP or 6\_GNP<sup>[136]</sup> by the unmodified upper rim of the calix[4]arene present on the gold nanoparticles was demonstrated.

Menon has introduced a simple route for the preparation of water soluble *para*-sulphonatocalix[4]arene thiol 7 capped gold nanoparticles<sup>[137]</sup> (Figure 22). 7 possesses an electron-rich cyclic cavity that can attract specifically cationic amino acids (lysine, arginine and histidine). These interactions between one amino acid molecule and two calix-modified gold nanoparticles tend to aggregate the assemblies more than the other amino acids (Figure 23). Similarly Han *et al.*<sup>[138]</sup> used *para*-sulphonato-calix[6]arene 9, gold nanoparticles in order to detect pollutant aromatic amines isomers (Figure 24).

Other studies have focused on the recognition of cations. Yan *et al.*<sup>[139]</sup> have developed 6 nm sized gold nanoparticles capped with methylthio-*para*-tert-butylcalixarene derivatives 11, 12 and 13 (Figure 25). They used the cationic recognition of structurally-tailored *para*-tert-butylcalixarenes to control access of the cationic guest to the cone cavity. This novel strategy has been shown to yield a specific red shift of the surface plasmon resonance band of gold nanoparticles, according to the cationic metal added. Solution of 0.4  $\mu\text{mol/L}$ , calix GNP showed apparent rates of  $1.4 \times 10^{-2} \text{ s}^{-1}$  for  $\text{Cu}^{2+}$  and  $2.5$

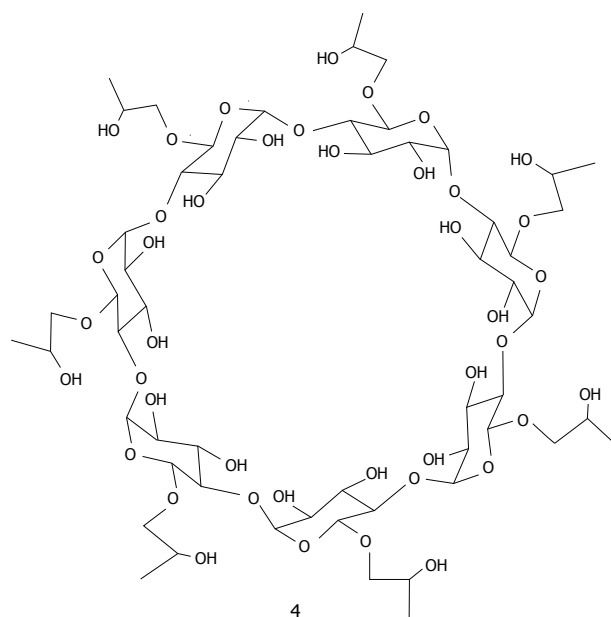


**Figure 19** Structure of  $\beta$ -cyclodextrin derivative 4.

$\times 10^{-1} \text{ s}^{-1}$  for  $\text{Cs}^{2+}$ .

Recently, Menon modified *para*-sulphonatocalix[4]arene with dithiocarbamate 14, for capping gold nanoparticles<sup>[140]</sup>. Sulfide ion recognition triggers particle aggregation through N-H-S hydrogen bonds and provides an easy way to measure color change (Figure 26). The lower detection limit was 10 nmol/L. This result validates the use of calix[n]arene capped gold nanoparticles in applications requiring high sensitivity and specificity.

**Silver:** Sanchez-Cortez used 25,27-diethyl-dithiocarbamic 26,28-dihydroxy *para*-tert-butylcalix[4]arene 15 in the functionalization of silver nanoparticles for pyrene detection by SERS<sup>[141]</sup>. SERS spectra provided information about the calix[4]arene orientation on the metal surface and the interaction mechanism (Figure 27).

Later Diao proposed a new method to change the surface properties of oleic acid stabilized silver nanoparticles and was successful in transferring silver nanoparticles from an organic phase into an aqueous phase<sup>[142]</sup>. By vigorous shaking of a biphasic mixture of the silver organosol protected with oleic acid and an aqueous solution of *para*-sulphonato-calix[4]arene 8, it is believed that an inclusion complex is formed between oleic acid molecules and 8, and the protective layer of the silver nanoparticles shifts from hydrophobic to hydrophilic in nature, which drives the transfer of silver nanoparticles from the organic phase into the aqueous phase. The 8-oleic acid inclusion complexation stabilized the nanoparticles for several weeks in the aqueous phase under ambient atmospheric conditions (Figure 28). Raston proposed new methods for environmentally friendly capping of silver nanoparticles with phosphonated derivatised calixarenes. *Para*-phosphonatedcalix[n]arenes 16, 17, 18 and 19 were used as stabilizers for evaluating the effect of hydrogen gas as an environmentally benign reductant of silver nanopar-

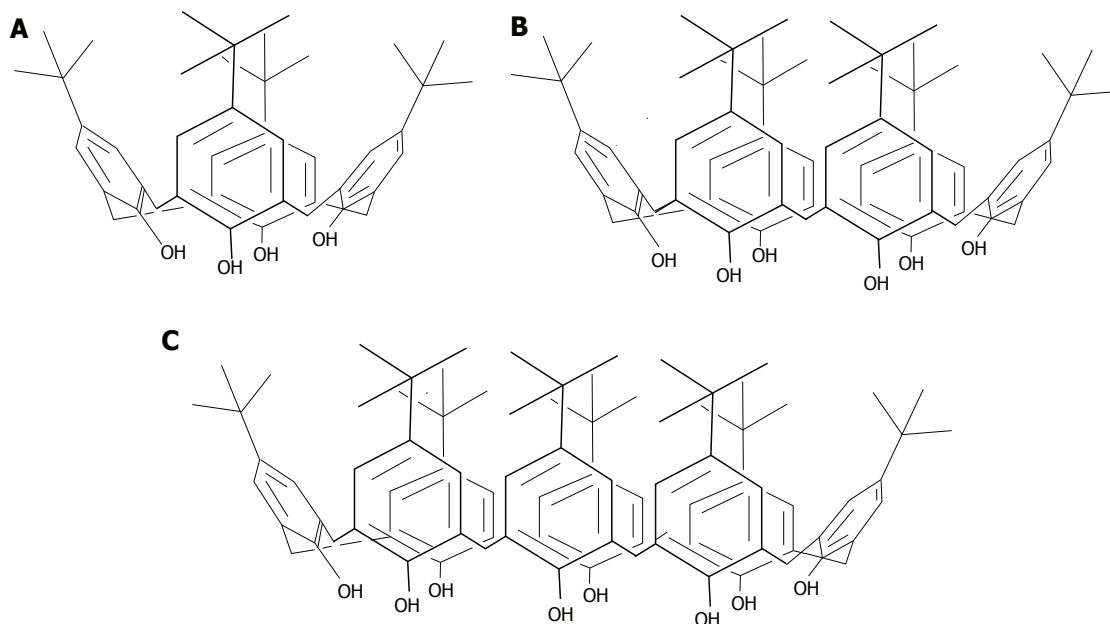


Figure 20 Structures of the t-Bu-calix[n]arenes,  $n = 4$  (A), 6 (B) and 8 (C).

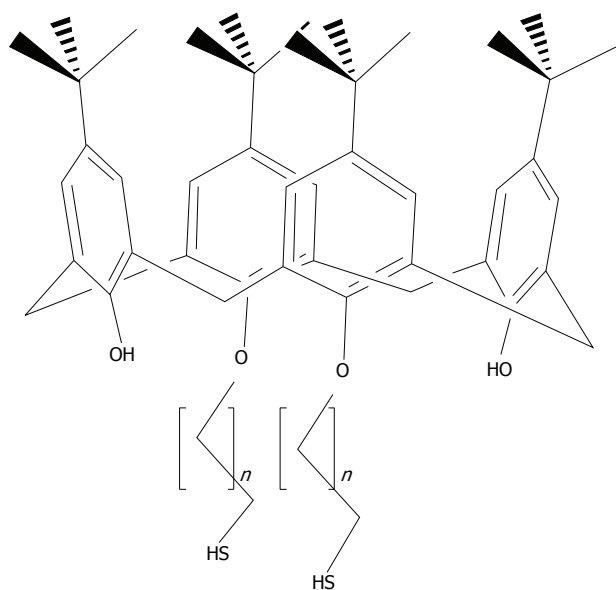


Figure 21 Structures of the thiolated-calix[n]arene derivatives. 5 corresponds to the present structure with  $n = 10$ ; 6 corresponds to the present structure with  $n = 5$ <sup>[136]</sup>.

ticles<sup>[143]</sup> (Figure 29). Other phosphonated derivatized calixarenes 20 and 21 have been tested for possible their effect on the growth of silver nanoparticles by photochemical synthesis<sup>[144]</sup> (Figure 29).

It is the work of Li which has made popular calix[n]arene capped silver nanoparticles with his easy route for producing them<sup>[145]</sup>. The group demonstrated the application of 8 capped silver nanoparticles for the recognition of cationic amino acids (Histidine, Lysine, Arginine) and pesticides including methyl parathion<sup>[146]</sup>.

Later, Coleman gave a more reasonable explanation for the structure of the assembly of 8 on the surface of

the silver nanoparticles<sup>[147]</sup>. It lies in the formation of the classic bilayer solid-state structure, where alternate coordinated *para*-sulphonato-calix[4]arene molecules give available cavities at the surface of the nanoparticle (Figure 30). Such assembly allows differentiation between the interactions, nucleic acids and nucleotides with 8 capped silver nanoparticles. Subsequently, the group investigated the assembly of the calixarene with one nucleotide (cytosine) in different states: in solution, in the solid-state and on the surface of silver nanoparticle<sup>[148]</sup>. The assembly was quite different according to the states involved, and needed the use of multiple physical methods to probe the complex assembly process. Recently, the group of Coleman has shown that 8 capped silver nanoparticles could interact with active pharmaceutical ingredients<sup>[149]</sup>. More interesting was the use of calixarene capped silver nanoparticles for the determination of the Critical Micellar Concentration (CMC) of some cationic surfactants<sup>[150]</sup>. This method generates a new means of studying CMC in media containing proteins and in particular membrane proteins.

**Copper:** Interestingly, only one study from 2007 reports on the use of copper as material support for calix[n]arenes<sup>[151]</sup>. Uniform cuprous oxide nanospheres with diameter of 10 nm were prepared by the reduction of  $\text{CuSO}_4$  in *para*-sulphonato-calix[8]arene 10 aqueous solution using hydrazine as a reducing agent. The host molecule, 10, was used as a bridge linker to make nanoparticles connect to each other and form large aggregations, which possess two types of properties: the photonic, catalytic and semiconductor properties of copper oxide and the supramolecular recognition function of 10-modified nanoparticles. As yet, there are no reports of any applications of this type of particle.

**Dendrimers:** Dendrimers are a class of hyper branched

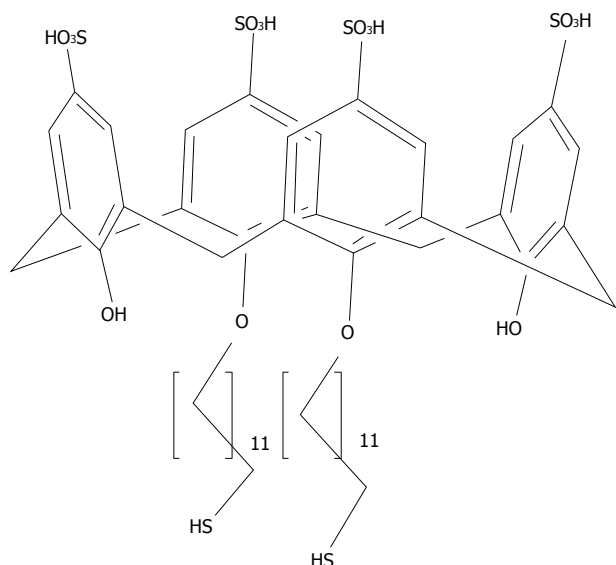
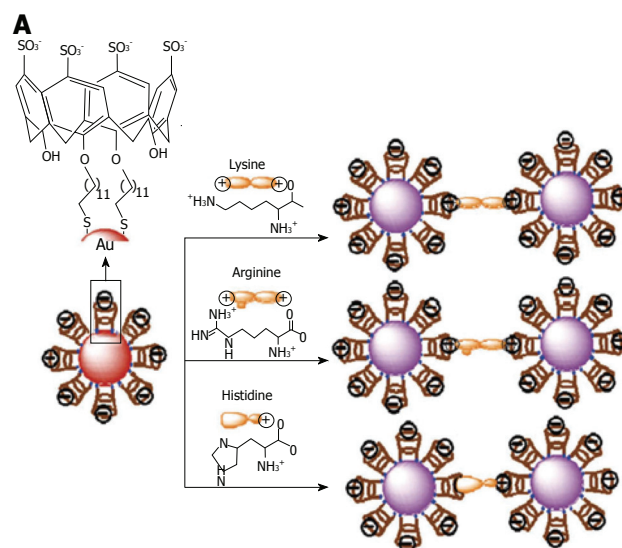


Figure 22 Structures of the *para*-sulphonato-calix[4]arene di-thiol 7.

oligomeric materials. Dendrimers are large and complex molecules having defined chemical structures. They possess three distinguishing architectural components, namely (a) an initiator core, (b) an interior layer (generations), composed of repeating units, radially attached to the initiator core and (c) exterior (terminal) functionality attached to the outermost interior generation (Figure 14). Dendrimers have been applied in biomedical applications, for drug-delivery systems and also for cancer therapy<sup>[152]</sup>. At this time, the major prospective applications of nanoparticle-dendrimer composites are in catalysis, biomedical research and electronic devices. The catalytic applications are mainly determined by properties of various mono- and bimetallic nanoparticles, while the dendrimer role is in templating or stabilization of nanoparticles, which, in turn, controls the nanoparticle size and morphology. There are a few examples where dendrimer generation (size) puts a limitation on the accessibility of the active centers for reacting molecules, due to a different size cavity in the dendrimer, thus creating size selectivity for a catalytic reaction. A similar effect was demonstrated for mesoporous catalysts with reactants of different sizes. The biomedical applications become possible due to the biocompatibility of many nanoparticle-dendrimer composites and their optical, magnetic and sensor properties<sup>[153]</sup>.

In the last decade dendrimeric gold nanoparticle systems have been widely studied. Crooks was the first to first encapsulated small gold nanoparticles (1-2 nm of diameter) by using a thiolated fourth-generation poly (amido-amine) (PAMAM) dendrimer 22 mixed with tetrachloroauric acid and reduced with an excess of  $\text{NaBH}_4$ <sup>[154]</sup> (Figure 31). Crooks also used dendrimeric gold nanoparticles in catalysis including intradendrimer hydrogenation and carbon-carbon coupling reactions in water, organic solvents, biphasic fluoruous/organic solvents and supercritical  $\text{CO}_2$ <sup>[155]</sup>.

Lu *et al.*<sup>[156]</sup> reported the use of RLS as a method for



B



Figure 23 A is given a schematic representation of the amino acid induced aggregation of calix-capped gold nanoparticles; and in B are given the photographic images of calix-capped gold nanoparticles solutions containing different amino acids. From Patel *et al.*<sup>[157]</sup>, reproduced with permission from Royal Society of Chemistry.

detecting trace quantities of protein. Here, RLS measures the change of light intensity scattered from the gold nanoparticles. The signal is known to be amplified upon aggregation. Generation of polypropylene imine hexadecane amine dendrimers 23 (PPIHA) was employed to synthesize uniform gold nanoparticles modified with amine groups on their surface (Figure 32). The amine groups strengthen the covalent coupling between gold nanoparticles and bovine serum albumin (BSA). As illustrated in Figure 33, the size of the gold nanoparticle-BSA conjugates was increased in the  $\text{HAuCl}_4\text{-NH}_4\text{OH-HCl}$  reaction system, enhancing the RLS intensity of the bioconjugates. The RLS intensity is related to the concentration of gold nanoparticle-BSA and has a lower detection limit of  $0.090 \mu\text{g/mL}$ . By employing BSA as a model protein, this work introduced a novel method for the quantitative detection of trace proteins<sup>[157]</sup>. Recently, Baker has developed a simple approach to fabricating multifunctional dendrimer-stabilized gold nanoparticles for cancer cell targeting and imaging<sup>[158]</sup>. In this work, amine-terminated generation 5 (G5) poly(amidoamine) (PAMAM) dendrimers pre-functionalized with folic acid and fluorescein isothiocyanate are complexed with Au (III) ions, followed by acetylation of the amine groups on the dendrimer surfaces. This one-step process leads to the spontaneous formation of 6 nm Au nanoparticles stabilized by

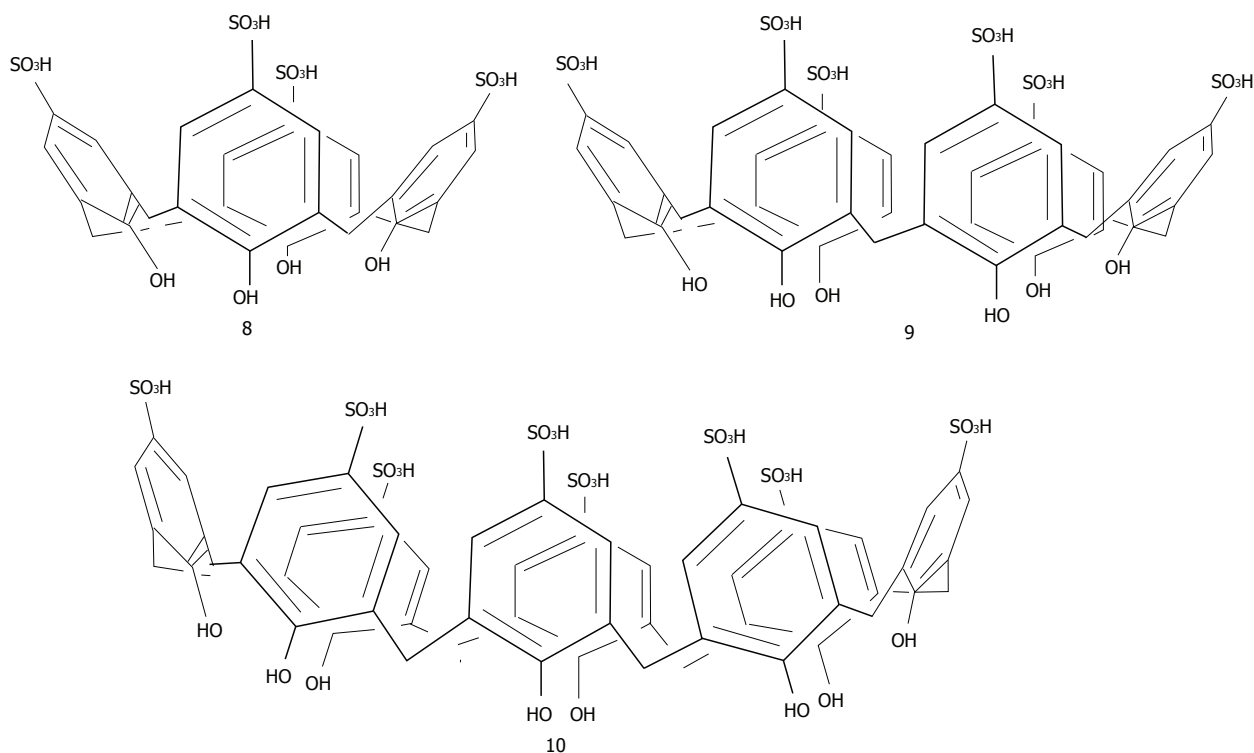


Figure 24 Structures of the para-sulphonato-calix[4, 6 and 8]arenes.

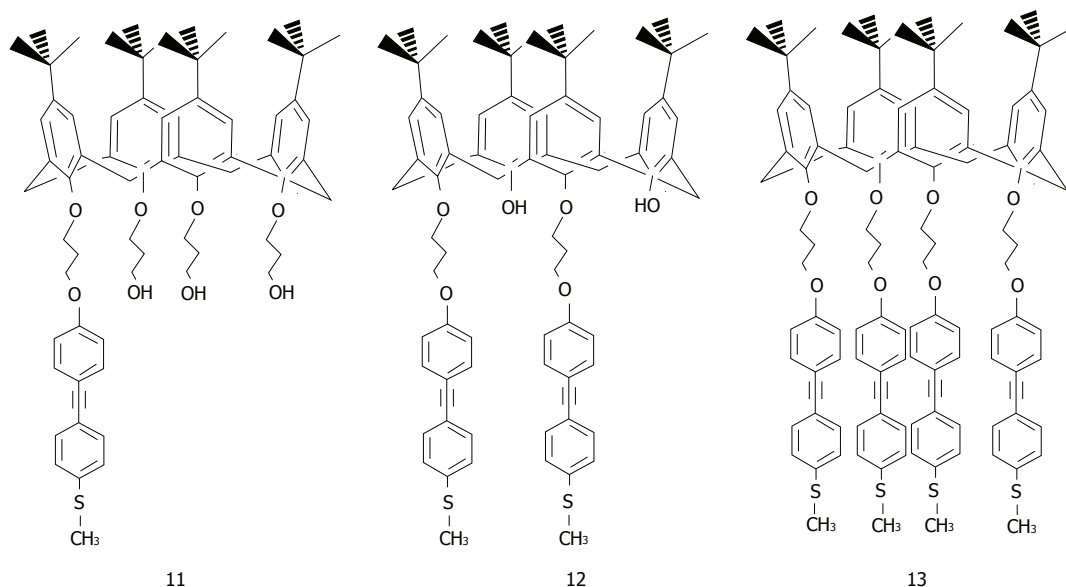


Figure 25 Structures of the methylthio-para-tert-butyl-calixarene derivatives.

multifunctional dendrimers bearing both targeting and imaging functionalities.

Wang used dendrons, segments of dendrimers that possess a focal point onto which the branching units of a dendritic architecture are attached to associated gold nanoparticles<sup>[159]</sup> (Figure 34). It was demonstrated that dendrons modified with a metal-coordinating functionality can be utilized as stabilizing media for the controlled growth of nanocrystals. The average size of the resulting nanoparticles is a direct function of the generation number of the capping dendron, with higher generation

dendrons producing larger particles. Astruc has made a large contribution in the research and development of dendronized gold nanoparticles<sup>[160]</sup>. Dendrons have been synthesized and used to assemble dendronized gold nanoparticles either by the ligand-substitution method from dodecanethiolate-gold nanoparticles (AB3 units) or Brust-type direct synthesis from a 1:1 mixture of dodecanethiol and dendronized thiol (AB9 units). Two nanoparticles have been made containing a nonasilylferrocenyl dendron 24 and 25 (Figure 35)<sup>[161]</sup>, bearing respectively 180 and 360 ferrocenyl units at the periphery.

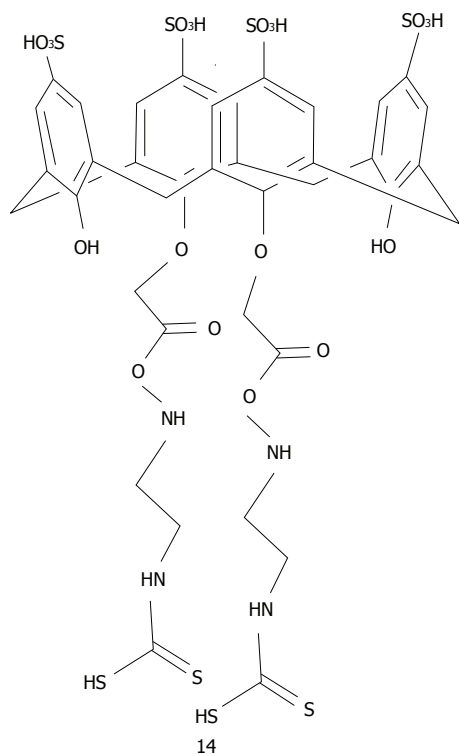


Figure 26 Structure of 25,27-bis(ethylaminecarbonylmethoxy)-26,28-dihydroxy-*para*-sulphonocalix[4]arene modified dithiocarbamate.

These colloids selectively recognize the anions  $\text{H}_2\text{PO}_4^-$  and adenosine-5'-triphosphate ( $\text{ATP}^{2-}$ ). Recognition has been monitored by cyclic voltammetry.

**Silver:** Recently Kakar reviewed dendrimer templated construction of silver nanoparticles. Up to now, synthesis assisted by dendrimers has led almost exclusively to formation of spherical-shaped silver nanoparticles. It is believed that dendrimers are likely to be more valuable for modulating the size of silver nanoparticles than their shape<sup>[162]</sup>.

Balogh *et al.*<sup>[163]</sup> reported that PAMAM Dendrimer 23 attached silver nanoparticles display considerable activity against *Staphylococcus aureus*, *Pseudomonas aeruginosa* and *E. coli* bacteria without the loss of solubility and activity in the presence of sulfate or chloride ions. Balogh has shown that dendrimer silver nanoparticles may find potential application as cell biomarkers<sup>[164]</sup>. They have synthesized hydroxyl-, and carboxyl-terminated ethylenediamine core generation 5 poly(amidoamine) dendrimers which were utilized to prepare aqueous silver-dendrimer nanoparticles. The hybrid particles are water-soluble, biocompatible, fluorescent, and stable below pH 7.5 The cellular uptake of nanoparticles was examined by transmission electron microscopy and confocal microscopy. Overall, cytotoxicity analysis indicates that the uptake of the hybrid particles is correlated with the surface charge of dendrimer and that the silver has no effect.

Mali reported the synthesis and characterization of a novel electrochemical label for sensitive electrochemical stripping metallo-immunoassays based on silver den-

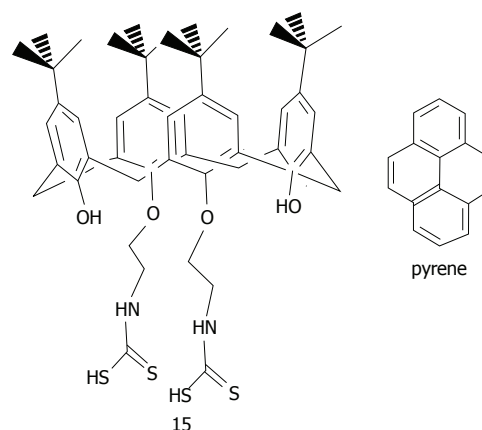


Figure 27 Structures of 25,27-diethyl-dithiocarbamic acid 26,28-dihydroxy *para*-*tert*-butylcalix[4]arene 15 and pyrene<sup>[141]</sup>.

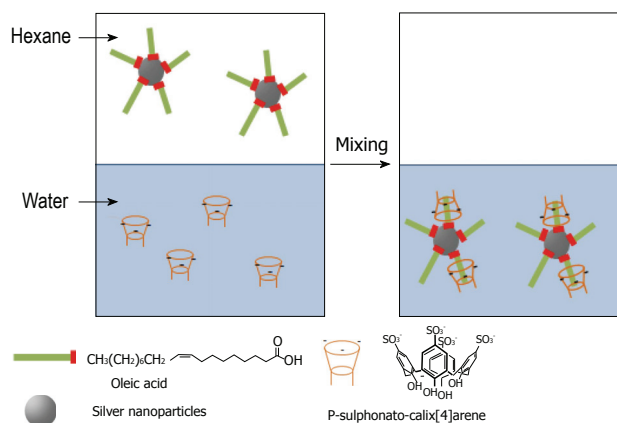


Figure 28 Phase transfer of Oleic acid stabilized silver nanoparticles from hexane to *para*-sulphonato-calix[4]arene aqueous solution.

dendrimer-encapsulated nanoparticles<sup>[165]</sup>. Several fixed ratios of  $\text{Ag}^+$ /dendrimer were prepared with the aim of obtaining stable nanocomposites with maximal silver loading in the interior of a polymeric shell. By combination of differential pulse voltammetry and anodic stripping analysis on a carbon electrode, individual silver dendrimer-encapsulated nanoparticles (limit of detection is 0.9 pMol) were detected down to  $1.35 \times 10^{10}$  after the dissolution of silver nanoparticles in dilute nitric acid.

Dendrimer silver nanoparticles have been shown to be good catalysts for reactions, such as the reduction of nitrophenol<sup>[166]</sup>, chloronitrobenzene<sup>[167]</sup> or the 2,7-dichloro-fluorescein dye<sup>[168]</sup>.

**Copper:** Various methods can be found in the literature to produce dendrimer copper nanoparticles, ranging from classical metal reduction using dendrimer as stabilizer<sup>[169]</sup> to more original electrochemical preparation<sup>[170]</sup>.

Using molecular assembly properties, Moore showed that dendrimer associated copper nanoparticles could be used as a catalyst of  $\text{Cu}^+$ -catalyzed azide-alkyne cycloaddition<sup>[171]</sup>. Reactivity was tested on a model reaction between azido propanol and propargyl alcohol in aqueous solution. The authors observed up to 120 fold faster con-

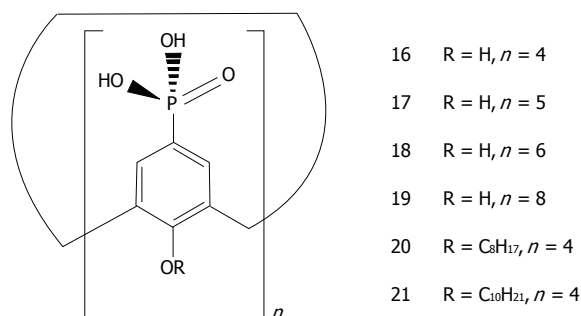


Figure 29 General structures of para-phosphonato-calix[n]arene derivatives.

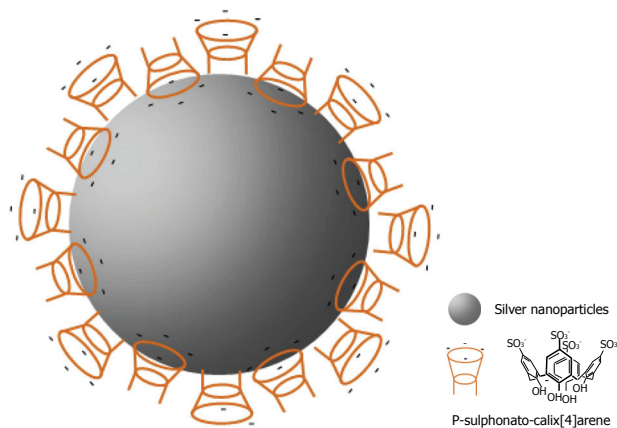


Figure 30 Schematic representation of the organization of para-sulphonato-calix[4]arene, 8 on silver nanoparticles.

version using PAMAM dendrimers as macromolecular  $\text{Cu}^+$  ligands compared to traditional small molecular ligand systems, and demonstrated that the macromolecular catalyst can be removed by ultrafiltration.

Huang has successfully synthesized mono-, di-, and tri-functionalized G5 PAMAM dendrimer conjugates with a copper-free click conjugation method<sup>[172]</sup>. An azido modified targeting moiety, a therapeutic drug and an imaging reagent were mixed with a G5 PAMAM dendrimer nanoplatfrom, simultaneously or sequentially, to give mono-, di- and tri-functional conjugates.

**Crown ethers:** Since Pedersen first reported the synthesis and cation complexation properties the crown ethers in 1967, these neutral synthetic heterocyclic compounds have attracted extensive and continuous attention through their unusual and powerful non-covalent cation binding properties. Classical crown ethers are macrocyclic polyethers that contain 3-20 oxygen atoms, each separated from the next by two or more carbon atoms (Figure 14)<sup>[173]</sup>. The most effective complexation agents, however, are macrocyclic oligomers of ethyleneoxy units, either substituted or unsubstituted, that contain 5-10 oxygen atoms. They are exceptionally versatile in selectively binding a range of metal ions and a variety of organic neutral and ionic species. Crown ethers are currently being studied and used in a variety of applications beyond

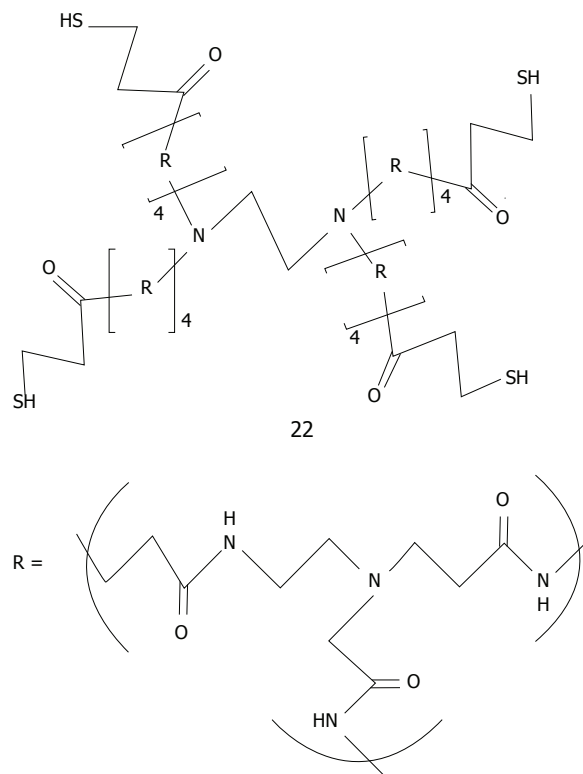


Figure 31 Structure of generation 4 thiolated dendrimer studied by Crooks<sup>[155]</sup>. The repeating unit R corresponds to poly(amido-amine).

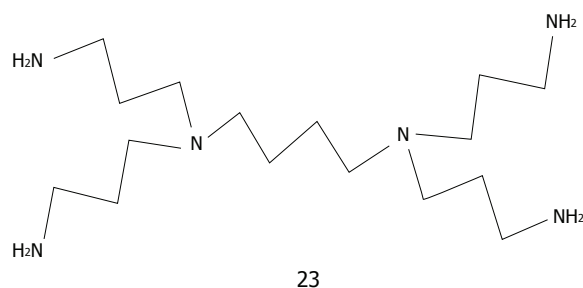
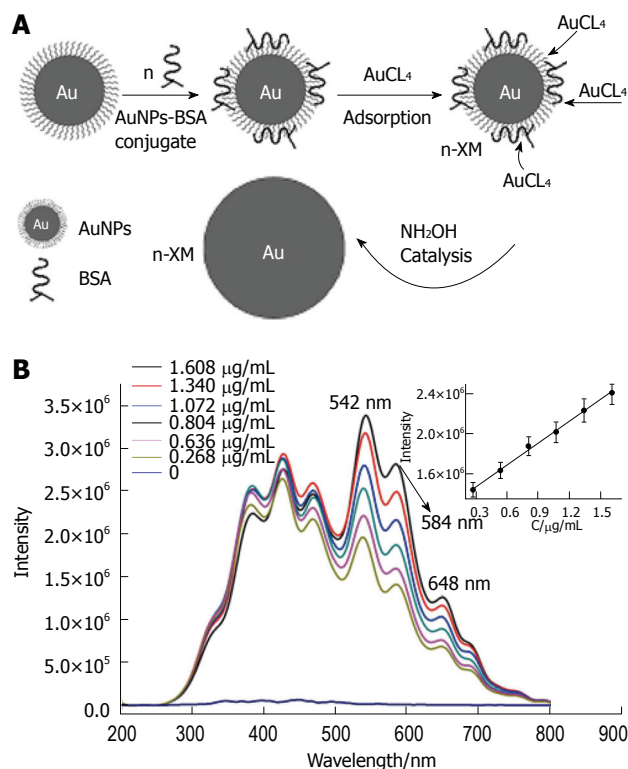


Figure 32 Structure of polypyrrolineiminehexadecaneamine (sic) dendrimer (PPHA generation 1<sup>st</sup>).

their traditional place in chemistry (used in the laboratory as phase transfer catalysts). In the biological context, they are being investigated as a promising anti-cancer compound<sup>[174]</sup>.

The combination of crown ethers with metallic nanoparticles has been mainly employed as a cation sensor. So far, crown ether capped gold nanoparticles have been used for cation detection using dithiocarbamate modified *N*-benzyl-4-aminobenzo-15-crown-5-ether 26 for  $\text{K}^+$ <sup>[175,176]</sup> or aza-15-crown-5-ether acridinedione 27 for  $\text{Ca}^{2+}$  and  $\text{Mg}^{2+}$ <sup>[176]</sup> (Figure 36). Li *et al.*<sup>[177]</sup> used silver because of its higher optical extinction ratio (stronger than gold). He capped dithiocarbamate modified aza-15-crown-5-ether 28 on silver nanoparticles with an average size of 8 nm of diameter (Figure 37). Li was able to detect  $\text{Ba}^{2+}$  with a detection limit of  $1 \times 10^{-8}$  mol/L. A possible explanation of the aggregation induced with  $\text{Ba}^{2+}$  is given by the formation of the sandwich structure with crown



**Figure 33** In A is given a schematic representation of the resonance light scattering amplification assay of biomolecules based on the biominalization of gold nanoparticles bioconjugates; in B is given the resonance light scattering spectrum of the biominalization product of concentration gradient of gold nanoparticles bioconjugates. From Liu *et al.*<sup>[157]</sup>, reproduced with permission from Elsevier. BSA: Bovine serum albumin; AuNP: gold nanoparticle.

ether (Figure 38).

Kwang has developed a colorimetric method of melamine detection, based on 18-crown-6 ether 29 (thiol derivatized) functionalized gold nanoparticles with an average diameter of 20 nm<sup>[178]</sup> (Figure 39). Melamine is a plant metabolite of cyromazine pesticides and a common chemical. It is also a highly toxic agent used fraudulently in the food industry. Crown ether capped gold nanoparticles enables the detection of melamine in milk after a pre-treatment consisting of centrifugation and purification. The crown ether GNP aggregation induced by the melamine is then monitored by UV-visible spectra with a LOD as low as 6 ppb, a wide linear range from 10 to 500 ppb, and acceptable reproducibility and specificity. This method could be extended to other toxins which show sufficient specificity in relation to the crown ethers and assembly ability (creating bridge between nanoparticles for aggregation).

**Cucurbiturils:** Cucurbiturils (CBs), are macrocycles derived from glycoluril units, which form stable host-guest complexes with various guest cationic molecules (Figure 14). Cucurbiturils have gained attention due to their unique structure and multiple recognition properties, as well as their potential applications for constructing sensors, drug delivery and biomimetic systems. Geckeler and collaborators initially reported a simple, green, one-pot

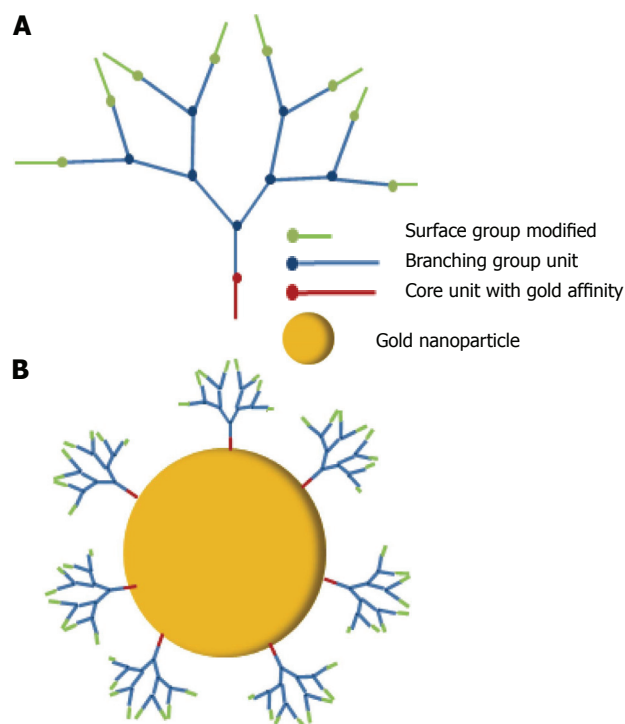


**Figure 34** Schematic representation of dendron generation 3 (A) and a dendron generation 3 capped gold nanoparticle (B).

synthesis of well-dispersed CB capped silver nanoparticles by the reaction of an aqueous silver nitrate solution with CB[7] in the presence of NaOH at room temperature<sup>[179]</sup>. Furthermore, they have investigated the *in vitro* cytotoxic properties of the prepared silver nanoparticles against two different human cancer cell types, namely human breast adenocarcinoma (MCF-7) and human lung bronchoalveolar (NCIH358) cells. It was demonstrated that the prepared CB[7]-protected silver nanoparticles, with an average size of about 5 nm, could be suitable candidates for cancer therapy applications. Mason prepared a series of CB capped silver nanoparticles and aggregates by reduction of silver nitrate with sodium borohydride in the presence of different CB<sup>[180]</sup>. They addressed the impact of CB[n] macrocycles ( $n = 5-8$ ) on the formation and stabilization of aqueous silver nanoparticles and Ag nanoaggregates obtained from silver nitrate and sodium borohydride, in the absence and presence of a set of positively charged guests shielding one or both portals of the cavitand. While CB[5] and CB[6] caused rapid aggregation and precipitation of Ag aggregates (diameters >13 nm), CB[7] and CB[8] allowed the formation and stabilization of monocrystalline, narrowly dispersed silver nanoparticles (diameters 5.3 and 3.7 nm, respectively). This could be explained by the rigidity of CB[5] and CB[6], and their possible lack of suitable arrangement at the silver surface, giving a poor stabilization of these silver assemblies, while the more flexible CB[7] and CB[8] may undergo some minor distortions and better adapt to the requirements of the metallic surface.

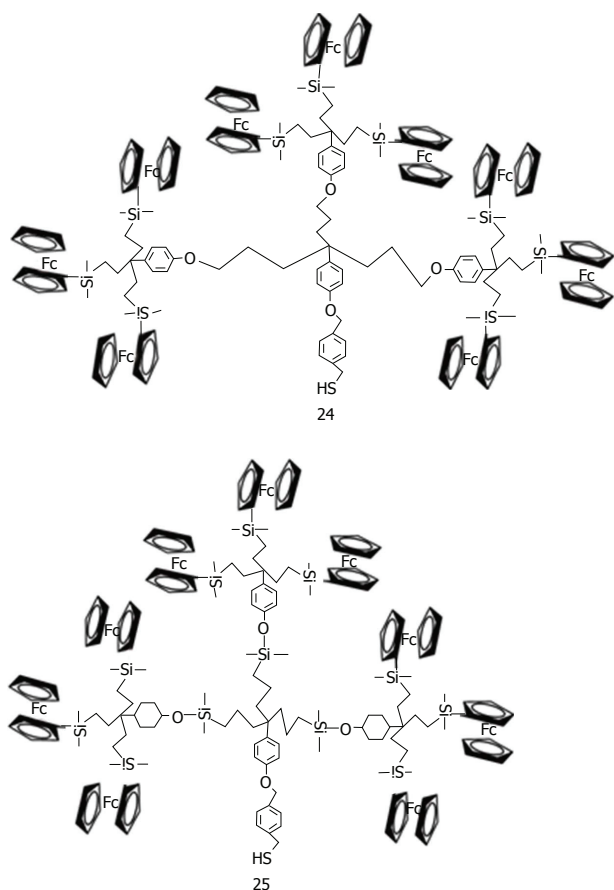


Figure 35 Structures of nonasilylferrocenyl dendron derivatives studied by Astruc *et al.*

## TOXICITY CONCERNS

Since hybrid nanoparticles have been investigated as therapeutic agents, a number of studies have investigated their toxicity<sup>[181]</sup>. More importantly, because of their numerous applications (described above) already high level of production of hybrid nanoparticles is growing and this inevitably leads to their appearance in air, water, soil and organisms<sup>[182]</sup>. As a consequence the risks to the environment and to human health are significant and should be treated as a concern.

Ray reviewed the different effects on health of different metal nanoparticle preparations<sup>[183]</sup>. Nanotoxicity studies revealed that the physicochemical characteristics of engineered nanomaterials play an important role in their interactions with living cells<sup>[184]</sup>. Physicochemical properties that affect the biological activity of hybrid nanoparticles include particle size, shape, surface chemistry, surface area, surface charge and their metallic composition<sup>[185]</sup>.

### Gold

While bulk gold is considered as “safe”, nanoscale particles of gold need to be examined for biocompatibility and environmental impact if they are to be manufactured on a large scale for *in vivo* usage<sup>[186]</sup>. Several researchers have reviewed the toxicity of gold nanoparticles in cells

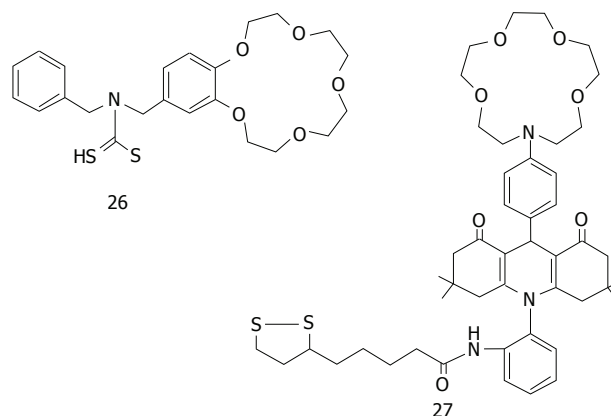


Figure 36 Structures of N-benzyl-4-aminobenzo-15-crown-5ether 26 for K<sup>+</sup> and aza-15-crown-5-ether acridinedione 27.

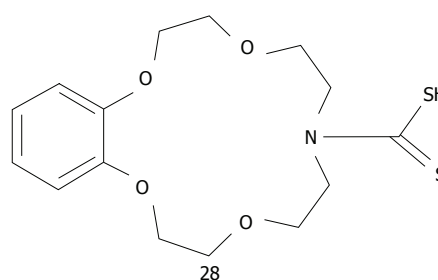
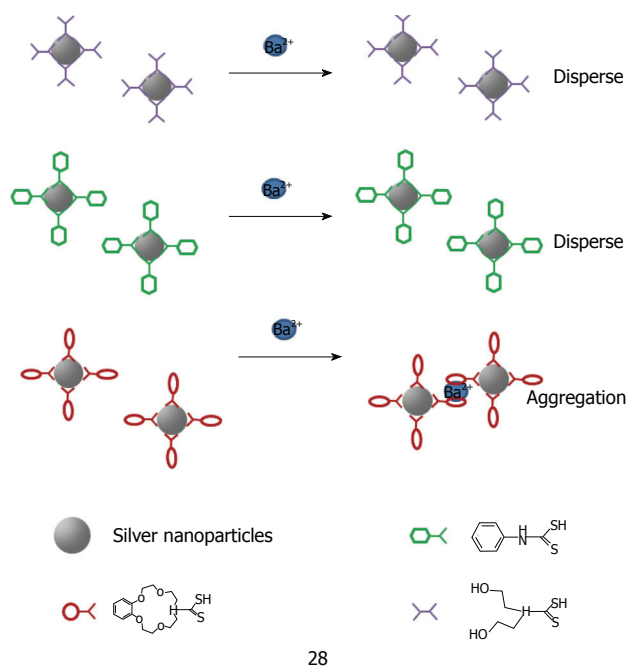


Figure 37 Structures dithiocarbamate modified aza-15-crown-5-ether 28 studied by Li *et al.*

(cytotoxicity) and *in vivo*<sup>[187,188]</sup>. Murphy reviewed these studies and highlighted some key parameters in the toxicity process<sup>[189]</sup>. First, the cell type is of critical importance. Patra studied the cell selective response to gold nanoparticles<sup>[190]</sup> and found that nanoparticles induced death in the A549 human carcinoma lung cell line while two other cell lines tested, BHK21 (baby hamster kidney) and HepG2 (human hepatocellular liver carcinoma), remained unaffected. The second key parameter is the surface charge. Cationic nanoparticles are much more cytotoxic than anionic particles. This may be related to their electrostatic interaction with the negatively charged cell membrane<sup>[191]</sup>. Size and shape are further critical parameters regarding potential toxicity. Chithrani *et al.*<sup>[192]</sup> observed that the cellular uptake of gold nanoparticles was greatly size dependent. Spheres of 50 nm were taken up more quickly by cells than either smaller or larger spheres in the 10-100 nm range and spheres were taken up more efficiently than nanorods that had dimensions in the 10-100 nm range<sup>[193]</sup>. Dikman has reviewed recently *in vivo* studies concerning gold nanoparticles and came to three conclusions<sup>[193]</sup>. Firstly, the dose and possible inflammatory processes are of paramount importance for the clearance (process avoiding accumulation in the organs of the reticuloendothelial system, such as spleen or liver) of 10-100 nm gold nanoparticles; Secondly, the effect of nanoparticle penetration *via* the hematoencephalic barrier depends critically on their size; 5-20 nm being the upper limit; Thirdly, gold nanoparticles of 1-2 nm in diameter

Tauran Y *et al.* Nanoparticle molecular recognition

28

**Figure 38** Schematic illustration of the aggregation of crown ether capped silver nanoparticles in the presence of metal ions  $Ba^{2+}$ .

could be more toxic due to the possibility of irreversible binding to biopolymers in cells. Also, numerous experiments on cell cultures have revealed no observable toxicity in colloidal particles with a size of 3-100 nm.

### Silver

Silver was originally used as an effective antimicrobial agent and as a disinfectant, as it was relatively free of adverse effects<sup>[194]</sup>. However even if silver is believed to be relatively nontoxic to mammalian cells, many *in vitro* studies have been performed to determine if this is still the case for silver nanoparticles. Several reviews summarize their effect on cells<sup>[195-197]</sup> *in vitro* studies have shown that silver nanoparticles have potential to induce toxicity in cells derived from a variety of organs. Chueh proposed a mechanism of cytotoxicity for fibroblast cells<sup>[198]</sup>. Silver nanoparticles induce cellular death (called apoptosis) by the generation of reactive oxygen species (ROS) and the activation of a specific biochemical pathway, JNK, *via* the mitochondria.

Despite the fact that silver nanoparticles have been increasingly applied in the biomedical and pharmacological fields, relatively little research has been done into their possible side-effects in clinical medicine<sup>[197]</sup>. Silver ingestion and topical application can induce the benign condition known as “argyria”, a grey-blue discoloration of the skin and liver caused by deposition of silver particles in the basal laminae of such tissues. Although argyria is not a life-threatening condition it is, however, cosmetically undesirable<sup>[199]</sup>. Wong *et al.*<sup>[200]</sup> reviewed and themselves investigated the effect on health of silver nanoparticles. They injected silver nanoparticles intravenously into experimental mice and did not observe any overt systemic effects, despite the silver nanoparticle solution used be-

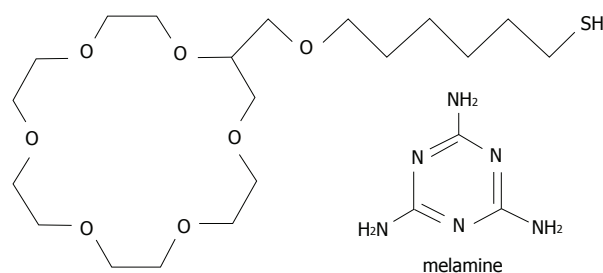


**Figure 39** Structures of thiolated crown ether 29 and melamine studied by Kuang *et al.*

ing at the relatively high concentration of 100 mmol/L. With to this administration route and dose application, silver nanoparticles can be potentially toxic. Intravenous administration may have more implications for adverse effects than dermal application<sup>[195]</sup>.

### Copper

Compared to gold and silver, the cytotoxicity of copper has been less studied<sup>[83]</sup>. However, Kim has recently investigated the toxicity of different metal nanoparticles<sup>[201]</sup>. They used the laser ablation method to generate Ag, Au, Co and Cu NPs in biocompatible aqueous solution. This method consists of intense laser irradiation of a material in solution and leads to an ejection of its constituents and the formation of nanoparticles<sup>[202]</sup>. This method allows generation of uncapped nanoparticles, allowing investigation of the toxicity of the metal itself. The cytotoxicity assay results demonstrate that nanoparticles possess moderate cytotoxicity to human cells in a cell-dependent manner. The half maximal inhibitory concentration ( $IC_{50}$ ) has been respectively determined for HeLa and PC3 cell lines: 78.9 and 88.6  $\mu\text{g}/\text{mL}$  of silver NP; 66.4 and 82.9  $\mu\text{g}/\text{mL}$  of gold NP and 85.5 and 91.7  $\mu\text{g}/\text{mL}$  of copper NP. Interestingly, the copper nanoparticles showed the lowest cytotoxicity. Valodkar produced 10 nm water soluble copper nanoparticles using starch as stabilizing agent and ascorbic acid as reducing agent<sup>[203]</sup>. These nanoparticles showed relatively low cytotoxicity (half maximal lethal dose of 100  $\mu\text{g}/\text{mL}$ ) and a strong bactericidal effect. The Minimum Bactericidal Concentration, the lowest concentration of antibiotic required to kill a particular bacterium, was determined as 3.2  $\mu\text{g}/\text{mL}$  for *S. Aureus* and 1.6  $\mu\text{g}/\text{mL}$  for *E. coli*. Because of their bactericidal effect at non-cytotoxic dose, these copper nanoparticles seem promising as possible therapeutic agents. However, clinical studies on silver and gold nanoparticles are required before considering copper nanoparticles as safe.

## CONCLUSION

In this review we have presented the preparation and physical properties of Noble metal capped nanoparticles. All aspects of molecular recognition of the various types of capping agent derived nanoparticles have been discussed in depth. Finally notice has been taken of the

concerns of many people with respect to the possible toxic effects of capped Noble metal nanoparticles.

## REFERENCES

- Hornayak GL, Patrissi CJ, Oberhauser EB, Martin CR, Valmalette JC, Lemaire L, Dutta J, Hofmann H. Effective medium theory characterization of Au/Ag nanoalloy-porous alumina composites. *NanoStructured Materials* 1997; **9**: 571-574 [DOI: 10.1016/S0965-9773(97)00127-X]
- Chabanne D, Bobin O, Schvoerer M, Ney C, Sciau PH. Metallic lustre of glazed ceramics: evolution of decorations in search for discriminating elements: Proceedings of 34th International Symposium on Archaeometry; 2004 May 3-7; Zaragoza, Spain. Zaragoza: Sociedad Cooperativa, Librería General, 2006: 327-332
- Needham J. Science and civilisation in China. 4th ed. Cambridge: Cambridge University Press, 1997: 268-269
- Kerker M. Founding fathers of light scattering and surface-enhanced Raman scattering. *Appl Opt* 1991; **30**: 4699-4705 [PMID: 20717272 DOI: 10.1364/AO.30.004699]
- Faraday M. The Bakerian Lecture: Experimental Relations of Gold (and Other Metals) to Light. *Philos Trans R Soc Lond* 1857; **147**: 145-181 [DOI: 10.1098/rstl.1857.0011]
- Strutt W, Rayleigh L. On the scattering of light by small particles. *Philos Mag Lett* 1871; **41**: 447-454
- Mie G. Contribution to the optics of turbid media particularly of colloidal metal solutions. *Ann Phys (Leipzig)* 1908; **25**: 377-445
- Turkeviche J, Stevenson PC, Hillier J. A study of the nucleation and growth processes in the synthesis of colloidal gold. *Discuss Faraday Soc* 1951; **11**: 55-75 [DOI: 10.1039/DF9511100055]
- Grzelczak M, Pérez-Juste J, Mulvaney P, Liz-Marzán LM. Shape control in gold nanoparticle synthesis. *Chem Soc Rev* 2008; **37**: 1783-1791 [PMID: 18762828 DOI: 10.1039/B711490G]
- Tréguer-Delapierre M, Majimel J, Mornet S, Duguet E, Ravaine S. Synthesis of non-spherical gold nanoparticles. *Gold Bulletin* 2008; **41**: 195-207 [DOI: 10.1007/BF03216597]
- Agasti SS, Rana S, Park MH, Kim CK, You CC, Rotello VM. Nanoparticles for detection and diagnosis. *Adv Drug Deliv Rev* 2010; **62**: 316-328 [PMID: 19913581 DOI: 10.1016/j.addr.2009.11.004]
- Hajipour MJ, Fromm KM, Ashkarran AA, Jimenez de Aberasturi D, de Larramendi IR, Rojo T, Serpooshan V, Parak WJ, Mahmoudi M. Antibacterial properties of nanoparticles. *Trends Biotechnol* 2012; **30**: 499-511 [PMID: 22884769 DOI: 10.1016/j.tibtech.2012.06.004]
- Arruebo M. Drug delivery from structured porous inorganic materials. *Wiley Interdiscip Rev Nanomed Nanobiotechnol* 2012; **4**: 16-30 [PMID: 21374827 DOI: 10.1002/wnan.132]
- Upadhyayula VK. Functionalized gold nanoparticle supported sensory mechanisms applied in detection of chemical and biological threat agents: a review. *Anal Chim Acta* 2012; **715**: 1-18 [PMID: 22244163 DOI: 10.1016/j.aca.2011.12.008]
- Jain PK, Huang X, El-Sayed IH, El-Sayed MA. Review of some interesting Surface Plasmon Resonance-enhanced properties of noble metal nanoparticles and their applications to biosystems. *Plasmonics* 2007; **2**: 107-118 [DOI: 10.1007/s11468-007-9031-1]
- Wang LH, Li J, Song SP, Li D, Fan C. Biomolecular Sensing via Coupling DNA-based Recognition with Gold Nanoparticles. *J Phys D Appl Phys* 2009; **42**: 203001 [DOI: 10.1088/0022-3727/42/20/203001]
- Li XM, Wang L, Fan YB, Feng QL, Cui FZ. Biocompatibility and Toxicity of Nanoparticles and Nanotubes. *J Nanomater* 2012; **2012**: 1-19 [DOI: 10.1155/2012/548389]
- Feldheim DL, Foss CA. Metal nanoparticles synthesis, characterization, and applications. New York: Marcel Dekker Inc, 2001: 360
- Katz E, Willner I. Integrated nanoparticle-biomolecule hybrid systems: synthesis, properties, and applications. *Angew Chem Int Ed Engl* 2004; **43**: 6042-6108 [PMID: 15538757 DOI: 10.1002/anie.200400651]
- Faulk WP, Taylor GM. An immunocolloid method for the electron microscope. *Immunochemistry* 1971; **8**: 1081-1083 [PMID: 4110101]
- Wilson R. The use of gold nanoparticles in diagnostics and detection. *Chem Soc Rev* 2008; **37**: 2028-2045 [PMID: 18762845 DOI: 10.1039/B712179M]
- Yu C, Irudayaraj J. Multiplex biosensor using gold nanorods. *Anal Chem* 2007; **79**: 572-579 [PMID: 17222022 DOI: 10.1021/ac061730d]
- Niemeyer CM. Nanoparticles, Proteins, and Nucleic Acids: Biotechnology Meets Materials Science. *Angew Chem Int Ed* 2001; **40**: 4128-4158 [DOI: 10.1002/1521-3773(20011119)]
- Doria G, Conde J, Veigas B, Giestas L, Almeida C, Assunção M, Rosa J, Baptista PV. Noble metal nanoparticles for biosensing applications. *Sensors (Basel)* 2012; **12**: 1657-1687 [PMID: 22438731 DOI: 10.3390/s120201657]
- Jain PK, Huang X, El-Sayed IH, El-Sayed MA. Noble metals on the nanoscale: optical and photothermal properties and some applications in imaging, sensing, biology, and medicine. *Acc Chem Res* 2008; **41**: 1578-1586 [PMID: 18447366 DOI: 10.1021/ar7002804]
- Chen Y, Ming H. Review of surface plasmon resonance and localized surface plasmon resonance sensor. *Photonics Sensors* 2012; **2**: 37-49 [DOI: 10.1007/s13320-011-0051-2]
- Colomban P. The Use of Metal Nanoparticles to Produce Yellow, Red and Iridescent Colour, from Bronze Age to Present Times in Lustre Pottery and Glass: Solid State Chemistry, Spectroscopy and Nanostructure. *Nano Res* 2009; **8**: 109-132 [DOI: 10.4028/www.scientific.net/JNanoR.8.109]
- Schmid G. Nanoparticles from Theory to Application. In: Blech K, Homberger M, Simon U. Electrical Properties of Metal Nanoparticles. 2nd ed. Germany: Wiley-VCH, 2004: 401-454
- Malaquin L, Vieu C, Genevieve M, Tauran Y, Carcenac F, Pourciel ML, Leberre V, Trevisiol V. Nanoelectrode-based devices for electrical biodetection in liquid solution. *Microelectron Eng* 2004; **73**: 887-892
- Chen YS, Hong MY, Huang GS. A protein transistor made of an antibody molecule and two gold nanoparticles. *Nat Nanotechnol* 2012; **7**: 197-203 [PMID: 22367097 DOI: 10.1038/nnano.2012]
- Sato K, Hosokawa K, Maeda M. Colorimetric biosensors based on DNA-nanoparticle conjugates. *Anal Sci* 2007; **23**: 17-20 [PMID: 17213617 DOI: 10.2116/analsci.23.17]
- Baptista P, Pereira E, Eaton P, Doria G, Miranda A, Gomes I, Quaresma P, Franco R. Gold nanoparticles for the development of clinical diagnosis methods. *Anal Bioanal Chem* 2008; **391**: 943-950 [PMID: 18157524 DOI: 10.1007/s00216-007-1768-z]
- Dykman L, Khlebtsov N. Gold nanoparticles in biomedical applications: recent advances and perspectives. *Chem Soc Rev* 2012; **41**: 2256-2282 [PMID: 22130549 DOI: 10.1039/c1cs15166e]
- Tiwari PM, Vig K, Dennis VA, Singh SR. Functionalized gold nanoparticles and their biomedical applications. *Nanomaterials* 2011; **1**: 31-63 [DOI: 10.3390/nano1010031]
- Mirkin CA, Letsinger RL, Mucic RC, Storhoff JJ. A DNA-based method for rationally assembling nanoparticles into macroscopic materials. *Nature* 1996; **382**: 607-609 [PMID: 8757129 DOI: 10.1038/382607a0]
- Stoltenburg R, Reinemann C, Strehlitz B. SELEX--a (r)evolutionary method to generate high-affinity nucleic acid ligands. *Biomol Eng* 2007; **24**: 381-403 [PMID: 17627883 DOI: 10.1016/j.biomoleng.2007.03.001]

Tauran Y *et al.* Nanoparticle molecular recognition

- 10.1016/j.bioeng.2007.06.001]
- 37 **Nelson DL**, Lehninger AL, Cox MM. Lehninger principles of biochemistry. 3rd ed. New York: Worth Publishers, 2008: 1100-44 Pustovit VN, Shahbazyan TV. SERS from molecules adsorbed on small Ag nanoparticles: a microscopic model. *Chem Phys Lett* 2006; **420**: 469-473
- 38 **Heller MJ**. DNA microarray technology: devices, systems, and applications. *Annu Rev Biomed Eng* 2002; **4**: 129-153 [PMID: 12117754 DOI: 10.1146/annurev.bioeng.4.020702.153438]
- 39 **Thompson DG**, Enright A, Faulds K, Smith WE, Graham D. Ultrasensitive DNA detection using oligonucleotide-silver nanoparticle conjugates. *Anal Chem* 2008; **80**: 2805-2810 [PMID: 18307361 DOI: 10.1021/ac702403w]
- 40 **Grabar KC**, Griffith Freeman R, Hommer MB, Natan MJ. Preparation and characterization of Au colloid monolayers. *Anal Chem* 1995; **67**: 735-743 [DOI: 10.1021/ac00100a008]
- 41 **Storhoff JJ**, Elghanian R, Mucic RD, Mirkin CA, Letsinger RL. One-Pot colorimetric differentiation of polynucleotides with single base imperfections using gold nanoparticle probes. *J Am Chem Soc* 1998; **120**: 1959-1964 [DOI: 10.1021/ja972332i]
- 42 **Taton TA**, Mirkin CA, Letsinger RL. Scanometric DNA array detection with nanoparticle probes. *Science* 2000; **289**: 1757-1760 [PMID: 10976070 DOI: 10.1126/science.289.5485.1757]
- 43 **Sun L**, Yu C, Irudayaraj J. Surface-enhanced Raman scattering based nonfluorescent probe for multiplex DNA detection. *Anal Chem* 2007; **79**: 3981-3988 [PMID: 17465531 DOI: 10.1021/ac700078z]
- 44 **Pustovit VN**, Shahbazyan TV. SERS from molecules adsorbed on small Ag nanoparticles: a microscopic model. *Chem Phys Lett* 2006; **420**: 469-473
- 45 **Rothmund PW**. Folding DNA to create nanoscale shapes and patterns. *Nature* 2006; **440**: 297-302 [PMID: 16541064 DOI: 10.1038/nature04586]
- 46 **Borovok N**, Gillon E, Kotlyar A. Synthesis and Assembly of Conjugates Bearing Specific Numbers of DNA Strands per Gold Nanoparticle. *Bioconjug Chem* 2012 Apr 30; Epub ahead of print [PMID: 22515478 DOI: 10.1021/bc200485r]
- 47 **Li H**, Sun Z, Zhong W, Hao N, Xu D, Chen HY. Ultrasensitive electrochemical detection for DNA arrays based on silver nanoparticle aggregates. *Anal Chem* 2010; **82**: 5477-5483 [PMID: 20550213 DOI: 10.1021/ac101193e]
- 48 **Zon VB**, Burley GA, Rant U. Photo-induced growth of DNA-capped silver nanoparticles. *Nanotechnology* 2012; **23**: 115607 [PMID: 22382001 DOI: 10.1088/0957-4484/23/11/115607]
- 49 **Latorre A**, Somoza Á. DNA-mediated silver nanoclusters: synthesis, properties and applications. *ChemBiochem* 2012; **13**: 951-958 [PMID: 22508551 DOI: 10.1002/cbic.201200053]
- 50 **Lan GY**, Chen WY, Chang HT. Characterization and application to the detection of single-stranded DNA binding protein of fluorescent DNA-templated copper/silver nanoclusters. *Analyst* 2011; **136**: 3623-3628 [PMID: 21776493 DOI: 10.1039/c1an15258k]
- 51 **Richards CI**, Hsiang JC, Senapati D, Patel S, Yu J, Vosch T, Dickson RM. Optically modulated fluorophores for selective fluorescence signal recovery. *J Am Chem Soc* 2009; **131**: 4619-4621 [PMID: 19284790 DOI: 10.1021/ja809785s]
- 52 **Rotaru A**, Dutta S, Jentsch E, Gothelf K, Mokhir A. Selective dsDNA-templated formation of copper nanoparticles in solution. *Angew Chem Int Ed Engl* 2010; **49**: 5665-5667 [PMID: 20629055 DOI: 10.1002/anie.200907256]
- 53 **Jia X**, Li J, Han L, Ren J, Yang X, Wang E. DNA-hosted copper nanoclusters for fluorescent identification of single nucleotide polymorphisms. *ACS Nano* 2012; **6**: 3311-3317 [PMID: 22417109 DOI: 10.1021/nn3002455]
- 54 **Pavlov V**, Xiao Y, Shlyahovsky B, Willner I. Aptamer-functionalized Au nanoparticles for the amplified optical detection of thrombin. *J Am Chem Soc* 2004; **126**: 11768-11769 [PMID: 15382892 DOI: 10.1021/ja046970u]
- 55 **Huang CC**, Huang YF, Cao Z, Tan W, Chang HT. Aptamer-modified gold nanoparticles for colorimetric determination of platelet-derived growth factors and their receptors. *Anal Chem* 2005; **77**: 5735-5741 [PMID: 16131089 DOI: 10.1021/ac050957q]
- 56 **Huang YF**, Chang HT. Analysis of adenosine triphosphate and glutathione through gold nanoparticles assisted laser desorption/ionization mass spectrometry. *Anal Chem* 2007; **79**: 4852-4859 [PMID: 17523592 DOI: 10.1021/ac070023x]
- 57 **Huang YF**, Lin YW, Lin ZH, Chang HT. Aptamer-modified gold nanoparticles for targeting breast cancer cells through light scattering. *J Nanopart Res* 2009; **11**: 775-783 [DOI: 10.1007/s11051-008-9424-x]
- 58 **Liu G**, Mao X, Phillips JA, Xu H, Tan W, Zeng L. Aptamer-nanoparticle strip biosensor for sensitive detection of cancer cells. *Anal Chem* 2009; **81**: 10013-10018 [PMID: 19904989 DOI: 10.1021/ac901889s]
- 59 **Wang Y**, Li Z, Li H, Vuki M, Xu D, Chen HY. A novel aptasensor based on silver nanoparticle enhanced fluorescence. *Biosens Bioelectron* 2012; **32**: 76-81 [PMID: 22209330 DOI: 10.1016/j.bios.2011.11.030]
- 60 **Aslan K**, Holley P, Geddes CD. Metal-enhanced fluorescence from silver nanoparticle-deposited polycarbonate substrates. *J Mater Chem* 2006; **16**: 2846-2852 [DOI: 10.1039/B604650A]
- 61 **Dreaden EC**, Alkilany AM, Huang X, Murphy CJ, El-Sayed MA. The golden age: gold nanoparticles for biomedicine. *Chem Soc Rev* 2012; **41**: 2740-2779 [PMID: 22109657 DOI: 10.1039/c1cs15237h]
- 62 **Kim SB**, Hattori M, Ozawa T. Intelligent design of nanoscale molecular imaging agents. *Int J Mol Sci* 2012; **13**: 16986-17005 [PMID: 23235326 DOI: 10.3390/ijms131216986]
- 63 **Van Dorst B**, Mehta J, Bekaert K, Rouah-Martin E, De Coen W, Dubruel P, Blust R, Robbens J. Recent advances in recognition elements of food and environmental biosensors: a review. *Biosens Bioelectron* 2010; **26**: 1178-1194 [PMID: 20729060 DOI: 10.1016/j.bios.2010.07.033]
- 64 **Willner I**, Basnar B, Willner B. Nanoparticle-enzyme hybrid systems for nanobiotechnology. *FEBS J* 2007; **274**: 302-309 [PMID: 17181543 DOI: 10.1111/j.1742-4658.2006.05602.x]
- 65 **Suresh Babu VV**. One hundred years of peptide chemistry. *Resonance* 2001; **2001**: 68-75
- 66 **Kogan MJ**, Olmedo I, Hosta L, Guerrero AR, Cruz LJ, Albericio F. Peptides and metallic nanoparticles for biomedical applications. *Nanomedicine (Lond)* 2007; **2**: 287-306 [PMID: 17716175 DOI: 10.2217/17435889.2.3.287]
- 67 **Pasquato L**, Pengo P, Scrimin P. Nanozymes: Functional nanoparticle-based catalysts. *Supramol Chem* 2005; **17**: 163-171 [DOI: 10.1080/10610270412331328817]
- 68 **Lévy R**. Peptide-capped gold nanoparticles: towards artificial proteins. *ChemBiochem* 2006; **7**: 1141-1145 [PMID: 16810658 DOI: 10.1002/cbic.200600129]
- 69 **Pengo P**, Baltzer L, Pasquato L, Scrimin P. Substrate modulation of the activity of an artificial nanoesterase made of peptide-functionalized gold nanoparticles. *Angew Chem Int Ed Engl* 2007; **46**: 400-404 [PMID: 17131436 DOI: 10.1002/anie.200602581]
- 70 **Wang Z**, Lévy R, Fernig DG, Brust M. Kinase-catalyzed modification of gold nanoparticles: a new approach to colorimetric kinase activity screening. *J Am Chem Soc* 2006; **128**: 2214-2215 [PMID: 16478166 DOI: 10.1021/ja058135y]
- 71 **Sun L**, Liu D, Wang Z. Microarray-based kinase inhibition assay by gold nanoparticle probes. *Anal Chem* 2007; **79**: 773-777 [PMID: 17222050 DOI: 10.1021/ac061687u]
- 72 **Yguerabide J**, Yguerabide EE. Resonance light scattering particles as ultrasensitive labels for detection of analytes in a wide range of applications. *J Cell Biochem Suppl* 2001; Suppl **37**: 71-81 [PMID: 11842431 DOI: 10.1002/jcb.10077]
- 73 **Wang Z**, Lévy R, Fernig DG, Brust M. The peptide route to multifunctional gold nanoparticles. *Bioconjug Chem* 2005; **16**:

- 497-500 [PMID: 15898714 DOI: 10.1021/bc050047f]
- 74 **Tkachenko AG**, Xie H, Coleman D, Glomm W, Ryan J, Anderson MF, Franzen S, Feldheim DL. Multifunctional gold nanoparticle-peptide complexes for nuclear targeting. *J Am Chem Soc* 2003; **125**: 4700-4701 [PMID: 12696875 DOI: 10.1021/ja0296935]
- 75 **Huang X**, Peng X, Wang Y, Wang Y, Shin DM, El-Sayed MA, Nie S. A reexamination of active and passive tumor targeting by using rod-shaped gold nanocrystals and covalently conjugated peptide ligands. *ACS Nano* 2010; **4**: 5887-5896 [PMID: 20863096 DOI: 10.1021/nn102055s]
- 76 **Graf P**, Manton A, Foelske A, Shkilnyy A, Masić A, Thüne-mann AF, Taubert A. Peptide-coated silver nanoparticles: synthesis, surface chemistry, and pH-triggered, reversible assembly into particle assemblies. *Chemistry* 2009; **15**: 5831-5844 [PMID: 19370744 DOI: 10.1002/chem.200802329]
- 77 **Garrido C**, Aliaga AE, Gomez-Jeria JS, Clavijo RE, Campos-Vallette MM, Sanchez-Cortes S. Adsorption of oligopeptides on silver nanoparticles: surface-enhanced Raman scattering and theoretical studies. *J Raman Spectrosc* 2010; **41**: 1149-1155 [DOI: 10.1002/jrs.2583]
- 78 **Cui Y**, Wang Y, Liu R, Sun Z, Wei Y, Zhao Y, Gao X. Serial silver clusters biomineralized by one peptide. *ACS Nano* 2011; **5**: 8684-8689 [PMID: 22023330 DOI: 10.1021/nn202566n]
- 79 **Wang X**, Wua L, Ren J, Miyoshi D, Sugimoto N, Qu X. Label-free colorimetric and quantitative detection of cancer marker protein using noncrosslinking aggregation of Au/Ag nanoparticles induced by target-specific peptide probe. *Biosens Bioelectron* 2011; **26**: 4804-4809 [DOI: 10.1016/j.bios.2011.06.012]
- 80 **Amato E**, Diaz-Fernandez YA, Taglietti A, Pallavicini P, Pasotti L, Cucca L, Milanese C, Grisoli P, Dacarro C, Fernandez-Hechavarria JM, Necchi V. Synthesis, characterization and antibacterial activity against Gram positive and Gram negative bacteria of biomimetically coated silver nanoparticles. *Langmuir* 2011; **27**: 9165-9173 [PMID: 21736306 DOI: 10.1021/la201200r]
- 81 **Taglietti A**, Diaz Fernandez YA, Amato E, Cucca L, Dacarro G, Grisoli P, Necchi V, Pallavicini P, Pasotti L, Patrini M. Antibacterial activity of glutathione-coated silver nanoparticles against Gram positive and Gram negative bacteria. *Langmuir* 2012; **28**: 8140-8148 [PMID: 22546237 DOI: 10.1021/la3003838]
- 82 **Wei QS**, Ji J, Fu JH, Shen JC. Norvancomycin-capped silver nanoparticles: Synthesis and antibacterial activities against *E. coli*. *Sci China B* 2007; **50**: 418-424 [DOI: 10.1007/s11426-007-0028-6]
- 83 **Valodkar V**, Jadeja RN, Thounaojam MC, Devkar RV, Thakore S. Biocompatible synthesis of peptide capped copper nanoparticles and their biological effect on tumor cells. *Mater Chem Phys* 2011; **128**: 83-89 [DOI: 10.1016/j.matchemphys.2011.02.039]
- 84 **Hosseini MR**, Schaffie M, Pazouki M, Darezereshki E, Ranjbar M. Biologically synthesized copper sulfide nanoparticles: Production and characterization. *Materials Science in Semiconductor Processing* 2012; **15**: 222-225 [DOI: 10.1016/j.mssp.2012.03.012]
- 85 **Lesk AM**, Chothia C. Evolution of proteins formed by  $\beta$ -sheets: II. The core of the immunoglobulin domains. *J Mol Biol* 1982; **160**: 325-342 [DOI: 10.1016/0022-2836(82)90179-6]
- 86 **Arruebo M**, Valladares M, Gonzalez-Fernandez A. Antibody-conjugated nanoparticles for biomedical applications. *J Nanomater* 2009; **2009**: 1-24 [DOI: 10.1155/2009/439389]
- 87 **Horisberger M**. Colloidal gold as a cytochemical marker in electron microscopy. *Gold Bull* 1981; **14**: 90-94 [DOI: 10.1007/BF03216735]
- 88 **Sokolov K**, Follen M, Aaron J, Pavlova I, Malpica A, Lotan R, Richards-Kortum R. Real-time vital optical imaging of precancer using anti-epidermal growth factor receptor antibodies conjugated to gold nanoparticles. *Cancer Res* 2003; **63**: 1999-2004 [PMID: 12727808]
- 89 **El-Sayed IH**, Huang X, El-Sayed MA. Surface plasmon resonance scattering and absorption of anti-EGFR antibody conjugated gold nanoparticles in cancer diagnostics: applications in oral cancer. *Nano Lett* 2005; **5**: 829-834 [PMID: 15884879 DOI: 10.1021/nl050074e]
- 90 **Popovtzer R**, Agrawal A, Kotov NA, Popovtzer A, Balter J, Carey TE, Kopelman R. Targeted gold nanoparticles enable molecular CT imaging of cancer. *Nano Lett* 2008; **8**: 4593-4596 [PMID: 19367807 DOI: 10.1021/nl8029114]
- 91 **Ankri R**, Peretz V, Motiei M, Popovtzer R, Fixler D. A new method for cancer detection based on diffusion reflection measurements of targeted gold nanorods. *Int J Nanomedicine* 2012; **7**: 449-455 [PMID: 22334777 DOI: 10.2147/IJN.S28424]
- 92 **Huang HC**, Barua S, Sharma G, Dey SK, Rege K. Inorganic nanoparticles for cancer imaging and therapy. *J Control Release* 2011; **155**: 344-357 [PMID: 21723891 DOI: 10.1016/j.jconrel.2011.06.004]
- 93 **Park C**, Youn H, Kim H, Noh T, Kook YH, Oh ET, Park HJ, Kim C. Cyclodextrin-covered gold nanoparticles for targeted delivery of an anti-cancer drug. *J Mater Chem* 2009; **19**: 2310-2315 [DOI: 10.1039/b816209c]
- 94 **Jiang W**, Kim BY, Rutka JT, Chan WC. Nanoparticle-mediated cellular response is size-dependent. *Nat Nanotechnol* 2008; **3**: 145-150 [PMID: 18654486 DOI: 10.1038/nnano.2008.30]
- 95 **Kennedy LC**, Bickford LR, Lewinski NA, Coughlin AJ, Hu Y, Day ES, West JL, Drezek RA. A new era for cancer treatment: gold-nanoparticle-mediated thermal therapies. *Small* 2011; **7**: 169-183 [PMID: 21213377 DOI: 10.1002/sml.201000134]
- 96 **Akhter S**, Ahmad MZ, Ahmad FJ, Storm G, Kok RJ. Gold nanoparticles in theranostic oncology: current state-of-the-art. *Expert Opin Drug Deliv* 2012; **9**: 1225-1243 [PMID: 22897613 DOI: 10.1517/17425247.2012.716824]
- 97 **Alkilany AM**, Thompson LB, Boulos SP, Sisco PN, Murphy CJ. Gold nanorods: their potential for photothermal therapeutics and drug delivery, tempered by the complexity of their biological interactions. *Adv Drug Deliv Rev* 2012; **64**: 190-199 [PMID: 21397647 DOI: 10.1016/j.addr.2011.03.005]
- 98 **Thanh NT**, Rees JH, Rosenzweig Z. Laser-based double beam absorption detection for aggregation immunoassays using gold nanoparticles. *Anal Bioanal Chem* 2002; **374**: 1174-1178 [PMID: 12474081 DOI: 10.1007/s00216-002-1599-x]
- 99 **Thanh NT**, Rosenzweig Z. Development of an aggregation-based immunoassay for anti-protein A using gold nanoparticles. *Anal Chem* 2002; **74**: 1624-1628 [PMID: 12033254 DOI: 10.1021/ac011127p]
- 100 **Murphy CJ**, Gole AM, Hunyadi SE, Stone JW, Sisco PN, Alkilany A, Kinard BE, Hankins P. Chemical sensing and imaging with metallic nanorods. *Chem Commun (Camb)* 2008; (5): 544-557 [PMID: 18209787 DOI: 10.1039/b711069c]
- 101 **Yuan Y**, Zhang J, Zhang H, Yang X. Silver nanoparticle based label-free colorimetric immunosensor for rapid detection of neurogenin 1. *Analyst* 2012; **137**: 496-501 [PMID: 22114758 DOI: 10.1039/C1AN15875A]
- 102 **Wang J**. Electrochemical biosensing based on noble metal nanoparticles. *Microchim Acta* 2012; **177**: 245-270 [DOI: 10.1007/s00604-011-0758-1]
- 103 **Szymanski M**, Turner APF, Porter R. Electrochemical dissolution of silver nanoparticles and its application in metalloimmunoassay. *Electroanalysis* 2010; **22**: 191-198 [DOI: 10.1002/elan.200900275]
- 104 **Hao N**, Li H, Long Y, Zhang L, Zhao X, Xu D, Chen HY. An electrochemical immunosensing method based on silver nanoparticles. *J Electroanal Chem* 2011; **656**: 50-54 [DOI: 10.1016/j.jelechem.2011.01.029]
- 105 **Duncan TV**. Applications of nanotechnology in food packaging and food safety: barrier materials, antimicrobials and

Tauran Y *et al.* Nanoparticle molecular recognition

- sensors. *J Colloid Interface Sci* 2011; **363**: 1-24 [PMID: 21824625 DOI: 10.1016/j.jcis.2011.07.017]
- 106 **Gilmartin N**, O'Kennedy R. Nanobiotechnologies for the detection and reduction of pathogens. *Enzyme Microb Technol* 2012; **50**: 87-95 [PMID: 22226193 DOI: 10.1016/j.enzmictec.2011.11.005]
- 107 **Lara HH**, Ixtepan-Turrent L, Garza Treviño EN, Singh DK. Use of silver nanoparticles increased inhibition of cell-associated HIV-1 infection by neutralizing antibodies developed against HIV-1 envelope proteins. *J Nanobiotechnology* 2011; **9**: 38 [PMID: 21923937 DOI: 10.1186/1477-3155-9-38]
- 108 **Zhang X**, Geng P, Liu H, Teng Y, Liu Y, Wang Q, Zhang W, Jin L, Jiang L. Development of an electrochemical immunoassay for rapid detection of *E. coli* using anodic stripping voltammetry based on Cu@Au nanoparticles as antibody labels. *Biosens Bioelectron* 2009; **24**: 2155-2159 [PMID: 19124236 DOI: 10.1016/j.bios.2008.11.019]
- 109 **Qu W**, Liu Y, Liu D, Wang Z, Jiang X. Copper-mediated amplification allows readout of immunoassays by the naked eye. *Angew Chem Int Ed Engl* 2011; **50**: 3442-3445 [PMID: 21387505 DOI: 10.1002/anie.201006025]
- 110 **Lehn JM**. Supramolecular chemistry. *Science* 1993; **260**: 1762-1763 [PMID: 8511582 DOI: 10.1126/science.8511582]
- 111 **Steed JW**, Atwood JL. Supramolecular Chemistry. 2nd ed. UK: John Wiley and Sons, 2009 [DOI: 10.1002/9780470740880]
- 112 **Saenger W**. Cyclodextrin inclusion compounds in research and industry. *Angew Chem Int Ed* 1980; **19**: 344-362 [DOI: 10.1002/anie.198003441]
- 113 **Atwood JL**, Davies JED, MacNicol DD, Vogtle F. Comprehensive Supramolecular Chemistry: Cyclodextrine. Vol. 3. 1st ed., Oxford: Pergamon, 1996
- 114 **Liu J**, Alvarez J, Kaifer AE. Metal nanoparticles with a knack for molecular recognition. *Adv Mater* 2000; **12**: 1381-1383 [DOI: 10.1002/1521-4095(200009)]
- 115 **Liu J**, Renliang X, Kaifer AE. In Situ modification of the surface of gold colloidal particles. Preparation of cyclodextrin-based rotaxanes supported on gold nanospheres. *Langmuir* 1998; **14**: 7337-7339 [DOI: 10.1021/la981385q]
- 116 **Liu J**, Ong W, Roman E, Lynn MJ, Kaifer AE. Cyclodextrin-modified gold nanospheres. *Langmuir* 2000; **16**: 3000-3002 [DOI: 10.1021/la991519f]
- 117 **Liu J**, Alvarez J, Ong W, Kaifer AE. Network aggregates formed by C60 and gold nanoparticles capped with gamma-Cyclodextrin hosts. *Nano Lett* 2001; **1**: 57-60 [DOI: 10.1021/nl0001813]
- 118 **Liu Z**, Jiang M. Reversible aggregation of gold nanoparticles driven by inclusion complexation. *J Mater Chem* 2007; **17**: 4249-4254 [DOI: 10.1039/B707910A]
- 119 **Chen Z**, Li J, Zhang X, Wu Z, Zhang H, Sun H, Yang B. Construction of nanoparticle superstructures on the basis of host-guest interaction to achieve performance integration and modulation. *Phys Chem Chem Phys* 2012; **14**: 6119-6125 [PMID: 22441168 DOI: 10.1039/c2cp40377c]
- 120 **Wei K**, Li J, Liu J, Chen G, Jiang M. Reversible vesicles of supramolecular hybrid nanoparticles. *Soft Matter* 2012; **8**: 3300-3303 [DOI: 10.1039/C2SM25178G]
- 121 **Li X**, Qi Z, Liang K, Bai X, Xu J, Liu J, Shen J. An artificial supramolecular nanozyme based on b-Cyclodextrin-modified gold nanoparticles. *Catal Letters* 2008; **124**: 413-417 [DOI: 10.1007/s10562-008-9494-5]
- 122 **Ng CHB**, Yang J, Fan WY. Synthesis and self-assembly of One-dimensional sub-10 nm Ag nanoparticles with cyclodextrin. *J Phys Chem C* 2008; **112**: 4141-4145 [DOI: 10.1021/jp710553c]
- 123 **Hebeish A**, El-Shafei A, Sharaf S, Zaghoul S. Novel precursors for green synthesis and application of silver nanoparticles in the realm of cotton finishing. *Carbohydr Polym* 2011; **84**: 605-613 [DOI: 10.1016/j.carbpol.2010.12.032]
- 124 **Jaiswal S**, Duffy B, Jaiswal AK, Stobie N, McHale P. Enhancement of the antibacterial properties of silver nanoparticles using beta-cyclodextrin as a capping agent. *Int J Antimicrob Agents* 2010; **36**: 280-283 [PMID: 20580208 DOI: 10.1016/j.ijantimicag.2010.05.006]
- 125 **Wang S**, Bai J, Li C, Zhang Y, Zhang J. Ag nanoparticle-embedded one-dimensional  $\beta$ -CD/PVP composite nanofibers prepared via electrospinning for use in antibacterial material. *Colloid Polym Sci* 2012; **290**: 667-672 [DOI: 10.1007/s00396-011-2581-y]
- 126 **Xie Y**, Wang X, Han X, Xue X, Ji W, Qi Z, Liu J, Zhao B, Ozaki Y. Sensing of polycyclic aromatic hydrocarbons with cyclodextrin inclusion complexes on silver nanoparticles by surface-enhanced Raman scattering. *Analyst* 2010; **135**: 1389-1394 [PMID: 20405060 DOI: 10.1039/c0an00076k]
- 127 **Chen X**, Parker SG, Zou G, Su W, Zhang Q.  $\beta$ -cyclodextrin-functionalized silver nanoparticles for the naked eye detection of aromatic isomers. *ACS Nano* 2010; **4**: 6387-6394 [PMID: 20973513 DOI: 10.1021/nn1016605]
- 128 **Xu JZ**, Xu S, Geng J, Li GX, Zhu JJ. The fabrication of hollow spherical copper sulfide nanoparticle assemblies with 2-hydroxypropyl-beta-cyclodextrin as a template under sonication. *Ultrason Sonochem* 2006; **13**: 451-454 [PMID: 16288896 DOI: 10.1016/j.ultsonch.2005.09.003]
- 129 **Premkumar T**, Geckeler KE. A green approach to fabricate CuO nanoparticles. *J Phys Chem Solids* 2006; **67**: 1451-1456 [DOI: 10.1016/j.jpcs.2006.01.122]
- 130 **Coleman AW**, Jebors S, Cecillon S, Perret P, Garin D, Marti-Battle D, Moulin M. Toxicity and biodistribution of para-sulfonato-calix[4]arene in mice. *New J Chem* 2008; **32**: 780-782 [DOI: 10.1039/B718962A]
- 131 **Perret F**, Coleman AW. Biochemistry of anionic calix[n]arenes. *Chem Commun (Camb)* 2011; **47**: 7303-7319 [PMID: 21552631 DOI: 10.1039/c1cc11541c]
- 132 **Danylyuk O**, Suwinska K. Solid-state interactions of calixarenes with biorelevant molecules. *Chem Commun (Camb)* 2009; (39): 5799-5813 [PMID: 19787105 DOI: 10.1039/b910331g]
- 133 **Acharya A**, Samanta K, Pulla Rao C. Conjugates of calixarenes emerging as molecular entities of nanoscience. *Coord Chem Rev* 2012; **256**: 2096-2125 [DOI: 10.1016/j.ccr.2012.05.018]
- 134 **Kim HJ**, Lee MH, Mutihac L, Vicens J, Kim JS. Host-guest sensing by calixarenes on the surfaces. *Chem Soc Rev* 2012; **41**: 1173-1190 [PMID: 21870018 DOI: 10.1039/c1cs15169j]
- 135 **Tshikhudo TR**, Demuru D, Wang Z, Brust M, Secchi A, Arduini A, Pochini A. Molecular recognition by calix[4]arene-modified gold nanoparticles in aqueous solution. *Angew Chem Int Ed Engl* 2005; **44**: 2913-2916 [PMID: 15818630 DOI: 10.1002/anie.200462909]
- 136 **Arduini A**, Demuru D, Pochini A, Secchi A. Recognition of quaternary ammonium cations by calix[4]arene derivatives supported on gold nanoparticles. *Chem Commun (Camb)* 2005; (5): 645-647 [PMID: 15672164 DOI: 10.1039/b411883a]
- 137 **Patel G**, Menon S. Recognition of lysine, arginine and histidine by novel p-sulfonatocalix[4]arene thiol functionalized gold nanoparticles in aqueous solution. *Chem Commun (Camb)* 2009; (24): 3563-3565 [PMID: 19521608 DOI: 10.1039/B905141D]
- 138 **Han C**, Zeng L, Li H, Xie G. Colorimetric detection of pollutant aromatic amines isomers with p-sulfonatocalix[6]arene-modified gold nanoparticles. *Sens Actuators B Chem* 2009; **137**: 704-709 [DOI: 10.1016/j.snb.2008.12.038]
- 139 **Yan H**, Luo J, Xie HM, Xie DX, Su Q, Yin J, Wanjala BN, Diao H, An DL, Zhong CJ. Cationic recognition by tert-butylcalix[4]arene-functionalized nanoproboscopes. *Phys Chem Chem Phys* 2011; **13**: 5824-5830 [PMID: 21327207 DOI: 10.1039/c0cp02658a]
- 140 **Pandya A**, Joshi KV, Modi NR, Menon SK. Rapid colorimetric detection of sulfide using calix[4]arene modified gold nanoparticles as a probe. *Sens Actuators B Chem* 2012; **168**: 54-

- 61 [DOI: 10.1016/j.snb.2012.01.023]
- 141 **Guerrini L**, Garcia-Ramos JV, Domingo C, Sanchez-Cortes S. Functionalization of Ag nanoparticles with dithiocarbamate calix[4]arene as an effective supramolecular host for the surface-enhanced Raman scattering detection of polycyclic aromatic hydrocarbons. *Langmuir* 2006; **22**: 10924-10926 [PMID: 17154566 DOI: 10.1021/la062266a]
  - 142 **Chen M**, Ding W, Kong Y, Diao G. Conversion of the surface property of oleic acid stabilized silver nanoparticles from hydrophobic to hydrophilic based on host-guest binding interaction. *Langmuir* 2008; **24**: 3471-3478 [PMID: 18278970 DOI: 10.1021/la704020j]
  - 143 **Hartlieb KJ**, Saunders M, Raston CL. Templating silver nanoparticle growth using phosphonated calixarenes. *Chem Commun (Camb)* 2009; (21): 3074-3076 [PMID: 19462091 DOI: 10.1039/B823067F]
  - 144 **Hartlieb KJ**, Martin AD, Saunders M, Raston CL. Photochemical generation of small silver nanoparticles involving multi-functional phosphonated calixarenes. *New J Chem* 2010; **34**: 1834-1837 [DOI: 10.1039/C0NJ00356E]
  - 145 **Xiong D**, Chen M, Li H. Synthesis of para-sulfonatocalix[4]arene-modified silver nanoparticles as colorimetric histidine probes. *Chem Commun (Camb)* 2008; (7): 880-882 [PMID: 18253535 DOI: 10.1039/b716270g]
  - 146 **Bian Y**, Li C, Li H. para-Sulfonatocalix[6]arene-modified silver nanoparticles electrodeposited on glassy carbon electrode: preparation and electrochemical sensing of methyl parathion. *Talanta* 2010; **81**: 1028-1033 [PMID: 20298889 DOI: 10.1016/j.talanta.2010.01.054]
  - 147 **Tauran Y**, Grosso M, Brioude A, Kassab R, Coleman AW. Colourimetric and spectroscopic discrimination between nucleotides and nucleosides using para-sulfonato-calix[4]arene capped silver nanoparticles. *Chem Commun (Camb)* 2011; **47**: 10013-10015 [PMID: 21833429 DOI: 10.1039/C1CC13175C]
  - 148 **Tauran Y**, Rhimi M, Ueno R, Grosso M, Brioude A, Janneau E, Suwinska K, Kassab R, Shahgaldian P, Cumbo A, Fenet B, Kim BJ, Coleman AW. Cytosine: para-sulfonatocalix[4]arene assemblies: in solution, in the solid-state and on the surface of hybrid silver nanoparticles. *J Incl Phenom Macrocycl Chem* 2012 [DOI: 10.1007/s10847-012-0235-4]
  - 149 **Perret F**, Tauran Y, Suwinska K, Kim BJ, Chassain-Nely C, Boulet M, Coleman AW. Molecular recognition and transport of active pharmaceutical ingredients on anionic calix[4]arene capped silver nanoparticles. *J Chem* 2013; **2013**: 1-9 [DOI: 10.1155/2013/191828]
  - 150 **Tauran Y**, Brioude A, Shahgaldian P, Cumbo A, Kim B, Perret F, Coleman AW, Montasser I. Calix-arene silver nanoparticles interactions with surfactants are charge, size and critical micellar concentration dependent. *Chem Commun (Camb)* 2012; **48**: 9483-9485 [PMID: 22899213 DOI: 10.1039/c2cc34670b]
  - 151 **Chen M**, Diao G, Zhou X. Formation of nanospheres of cuprous oxide with a bridge linker of p-sulfonated calix[8]arene host. *Nanotechnology* 2007; **18**: 1-10 [DOI: 10.1088/0957-4484/18/27/275606]
  - 152 **Nanjwade BK**, Bechra HM, Derkar GK, Manvi FV, Nanjwade VK. Dendrimers: emerging polymers for drug-delivery systems. *Eur J Pharm Sci* 2009; **38**: 185-196 [PMID: 19646528 DOI: 10.1016/j.ejps.2009.07.008]
  - 153 **Bronstein LM**, Shifrina ZB. Dendrimers as encapsulating, stabilizing, or directing agents for inorganic nanoparticles. *Chem Rev* 2011; **111**: 5301-5344 [PMID: 21718045 DOI: 10.1021/cr2000724]
  - 154 **Chechik V**, Crooks RM. Monolayers of thiol-terminated dendrimers on the surface of planar and colloidal gold. *Langmuir* 1999; **15**: 6364-6369 [DOI: 10.1021/la9817314]
  - 155 **Crooks RM**, Zhao M, Sun L, Chechik V, Yeung LK. Dendrimer-encapsulated metal nanoparticles: synthesis, characterization, and applications to catalysis. *Acc Chem Res* 2001; **34**: 181-190 [PMID: 11263876 DOI: 10.1021/ar000110a]
  - 156 **Lu W**, Shang J. A resonance light-scattering (RLS) serving for various quantitative events since 1995: a comment proposed towards how to apprehend well the meaning of RLS and its corresponding guiding role. *Spectrochim Acta A Mol Biomol Spectrosc* 2009; **74**: 285-291 [PMID: 19648054 DOI: 10.1016/j.saa.2009.06.058]
  - 157 **Liu Z**, Luo L, Dong Y, Weng G, Li J. Resonance scattering amplification assay of biomolecules based on the biomimicrization of gold nanoparticles bioconjugates. *J Colloid Interface Sci* 2011; **363**: 182-186 [PMID: 21851949 DOI: 10.1016/j.jcis.2011.07.073]
  - 158 **Shi X**, Wang SH, Van Antwerp ME, Chen X, Baker JR. Targeting and detecting cancer cells using spontaneously formed multifunctional dendrimer-stabilized gold nanoparticles. *Analyst* 2009; **134**: 1373-1379 [PMID: 19562204 DOI: 10.1039/b902199j]
  - 159 **Wang R**, Yang J, Zheng Z, Carducci MD, Jiao J, Seraphin S. Dendron-Controlled Nucleation and Growth of Gold Nanoparticles We thank the University of Arizona and the Research Corporation for financial support. Acknowledgement is also made to the donors of the Petroleum Research Fund, administered by the American Chemical Society, for partial support of this research. The X-ray diffractometer was purchased with support from the U.S. National Science Foundation (CHEM-9610374). We thank Dr. K. Nebesny for help with the XPS experiments. *Angew Chem Int Ed Engl* 2001; **40**: 549-552 [PMID: 11180366 DOI: 10.1002/1521-3773(20010202)]
  - 160 **Astruc D**, Daniel MC, Ruiz J. Dendrimers and gold nanoparticles as exo-receptors sensing biologically important anions. *Chem Commun (Camb)* 2004; (23): 2637-2649 [PMID: 15568050 DOI: 10.1039/B410399H]
  - 161 **Daniel MC**, Ruiz J, Nlate S, Blais JC, Astruc D. Nanoscopic assemblies between supramolecular redox active metallo-dendrons and gold nanoparticles: synthesis, characterization, and selective recognition of H<sub>2</sub>PO<sub>4</sub><sup>-</sup>, HSO<sub>4</sub><sup>-</sup>, and adenosine-5'-triphosphate (ATP<sup>2-</sup>) anions. *J Am Chem Soc* 2003; **125**: 2617-2628 [PMID: 12603150 DOI: 10.1021/ja021325d]
  - 162 **Castonguay A**, Kakkar AK. Dendrimer templated construction of silver nanoparticles. *Adv Colloid Interface Sci* 2010; **160**: 76-87 [PMID: 20708163 DOI: 10.1016/j.cis.2010.07.006]
  - 163 **Balogh L**, Swanson DR, Tomalia DA, Hagnauer GL, McManus AT. Dendrimer-silver complexes and nanocomposites as antimicrobial agents. *Nano Letters* 2001; **1**: 18-21 [DOI: 10.1021/nl005502p]
  - 164 **Lesniak W**, Bielinska AU, Sun K, Janczak KW, Shi X, Baker JR, Balogh LP. Silver/dendrimer nanocomposites as biomarkers: fabrication, characterization, in vitro toxicity, and intracellular detection. *Nano Lett* 2005; **5**: 2123-2130 [PMID: 16277438 DOI: 10.1021/nl051077u]
  - 165 **Stofik M**, Stryhal Z, Malý J. Dendrimer-encapsulated silver nanoparticles as a novel electrochemical label for sensitive immunosensors. *Biosens Bioelectron* 2009; **24**: 1918-1923 [PMID: 19022648 DOI: 10.1016/j.bios.2008.09.028]
  - 166 **Esumi K**, Isono R, Yoshimura T. Preparation of PAMAM and PPI-metal (silver, platinum, and palladium) nanocomposites and their catalytic activities for reduction of 4-nitrophenol. *Langmuir* 2004; **20**: 237-243 [PMID: 15745027 DOI: 10.1021/la035440t]
  - 167 **Manna A**, Imae T, Aoi K, Okada M, Yogo T. Synthesis of dendrimer-passivated noble metal nanoparticles in a polar medium: comparison of size between silver and gold particles. *Chem Mater* 2001; **13**: 1674-1681 [DOI: 10.1021/cm000416b]
  - 168 **Li L**, Cao X, Yu F, Yao Z, Xie Y. G1 dendrimers-mediated evolution of silver nanostructures from nanoparticles to solid spheres. *J Colloid Interface Sci* 2003; **261**: 366-371 [PMID: 16256543 DOI: 10.1016/S0021-9797(03)00122-X]
  - 169 **Wei X**, Zhu B, Xu Y. Preparation and stability of copper

Tauran Y *et al.* Nanoparticle molecular recognition

- particles formed using the template of hyperbranched poly(amine-ester). *Colloid Polym Sci* 2005; **284**: 102-107 [DOI: 10.1007/s00396-005-1344-z]
- 170 **Berchmans S**, Vergeheese TM, Kavitha AL, Veerakumar M, Yegnaraman V. Electrochemical preparation of copper-dendrimer nanocomposites: picomolar detection of Cu<sup>2+</sup> ions. *Anal Bioanal Chem* 2008; **390**: 939-946 [PMID: 18004548 DOI: 10.1007/s00216-007-1723-z]
- 171 **Moore E**, McInnes SJ, Vogt A, Voelcker NH. Rapid aqueous 'click chemistry' using Cu(I)-loaded dendrimers as macromolecular catalysts. *Tetrahedron Lett* 2011; **52**: 2327-2329 [DOI: 10.1016/j.tetlet.2011.02.090]
- 172 **Huang B**, Kukowska-Latalo JF, Tang S, Zong H, Johnson KB, Desai A, Gordon CL, Leroueil PR, Baker JR. The facile synthesis of multifunctional PAMAM dendrimer conjugates through copper-free click chemistry. *Bioorg Med Chem Lett* 2012; **22**: 3152-3156 [PMID: 22480432 DOI: 10.1016/j.bmcl.2012.03.052]
- 173 **Kralj M**, Tusek-Bozić L, Frkanec L. Biomedical potentials of crown ethers: prospective antitumor agents. *ChemMedChem* 2008; **3**: 1478-1492 [PMID: 18683175 DOI: 10.1002/cmdc.200800118]
- 174 **Patel G**, Kumar A, Pal U, Menon S. Potassium ion recognition by facile dithiocarbamate assembly of benzo-15-crown-5-gold nanoparticles. *Chem Commun (Camb)* 2009; (14): 1849-1851 [PMID: 19319422 DOI: 10.1039/b822734a]
- 175 **Ho ML**, Hsieh JM, Lai CW, Peng HC, Kang CC, Wu IC, Lai CH, Chen YC, Chou PT. 15-Crown-5 Functionalized Au nanoparticles synthesized via single molecule exchange on silica nanoparticles: Its application to probe 15-crown-5/K<sup>+</sup>/15-crown-5 "sandwiches" as linking mechanisms. *J Phys Chem C* 2009; **113**: 1686-1693 [DOI:10.1021/jp807256h]
- 176 **Velu R**, Ramakrishnan VT, Ramamurthy P. Colorimetric and fluorometric chemosensors for selective signaling toward Ca<sup>2+</sup> and Mg<sup>2+</sup> by aza-crown ether acridinedione-functionalized gold nanoparticles. *Tetrahedron Lett* 2010; **51**: 4331-4335 [DOI: 10.1016/j.tetlet.2010.06.041]
- 177 **Li H**, Zhang L, Yao Y, Han C, Jin S. Synthesis of aza-crown ether-modified silver nanoparticles as colorimetric sensors for Ba<sup>2+</sup>. *Supramol Chem* 2010; **22**: 544-547 [DOI: 10.1080/10610278.2010.497209]
- 178 **Kuang H**, Chen W, Yan W, Xu L, Zhu Y, Liu L, Chu H, Peng C, Wang L, Kotov NA, Xu C. Crown ether assembly of gold nanoparticles: melamine sensor. *Biosens Bioelectron* 2011; **26**: 2032-2037 [PMID: 20884195 DOI: 10.1016/j.bios.2010.08.081]
- 179 **Premkumar T**, Lee Y, Geckeler KE. Macrocycles as a tool: a facile and one-pot synthesis of silver nanoparticles using cucurbituril designed for cancer therapeutics. *Chemistry* 2010; **16**: 11563-11566 [PMID: 20803582 DOI: 10.1002/chem.201001325]
- 180 **Lu X**, Masson E. Formation and Stabilization of Silver Nanoparticles with Cucurbit[n]urils (n = 5-8) and Cucurbituril-Based Pseudorotaxanes in Aqueous Medium. *Langmuir* 2011 Feb 15; Epub ahead of print [PMID: 21322592 DOI: 10.1021/la104729j]
- 181 **Klien K**, Godnić-Cvar J. Genotoxicity of metal nanoparticles: focus on in vivo studies. *Arh Hig Rada Toksikol* 2012; **63**: 133-145 [PMID: 22728795 DOI: 10.2478/10004-1254-63-2012-2213]
- 182 **Elsaesser A**, Howard CV. Toxicology of nanoparticles. *Adv Drug Deliv Rev* 2012; **64**: 129-137 [PMID: 21925220 DOI: 10.1016/j.addr.2011.09.001]
- 183 **Ray PC**, Yu H, Fu PP. Toxicity and environmental risks of nanomaterials: challenges and future needs. *J Environ Sci Health C Environ Carcinog Ecotoxicol Rev* 2009; **27**: 1-35 [PMID: 19204862 DOI: 10.1080/10590500802708267]
- 184 **Auffan M**, Rose J, Wiesner MR, Bottero JY. Chemical stability of metallic nanoparticles: a parameter controlling their potential cellular toxicity in vitro. *Environ Pollut* 2009; **157**: 1127-1133 [PMID: 19013699 DOI: 10.1016/j.envpol.2008.10.002]
- 185 **Oberdörster G**, Oberdörster E, Oberdörster J. Nanotoxicology: an emerging discipline evolving from studies of ultrafine particles. *Environ Health Perspect* 2005; **113**: 823-839 [PMID: 16002369 DOI: 10.1289/ehp.7339]
- 186 **Fadeel B**, Garcia-Bennett AE. Better safe than sorry: Understanding the toxicological properties of inorganic nanoparticles manufactured for biomedical applications. *Adv Drug Deliv Rev* 2010; **62**: 362-374 [PMID: 19900497 DOI: 10.1016/j.addr.2009.11.008]
- 187 **Lewinski N**, Colvin V, Drezek R. Cytotoxicity of nanoparticles. *Small* 2008; **4**: 26-49 [PMID: 18165959 DOI: 10.1002/smll.200700595]
- 188 **Papasanani MR**, Wang G, Hill RA. Gold nanoparticles: the importance of physiological principles to devise strategies for targeted drug delivery. *Nanomedicine* 2012; **8**: 804-814 [PMID: 22306155]
- 189 **Murphy CJ**, Gole AM, Stone JW, Sisco PN, Alkilany AM, Goldsmith EC, Baxter SC. Gold nanoparticles in biology: beyond toxicity to cellular imaging. *Acc Chem Res* 2008; **41**: 1721-1730 [PMID: 18712884 DOI: 10.1021/ar800035u]
- 190 **Patra HK**, Banerjee S, Chaudhuri U, Lahiri P, Dasgupta AK. Cell selective response to gold nanoparticles. *Nanomedicine* 2012; **8**: 897-900 [DOI: 10.1016/j.nano.2012.01.008]
- 191 **Goodman CM**, McCusker CD, Yilmaz T, Rotello VM. Toxicity of gold nanoparticles functionalized with cationic and anionic side chains. *Bioconjug Chem* 2004; **15**: 897-900 [PMID: 15264879 DOI: 10.1021/bc049951i]
- 192 **Chithrani BD**, Ghazani AA, Chan WC. Determining the size and shape dependence of gold nanoparticle uptake into mammalian cells. *Nano Lett* 2006; **6**: 662-668 [PMID: 16608261 DOI: 10.1021/nl052396o]
- 193 **Dykman LA**, Khlebtsov NG. Gold nanoparticles in biology and medicine: recent advances and prospects. *Acta Naturae* 2011; **3**: 34-55 [PMID: 22649683]
- 194 **Uygur F**, Oncül O, Evinç R, Diktas H, Acar A, Ulkür E. Effects of three different topical antibacterial dressings on *Acinetobacter baumannii*-contaminated full-thickness burns in rats. *Burns* 2009; **35**: 270-273 [PMID: 18789593 DOI: 10.1016/j.burns.2008.05.020]
- 195 **Yıldırım L**, Thanh NT, Loizidou M, Seifalian AM. Toxicology and clinical potential of nanoparticles. *Nano Today* 2011; **6**: 585-607 [PMID: 23293661 DOI: 10.1016/j.nantod.2011.10.001]
- 196 **Chernousova S**, Epple M. Silver as antibacterial agent: ion, nanoparticle, and metal. *Angew Chem Int Ed Engl* 2013; **52**: 1636-1653 [PMID: 23255416 DOI: 10.1002/anie.201205923]
- 197 **Ahamed M**, Alsalhi MS, Siddiqui MK. Silver nanoparticle applications and human health. *Clin Chim Acta* 2010; **411**: 1841-1848 [PMID: 20719239 DOI: 10.1016/j.cca.2010.08.016]
- 198 **Hsin YH**, Chen CF, Huang S, Shih TS, Lai PS, Chueh PJ. The apoptotic effect of nanosilver is mediated by a ROS- and JNK-dependent mechanism involving the mitochondrial pathway in NIH3T3 cells. *Toxicol Lett* 2008; **179**: 130-139 [PMID: 18547751 DOI: 10.1016/j.toxlet.2008.04.015]
- 199 **Fung MC**, Bowen DL. Silver products for medical indications: risk-benefit assessment. *J Toxicol Clin Toxicol* 1996; **34**: 119-126 [PMID: 8632503 DOI: 10.3109/15563659609020246]
- 200 **Wong KKY**, Liu X. Silver nanoparticles-the real "silver bullet" in clinical medicine. *Med Chem Commun* 2010; **1**: 125-131 [DOI: 10.1039/c0md00069h]
- 201 **Kim YS**, Kim KK, Shin S, Park SM, Hah SS. Comparative toxicity studies of ultra-pure Ag, Au, Co, and Cu nanoparticles generated by Laser Ablation in biocompatible aqueous solution. *Bul Korean Chem Soc* 2012; **33**: 3265-3268 [DOI: 10.5012/bkcs.2012.33.10.3265]
- 202 **Ullmann M**, Friedlander SK, Schmidt-Ott A. Nanoparticle formation by laser ablation. *J Nanopart Res* 2002; **4**: 499-509 [DOI: 10.1023/A:1022840924336]
- 203 **Valodkar M**, Rathore PS, Jadeja RN, Thounaojam M,

Tauran Y *et al.* Nanoparticle molecular recognition

- Devkar RV, Thakore S. Cytotoxicity evaluation and antimicrobial studies of starch capped water soluble copper nanoparticles. *J Hazard Mater* 2012; **201-202**: 244-249 [PMID: 22178277 DOI: 10.1016/j.jhazmat.2011.11.077]
- 204 **Ma Z**, Wu J, Zhou T, Chen Z, Dong Y, Tang J, Sui SF. Detection of human lung carcinoma cell using quartz crystal microbalance amplified by enlarging Au nanoparticles in vitro. *New J Chem* 2002; **26**: 1795-1798 [DOI: 10.1039/b206248h]
- 205 **Sylvestre JP**, Kabashin AV, Sacher E, Meunier M, Luong JH. Stabilization and size control of gold nanoparticles during laser ablation in aqueous cyclodextrins. *J Am Chem Soc* 2004; **126**: 7176-7177 [PMID: 15186145 DOI: 10.1021/ja048678s]
- 206 **Biji P**, Patnaik A. Novel crown ether-capped cationic gold nanoclusters in an aqueous medium and their single-electron charging features. *Langmuir* 2007; **23**: 12048-12054 [PMID: 17918974 DOI: 10.1021/la701636h]
- 207 **Yeh CH**, Chen WT, Lin HP, Chang TC, Lin YC. Development of an immunoassay based on impedance measurements utilizing an antibody-nanosilver probe, silver enhancement, and electro-microchip. *Sens Actuators B Chem* 2009; **139**: 387-393 [DOI: 10.1016/j.snb.2009.03.029]
- 208 **Yang Y**, Liu S, Kimura K. Cyclodextrin as a capturing agent for redundant surfactants on Ag nanoparticle surface in phase transfer process. *Colloids Surf A Physicochem Eng Asp* 2006; **290**: 143-149 [DOI: 10.1016/j.colsurfa.2006.05.016]

**P- Reviewer** Tanaka T **S- Editor** Wen LL **L- Editor** A  
**E- Editor** Yan JL





Part A

Section 4

Bio-applications of calix[n]arene  
capped silver nanoparticles



## Bio-applications of calix[n]arene capped silver nanoparticles

Yannick Tauran\*<sup>1,2</sup>, Beomjoon Kim<sup>2,3</sup> Anthony W. Coleman FRSC\*<sup>1</sup>

- 1 LMI CNRS UMR 5615, Université Lyon 1, Villeurbanne, F69622, France.
- 2 LIMMS/CNRS-IIS (UMI 2820), University of Tokyo, Tokyo, Japan
- 3 CIRMM, Institute of Industrial Science, University of Tokyo, Tokyo, Japan.

\*Authors for correspondance :

Phone : +33 4 4243 1027

E-mail: anthony.coleman@univ-lyon1.fr

E-mail : yannick.tauran@univ-lyon1.fr

### Keywords

Calix[n]arenes – Silver nanoparticles – Biomolecules – Optical biosensors – Therapeutically agents – Antibacterial – Antiviral – Reactive Oxygen Species

### Summary

During the 10 last years, there has been a growing interest in calix[n]arene capped silver nanoparticles for their uses in biosensing and much more recently for their intrinsic therapeutic properties. Cost effective, portable and ultra-sensitive analytical tools are one of the major expectations of silver nanoparticles capped with calix[n]arenes. Their uses for detecting a wide range of hazardous molecules and biological compounds by different physical approaches (optical or electrical) are reviewed in depth here. A second part deals with their biological activities. These hybrid nanoparticles have been shown to possess antibacterial properties, and to reach antiviral and anti-cancer targets.

## 1. Introduction

The calix[n]arenes represent one of the major classes among the supramolecular family [Steed\_2009] with regard to their popularity in academic research. These macrocyclic molecules consist of  $n$  phenolic units linked to each other by methylene bridges (Figure 1A).

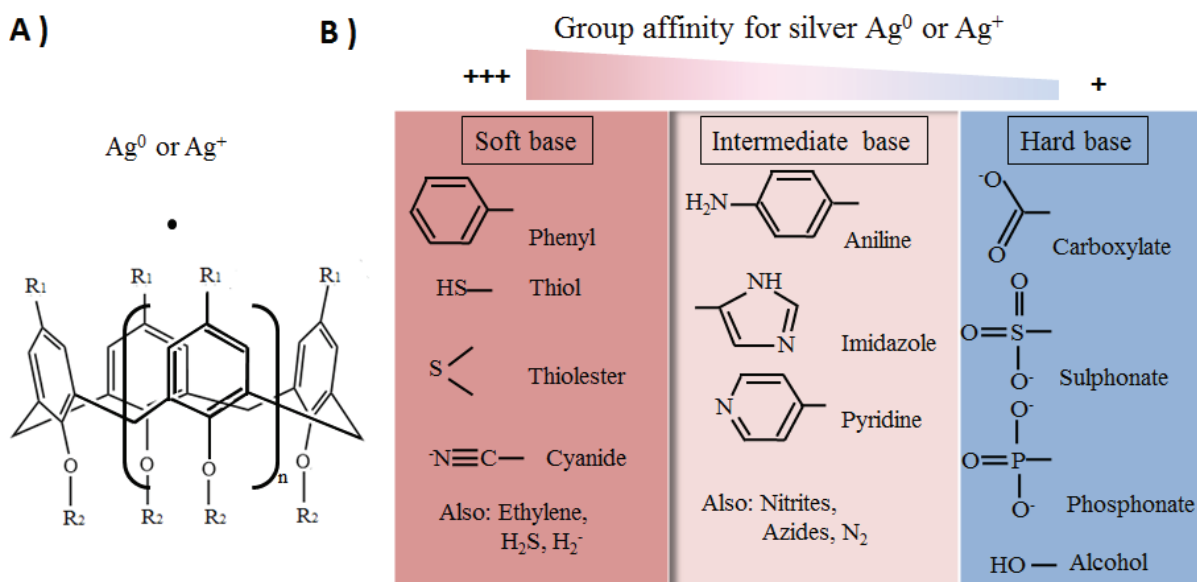


**Figure 1-** A) General structure of calix[n]arene and silver.  $\text{R}_1$  and  $\text{R}_2$  represent respectively functional groups at upper and lower rim and  $n$  corresponds to the number of phenolic unit B) Argentophilic level of various functional groups according to the hard soft acid base theory. Soft acid silver  $\text{Ag}^+$  or  $\text{Ag}^0$  reacts more strongly with soft base (in red) than hard base (in blue) [Lemire *et al.*, 2013].

When  $n$  is four or five the molecules are bucket shaped but conformationally mobile and can act as hosts for capturing small molecular guests in their cavities by non-covalent bonds [Gutsche\_2008]. For the calix[n]arenes where  $n$  is 6 or greater, a large number of possible conformations exist and various geometries for complexation exist. This ability to endo-complex has been described for a wide range of biomolecules such nucleic acids, amino acids or Active Pharmaceutical Ingredients (API) [Perret *et al.*, 2006]. Exo-complexation is also well known with regard to various bio-macromolecules including peptides, oligo-nucleotides, DNA and proteins [McGovern *et al.*, 2012]. As a consequence, their biochemical properties have been extensively studied *in vitro* for various applications. They have been shown to be protein stabilisers, transporters of API, intrinsic APIs, metabolic agents and can act as biomolecular recognition agents for sensing [Coleman *et al.*, 2007a]. A particular interest in therapeutic applications has grown dramatically with the development of water soluble and non-toxic anionic calix[n]arenes [Perret *et al.*, 2011][Shinkai *et al.*, 1984]. Haemotoxicity is a critical element in the evaluation of side effects of drugs. The index to evaluate the haemotoxicity is  $\text{EH}_{50}$  corresponding to the concentration of compound that kill 50% of blood cell. However, sometimes it is not possible to reach 50% ratio of cellular death, in that case the haemolytic activity is expressed as % of cellular death at a specific concentration.

Anionic and amphiphilic calix[n]arene derivatives show very low haemotoxicity with regard to human blood erythrocytes with up to 200mM for *para*-sulphonate calix[n]arene derivatives (See table1) [DaSilva *et al.*, 2004] [Shahgaldian *et al.*, 2003]. On the other hand, cationic calix[n]arene derivatives, *para*-tetra (trimethylammonioethyloxymethyl) tetra(propoxy)calix[4]arene and *para*-tetra-(trimethylammonioethyloxymethyl) tetra(propoxy)calix[4]arene, have shown to possess hemotoxic activity with an EH<sub>50</sub> superior or equal to 50 μM. Only *para*-tetra (trimethylammoniomethyl) tetra(propoxy)calix[4]arene, has shown an EH<sub>50</sub> superior to 100 μM [Ukhatskaya *et al.*, 2013]. Moreover, *para*-sulphonato-calix[4]arene has shown low toxicity *in vivo* when administrated to mice [Coleman *et al.*, 2008]. The same calix[4]arene has been also used as *in vivo* de-toxifying agents against paraquat [Wang *et al.*, 2009]. Calix[n]arene derivatives have also been demonstrated as antibacterial, anti-coagulant, antiviral and antifungal agents [Perret *et al.*, 2013a]. Our group has recently reviewed the biological activity of calix[n]arene in cellular bio assays and *in vivo* [Tauran *et al.*, 2014a]. As an example illustrating the activity of calix[n]arene over the animal cell growth, calix[4]arene-O-diphosphorus acid derivatives have shown to possess a higher toxicity toward cancer cell lines growth compared to normal blood cells, thus possessing a large pharmaceutical window [Coleman *et al.*, 2007b].

**Table 1** – Haemolytic activity of various calix[n]arenes

Reference	Calixarene	Ion	Hemotoxicity (% of hemolysis at a specific concentration)
[Ukhatskaya <i>et al.</i> , 2013]	<i>para</i> -tetra (trimethylammonioethyloxymethyl) tetrapropoxycalix[4]arene	Cationic	60% at 50μM
	<i>para</i> -tetra (trimethylammonioethyloxymethyl) tetraoctoxycalix[4]arene		70% at 50μM
	<i>para</i> -tetra (trimethylammoniomethyl) tetrapropoxycalix[4]arene		1.1% at 100μM
[Shahgaldian <i>et al.</i> , 2003]	tetra(hexanoyl)-calix[4]arene	Neutral	0 % at 183μM
	tetra(octanoyl)-calix[4]arene		0.5 % at 48μM
	tetra(decanoyl)-calix[4]arene		0 % at 144μM
	tetra(dodecanoyl)-calix[4]arene		0 % at 130μM
	tetra(dodecanoyl) di(diethylphosphoriloxy)-calix[4]arene	Anionic	0.25 % at 700μM
	tetra(dodecanoyl) di(dihydroxyphosphoriloxy)-calix[4]arene		1.8 % at 38μM
[Da Silva <i>et al.</i> , 2004]	<i>para</i> -tetra(sulphonato)-calix[4]arene	Anionic	0.6% at 200mM
	<i>para</i> -hexa(sulphonato)-calix[6]arene		8% at 200mM
	<i>para</i> -octa(sulphonato)-calix[8]arene		31% at 200mM
	<i>para</i> -tetra(sulphonato) di(methoxycarboxylate)calix[4]arene		0.1% at 200mM

<i>para</i> -hexa(sulphonato)tri(methoxycarboxylate)calix[4]arene		3% at 200mM
<i>para</i> -octa(sulphonato)tetra(methoxycarboxylate)calix[4]arene		20% at 200mM
<i>para</i> -tetra(sulphonato)di(ethoxyamido)calix[4]arene	Neutral	0.8% at 200mM
<i>para</i> -hexa(sulphonato)tri(ethoxyamido)calix[4]arene		2% at 200mM
<i>para</i> -octa(sulphonato)tetra(ethoxyamido)calix[4]arene		5% at 200mM
<i>para</i> -tetra(sulphonato)di(ethoxyamino)calix[4]arene		1% at 200mM
<i>para</i> -hexa(sulphonato)tri(ethoxyamino)calix[4]arene		12% at 200mM
<i>para</i> -octa(sulphonato)tetra(ethoxyamino)calix[4]arene		16% at 200mM

The complexation of *para*-di(tert-butyl) tetra(ethylester)-calix[4]arene *exo*-annularly (bridged at *para* face in alternate conformation by an octane) and silver ions was first described by Bohmer in 1992 [Arnaud-Neu *et al.*, 1992]. Their affinity is well described by the hard-soft acid base theory. This theory is an empirically derived chemical theory that explains how organic and inorganic compound react [Pearson *et al.*, 1963]. Hard acids and bases have a smaller ionic radius, a high oxidation state and weak polarizability. By contrast, soft acids tend to have a large ionic radius, a low oxidation state and strong polarizability [Lemire *et al.*, 2013]. In accord with this theory (Figure 1B), the functionalizing of calix[n]arene molecules by groups containing soft donor atoms such as nitrogen and, especially, sulphur atoms yields a high binding efficiency towards soft metal ions ( $\text{Ag}^+$  and  $\text{Hg}^+$ ). O'Connor *et al.* demonstrated that specifically one calix[n]arene, *para*-tetra(tert-butyl)-tetra(methylmercaptopropanoylmethoxy)calix[4]arene, could be used as silver ions ionophores when coated on carbon glass electrodes. Silver and mercury ions have shown best selectivity over other metal ions  $\text{Na}^+$ ,  $\text{Pb}^+$ ,  $\text{K}^+$ ,  $\text{Cd}^+$ ,  $\text{Co}^{2+}$ ,  $\text{Ni}^{2+}$ ,  $\text{Cu}^{2+}$  [O'Connor *et al.*, 1992]. Since then, calix[n]arenes have been applied, such as  $\text{Ag}^+$  extracting agents [Podyachev *et al.*, 2014], templates for the synthesis of silver nanoparticles [Baghayeri\_2013], and as biosensors using silver ions as marker. Tuntulani *et al.* developed a membrane electrode coated with a benzothiazole calix[4]arene derivative which was able to detect  $\text{Ag}^+$  at low detection limit of 500 nM [Ngeontae *et al.*, 2008]. This electrode has detected DNA oligonucleotide sequences [Janrungsakul *et al.*, 2013] or glucose [Ngeontae *et al.*, 2009] with silver nanoparticles labelling. For example, this reaction can use glucose oxidase to catalyse the reaction of glucose and oxygen to gluconic acid and hydrogen peroxide. In the reaction cascade, silver nanoparticles are oxidized to  $\text{Ag}^+$  and can finally be detected by calix[n]arene.

In recent years, nanoparticle conjugates of calix[n]arenes have emerged, combining the advantages of calix[n]arene with the properties of the associated particles (quantum dots, gold or silver nanoparticles) [Acharya *et al.*, 2012]. Kim *et al.* have reviewed the methods for preparing and characterizing various conjugates and have discussed about sensing applications [Kim *et al.*, 2012]. Their biomolecular recognition properties and their methods of preparation for noble metal, along with their applications have been described in a recent review [Tauran *et al.*, 2013a]. Very recently, Yang *et al.* provided an overview of nano-devices utilizing host-guest system like calix[n]arenes [Yang *et al.*, 2014]. The review presents possible future applications such as the development of a mechanical actuator based on molecular muscles or active molecular plasmonic device based on molecular switches. This review highlights the challenge to integrate these supramolecular systems on a surface instead of in solution.

Compared to other conjugates, silver at the nanometric scale shows unique optical, electrical and biological properties. The localized surface plasmon resonance (LSPR) in silver nanoparticles possesses a higher extinction coefficient when compared to gold nanoparticles, making it ideal for optical sensing [Vilela *et al.*, 2012]. Navarro and Werts have estimated that the extinction coefficient of spherical silver nanoparticles is around 5 times higher than spherical gold nanoparticles, under 35 nm of diameter [Navarro *et al.*, 2012]. Silver nanoparticles are considered also less toxic than quantum dots for biological applications [Nguyen *et al.*, 2013]. Ju-Nam and Lead have reported in an environmental study that quantum dots have multiple deleterious effects such as the induction of human neuroblastoma cell death, increase immunotoxicity and can damage DNA [Ju-Nam *et al.*, 2008]. On the other hand, the toxicity of silver nanoparticles has been established against bacteria but still debated for animal cells. Silver nanoparticle toxicity has been shown to depend on several factors (size, solubility, coating, morphology, surface charge and surface area) [Foldbjerg *et al.*, 2013].

The present review will provide a comprehensive analysis of the bio-applications of calix[n]arene capped silver nanoparticles. After describing in a first part, the state of the art, for bio detection using calix[n]arene capped silver nanoparticles, the recent advances will be presented with regard to possible future therapeutic applications of these novel systems. All along the review, the argentophilic functional group of calix[n]arene will be highlighted in the figures and described according to their strength (blue and red correspond respectively from high to very high).

## **2. Synthesis of calix[n]arene capped silver nanoparticles**

The synthesis of calix[n]arene capped silver nanoparticles can be performed using several methods. The method of choice for argentophilic calix[n]arenes was introduced by Xiong *et al.* and consists of mixing silver salts and a calix[n]arene [Xiong *et al.*, 2008]. Then the addition of a suitable reagent, such as sodium borohydride reduces the  $\text{Ag}^+$  ions to dispersions of metallic Ag. This method provides dispersed and uniform spherical nanoparticles and has proved to be efficient over a wide range of calix[n]arene derivatives bearing argentophilic

group. The solubility of calix[n]arene in water will be also a critical factor. Calix[n]arene is used here as capping agent having silver affinity and properties for maintaining the silver nanoparticles as non-aggregated colloids by electrostatic repulsion. More recently, new methods have been reported and are described in Table 2, along with nanoparticle geometries. They present some particularities in the synthesis of nanoparticles with specific sizes and shapes. The shape/size parameter strongly influences the optical and biological properties of hybrid silver nanoparticle [Sun *et al.*, 2013]. As an example, it has been recently demonstrated that smaller silver nanoparticles are more cytotoxic than larger ones (between 20 and 50 nm) [Liu *et al.*, 2010]. When the size of silver nanoparticle decreases, the ratio surface / volume increases. This could enhance the reactivity of nanoparticle and release higher concentration of silver ions [Foldbjerg *et al.*, 2013].

Raston *et al.* have reported the interest of using a green synthetic route for the preparation of calix[n]arene capped silver nanoparticles by reducing silver ions with light (at 365 nm) instead of classis toxic reducer agents [Hartlieb *et al.*, 2010]. This reduction might occur through the photolytic excitation of the calix[n]arene with transfer of an electron to the silver ion. However the yield for producing *para*-phosphonated calix[4]arene capped silver nanoparticle is 50% lower than chemical reduction synthesis. Recently, a similar green approach has been considered for the synthesis of silver nanoparticles by biogenic method. This method consists of reducing silver ions by biological means from a whole cell or cellular extract [Rai *et al.*, 2011]. Some biological species produce enzyme able to reduce silver ions in nanoparticles and to stabilize them mostly by proteins. Compared to previous chemical and physical methods, the advantages of biogenic method are mainly the non-toxicity of synthesis (with no toxic chemical required for their synthesis) but cells can also produce silver nanoparticles continuously, shape/size of nanoparticles can be tuned according to pH, temperature and biological species used [Sintubin *et al.*, 2012]. Moreover, biogenic nanoparticles produced at the outer membrane of cells can be functionalized by other molecules [Hennebel *et al.*, 2009]. This biogenic method is a possible future route for synthesizing calix[n]arene capped silver nanoparticles. A work of our research group is currently underway to synthesize the calix[n]arene capped silver nanoparticles using tea plant extract as reducing agent.

**Table 2** – Synthetic methods for the preparation of calix[n]arene capped silver nanoparticles synthesis

Reference	Method	Description	Result
Xiong <i>et al.</i> , 2008	Chemical reduction	A mixture of <i>para</i> -sulphonato-calixa[4]arene <b>1</b> and silver nitrate are reduced by sodium borohydrate.	Calixarene capped silver nanoparticles are highly dispersed and uniform in aqueous solution, with a diameter $8 \pm 1$ nm

Harlieb <i>et al.</i> , 2010	Photochemical	A mixture of <i>para</i> -phosphonated calix[4]arene and <i>para</i> -sulphonated calix[4]arene <b>1</b> and silver salt is reduced by light to yield calixarene capped silver nanoparticle.	Silver nanoparticle with an average size of $18.5 \pm 6$ nm surrounded by 20-30 nm of calixarene. This method function preferentially with phosphonated calix[4]arene
Pandya <i>et al.</i> , 2013	Microwave	A mixture of calix[4]arene thiol derivative <b>11</b> , sodium hydroxide and formaldehyde solution was taken in an open vessel and was irradiated with 50 W power in a microwave	Spherical silver nanoparticles with an average diameter of $40 \pm 10$ nm are produced.
Brown <i>et al.</i> , 2006	In situ	<i>Para</i> -tert-butyl-calix[4]arene complexes silver ions and ethylenediamine. Silver ions are reduced in calixarene cavities and yields silver nanocrystals	Silver nanocrystals have an average diameter of 9.4 nm.
Gao <i>et al.</i> , 2010	In situ synthesis and layer by layer	<i>Para</i> -amino calix[4]arene are previously coated on a negative charged surface then silver is added and reduced in calixarene cavity. Then a new cycle of layer is added.	Produce uniform small nanoparticle with average diameter of $6 \pm 2$ nm.
Zhou <i>et al.</i> , 2014	In situ synthesis by one layer	Calix[7]arene-hydroquinone are attached on a surface, and reduce silver nitrate ions in their cavities.	Nanoplates are produced with an average diameter of $9.5 \pm 2.9$ nm and a thickness less than 2 nm.
Cho <i>et al.</i> , 2008	Metallization on self-assembled calixarene	An amphiphilic calixarene, para-Tetra(D-AlaOEt)-tetra(decanyloxy) calix[4]arene, is self-assembled by heating at 95°C and colled down at room temperature. Then silver nitrate is added and reduced with ascorbic acid.	Dendritic silver nanostructures are obtained with branch of nanometer size range.

### 3. Bio-detection

Because of their unique optical and electrical properties, a variety of physical approach have been proposed for detecting molecules by calix[n]arene capped silver nanoparticles. Table 3 summarizes the advantages and disadvantages of each method. Moreover, a comparison is done with conventional methods using calix[n]arene as recognition molecule. The table shows that there is not yet a gold technique enable to detect biomolecule with all advantages (high specificity, fast, cost effective, ultra-sensitive and portable). Each method offers its own characteristics and will be described in the following sections.

**Table 3** - Advantages and disadvantages of bio-detection method using calix[n]arene and calix[n]arene capped silver nanoparticles.

Material used	Method of bio-detection	Reference	Advantages	Disadvantages
Calix[n]arene capped silver nanoparticles	Optical (naked eye)	[Xiong <i>et al.</i> , 2008]	Cost effective, Fast, Portable	Low detection limit ( $\mu\text{M}$ concentration range)
	Optical (with DLS)	[Pandya <i>et al.</i> , 2013]	Cost effective, Fast, Very sensitive (10 nM)	Not portable
	SERS	[Guerrini <i>et al.</i> , 2009]	Provide structural data, Fast, Ultra sensitive (10 nM)	Not portable, Expensive
	Electrical	[Evtugyn <i>et al.</i> , 2011] [Bian <i>et al.</i> , 2010]	Fast, Portable, Ultra-sensitive (1nM [Evtugyn_2011] and 4nM[Bian_2010])	Expensive
Calix[n]arene	ELISA	[Cecillon <i>et al.</i> , 2005]	Highly specific and very sensitive (10nM concentration range)	Expensive and slow (Need a revelation step of the complex by antibody).
	Mass Spectrometry	[Da Silva <i>et al.</i> , 2006]	Provide structural data. Fast and Sensitive (100nM concentration range)	Not portable and very expensive.
	Western blot	[Cecillon <i>et al.</i> , 2005]	Highly specific, very sensitive (10nM concentration range)	Not portable and slow (Need a revelation step of the complex by antibody).

### 3.1 Colorimetric methods

The interaction of the electric field of light over metal generates a plasmon described as the resonance (or collective oscillation) of the electronic conduction band along a metallic surface. This surface plasmon resonance is called more specifically Localized Surface Plasmon Resonance (LSPR) when it occurs on nanoparticles [Derkachova *et al.*, 2013]. In LSPR, the particle's absorbance band reaches a maximum at the plasmon resonance frequency. This occurs at visible wavelength for spherical noble metal nanoparticles (400 nm for silver and 570 nm for gold). For observing LSPR, two conditions should be filled: 1) the dielectric permittivity of the metal needs to be negative 2) the free-space wavelength should be large in comparison to the nanoparticle diameter [Mayergoysz *et al.*, 2013].

LSPR and its optical effects on nanoparticles depend on the size, shape, the nature of metal and the molecular environment surrounding the nanoparticles. The depolarization of the electronic conduction band induced by light will be strongly influenced by the geometry of metal surface (size, shape) [Amendola *et al.*, 2010]. The nature of metal is also a critical parameter. Silver exhibits higher dielectric permittivity ratio than gold, giving higher polarization and better absorbance of light [Ghosh *et al.*, 2007]. Finally, the dielectric permittivity of the molecular environment surrounding the metal nanoparticles influences greatly the plasmonic response by depolarizing the conductive electrons. A medium with a higher dielectric permittivity enhances the depolarization and then increases the absorbance of metal nanoparticles and red-shifts their plasmonic band [Mayer *et al.*, 2011]. The dependence of the plasmonic frequency and the dielectric component of the molecular environment surrounding the metal nanoparticle is the key factor for using nanoparticles as optical molecular sensor.

Silver nanoparticles as optical sensor for the identification of or discrimination between chemical or biological agents offer many advantages in medical and environmental sciences. They are cost effective, stable in time, show rapid response times and can be very sensitive. In order to be used as optical molecule sensors, silver nanoparticles need to be functionalized with a molecule able to recognize the targeted ligand. Nanomolar level detection can be achieved in cases of a strong affinity between the ligand and the receptor present at the surface of the nanoparticles [Doria *et al.*, 2012].

One of the physical consequences of the complexation of ligand onto the surface of the hybrid nanoparticles, are changes of both the wavelength and the intensity of maximum absorbance [Jain *et al.*, 2007]. For example, the plasmonic absorption band of spherical shaped silver nanoparticles is typically in the range 390-400 nm, yielding a yellow colour for the colloidal dispersion. Aggregation provoked by the complexation of a ligand to the receptor which can bridge between the nanoparticles, induces a change in the polarity of the local environment and a change in size. At higher size, the resonance of electronic shift from a simple mode to multipolar mode which are characterized optically by a strong red shift and an enlargement of the plasmonic band. This can be readily observed, even by the naked eye [Agasti *et al.*, 2010]. An example of this phenomenon is illustrated by the addition of cytosine to a *para*-sulphonato-calix[4]arene **1** capped silver nanoparticle suspension (Figure 2 and 3). Indeed, *para*-sulphonato-calix[4]arene is known to interact with nucleic bases [Atwood *et al.*, 1996] Recently, **1** capped silver nanoparticles have been showed to aggregate

particularly upon the addition of pyrimidine family bases (consisting of one heterocycle) including cytosine, thymine and uracil [Tauran *et al.*, 2011]. More details are given in the biomolecules section.

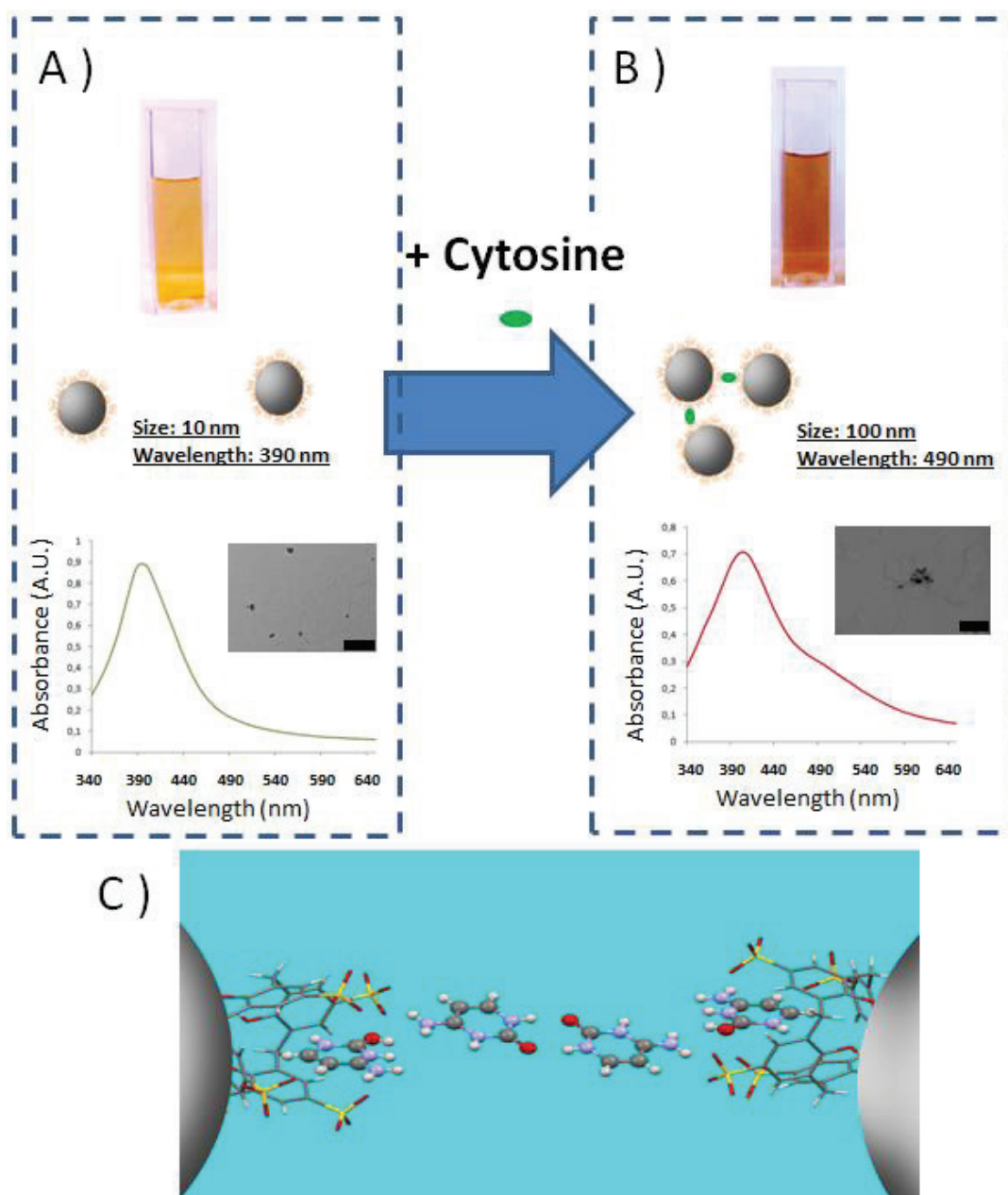


**Figure 2** - Illustration of the optical effects induced by aggregation of nanoparticles. A) before and B) after the addition of cytosine to a *para*-sulphonato-calix[4]arene 1 capped silver nanoparticle suspension. In a blue dashed line panel, from top to bottom: at the top part there is a picture of the nanoparticle solution, in the middle part there is a schematic representation of silver nanoparticles dispersion, and at the bottom there is UV-Visible spectrum of the silver nanoparticles with a TEM picture in the inset. C) Schematic representation of the aggregation mechanism proposed by Coleman *et al.* [Tauran\_2012]. Grey areas represent the surface of silver nanoparticles capped by *para*-sulphonato-calix[4]arene 1. 4 cytosine nucleic bases bridge the nanoparticles, leading to the aggregation process.

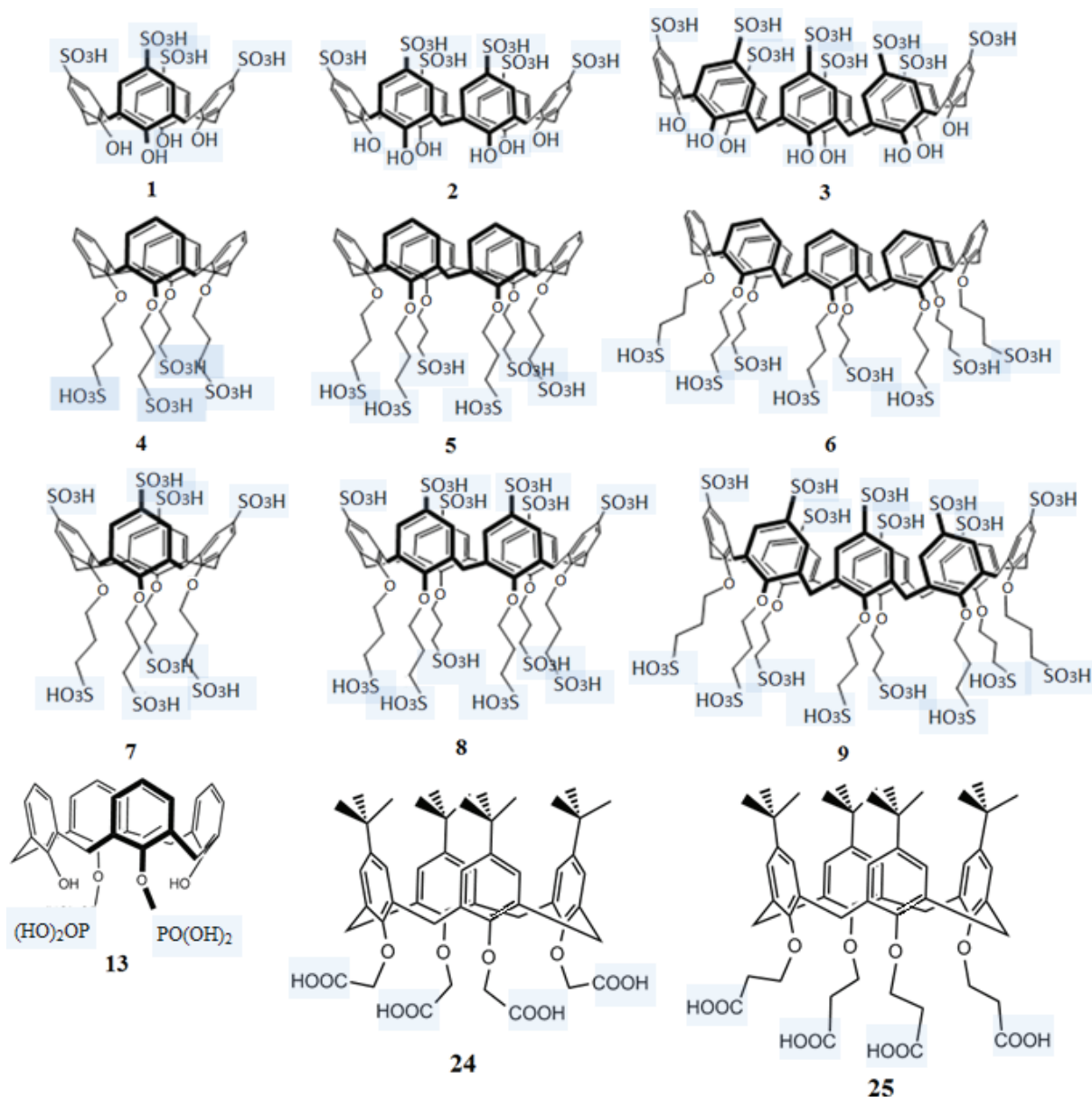


**Figure 3** - Structures of calix[n]arene derivatives studied by Coleman *et al.*

### 3.1.1 Ferric ions

Ferric ions, Fe<sup>3+</sup> are involved in two main biochemical functions: the transport and storage of dioxygen and also in electron transport. In dioxygen transport, Fe<sup>3+</sup> allows the coordination between oxygen and the heme function groups of circulating haemoglobin [Tsiftoglou *et al.*, 2006]. With regard to electron transport, Fe<sup>3+</sup> coordinated to the metallo-protein cytochrome C catalyses either reduction or oxidation of small substrate molecules present inside the mitochondria. Thus, perturbation of Fe<sup>3+</sup> concentration can lead to several human diseases, such as anaemia when Fe<sup>3+</sup> is at low concentration or endometriosis when Fe<sup>3+</sup> is at high concentration [Toyokuni *et al.*, 2008].

Hybrid silver nanoparticles have been investigated to identify this ion diluted in solution or from collected blood. The pyridyl appended calix[4]arene **10** has been capped onto silver nanoparticles by chemical reduction and used for the detection of Fe<sup>3+</sup> in methanol

solution (Figure 4). The hybrid nanoparticles specifically recognized  $\text{Fe}^{3+}$  over a wide range of other metal ions ( $\text{Li}^+$ ,  $\text{Na}^+$ ,  $\text{K}^+$ ,  $\text{Cs}^+$ ,  $\text{Mg}^{2+}$ ,  $\text{Ca}^{2+}$ ,  $\text{Sr}^{2+}$ ,  $\text{Ba}^{2+}$ ,  $\text{Cu}^{2+}$ ,  $\text{Mn}^{2+}$ ,  $\text{Ni}^{2+}$ ,  $\text{Zn}^{2+}$ ,  $\text{Co}^{2+}$ ,  $\text{Fe}^{2+}$ ,  $\text{Cr}^{3+}$ ) and  $\text{Fe}^{3+}$  could be detected at a lowest concentration of  $125\mu\text{M}$  [Zhan *et al.*, 2012].

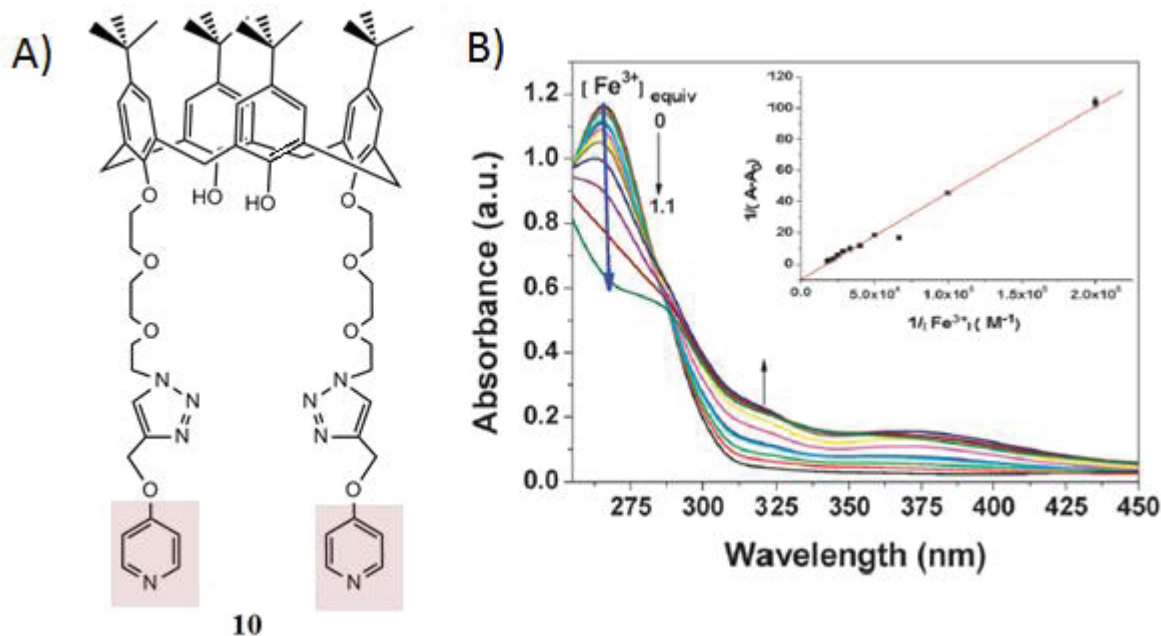


**Figure 4** – (A) Structure of Pyridyl appended calix[4]arene **10** (B) UV-Visible spectra titration of **10** capped silver nanoparticles mixed with various concentration of  $\text{Fe}^{3+}$ . Inset shows calibration curve. From Zhan *et al.* [Zhan *et al.*, 2012], reproduced with permission from Royal Society of Chemistry.

Recently Pandya *et al.* have used a para-sulphonato-calix[4]arene thiolated derivative **11** functionalized silver nanoparticles for the selective recognition of  $\text{Fe}^{3+}$  in phosphate buffer and in human blood. The hybrid colloids were prepared by a microwave assisted method, see Table 1 [Pandya *et al.*, 2012]. They have shown pH stability over a range of pH between 4 and 10 and a selectivity over a wide range of metal ions ( $\text{Zn}^{2+}$ ,  $\text{Cu}^{2+}$ ,  $\text{Ca}^{2+}$ ,  $\text{Co}^{2+}$ ,  $\text{Mg}^{2+}$ ,  $\text{Cd}^{2+}$ ,  $\text{Ba}^{2+}$ ,  $\text{Na}^+$ ,  $\text{K}^+$ ,  $\text{Mn}^{2+}$ ,  $\text{Fe}^{2+}$ ,  $\text{Pb}^{2+}$ ,  $\text{Ni}^{2+}$ ,  $\text{Pd}^{2+}$ , and  $\text{Hg}^{2+}$ ) and bio-macro-molecules such as pepsin, cytochrome C, BSA and myoglobin. The selectivity of  $\text{Fe}^{3+}$  has been assessed by measuring the ratio absorbance of aggregated nanoparticles over plasmon absorption peak for each molecule.  $\text{Fe}^{3+}$  has shown a ratio 10 times higher than other metal ions and proteins at the same concentration. The plasmon absorption peak was linearly red shifted up to 10 nm of  $\text{Fe}^{3+}$  (Figure 5). This calix[n]arene nanoparticle is 10000 times more sensitive than previous case. Anionic sulphonate functions of **11** might enhance the capture of highly positive charges of metal ions like  $\text{Fe}^{3+}$ . However, the use of Dynamic Light Scattering (DLS) is preferred at lower concentrations ( $<10\text{nM}$ ) because of its higher selectivity [Pandya *et al.*, 2013]. A suitable pre-treatment (chemical lysis followed by one cycle of centrifugation) liberates the ferric ions from the blood cells for subsequent detection.

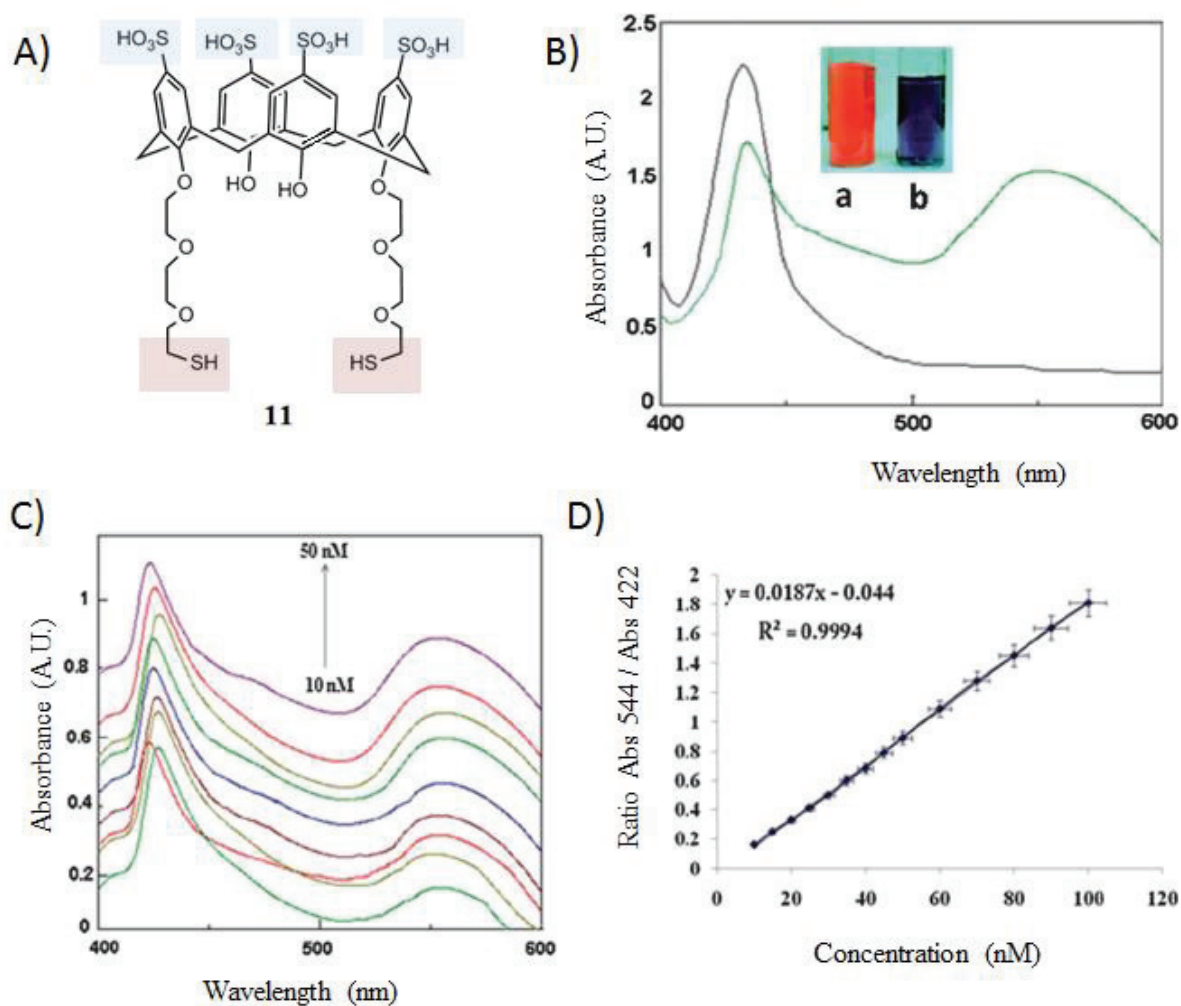


**Figure 5** – (A) Structure of calix[4]arene thiol derivative **11** (B) UV-Visible spectra of **1** capped silver nanoparticle (a) alone or (b) in presence of 100nM of  $\text{Fe}^{3+}$  (C) UV-Visible spectra of **1** capped silver nanoparticle with various concentration of  $\text{Fe}^{3+}$  (D) Ratio of the absorbance of the aggregation band at 544 nm over the absorbance of dispersed silver nanoparticles at 422 nm as a matter of concentration. A linear correlation is obtained. From Pandya *et al.* [Pandya *et al.*, 2012], reproduced with permission from Royal Society of Chemistry.

### 3.1.2 Organophosphates

Organophosphate esters often present toxicity to various living species, because of their ability to inhibit acetyl cholinesterase, an enzyme essential for maintaining the function of the central nervous system. Organophosphates can be found as insecticides, pesticides and chemical warfare agents [Namba *et al.*, 1971]. The use of calix[n]arene capped silver nanoparticles has emerged as a way to identify the presence of these toxic compounds in the environment in a simple, cost effective way with high selectivity and sensitivity. The structures of organophosphate described here are given in figure 6.

Bian *et al.* have developed *para*-sulphonato-calix[6]arene **2** for detection the methyl parathion nitroaromatic organophosphate [Bian *et al.*, 2010]. The detection was undertaken using an electrochemical sensor in order to enhance the specificity and sensitivity (see Electrical sensing section).

Recently, Menon *et al.* have prepared silver nanoparticles capped with *para*-sulphonato-calix[4]resorcinarene **12** for the specific detection of dimethoate, an organophosphate insecticide (figure 6) [Menon *et al.*, 2013]. The addition of this chemical to the hybrid particles solution induces aggregation of nanoparticles, generating a red shift in the wavelength of the surface plasmon band. The initial absorption band of the hybrid nanoparticle at 420nm disappears in favour of the apparition of a new absorption band at 519nm corresponding to the aggregated form of nanoparticle. DLS confirms the change of nanoparticle size from 38nm to an aggregate of 700 nm size. Finally, these hybrid nanoparticles have shown no reactivity with regard to 6 other organophosphate derivatives and have demonstrated a detection limit of 80 nM (Figure 6).

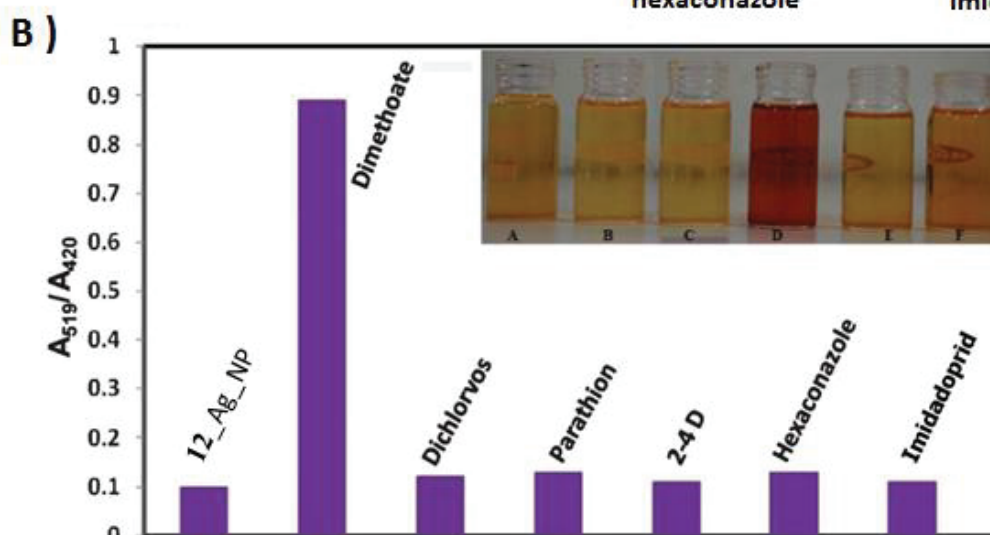
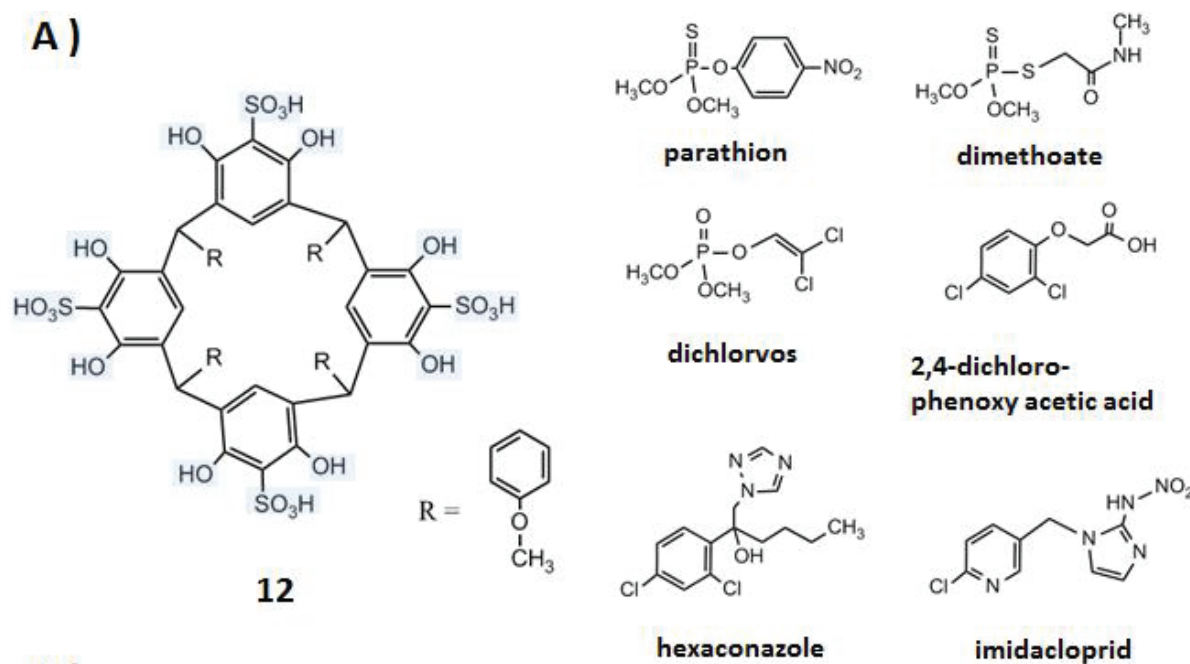


**Figure 6** – (A) Structure of sulphonato-calix[4]resorcinarene **12** and a series of organophosphates studied by Menon *et al.* [Menon *et al.*, 2013], (B) The relative absorbance  $A_{519}/A_{420}$  change of **12** capped silver nanoparticles (**12\_Ag\_NP**) mixed with different pesticides. In the inset, the photographic images of the corresponding solutions. From [Menon *et al.*, 2013], reproduced with permission from Royal Society of Chemistry.

### 3.1.3 Biomolecules

In 2007, Xiong *et al.* began research in the area of non-covalently capped silver nanoparticles by combining calix[n]arenes and silver nanoparticles for the specific detection of histidine, one of the 20 amino acids found in proteins. Because of the involvement of histidine in the growth and the repair of human tissue, as well as its role in nerve cell protection, the identification and dosing of histidine is a medical concern. Here, the water soluble *para*-sulphonato-calix[4]arene **1** capped silver nanoparticles were prepared, by chemical reduction with sodium borohydride. The hybrid nanoparticles thus prepared were

shown to be stable in aqueous solution, and to be able to colourimetrically detect histidine down to a concentration of 5  $\mu\text{M}$  and with selectivity with respect to 11 other amino acids [Xiong\_2008]. However, the amino acids lysine ( $K_d = 737 \mu\text{M}$ ) and arginine ( $K_d = 737 \mu\text{M}$ ) both known to complex the calix[n]arenes with higher affinity than histidine ( $K_d = 1.9 \text{ mM}$ ) have not been tested [DaSilva *et al.*, 2003][Perret *et al.*, 2007].

Coleman *et al.* have used the ability of **1** and 1,3-di-O-phosphonato-calix[4]arene **13** to interact with some amino acids and proteins such as serum albumins for discriminating between proteins of different animal species (Figure 3). These calix[n]arenes were selected for their argentophilic nature and their known or supposed affinities for serum albumins. Complexation of Bovine Serum Albumin (BSA) and **1** have been already determined in a previous study [Memmi *et al.*, 2001]. Calix[4]arene diphosphonate **13** has been demonstrated to interact in a ternary complex with zinc and histidine [Perret *et al.*, 2002]. BSA is a major zinc transporter in plasma, typically binds about 80% of all plasma zinc and is composed of 2.8% of histidine (Information collected from reference P02769 on Protein Data Base). Therefore, it has been supposed that **13** could interact with serum albumin. The serum albumins represent the most common protein class in animal physiological fluids with concentrations of up to 40 g/L (0.6 mM) in blood. Discrimination between albumins of different species could be a fast, cost effective and selective method for identifying meat species in food industry, and in particular with regard to the presence of pork in 'so-called' halal food [Che\_Man *et al.*, 2007]. Two types of calix[n]arene capped silver nanoparticles have been prepared by chemical reduction and have shown high stability in aqueous solution (for months). First, the interaction between albumin and the hybrid nanoparticles **1** and **13** have been characterized by fluorimetry, and then specific optical behaviour of the hybrid nanoparticles mixed with albumin from different animal species has been studied as a matter of temperature and time [Tauran *et al.*, 2013b]. The analysis of the results allows discrimination between the serum albumins of the various species.

The use of noble metal nanoparticles for the complexation with DNA or RNA has received considerable attention. A large number of studies have shown the interest of such complexation for biological uses including diagnostics and medical applications.

Coleman *et al.* have prepared **1** capped silver nanoparticles and have described their interactions with the 5 nucleic bases (Adenine, Guanine, Cytosine, Thymine and Uracil). Nucleic bases are divided in two classes, pyrimidines that contain only one heterocycle while purines that are composed of two heterocycles. **1** capped silver nanoparticles mixed with nucleic bases yield selective complexation reflected in the change of colour due to the aggregation. Particularly, for the pyrimidines there is colour change from yellow to orange red and pink, allowing the discrimination between the 2 classes of molecules. Nucleoside (nucleic base conjugated to a ribose) and deoxyribonucleoside (nucleic base conjugated to a deoxy-ribose) constituting respectively RNA and DNA were also investigated against **1** capped silver nanoparticles. Their interaction have shown different optical effects suggesting this colorimetric method for discriminating DNA from RNA. Furthermore, for the first time a reasonable model of the organization of **1** over silver nanoparticles has been given [Tauran *et al.*, 2011].

Subsequently, the group investigated the complex assembly process induced by the interaction of cytosine and calix[n]arene **1** capped silver nanoparticles. Multiple physical methods have been used, including DOSY NMR, fluorescence and visible spectroscopies, DLS, Single Crystal Solid State Diffraction and Electron microscopy. The complexation assembly is assumed to be in 2 steps. First, there is a binding event between cytosine and **1** capped silver nanoparticles with a constant of dissociation  $K_d$  of 2  $\mu\text{M}$ . Then cytosine bridges silver nanoparticles in a 1 : 2 complex, the formation of this super complex induces aggregation assembly (figure 6) and change of the colloidal solution colour from yellow to red orange. Here, the presence of cytosine can be determined at a minimum concentration of 1  $\mu\text{M}$  using UV-visible spectrometry [Tauran *et al.*, 2013c].

Recently, Georghiou and Coleman have shown that sulphonate calixnaphthalene capped silver nanoparticles can discriminate different nucleic bases and amino acids, [Valluru *et al.*, 2014], preferentially complexing the aromatic amino acids phenylalanine and tryptophan. This effect is promising for new applications such as the extraction, the transport or the activity modulation of proteins rich in aromatic amino acids.

As a last example of studies relevant to biomolecules, surfactant aggregation and micelle formation has been investigated using calix[n]arene capped silver nanoparticles [Tauran *et al.*, 2012]. Surfactants are usually amphiphilic organic compounds containing both hydrophobic groups (their tails) and hydrophilic groups (their heads). Above a specific concentration termed the Critical Micelle Concentration (CMC), surfactants form various aggregate structures including micelles. The CMC determination of mixed compounds ( $C^M$ ) is particularly interesting in biochemistry because it is critical to know the exact concentrations of multiple surfactants needed for extracting a specific membrane protein or for transporting drugs in micelle. In this study, calix[n]arene capped silver nanoparticles have been evaluated for determining CMC and  $C^M$ . Various sulphonato-calix[n]arene derivatives capped on silver nanoparticles in aqueous solution have been prepared by the method described previously [Tauran *et al.*, 2011] and mixed with 4 different surfactants (cetyl pyridium bromide, cetyl trimethyl ammonium bromide, triton X 100 and N-octyl glucopyranoside). Sulphonato-calix[4]arene derivatives **1**, **4** and **7** have shown changes both in intensity and wavelength of the plasmonic absorption band upon the addition of cationic surfactants in a manner strictly equivalent to that observed in the CMC behaviour. This is probably coming from the difference of dielectric permittivity between a surfactant monomer and micelle assembled surfactant. Furthermore, the study has reported the use of these hybrid nanoparticles for the determination of  $C^M$  values for different ratio of cationic and neutral surfactants (Figure 7). The non-linear behaviour of micelle formation as a matter of surfactant ratio has been followed by hybrid nanoparticles and has been successfully compared to data from more classical methods. These hybrid nanoparticles could be investigated in the future on membrane proteins and surfactants in order to discriminate their various assembly forms.

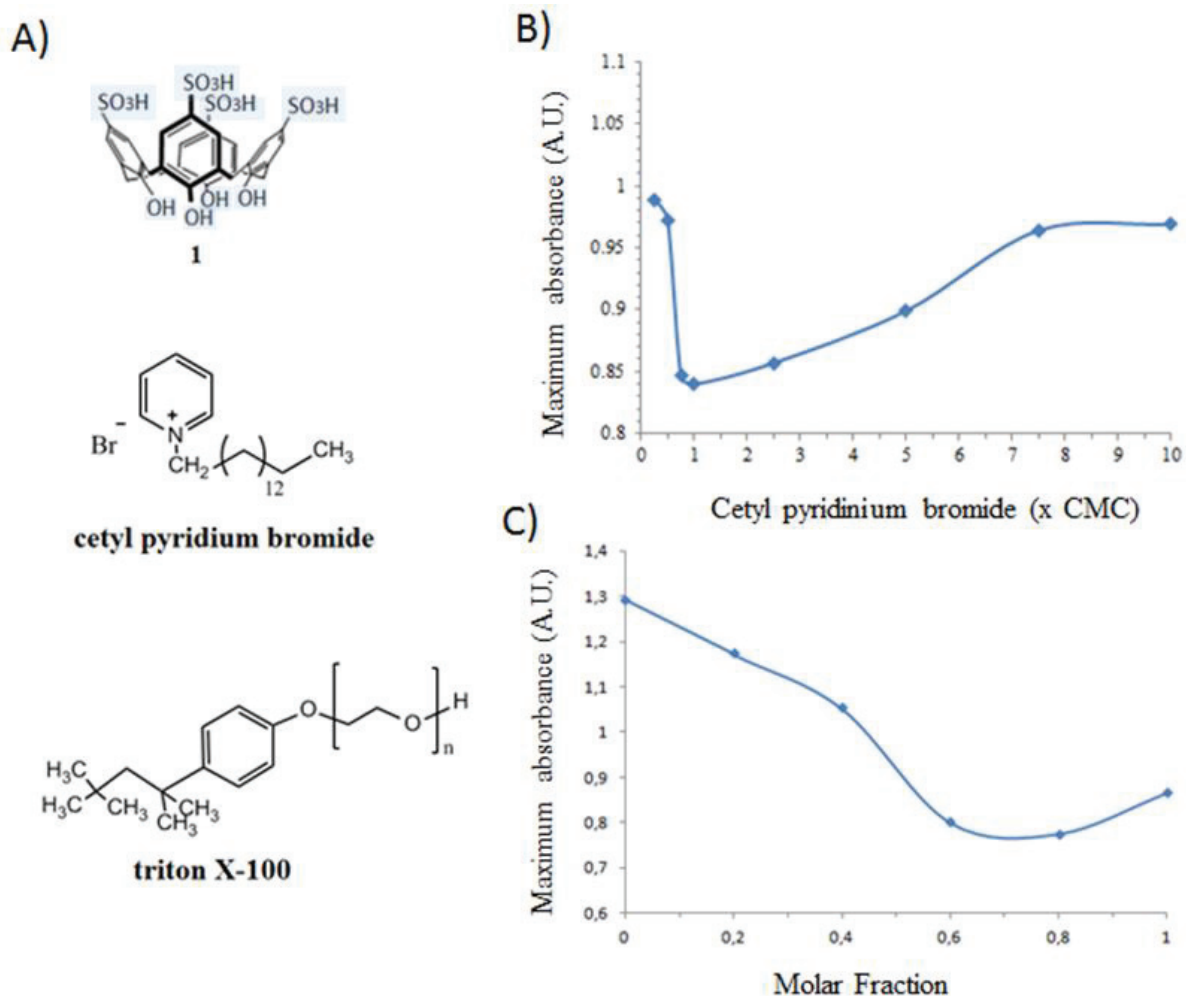


**Figure 7** – (A) Structure of **1** and the surfactants cetyl pyridinium bromide and triton X100 investigated in [Tauran *et al.*, 2012] (B) Maximum absorbance of **1** capped silver nanoparticles mixed with different concentration of cetyl pyridinium bromide (C) Dependencies of the maximum absorbance of **1** capped silver nanoparticles with a neutral/cationic surfactant mixture (cetyl pyridinium bromide / triton X100). From Tauran *et al.* [Tauran *et al.*, 2012] reproduced with permission from Royal Society of Chemistry.

### 3.2 SERS

Surface-Enhanced Raman Scattering (SERS) is a surface-sensitive technique that enhances the scattering of light by molecules adsorbed on nanostructured metal surfaces. The amplification of the SERS signals comes (mainly) through the electromagnetic interaction of light with the metal, which produces large amplifications of the laser field through excitation of the plasmonic resonance. This method is extensively used to identify and understand the orientation of molecules adsorbed on the metal surface. The enhancement factor can be as much as  $10^{10}$  to  $10^{11}$  allowing the technique to detect single molecules [Le Ru *et al.*, 2009]. As they are composed of nanostructured metal, silver nanoparticles can be used for SERS analysis in bio-detection. Sanchez-Cortes *et al.* have investigated in-depth SERS for studying

the interaction between calix[n]arene capped silver nanoparticles and some substrates such as pigments or Polycyclic Aromatic Hydrocarbons (PAHs) [Guerrini *et al.*, 2007].

### 3.2.1 PAH detection

PAHs are organic molecules with a condensed polyaromatic structure. They can be found in coal, oil, gas or other organic substances such as tobacco and cooked meats. The formation of PAHs occurs when insufficient oxygen or other factor result in incomplete combustion of organic matter (Figure 7A). Many possess carcinogenic and mutagenic properties, and it is a public concern to detect and quantify these pollutants in the environment.

First, Sanchez-Cortes *et al.* have prepared calix[4]arene derivatives **14**, **15** and **16** capped silver nanoparticles by chemical reduction (Figure 7B). Compound **15** has been founded to be the most appropriate host with regard to both the sensitivity and selectivity of PAH detection (Figure 7C). The complexation of a PAH induces a significant change in the calix[n]arene structure. A host-guest interaction between the aromatic rings of PAH and those composing the cavity of the calix[n]arene through  $\pi$ - $\pi$  stacking is proposed. Therefore, a change of orientation into a closed cavity will oriented the complex in a perpendicular axe to the surface. This could lead to an increase in the charge transfer of the complex to the metal surface and SERS bands intensity. Among all the PAHs tested pyrene and benzo[c]phenanthrene have shown the strongest signals, with the detection at a lowest concentration of 10  $\mu$ M [Leyton *et al.*, 2004].

Another study have compared calix[4]arene derivatives functionalized with dithiocarbamate, **17** without and **18** with, for detecting PAHs by SERS (Figure 14). **18** was more appropriate to improve the affinity of the calix[n]arene host toward the nanoparticle surface. Dithiocarbamate was chosen for its high argentophilic nature thus attaching strongly the calix[n]arene to the silver surface, allowing a better charge transfer for SERS measurement [Guerrini *et al.*, 2006]. Then, the limit of detection has been estimated to range from 10 to 100 nM for PAHs containing four benzene rings: pyrene, benzo[c]phenanthrene, triphenylene and coronene (Figure 7D) [Guerrini *et al.*, 2009]. This study highlights the need for the design of molecules targeting PAHs with the highest affinity for improving the level of detection

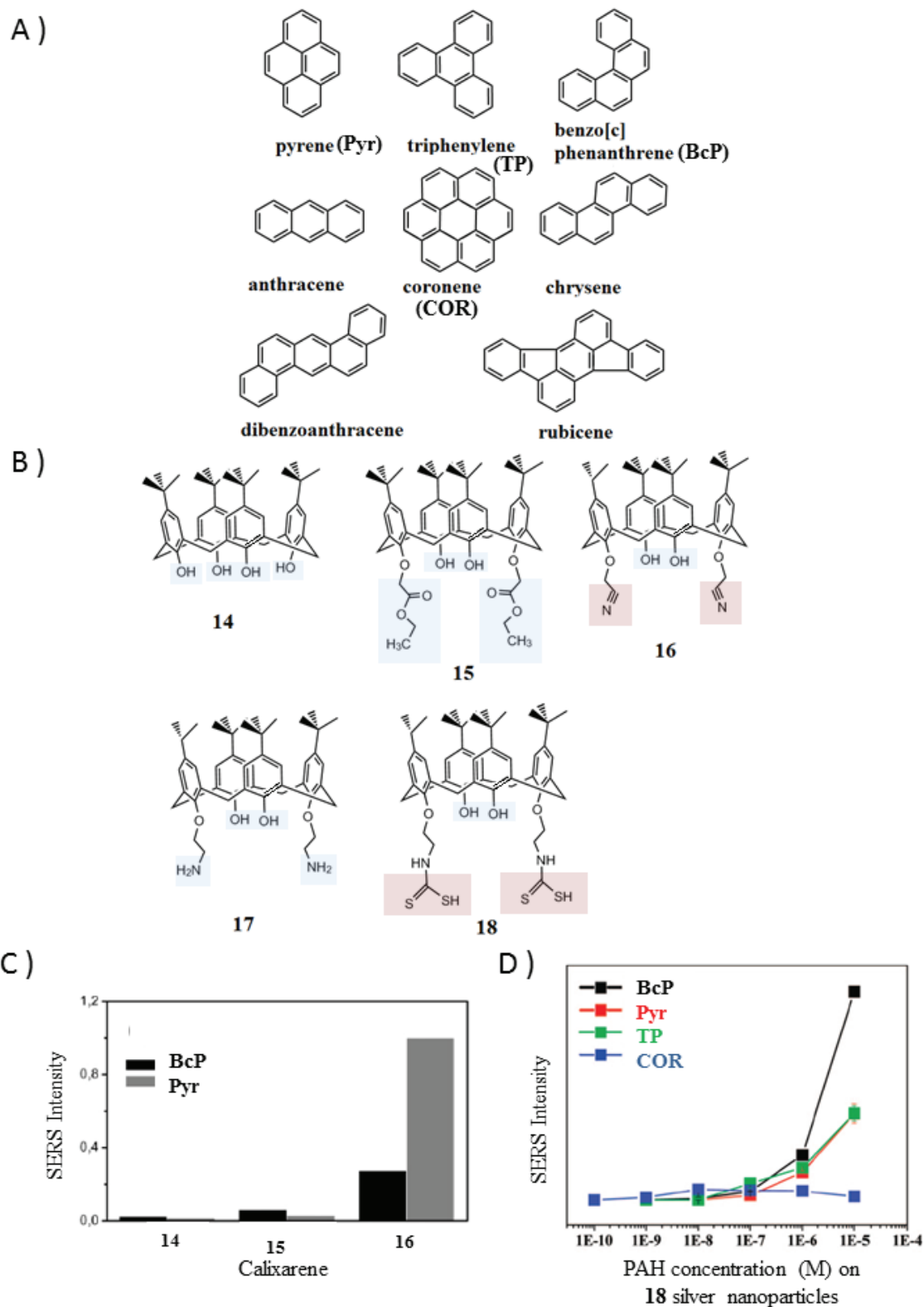


**Figure 8** – A) Structures of PAHs and B) calix[n]arenes studied by Sanchez-Cortes *et al.* [34-36] C) Intensity SERS bands of Pyr and BcP complexed to 3 different calix[n]arenes capped silver nanoparticles D) Intensity SERS bands at various concentrations of Pyr, BcP, TP and COR complexed with **18** capped silver nanoparticles. From [Leyton *et al.*, 2004][Guerrini *et al.*, 2009] with permission from ACS.

### 3.2.2 Pigment detection

Recently, the quinacridone pigment has been detected by calix[n]arene capped silver nanoparticles using SERS. Quinacridone is an organic synthetic pigment which has found extensive use in industrial colorant applications, such as robust outdoor paints and inkjet toners. Its identification is still challenging mainly because of its insolubility in many solvents. In this study, the authors selected calix[n]arenes for their ability to solubilize the pigment by inclusion within the molecular cavity. Four different calix[n]arenes **14**, **19**, **20** and **21** (Figure 10) have been capped on silver nanoparticles by chemical reduction [Del\_Puerto\_2011]. Carboethoxy-calix[n]arene derivatives have been shown to be more efficient than the simple phenolic calix[n]arenes for attachment to the silver surface. Moreover, the carboethoxy calix[n]arene possessing the largest cavity size (with 8 phenolic units) **21** is reported as the most effective molecule for disaggregating quinacridone. Finally, **20** and **21** capped silver nanoparticles have been found to disperse and detect quinacridone at concentrations in the range of 1  $\mu$ M to 1mM.

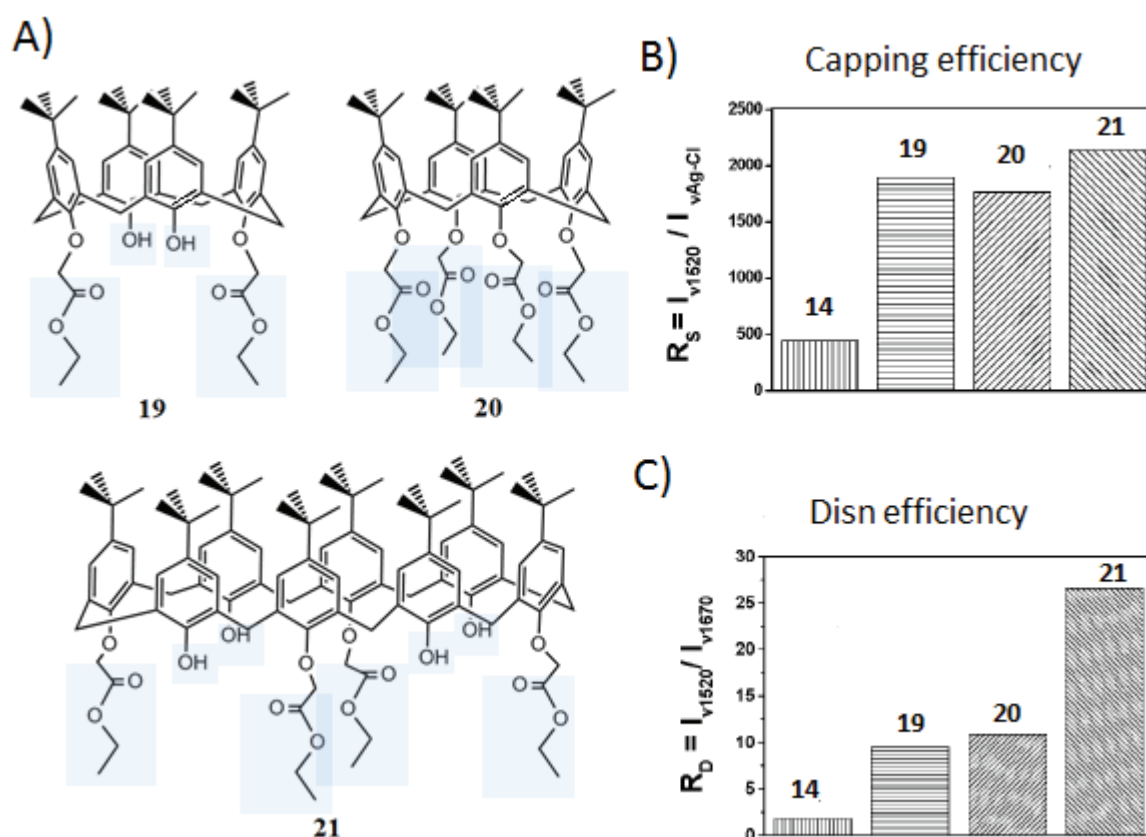


**Figure 9** – A) Structures of calix[n]arenes studied by Del Puerto *et al.* [Del Puerto *et al.*, 2011] B) Ratio  $R_S$  of the intensity of Raman band of calix[n]arene over silver, considered as an efficiency index of capping. C) Ratio  $R_D$  of the intensity of Raman band of calix[n]arene over quinone, considered as a dispersion index of capping. From [Del Puerto *et al.*, 2011] with permission from The Royal Society of Chemistry.

### 3.3 Electrical sensing

In view of its high electrical conductivity, the silver nanoparticle presents an interest in electronic device applications and notably by converting a biomolecular recognition event into an electrical signal. Electrical detection methods offer the possibility of portable assays that could be used in a variety of point-of-care environments. Silver nanoparticles are generally used as markers for the electrical revelation of the presence of a targeted ligand in solution [Rosi *et al.*, 2005]. The use of a calix[n]arene as the receptor molecule has been reported for detecting organophosphate and dopamine.

*Para*-sulphonatocalix[6]arene **2** capped silver nanoparticles have been used in an electrochemical sensor for detecting methyl parathion, one of the most toxic organophosphate pesticides [Bian *et al.*, 2010]. The hybrid nanoparticles were coated on a glassy carbon electrode and were shown to capture the nitroaromatic organophosphate (the responsible interactions were assumed to be cation- $\pi$  or  $\pi$ - $\pi$  interactions) on the electrochemical surface. Under electrical current, the reduction of methyl parathion is enhanced by its complexation to the calix[n]arene. Thus, the differential pulse voltammogram profile allows the determination of the ligand with a detection limit of 4 nM (Figure 11). The method has shown selectivity over  $\text{PO}_4^{3-}$ ,  $\text{SO}_4^{2-}$ ,  $\text{CO}_3^{2-}$  and  $\text{NO}_3^-$  anionic ions with no interference when they are 1000 fold more concentrated than methyl parathion. However interferences have been shown for *p*-nitrophenol or nitrobenzene when they were 10 times more concentrated than methyl parathion.

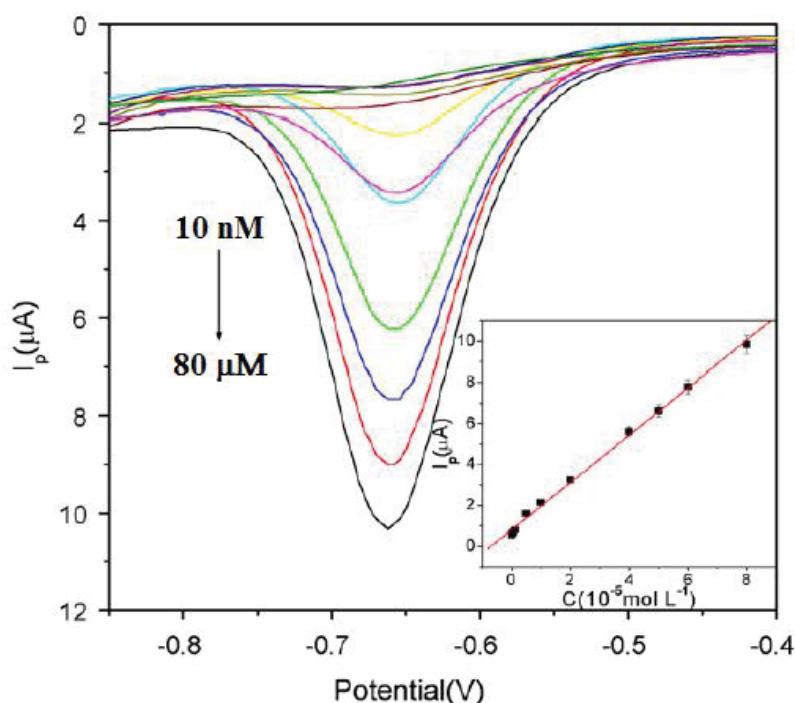


**Figure 10** – Differential pulse voltammograms for **2** capped silver nanoparticles mixed with different concentration of methyl parathion. Inset shows maximum current against concentration of methyl parathion. From Bian *et al.* [Bian *et al.*, 2010] reproduced with permission from Elsevier.

A second approach has been developed for detecting Dopamine with an electrochemical sensor using hybrid silver nanoparticles coated on electrode surface. Dopamine is a neurotransmitter that plays a key role in human organ functions, such as kidney, heart and the central nervous system. Its deregulation can lead to several diseases like Parkinsons, Schizophrenia and other neuro-psychiatric disorders. Here, a thiacalix[4]arene bearing catechol groups at the lower rim derivative has been obtained by mixing a thiacalix[4]arene with dopamine solutions. This new calix[n]arene derivative exhibits strong redox activity and can produce silver nanoparticles of 4-6 nm size range. The detection has been also performed by differential pulse voltammetry. Dopamine concentration detection is linear in the concentration range from 1 nM to 1  $\mu$ M with a detection limit of 0.5 nM [Evtugyn *et al.*, 2011].

## 4. Therapeutical Applications

### 4.1 Antibiotic Activity

Since the accidental discovery in 1928 by A. Fleming [Fleming *et al.*, 1929] of penicillin antibiotic, medicine has been revolutionised through the increase of human life expectancy. Many new antibiotic compounds were rapidly found in the years after the discovery of penicillin. In fact, nearly all the antibiotics in use today are compounds that were discovered during the 1940s to 1960s. Indeed, since the 1990s, no major antibiotic has been delivered to the market. The emergence of antibiotic resistance, its rise and spread over the world is possibly the major public health concern of the 21<sup>st</sup> century [Lewis *et al.*, 2013]. Even if their human toxicity is still debated, silver nanoparticles have demonstrated high ability to kill bacteria while not affecting animal cells [Wong *et al.*, 2010]. Their complexation with antibiotics has shown promising synergistic bactericidal effects which could be very effective against persistent bacterial infection involving antibiotic resistance [Li *et al.*, 2005]. Rhimi and Coleman have investigated the use of calix[n]arene silver nanoparticles as potential antibacterial agents and also for their ability to transport antibiotics.

8 different anionic calix[n]arene capped silver nanoparticles varying in their size (4, 6 or 8 phenolic units) and the position of the sulphonato group (upper rim, lower rim, or both faces), Figure 3 1-9, were evaluated for anti-bacterial activity with regard to the two classes of bacteria; Gram positive and Gram negative [Boudebouze *et al.*, 2013]. Gram positive bacteria possess a thick peptidoglycan layer without outer membrane while Gram negative bacteria have a thin peptidoglycan layer surrounded by an outer membrane (Figure 12) [Gunsalus *et al.*, 1986].

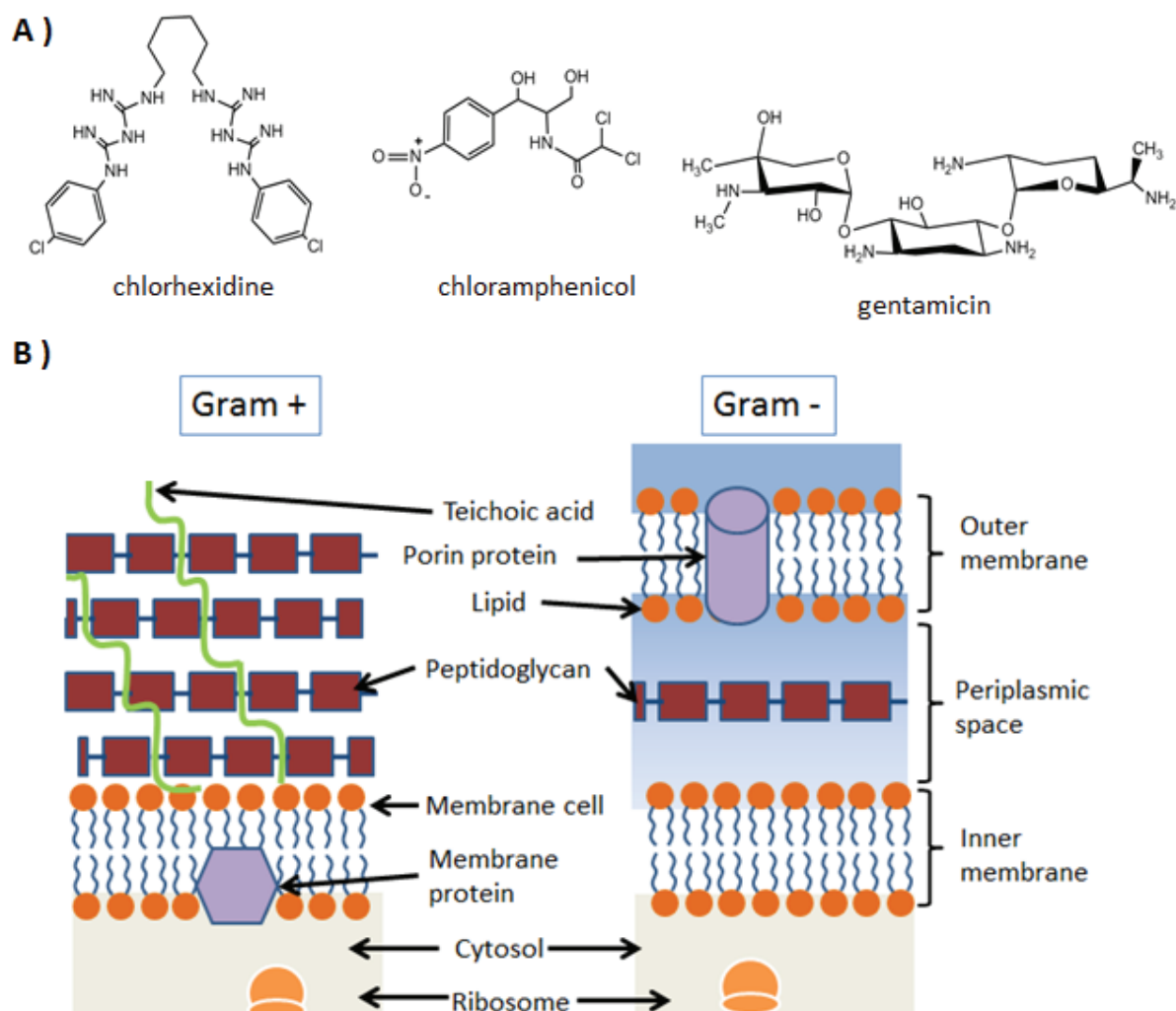


**Figure 11** – (A) Series of APIs investigated in by Perret *et al.* [Perret *et al.*, 2012] (B) Typical cell wall composition of bacteria Gram + and Gram –

*Para*-sulphonato-calix[n]arenes **1**, **2** and **3**, were shown to possess bactericidal activity against *E. Coli* Gram positive bacteria. In contrast to this behaviour, the molecules with sulphonato groups at both *para* and O-alkyl terminal positions, **7** and **8** are active against *B. Subtilis* Gram negative bacteria. The antibiotic effect has been observed for a concentration of hybrid nanoparticles equal to 100nM, with a *B. Subtilis* growth inhibition of 80% for **3** and an *E. Coli* growth inhibition of 60 % for **5**. These values can be compared to the results obtained by Grare *et al.* [Grare *et al.*, 2007], where growth inhibition on both bacterial classes have been determined at above 1  $\mu$ M for classical antibiotics (hexamidine and chlorhexidine) and an antibacterial amino-calix[n]arene derivative. The discriminatory effect reported in the paper presents interest for future work.

Transportation of Active Pharmaceutical Ingredients (API) including antibiotics has also been investigated for anionic calix[4]arene capped silver nanoparticles [Perret *et al.*, 2013b]. In this new study, Perret and Coleman used a series of six anionic calix[4]arenes, having sulphonate **1**, **4** and **7**, carboxylate **24** and **25**, or phosphonate **13** functions at either the *para* aromatic position or the phenolic face for capping silver nanoparticles (Figure 3).

The choice of the three APIs studied was based on the fact that they all possess antibacterial properties and are known for interacting or not with anionic calix[n]arenes (Figure 12). Chlorhexidine is able to form co-crystals with anionic calix[4]arenes [Dupont *et al.*, 2008], gentamicin sulphate has been shown to interact with **1** [Grare *et al.*, 2014] and finally chloramphenicol is a neutral apolar antibiotic taken as a negative control. The evolution of the interaction between the hybrid nanoparticles and the API was followed by UV-Visible spectrophotometry. As expected, chloramphenicol has shown a small or inexistent effect. In contrast, there is a strong shift in the plasmon resonance bands and intensity variation for chlorhexidine and gentamicin. This is directly related to a slight aggregation induced by the complexation of the API to nanoparticles. Moreover, the affinity between calix[4]arene and API varies, **1** capped silver nanoparticle has the highest affinity for the two interacting APIs while **24** shows little or no affinity for these APIs. This study has demonstrated that anionic calix[4]arene capped silver nanoparticle can be associated with molecules having antibacterial properties. Future work will evaluate if any synergistic effects exist on Gram + and Gram – bacteria strains and more importantly extend the range of APIs.

## 4.2 Enzyme Inhibition

Very recently, groups in Lyon and Tokyo have investigated the ability of organic host molecules including calix[n]arenes **1**, **2**, **3** and **13** or cyclodextrins **26** and **27** as inhibitors of endonucleases (Figure 22) [Tauran *et al.*, 2014]. Endonucleases are a class of enzyme whose biological role is to digest DNA. They are involved in many biochemical processes such as DNA repair and they are a key element in viral infection. A number of studies have already pointed to endonucleases as targets for anti-viral medications. For example, endonuclease encoded by influenza virus, are required for initiating the translation from viral mRNA to viral proteins inside the infected cell.

Of the six molecules studied with regard to two different classes of DNase (restriction enzymes and rhDNase I), inhibitory effects were demonstrated only for **2**, **3** and **27**, that is molecules with a minimum of 6 units in the macrocycle) and also possessing a strong negative charge. The lowest half maximal inhibitory concentration ( $IC_{50}$ ) has been determined to be at the  $\mu M$  level with regard to certain restriction enzymes, representing a very strong inhibition efficacy compared to standard antiviral drugs. Moreover, the inhibition is still effective after capping **27** on silver nanoparticles and dialyzing the system against deionised water (Figure 12).



anionic calix[n]arene capped silver nanoparticles. ROS are chemically reactive molecules such as oxygen ions and peroxides. ROS are formed as a natural byproduct of the normal human metabolism of oxygen and have important roles in cell signaling and homeostasis [Bolisetty\_2013]. However, during times of environmental stress (UV or heat exposure), ROS levels can increase dramatically and induce chemical reactions leading to DNA, RNA or protein damage that contribute to carcinogenesis [Choudhari\_2014]. Here PC12 neuronal like cells have been stressed by glutamate in order to increase their ROS levels. Then, cells were treated with the same concentrations of various macrocyclic molecules either capped on silver nanoparticles or as free molecules. Firstly it has been shown that the viability of cells is not affected upon the addition of any of the macrocycles whether capped or not on silver nanoparticles. Moreover, anti-oxidant properties have been demonstrated for sulphonato-calix[4]arene derivatives **1**, **4**, **7** and to a lesser extent for sulphonato-calix[6]arene derivatives **2**, **5** and **8** (see table 4). No anti-oxidant properties have been shown for sulphonato-calix[8]arene derivatives **3**, **6** and **9**, 1,3-di-O-phosphonato-calix[4]arene **13** and  $\beta$  cyclodextrin sulphate **27**. Interestingly, the calix[n]arenes **1** and **4** appear to have greater ROS reducing abilities when linked to the silver nanoparticles. This study highlights the potential benefits of combining calix[n]arenes and silver nanoparticles in the development of new bio-active systems.

**Table 4** – ROS level assessed after incubation during one hour, of various macrocyclic molecules capped or not on silver nanoparticles at 10  $\mu$ M. The percentages reported are normalized to the ROS level monitored after incubation of glutamate during one hour (0%). In dark blue are ROS levels inferior to -50%; in light blue are ROS levels inferior to -20%; in white are ROS levels superior to -20%.

Molecule	ROS level (%) compared to blank	Molecule capped on silver nanoparticles	ROS level (%) compared to blank
<b>1</b>	-32	<b>1_Ag_NP</b>	-59
<b>2</b>	-22	<b>2_Ag_NP</b>	-33
<b>3</b>	-7	<b>3_Ag_NP</b>	-5
<b>4</b>	-21	<b>4_Ag_NP</b>	-49
<b>5</b>	-35	<b>5_Ag_NP</b>	-35
<b>6</b>	17	<b>6_Ag_NP</b>	-2
<b>7</b>	-49	<b>7_Ag_NP</b>	-46
<b>8</b>	-31	<b>8_Ag_NP</b>	-37
<b>9</b>	1	<b>9_Ag_NP</b>	25
<b>13</b>	1	<b>13_Ag_NP</b>	-7
<b>27</b>	-14	<b>27_Ag_NP</b>	1

## 5. Conclusion and future perspective

Calix[n]arene capped silver nanoparticles have unexpected properties and interesting possible applications. In the first part of this review, their use as biosensors for a wide range of molecules has been described. They have been used detecting various types of biomolecules, including amino acids, nucleobases and proteins or hazardous compounds, such as organophosphates, and also inorganic systems such as ferric ions with a nanomolar detection limit. Micro-electronic devices have shown particularly high sensitivity but also many other advantages such fast and portable compared to conventional detection methods (see table 3). Device coming from micro and nanotechnologies using such hybrid nanoparticles represent probably the future biodetection methods. However, the specificity of the detection is still limited and a pre-treatment of purification appears necessary for analyzing complex mixtures without false positives. The integration and automation of sample treatment step in such electronic device should be one of the main works in future years.

In the second part, evidence for their promising interest potential as antibiotic, antiviral or anticancer medications is presented. Collaborative work on several research axes including the relationship between the decrease of ROS level, their antibiotic effect, and protein inhibition *in vitro* appears to have promise, in the long term.

Even if calix[n]arene capped silver nanoparticles have shown no cytotoxicity, their toxicity *in vivo* is a concern that should be addressed in the future. Toxicity of hybrid silver nanoparticles in human is still not well understood because of the low number of cases studied. Caraglia *et al.* have recently compared the advantages and risks of various nanoparticle systems in such a context [Lamberti *et al.*, 2014]. Even if these nanosystems offer promising therapeutic effect, they may present unexpected toxic side-effects.

Liposome can trigger immune response [Marra *et al.*, 2012] and polymeric micelles can be cytotoxic with regards to their stability, uptake and release in cell culture media [Ostacolo\_2010], in this context the lack of immune response towards calix[n]arenes is promising [Schrader *et al.*, 2006]. Carbon nanotubes have shown to be carcinogenic for lung, gastrointestinal tract, and blood [Magrini *et al.*, 2006]. Again the calix[n]arenes are promising in view of their anti-cancer properties [Rodik *et al.*, 2009]. Finally, the toxicity of metallic nanoparticles is generally related to the metal toxicity itself because of their release under ionic state after being oxidized. Generation of Reactive Oxygen Species, induced by the metal ion, appears to be one the main way leading to genotoxic and cytotoxic effects. Beside, their behavior as free metal ions increases the local ionic concentration and subsequently disturbs the cellular functions. As examples,  $Zn^{2+}$  can inhibit the cellular respiration, and  $Ag^+$  can act an analog on  $Ca^{2+}$  receptor sites [Frohlich *et al.*, 2013]. However, *in vitro* and *in vivo* studies have shown that hybrid silver nanoparticles possess various levels of toxicity according to their size, shape, functionalization and mode of exposition [Dos Santos *et al.*, 2014]. Under some conditions, silver nanoparticles have shown to pass the blood-brain barrier and accumulate in different region of brain. This could be interesting for targeting brain tumor but maybe also dangerous for neural toxicity [Sarin *et al.*, 2008].

Such toxicity problems will only be resolved by suitable testing *in vivo* on several animal species and thus will require a lengthy period of waiting.

### Financial & competing interest disclosure

The authors are funded in whole or in part by Université Lyon 1 and LIMMS, University of Tokyo. The authors have no other relevant affiliations or financial involvement with any organization or entity with a financial interest in or financial conflict with the subject matter or materials discussed in the manuscript apart from those disclosed. No writing assistance was utilized in the production of this manuscript.

### References

Papers of special note have been highlighted as:

\* of interest

\*\* of considerable interest

Acharya A, Samanta K, Rao CP. **Conjugates of calixarenes emerging as molecular entities of nanoscience.** *Cood. Chem. Rev.* 256, 2096-2125 (2012).

Agasti SS, Rana S, Park MH, Kim CK, You CC, Rotello VM. **Nanoparticles for detection and diagnosis.** *Adv. Drug Deliver. Rev.* 62, 316–328 (2010).

Amendola V, Bakr OM, Stellacci F. **A study of the surface plasmon resonance of silver nanoparticles by the discrete dipole approximation method: Effect of shape, size, structure and assembly.** *Plasmonic.* 5, 85-97 (2010).

Atwood JL, Barbour LJ, Dawson ES, Junk PC, Kienzle J. **X-ray structure of the water soluble [adeninium][p-sulfonatocalix[4]arene] which displays cationic and anionic bilayers.** *Supra. Chem.* 7, 271-274 (1996).

Arnaud Neu F, Bohmer V, Guerra L, McKervey MA, Paulus AF, Rodriguez A, *et al.* **Metal ion complexation by tetraester derivatives of bridged calix[4]arenes.** *J. Phys. Org. Chem.* 5, 471-481 (1992).

Baghayeri M, Namadchian M, Karimi-Maleh H, Beitollahi H. **Determination of nifedipine using nanostructured electrochemical sensor based on simple synthesis of Ag nanoparticles at the surface of glassy carbon electrode: Application to the analysis of some real sample.** *J. Electroanal. Chem.* 697, 53-59 (2013).

Bian Y, Li C, Li H. **para-Sulfonatocalix[6]arene-modified silver nanoparticles electrodeposited on glassy carbon electrode: Preparation and electrochemical sensing of methyl parathion.** *Talanta.* 81, 1028–1033 (2010).

Bolisetty S, Jaimes EA. **Mitochondria and Reactive Oxygen Species: Physiology and Pathophysiology.** *Int. J. Mol. Sci.* 14, 6306-6344 (2013).

Boudebouze S, Coleman AW, Tauran Y *et al.* **Discriminatory antibacterial effects of calix[n]arene capped silver nanoparticles with regard to Gram positive and Gram negative bacteria.** *Chem. Commun.* 49, 7150-7152 (2013).

\*\* shows that *para*-sulphonato-calix[n]arenes are active against Gram positive bacteria and the derivatives having sulphonate groups at both para and alkyl terminal positions are active against Gram negative bacteria.

Brown PO, Enright GD, Ripmeester JA. **Nanocrystalline Ag from supramolecular stabilization of metals in 4-tert-butylcalix[4]arene lattices.** *Chem. Asian J.* 1, 529–535 (2006).

Cecillon S, Coleman AW, Eveno-Nobile A, Perron H, Rodrigue M. **Method for detecting aggregate-forming circulating protein forms using an agent for aggregating said forms and an agent for capturing formed aggregates.** Patent US 8158441 B2 (2005).

Che Man YB, Aida AA, Raha AR, Son R. **Identification of pork derivatives in food products by species-specific polymerase chain reaction (PCR) for halal verification.** *Food Control.* 18, 885–889 (2007).

Cho EJ, Kang JK, Han WS, Jung HJ. **Stimuli-responsive supramolecular nanostructure from amphiphilic calix[4]arene and its three-dimensional dendritic silver nanostructure.** *Langmuir.* 24, 5229-5232 (2008).

Choudhari SK, Chaudhary M, Gadbañal AR, Sharma A, Tekade S. **Oxidative and antioxidative mechanisms in oral cancer and precancer: A review.** *Oral Oncology.* 50, 10–18 (2014).

Coleman AW, Perret F, Moussa A, Dupin M, Guo Y, Perron H. Calixarenes as Protein Sensors. In: *Creative Chemical Sensor Systems.* Schrader T (Ed.) Springer, Berlin, Germany, 2007, 31–88 (2007a).

Coleman AW, Baggetto LG, Lazar AN, Michaud MH, Magnard S. **Calixarene derivatives as anticancer agent.** Patent WO2007119027 A1. (2007b).

Coleman AW, Jebors S, Cecillon S, Perret P, Garin D, Marti-Battle D, Moulin M. **Toxicity and biodistribution of *para*-sulphonato-calix[4]arene in mice.** *New J. Chem.* 32, 780-782 (2008).

Da Silva E, Coleman A.W. **Synthesis and complexation properties towards amino acids of mono-substituted *p*-sulphonato-calix-[n]-arenes.** *Tetrahedron.* 59, 7357–7364 (2003).

Da Silva E, Shahgaldian P, Coleman AW. **Haemolytic properties of some water-soluble *para*-sulphonato-calix-[n]-arenes.** *Int. J. Pharm.* 273, 57–62 (2004).

Da Silva E, Rousseau CF, Zanella-Cleon I, Becchi M, Coleman AW. **Mass spectrometric determination of association constants of Bovine Serum Albumin (BSA) with *para*-sulphonato-calix[n]arene derivatives.** *J. Inc. Phenom. Macro. Chem.* 54, 53–59 (2006).

Del Puerto E, Sanchez-Cortes S, Garcia-Ramos JV, Domingo C. **Solution SERS of an insoluble synthetic organic pigment-quinacridone quinone-employing calixarenes as dispersive cavitands.** *Chem. Commun.* 47, 1854–1856 (2011).

Derkachova A, Kolwas K. **Simple analytic tool for spectral control of dipole plasmon resonance frequency for gold and silver nanoparticles.** *Photonics Letters of Poland.* 5(2), 69-71 (2013).

\* gives a mathematically simple tool allowing us to predict dipole localized surface plasmon resonance frequency as a function of size of gold and silver nanoparticles in water.

Doria G, Conde J, Veigas B *et al.* **Noble Metal Nanoparticles for Biosensing Applications.** *Sensors.* 12, 1657-1687 (2012).

\* reviews the use of noble metal nanoparticles for biosensing strategies from synthesis and functionalization to integration in molecular diagnostics platforms.

Dos Santos CA, Seckler MM, Inle AP, Gupta I, Galdiero S, Galdiero M, *et al.* **Silver nanoparticles: therapeutical uses, toxicity, and safety issues.** *J. Pharm. Sci.* 103, 1931–1944 (2014).

Dupont N, Lazar AN, Perret F *et al.* **Solid state structures of the complexes between the antiseptic chlorhexidine and three anionic derivatives of calix[4]arene.** *Cryst. Eng. Comm.*, 10, 975–977 (2008).

Evtugyn GA, Shamagsumova RV, Sitdikov RR. **Dopamine sensor based on a composite of silver nanoparticles implemented in the electroactive matrix of calixarenes.** *Electroanalysis*, 23(10), 2281 – 2289 (2011).

Fleming A. **On the antibacterial action of cultures of a penicilium, with special reference to their use in the isolation of B. Influenzae.** *Brit. J. Exp. Pathol.* 10(3), 226-236 (1929).

Foldbjerg R, Autrup H. **Mechanisms of silver nanoparticle toxicity.** *Arch. Bas. App. Med.* 1, 5-15 (2013).

Fröhlich E. **Cellular targets and mechanisms in the cytotoxic action of non-biodegradable engineered nanoparticles.** *Curr Drug Metab.* 14, 976–988 (2013).

Gao S, Yuan D, Lü J, Cao R. **In situ synthesis of Ag nanoparticles in aminocalix[4]arene multilayers.** *J. Coll. Int. Sci.* 341, 320–325 (2010).

Guerrini L, Garcia-Ramos JV, Domingo C, Sanchez-Cortes S. **Functionalization of Ag nanoparticles with dithiocarbamate calix[4]arene as an effective supramolecular host for the surface-enhanced raman scattering detection of polycyclic aromatic hydrocarbons.** *Langmuir.* 22, 10924-10926 (2006).

Guerrini L, Jurasekova Z, Domingo C *et al.* **Importance of metal–adsorbate interactions for the surface-enhanced raman scattering of molecules adsorbed on plasmonic nanoparticles.** *Plasmonics.* 2, 147–156 (2007).

Guerrini L, Garcia-Ramos JV, Domingo C, Sanchez-Cortes S. **Sensing polycyclic aromatic hydrocarbons with dithiocarbamate-functionalized Ag nanoparticles by surface-enhanced raman scattering.** *Anal. Chem.* 81, 953–960 (2009).

\* demonstrates that the functionalization of silver nanoparticles with a dithiocarbamate calix[4]arene host led to a sensitive and selective system in the detection of PAHs by Surface Enhanced Raman Spectroscopy.

Ghosh S.K., Pal T. **Interparticle coupling effect on the surface plasmon resonance of gold nanoparticles: From theory to application.** *Chem. Rev.* 107, 4797-4862 (2007).

Grare M, Massimba Dibama H, Lafosse S *et al.* **Cationic compounds with activity against multidrug-resistant bacteria : interest of a new compound compared with two older antiseptics, hexamidine and chlorhexidine.** *Clin. Microbiol. Infect.* 16, 432-438 (2009).

Grare M, Duval RE. **Use of calixarenes associated with an antibiotic in the treatment of bacterial infections.** Patent n° US 2014/0066365 A1 (2014).

Gunsalus IC. The structure and biosynthesis of bacteria cell walls (Chapter 6). In: *The Bacteria: A Treatise on Structure and Function.* Spkatch JR (Ed.) Academic Press Inc. London, UK. 291-415 (1986).

Gutsche CD. Shaping the Baskets: Conformations of Calixarenes (Chapter 4). In: *Calixarenes an Introduction, 2<sup>nd</sup> Edition.* The Royal Society of Chemistry, Cambridge, UK, 77-115 (2008).

Hartlieb KL, Martin AD, Saunders M, Raston CL. **Photochemical generation of small silver nanoparticles involving multi-functional phosphonated calixarenes.** *New J. Chem.* 34, 1834–1837 (2010).

Hennebel T, De Gusseme B, Boon N, Verstraete W. Biogenic metals in advanced water treatment. *Trends Biotechnol* 27, 90–98 (2009).

Jain PK, Huang X, El-Sayed IH, El-Sayed MA. **Review of Some Interesting Surface Plasmon Resonance-enhanced Properties of Noble Metal Nanoparticles and Their Applications to Biosystems.** *Plasmonics*. 2, 107–118 (2007).

Janrungratsakul W, Vilaivan T, Vilaivan C, Watchasit S, Suksai C, Ngeontae W, *et al.* **New calix[4]arene derivatives as ionophores in polymeric membrane electrodes for Ag(I): Comparative selectivity studies and detection of DNA hybridization.** *Talanta*. 105, 1–7 (2013).

Ju-Nam Y, Lead JR. **Manufactured nanoparticles: An overview of their chemistry, interactions and potential environmental implications.** *Sci. Total Environ*. 400, 396–414 (2008).

Kim HJ, Lee HM, Mutihac L, Vicens J, Kim SJ. **Host-guest sensing by calixarenes on the surfaces.** *Chem. Soc. Rev*. 41, 1173–1190 (2012).

Lemire JA, Harrison JJ, Turner RJ. **Antimicrobial activity of metals: mechanisms, molecular targets and applications.** *Nature Reviews Microbiology*. 11: 371–384 (2013).

Le Ru E, Etchegoin P. A quick overview of surface-enhanced Raman spectroscopy (Chapter 1). In: *Principles of Surface Enhanced Raman Spectroscopy, 1st Edition*. Elsevier, Amsterdam, The Netherlands. 1–27 (2009).

Leyton P, Sanchez-Cortes S, Garcia-Ramos JV *et al.* **Selective molecular recognition of Polycyclic Aromatic Hydrocarbons (PAHs) on calix[4]arene-functionalized Ag nanoparticles by Surface-Enhanced Raman Scattering.** *J. Phys. Chem. B*. 108, 17484–17490 (2004).

Liu W, Wu Y, Wang C, Li HC, Wang T, Liao CY, *et al.* **Impact of silver nanoparticles on human cells: effect of particle size.** *Nanotoxicol*. 4, 319–330 (2010).

Magrini A, Bergamaschi A, Bergamaschi E. **Carbon nanotubes (CNT) and nanoparticles (NP): interaction with lung epithelium and other biological systems.** *G. Ital. Med. Lav. Ergon*. 28, 266–269 (2006).

Marra M, Salzano G, Leonetti C, Porru M, Franco R, Zappavigna S, *et al.* **New self-assembly nanoparticles and stealth liposomes for the delivery of zoledronic acid: a comparative study.** *Biotechnology Advances*. 30, 302–309 (2012).

Mayer KM, Hafner JH. **Localized surface plasmon resonance sensors.** *Chem. Rev*. 111, 3828–3857 (2011).

Mayergoz ID. Volume 6: **Plasmon resonances in nanoparticles.** Ed. World Scientific Publishing. Singapore, Singapore. (2013).

McGovern RE, Fernandes H, Khan AR, Power NP, Crowley PB. **Protein camouflage in cytochrome c–calixarene complexes.** *Nat. Chem*. 4, 527–533 (2012).

Memmi L., Lazar A., Brioude A., Ball V., Coleman A.W. **Protein–calixarene interactions: complexation of Bovine Serum Albumin by sulfonatocalix[n]arenes.** *Chem. Commun.*, 7, 2474–2475 (2001).

Namba T, Nolte CT, Jackrel J, Grob D. **Poisoning due to organophosphate insecticides.** *Am. J. Med*. 50, 475–492 (1971).

Navarro JRG, Werts MHV. Resonant light scattering spectroscopy of gold, silver and gold–silver alloy nanoparticles and optical detection in microfluidic channels. *Analyst*. 138, 583–592 (2013).

Ngeontae W, Janrungratsakul W, Morakot N, Aeungmaitrepirom W, Tuntulani T. **New silver selective electrode fabricated from benzothiazole calix[4]arene: Speciation analysis of silver nanoparticles.** *Sensors and Actuators B*. 134, 377–385 (2008).

Ngeontae W, Janrungratsakul W, Maneewattanapinyo P, Ekgasit S, Aeungmaitrepirom W, Tuntulani T. **Novel potentiometric approach in glucose biosensor using silver nanoparticles as redox marker.** *Sensors and Actuators B.* 137, 320–326 (2009).

Nguyen KC, Seligy VL, Massarsky A. **Comparison of toxicity of uncoated and coated silver nanoparticles.** *Journal of Physics: Conference Series.* 429, 1-15 (2013).

Menon SK, Modi NR, Pandya A, Lodha A. **Ultrasensitive and specific detection of dimethoate using a p-sulphonato-calix[4]resorcinarene functionalized silver nanoprobe in aqueous solution.** *RSC Advances,* 3, 10623-10627 (2013).

\* demonstrates a facile strategy for preparing highly stable silver nanoprobe modified *para*-sulphonato-calix[4]resorcinarene which were utilized for the selective recognition of insecticide dimethoate.

Lamberti M, Zappavigna S, Sannolo N, Porto S, Caraglia M. **Advantages and risks of nanotechnologies in cancer patients and occupationally exposed worker.** *Expert Opin. Drug Deliv.* 11: 1087-1101 (2014)

Lewis K. **Platforms for antibiotic discovery.** *Nat. Rev.* 12, 371-387 (2013).

Li P, Li J, Wu C, Wu Q, Li J. **Synergistic antibacterial effects of  $\beta$ -lactam antibiotic combined with silver nanoparticles.** *Nanotechnology.* 16, 1912–1917 (2005).

O'Connor KM, Svehla G, Harris SJ, McKervey MA. **Calixarene potentiometric ion-selective electrodes for silver.** *Talanta.* 39, 1549-1554 (1992).

Ostacolo L, Marra M, Ungaro F, Zappavigna S, Maglio G, Quaglia F, *et al.* **In vitro anticancer activity of docetaxel-loaded micelles based on poly(ethylene oxide)-poly(epsilon-caprolactone) block copolymers: Do nanocarrier properties have a role?** *J. Cont. Releas.* 148, 255-263 (2010).

Pandya A, Joshi KV, Modi NR, Menon SK. **Rapid colorimetric detection of sulfide using calix[4]arene modified gold nanoparticles as a probe.** *Sensor. Actuat. B-Chem.* 168, 54– 61 (2012).

Pandya A, Sutariya PG, Lodha A, Menon SK. **A novel calix[4]arene thiol functionalized silver nanoprobe for selective recognition of ferric ion with nanomolar sensitivity via DLS selectivity in human biological fluid.** *Nanoscale.* 5, 2364-2371 (2013).

\*\* developed a rapid response and sensitive calix[4]arene functionalized silver nanoprobe based system that can selectively detect  $Fe^{3+}$  in an aqueous medium.

Pearson RG. **Hard and Soft Acids and Bases.** *J. Am. Chem. Soc.* 85, 3533–3539 (1963).

Perret F., Morel-Desrosiers N., Coleman A.W. **An ESI/MS study of the formation of ternary 25,27-bis(dihydroxy-phosphoryloxy) calix[4]arene-metal ion-aminoacid complexes.** *J Supra. Chem.* 2, 533–536 (2002).

Perret F, Lazar AN, Coleman AW. **Biochemistry of the para-sulfonato-calix[n]arenes.** *Chem. Commun.* 23, 2425-2438 (2006).

Perret F. , Peron H. , Dupin M., Coleman A.W. **Calixarenes as protein sensors,** in **Topic in current chemistry, Creative chemical sensor systems,** ed. T. Schrader, Springer, Berlin, vol. 277, pp. 31–88 (2007).

Perret F, Coleman AW. **Biochemistry of anionic calix[n]arenes.** *Chem. Commun.* 47, 7303-7319 (2011).

\*\* Reviews the biological properties of the various anionic calix[n]arenes, both as soluble forms and in the colloidal state, best used in combination with reference (McGovern *et al* 2013).

Perret F, Coleman AW. Interactions of calix[n]arenes and other organic supramolecular systems with proteins (Chapter 6). In: *Supramolecular Systems in Biomedical Fields*. Schneider H-J (Ed.), The Royal Society of Chemistry, Cambridge, UK, 140-163 (2013a).

\*\* discusses how various proteins recognize, stabilize or are inhibited by organic supramolecular systems, with emphasis on the actions of the calix[n]arenes.

Perret F, Tauran Y, Suwinska K *et al.* **Molecular recognition and transport of Active Pharmaceutical Ingredients on anionic calix[4]arene capped silver nanoparticles.** *Journal of Chemistry*, 2013, 1-9 (2013b). DOI: 10.1155/2013/191828.

Podyachev SN, Kashapova NE, Syakaev VV, Sudakova SN, Zainullina RR, Gruner M, *et al.* **Mercury(II) and silver(I) receptors based on tetrathiacalix[4]arene hydrazones.** *J. Incl. Phenom. Macrocycl. Chem.* 78, 371–380 (2014).

Rai M, Gade A, Yadav A. Biogenic nanoparticles: An introduction to what they are, how they are synthesized and their applications. In: *Metal nanoparticles in microbiology*. Rai M Duran N (Ed.) Springer-Verlag Berlin Heidelberg, Berlin, Germany (2011)

Rodik R.V., Boyko V.I., Kalchenko V.I. **Calixarenes in Bio-Medical Researches.** *Curr. Med. Chem.* 16, 1630-1655 (2009).

Rosi NL, Mirkin CA. **Nanostructures in biodiagnostics.** *Chem. Rev.* 105, 1547-1562 (2005).

Sarin H, Kanevsky AS, Wu H, Brimacombe KR, Fung SH, Sousa AA, *et al.* **Effective transvascular delivery of nanoparticles across the blood-brain tumor barrier into malignant glioma cells.** *Journal of Translational Medicine.* 6, 80 (2008).

Schrader T., Klaerner F.G., Fokkens M., Zadnani R., Polkowska J., Bastkowski F., Less C.J. **Novel active substances for treating, diagnosing and preventing macular degeneration.** WO 2006056182 A1 (2006).

Sintubin L, Verstraete W, Boon N. Biologically produced nanosilver: Current state and future perspectives. *Biotech. Bioeng.* 109, 2422-2436 (2012).

Shahgaldian P, Da Silva E, Coleman AW. **A First Approach to the study of calixarene Solid Lipid Nanoparticle (SLN) toxicity.** *J. Incl. Phenom. Macrocycl. Chem.* 46: 175-177 (2003).

Shinkai S, Tsubaki T, Sone T, Manabe O. **New water-soluble host molecules derived from calix[6]arene.** *Tetrahedron Lett.* 25: 5315-5318 (1984).

Steed JW, Atwood JL. Molecular Guests in Solution (Chapter 6). In: *Supramolecular Chemistry, 2<sup>nd</sup> Edition*. John Wiley & Sons, Chichester, UK, 307 - 380 (2009).

Sun Y. **Controlled synthesis of colloidal silver nanoparticles in organic solutions: empirical rules for nucleation engineering.** *Chem. Soc. Rev.* 42, 2497-2511(2013).

Tauran Y, Grosso M, Brioude A, Kassab R, Coleman AW. **Colourimetric and spectroscopic discrimination between nucleotides and nucleosides using para-sulfonato-calix[4]arene capped silver nanoparticles.** *Chem. Commun.* 47(36), 10013-10015 (2011).

\* shows that the interactions of para-sulphonatocalix[4]arene capped silver nanoparticles with nucleotides, nucleosides and deoxynucleosides yield selective complexation reflected both in changes in colour and in the visible spectrum due to aggregate formation.

Tauran Y, Brioude A, Shahgaldian P *et al.* **Calixarene silver nanoparticles interactions with surfactants are charge, size and critical micellar concentration dependent.** *Chem. Commun.* 48, 9483-9485 (2012).

Tauran Y, Brioude A, Coleman AW, Rhimi M, Kim B. **Molecular recognition by gold, silver and copper nanoparticles.** *World Journal of Biological Chemistry.* 4, 35-63 (2013a).

Tauran Y, Brioude A, Kim B, Perret F, Coleman AW. **Anionic Calixarene-Capped Silver Nanoparticles Show Species-Dependent Binding to Serum Albumins.** *Molecules.* 18, 5993-6007 (2013b).

Tauran Y, Rhimi M, Ueno R *et al.* **Cytosine: *para*-sulphonato-calix[4]arene assemblies: in solution, in the solid-state and on the surface of hybrid silver nanoparticles.** *J Incl Phenom Macrocycl Chem.* 77, 213-221 (2013c).

Tauran Y, Anjard C, Kim B, Rhimi M, Coleman AW. **Large supramolecular organic macrocycles as inhibitors of endonuclease enzymes.** *Chem. Commun.* (2014) DOI:10.1039/c4cc04805a.

Tauran Y, Kim B, Coleman AW. **Biological activities of calixarene in cellular bioassays and in vivo.** *EXCLI Journal.* Submitting (2015).

Toyokuni S. **Role of iron in carcinogenesis: Cancer as a ferrotoxic disease.** *Cancer Sci.* 100, 9-16 (2009)

Tsiftoglou AS, Tsamadou AI, Papadopoulou LC. **Heme as key regulator of major mammalian cellular functions: Molecular, cellular, and pharmacological aspects.** *Pharmacol. Therapeut.* 111, 327-345 (2006).

Ukhatskaya EV, Kurkov SV, Hjálmarsson MA, Karginov VA, Matthews SE, Rodik RV, *et al.* **Cationic quaternized aminocalix[4]arenes: cytotoxicity, haemolytic and antibacterial activities.** *Int J Pharm.* 458, 25-30 (2013).

Valluru G, Georghiou PE, Sleem HF, Perret F, Montasser I, Grandvoinet A, *et al.* **Molecular recognition of nucleobases and amino acids by sulphonato-calixnaphthalene-capped silver nanoparticles.** *Supra. Chem.* 26, 561-568 (2014).

Vilela D, González MC, Escarpa A. **Sensing colorimetric approaches based on gold and silver nanoparticles aggregation: Chemical creativity behind the assay. A review.** *Analytica Chimica Acta.* 751, 24- 43 (2012).

\* reports the main achievements of gold nanoparticles and silver nanoparticles aggregation for sensing colorimetric methods.

Wang K, Guo DS, Zhang HQ, Li D, Zheng XL, Liu Y. **Highly effective binding of viologens by *p*-sulfonatocalix[n]arenes for the treatment of viologen poisoning.** *J Med Chem* 52,6402-6412 (2009).

Wong K.K.Y, Liu X. **Silver nanoparticles—the real “silver bullet” in clinical medicine?** *Med. Chem. Commun.* 1, 125-131 (2010).

Xiong D, Chen M, Li H. **Synthesis of *para*-sulfonatocalix[4]arene-modified silver nanoparticles as colorimetric histidine probes.** *Chem. Commun.* (7), 880-882 (2008).

Yang YW, Sun YL, Song N. **Switchable host guest systems on surfaces.** *Acc. Chem. Res.* 47, 1950-1960 (2014).

Zhan J, Wen L, Miao F, Tian D, Zhu X, Li H. **Synthesis of a pyridyl-appended calix[4]arene and its application to the modification of silver nanoparticles as Fe<sup>3+</sup> colorimetric sensor.** *New J. Chem.* 36, 656-661 (2012).

Zhou R, Shileng T, Srinivasan MP. **In situ formation of silver nanoparticle layer by supramolecule-directed assembly.** *Thin Solid Films.* 550, 210-219 (2014).



## Part B

# Results



## Part B

### Section 1

# Biosensing by calix[n]arene capped silver nanoparticles



## **Colourimetric and spectroscopic discrimination between nucleotides and nucleosides using para-sulfonato-calix[4]arene capped silver nanoparticles**

Titre: Spectroscopique et colorimétrique distinction entre nucléotides et nucléosides utilisant des nanoparticules d'argent fonctionnalisées par le *para*-sulphonato-calix[4]arene

Résumé: La complexation entre nucleosides et nucléotides par des nanoparticules hybrides fonctionnalisées à base de *para*-sulphonato-calix[4]arene montre un comportement optique distinct entre les molécules à base purine ou pyrimidine. Pour les nucléotides pyrimidine, il y a apparition d'une nouvelle bande d'absorption autour de 550nm, et un changement de couleur du jaune au rouge orange et rose.

Cite this: DOI: 10.1039/c1cc13175c

www.rsc.org/chemcomm

## COMMUNICATION

Colourimetric and spectroscopic discrimination between nucleotides and nucleosides using *para*-sulfonato-calix[4]arene capped silver nanoparticles†Yannick Tauran,<sup>a</sup> Marie Grosso,<sup>a</sup> Arnaud Brioude,<sup>a</sup> Rima Kassab<sup>b</sup> and Anthony W. Coleman<sup>\*a</sup>

Received 30th May 2011, Accepted 24th July 2011

DOI: 10.1039/c1cc13175c

The complexation of nucleosides and nucleotides by hybrid nanoparticles capped by *para*-sulfonato-calix[4]arene shows clear discrimination between purine and pyrimidine based molecules. For the pyrimidine nucleotides there is appearance of a new absorption band around 550 nm, and a colour change from yellow to orange red and pink.

The calix[*n*]arenes are one of the most widely studied organic host classes.<sup>1</sup> In recent years their interactions with biological molecules,<sup>2</sup> and indeed their biochemistry<sup>3,4</sup> have been widely studied. In contrast to the large body of work on their complexation with amino acids,<sup>5</sup> peptides<sup>6</sup> or proteins<sup>7</sup> the study of their interactions with nucleosides,<sup>8</sup> nucleotides<sup>9</sup> and RNA<sup>10</sup> or DNA<sup>11</sup> is sparse. Generally the work has concentrated on coupling nucleosides onto the calix[*n*]arene skeleton,<sup>12</sup> although Goto *et al.* have studied the extraction of various nucleosides where a strong selectivity for adenine was observed.<sup>13</sup> The solid-state structures between *para*-sulfonato-calix[4]arene and the adeninium cation,<sup>14</sup> and also the mixed system guanine and cytosine,<sup>15</sup> have been reported.

Recently Xiong *et al.* have developed stable nanoparticles of silver or gold capped with *para*-sulfonato-calix[4]arene.<sup>16,17</sup> These have been shown to colourimetrically recognise amino acids with a high selectivity for histidine.

The use of metal nanoparticles for the complexation and detection of nucleic acids,<sup>18</sup> has received a large amount of attention, particularly as the method is sensitive enough to detect heavy metal ion induced DNA damage.<sup>19</sup>

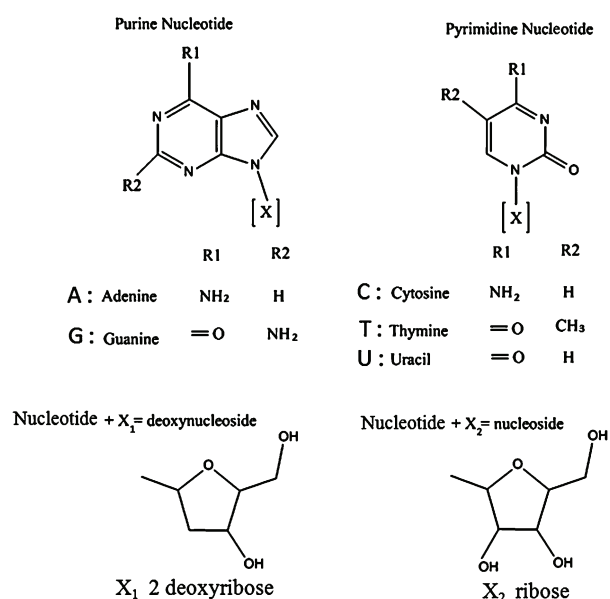
In this communication we describe the interactions between nucleic bases and *para*-sulfonato-calix[4]arene capped silver nanoparticles. New absorbances at around 530 nm occur for

pyrimidine bases accompanied by a colour shift from yellow to orange red and pink; these changes arise from nanoparticle aggregation.

The chemical structures of the nucleic bases and nucleotides are given in Scheme 1, in which it can be seen that the purines are composed of two heterocycles whereas the pyrimidines contain only one heterocycle.

The *para*-sulfonato-calix[4]arene capped silver nanoparticles, SC4:Ag NPs, were prepared by the method reported by Xiong *et al.*,<sup>16</sup> to these NPs were added solutions of the nucleic bases and nucleotides at a concentration of 10<sup>-2</sup> M and then diluted to 10<sup>-3</sup> M. The spectra were measured directly using a 96 titre well visible spectrometer.

The spectra are shown, at 1 hour after addition, in Fig. 1a–c and at 24 hours after addition, in Fig. 2a–c.



**Scheme 1** Aromatic purine and pyrimidine ring structure of nucleotide bases. Differing side groups for all five different bases are indicated by R1 and R2. Deoxyribose or ribose conjugated with nucleotides gives deoxynucleoside or nucleoside.

<sup>a</sup> LMI CNRS UMR 5615, Univ. Lyon 1, Villeurbanne, F69622, France. E-mail: antony.coleman@adm.univ-lyon1.fr; Tel: +33 4 4243 1027

<sup>b</sup> University of Balamand, Faculty of Sciences, Department of Chemistry, P.O. Box: 100, Tripoli, Lebanon. E-mail: rima.kassab@balamand.edu.lb; Tel: +961 6 930250

† Electronic supplementary information (ESI) available. See DOI: 10.1039/c1cc13175c

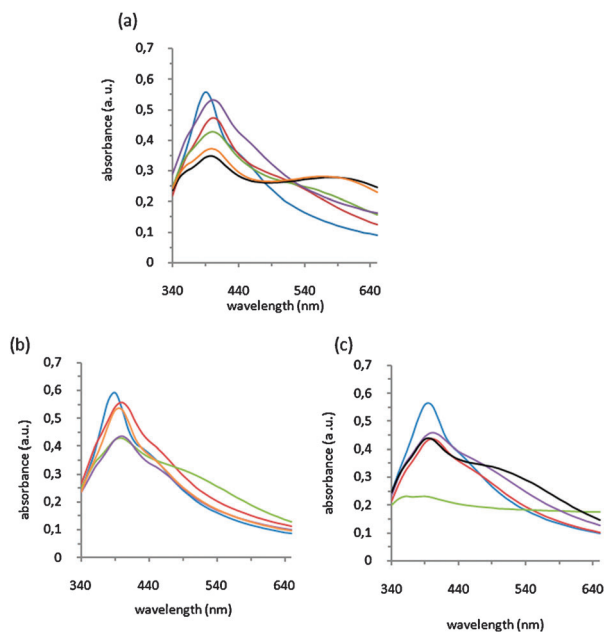


**Fig. 1** Visible spectra of the complexation of (a) nucleotide, (b) nucleoside and (c) deoxy-nucleoside bases with SC4:Ag NPs after one hour at a final concentration of  $10^{-3}$  M. Blue line: pSC4:Ag NP; red line: pSC4-Ag NP + A; purple line: pSC4-Ag NP + G; green line: pSC4-Ag NP + C; orange line: pSC4-Ag NP + U; black line: pSC4-Ag NP + T.

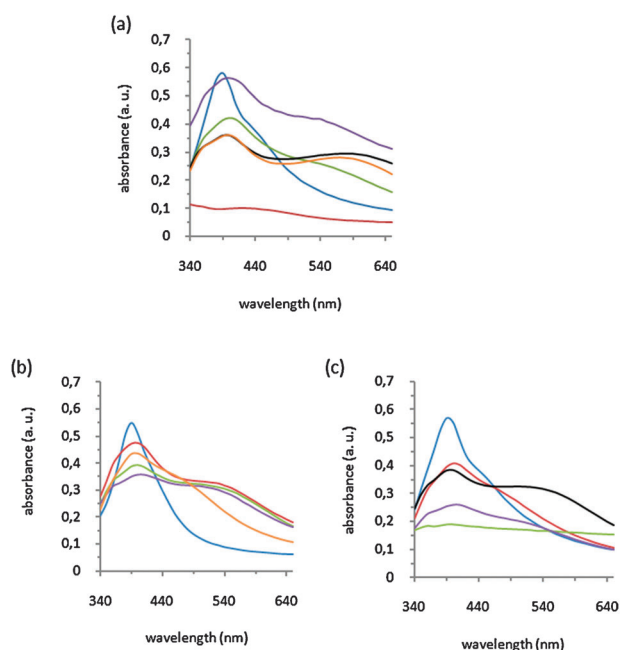


**Fig. 2** Visible spectra of the complexation of (a) nucleotide, (b) nucleoside and (c) deoxy-nucleoside bases with SC4:Ag NPs after one hour at a final concentration of  $10^{-3}$  M. Blue line: pSC4-Ag NP; red line: pSC4-Ag NP + A; purple line: pSC4-Ag NP + G; green line: pSC4-Ag NP + C; orange line: pSC4-Ag NP + U; black line: pSC4-Ag NP + T.

In Fig. 3 are given photographic images of the solutions. There are clear visible differences between the various nucleotides and nucleosides. For the nucleotides the pyrimidine bases are red to violet. For the nucleosides only cytosine leads to a visible change.

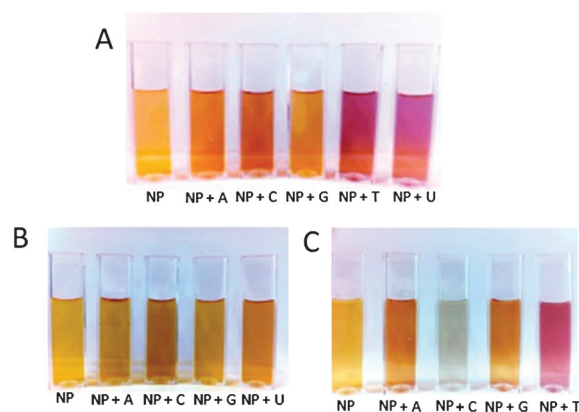


**Fig. 3** Photographs of the complexation of (A) nucleotide, (B) nucleoside and (C) deoxy-nucleoside bases with SC4:Ag NPs after one hour at a final concentration of  $10^{-3}$  M.

However for the deoxy-nucleotides with thymidine the solution turns violet and with cytosine there is a pale grey solution without the presence of the plasmon resonance.

With regard to the visible spectra a redshift occurs in the plasmonic absorption for all systems. This shift, see Table S1 (ESI<sup>†</sup>), indicates that there is complexation on the nanoparticle of the nucleotides, nucleosides and deoxy-nucleotides. The red shift of 10 nm is constant for all the systems studied here. Considering the thickness and the refractive index of layers formed at the metallic nanoparticles surface by those organic molecules, such behaviour is consistent with red shifts already observed in many systems.<sup>20</sup>

In the case of the nucleotides, after one hour for adenine and guanine, the spectra are essentially identical to the SC4:AgNPs. For cytosine a second peak appears at 540 nm, now for thymine and uracil this peak is strongly red shifted to 580 nm. After 24 hours the situation has again changed considerably; now for guanine a peak appears at 540 nm, while the peak for the cytosine complex remains at 540 nm. The peak arising from uracil remains at 580 nm while that for thymine shifts slightly to 590 nm. Intriguingly for adenine after 24 hours a clear solution of SC4:AgNPs was obtained, this is a highly reproducible phenomenon.

This effect is of considerable interest as cytosine and thymidine are present in RNA and DNA whereas uracil is present only in RNA. This suggests a possible spectroscopic means of determining RNA and DNA contents.

For the nucleosides after 1 hour, a second peak at higher wavelength appears at 450 nm for adenosine, uridine, guanosine and at 490 nm for cytidine. Such plasmon resonance bands can be attributed to the formation of metallic nanoparticle aggregates.<sup>20</sup> The situation changes radically after 24 hours now in all cases there is the presence of a peak at 520 nm except for uridine where the band is shifted to 470 nm. Thus it is possible to discriminate between the two sets of nucleosides by the kinetics of their aggregation behaviour.

With regard to the deoxy-nucleosides, after one hour, the behaviour is somewhat different, again there is a red shift in the peaks associated with the plasmon resonance. For deoxy-adenosine and deoxy-guanosine an aggregation peak at 460 nm is present. The aggregation peak of deoxy-thymidine has been

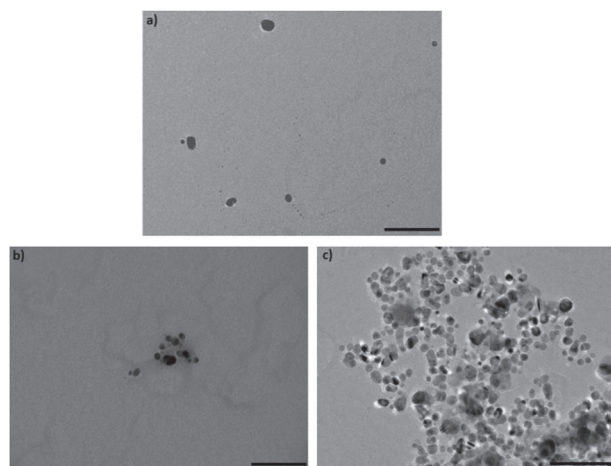


**Fig. 4** TEM images of pSC4-Ag NPs (a) alone, (b) after addition of adenosine at a final concentration of  $10^{-3}$  M, (c) after addition of thymidine at a final concentration of  $10^{-3}$  M. The scale bars are for all pictures 100 nm.

strongly red-shifted to 520 nm. However for the mixture of SC4:AgNPs with deoxy-cytidine the result is the loss of all peaks and the solution turns grey.

In general, there is also appearance of weak peaks and shoulders in the region of 360 nm which may be attributed to the presence of multipolar plasmon resonances (quadrupolar mode). This particular resonance is well-known in the silver case for nanoparticles size greater than 50 nm.<sup>21</sup>

Transmission electron microscopy, as shown above in Fig. 4, confirms the aggregation caused by deoxy-nucleosides. It can be clearly seen that the SC4:AgNPs are present alone as well separated objects around 20 nm in size. For adenosine where the spectrum shows a weak peak for the aggregation of small clumps of the nanoparticles is present. However in the case of thymidine where a strong peak at 540 nm is observed and there is a colour change to pink, the nanoparticles are strongly aggregated. Dynamic light scattering shows a population at 30 nm for SC4:AgNPs and for the thymidine complexed SC4:AgNPs a high degree of polydispersity is observed with populations up to 300 nm in diameter. For the less aggregated systems in addition to single particles there are in general populations of about 100 nm in diameter.

For the SC6:AgNPs and the SC8:NPs the situation is very different, here there is in most cases the 10 nm red shift, ESI<sup>+</sup> figures, but no aggregation takes place and hence no peaks are observed in the region 500–600 nm and no colour changes are observed.

The results obtained point to an association between the various types of nucleotides and nucleosides with the cavity of *para*-sulfonatocalix[4]arene, that is inconsistent with the proposition of Xiong *et al.*<sup>16</sup> where the *para*-sulfonatocalix[4]arene molecules coordinate to the NPs *via* the sulfonate groups thus blocking the cavity. A more reasonable explanation lies in the formation of the classic bilayer solid-state structure,<sup>22</sup> where alternate coordinated *para*-sulfonatocalix[4]arene molecules and available cavities are present at the surface of the

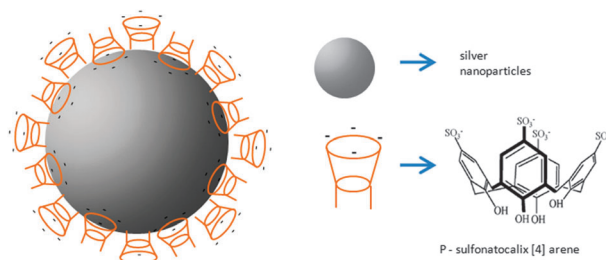


**Fig. 5** Schematic representation of the organization of *para*-sulfonatocalix[4]arene on silver nanoparticles.

nanoparticles, as shown in Fig. 5. This would be associated with a population of between 400 and 1000 molecules at the SC4:AgNPs surface.

In conclusion we have shown that the interactions of SC4:AgNPs with nucleotides, nucleosides and deoxy-nucleosides yield selective complexation reflected both in changes in colour and in the visible spectrum due to aggregate formation.

## Notes and references

- C. D. Gutsche, *Calixarenes an Introduction*, 2nd edn, The Royal Society of Chemistry, Cambridge, 2008.
- R. V. Rodik, V. I. Boyko and V. Kalchenko, *Curr. Med. Chem.*, 2009, **16**, 1630–1655.
- A. W. Coleman, F. Perret, A. Moussa, M. Dupin, Y. Gu and H. Perron, *Top. Curr. Chem.*, 2007, **277**, 31–88.
- F. Perret, A. N. Lazar and A. W. Coleman, *Chem. Commun.*, 2006, 2425–2438.
- E. Da Silva and A. W. Coleman, *Tetrahedron*, 2003, **59**, 7357–7364.
- N. Douteau-Guevel, F. Perret, A. W. Coleman, J. P. Morel and N. Morel-Desrosiers, *J. Chem. Soc., Perkin Trans. 2*, 2002, 524–532.
- R. Zadnurd and T. Schrader, *J. Am. Chem. Soc.*, 2005, **127**, 904–915.
- F. Sansone, L. Baldini, A. Casnati and R. Ungaro, *New J. Chem.*, 2010, **34**, 2715–2728.
- G. M. L. Consoli, G. Granata, R. Lo Nigro, G. Malandrino and C. Geraci, *Langmuir*, 2008, **24**, 6194–6200.
- R. Zadnurd and T. Schrader, *Angew. Chem., Int. Ed.*, 2006, **45**, 2703–2706.
- S. J. Kim and B. H. Kim, *Tetrahedron Lett.*, 2002, **43**, 6367–6371.
- G. M. L. Consoli, G. Granata, D. Garozzo, T. Mecca and C. Geraci, *Tetrahedron Lett.*, 2007, **48**, 7974–7977.
- K. Shimajo, T. Oshima and M. Goto, *Anal. Chim. Acta*, 2004, **521**, 163–171.
- J. L. Atwood, L. J. Barbour, E. S. Dawson, P. C. Junk and J. Kienzle, *Supramol. Chem.*, 1996, **7**, 271–274.
- P. J. Nichols, M. Makha and C. L. Raston, *Cryst. Growth Des.*, 2006, **6**, 1161–1167.
- D. Xiong, M. Chen and H. Li, *Chem. Commun.*, 2008, 880–882.
- T. T. Jiang, R. R. Liu, X. F. Huang, H. J. Feng, W. L. Teo and B. G. Xing, *Chem. Commun.*, 2009, 1972–1974.
- Y. Cai, J. Wang, Y. Xu and G. Li, *Biosens. Bioelectron.*, 2010, **25**, 1032–1036.
- Q. Zhang, P. Dai and Z. Yang, *Microchim. Acta*, 2011, **173**, 347–352.
- D. D. Lekeufack, A. Brioude, A. W. Coleman, P. Miele, J. Bellessa, L. D. Zeng and P. Stadelmann, *Appl. Phys. Lett.*, 2010, **96**, 253107.
- K. L. Kelly, E. Coronado, L. L. Zhao and G. C. Schatz, *J. Phys. Chem. B*, 2003, **107**, 668–677.
- A. W. Coleman, S. G. Bott, D. S. Morley, C. M. Means, K. D. Robinson, H. Zhang and J. L. Atwood, *Angew. Chem., Int. Ed. Engl.*, 1988, **27**, 1361–1362.

## **Cytosine: para-sulphonato-calix[4]arene assemblies: in solution, in the solid-state and on the surface of hybrid silver nanoparticles**

Titre: Assemblage cytosine : *para*-sulphonato-calix[4]arene : en solution, en état solide et à la surface de nanoparticules d'argent hybride

Résumé: La reconnaissance moléculaire de la cytosine par le *para*-sulphonato-calix[4]arene se passe en solution, à l'état solide, et par l'assemblage de *para*-sulphonato-calix[4]arene à la surface de nanoparticules d'argent. Chacun de ces états montre différents modes d'assemblage. En solution un complexe 1 : 1 est formé. A l'état solide un assemblage 4 : 1 existe, toutefois certaines des molécules cytosines sont présentes comme remplisseurs d'espace et ne participent pas dans le complexe avec le calix[n]arene hôte. Finalement, à la surface de nanoparticules d'argent hybrides *para*-sulphonato-calix[4]arene, un complexe cytosine / *para*-sulphonato-calix[4]arene 2 : 1 est observé. Le processus d'assemblage a été étudié par DOSY RMN, spectroscopie à fluorescence, diffusion dynamique de la lumière, Diffraction d'un seul cristal à l'état solide, spectroscopie UV-Visible et microscopie électronique. Les résultats démontrent comment la cytosine initie l'agrégation des nanoparticules d'argent hybrides *para*-sulphonato-calix[4]arene.

# Cytosine: *para*-sulphonato-calix[4]arene assemblies: in solution, in the solid-state and on the surface of hybrid silver nanoparticles

Yannick Tauran · Moez Rhimi · Ryohei Ueno · Marie Grosso · Arnaud Brioude ·  
Erwann Janneau · Kinga Suwinska · Rima Kassab · Patrick Shahgaldian ·  
Alessandro Cumbo · Bernard Fenet · Beomjoon Kim · Anthony W. Coleman

Received: 11 May 2012 / Accepted: 8 August 2012  
© Springer Science+Business Media B.V. 2012

**Abstract** The molecular recognition by *para*-sulphonato-calix[4]arene of cytosine, occurs in solution, in the solid-state and by assembly on the surface of *para*-sulphonato-calix[4]arene capped silver nanoparticles. Each of these states shows different modes of assembly; in solution a 1:1 complex is formed; in the solid state a 4:1 assembly exists, however some of the cytosine molecules are present as space fillers and do not participate in the host (guest complexes, finally on the surface of the hybrid silver/*para*-sulphonato-calix[4]arene nanoparticles a 2:1 cytosine/

*para*-sulphonato-calix[4]arene assembly is observed. The assembly processes have been studied by DOSY NMR, fluorescence spectroscopy, Dynamic Light Scattering (DLS), Single Crystal Solid State Diffraction, Visible Spectroscopy and Electron Microscopy. The results demonstrate how cytosine initiates the aggregation of the hybrid silver/*para*-sulphonato-calix[4]arene hybrid nanoparticles.

**Keywords** Cytosine · *Para*-sulphonato-calix[4]arene · Hybrid silver nanoparticles · Solution · Solid-state · Colloids

**Electronic supplementary material** The online version of this article (doi:10.1007/s10847-012-0235-4) contains supplementary material, which is available to authorized users.

Y. Tauran · M. Grosso · A. Brioude · A. W. Coleman (✉)  
LMI, CNRS UMR 5615, Univ. Lyon 1, Villeurbanne 69622,  
France  
e-mail: aw.coleman@ibcp.fr; antony.coleman@adm.univ-lyon1.fr

Y. Tauran · B. Kim  
LIMMS/CNRS-IIS (UMI 2820), University of Tokyo, Tokyo,  
Japan

M. Rhimi  
BMSSI UMR5086-CNRS, Institut de Biologie Et Chimie des  
Protéines FR3302, Univ. Lyon 1, 7 Passage du Vercors, Lyon  
69367, France

R. Ueno · B. Kim  
CIRMM, Institute of Industrial Science, University of Tokyo,  
Tokyo, Japan

E. Janneau  
Centre de diffractométrie Henri Longchambon, Univ. Lyon 1,  
Villeurbanne 69622, France

K. Suwinska  
Institute of Physical Chemistry, Polish Academy of Sciences,  
Kasprzaka 44/52, 01 224 Warszawa, Poland

K. Suwinska (✉)  
Faculty of Biology and Environmental Sciences, Cardinal  
Stefan, Wyszynski University in Warsaw, Wóycickiego 1/3, 01  
938 Warszawa, Poland  
e-mail: ksuwinska@ichf.edu.pl

R. Kassab  
Department of Chemistry, Faculty of Sciences, University of  
Balamand, P.O. Box 100, Tripoli, Lebanon

P. Shahgaldian · A. Cumbo  
Fachhochschule Nordwestschweiz, Hochschule für Lifesciences,  
Gründenstrasse 40, 4132 Muttenz, Switzerland

B. Fenet  
Centre Commun RMN, Univ. Lyon 1, Villeurbanne 69622,  
France

## Introduction

Molecular recognition events involving capped noble metal nanoparticles are generally associated with colour changes due to aggregation of the capped nanoparticles, for example in the recognition of oligonucleosides on gold nanoparticles [1]. Such aggregation events are sensitive enough to allow detection of a single base pair mutation [2]. Binding of strands of oligonucleosides will involve a large number of hydrogen bonds leading to strong binding in the aggregates.

The calix[*n*]arenes are one of the most widely studied organic host classes [3]. In recent years their interactions with biological molecules [4], and indeed the biochemistry of the *para*-sulphonato-calix[*n*]arenes [5, 6] and other calix[*n*]arenes have been widely studied [7]. With regard to the interactions between *para*-sulphonato-calix[4]arene and nucleic bases there exists the study by Atwood et al. [8] of the solid-state structure of the complex between *para*-sulphonato-calix[4]arene and the adeninium cation, and there is also an extensive study by Raston and co-workers [9] of mixed complexes between *para*-sulphonato-calix[4]arene and guanine and cytosine.

Recently Xiong et al. [10, 11] has developed stable hybrid nanoparticles of silver capped with *para*-sulphonato-calix[4]arene, which show colorimetric responses both to pesticides and also to amino-acids with a high selectivity for histidine, however it should be noted that neither lysine nor arginine were cited as a substrate in spite of their known binding to *para*-sulphonato-calix[4]arene. The complexation induces a clear diminution in the absorbance arising from the plasmonic resonance at 390 nm and an increase in the intensity of the aggregate band at 540 nm leading to a visible change in the colour of the solutions allowing easy detection. Very recently we have shown that nucleotides, nucleosides and deoxynucleosides bind differentially to *para*-sulphonato-calix[4]arene capped silver nanoparticles again inducing colour changes [12].

In this paper we have studied the assembly processes for the interaction of *para*-sulphonato-calix[4]arene with cytosine, in solution, in the solid state and as assemblies on the surface of hybrid *para*-sulphonato-calix[4]arene capped silver nanoparticles. The behavior and stoichiometries of the complexes in the three states would appear to be quite different. Given that we are treating assemblies in very different states the use of multiple physical methods is obviously required to probe the various assembly processes.

## Experimental

### Synthesis and analysis of *para*-sulphonato-calix[4]arene

The synthesis of *para*-sulphonato-calix[4]arene was carried out according to the method described by Coleman [13].

1 g of *para*-H-calix[4]arene was added to 4 mL of H<sub>2</sub>SO<sub>4</sub>. Then the mixture has been heated for 4 h at 90 °C. After cooling to room temperature, 1 mL of methanol was added, and the resulting solution was mixed with 300 mL of ethyl acetate. After stirring for 30 min, the product was obtained by filtration and drying. Yield of 85 % with purity superior to 95 %.

### *para*-sulphonato-calix[4]arene analysis

<sup>1</sup>H NMR (500 MHz, [dms<sub>o</sub>-d<sub>6</sub>, tetramethylsilane):  $\delta = 3.72\text{--}3.94$  (–CH<sub>2</sub>–), 7.14–7.36 (Ar–H); MALDI-TOF-MS: *m/z* [M + H] + calculated for (C<sub>28</sub>H<sub>24</sub>O<sub>16</sub>S<sub>4</sub> + H): 744.8, found: 745.8.

### Synthesis of *para*-sulphonato-calix[4]arene modified silver nanoparticles

The procedure of Xiong [11] was slightly modified as follows. 10 mL of 10<sup>–2</sup> M AgNO<sub>3</sub> solution was added to 80 mL of deionized water. To this solution, 10 mL of 10<sup>–2</sup> M *para*-sulphonato-calix[4]arene aqueous solution was added as stabilizer with stirring for 30 min. And then, 44 mg of NaBH<sub>4</sub> was added to the solution. The *para*-sulphonato-calix[4]arene capped silver colloidal suspensions were obtained after 5 min.

### UV–visible absorption assays

The mixture experiments were conducted by monitoring the change in absorbance between 340 and 650 nm, using a 96 titer well visible spectrometer, (BioTek Power Wave 340).

### Fluorescence experiments

All the fluorescence spectra were measured at 25.0 °C.

Fluorescence studies of *para*-sulphonato-calix[4]arene capped silver nanoparticles at varying concentrations of cytosine.

Fluorescence spectra and fluorescence intensities measurements were recorded on a Tecan InfiniteH M1000 spectrofluorimeter. The excitation wavelength was set at 280 nm. Emission spectra were collected in the range 290–500 nm (with 2 nm-increments), using a black flat-bottomed, and low-binding 96-well microplate (Greiner Bio one).

Studies of cytosine with different concentrations of *para*-sulphonato-calix[4]arene or *para*-sulphonato-calix[4]arene capped silver nanoparticles.

Fluorescence spectra and fluorescence intensities were measured on a model F-6500 fluorescence spectrophotometer (Hitachi, Japan) using a 1(W) × 3(D) × 35(H) mm

micro-quartz cell. The slits for the excitation and emission monochromators were fixed at 10.0 and 1.0 nm, respectively. The excitation wavelength was set at 320 nm.

### NMR diffusion spectroscopy

The NMR experiments were performed on a Bruker DRX400 spectrometer. A series of five solutions containing different ratios of cytosine/*para*-sulphonato-calix[4]-arene were prepared in D<sub>2</sub>O (See Table S1).

Data were collected at 298 K. Signal averaging ranged from 40 scans to 1,024 scans as required for adequate signal to noise. The experimentally observed diffusion coefficients were then determined by the single point method well described by Fielding and co-workers [17]. Only data from the samples with a ratio of cytosine/*para*-sulphonato-calix[4]-arene 1:1 were used to calculate a  $K_a$  average.

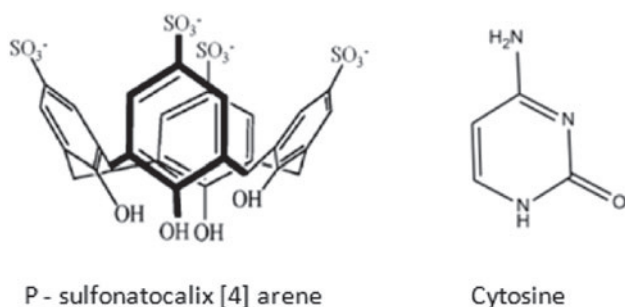
### SEM imaging

Samples for SEM acquisitions were prepared by spreading 3  $\mu$ L of the nanoparticle suspensions on freshly cleaved mica surfaces. After drying at room temperature and Au–Pd sputter coating (15 s at 15 mA), micrographs were acquired using a Supra 40 V system (Carl Zeiss, Switzerland) at an accelerating voltage of 20 kV using an in-lens detector. Statistical size measurements were performed measuring the diameter of at least 50 nanoparticles using the analysis<sup>®</sup> (Olympus, Germany) software package.

## Results and discussion

The molecular structures of cytosine and *para*-sulphonato-calix[4]-arene are shown in Scheme 1.

*Para*-sulphonato-calix[4]-arene was synthesized by the literature method [13], and the capped *para*-sulphonato-calix[4]-arene silver nanoparticles by sodium borohydride reduction of silver nitrate in the presence of the capping



**Scheme 1** Structure of *para*-sulphonato-calix[4]-arene (on the left side) and cytosine (on the right side)

agent. The use of sodium borohydride in the reduction is known to generate monodisperse colloidal assemblies [14].

We have previously demonstrated that hybrid *para*-sulphonato-calix[4]-arene nanoparticles interact with nucleic bases, nucleotides, and that for certain nucleosides such complexation leads to aggregation accompanied by clearly visible colour changes. In an attempt to better understand the aggregation processes we have studied the interactions between cytosine and *para*-sulphonato-calix[4]-arene in solution, in the solid state and on colloidal nanoparticles. Here we discuss the results and attempt to correlate the assembly behavior in the three different states.

### Solution complexation

Firstly we studied assembly behavior in solution using both fluorescence spectroscopy and NMR DOSY spectroscopy.

As cytosine has an intrinsic fluorescence the use of the emission quenching by *para*-sulphonato-calix[4]-arene can provide useful information.

Fluorescence spectroscopy experiments on the complexation of cytosine by *para*-sulphonato-calix[4]-arene were carried out to investigate the interaction. 20  $\mu$ L of different concentrations of *para*-sulphonato-calix[4]-arene solution were added to 0.18 mL of a  $1 \times 10^{-3}$  M cytosine solution in a micro quartz cell.

Fluorescence spectra and relative fluorescence intensities were measured on a model F-6500 fluorescence spectrophotometer (Hitachi, Japan) at room temperature.

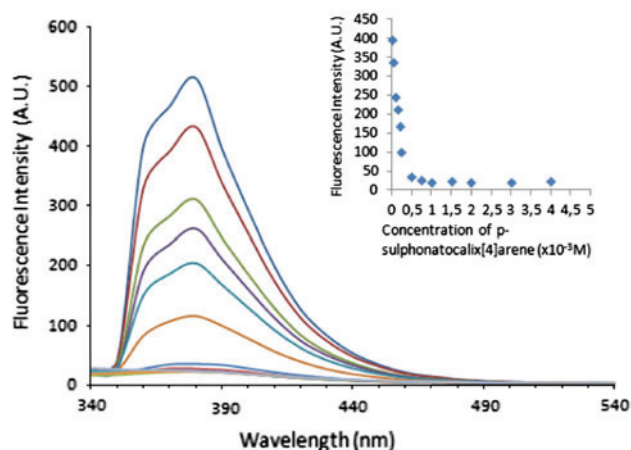


**Fig. 1** Fluorescence spectra of cytosine at  $1 \times 10^{-3}$  M varying concentrations of *para*-sulphonato-calix[4]-arene (thick blue 0 M; thick red  $0.5 \times 10^{-4}$  M; thick green  $1 \times 10^{-4}$  M; thick violet  $1.5 \times 10^{-4}$  M; thick sky blue  $2 \times 10^{-4}$  M; thick orange  $2.5 \times 10^{-4}$  M; thin blue  $5 \times 10^{-4}$  M; thin red  $7.5 \times 10^{-4}$  M; thin green  $1 \times 10^{-3}$  M; thin violet  $1.5 \times 10^{-3}$  M; thin sky blue  $2 \times 10^{-3}$  M; thin orange  $3 \times 10^{-3}$  M; light color  $4 \times 10^{-3}$  M). In the inset, cytosine maximum fluorescence intensity as a function of *para*-sulphonato-calix[4]-arene. (Color figure online)

For cytosine in water, the excitation and emission peaks are 320 and 380 nm, respectively. When *para*-sulphonatocalix[4]arene was added to cytosine, a rapid fluorescence quenching was observed, complete quenching is achieved at  $0.5 \times 10^{-3}$  M (Fig. 1).

The stoichiometry of the inclusion complex was determined following the classic method of Benesi and Hildebrand [15]. The fluorescence intensity variation of cytosine ( $1 \times 10^{-3}$  mol/L) in the concentration range of *para*-sulphonatocalix[4]arene from  $5 \times 10^{-5}$  to  $4 \times 10^{-3}$  mol/L was determined. According to the Benesi–Hildebrand equation:

$$\frac{1}{\Delta I_f} = \frac{1}{K_n \alpha} \frac{1}{[H]_0^n} + \frac{1}{\alpha}$$

in which,  $\Delta I_f = I_{f_{h-g}} - I_{f_g} - I_{f_h}$ , where  $I_{f_{h-g}}$ ,  $I_{f_g}$  and  $I_{f_h}$  are the fluorescence intensity of the host–guest complex, the guest molecule and the host molecule, respectively.  $[H]_0$  is the original concentration of the calix[*n*]arene,  $K$  is the association constant,  $n$  is the number of host molecule (s) in a complex and  $\alpha$  is a constant.

By plotting  $1/\Delta I_f$  versus  $1/[H]_0^n$  for different values  $n$ , the value of  $n$  that results a straight line can be taken as the number of host molecules, consequently, the inclusion ratio can be obtained as 1: $n$ . From Fig. 2, the excellent linearity relationship (with  $r^2 = 0.9940$ ) indicated that the composition ratio of the inclusion complex is 1:1 for *para*-sulphonatocalix[4]arene: cytosine, for all other values of  $n$  the  $r^2$  values are much lower, see ESI. The association constant,  $K$  was determined to be  $9,500 \text{ M}^{-1}$ .

While the global stoichiometry of the complex can be determined by fluorescence spectroscopy as being at a 1:1 ratio, the method does not allow determination of the absolute stoichiometry whether the complex is monomeric of a higher order, for example 2:2. The use of DOSY NMR spectrometry [16] allows determination of both diffusion

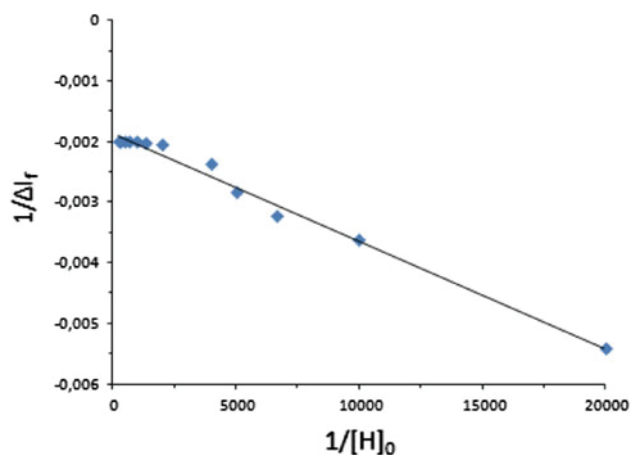


**Fig. 2** Graph of  $1/\Delta I_f$  versus  $1/[H]_0$  for cytosine/*para*-sulphonatocalix[4]arene complexation

coefficient and also the apparent molecular mass of host and complex. The technique has been widely used by Fielding and co-workers for cyclodextrin inclusion complexes [17], and Raston and co-workers has been the guiding force in the use of DOSY in calix[*n*]arene complexation [18].

The changes in diffusion coefficients of cytosine and *para*-sulphonatocalix[4]arene, as a function of their concentration ratio are depicted graphically in Fig. 3. Cytosine the small guest in the current work diffuses several times faster than the host molecule. Upon the addition of increasing concentrations of the host (*para*-sulphonatocalix[4]arene) the observed diffusion coefficient of cytosine decreases dramatically. Using the “single point method” described by Raston and co-workers [18], the  $K_a$  value of the complex was estimated to  $1,400 \text{ M}^{-1}$  (see ESI) which is difference from the  $K$  previously determined by spectrofluorimetry. This difference could be explained by the nature of the constant (diffusion or inclusion) specific of each method. It should also be noted that spectrofluorimetry analyses the behavior of cytosine whereas the NMR analyses the behavior of the calix-arene

On the other hand, at host/guest ratio above 1:1, the observed diffusion of the host does not change. This suggests that when cytosine is complexed by *para*-sulphonatocalix[4]arene the apparent molecular weight of the complex remains unchanged.

Based on the work of Raston and co-workers [18], the molecular weight of the complex is in the range of 1,100 Da showing a 1:1 monomeric complex is formed. Intriguingly at low ratios of cytosine to *para*-sulphonatocalix[4]arene, the diffusion coefficient shows a small but

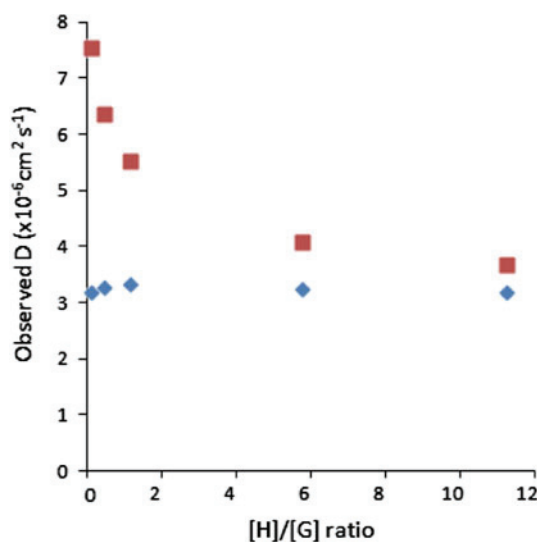


**Fig. 3** The apparent diffusion coefficients ( $D_{\text{obs}}$ ) of Cytosine (filled square) and *para*-sulphonatocalix[4]arene (filled diamond) as a function of solution composition as the concentration ratio  $[H]/[G]$ .  $K_a$  was determined as  $1,400 \text{ M}^{-1}$

**Table 1** Crystal data and structure refinement details

Empirical formula	$2(\text{C}_{28}\text{H}_{20}\text{O}_{16}\text{S}_4) \cdot 8(\text{C}_4\text{H}_6\text{N}_3\text{O}) \cdot \text{CH}_4\text{O} \cdot 18(\text{H}_2\text{O})$
Formula weight	2734.71
Temperature (K)	100 (2)
Diffractometer	Xcalibur, Atlas, Gemini ultra
Wavelength (Å)	0.71073
Crystal	Needle, colourless
Crystal size (mm <sup>3</sup> )	0.42 × 0.17 × 0.15
Crystal system	Triclinic
Space group	<i>P</i> -1
Unit cell	
Dimensions	12.423(1)
<i>a</i> (Å)	14.894(2)
<i>b</i> (Å)	17.357(1)
<i>c</i> (Å)	
$\alpha$ (°)	71.444(9)
$\beta$ (°)	71.745(8)
$\gamma$ (°)	75.420(9)
Volume (Å <sup>3</sup> )	2849.8(5)
<i>Z</i>	1
Calculated density (g cm <sup>-3</sup> )	1.593
<i>F</i> (000)	1430
Absorption coefficient (mm <sup>-1</sup> )	0.27
$\theta$ range for data collection (°)	3.4–29.4
<i>hkl</i> ranges	$-15 \leq h \leq 15, -17 \leq k \leq 19, 0 \leq l \leq 23$
Reflections collected/unique	25,102/12,946
Completeness (%) to $\theta$	81.5
<i>T</i> <sub>min</sub> , <i>T</i> <sub>max</sub>	0.936, 0.965
Refinement method	Full-matrix least-squares on <i>F</i> <sup>2</sup>
Data/restraints/parameters	12,946/57/883
Goodness-of-fit on <i>F</i> <sup>2</sup>	0.95
Final <i>R</i> indices [ <i>I</i> > 2 $\sigma$ ( <i>I</i> )]	<i>R</i> = 0.067, <i>wR</i> = 0.153
<i>R</i> indices (all data)	<i>R</i> = 0.095, <i>wR</i> = 0.196

significant increase implying a decrease in the size of the assembly. This may be ascribed to a reduction in the size of the complex as the cytosine is included into the cavity and hydrogen bonds to the sulphonate groups.

#### Solid state complexation

The solid state structure of one complex between *para*-sulphonato-calix[4]arene and cytosine has been determined, Table 1 for crystallographic data.

The structure shows the *para*-sulphonato-calix[4]arene molecules in the expected cone conformation. One of the four crystallographically independent cytosine molecules is located in the macrocycle cavity, and two such inclusion complexes, related by centre of symmetry, form a molecular

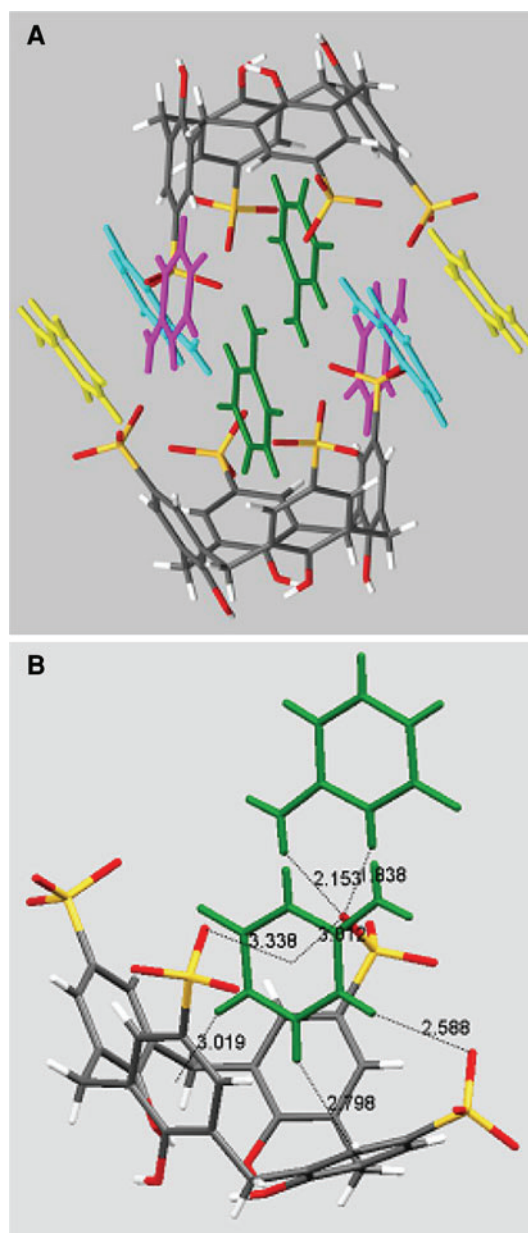


**Fig. 4** Capsule formation, **a** the four symmetry independent cytosine molecules are represented by different colors. The pair of green molecules related by center of symmetry is located within the capsule and **b** interaction distances for one the included cytosine molecules. (Color figure online)

capsule accommodating two cytosine molecules. There are five types of interactions within the capsule: host–guest and guest–guest  $\pi \cdots \pi$  interactions, and host–guest S–O $\cdots$  $\pi$ , C–H $\cdots$  $\pi$ , C–H $\cdots$ O and N–H $\cdots$ O interactions (Fig. 4).

Capsules are connected via host–guest<sub>exo</sub> and guest<sub>endo</sub>–guest<sub>exo</sub> N–H $\cdots$ O hydrogen bonds (Fig. 5). A hydrogen bonded dimer of cytosine molecules links diagonally two capsules, looking almost like a goeyduck clam. The dimer is held in place by strong hydrogen bonds to sulphonate

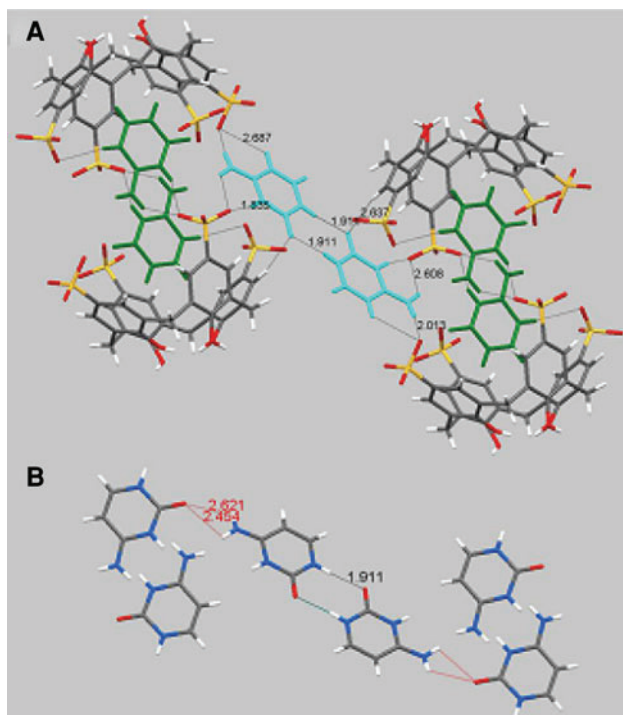


**Fig. 5** **a** Hydrogen bond interactions between capsules. Interactions with solvent molecules are not shown for the clarity and **b** hydrogen bond interactions in the bridging dimer

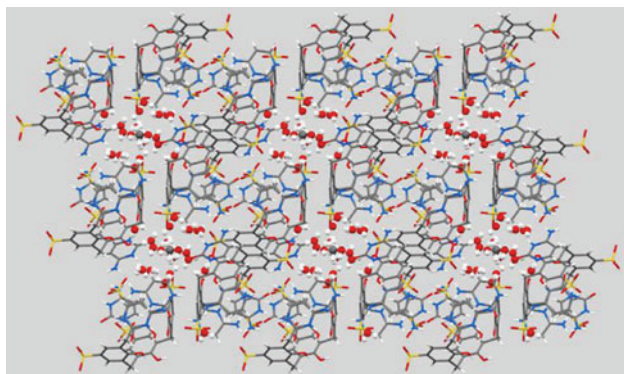


**Fig. 6** Packing viewed along *b* crystallographic axis. Solvent molecules shown in *ball and stick* mode to illustrate the channel formation

groups, Fig. 5a and not to the encapsulated cytosine molecules, Fig. 5b.

The packing observed here is quite different from the classic bilayer structure [19]. Solvent molecules (water and methanol) are hydrogen bonded both to *para*-sulphonato-calix[4]arene and cytosine molecules, and are located in channels along *b* crystallographic axis (Fig. 6).

#### Colloidal assembly

As observed previously for *para*-sulphonato-calix[4]arene capped silver nanoparticles for a silver concentration of

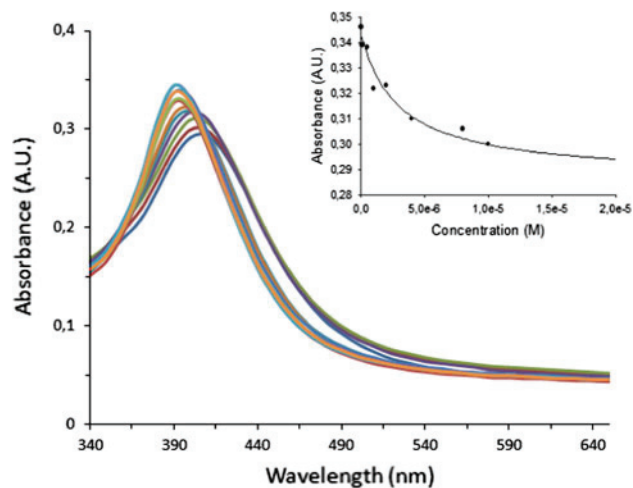


**Fig. 7** Visible spectroscopy titration curves for *para*-sulphonato-calix[4]arene capped silver nanoparticles with cytosine, *inset* maximum absorbance versus concentration

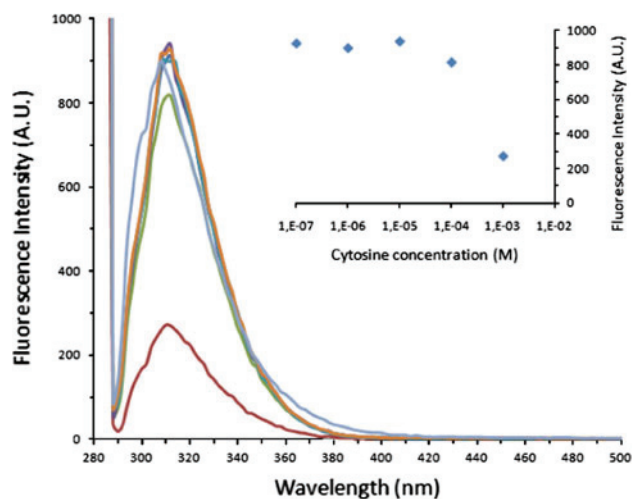


**Fig. 8** Fluorescence spectra of *para*-sulphonato-calix[4]arene capped silver nanoparticles at varying concentrations of cytosine, *inset* maximum fluorescence emission intensity as a function of cytosine concentration

$10^{-3}$  M, addition of cytosine at higher concentrations induces a change in colour of the colloidal solution from yellow to red with the appearance of an aggregation associated adsorption band at 540 nm.

However titration of the *para*-sulphonato-calix[4]arene silver nanoparticles with cytosine at lower concentrations, as shown in Fig. 7, reveals a binding event not associated with the aggregation. Plotting maximum absorbance against cytosine concentration shows a typical binding curve with saturation at  $10^{-5}$  M, well below the aggregation point. Based on calculation of the binding sites on the capped nanoparticles an approximate KD of  $2 \times 10^{-6}$  M can be determined.

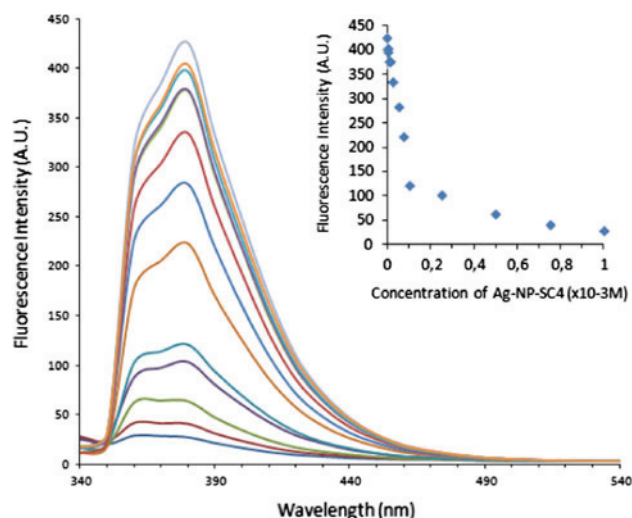


**Fig. 9** Fluorescence spectra of cytosine at  $1 \times 10^{-3}$  M varying concentrations of *para*-sulphonato-calix[4]arene AgNPs (*thick blue*  $1 \times 10^{-3}$  M; *thick red*  $7.5 \times 10^{-4}$  M; *thick green*  $5 \times 10^{-4}$  M; *thick violet*  $2.5 \times 10^{-4}$  M; *thick sky blue*  $1 \times 10^{-4}$  M; *thick orange*  $7.5 \times 10^{-5}$  M; *thick dark blue*  $5 \times 10^{-5}$  M; *thick dark red*  $2.5 \times 10^{-5}$  M; *thin light green*  $1 \times 10^{-5}$  M; *thick violet*  $7.5 \times 10^{-6}$  M; *thick sky blue*  $5 \times 10^{-6}$  M; *thick orange*  $2.5 \times 10^{-6}$  M; *light color* 0 M). In the *inset*, cytosine maximum fluorescence intensity as a function of *para*-sulphonato-calix[4]arene silver nanoparticles. (Color figure online)

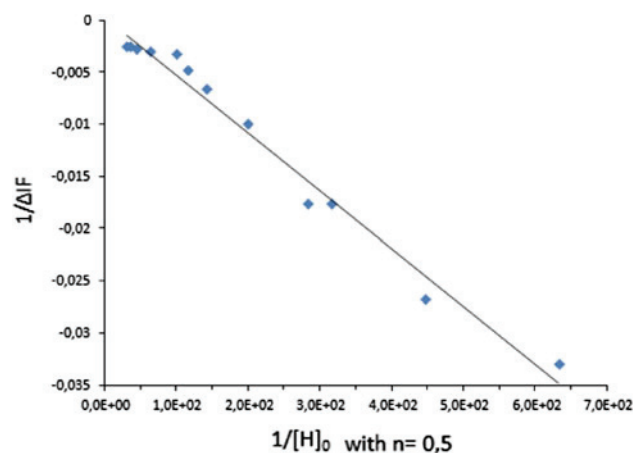


**Fig. 10** Graph of the  $1/\Delta I_f$  versus  $1/[H]_0$  for cytosine/*para*-sulphonato-calix[4]arene capped silver nanoparticle complex

More generally the bridging capacity of ligands such as cytosine applies also to basic amino acids such as lysine, arginine and histidine, where two or more bridging hydrogen may link capsules together.

The system was shown to be fluorescent when excited at 280 nm with a strong emission at 320 nm, the intensity of this emission is independent of cytosine concentration below  $10^{-4}$  M but decreases dramatically at a cytosine concentration of  $10^{-3}$  M. Such behaviour is characteristic of the aggregation of capped nanoparticles, Fig. 8.

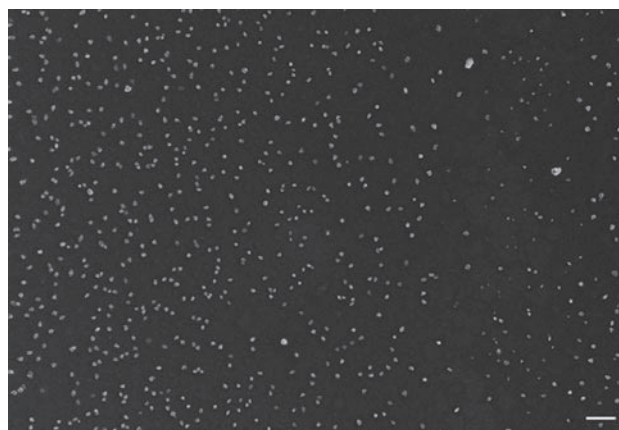


**Fig. 11** SEM images of *para*-sulphonato-calix[4]arene capped silver nanoparticles mixed with cytosine at a final concentration of  $10^{-4}$  M (molar ratio nanoparticles:cytosine = 1:1). The scale bar for the image is 2  $\mu$ m

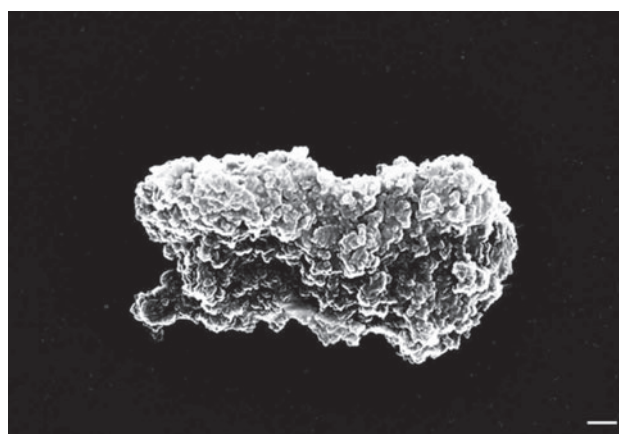


**Fig. 12** SEM images of *para*-sulphonato-calix[4]arene capped silver nanoparticles mixed with cytosine at a final concentration of  $10^{-3}$  M (molar ratio nanoparticles:cytosine = 1:10). The microscope is focused on one aggregate. The scale bar for the image is 200 nm

Similarly the fluorescence quenching of cytosine in the presence of *para*-sulphonato-calix[4]arene capped silver nanoparticles was studied, see Figs. 9 and 10. For monitoring the fluorescence emission of cytosine, we set the excitation wavelength at 320 nm. Quenching of the cytosine fluorescence again occurred, and was complete for a nominal concentration in *para*-sulphonato-calix[4]arene capped nanoparticles of  $1 \times 10^{-4}$  M. Surprisingly the use of the Benesi-Hildebrand equation, led to a stoichiometry of 1 cytosine:1*para*-sulphonato-calix[4]arene, assuming *para*-sulphonato-calix[4]arene at the surface of the capped silver nanoparticles to be the quencher. To the best of our knowledge this is a rare example of how coupling to the surface of a nanoparticle induces a change in the complex stoichiometry as compared to that observed for the complex in solution.

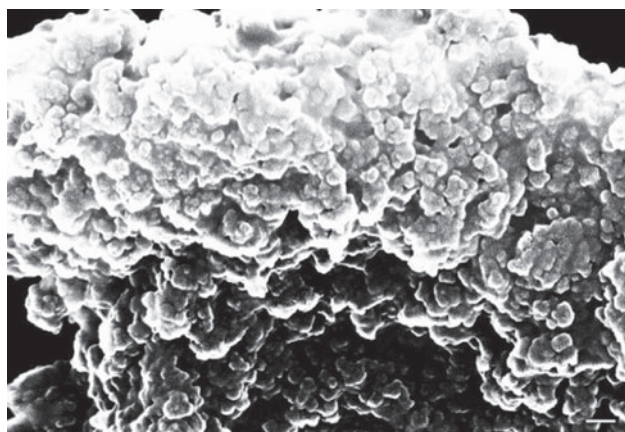


**Fig. 13** SEM images of *para*-sulphonato-calix[4]arene capped silver nanoparticles mixed with cytosine at a final concentration of  $10^{-3}$  M (molar ratio nanoparticles:cytosine = 1:10). The microscope is focused on one aggregate. The scale bar for the image is 100 nm

Interestingly in the solid state it was observed that both 1:1 capsules and extended capsules containing 2 or more cytosine molecules per capsule can exist. Thus there is agreement between solid state information and fluorescence as to how cytosine can participate in linking together *para*-sulphonato-calix[4]arene capped silver nanoparticles to form aggregates.

This explains the histidine selective colorimetric determination for amino acids observed by Xiong et al. [11] as in that series only histidine presented the possibility of bridging between nanoparticles.

Thus it would appear that at two distinct binding events occur, firstly at low cytosine concentrations there is a strong interaction in the low micro molar range but with no aggregation and secondly a binding event above  $10^{-4}$  M with a KD which is associated with aggregation with bridging of organic material between nanoparticles.

The aggregation behaviour of the *para*-sulphonato-calix[4]arene capped silver nanoparticles can be observed using Electron Microscopy. For this, we used two different molar ratio of nanoparticles:cytosine. One with a 1:1 ratio and another with an excess of cytosine 1:10.

At a final concentration of  $10^{-4}$  M (with a molar ration 1:1), individual nanoparticles are observed (see Fig. 11). The size of the observed nanoparticles has been calculated as 290 nm, this can be compared to the value of 250 nm observed from Dynamic Light Scattering (DLS). The small difference results undoubtedly from the coating the sample by gold prior to observation. In the DLS measurements a smaller population of diameter 30 nm are also observed. These can be observed on the left hand side of the micrograph. The surface is quite heterogeneous with both populations of *para*-sulphonato-calix[4]arene capped silver nanoparticles and areas which can be ascribed to sodium

borate depositions. Moreover, TEM experiments confirm that *para*-sulphonato-calix[4]arene capped silver nanoparticles alone in water were observed to be dispersed with a mono sized population of 30 nm (see ESI, figure S5).

For high ratios of nanoparticles to cytosine, (molar ratio *para*-sulphonato-calix[4]arene capped silver nanoparticles:cytosine = 1:10), the aggregates can clearly be seen with particles involving diameters of around 30 nm, which are bound together by amorphous material (see Figs. 12, 13).

At this stage it is unclear whether only the smaller nanoparticles are active in the aggregation process or whether the larger nanoparticles are small supramolecular assemblies of the smaller nanoparticles and that this aggregation is an equilibrium process in which case there will be a free population of small nanoparticles to participate in the aggregation assembly.

## Conclusions

The assembly process between *para*-sulphonato-calix[4]arene and cytosine is quite different between the states of matter involved; in solution a monomeric 1:1 complex is involved, in the solid state a 1:4 complex is involved of which one cytosine molecule is there as a space filler, on the surface of the colloidal *para*-sulphonato-calix[4]arene capped silver nanoparticles there is initially a 1:2 complex formation followed by aggregation involving organic material to yield agglomerates.

The use of multiple physical methods is obligatory to probe such complex assembly processes, we currently looking at other microscopy methods to give further information and to extend the work to other molecules such as, Active Pharmaceutical Ingredients, surfactants and even proteins which can provoke the aggregation of hybrid *para*-sulphonato-calix[4]arene capped silver nanoparticles.

**Acknowledgments** One of us, Y.T., acknowledges support from the Department of Chemistry and Biochemistry, University of Lyon 1. We thank Professor Shoji Takeuchi, his lab members and Dr. Yannick Rondelez for fluorescence experiments.

## References

1. He, W., Huang, C.Z., Li, Y.F., Xie, J.P., Yang, R.G., Zhou, P.F., Wang, J.: One-step label-free optical genosensing system for sequence-specific DNA related to the human immunodeficiency virus based on the measurements of light scattering signals of gold nanorods. *Anal. Chem.* **80**, 8424–8430 (2008)
2. Storhoff, J.J., Elghanian, R., Mucic, R.C., Mirkin, C.A., Letsinger, R.L.: One-pot colorimetric differentiation of polynucleotides with single base imperfections using gold nanoparticle probes. *J. Am. Chem. Soc.* **120**, 1959–1964 (1998)
3. Gutsche, C.D.: *Calixarenes: An Introduction*, 2nd edn. The Royal Society of Chemistry, Cambridge (2008)

- Danylyuk, O., Suwinska, K.: Solid-state interactions of calixarenes with biorelevant molecules. *Chem. Commun.* **39**, 5799–5813 (2009)
- Perret, F., Lazar, A.N., Coleman, A.W.: Biochemistry of the *para*-sulphonato-calix[n]arenes. *Chem. Commun.* **23**, 2425–2438 (2006)
- Perret, F., Coleman, A.W.: Biochemistry of anionic calix[n]arenes. *Chem. Commun.* **47**, 7303–7319 (2011)
- Rodik, R.V., Boyko, V.I., Kalchenko, V.I.: Calixarenes in biomedical researches. *Curr. Med. Chem.* **16**, 1630–1655 (2009)
- Atwood, J.L., Barbour, L.J., Dawson, E.S., Junk, P.C., Kienzle, J.: X-ray structure of the water soluble adeninium *para*-sulfonatocalix[4]arene which displays cationic and anionic bilayers. *Supramol. Chem.* **7**, 271–274 (1996)
- Nichols, P.J., Makha, M., Raston, C.L.: Confinement of nucleic acid bases and related compounds using tetra-*para*-sulfonatocalix[4] arene. *Cryst. Growth Des.* **6**, 1161–1167 (2006)
- Xiong, D., Li, H.: Colorimetric detection of pesticides based on calixarene modified silver nanoparticles in water. *Nanotechnology* (2008). doi:10.1088/0957-4484/19/46/465502
- Xiong, D., Chen, M., Li, H.: Synthesis of *para*-sulfonatocalix[4]arene-modified silver nanoparticles as colorimetric histidine probes. *Chem. Commun.* **7**, 880–882 (2008)
- Tauran, Y., Grosso, M., Brioude, A., Kassab, R., Coleman, A.W.: Colourimetric and spectroscopic discrimination between nucleotides and nucleosides using *para*-sulphonato-calix[4]arene capped silver nanoparticles. *Chem. Commun.* **47**, 10013–10015 (2011)
- Coleman, A.W., Jebors, S., Cecillon, S., Perret, P., Garin, D., Marti-Battle, D., Moulin, M.: Toxicity and biodistribution of *para*-sulphonato-calix[4]arene in mice. *New J. Chem.* **32**, 780–782 (2008)
- Tan, Y.W., Wang, Y., Jiang, L., Zhu, D.B.: Thiosalicylic acid-functionalized silver nanoparticles synthesized in one-phase system. *J. Colloid Interface Sci.* **249**, 336–345 (2002)
- Benesi, H., Hildebrand, J.: A spectrophotometric investigation of the interaction of iodine with aromatic hydrocarbons. *J. Am. Chem. Soc.* **71**, 2703–2707 (1949)
- Schalley, C.: *Analytical Methods in Supramolecular Chemistry*. Wiley-VCH Verlag GmbH, Weinheim (2007)
- Cameron, K.S., Fielding, L.: NMR diffusion spectroscopy as a measure of host–guest complex association constants and as a probe of complex size. *J. Org. Chem.* **66**, 6891–6895 (2001)
- Dalgarno, S.J., Fisher, J., Raston, C.L.: Interplay of *para*-sulfonatocalix[4]arene and crown ethers en route to molecular capsules and “Russian dolls”. *Chem. Eur. J.* **12**, 2772–2777 (2006)
- Coleman, A.W., Bott, S.G., Morley, S.D., Means, C.M., Robinson, K.D., Zhang, H.M., Atwood, J.L.: Novel layer structure of sodium calix[4]arenesulfonate complexes – a class of organic clay mimics. *Angew. Chem. Int. Ed.* **2**, 1361–1362 (1988)

## **Anionic calixarene-capped silver nanoparticles show species-dependent binding to serum albumins**

Titre: Les nanoparticules d'argent fonctionnalisées par des calix[n]arene anioniques montrent une liaison dépendante des espèces albumines sériques

Résumé: Les calix[n]arenes anioniques *para*-sulphonato-calix[4]arene et 1,3-di-Ophosphonato-calix[4]arene ont été utilisés pour fonctionnaliser des nanoparticules d'argent. La liaison de ces particules fonctionnelles pour différentes espèces d'albumines (bovine, humaine, porcine et ovine) a été étudiée par spectroscopie fluorescente et visible à température variable. Le *quenching* de la fluorescence de l'albumine varie en fonction du calix[n]arene utilisé et le spectre visible des nanoparticules d'argents hybrides est aussi fonction de l'origine de l'albumine sérique. Il devient alors possible de distinguer les différentes espèces.

Article

## Anionic Calixarene-Capped Silver Nanoparticles Show Species-Dependent Binding to Serum Albumins

Yannick Tauran <sup>1,2</sup>, Arnaud Brioude <sup>1</sup>, Beomjoon Kim <sup>2</sup>, Florent Perret <sup>3</sup> and Anthony W. Coleman <sup>1,2,\*</sup>

<sup>1</sup> LMI, CNRS UMR 5615, Université Lyon 1, Villeurbanne F69622, France

<sup>2</sup> Institute of Industrial Science, the University of Tokyo, 4-6-1 Komaba, Meguro-ku, Tokyo 153-0041, Japan

<sup>3</sup> ICBMS, UMR 5246, Université Lyon 1, Villeurbanne F69622, France

\* Author to whom correspondence should be addressed; E-Mail: antony.coleman@adm.univ-lyon1.fr; Tel.: +33-4-7243-1027; Fax: +33-4-7244-0618.

Received: 28 February 2013; in revised form: 25 April 2013 / Accepted: 9 May 2013 /

Published: 21 May 2013

---

**Abstract:** The anionic calixarenes *para*-sulphonatocalix[4]arene and 1,3-di-O-phosphonatocalix[4]arene, have been used to cap silver nanoparticles. The binding of these functional particles with regard to various serum albumins (bovine serum albumin, human serum albumin, porcine serum albumin and sheep serum albumin) has been studied by variable temperature fluorescence spectroscopy. The quenching of the fluorescence of the proteins was shown to vary as a function of the anionic calixarene capping molecule and also as a function of the origin of the serum albumin. It is thus possible to discriminate between the different species.

**Keywords:** calixarenes; molecular recognition; serum albumins; species dependence

---

### 1. Introduction

In late 2012 and early 2013, a number of public health scandals erupted in Asia and Europe [1]. The first of these concerned the Chinese subsidiary of a multinational food company; here a plethora of disparate Active Pharmaceutical Ingredients (APIs) were found to be contaminants in chicken meat [2]. They included caffeine, amantadine, an anti-Parkinson AP, antibiotics including the banned fluoroquinolones and intriguingly, Prozac. This represents a true public health safety risk and will be

treated in a separate publication. In Europe there was recently a media explosion concerning the presence of horsemeat in a wide range of frozen and prepared beef products [3]. However more careful analysis of the readily available data shows that is a minor problem as there is no true health risk, although the UK there is undoubtedly disgust about the consumption of horse, a widely loved animal. In reality this crisis concerns a fraud of deliberate mislabeling of horsemeat as beef, however it was widely trumpeted by the media and government agencies [4]. Yet there are two more problems associated with contaminated beef products. Firstly, the presence of the banned veterinary API phenylbutazone, as despite government assurances that there the level was not dangerous, the permitted level of this API in the human food chain is zero [5]. The second contamination does not represent a true health risk but is far more serious, as compared to horsemeat, from an ethical point of view as it concerns the contamination by pork of beef products, including in at least one case, a product labeled Halal [6]. Interestingly the Irish Food Safety Agency published an analysis of the presence of pork and horsemeat in frozen beef products. The results are striking, of the 27 products tested only three were not contaminated with meat from other species; only 10 samples showed the presence of horsemeat, however 23 products showed the presence of pork. In view of the above, methods to check for the presence of pork in food products would seem to be useful [7].

Aside from DNA testing, detection of serum albumins would appear to be an interesting route for the investigation of contaminants in food stuffs [8]. The serum albumins represent the most common proteins in animal physiological fluids with up to 40 g per liter being present. This class of proteins is capable of transporting a wide variety of molecules and ions, including copper, various carboxylic acids and a large range of APIs [9]. Recently a crystallographic study on a number of serum albumins has demonstrated that despite a high degree of homology, the binding pockets in these proteins differ both in nature and also in their capacity to bind substrate molecules [10].

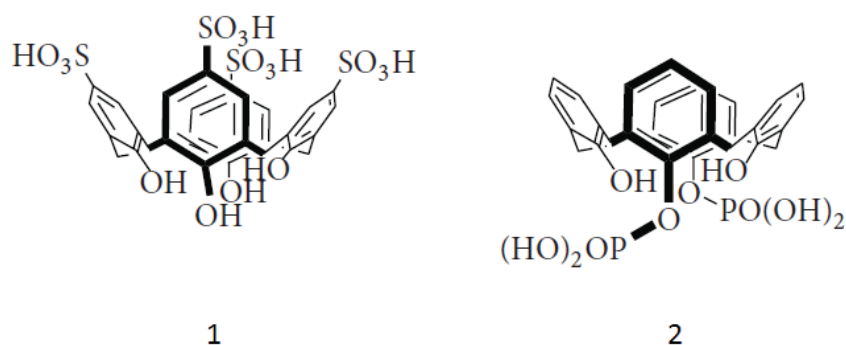
The anionic calixarenes have been investigated over a number of years for their capacity to complex biomolecules, including a wide range of proteins [11]. Examples of such complexation include proteins of the blood coagulation cascade [12], ATP binding domains of ABC transporters [13], calcium dependent ion channels [14], histones [15], the protease resistant protein, prion protein [16], other proteins associated with neurodegenerative diseases [17] and especially the serum albumins [18]. Previous work has shown that the *para*-sulphonatocalix[n]arenes interact with several binding sites of the serum albumins but also that such binding depends on the nature of the source of the serum albumins [19]. In this last case the studies used Electrospray Mass Spectrometry under partially denaturing conditions, in view of this we have turned to the use of calixarene-capped silver nanoparticles to generate systems with internal probes for the complexation. Previous work by Xiong on amino acid binding [20] and by ourselves on nucleic acid [21] or API [22] binding has demonstrated the interest of such an approach.

In the current work we treat the dependent temperature binding of bovine serum albumin (BSA), human serum albumin (HSA), porcine serum albumin (PSA) and sheep serum albumin (SSA) with silver nanoparticles capped by *para*-sulphonatocalix[4]arene (**1\_Ag\_NP**) and 1,3-di-O-phosphonatocalix[4]arene (**2\_Ag\_NP**) by spectroscopic methods. The results show that the use of only two types of capped nanoparticles allows the discrimination of serum albumins from different mammalian species.

## 2. Results and Discussion

The molecular structures of *para*-sulphonatocalix[4]arene, (**1**) and 1,3-di-O-phosphonato-calix[4]arene (**2**) are shown below in Scheme 1.

**Scheme 1.** Structure of the anionic calix[4]arenes studied. Compound **1** is *para*-sulphonato-calix[4]arene and **2** is 1,3-di-O-phosphonato-calix[4]arene.



*Para*-sulphonatocalix[4]arene (**1**) and 1,3-di-O-phosphonatocalix[4]arene (**2**) were synthesised as per the literature methods, in particular for **1** the method for use *in vivo* was used [23].

Compound **1** is well known for its capacity to complex basic amino-acids both in solution [24], for lysine  $K_{\text{ass}} = 1356 \text{ M}^{-1}$  and for arginine  $K_{\text{ass}} = 1546 \text{ M}^{-1}$ , the solid state structures of both complexes have been determined. That of the lysine complex shows the hydrophobic chain embedded in the macrocyclic cavity, this structure is in complete concordance with that obtained in solution [25]. For the arginine complex, four different orientations for the amino acid side chain are observed within the cavity [26]. In the case of **2** binding of basic amino acids occurs, but is dependent on the presence of co-solute cations [27], the solid-state structure with lysine has been determined and shows complexation at the phosphonate groups externally to the macrocyclic cavity [28]. The relevant physical data on the four serum albumins in the current work are given in Table 1 below.

**Table 1.** Physical molecular data of different albumin species.

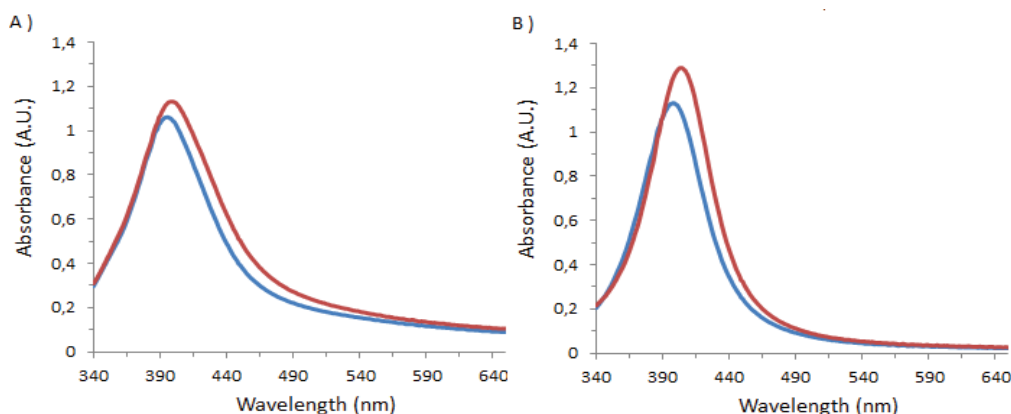
	BSA	HSA	PSA	SSA
Molar Mass	69,323.44	66,472.21	69,692.17	69,188.28
Iso Electric Point	5,82	5,67	6,08	5,8
Amino Acid number	607	585	607	607
Lysine Residues	60	59	58	61
Arginine Residues	26	24	29	25
Histidine Residues	17	16	19	18
Aspartic Acid Residues	40	36	36	44
Glutamic Acid Residues	59	62	61	56
Homology	100%	76%	80%	92%
Structure (reference)	[10]	[29]	ND *	ND *
Accession Number PDB	PDB: 4F5S	PDB ID: 1AO6		
Accession Number NCBI	NP_851335.1	PMID: 10388840	NP_001005208.1	NP_001009376.1

\* ND: Not Determined.

The serum albumins show molecular masses in the range 65 to 70 kD and have iso-electric points below pH 7. The solid-state structures show the presence of binding pockets, in general lined with basic aminoacids, and indeed the serum albumins are known as transporters of anionic organic molecules, but also are capable of transporting various metal cations. While there is a good homology between the serum albumins, the differences, particularly in the anion binding pockets, led us to consider that differential binding with the two anionic calixarenes **1** and **2** might occur.

Previous studies, using Electrospray Mass Spectrometry (ES/MS) have shown that **1** binds strongly to the various serum albumins, and that several binding sites are present. The  $K_{\text{ass}}$  values vary from  $7.69 \times 10^5 \text{ M}^{-1}$  to  $3.85 \times 10^5 \text{ M}^{-1}$  to  $0.33 \times 10^5 \text{ M}^{-1}$  for binding to BSA, and sequential but differentiated binding occurs for the other serum albumins [19]. However there is some doubt as to whether partial denaturation may occur under the particular conditions required for the ES/MS experiment which has led us to attempt to use true solution methods. The capped silver nanoparticles using **1** and **2** were prepared as previously described [20]. Both systems showed a strong plasmon resonance absorption at 390 nm and 398 nm, respectively. Initial experiments confirmed by visible spectroscopy the complexation of BSA on the surface of the capped nanoparticles, this was accompanied by a shift in the resonance band to higher frequency, for **1** to 398 nm and for **2** to 404 nm and a clear increase in the intensity of the resonance band, Figure 1, below. In neither case was a band typical of aggregation observed.

**Figure 1.** UV-Visible spectra of (A) **1**\_Ag\_NP or (B) **2**\_Ag\_NP mixed with DI water (in blue) or with BSA (in red).



The use of fluorescence spectroscopy, Figures 2 and 3 below, allowed the determination of the association constants, by the well-known method of Benesi-Hildebrand [30]. Starting from the equation:

$$\frac{1}{\Delta I_f} = \frac{1}{K_n \alpha} \frac{1}{[H]_0^n} + \frac{1}{\alpha} \quad (1)$$

in which,  $\Delta I_f = I_{f_{h-g}} - I_{f_g} - I_{f_h}$ , where,  $I_{f_{h-g}}$ ,  $I_{f_g}$  and  $I_{f_h}$  are the fluorescence intensity of the host–guest complex, the guest molecule and the host molecule, respectively.  $[H]_0$  is the original concentration of the calix[n]arenes,  $K$  is the inclusion constant,  $n$  is the number of host molecule (s) in a complex and  $\alpha$  is a constant. Then, it is possible to determine the inclusion constant by plotting  $1/\Delta I_f$  versus  $1/[H]_0^n$  for different values  $n$ , the value of  $n$  that results a straight line can be taken as the number of host molecules.

**Figure 2.** Fluorescence spectra of BSA at  $1 \times 10^{-5}$  M with varying concentrations of (A) **1** or (B) **1\_Ag\_NP**. In the inset, BSA maximum fluorescence intensity as a function of (A) **1** or (B) **1\_Ag\_NP**. (— DI Water; —  $1 \times 10^{-6}$  M; —  $2.5 \times 10^{-6}$  M; —  $5 \times 10^{-6}$  M; —  $1 \times 10^{-5}$  M; —  $2.5 \times 10^{-4}$  M; —  $5 \times 10^{-5}$  M; —  $7.5 \times 10^{-5}$  M; —  $1 \times 10^{-4}$  M; —  $2 \times 10^{-4}$  M; —  $3 \times 10^{-4}$  M; —  $4 \times 10^{-4}$  M; —  $5 \times 10^{-4}$  M; —  $7 \times 10^{-4}$  M; —  $9 \times 10^{-4}$  M).

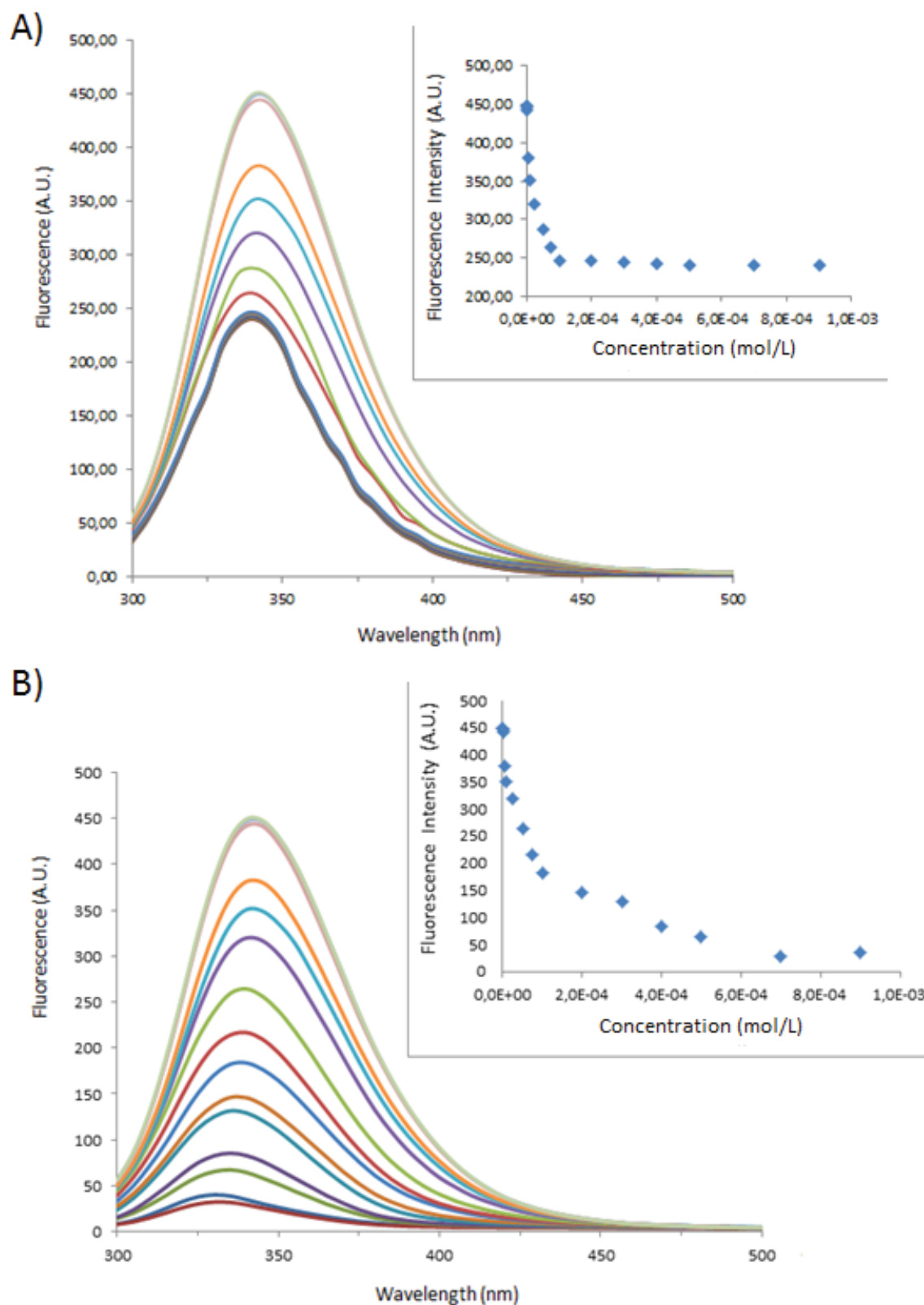
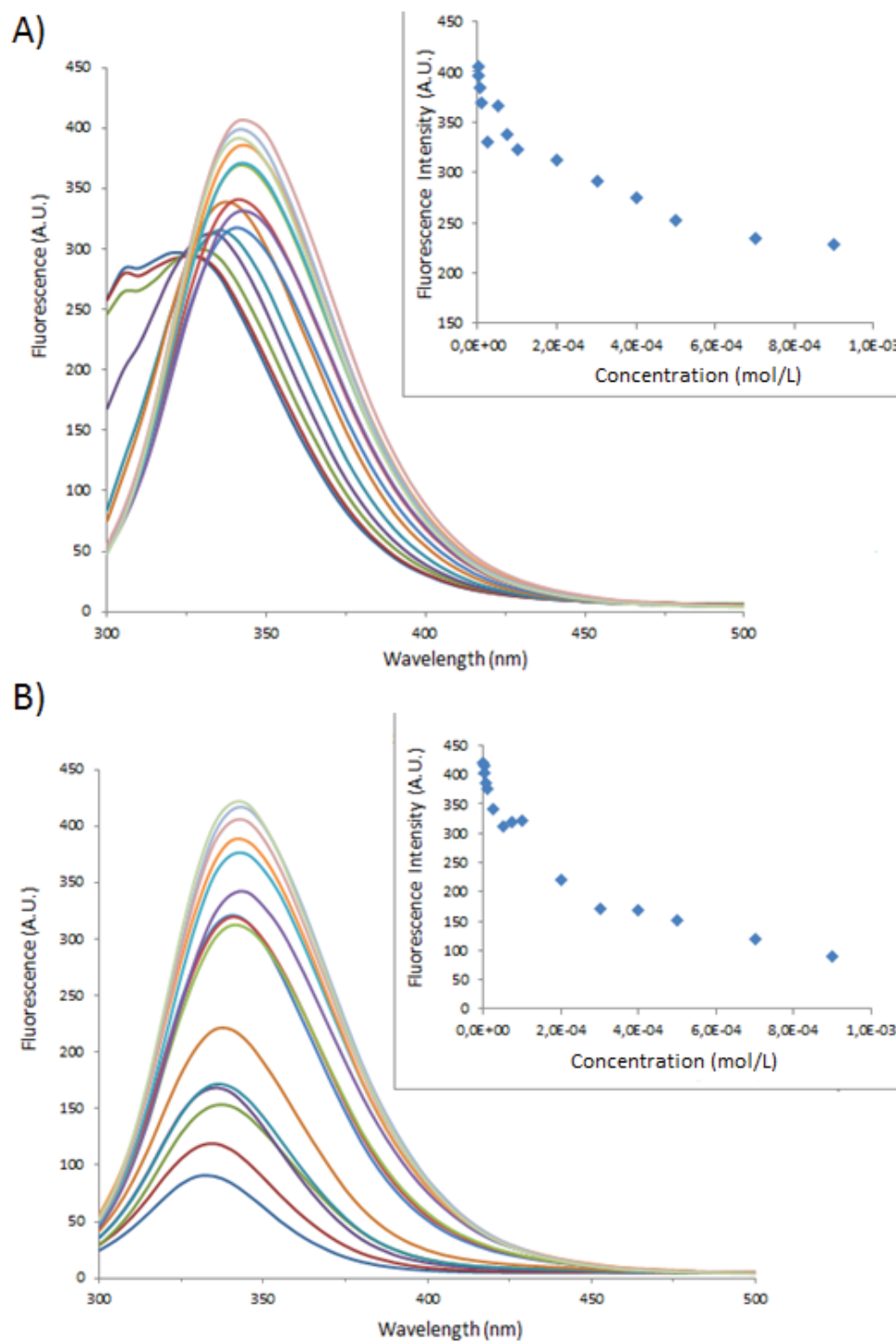


**Figure 3.** Fluorescence spectra of BSA at  $1 \times 10^{-5}$  M varying concentrations of (A) **2** or (B) **2\_Ag\_NP**. In the inset, BSA maximum fluorescence intensity as a function of (A) **2** or (B) **2\_Ag\_NP**. (— DI Water; —  $1 \times 10^{-6}$  M; —  $2.5 \times 10^{-6}$  M; —  $5 \times 10^{-6}$  M; —  $1 \times 10^{-5}$  M; —  $2.5 \times 10^{-4}$  M; —  $5 \times 10^{-5}$  M; —  $7.5 \times 10^{-5}$  M; —  $1 \times 10^{-4}$  M; —  $2 \times 10^{-4}$  M; —  $3 \times 10^{-4}$  M; —  $4 \times 10^{-4}$  M; —  $5 \times 10^{-4}$  M; —  $7 \times 10^{-4}$  M; —  $9 \times 10^{-4}$  M).



The fluorescence emission of the tryptophan amino acids is quenched with increasing concentrations of **1**, **2**, **1\_Ag\_NP** and **2\_Ag\_NP**, in the insets the maximum fluorescence is plotted as a function of the concentration of the various systems. While the spectra and maximum emission values

for **1** and **1\_Ag\_NP**, follow typical binding curves; those for **2** show red shifts at high concentrations of **2**, suggesting an increase in the polarity of the local environment of the tryptophan residues.

The observed value for **1** at  $7.2 \times 10^5$  is reasonably close to the average value obtained from ES/MS experiments, at  $3.95 \times 10^5$ , however for **2** the  $k_{\text{ass}}$  value is much lower at  $1.0 \times 10^5$  [19], this difference undoubtedly reflects the capacity of **1** to bind the basic amino acid side chains within the macrocyclic cavity [26], whereas **2** binds the basic amino acids externally to the cavity [28].

The calculated association constant values for the capped nanoparticles are considerably lower ( $2.4 \times 10^4 \text{ M}^{-1}$  for **1\_Ag\_NP**), in particular in the case of **2\_Ag\_NP** ( $3.5 \times 10^3 \text{ M}^{-1}$  for **2\_Ag\_NP**) implying that at least one of the stronger binding pockets on BSA is not available for interaction with the anionic calix[4]arene-capped nanoparticles. The observed results and stoichiometries are summarized in Table 2, below. It is interesting to note that the rule of thumb calculation that the concentration at half-height is equal to the  $K_{\text{dis}}$  value gives values which are at a first approximation close to those calculated from the method of Benesi [30].

**Table 2.** Stoichiometry S and Association Constants  $K_{\text{ass}}$  of different samples toward BSA.  $K_{\text{ass}}$  has been calculated according 2 different methods, that of Benesi, [30] and a simplistic method where  $K_{\text{dis}}$  is calculated as the half height of the binding curve and  $K_{\text{ass}}$  is taken simply as the inverse.

Sample	Type of Bovine Albumin	Stoichiometry determined according to the method of Benesi [30]	$K_{\text{ass}}$ determined according to the method of Benesi [30] ( $\text{M}^{-1}$ )	$K_{\text{ass}}$ apparent ( $\text{M}^{-1}$ )
<b>1</b>	BSA	1 : 1	71,666	100,000
<b>1_Ag_NP</b>	BSA	1 : 1	24,000	16,600
<b>1_Ag_NP</b>	BSA-FITC	1 : 1	5,200	4,540
<b>2</b>	BSA	1 : 1	10,000	5,500
<b>2_Ag_NP</b>	BSA	1 : 1	3,500	5,500
<b>2_Ag_NP</b>	BSA-FITC	1 : 1	5,400	3,300

In Figure 4 below are given the plots of  $1/\Delta f$  versus  $1/[H]_0$  as per Benesi, [30] this allows the calculation of an approximate stoichiometry of the complexation events, the best straight lines are obtained for 1:1 stoichiometries. It must be underlined that such deductions should be treated with some care as the exact nature of the binding events between serum albumins and nanoparticles are not completely clear.

We were hopeful that the use of FITC capped albumins would open up a second spectroscopic probe with higher inherent fluorescence intensity than that of the aromatic amino acids. As there are only two fluorescent tryptophan, 21 fluorescent tyrosine and 30 fluorescent phenylalanine amino acids; this should allow enhancement of the fluorescence signal and thus diminution of the minimum detectable limit. The results are shown in Figure 5 below, and the global results are summarized in Table 2. Here the binding is far lower than that observed with BSA alone, at  $5.2 \times 10^3 \text{ M}^{-1}$  for **1\_Ag\_NP** and  $5.4 \times 10^3 \text{ M}^{-1}$  for **2\_Ag\_NP**, Figure 6. On reflection this is not surprising as FITC selectively couples to lysine residues which are one of the main recognition sites for the anionic calix[4]arenes [11].

**Figure 4.** Graph of  $1/\Delta I_f$  versus  $1/[H]_0$  for BSA above (A) 1, (B) 1\_Ag\_NP, (C) 2, (D) 2\_Ag\_NP. In the inset, the straight line equation with the coefficient of determination  $R^2$ .

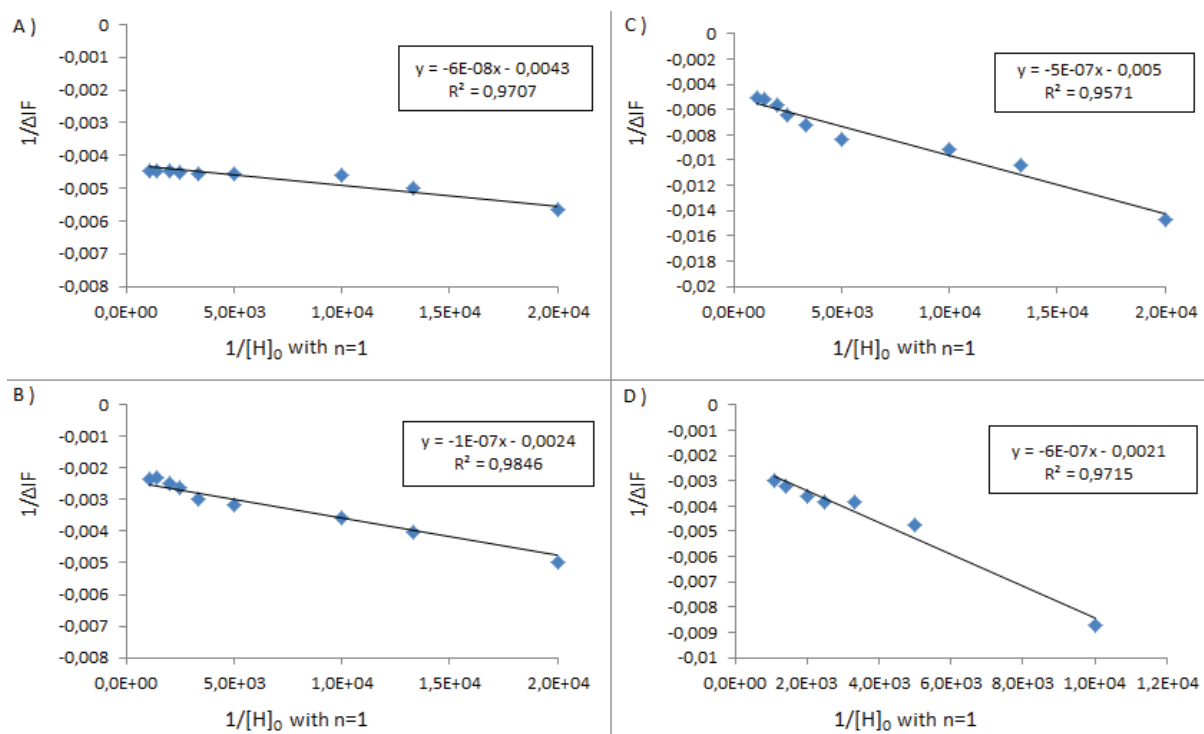


**Figure 5.** Fluorescence spectra of BSA-FITC at  $1 \times 10^{-5}$  M varying concentrations of (A) 1\_Ag\_NP or (B) 2\_Ag\_NP. In the inset, BSA maximum fluorescence intensity as a function of (A) 1\_Ag\_NP or (B) 2\_Ag\_NP. (— DI Water; —  $1 \times 10^{-6}$  M; —  $2.5 \times 10^{-6}$  M; —  $5 \times 10^{-6}$  M; —  $1 \times 10^{-5}$  M; —  $2.5 \times 10^{-4}$  M; —  $5 \times 10^{-5}$  M; —  $7.5 \times 10^{-5}$  M; —  $1 \times 10^{-4}$  M; —  $2 \times 10^{-4}$  M; —  $3 \times 10^{-4}$  M; —  $4 \times 10^{-4}$  M; —  $5 \times 10^{-4}$  M; —  $7 \times 10^{-4}$  M; —  $9 \times 10^{-4}$  M).

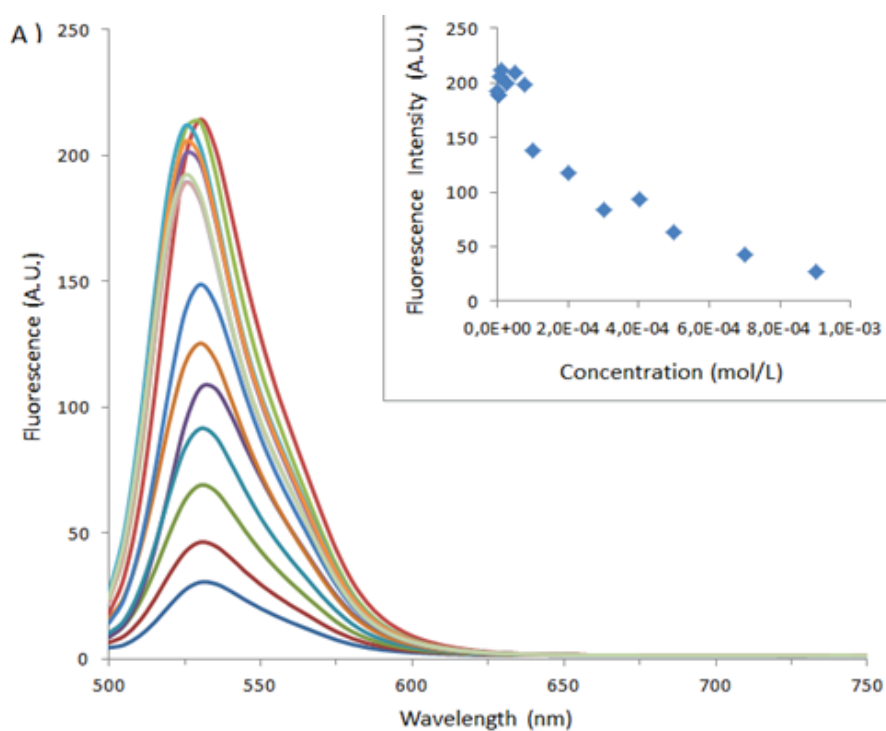
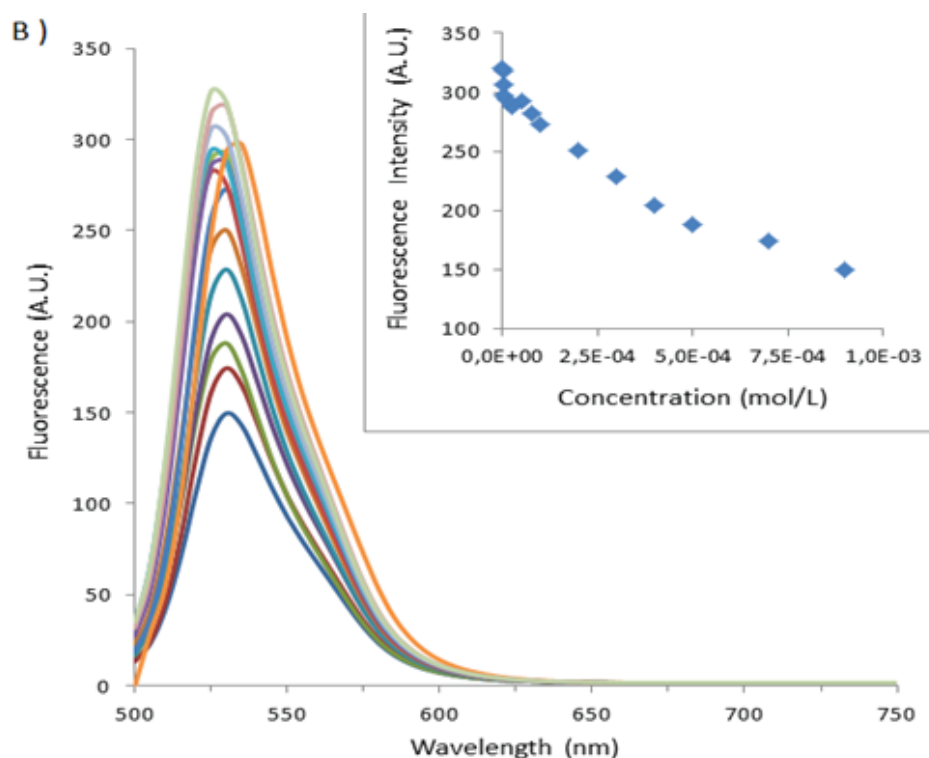
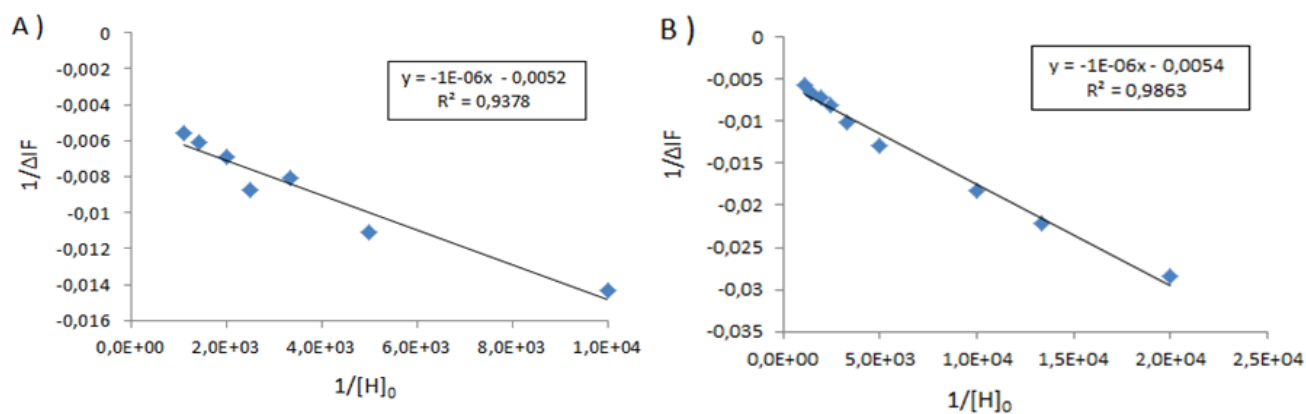


Figure 5. Cont.



**Figure 6.** Graph of  $1/\Delta I_f$  versus  $1/[H]_0$  for BSA-FITC above (A) 1\_Ag\_NP, (B) 2\_Ag\_NP. In the inset, the straight line equation with the coefficient of determination  $R^2$ .



Initial experiments with the complexation of the anionic calix[4]arene capped silver nanoparticles with different serum albumins showed a time dependent variation in the intensities of the plasmon resonance peak. Subsequent experiments showed that this variation was temperature dependent and quite rapid, taking place over about 20 minutes. The known values of the denaturing temperatures of the serum albumins, *i.e.*, bovine serum albumin (BSA), human serum albumin (HAS), porcine serum albumin (PSA) and sheep serum albumin (ssa) are given below in Table 3 [31–34]. The quite large span of temperatures for BSA is known to be associated with partial unfolding of the protein [31].

**Table 3.** Denaturation temperatures of different albumins.

	BSA	HSA	PSA	SSA
Denaturation Temperature (°C)	50–80	50	68	60

In Figure 7, above are shown the temporal variations in the intensity of the plasmon resonance peak as a function of temperature for the two nanoparticles in the presence of different serum albumins. The relevant percentage changes after 5 min and 15 min are summarized in Tables 4 and 5, respectively. It can clearly be seen that it is possible to differentiate between species using this data, for example at 50 °C for BSA with **1\_Ag\_NP** there is a change of −8% after 5 min −11% after 15 min, for **2\_Ag\_NP** the changes are −3% after 5 min and −32% after 15 min whereas for PSA the same data gives 13%, −0.5% for **1\_Ag\_NP** and −15% and −0.5% for **2\_Ag\_NP**. The diminution in the intensity of the plasmon resonance absorption of **2\_Ag\_NP** in the presence of BSA is quite singular at over 30% for temperatures above the initial partial unfolding [31]. It thus becomes possible with a quite simple methodology to discriminate between the species

**Figure 7.** Maximum absorbance, normalized to 1 at time zero of calix[n]arene capped silver nanoparticles mixed with different albumin species as a function of time and temperature (thick blue: 20 °C, red: 30 °C, green: 40 °C, purple: 50 °C and sky blue: 60 °C). On the left, **1\_Ag\_NP** mixed with BSA (A), HSA (B), PSA (C), and SSA (D); on the right **2\_Ag\_NP** mixed with BSA (E), HSA (F), PSA (G) and SSA (H).

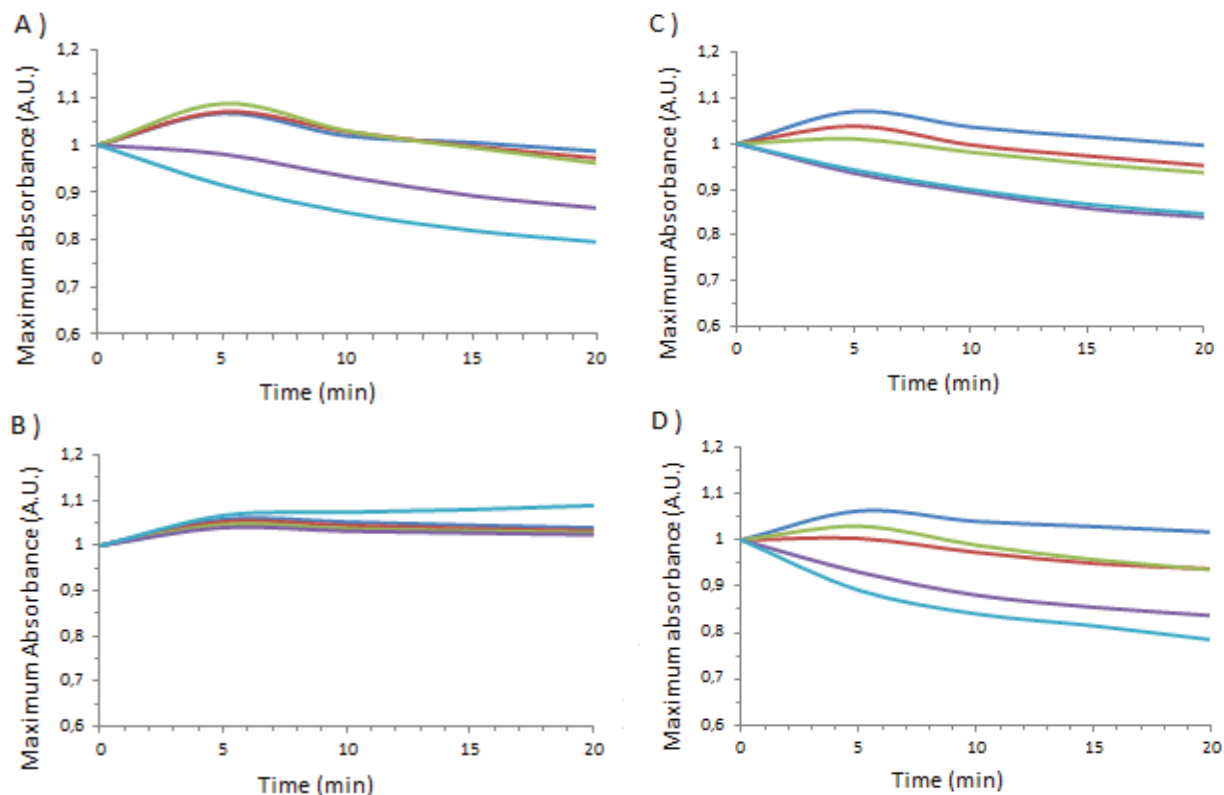
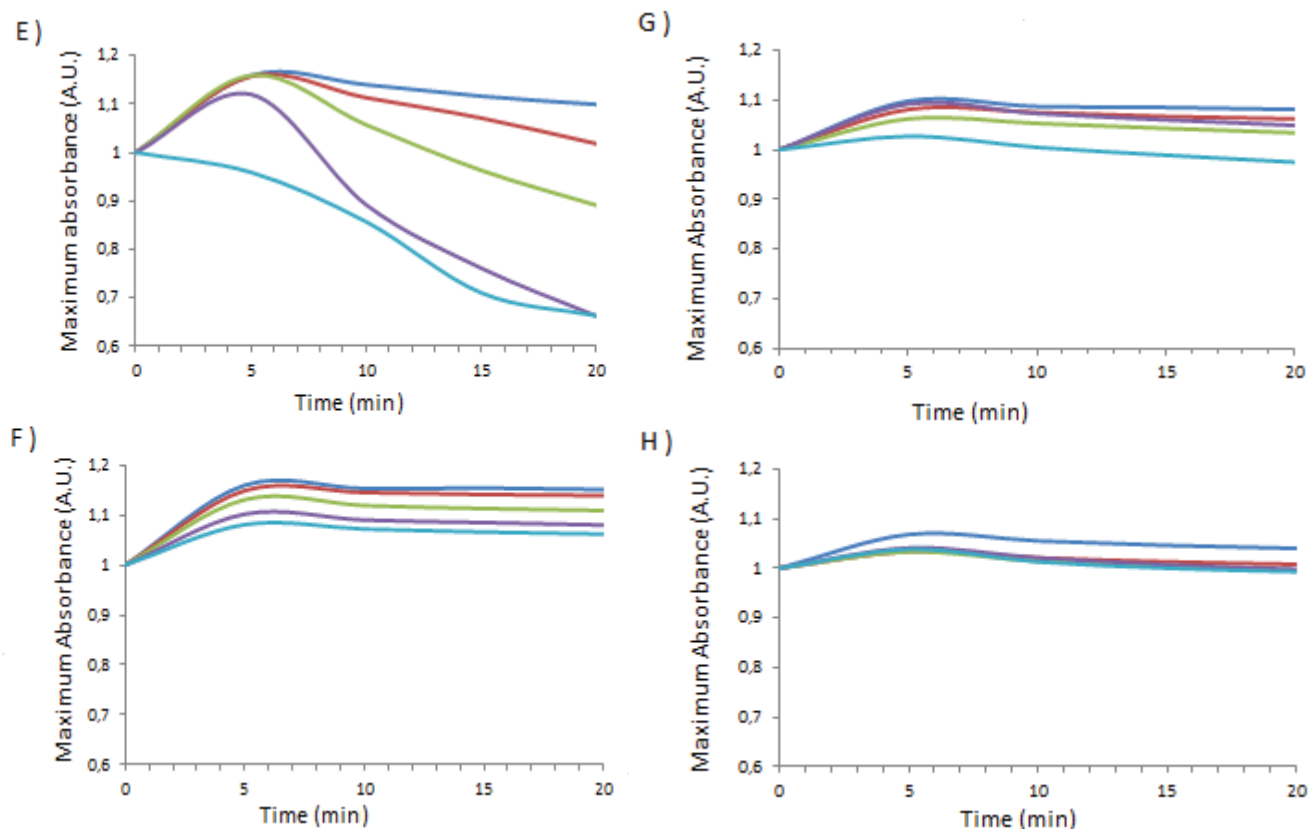


Figure 7. Cont.



**Table 4.** Percentage changes of the maximum absorption of calixarenes-capped silver nanoparticles against Serum Albumin as a function of temperature, after 5 min.

Temperature applied (°C)	1_Ag_NP / BSA	1_Ag_NP / HSA	1_Ag_NP / PSA	1_Ag_NP / SSA	2_Ag_NP / BSA	2_Ag_NP / HSA	2_Ag_NP / PSA	2_Ag_NP / SSA
20	0	0	0	0	0	0	0	0
30	0.3	-0.5	-3	-5.62	-0.17	-0.95	-1.55	-3.18
40	1.93	-1.1	-5.6	-3.13	0	-2.5	-3.28	-3.28
50	-8.08	-1.71	-12.61	-12.46	-3.36	-5	-0.55	-2.53
60	-14.26	0.8	-11.95	-16.16	-17.26	-6.81	-6.47	-2.81

**Table 5.** Percentage changes of the maximum absorption of calixarene-capped silver nanoparticles as a function of temperature, after 15 min.

Temperature applied (°C)	1_Ag_NP / BSA	1_Ag_NP / HSA	1_Ag_NP / PSA	1_Ag_NP / SSA	2_Ag_NP / BSA	2_Ag_NP / HSA	2_Ag_NP / PSA	2_Ag_NP / SSA
20	0	0	0	0	0	0	0	0
30	-0.78	-0.7	-4.14	-7.74	-4.03	-1.13	-1.55	-3.15
40	-1.04	-1.21	-5.81	-6.93	-13.71	-3.55	-3.28	-3.92
50	-11.17	-1.64	-15.46	-16.95	-31.81	-5.98	-0.55	-3.73
60	-18.52	3.3	-14.57	-20.87	-36.38	-7.63	-6.47	-4.4

### 3. Experimental

#### 3.1. Synthesis

*para*-Sulphonatocalix[4]arene (**1**) was synthesized as per the literature method and physical characteristics correspond to the literature values [23]. The diphosphonate derivative **2** was synthesized as per the method of Markovsky and Kalchenko [35], and all spectral values were in accord with their reported values.

#### 3.2. Nanoparticle Preparation and Characterization

The procedure of Xiong [20] was slightly modified as follows:  $1 \times 10^{-2}$  M AgNO<sub>3</sub> solution (10 mL) was added to deionized water (80 mL). To this solution,  $1 \times 10^{-2}$  M calix[n]arene aqueous solution (10 mL) was added as stabilizer and the mixture stirred during 30 min. Then, NaBH<sub>4</sub> (44 mg) was added to the solution. The calix[n]arene capped silver colloidal suspensions were characterized by UV-Visible absorption assays. The change in absorbance between 340 nm and 650 nm was monitored, using a 96 titer well visible spectrometer, (BioTek Power Wave 340, Bad Friedrichshall, Germany).

#### 3.3. Fluorimetry Experiments

All the fluorescence spectra were measured at 20 °C. The albumin was diluted at a final concentration of  $1 \times 10^{-5}$  M and was mixed with a varying concentration of calix[n]arene (or calix[n]arene-capped silver nanoparticles) from  $9 \times 10^{-4}$  to  $1 \times 10^{-6}$  M. Fluorescence spectra and fluorescence intensities were measured on a model F-6500 fluorescence spectrophotometer (Hitachi, Tokyo, Japan) using a 1(W) × 3(D) × 35(H) mm micro-quartz cell. The slits for the emission monochromators were fixed at 5.0 nm. The excitation wavelength was set at 290 nm for bovine serum albumin (BSA) and 495 nm for the BSA-fluorescein conjugate. The emission spectra were monitored from 300 to 500 nm for BSA and 500 to 750 nm for the BSA-fluorescein conjugate.

#### 3.4. Thermal Complexation Titrations

All albumins were purchased from Sigma Aldrich (Sigma Aldrich, Saint-Quentin, France), and used without further purification. The calix[n]arene capped silver colloidal suspensions and the albumin were heated independently 10 min before mixing. Then, the complexation between albumin and calix[n]arene capped silver colloidal suspensions was monitored using a thermoregulated cell accessory for the Jasco spectrophotometer FP-6200 (Tokyo, Japan). The value at 490 nm corresponding to the absorption band of aggregated nanoparticles was measured, every 5 minutes during 20 min at 20, 30, 40, 50 and 60 °C.

### 4. Conclusion

We have studied the use of fluorescence spectroscopy and visible spectroscopy to obtain discrimination between the behaviour of four different types of serum albumins. The temperature and time dependent variation in the intensity of the plasmon resonance peak in calix[n]arene capped nanoparticles provides a suitable method to differentiate between different animal species.

## Conflict of Interest

The authors declare no conflict of interest.

## References

1. FSA statement on horse meat investigation. *Food Standard Agency*, 8 February 2013.
2. Shen, S.; Lee, M. Yum's China chicken antibiotics within limits: Shanghai government. *Reuters Agency*, 24 December 2012.
3. Dunmore, C.; Croft, A. Horsemeat scandal set to spur tougher EU food tests. *Reuters Agency*, 13 February 2013.
4. How the horsemeat scandal unfolded—Timeline. *The Guardian. Press Association* (London: Guardian News and Media), 15 February 2013.
5. Reilly, A. CEO Statement to the Joint Oireachtas Committee on Agriculture, Food and the Marine. *Food Safety Authority of Ireland*, 5 February 2013.
6. Supplier of halal meat containing pork DNA is named. *BBC Press Association*, 3 February 2013.
7. FSAI Survey Finds Horse DNA in Some Beef Burger Products. *Food Safety Authority of Ireland*. 15 January 2013.
8. Winter, A.K.; Thomsen, P.D. A comparison of DNA-hybridization, immunodiffusion, countercurrent immunoelectrophoresis and isoelectric focusing for detecting the admixture of pork to beef. *Meat Sci.* **1990**, *27*, 75–85.
9. Curry, S.; Brick, P.; Franks, N.P. Fatty Acid Binding to Human Serum Albumin: New Insights from Crystallographic Studies. *Biochim. Biophys. Acta* **1999**, *1441*, 131–140.
10. Bujacz, A. Structures of bovine, equine and leporine serum albumin. *Acta Crystallogr. Sect. D Biol. Crystallogr.* **2012**, *D68*, 1278–1289.
11. Perret, F.; Coleman, A.W. Biochemistry of the anionic calix[n]arenes. *Chem. Commun.* **2011**, *47*, 7303–7319.
12. Da Silva, E.; Ficheux, D.; Coleman, A.W. Anti-thrombotic activity of water-soluble calix[n]arenes. *J. Inclusion Phenom. Macrocyclic Chem.* **2005**, *52*, 201–206.
13. Matar-Merheb, R.; Rhimi, M.; Leydier, A.; Huche, F.; Galian, C.; Desuzinges-Mandon, E.; Ficheux, D.; Flot, D.; Aghajari, N.; Kahn, R.; *et al.* Structuring Detergents for Extracting and Stabilizing Functional Membrane Proteins. *PLoS One* **2011**, *6*, e18036.
14. Atwood, J.L.; Bridges, R.J.; Juneja, R.K.; Singh, A.K. Calixarene chloride channel blockers. U.S. Patent 5489612, 1996.
15. Beshara, C.S.; Jones, C.E.; Daze, K.D.; Lilgert, B.J.; Hof, F. A Simple Calixarene Recognizes Post-translationally Methylated Lysine. *ChemBioChem* **2010**, *11*, 63–66.
16. Coleman, A.W.; Perret, F.; Cecillon, S.; Moussa, A.; Martin, A.; Dupin, M.; Perron, H. Enhanced detection of the pathogenic prion protein by its supramolecular association with para-sulfonato-calix[n]arene derivatives. *New J. Chem.* **2007**, *31*, 711–717.
17. Cecillon, S.; Coleman, A.W.; Eveno-Nobile, A.; Perron, H.; Rodrigue, M. Method for detecting aggregate-forming circulating protein forms and agent for capturing formed aggregates. U.S. Patent 8158441, 2006.

18. Memmi, L.; Lazar, A.; Brioude, A.; Ball, V.; Coleman, A.W. Protein–calixarene interactions: Complexation of Bovine Serum Albumin by sulfonatocalix[n]arenes. *Chem. Commun.* **2001**, *23*, 2474–2475.
19. Da Silva, E.; Rousseau, C.F.; Zanella-Cleon, I.; Becchi, M.; Coleman, A.W. Mass Spectrometric Determination of Association Constants of Bovine Serum Albumin (BSA) with para-Sulphonato-Calix[n]arene Derivatives. *J. Inclusion Phenom. Macrocyclic Chem.* **2006**, *54*, 53–59.
20. Xiong, D.; Chen, M.; Li, H. Synthesis of para-sulfonatocalix[4]arene-modified silver nanoparticles as colorimetric histidine probes. *Chem. Commun.* **2008**, *7*, 880–882.
21. Tauran, Y.; Grosso, M.; Brioude, A.; Kassab, R.; Coleman, A.W. Colourimetric and spectroscopic discrimination between nucleotides and nucleosides using para-sulphonato-calix[4]arene capped silver nanoparticles. *Chem. Commun.* **2011**, *47*, 10013–10015.
22. Perret, F.; Tauran, Y.; Suwinska, K.; Kim, B.J.; Chassain-Nely, C.; Boulet, M.; Coleman, A.W. Molecular recognition and transport of active pharmaceutical ingredients on anionic calix[4]arene-capped silver nanoparticles. *J. Chem.* **2013**, *2013*, doi:10.1155/2013/191828.
23. Coleman, A.W.; Jebors, S.; Cecillon, S.; Perret, P.; Garin, D.; Marti-Battle, D.; Moulin, M. Toxicity and biodistribution of para-sulfonato-calix[4]arene in mice. *New J. Chem.* **2008**, *32*, 780–782.
24. Da Silva, E.; Coleman, A.W. Synthesis and complexation properties towards amino acids of mono-substituted p-sulphonato-calix-[n]-arenes. *Tetrahedron* **2003**, *59*, 7357–7364.
25. Selkti, M.; Tomas, A.; Coleman, A.W.; Douteau-Guevel, N.; Nicolis, I.; Villain, F.; de Rango, C. The first example of a substrate spanning the calix[4]arene bilayer: the solid state complex of p-sulfonatocalix[4]arene with L-lysine. *Chem. Commun.* **2000**, 161–162.
26. Adina, L.; Da Silva, E.; Navaza, A.; Barbey, C.; Coleman, A.W. A new packing motif for para-sulfonatocalix[4]arene: the solid state structure of the para-sulfonatocalix[4]arene D-arginine complex. *Chem. Comm.* **2004**, 2162–2163.
27. Perret, F.; Morel-Desrosiers, N.; Ficheux, D.; Coleman, A.W. An ESI/MS study of the formation of ternary 25,27-bis(dihydroxy-phosphoryloxy) calix[4]arene- metal ion-aminoacid complexes. *J. Supramol. Chem.* **2004**, *2*, 533–536.
28. Lazar, A.N.; Danylyuk, O.; Suwinska, K.; Coleman, A.W. Hydrogen Bonding Effects in the structure of Calix[4]arene dihydroxyphosphonic acid and L-Lysine. *J. Mol. Struct.* **2006**, *825*, 20–25.
29. Sugio, S.; Kashima, A.; Mochizuki, S.; Noda, M.; Kobayashi, K. Crystal structure of human serum albumin at 2.5 Å resolution. *Protein Eng.* **1999**, *12*, 439–446.
30. Benesi, H.; Hildebrand, J. A spectrophotometric investigation of the interaction of iodine with aromatic hydrocarbons. *J. Am. Chem. Soc.* **1949**, *71*, 2703–2707.
31. Aoki, K.; Hiramatsu, K.; Kimura, K.; Kaneshina, S.; Nakamura, Y.; Sato, K. Heat Denaturation of Bovine Serum Albumin. I. Analysis by Acrylamide-gel Electrophoresis. *Bull. Inst. Chem. Res.* **1969**, *47*, 274–282.
32. Wetzel, R.; Becker, M.; Behlke, J.; Billwitz, H.; Böhm, S.; Ebert, B.; Hamann, H.; Krumbiegel, J.; Lassmann, G. Temperature behaviour of human serum albumin. *Eur. J. Biochem.* **1980**, *104*, 469–478.
33. Saguer, E.; Alvarez, P.; Ismail, A.A. Heat-induced denaturation/aggregation of porcine plasma and its fractions studied by FTIR spectroscopy. *Food Hydrocolloids* **2012**, *27*, 208–219.

34. Ghazaei, C.; Ahmadi, M.; Hosseini, J.N. Optimization and comparative characterization of neuraminidase activities from *Pseudomonas aeruginosa* with *Klebsiella pneumoniae*, Hep-2 cell, sheep kidney and rat liver lysosome. *Iran. J. Microbiol.* **2010**, *2*, 33–40.
35. Kalchenko, V.I.; Rudkevich, D.M.; Markovskii, L.N. Phosphorylation of 3,5,10,12,17,19,24,26-octahydroxy-1,8,14,22-tetramethyl[1–4]metacyclophane. *Zh. Obshch. Khim.* **1990**, *60*, 2813–2814.

*Sample Availability:* Samples of the compounds **1** and **2** are available from the authors.

© 2013 by the authors; licensee MDPI, Basel, Switzerland. This article is an open access article distributed under the terms and conditions of the Creative Commons Attribution license (<http://creativecommons.org/licenses/by/3.0/>).

## **Calix[n]arene silver nanoparticles interactions with surfactants are charge, size and critical micellar concentration dependent**

Titre: Les interactions entre les nanoparticules d'argent calix[n]arene et les surfactants sont dépendantes de la charge, de la taille et de la concentration micellaire critique des surfactants

Résumé: Les interactions entre les nanoparticules d'argent fonctionnalisées par différents calix[n]arenes (portants des groupes sulfonates en position phénolique et/ou *para*) et des surfactants (anioniques, neutres et cationiques) ont été étudiées. Les changements d'absorbance plasmonique ont été observés pour seulement les calix[4]arenes sulfonates à la position *para* avec les surfactants cationiques. Les interactions suivent les valeurs de concentration micellaire critique CMC des surfactants aussi bien sous forme de monomères ou de micelles mixtes.

Cite this: DOI: 10.1039/c2cc34670b

www.rsc.org/chemcomm

## COMMUNICATION

## Calix-arene silver nanoparticles interactions with surfactants are charge, size and critical micellar concentration dependent†

Yannick Tauran,<sup>ab</sup> Arnaud Brioude,<sup>a</sup> Patrick Shahgaldian,<sup>c</sup> Alessandro Cumbo,<sup>c</sup> Beomjoon Kim,<sup>bd</sup> Florent Perret,<sup>e</sup> Anthony W. Coleman<sup>\*a</sup> and Imed Montasser<sup>f</sup>

Received 29th June 2012, Accepted 8th August 2012

DOI: 10.1039/c2cc34670b

The interactions of silver nanoparticles capped by various calix[*n*]arenes bearing sulphonate groups at the *para* and/or phenolic faces with cationic, neutral and anionic surfactants have been studied. Changes in the plasmonic absorption show that only the calix[4]arene derivatives sulphonated at the *para*-position interact and then only with cationic surfactants. The interactions follow the CMC values of the surfactants either as simple molecules or mixed micelles.

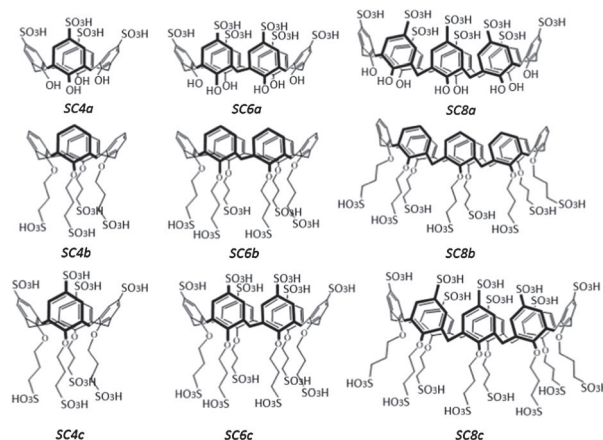
Micelles are formed by the aggregation of surfactants having a cone like geometry,<sup>1</sup> they are characterised by the critical micellar concentration (CMC), above which no free surfactant molecules go into solution.<sup>2</sup> The CMCs can be determined by a quite large number of physical measurements of which the surface tension is the most widely used.<sup>3</sup> Micelles are used in a vast range of applications varying from soaps and detergents,<sup>4</sup> through butter or margarine<sup>5</sup> to the extraction of membrane proteins.<sup>6</sup> Such applications as the last require detailed knowledge of the micellar aggregations whereas the former applications are dependent on a subjective feeling by a consumer. It is the field of membrane protein biochemistry that the use of supramolecular surfactants is starting to make an impact.

The calix[*n*]arenes are one of the most widely studied classes of organic host molecules, their biological,<sup>7</sup> solid-state complexation<sup>8</sup>

and assembly properties<sup>9</sup> have been widely studied. They are known to complex a wide range of organic cations,<sup>10</sup> including alkyl ammonium,<sup>11</sup> and alkylated pyridinium<sup>12</sup> salts. Amphiphilic calix[*n*]arenes have been demonstrated to form various types of assembly in aqueous media. One minor drawback is that calix[*n*]arenes require very considerable modification to introduce reporter groups, with the possible perturbation of the complexation properties. The discovery by Xiong *et al.* that *para*-sulphonato-calix[*n*]arenes can cap silver nanoparticles and that the plasmon resonance bands of the hybrid colloids show strong spectral shifts upon selective interaction with histidine introduces the needed reporter functions.<sup>13</sup> Recently we have shown that the hybrid nanoparticles interact with nucleic bases in a similar manner and that the interactions can lead to aggregation of the colloids.<sup>14</sup>

In the present work we report the interactions of three types of sulphonato-calix[*n*]arene silver nanoparticles with various cationic, neutral and anionic surfactants. The measured spectral shifts can be used as a novel way to determine CMC values for cationic surfactants. Moreover this behaviour can be used to study the highly non-ideal behaviour of mixed surfactant assemblies.

The chemical structures of the various calix[*n*]arenes are given in Scheme 1 and those of the surfactants in Scheme 2.



**Scheme 1** Structures of the sulphonato calix[*n*]arenes studied. SC(*n*)a, SC(*n*)b and SC(*n*)c correspond, respectively, to *para*-sulphonato-calix[*n*]arene, *O*-propyl sulphonate calix[*n*]arene and *O*-propyl *para*-sulphonato-calix[*n*]arene; with (*n*) corresponding to the number of phenolic units in the macrocycle.

<sup>a</sup> LMI CNRS UMR 5615, Univ. Lyon 1, Villeurbanne, F69622, France. E-mail: antony.coleman@adm.univ-lyon1.fr; Tel: +33 4 4243 1027

<sup>b</sup> LIMMS/CNRS-IIS (UMI 2820), University of Tokyo, Tokyo, Japan

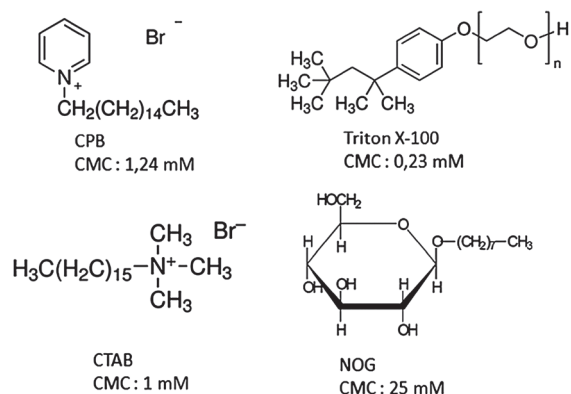
<sup>c</sup> Fachhochschule Nordwestschweiz, Hochschule für Lifesciences, Gründenstrasse 40, 4132 Muttenz, Switzerland. E-mail: patrick.shahgaldian@fhnw.ch

<sup>d</sup> CIRMM, Institute of Industrial Science, University of Tokyo, Tokyo, Japan. E-mail: bjoonkim@iis.u-tokyo.ac.jp

<sup>e</sup> ICBMS, UMR 5246, Univ. Lyon 1, Villeurbanne, F69622, France. E-mail: florent.perret@univ-lyon1.fr; Tel: +33 4 2623 4404

<sup>f</sup> Institut National de Recherche et d'Analyse physico-chimique Technopôle de Sidi Thabet, Tunisia. E-mail: imed.montasser@inrap.rnrt.tn

† Electronic supplementary information (ESI) available: Full details of the syntheses, along with electrospray mass spectrometry and <sup>1</sup>H NMR spectral details, preparation of the hybrid nanoparticles via sodium borohydride reduction, full details of the visible spectrometric characterisation of the formation and stability of the hybrid nanoparticles and the spectrometric titrations. See DOI: 10.1039/c2cc34670b



**Scheme 2** Structures of cationic and neutral surfactants. CPB, CTAB and NOG correspond, respectively, to cetyl pyridium bromide, cetyl trimethyl ammonium bromide and *N*-octyl glucopyranoside.

The calix[*n*]arenes carrying *O*-propylsulphonate groups at the phenolic functions were synthesised by treating the parent calix[*n*]arenes with butyl sultone and a large excess of sodium hydride in tetrahydrofuran as per the method of Shinkai *et al.*<sup>15,16</sup> The reaction was followed using electrospray mass spectrometry and further additions of the reactants were continued until total substitution was achieved.

Suspensions of nine calix[*n*]arene capped silver nanoparticles at a concentration of  $10^{-3}$  M were titrated against five surfactants; with CPB and CTAB as cationics; Triton X-100 and NOG as neutral; and SDS as an anionic.

Of the calix[*n*]arenes only for **SC4a**, **SC4b** and **SC4c** were there changes in the visible spectra, see ESI†, with both intensity changes and small changes in maximum wavelength, Fig. 1. The shifts in the plasmon resonance peaks are in accordance with interactions but not aggregation. Thus the presumed cone conformation of these molecules on the surface of the silver nanoparticles is important for complexation.

The work was extended for **SC4a** to cover a range of surfactant concentrations up to ten times the CMC values, shown in Fig. 1. Here there is a clear differentiation between cationic and anionic or neutral surfactants. Measuring the absorbance at 390 nm corresponding to the maximum absorbance in the absence of surfactants or using the maximum absorbance

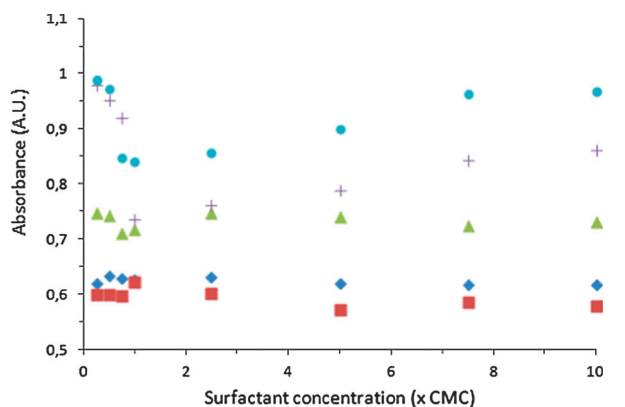


**Fig. 1** Maximum absorbance of *para*-sulphonato-calix[4]arene capped silver nanoparticles ( $\text{Ag\_NP\_SC4a}$ ) as a function of surfactant concentration. ● is CPB; + is CTAB; ◆ is NOG; ■ is Triton X 100; ▲ is SDS.

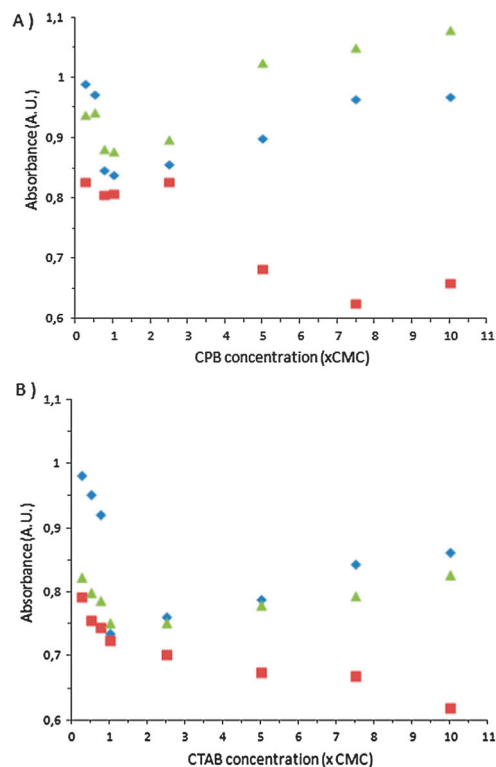


**Fig. 2** Maximum absorbance of calix[*n*]arene capped silver nanoparticles ( $\text{Ag\_NP\_Calix}[n]\text{arene}$ ) as a function of cationic surfactant concentration. (A) With CPB and (B) with CTAB. ◆ is  $\text{Ag\_NP\_SC4a}$ ; ■ is  $\text{Ag\_NP\_SC4b}$ ; ▲ is  $\text{Ag\_NP\_SC4c}$ .

shows identical behaviour. Extending further to all calix[4]arene derivatives, for **SC4a** and **SC4c** there is a minimum in the absorbance at the CMC value for both CPB and CTAB, Fig. 2. Interestingly with **SC4b** the behaviour is totally different. Here a decrease in the absorbance to reach a plateau is observed. Such behaviour seems more typical of a molecular interaction independent of the micellisation process. DLS and electron microscopy indicate a lack of aggregation up to surfactant to nanoparticle ratios of 5 : 1, see ESI†. However for **SC4b** the observed DLS values are almost invariant. In the electron microscopy it was observed that at the CMC concentration there is a large degree of variation in the geometry of the objects. Intriguingly for **SC4c** at 1 : 1 and 5 : 1 ratios, there is formation of small crystallites. Such behaviour might have an impact on nucleation of bio-macromolecules. Thus the presence of the sulphonate group in the *para*-position is required for CMC dependent interactions.

We have demonstrated how capped nanoparticles can be used as probes for CMC determination in the case of cationic surfactants.

Applications of micellar suspensions often involve the use of mixtures of two or more surfactants, as for example in the extraction of membrane proteins. Here one detergent is used to remove the protein from its lipid bilayer environment and then the first surfactant is stripped away by a stabilising detergent.<sup>17</sup> Obviously while the CMC values of the pure detergents are known, the effects of surfactant protein and how CMC values will change as a function of mole fractions of the various components are non-trivial problems.

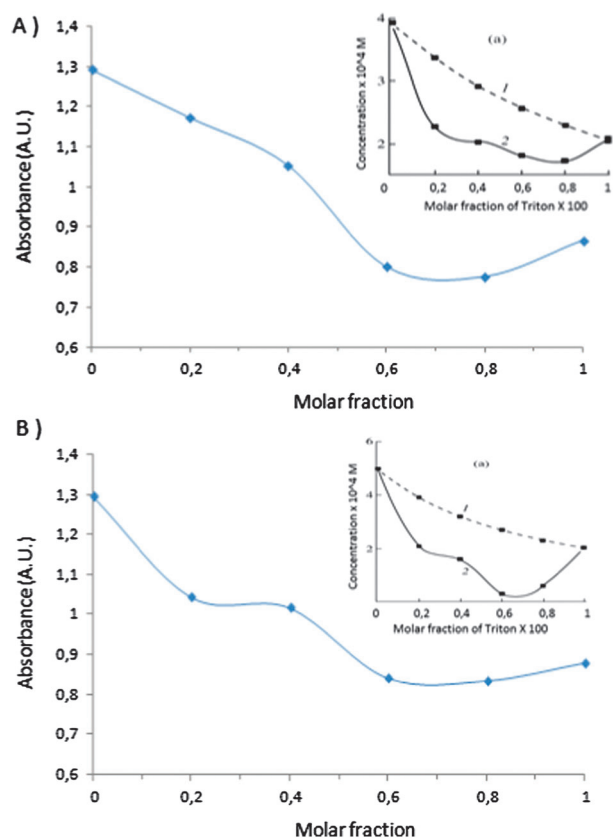


**Fig. 3** Dependencies of the maximum absorbance of Ag\_NP\_SC4a mixed with a neutral-cationic surfactant mixture on the molar fraction of Triton X100. (A) With CPB and (B) with CTAB. Inset: Dependencies of the CMC of the cationic surfactant Triton X100 mixture required to reach surface pressure on the molar fraction of Triton X100 in solution. (1) refers to the calculation for the ideal system and (2) denotes experimental data. See ref. 18.

A study by Kharitonova *et al.*<sup>18</sup> on the behaviour of CTAB/Triton-X100 and CPB/Triton X-100 mixed micelles demonstrated that there was a very strong non-ideal behaviour of the  $C^M$  (CMC of a mixture). Diminutions of a factor of ten between the ideal behaviour and the experimental values were found. The measurements are quite complicated and time consuming.

In view of this, we used the simple spectroscopic determination of the  $C^M$  values by using various mole fractions of the mixture in the 96 titre well visible spectrometer. Such measurements require only a few minutes and indeed sample preparation is more time consuming in the experiments. The spectra are given in the ESI†, and the variations of the maximum absorbance as a

function of the surfactant mole fractions are given in Fig. 3. For comparison the values obtained by Kharitonova are given as insets. It can be clearly seen that values obtained here parallel those previously observed using surface tension isotherms as the analytical tool.

In conclusion we have shown that hybrid silver nanoparticles capped by *para*-sulphonato-calix[4]arene derivatives interact in a critical micellar concentration dependent manner with cationic surfactants. Intensity changes in the plasmon resonance absorption spectral peak intensity can be used to determine the CMC. More importantly the method can be applied directly to the determination of critical micellar concentrations in mixed micellar systems. The method generates a new means of studying critical micellar concentrations in media containing proteins and in particular membrane proteins, work is underway to confirm this application.

This work was funded in part by the ANR PiriBio program, grant number ANR-09-PIRI-0002.

## Notes and references

- I. D. Robb, *Specialist Surfactants*, Chapman and Hall, London, 1st edn, 1997.
- Y. Moroi, *Micelles: Theoretical and Applied Aspects*, Plenum Press, New York, 1992.
- C. E. Lin, *J. Chromatogr., A*, 2004, **1037**, 467–478.
- W. L. Hinze and E. Pramauro, *CRC Crit. Rev. Anal. Chem.*, 1993, **24**, 133–177.
- J. D. Dziezak, *Food Technol.*, 1988, **42**, 172.
- A. M. Seddon, P. Curnow and P. J. Booth, *Biochim. Biophys. Acta*, 2004, **1666**, 105–117.
- A. W. Coleman, S. Jebors, S. Cecillon, P. Perret, D. Garin, D. Marti-Battle and M. Moulin, *New J. Chem.*, 2008, **32**, 780–782.
- O. Danylyuk and K. Suwinska, *Chem. Commun.*, 2009, 5799–5813.
- F. Perret, A. N. Lazar and A. W. Coleman, *Chem. Commun.*, 2006, 2425–2438.
- F. Perret and A. W. Coleman, *Chem. Commun.*, 2011, **47**, 7303–7319.
- Y. J. Lee, S. W. Ko, H. M. Yeo, H. Jeong and K. C. Nam, *Bull. Korean Chem. Soc.*, 2006, **27**, 1227–1230.
- K. Araki, H. Shimizu and S. Shinkai, *Chem. Lett.*, 1993, 205–208.
- D. Xiong, M. Chen and H. Li, *Chem. Commun.*, 2008, 880–882.
- Y. Tauran, M. Grosso, A. Brioude, R. Kassab and A. W. Coleman, *Chem. Commun.*, 2011, **47**, 10013.
- S. Shinkai, S. Mori, T. Tsubaki, T. Sone and O. Manabe, *Tetrahedron Lett.*, 1984, **25**, 5315–5318.
- S. Shinkai, S. Mori, H. Koreishi, T. Tsubaki and O. Manabe, *J. Am. Chem. Soc.*, 1986, **108**, 2409–2416.
- R. Matar-Merheb, M. Rhimi, A. Leydier, F. Huché, C. Galián, E. Desuzinges-Mandon, D. Ficheux, D. Flot, N. Aghajari, R. Kahn, A. Di Pietro, J. M. Jault, A. W. Coleman and P. Falson, *PLoS One*, 2011, **6**, 18036.
- T. V. Kharitonova, N. I. Ivanova and B. D. Summ, *Colloid J.*, 2002, **64**, 620–630.

## Part B

### Section 2

# Biological activities of calix[n]arene nanoparticles



## **Discriminatory antibacterial effects of calix[n]arene capped silver nanoparticles with regard to Gram positive and Gram negative bacteria**

Titre: Effet antibactérien discriminant les bactéries à Gram positif ou Gram négatif causé par des nanoparticules d'argent fonctionnalisées de calix[n]arènes

Résumé: Les nanoparticules d'argent ont été fonctionnalisées avec 9 calix[n]arènes sulfonates différents et leurs effets antibactériens ont été évalués sur *B. subtilis* et *E. coli* à une concentration de 100 nM en calix[n]arène. Les résultats ont montré que les *para*-sulfonato-calix[n]arènes sont actifs contre les bactéries à Gram positif alors que les calix[n]arènes ayant des groupes sulfonates aux positions terminales *para* et alkyl sont actifs contre les bactéries à Gram négatif. Enfin, le calix[6]arène portant des groupements sulfonates seulement en position O-alkyl a montré aussi une activité antibactérienne.

## Discriminatory antibacterial effects of calix[*n*]arene capped silver nanoparticles with regard to Gram positive and Gram negative bacteria†

Cite this: DOI: 10.1039/c3cc42838a

Received 17th April 2013,  
Accepted 28th June 2013

DOI: 10.1039/c3cc42838a

www.rsc.org/chemcomm

Samira Boudebouze,<sup>a</sup> Anthony W. Coleman,<sup>\*b</sup> Yannick Tauran,<sup>b</sup> Hela Mkaouer,<sup>a</sup> Florent Perret,<sup>c</sup> Alexandrine Garnier,<sup>a</sup> Arnaud Brioude,<sup>b</sup> Beomjoon Kim,<sup>d</sup> Emmanuelle Maguin<sup>a</sup> and Moez Rhimi<sup>\*a</sup>

Silver nanoparticles capped with nine different sulphonated calix[*n*]arenes were tested for their anti-bacterial effects against *B. subtilis* and *E. coli* at an apparent concentration of 100 nM in calix[*n*]arene. The results show the *para*-sulphonato-calix[*n*]arenes are active against Gram positive bacteria and the derivatives having sulphonate groups at both *para* and alkyl terminal positions are active against Gram negative bacteria. The calix[6]arene derivative with only *O*-alkyl sulphonate groups shows bactericidal activity.

With rise of drug resistant bacteria,<sup>1</sup> the search for new anti-bacterial drugs and especially those with structures unrelated to current active pharmaceutical ingredients has become a key theme in biological and medicinal chemistry. Different approaches are needed as the Gram<sup>+</sup> bacteria possess no outer membrane whereas the Gram<sup>-</sup> bacteria possess a thick peptidoglycan outer membrane.<sup>2</sup>

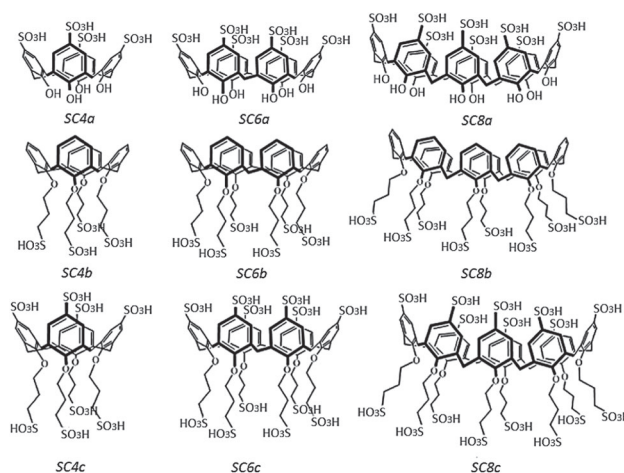
Silver nanoparticles have attracted much interest in academic research and industrial applications due to their low cost and their ease of production.<sup>3</sup> They have been used as optical sensors,<sup>4</sup> cosmetic coatings,<sup>5</sup> colorimetric sensors<sup>6</sup> or even as photo thermal therapeutic agents.<sup>7</sup> Silver nanoparticles have been shown to be efficient antimicrobial agents,<sup>8</sup> this combined a limited human toxicity<sup>9</sup> has promoted their use in consumer products such as phone protection, food packaging, clothes or skin care.<sup>10</sup>

The calix[*n*]arene class of molecules is one of the most studied in supramolecular chemistry.<sup>11</sup> The molecular recognition ability of such molecules allows complexation with a wide range of biomolecules including active pharmaceutical ingredients (APIs),<sup>12</sup> nucleotides,<sup>13</sup> amino-acids<sup>14</sup> and proteins.<sup>15,16</sup> The biological activity of the anionic calix[*n*]arenes has been reviewed in depth.<sup>17</sup> With regard to anti-bacterial activity Cornforth and later

authors demonstrated that certain calix[*n*]arene could be used as an anti-tubercular agents.<sup>18,19</sup> Additionally the sulphonated calix[*n*]arenes show low toxicity both *in vitro* and *in vivo*<sup>17,20</sup> a property which increases interest in their application as possible capping agents for silver nanoparticles. Calix[*n*]arenes capped silver nanoparticles have been shown to complex amino acids<sup>21</sup> nucleic acids<sup>22</sup> and APIs.<sup>23</sup>

Here we report the discriminatory antibacterial effects of eight different anionic calix[*n*]arene capped silver nanoparticles varying in their size (4, 6 or 8 phenolic unit) and the position of the sulphonato group (upper rim, lower rim, or both faces) with regard to Gram positive and Gram negative bacteria.

As previously described,<sup>23</sup> silver nanoparticles capped by the nine different calix[*n*]arenes, as shown in Scheme 1, were prepared at a concentration of 100 μM in calix[*n*]arene. The hybrid nanoparticles were characterized by UV-visible spectroscopy, Dynamic Light Scattering and zeta potential, see ESI.†



**Scheme 1** Structures of the sulphonato calix[*n*]arenes studied. SC(*n*)a, SC(*n*)b and SC(*n*)c correspond respectively to *para*-sulphonato-calix[*n*]arenes, *O*-butyl sulphonato calix[*n*]arenes and *O*-butyl *para*-sulphonato-calix[*n*]arenes. The value of (*n*) corresponds to the number of phenolic units in the macrocycle.

<sup>a</sup> INRA, UMR 1319 Micalis, F-78350 Jouy-en-Josas, France.

E-mail: moez.rhimi@jouy.inra.fr; Tel: +33 1 3465 2294

<sup>b</sup> LMI CNRS UMR 5615, Univ. Lyon 1, Villeurbanne, F69622, France.

E-mail: antony.coleman@adm.univ-lyon1.fr; Tel: +33 4 4243 1027

<sup>c</sup> ICBMS, UMR 5246, Univ. Lyon 1, Villeurbanne, F69622, France<sup>d</sup> Institute of Industrial Science, University of Tokyo, Tokyo, Japan

† Electronic supplementary information (ESI) available. See DOI: 10.1039/c3cc42838a

*Bacillus subtilis* 168 and *Escherichia coli* were cultivated on Luria Bertani medium at 37 °C (220 rpm). Kinetics of growth was studied by measuring the optical density at 600 nm each hour.<sup>24</sup> Full details are available in ESI.†

The effect of calix[*n*]arene capped silver nanoparticles on bacterial growth was determined by their addition into the corresponding *B. subtilis* and *E. coli* cultures. The silver nanoparticles were added so as to give a final concentration of 100 nM in the relevant calix[*n*]arene. The use of a single, very low concentration proscribed the determination of an IC<sub>50</sub> value this is in contrast to the large body of work by Regnouf de Vains on various calix[4]arene derivatives where IC<sub>50</sub> values have been calculated for Gram<sup>−</sup> and Gram<sup>+</sup> bacteria, in the case of water soluble carboxylate derivatives IC<sub>50</sub> in the range >50 μM were found.<sup>25</sup>

The results are summarised in Table 1 for *B. subtilis* and in Table 2 for *E. coli*, given in bold are values which are significantly different from those observed for culture in the absence of the calix[*n*]arene capped silver nanoparticles.

In the absence of the calix[*n*]arene nanoparticles the bacterial colonies grow with a maximum OD of 2.7 for *B. subtilis* and 3.2 for *E. coli* obtained after 16 hours of culture. After this time a plateau is reached and no effective change in the OD is observed (Fig. 1). In the absence of the calix[*n*]arene capping the silver nanoparticles decomposed within two hours and consequently no measurements using uncapped silver nanoparticles were possible.

For the of series *para*-sulphonato-calix[*n*]arene capped silver nanoparticles there are effects on the growth of the Gram<sup>+</sup> bacteria *B. subtilis* but there are no effects on the Gram<sup>−</sup>

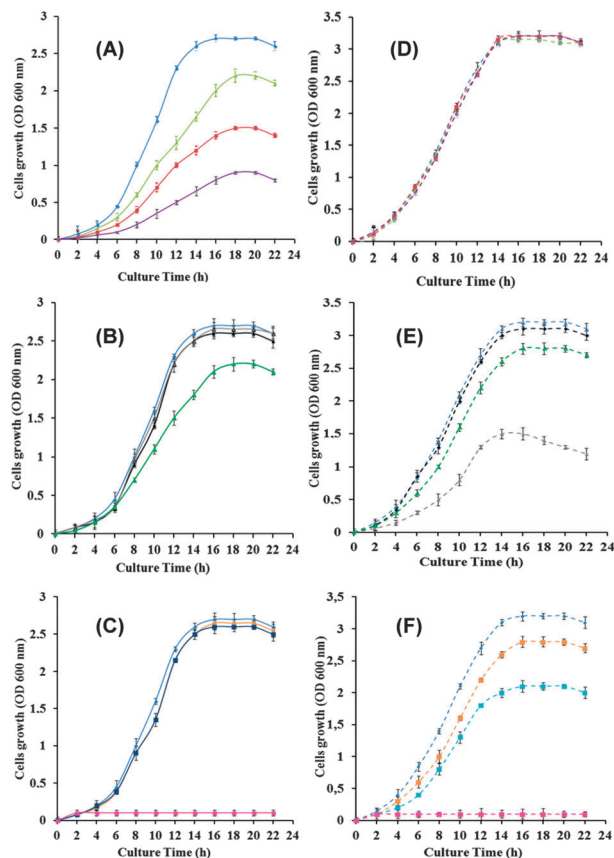


**Fig. 1** Effect of calix[*n*]arene capped silver nanoparticles effect on Gram<sup>+</sup> and Gram<sup>−</sup> bacterial growth. A, B, and C represent *B. subtilis* cultures (Gram<sup>+</sup>) and D, E and F represent *E. coli* cultures (Gram<sup>−</sup>). Solid and dashed blue line corresponds to *B. subtilis* and *E. coli* curves growth, respectively, without addition of nanoparticles. In A and D light green color correspond to SC4a\_NP, red color correspond to SC6a\_NP, purple color correspond to SC8a\_NP, in B and E dark color corresponds to SC4b\_NP, grey color corresponds to SC6b\_NP, dark green corresponds to SC8b\_NP. In C and F orange color corresponds to SC4c\_NP, light blue color corresponds to SC6c\_NP and pink color corresponds to SC8c\_NP which precipitated under the conditions for cell growth and in consequence was not studied.

**Table 1** Summary of bacterial culture data for *B. subtilis*

Nanoparticle	OD <sub>max</sub> at 600 nm	Time to attain OD <sub>max</sub> (hours)	ΔOD <sub>22H</sub>
<i>B. subtilis</i>	2.7	16	−0.1
SC4a	2.2	<b>18</b>	−0.1
SC4b	2.6	16	−0.1
SC4c	<b>2.65</b>	16	−0.1
SC6a	1.5	<b>18</b>	−0.1
SC6b	2.65	16	−0.05
SC6c	2.6	16	−0.1
SC8a	<b>0.9</b>	<b>18</b>	−0.1
SC8b	2.2	<b>18</b>	−0.1
SC8c	N.A.	N.A.	N.A.

N.A: not tested.

**Table 2** Summary of bacterial culture data for *E. coli*

Nanoparticle	OD <sub>max</sub> at 600 nm	Time to attain OD <sub>max</sub> (hours)	ΔOD <sub>22H</sub> − OD <sub>max</sub>
<i>E. coli</i>	3.2	16	−0.1
SC4a	3.15	16	−0.1
SC4b	3.1	16	−0.1
SC4c	2.7	16	−0.1
SC6a	3.2	16	−0.1
SC6b	<b>1.5</b>	<b>14</b>	−0.3
SC6c	2.1	16	−0.1
SC8a	3.2	16	−0.1
SC8b	2.8	16	−0.1
SC8c	N.A.	N.A.	N.A.

N.A: not tested.

bacteria *E. coli*, Fig. 1A and D. The action causes a significant retardation in the growth of the bacterial culture with a maximum in the OD achieved two hours later than in the case of *B. subtilis* alone. There is a strong decrease in the maximum observed OD, which is dependent on the ring size, thus for SC6a and SC8a capped silver nanoparticles the final OD is less than 50% of that observed for the bacteria alone, it is possible to ascribe this to an IC<sub>50</sub> value which will be less than 100 nM. For the *para*-sulphonato-calix[*n*]arenes interactions with proteins such as heparin Cofactor II, and the protease resistant prion protein follow a similar behaviour whereas the interactions with serum albumins are stronger for the smallest macrocycle.<sup>15</sup> The hematoxic effects of the *para*-sulphonato-calix[*n*]arenes show similar behaviour with the haemolytic effect increasing with ring size.<sup>26</sup>

In the SCnb series, the sulphonate group is present at the terminus of an *−O*-butyl chain. Neither the four nor six membered calix[*n*]arenes have any significant effects on *B. subtilis* while system having an eight membered ring has a small but significant effect on the growth with a final OD of 2.2 being achieved after 18 hours. In the case of *E. coli*, the four and eight membered

calix[n]arenes have no effects. For SC6b capped silver nanoparticles the observed effects are quite spectacular. Here a maximum OD of 1.5, that is 47%, of the OD for *E. coli* alone is reached after 14 hours and then the OD declines to 1.2, (37%) after 22 hours. It would seem that this compound both inhibits bacterial growth and also is bactericidal. With regard to the physical characterisation of this system, the visible spectrum shows the plasmon resonance to be at lower frequency than the other nanoparticles and this is associated with an observable aggregation peak at 450 nm. Both the apparent diameter (74.5 nm) and the zeta potential (−26.7 mV) differ from all those observed for all other nanoparticles. Thus a combination of physicochemical factors may account for the activity against Gram<sup>−</sup> bacteria.

In the final series in which sulphonate groups are present both in the *para*-position and at the terminal position of an *−O*-butyl chain, the behaviour is totally different than in the preceding cases. Here the nanoparticles prepared using SC8c are unstable and precipitate under cell culture conditions. The Gram positive *B. subtilis* is unaffected by either SC4c or SC6c silver nanoparticles. However, for *E. coli* both nanoparticle systems cause a significant decrease in the observed OD<sub>max</sub>, decreasing to 2.7 for SC4c and 2.1 for SC6c, but without a decrease with time.

The mechanisms of the anti-bacterial activity of Ag nanoparticles are even now unclear,<sup>8</sup> but may involve both release of Ag<sup>+</sup>, electrostatic interactions and cell wall damage for *B. subtilis* and perturbation of membrane permeability for *E. coli*, along with membrane interaction. In the present systems the concentration are several orders of magnitude lower than those cited Mahmoudi,<sup>8</sup> the strong anionic charge on the calix[n]arenes will enhance electrostatic interactions and there may be perturbation of membrane transport as shown for the *para*-sulphonato-calix[n]arenes with regard to calcium dependent ion channels, where activity increased with increasing ring size.<sup>27</sup>

In conclusion, the anti-bacterial effects of the calix[n]arene capped Ag nanoparticles depend on the structure of the sulphonated calix[n]arenes and also on the size of the macrocycle ring.

These discriminatory effects of silver nanoparticles seem to be a promising tool to limit the growth of numerous pathogenic bacteria. For this purpose, work is currently being undertaken to extend the study to other bacteria and also to other calix[n]arene derivatives. From a fundamental point of view, these chemical compounds appear to possess a high potential for selective action

against either Gram<sup>+</sup> or Gram<sup>−</sup> bacteria in complex cultures (micro bacrobial consortium) having immunomodulatory effects.

## Notes and references

- 1 J. F. Fisher and S. Mobashery, *Enzymology of Bacterial Resistance*, in *Comprehensive Natural Products II. Volume 8: Enzymes and Enzyme Mechanisms*, Elsevier, Holland, 2010, pp. 443–487.
- 2 H. C. Gram, *Fortschr. Med.*, 1884, **2**, 185–189.
- 3 P. K. Jain, X. Huang, I. H. El-Sayed and M. A. El-Sayed, *Plasmonics*, 2007, **2**, 107–118.
- 4 M. Szymanski, A. P. F. Turner and R. Porter, *Electroanalysis*, 2010, **22**, 191–198.
- 5 P. Colomban, *J. Nano Res.*, 2009, **8**, 109–132.
- 6 G. Doria, J. Conde, B. Veigas, L. Giestas, C. Almeida, M. Assunção, J. Rosa and P. V. Baptista, *Sensors*, 2012, **12**, 1657–1687.
- 7 S. C. Boca, M. Potara, A. M. Gabudean, A. Juhem, P. L. Baldeck and S. Astilean, *Cancer Lett.*, 2011, **311**, 131–140.
- 8 M. J. Hajipour, K. M. Fromm, A. A. Ashkarran, D. J. Aberasturi, I. R. Larramendi, T. Rojo, V. Serpooshan, W. J. Parak and M. Mahmoudi, *Trends Biotechnol.*, 2012, **30**, 499–511.
- 9 K. K. Y. Wong and X. Liu, *MedChemCommun.*, 2010, **1**, 125–131.
- 10 M. Epple and S. Chernousova, *Angew. Chem., Int. Ed.*, 2013, **52**, 1636–1653.
- 11 J. W. Steed and J. L. Atwood, *Supramolecular Chemistry*, 2nd edn, John Wiley & Sons, UK, 2009.
- 12 O. Danylyuk and K. Suwinska, *Chem. Commun.*, 2009, 5799–5813.
- 13 M. S. Peters, M. Li and T. Schrader, *Nat. Prod. Commun.*, 2012, **7**, 409–417.
- 14 E. Da Silva and A. W. Coleman, *Tetrahedron*, 2003, **59**, 7357–7364.
- 15 F. Perret and A. W. Coleman, in *Supramolecular Systems in Biomedical Fields*, ed. Hans-Jörg Schneider, RSC, Cambridge, 2013.
- 16 R. E. McGovern, H. Fernandes, A. R. Khan, N. P. Power and P. B. Crowley, *Nat. Chem.*, 2012, **4**, 527–533.
- 17 F. Perret and A. W. Coleman, *Chem. Commun.*, 2011, **47**, 7303–7319.
- 18 J. W. Cornforth, P. D. Hart, G. A. Nicholls, R. J. Rees and J. A. Stock, *Br. J. Pharmacol. Chemother.*, 1955, **10**, 73–88.
- 19 P. D. Hart, J. A. Armstrong and E. Brodaty, *Infect. Immun.*, 1996, **64**, 1491–1493.
- 20 A. W. Coleman, S. Jebors, S. Cecillon, P. Perret, D. Garin, D. Marti-Battle and M. Moulin, *New J. Chem.*, 2008, **32**, 780–782.
- 21 D. Xiong, M. Chen and H. Li, *Chem. Commun.*, 2008, 880–882.
- 22 Y. Tauran, M. Grosso, A. Brioude, R. Kassab and A. W. Coleman, *Chem. Commun.*, 2011, **47**, 100013–100015.
- 23 Y. Tauran, A. Brioude, P. Shahgaldian, A. Cumbo, B. J. Kim, F. Perret, A. W. Coleman and I. Montasser, *Chem. Commun.*, 2012, **48**, 9483–9485.
- 24 G. Sezonov, D. Joseleau-Petit and R. D'Ari, *J. Bacteriol.*, 2012, **189**, 8746–8749.
- 25 M. Mourer, S. Fontanay, R. E. Duval, E. Raphael and J.-B. Regnouf-de-Vains, *Helv. Chim. Acta*, 2012, **95**, 1373–1386.
- 26 E. Da Silva, P. Shahgaldian and A. W. Coleman, *Int. J. Pharm.*, 2004, **273**, 57–62.
- 27 J. L. Atwood, R. J. Bridges, R. K. Juneja and A. K. Singh, *US Pat.*, 5489612, 1996.

## **Molecular recognition and transport of Active Pharmaceutical Ingredients on anionic calix[4]arene capped silver nanoparticles**

Titre: Reconnaissance moléculaire et transport d'ingrédients pharmaceutiques actifs sur des nanoparticules d'argent fonctionnalisées par des calix[n]arènes

Résumé: Une série de 6 calix[4]arènes anioniques, ayant des fonctions sulfonates, carboxylates ou phosphonates à la position phénolique ou *para* a été utilisée pour fonctionnaliser des nanoparticules d'argent. Leurs propriétés de reconnaissance moléculaire ont été étudiées pour 3 ingrédients pharmaceutiques actifs (API): Chlorhexidine, Chloramphenicol and Gentamycin Sulfate. Parmi ces APIs, la Chlorhexidine est connue pour former des co-cristaux avec les calix[4]arènes anionique. La Gentamycine sulfate est un antibiotique amino-glycosidique et le Chloramphenicol est un antibiotique neutre. Comme attendu, les deux premiers APIs ont montré un comportement complexant observé par un déplacement dans le spectre visible alors que le dernier API n'a montré aucune modification dans la longueur d'onde de la bande plasmonique des nanoparticules d'argent.

## Research Article

# Molecular Recognition and Transport of Active Pharmaceutical Ingredients on Anionic Calix[4]arene-Capped Silver Nanoparticles

Florent Perret,<sup>1</sup> Yannick Tauran,<sup>2,3</sup> Kinga Suwinska,<sup>4,5</sup> Beomjoon Kim,<sup>3,6</sup> Cyrielle Chassain-Nely,<sup>2</sup> Maxime Boulet,<sup>2</sup> and Anthony W. Coleman<sup>2</sup>

<sup>1</sup> ICBMS-UMR 5246, Université Claude Bernard Lyon 1, 69622 Villeurbanne, France

<sup>2</sup> LMI-UMR 5615, CNRS, Université Claude Bernard Lyon 1, 69622 Villeurbanne, France

<sup>3</sup> LIMMS/CNRS-IIS (UMI 2820), University of Tokyo, Tokyo, Japan

<sup>4</sup> Institute of Physical Chemistry, Polish Academy of Sciences, Kasprzaka 44/52, 01 224 Warszawa, Poland

<sup>5</sup> Faculty of Biology and Environmental Sciences, Cardinal Stefan Wyszyński University in Warsaw, Wóycickiego 1/3, 01 938 Warszawa, Poland

<sup>6</sup> CIRMM, Institute of Industrial Science, University of Tokyo, Tokyo, Japan

Correspondence should be addressed to Anthony W. Coleman; [antony.coleman@adm.univ-lyon1.fr](mailto:antony.coleman@adm.univ-lyon1.fr)

Received 29 June 2012; Accepted 14 August 2012

Academic Editor: Kevin Shuford

Copyright © 2013 Florent Perret et al. This is an open access article distributed under the Creative Commons Attribution License, which permits unrestricted use, distribution, and reproduction in any medium, provided the original work is properly cited.

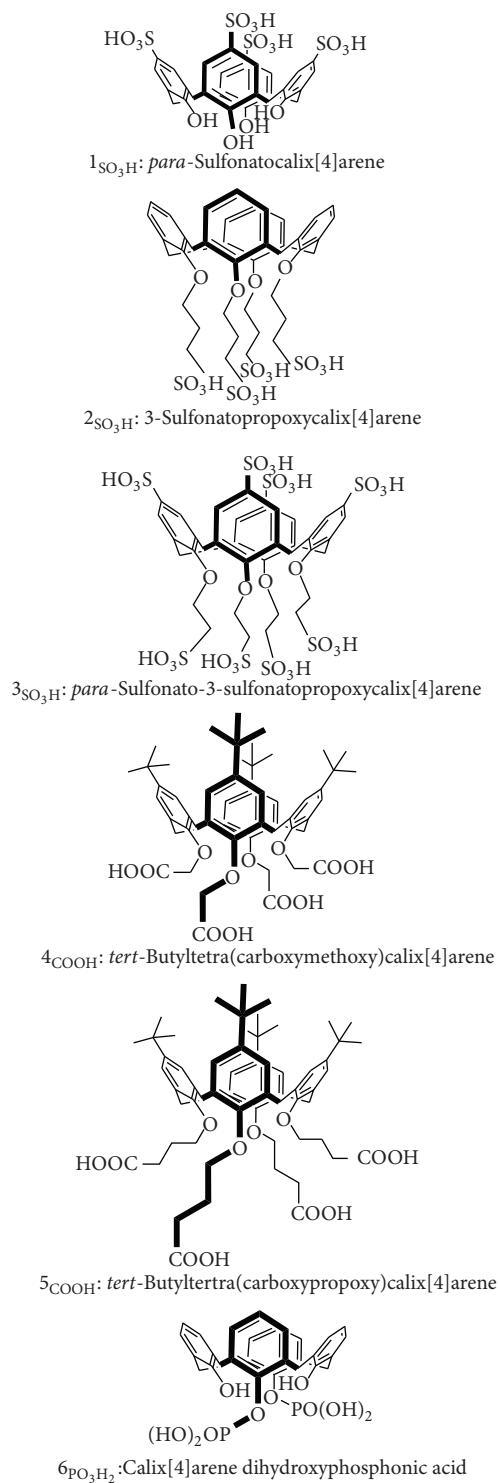
A series of six anionic calix[4]arenes, having sulphonate, carboxylate, or phosphonate functions at either the para-aromatic position or the phenolic face were used to cap silver nanoparticles. Their molecular recognition properties were studied with regard to three active pharmaceutical ingredients, chlorhexidine, chloramphenicol, and gentamycin sulfate. Of these APIs chlorhexidine is known to form cocrystals with the anionic calix[4]arenes, gentamycin sulfate is an aminoglycosidic antibiotic, and chloramphenicol is a neutral antibiotic. As expected the former two APIs show clear complexation behavior as demonstrated by shifts in the visible spectra whereas the last shows no modification in the wavelength of the plasmon resonance of the silver nanoparticles.

## 1. Introduction

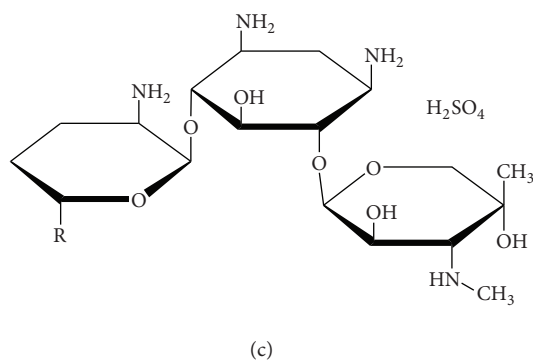
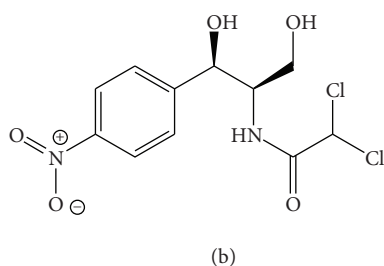
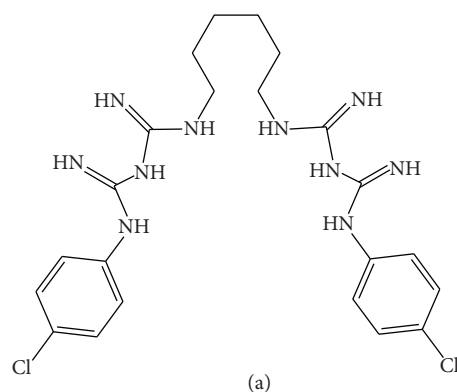
The noble metal nanoparticles are formed by the reduction of a suitable metal salt, for example, chloroauric acid or silver nitrate to the zero oxidation state in the presence of a suitable capping molecule or polymer to stabilize them [1]. They are well known for their ability to act as sensors for molecular interactions by means of shifts in the plasmon resonance absorption [2]. A great amount of work exists concerning their biological properties [3], including biological imaging [4], of particular interest are the antibacterial effects of both the silver and gold nanoparticles [5, 6]. Indeed the silver nanoparticles have seen commercial usage in areas ranging from hygiene (disinfection of socks) [7] to treatment of computer keyboards [8].

The calix[n]arenes are a group of supramolecular systems [9] widely studied for their ability to complex a very wide

range of molecules and ions [10]. The relative ease with which the calix[n]arenes can be modified at either aromatic para-position or at the phenolic face, [11] has made them perhaps the most attractive of organic hosts. Interest in the biochemistry of the calix[n]arenes has grown dramatically with emergence of a wide range of water soluble derivatives [12]. Their direct behavior to act as Active Pharmaceutical Ingredients (APIs) is now emerging, [13] with activities ranging from anti-viral, [14] anti-bacterial, [15] enzyme activators [16] or blockers [17] anti-coagulant, [18] through anti-cancer [19] to detoxification [20]. As with other supramolecular systems the calix[n]arenes provide means to transport APIs in the solid-state as co-crystals, [21], as solubilizing agents, [22], or as colloidal suspensions, via solid lipid nanoparticle formation [23] or via the formation of cocolloidal complexes with highly hydrophobic partners [24]. Their possible pharmaceutical applications have been made more attractive by a lack of



SCHEME 1: Structures of the calix[n]arene studied.



SCHEME 2: Structures of the APIs evaluated: (a) chlorhexidine, (b) chloramphenicol, and (c) gentamycin sulfate.

hemolytic effects [25], an absence of an immune response [26], and a clear lack of in vivo toxicity [27].

The combination of the useful biopharmaceutical properties of the calix[n]arenes with known biological properties thus makes them attractive as biosensors [28] or as transporters or more interestingly by using the calix[n]arenes to act capping stabilisers for nanoparticles and the using their complexation capacities towards APIs to form multifunction APU cocktails.

## 2. Experimental

**2.1. Synthesis.** *para*-Sulfonatocalix[4]arene,  $1_{SO_3H}$ , was synthesized as per the literature method and physical characteristics correspond to the literature values [27]. The two

TABLE 1: Maximum wavelength of each Ag\_NP\_Calix[n]arene as a matter of time of preparation.

Compounds	$\lambda$ after 1 hour mixing	$\lambda$ after 24 hours mixing
Ag_NP_1 <sub>SO<sub>3</sub>H</sub>	400 nm	390 nm
Ag_NP_2 <sub>SO<sub>3</sub>H</sub>	390 nm	390 nm
Ag_NP_3 <sub>SO<sub>3</sub>H</sub>	390 nm	380 nm
Ag_NP_4 <sub>COOH</sub>	410 nm	420 nm
Ag_NP_5 <sub>COOH</sub>	390 nm	400 nm
Ag_NP_6 <sub>PO<sub>3</sub>H<sub>2</sub></sub>	390 nm	400 nm

3-sulfonatopropoxy derivatives,  $2_{SO_3H}$  and  $3_{SO_3H}$ , were prepared by the method of Hwang et al. [29] or Shinkai et al. [30] and the physical properties are in accord with the literature values. *tert*-Butyltetra carboxymethoxy calix[4]arene  $4_{COOH}$

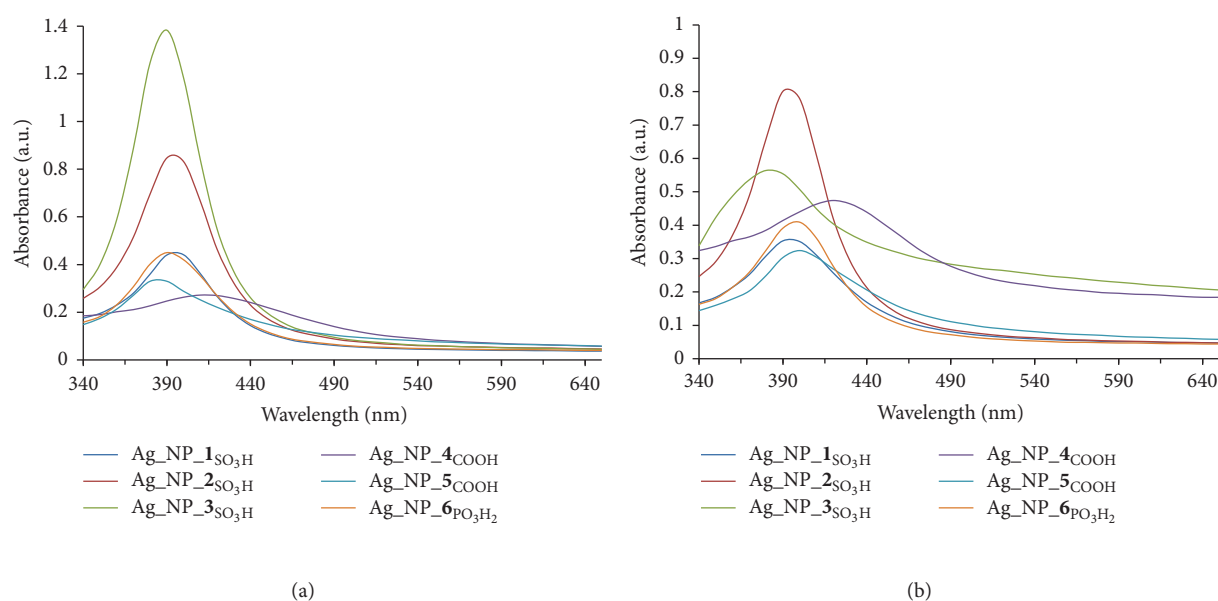


FIGURE 1: The UV visible spectra of Ag\_NP\_Calix[n]arene after (a) 1 hour and after (b) 24 hours.

TABLE 2: The slopes of the variation of the maximum wavelength of Ag\_NP\_Calix[n]arene against the concentration of chlorhexidine.

Compounds	Slope (nm/M)	Rank
After 1 hour mixing with chlorhexidine		
Ag_NP_3SO <sub>3</sub> H	$1.1 \times 10^6$	1
Ag_NP_6PO <sub>3</sub> H <sub>2</sub>	$4 \times 10^5$	2
Ag_NP_1SO <sub>3</sub> H	$3.6 \times 10^5$	3
Ag_NP_2SO <sub>3</sub> H	$2 \times 10^5$	4
Ag_NP_5COOH	$2 \times 10^5$	4
Ag_NP_4COOH	0	5
After 24 hours mixing with chlorhexidine		
Ag_NP_2SO <sub>3</sub> H	$1 \times 10^6$	1
Ag_NP_1SO <sub>3</sub> H	$5 \times 10^5$	2
Ag_NP_3SO <sub>3</sub> H	$3 \times 10^5$	3
Ag_NP_6PO <sub>3</sub> H <sub>2</sub>	$3 \times 10^5$	3
Ag_NP_5COOH	$3 \times 10^5$	3
Ag_NP_4COOH	0	4

and *tert*-butyltetra carboxypropoxy calix[4]arene 5<sub>COOH</sub> were synthesized as per Ohto [31] and purity confirmed by spectral means. The diphosphonate derivative, 6<sub>PO<sub>3</sub>H<sub>2</sub></sub>, was synthesized as per the method of Markovsky and Kalchenko [32]; all spectral values are in accord with their values.

**2.2. Nanoparticle Preparation and Characterization.** The procedure of Xiong et al. [33] was slightly modified as follows. 10 mL of  $1 \times 10^{-2}$  M AgNO<sub>3</sub> solution was added to 80 mL of deionized water. To this solution, 10 mL of  $1 \times 10^{-2}$  M calix[n]arene aqueous solution was added as stabilizer with stirring for 30 min. And then, 44 mg of NaBH<sub>4</sub> was added to the solution. Then the calix[n]arene-capped silver colloidal

TABLE 3: The slopes of the variation of the maximum wavelength of Ag\_NP\_Calix[n]arene against the concentration of gentamycine sulfate.

Compounds	Slope (nm/M)	Rank
After 1 hour mixing with gentamycine sulfate		
Ag_NP_2SO <sub>3</sub> H	$9 \times 10^6$	1
Ag_NP_5COOH	$9 \times 10^6$	1
Ag_NP_3SO <sub>3</sub> H	$2 \times 10^6$	2
Ag_NP_6PO <sub>3</sub> H <sub>2</sub>	$1.3 \times 10^6$	3
Ag_NP_1SO <sub>3</sub> H	$9 \times 10^5$	4
Ag_NP_4COOH	NA*	
After 24 hours mixing with gentamycine sulfate		
Ag_NP_2SO <sub>3</sub> H	$1.4 \times 10^7$	1
Ag_NP_6PO <sub>3</sub> H <sub>2</sub>	$1.3 \times 10^7$	2
Ag_NP_3SO <sub>3</sub> H	$3 \times 10^6$	3
Ag_NP_5COOH	$1.2 \times 10^6$	4
Ag_NP_1SO <sub>3</sub> H	$1 \times 10^6$	5
Ag_NP_4COOH	NA*	

NA\*: not applicable.

suspensions were characterized by UV-visible absorption assays. We monitored the change in absorbance between 340 nm and 650 nm, using a 96-titer well-visible spectrometer, (BioTek Power Wave 340).

**2.3. Complexation Titration.** All APIs were purchased from Sigma Aldrich; chlorhexidine (Merck index no. 55-56-1), chloramphenicol (Merck index no. 56-75-7) and gentamycine sulfate (Merck index no. 1403-66-3).

The complexation between API and calix[n]arene-capped silver colloidal suspensions was monitored with UV-visible absorption spectra after mixing for 1 hour and 24 hours.

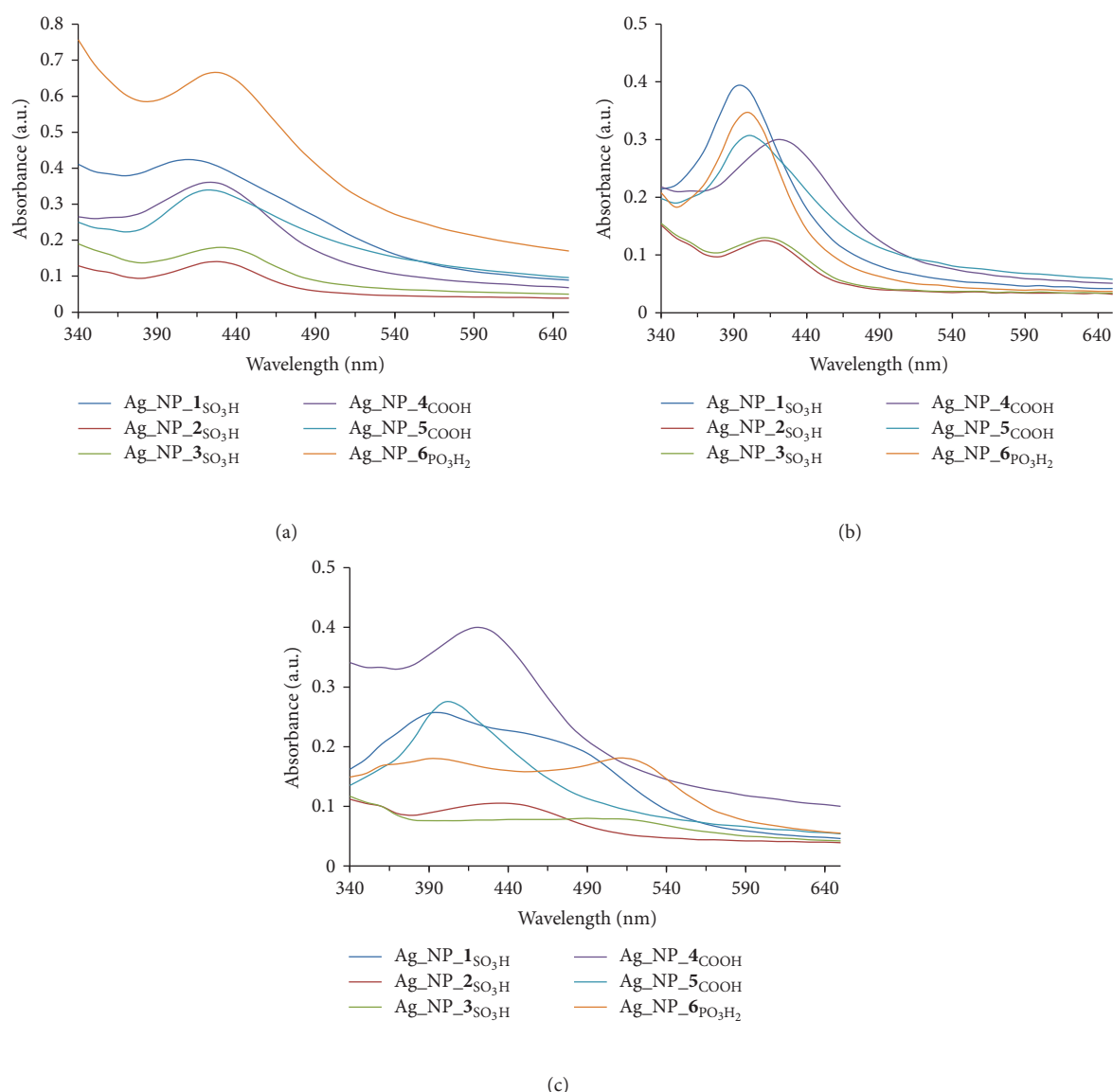


FIGURE 2: The UV-visible spectra of Ag\_NP\_Calix[n]arene mixed for 1 hour with (a)  $1 \times 10^{-4}$  M chlorhexidine (b)  $1 \times 10^{-4}$  M chloramphenicol (c)  $1 \times 10^{-4}$  M gentamycin sulfate.

The calix[n]arene-capped silver colloidal suspensions are at a final concentration of  $1 \times 10^{-4}$  M. The API will be mixed at different final concentrations:  $1 \times 10^{-3}$  M,  $1 \times 10^{-4}$  M,  $1 \times 10^{-5}$  M,  $1 \times 10^{-6}$  M, and  $1 \times 10^{-7}$  M.

### 3. Results and Discussion

The chemical structures of the calix[n]arene derivatives are given in Scheme 1. The chemical structures of the APIs are given in Scheme 2 below.

The stability over the time of the different calix[n]arene-capped silver nanoparticles (Ag\_NP\_Calix[n]arene) solutions as characterized using UV-visible spectroscopy 1 hour and 24 hours after their preparation (Figure 1). Even if the intensity of absorbance decreases for some silver nanoparticle

solutions, in particular with Ag\_NP\_3<sub>SO<sub>3</sub>H</sub>, Table 1 shows that the maximum wavelength of all Ag\_NP\_Calix[n]arene remains stable. This shows that silver nanoparticles are still present after 24 hours of their preparation. For all but Ag\_NP\_3<sub>SO<sub>3</sub>H</sub>, the plasmon resonance absorption peak is sharp and centered at 390 nm; however in the case of Ag\_NP\_3<sub>SO<sub>3</sub>H</sub>, the plasmonic peak is quite broad and centered at 420 nm suggesting a different assembly mode and also some aggregation.

Titration experiments were carried out between the six different types of calix[4]arene-capped nanoparticles and three APIs, chlorhexidine, chloramphenicol, and gentamycin.

Chlorhexidine is a clinically important antiseptic, disinfectant, and preservative. It is a potent membrane-active

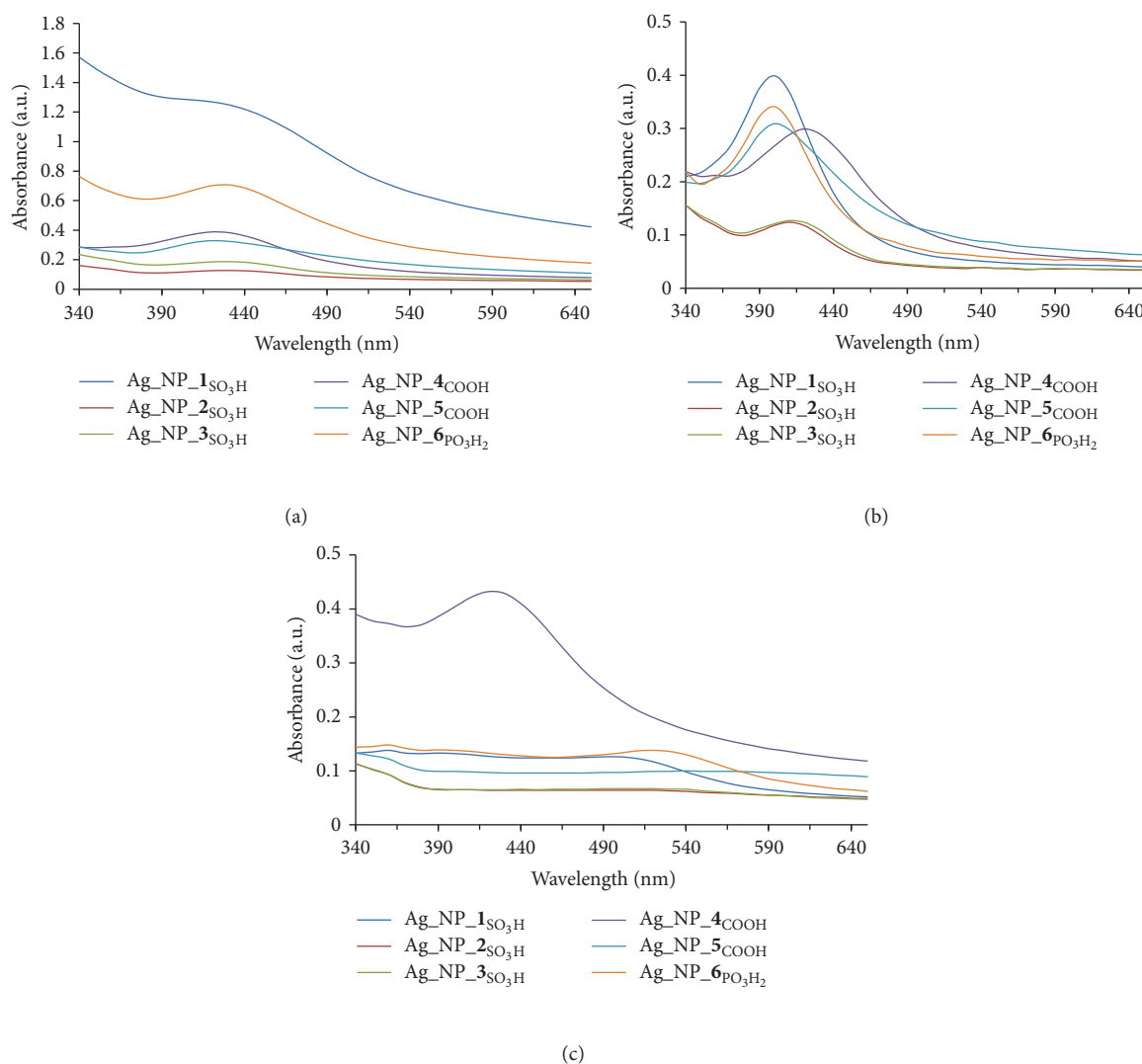


FIGURE 3: The UV visible spectra of Ag\_NP\_Calix[n]arene mixed 24 hours with (a)  $1 \times 10^{-4}$  M chlorhexidine, (b)  $1 \times 10^{-4}$  M chloramphenicol, and (c)  $1 \times 10^{-4}$  M gentamycin sulfate.

agent against bacteria and inhibits outgrowth, but not germination, of bacterial spores. Chloramphenicol is considered a prototypical broad-spectrum antibiotic, alongside the tetracyclines. The most serious adverse effect associated with chloramphenicol treatment is bone marrow toxicity, which is rare (0.1% of the cases), unpredictable, unrelated to dose and in general fatal. As a consequence, it is no longer a first-line agent for any infection in developed nations, although it is sometimes used topically for eye infections. Nevertheless, the global problem of advancing bacterial resistance to newer drugs has led to renewed interest in its use.

Gentamycin sulfate is an aminoglycoside antibiotic, used to treat many types of bacterial infections, particularly those caused by Gram-negative organisms. Its bactericidal effect involves binding the 30S subunit of the bacterial ribosome, interrupting protein synthesis. Like all aminoglycosides, when gentamicin is given orally, it is not systemically active. This is because it is not absorbed to any appreciable extent

from the small intestine. It is administered intravenously, intramuscularly, or topically to treat infections.

The choice of the APIs was based on the facts that chlorhexidine is known to complex with all three types of calix[4]arene derivatives; the conformational flexibility of the molecule led to the presence of three distinct isomers in the solid state [34]. In the case of gentamycin it has already been shown that aminoglycosides complex with  $1\text{SO}_3\text{H}$  [10]; however for streptomycin the complexation was associated over several weeks with glycosidic bond cutting [35]. With regard to chloramphenicol, preliminary studies had shown a total lack of interaction and the molecule was chosen as a negative control.

Representative visible spectratitration curves at 1H and 24H are shown in Figures 2 and 3; for both gentamycin and chlorhexidine there are strong shifts in the plasmon resonance and intensity variations. For gentamycin in particular the changes in wavelength clearly arise from complexation on the nanoparticles by the API [28].

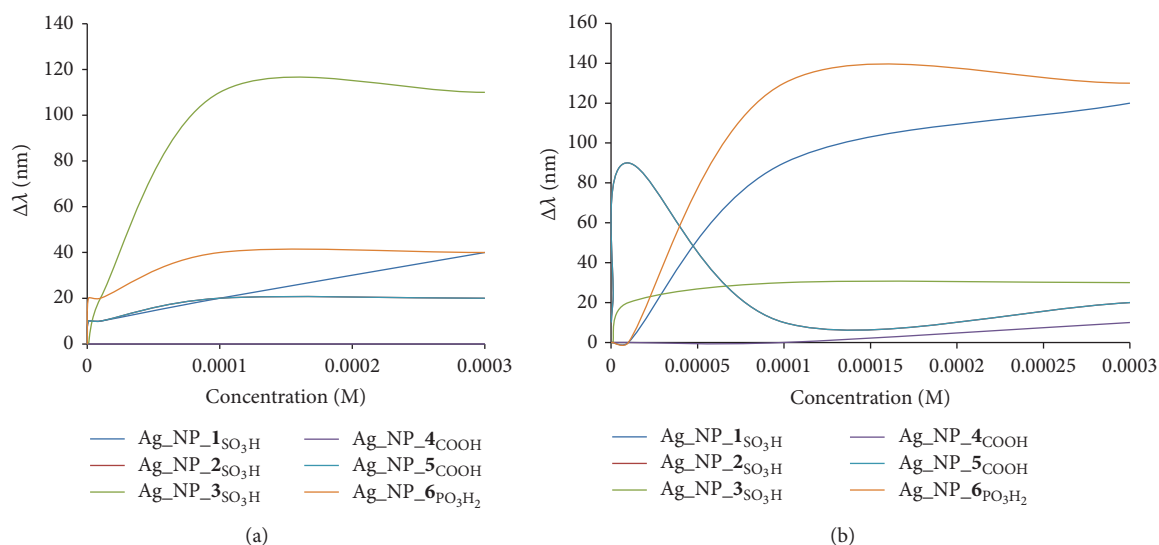


FIGURE 4: The delta values of the maximum wavelength of Ag\_NP\_Calix[n]arene as a matter of concentration of API mixed during 1 hour with (a) chlorhexidine and (b) gentamycin sulfate.

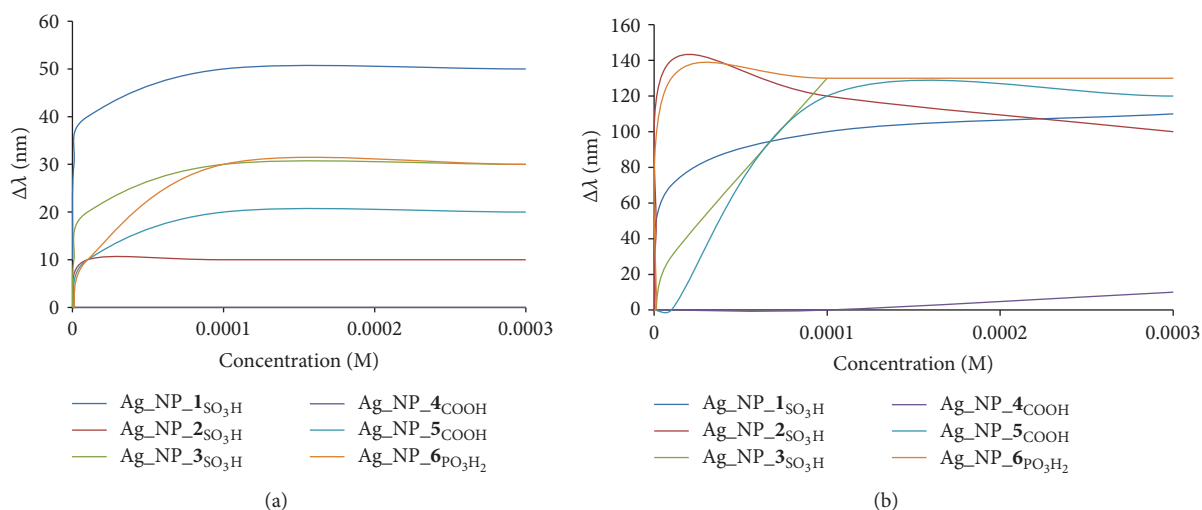


FIGURE 5: The delta of the maximum wavelength of Ag\_NP\_Calix[n]arene as a matter of concentration of API mixed during 24 hours with (a) chlorhexidine (b) gentamycin sulfate.

Given the large shifts in wavelength observed for the absorption associated with the plasmon resonance, the change in wavelength was plotted as a function of API concentration; see Figures 4 and 5.

For chloramphenicol, no change in the wavelength is observed; this is expected in view of the lack of complexation. For chlorhexidine and gentamycin, the curves show a typical concentration-dependent absorption associated with saturation. These reflect the different binding affinities of the various calix[4]arene derivatives with regard to the two APIs.

Given the uncertainty in the exact concentration of complexation sites on the surfaces of the nanoparticles we consider it unwise to calculate association constants.

However comparative values can be extracted from the initial slopes of the curves and these are summarized in Tables 2 and 3.

There are clear variations in the affinity, while in general the hybrid silver nanoparticles capped with Ag\_NP\_2SO<sub>3</sub>H show the highest affinity with chlorhexidine; after 1H the system is fourth in respect to affinity. Of the systems studied only Ag\_NP\_4COOH shows little or no affinity for these two APIs.

Thus we have observed selectivity in the interactions between the calix[4]arene capped nanoparticles and the APIs studied. This variation is dependent on the nature of the calix[n]arene, the API, and the kinetics of the interaction.

#### 4. Conclusion

A series of novel calix[n]arene-capped silver nanoparticles have been prepared and their stability demonstrated. We have been able to couple calix[4]arenes having sulfonate, carboxylate, and phosphonate functions onto the silver nanoparticles. Tests with the APIs, chlorohexidine, chloramphenicol, and gentamycine sulfate, show strong affinity towards chlorohexidine and gentamycine, whereas for chloramphenicol little or no affinity exists. The affinities for the APIs depend on the nature of the calix[4]arene and on the nature of the API, and the kinetics of interaction vary as a function of both of the above.

#### Acknowledgments

The authors thank the CNRS and the University Lyon 1 for financial support.

#### References

- [1] J. Turkevich, P. C. Stevenson, and J. Hillier, "A study of the nucleation and growth processes in the synthesis of colloidal gold," *Discussions of the Faraday Society*, vol. 11, pp. 55–75, 1951.
- [2] P. K. Jain, W. Huang, and M. A. El-Sayed, "On the universal scaling behavior of the distance decay of plasmon coupling in metal nanoparticle pairs: a plasmon ruler equation," *Nano Letters*, vol. 7, no. 7, pp. 2080–2088, 2007.
- [3] P. K. Jain, X. Huang, I. H. El-Sayed, and M. A. El-Sayed, "Noble metals on the nanoscale: optical and photothermal properties and some applications in imaging, sensing, biology, and medicine," *Accounts of Chemical Research*, vol. 41, no. 12, pp. 1578–1586, 2008.
- [4] M. A. Hahn, A. K. Singh, P. Sharma, S. C. Brown, and B. M. Moudgil, "Nanoparticles as contrast agents for in-vivo bioimaging: current status and future perspectives," *Analytical and Bioanalytical Chemistry*, vol. 399, no. 1, pp. 3–27, 2011.
- [5] R. T. Tom, V. Suryanarayanan, P. G. Reddy, S. Baskaran, and T. Pradeep, "Ciprofloxacin-protected gold nanoparticles," *Langmuir*, vol. 20, no. 5, pp. 1909–1914, 2004.
- [6] K. K. Y. Wong and X. Liu, "Silver nanoparticles—the real "silver bullet" in clinical medicine?" *Medical Chemical Communications*, vol. 1, no. 2, pp. 125–131, 2010.
- [7] X. Chen and H. J. Schluesener, "Nanosilver: a nanoproduct in medical application," *Toxicology Letters*, vol. 176, no. 1, pp. 1–12, 2008.
- [8] J. Markarian, "Antimicrobials find new healthcare applications," *Plastics, Additives and Compounding*, vol. 11, no. 1, pp. 18–22, 2009.
- [9] C. D. Gutsche, *Calixarenes An Introduction*, The Royal Society of Chemistry, Cambridge, UK, 2nd edition, 2008.
- [10] F. Perret, A. N. Lazar, and A. W. Coleman, "Biochemistry of the para-sulfonato-calix[n]arenes," *Chemical Communications*, no. 23, pp. 2425–2438, 2006.
- [11] S. Shinkai, S. Mori, T. Tsubaki, T. Sone, and O. Manabe, "New water-soluble host molecules derived from calix[6]arene," *Tetrahedron Letters*, vol. 25, no. 46, pp. 5315–5318, 1984.
- [12] F. Perret and A. W. Coleman, "Biochemistry of anionic calix[n]arenes," *Chemical Communications*, vol. 47, no. 26, pp. 7303–7319, 2011.
- [13] E. Da Silva, A. N. Lazar, and A. W. Coleman, "Biopharmaceutical applications of calixarenes," *Journal of Drug Delivery Science and Technology*, vol. 14, no. 1, pp. 3–20, 2004.
- [14] L. K. Tsou, G. E. Dutschman, E. A. Gullen, M. Telpoukhovskaia, Y. C. Cheng, and A. D. Hamilton, "Discovery of a synthetic dual inhibitor of HIV and HCV infection based on a tetrabutoxycalix[4]arene scaffold," *Bioorganic and Medicinal Chemistry Letters*, vol. 20, no. 7, pp. 2137–2139, 2010.
- [15] R. Lamartine, M. Tsukada, D. Wilson, and A. Shirata, "Antimicrobial activity of calixarenes," *Comptes Rendus Chimie*, vol. 5, no. 1, pp. 163–169, 2002.
- [16] P. Molenveld, J. F. J. Engbersen, and D. N. Reinhoudt, "Dinuclear bisimidazolyl-Cu(II) calix[4]arenes as metalloenzyme models. Synthesis and bifunctional catalysis in phosphate diester transesterification," *Journal of Organic Chemistry*, vol. 64, no. 17, pp. 6337–6341, 1999.
- [17] A. I. Vovk, V. I. Kalchenko, S. A. Cherenok, V. P. Kukhar, O. V. Muzychka, and M. O. Lozynsky, "Calix[4]arene methylenebisphosphonic acids as calf intestine alkaline phosphatase inhibitors," *Organic and Biomolecular Chemistry*, vol. 2, no. 21, pp. 3162–3166, 2004.
- [18] E. Da Silva, D. Ficheux, and A. W. Coleman, "Anti-thrombotic activity of water-soluble calix[n]arenes," *Journal of Inclusion Phenomena*, vol. 52, no. 3–4, pp. 201–206, 2005.
- [19] R. Kamada, W. Yoshino, T. Nomura et al., "Enhancement of transcriptional activity of mutant p53 tumor suppressor protein through stabilization of tetramer formation by calix[6]arene derivatives," *Bioorganic and Medicinal Chemistry Letters*, vol. 20, no. 15, pp. 4412–4415, 2010.
- [20] R. Kumar Pathak, V. Kumar Hinge, M. Mondal, and C. Pulla Rao, "Triazole-linked-thiophene conjugate of calix[4]arene: its selective recognition of Zn<sup>2+</sup> and as biomimetic model in supporting the events of the metal detoxification and oxidative stress involving metallothionein," *Journal of Organic Chemistry*, vol. 76, pp. 10039–10049, 2011.
- [21] O. Danylyuk and K. Suwinska, "Solid-state interactions of calixarenes with biorelevant molecules," *Chemical Communications*, no. 39, pp. 5799–5813, 2009.
- [22] W. Yang, D. P. Otto, W. Liebenberg, and M. M. De Villiers, "Effect of para-sulfonato-calix[n]arenes on the solubility, chemical stability, and bioavailability of a water insoluble drug nifedipine," *Current Drug Discovery Technologies*, vol. 5, no. 2, pp. 129–139, 2008.
- [23] S. Jebors, A. Leydier, Q. Wu, B. Bertino Ghera, M. Malbouyre, and A. W. Coleman, "Solid lipid nanoparticles (SLNs) derived from para-acyl-calix[9]-arene: preparation and stability," *Journal of Microencapsulation*, vol. 27, no. 7, pp. 561–571, 2010.
- [24] J. Gualbert, P. Shahgaldian, and A. W. Coleman, "Interactions of amphiphilic calix[4]arene-based Solid Lipid Nanoparticles with bovine serum albumin," *International Journal of Pharmaceutics*, vol. 257, no. 1–2, pp. 69–73, 2003.
- [25] E. Da Silva, P. Shahgaldian, and A. W. Coleman, "Haemolytic properties of some water-soluble para-sulphonato-calix-[n]-arenes," *International Journal of Pharmaceutics*, vol. 273, no. 1–2, pp. 57–62, 2004.
- [26] M. H. Paclat, C. F. Rousseau, C. Yannick, F. Morel, and A. W. Coleman, "An absence of non-specific immune response towards para-sulphonato-calix[n] arenes," *Journal of Inclusion Phenomena and Macrocyclic Chemistry*, vol. 55, no. 3–4, pp. 353–357, 2006.

- [27] A. W. Coleman, S. Jebors, S. Cecillon et al., "Toxicity and biodistribution of para-sulfonato-calix[4]arene in mice," *New Journal of Chemistry*, vol. 32, no. 5, pp. 780–782, 2008.
- [28] Y. Tauran, M. Grosso, A. Brioude, R. Kassab, and A. W. Coleman, "Colourimetric and spectroscopic discrimination between nucleotides and nucleosides using para-sulphonato-calix[4]arene capped silver nanoparticles," *Chemical Communications*, vol. 47, pp. 10013–10015, 2011.
- [29] K. M. Hwang, Y. M. Qi, S. Liu, T. C. Lee, W. Choy, and J. Chen, "Antithrombotic treatment with calixarene compounds," Patent, US54099959, p. 46, 1995.
- [30] S. Shinkai, S. Mori, H. Koreishi, T. Tsubaki, and O. Manabe, "Hexasulfonated calix[6]arene derivatives: a new class of catalysts, surfactants, and host molecules," *Journal of the American Chemical Society*, vol. 108, no. 9, pp. 2409–2416, 1986.
- [31] K. Ohto, M. Yano, K. Inoue et al., "Solvent extraction of trivalent rare earth metal ions with carboxylate derivatives of calixarenes," *Analytical Sciences*, vol. 11, no. 6, pp. 893–899, 1995.
- [32] L. N. Markovskiy, V. I. Kalchenko, and N. A. Parkhomenko, "O-phosphorylated p-tert-butylcalixarenes," *Zhurnal Obshchei Khimii*, vol. 60, pp. 2811–2812, 1990.
- [33] D. Xiong, M. Chen, and H. Li, "Synthesis of para-sulfonatocalix[4]arene-modified silver nanoparticles as colorimetric histidine probes," *Chemical Communications*, no. 7, pp. 880–882, 2008.
- [34] N. Dupont, A. N. Lazar, F. Perret et al., "Solid state structures of the complexes between the antiseptic chlorhexidine and three anionic derivatives of calix[4]arene," *CrystEngComm*, vol. 10, no. 8, pp. 975–977, 2008.
- [35] B. Leśniewska, S. Jebors, A. W. Coleman, and K. Suwińska, "Streptidinium sulfate monohydrate," *Acta Crystallographica Section C*, vol. 65, no. 6, pp. o290–o292, 2009.

## **Large negatively charged organic host molecules as inhibitors of endonuclease enzymes**

Titre: Molécules hôtes organiques chargées négativement en tant qu'inhibiteurs d'enzymes endonuclease

Résumé: Parmi six molécules macrocycliques étudiées, trois larges molécules hôtes chargées négativement,  $\beta$ -cyclodextrin sulphate, *para*-sulphonato-calix[6]arene and *para*-sulphonato-calix[8]-arene ont été caractérisées comme d'efficace inhibiteurs d'endonucléase à une gamme de concentration micro-molaire. De plus, il a été démontré que le *para*-sulphonato-calix[8]arene est un inhibiteur partiel de la rhDNAse I.

## Large negatively charged organic host molecules as inhibitors of endonuclease enzymes†

Cite this: *Chem. Commun.*, 2014, 50, 11404

Received 24th June 2014,  
Accepted 13th August 2014

DOI: 10.1039/c4cc04805a

www.rsc.org/chemcomm

Yannick Tauran,<sup>ab</sup> Christophe Anjard,<sup>c</sup> Beomjoon Kim,<sup>bd</sup> Moez Rhimi<sup>e</sup> and Anthony W. Coleman<sup>\*a</sup>

**Three large negatively charged organic host molecules;  $\beta$ -cyclodextrin sulphate, *para*-sulphonato-calix[6]arene and *para*-sulphonato-calix[8]arene have been shown to be effective inhibitors of endonuclease in the low micromolar range, additionally *para*-sulphonato-calix[8]arene is a partial inhibitor of rhDNase I.**

The endonucleases are a class of enzymes whose biological role is to digest DNA.<sup>1</sup> As such, they play a role in human cell repair<sup>2</sup> but also are key elements in viral infection.<sup>3</sup> The endonucleases also act as protective elements in bacterial defense strategy against bacteriophages.<sup>4</sup> They represent a valid target in drug design for anti-cancer, anti-viral and antibiotic treatments, however new compounds compatible with pharmaceutical criteria (high solubility, non-toxic) are needed.<sup>5</sup>

A number of studies have pointed to endonucleases as potential targets for influenza treatment.<sup>6</sup> The few anti-influenza medications currently available are often associated with severe side-effects. Commercial treatments target the viral membrane protein M2 (amantadine and rimantadine);<sup>7</sup> or neuraminidases, oseltamivir (Tamiflu) and zanamivir (Relenza).<sup>8</sup>

PA endonuclease is a domain belonging to the RNA-dependent RNA polymerase (RdRp) and it initiates the translation from viral mRNA to viral proteins. Its contribution is essential to viral production inside the infected cell.<sup>9</sup> Pharmaceutically active soluble endonuclease inhibitors would thus appear to be excellent target as antiviral medications.<sup>10</sup>

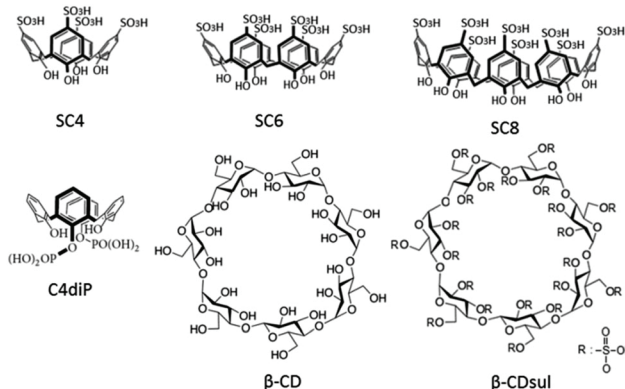
Secondly, human endonucleases present an interest as oncotherapeutic targets. AP endonuclease is a human enzyme involved in DNA lesion repairing system. This endonuclease is

overexpressed in cancers such as glioblastoma leading to resistant to radio- and chemo-therapy. While development of AP endonuclease inhibitors is underway none are presently available due to their incompatibility with desirable clinical criteria (high solubility, non-toxic, low efflux transport, enzyme-resistant).<sup>11</sup>

Supramolecular organic macrocycles,<sup>12</sup> present considerable interest in biopharmaceutical science, the cyclodextrins are well known as transporters for bioactive compounds<sup>13</sup> but are somewhat less well known for direct biological activity against proteins.<sup>14</sup> The calix[*n*]arenes are well documented both as transporter molecules and also for their direct biological activity,<sup>15</sup> particularly with regard to protein complexation.<sup>16</sup>

In the current paper we describe the inhibitory activity of a series of organic host molecules, Scheme 1, with regard to four site specific endonucleases, Scheme 2, and the non-specific human rhDNase I enzyme.

The negatively charged organic host molecules, were chosen for the possible binding affinity for the DNA binding site and cleavage site, using the crystallographic information on the influenza virus PA endonuclease as the lead structure. The endonuclease enzymes were chosen for their known cleavage



Scheme 1 Structures of the organic host molecules evaluated as endonucleases inhibitors.

<sup>a</sup> LMI CNRS UMR 5615, Univ. Lyon 1, Villeurbanne, F69622, France.

E-mail: antony.coleman@adm.univ-lyon1.fr; Tel: +33 4 4243 1027

<sup>b</sup> LIMMS/CNRS-IIS (UMI 2820), University of Tokyo, Tokyo, Japan

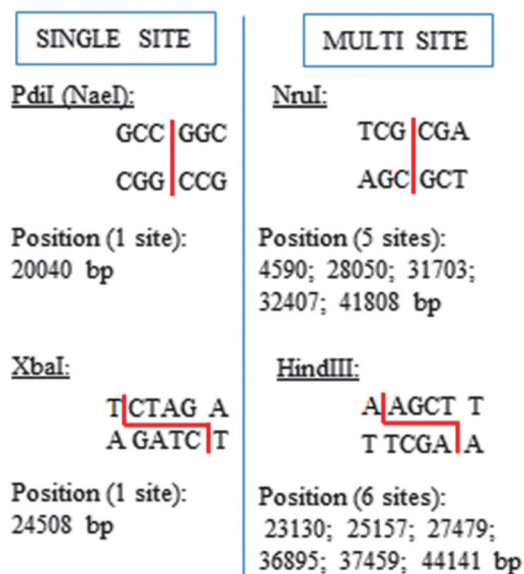
<sup>c</sup> CGPhIMC UMR5534, Univ. Lyon 1, Villeurbanne, F69622, France

<sup>d</sup> CIRMM, Institute of Industrial Science, University of Tokyo, Tokyo, Japan.

E-mail: hjoonkim@iis.u-tokyo.ac.jp

<sup>e</sup> INRA, UMR 1319 Micalis, Jouy-en-Josas, F-7835, France

† Electronic supplementary information (ESI) available: Full experimental values. See DOI: 10.1039/c4cc04805a



Scheme 2 Sequence of cleavage site for different restriction enzymes and their positions on Lambda DNA phage.

properties on the lambda phage DNA. Two, NruI, (CG site cleavage) and HindIII (AA) give rise to multisite cleavage of the DNA chain. The other two PdiI (CG) and XbaI (TT) cause cleavage at only a single site on the DNA chain.<sup>17</sup> Our aim was to determine the factors which influence the inhibitory effects of the organic host molecules for possible use as therapeutic agents for influenza treatment.

In the inhibition experiments, the half maximal inhibitory concentration ( $IC_{50}$ ) was measured. The digestion activity of endonuclease was evaluated using agarose gel electrophoresis at varying inhibitor concentrations. After quantifying the intensity of the digested bands on the gel the concentration of inhibitor needed for 50% ( $IC_{50}$ ) inhibition of the endonuclease activity, was determined. See ESI.†

The  $IC_{50}$  concentrations for the six organic host molecules tested are given below in Table 1, of these three,  $\beta$ -CD, C4diP and SC4 show no inhibitory activity. The other three  $\beta$ -CDsul, SC6 and SC8 all show  $IC_{50}$  values in the low micromolar range with regard to NruI and slightly lower values for HindIII. All three molecules are characterised by a combination of high

Table 1 Half maximal inhibitory concentration ( $IC_{50}$ ) of different organic host molecules determined for restriction enzymes NruI and HindIII. N.I. corresponds to an absence of endonuclease inhibition

Molecules	$IC_{50}$ ( $\mu$ M)	
	NruI	HindIII
$\beta$ -CD	N.I.*	N.I.*
$\beta$ -CDsul	3	6
C4diP	N.I.*	N.I.*
SC4	N.I.*	N.I.*
SC6	3	1.1
SC8	1.8	0.6

N.I.\*: no inhibition.

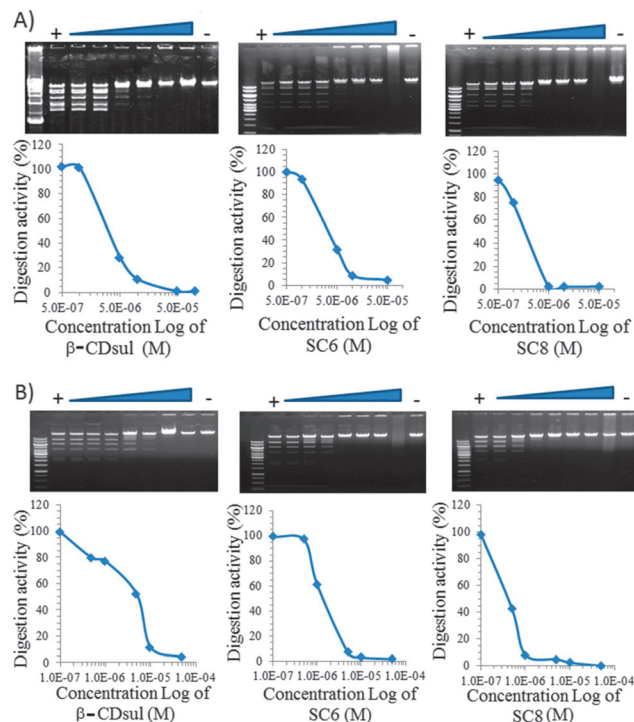


Fig. 1  $IC_{50}$  values for three different supramolecular organic macrocycles acting on the restriction enzymes (A) NruI and (B) HindIII. Gel electrophoresis was used to determine the activity of the enzyme in the presence of increasing concentration of inhibitor. After quantification of the band intensities the digestion activity is then plotted as a factor of inhibitor concentration.

negative charge and a size capable of spanning both the DNA binding site and the cleavage site in an endonuclease.<sup>10</sup> As both these sites are characterised, in influenza PA Endonuclease by the presence of basic amino-acids (DNA binding site, K34 and R124) and (Catalytic site, R84 and K184), blockage of the sites, by large anionic macrocycles, is not unexpected and is a requirement for enzyme inhibition (Fig. 1).<sup>15</sup>

The results obtained can be compared to known inhibition activities, for example for small molecule inhibitors of apurinic/aprimidinic (AP) endonuclease 1 (Ape1) four were reported to have  $IC_{50}$  values of less than 10  $\mu$ M and one, Ape1 repair inhibitor 03 [2,4,9-trimethylbenzo[*b*][1,8]-naphthyridin-5-amine; AR03], inhibited cleavage of AP sites in SF767 glioblastoma cells, in whole cell extracts and inhibited purified human Ape1 *in vitro*.<sup>18</sup> With regard to influenza PA Endonuclease inhibition, values are in the range high nanomolar to sub 10  $\mu$ M for effective inhibitors.<sup>10</sup> The observed values in this work are in the same range and  $IC_{50}$  of SC8 with regard to HindIII is comparable to the best published value.

We have previously shown that supramolecular hybrid silver nanoparticles have anti-bacterial activity,<sup>19</sup> thus it was of interest to investigate if such systems possess enzyme inhibitory activity. However, of the current systems only hybrid nanoparticles capped by  $\beta$ -CDsul proved stable under the conditions of the enzyme inhibition experiments.

The results are given in Fig. 2. In order to ascertain that free  $\beta$ -CDsul was not responsible for the inhibitory effect the

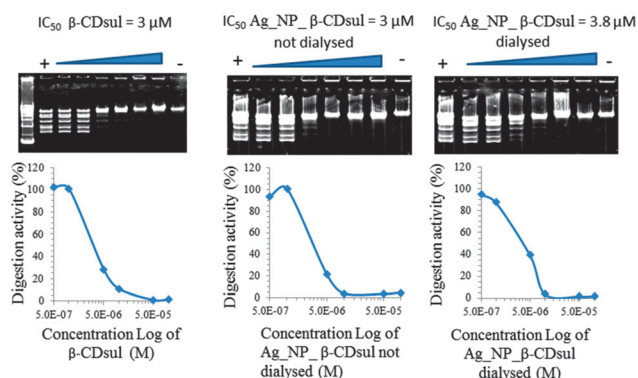


Fig. 2  $IC_{50}$  of  $\beta$ -cyclodextrin sulphate and  $\beta$ -cyclodextrin sulphate capped on silver nanoparticles (dialysed in DI water or not) have been determined on the restriction enzyme NruI.

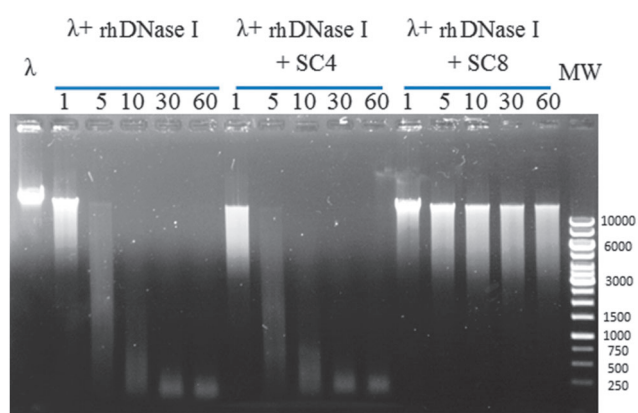


Fig. 3 Agarose gel electrophoresis showing the kinetics of Lambda DNA (annotated  $\lambda$ ) digestion by rhoDNase I in the presence of SC4 and SC8 at 100  $\mu$ M. Time of incubation was 1, 5, 10, 30 and 60 minutes. MW correspond to the Molecular Weight ladder (bp is shown on the right).

suspension was dialysed; the observed values decrease from an  $IC_{50}$  of 3  $\mu$ M for the free ligand to 3.8  $\mu$ M for the  $\beta$ -CDSul capped silver nanoparticles. This decrease is similar to the small decrease in the plasmon resonance intensity observed, given in ESI,<sup>†</sup> Fig. S1.

In contrast to the endonucleases, the super family of the DNases are a family of enzymes that non-specifically cleave phosphodiester bonds. It is, also, to be noted that these enzymes do not conserve the aminoacid geometry around the active site. Thus rhoDNase I has an active site with histidine, asparagine and aspartic acid and glutamic acid residues. In contrast, in bDNase I there are additional basic (Arg) residues. Both are characterised by a need for divalent cations in the active sites.<sup>20</sup>

The inhibition experiments, using rhoDNase I, were initially carried out at the same concentration as the endonuclease

experiments. However, the evidence for enzyme inhibition was un-convincing. Reducing the rhoDNase I concentration to 100  $\mu$ M and observing the kinetics of digestion led to the results shown in Fig. 3. Here SC8 inhibits the action of rhoDNase I during 60 minutes. The partial inhibition at low enzyme concentrations is not unexpected as rhoDNase I only contains histidine residues, which bind weakly to SC8, in the active site.

In conclusion we have demonstrated that large organic host molecules with a size above four units in the macrocycle and possessing strong negative charge are effective inhibitors of endonuclease enzymes. Work is currently underway to extend the work to influenza endonucleases and to study the cellular efficacy of the molecules.

Y.T. thanks the Université of Lyon 1 and LIMMS for financial aid.

## Notes and references

- 1 D. L. Nelson and M. M. Cox, *Lehninger Principles of Biochemistry*, Worth Publishers, New York, 3rd edn, 2003, ch. 29, pp. 931–978.
- 2 M. R. Kelley and M. L. Fishel, *Mol. Aspects Med.*, 2007, **28**, 375–395.
- 3 E. De Clercq, *Nat. Rev. Drug Discovery*, 2006, **5**, 1015–1025.
- 4 S. J. Labrie, J. E. Samson and S. Moineau, *Nat. Rev. Microbiol.*, 2010, **8**, 317–327.
- 5 D. Dorjsuren, D. Kim, D. J. Maloney, D. M. Wilson III and A. Simeonov, *Nucleic Acids Res.*, 2011, **39**, 1–11.
- 6 E. Nistal-Villán and A. García-Sastre, *Nat. Med.*, 2009, **15**, 1253–1254.
- 7 P. Intharathep, C. Laohpongspaisan, T. Rungrotmongkol, A. Loiruangsinsin, M. Malaisree, P. Decha, O. Aruksakunwong, K. Chuenpenit, N. Kaiyawet, P. Sompornpisut, S. Pianwanit and S. Hannongbua, *J. Mol. Graphics Modell.*, 2008, **27**, 342–348.
- 8 A. Moscona, *N. Engl. J. Med.*, 2005, **353**, 1363–1373.
- 9 A. Dias, D. Bouvier, T. Crepin, A. A. McCarthy, D. J. Hart, F. Baudin, S. Cusack and R. W. H. Ruigrok, *Nature*, 2009, **458**, 914–918.
- 10 R. M. DuBois, P. J. Slavish, B. M. Baughman, M. K. Yun, J. Bao, R. J. Webby, T. R. Webb and S. W. White, *PLoS Pathog.*, 2012, **8**, 1–13.
- 11 M. Z. Mohammed, V. N. Vyjayanti, C. A. Loughton, L. V. Dekker, P. M. Fischer, D. M. Wilson III, R. Abbotts, S. Shah, P. M. Patel, I. D. Hickson and S. Madhusudan, *Br. J. Cancer*, 2001, **104**, 653–663.
- 12 J. W. Steed and J. L. Atwood, *Supramolecular Chemistry*, Wiley & Sons, Chichester, 2nd edn, 2009.
- 13 E. Biensoy, *Cyclodextrins in Pharmaceuticals, Cosmetics and Biomedicine*, Wiley & Sons, Chichester, 2011.
- 14 F. Perret and A. W. Coleman, in *Supramolecular Systems in Biomedical Fields*, ed. H. J. Schneider, RSC, Cambridge, 2013, ch. 6.
- 15 F. Perret, H. Peron, M. Dupin and A. W. Coleman, in *Calix-arenes as Protein Sensors*, in *Creative Chemical Sensor Systems*, ed. T. Schrader, Topics in Current Chem., Springer, Berlin, 2007, vol. 277, pp. 31–88.
- 16 F. Perret and A. W. Coleman, *Chem. Commun.*, 2011, **47**, 7303–7319.
- 17 N. Cunningham, J. Tomlinson and F. Journak, *Biochem. Educ.*, 1983, **11**, 130–134.
- 18 A. Bapat, L. S. Glass, M. Luo, M. L. Fishel, E. C. Long, M. M. Georgiadis and M. R. Kelly, *J. Pharmacol. Exp. Ther.*, 2010, **334**, 988–998.
- 19 S. Boudebouze, A. W. Coleman, Y. Tauran, H. Mkaouer, F. Perret, A. Garnier, A. Brioude, B. J. Kim, E. Maguin and M. Rhimi, *Chem. Commun.*, 2013, **49**, 7150–7152.
- 20 G. Parsieglia, C. Noguere, L. Santell, R. A. Lazarus and Y. Bourne, *Biochemistry*, 2012, **51**, 10250–10258.

## **Multifunctional curcumin-nanocarriers based on host-guest interaction for Alzheimer Disease diagnostic**

Titre: Nano-transporteurs de curcumin multifonctionnels basés sur une interaction hôte / invité pour le diagnostic de la maladie d'Alzheimer

Résumé: L'utilisation de ratio stœchiométrique contrôlé entre le curcumin et les molécules hôtes  $\beta$ -cyclodextrine, *para*-sulphonato-calix[4]arene et *para*-sulphonato-calix[6]arene permettent la formation de nano-transporteurs stables. Les nano-transporteurs obtenus présentent du curcumin disponible à leurs surfaces. Les nanoparticules préviennent la toxicité A $\beta$ 42 induites, sont capable d'interagir avec le peptide A $\beta$ , réduisent son agrégation et montre une grande affinité pour les dépôts d'amyloïdes. Fortement marquées, les nanoparticules complexent non seulement les plaques séniles mais aussi les dépôts diffus d'A $\beta$  dans le tissu cérébral de patients atteint de la maladie d'Alzheimer.

## ARTICLE

# Multifunctional curcumin-nanocarriers based on host-guest interaction for Alzheimer Disease diagnostic

Cite this: DOI: 10.1039/x0xx00000x

Received 00th January 2012,  
Accepted 00th January 2012

DOI: 10.1039/x0xx00000x

[www.rsc.org/](http://www.rsc.org/)L. Ramdani,<sup>a</sup> R. Bourboulou,<sup>a</sup> M. Belkouch,<sup>a,b</sup> D. Langui,<sup>a</sup> S. Jebors,<sup>c</sup> Y. Tauran,<sup>c</sup> C. Parizot,<sup>d</sup> K. Suwinska,<sup>e</sup> A.W. Coleman,<sup>c</sup> and C. Duyckaerts<sup>a,b,\*</sup>, A.N. Lazar,<sup>a,b,\*</sup>

**Abstract** The use of controlled stoichiometric ratios between curcumin and the host molecules  $\beta$ -cyclodextrin, *para*-sulphonato-calix[4]arene and *para*-sulphonato-calix[6]arene allows the formation of stable nanocarriers. The obtained nanocarriers have available curcumin at their surfaces. They show high affinity for the amyloid deposits, strongly labelling not only the senile plaques but also the diffuse deposits of Alzheimer Disease brains; they are able to interact with the A $\beta$  peptide, reducing its aggregation and preventing its toxicity.

## Introduction

Alzheimer Disease (AD) is the most common form of dementia, currently concerning more than 26 million people worldwide. The two pathological features characterizing AD are the intraneuronal accumulation of tau protein (neurofibrillary tangles) and the extracellular aggregation of Amyloid beta peptide (senile plaques). Their detection on post-mortem tissue is still indispensable for the diagnosis.<sup>1</sup> The A $\beta$  peptide, the main component of senile plaques is considered as the driving actor in the progression of Alzheimer Disease. According to the amyloid cascade hypothesis,<sup>2,3</sup> the accumulation of A $\beta$  peptide is the initial event in the cascade of reactions that lead to cortical dysfunction. A $\beta$  plaques are present in moderate to frequent numbers in the cortical grey matter of AD patients, years before the onset of dementia. The possibility of targeting A $\beta$  pathology in the brain is an important strategy in AD. Still, the development of probes with selective affinity for the amyloid plaques is a challenge.

Several studies showed the potential of curcumin in the treatment of AD. Curcumin not only impedes the aggregation of the amyloid peptide but is also able to disaggregate the already formed fibrils, according to *in vitro* studies<sup>4-7</sup>. Curcumin as well as curcumin derivatives proved also their potential for the diagnosis of AD, being able to bind to the

amyloid deposits *in vitro*, *in vivo* or on post-mortem tissue<sup>8-13</sup>. Moreover, curcumin is known to have numerous other protective and curative properties: anti-oxidant,<sup>14-19</sup> anti-inflammatory,<sup>20-22</sup> anti-cancerous,<sup>23-27</sup> confirming its potential bio-compatibility.

Despite such encouraging reports, the study of curcuminoids is severely limited by their exceedingly low bioavailability, due to their poor solubility and instability in aqueous solutions. Thus, curcuminoids are often prepared in dimethyl sulfoxide (DMSO) or methanol, and this has raised questions about its clinical efficacy. As the need for probes suitable for the identification of A $\beta$  pathology in Alzheimer disease at early stages is becoming imperative, efforts have been made to improve the solubility of these compounds.<sup>28</sup> Nanoparticle-based delivery has the potential of rendering hydrophobic agents, such as curcumin, dispersible in aqueous media. Liposomes and polymeric nanoparticles are widely used as delivery systems.<sup>29-33</sup> An alternative of increasing the water solubility of active principles is the complexation with macromolecules. Cyclodextrins<sup>34</sup> and calix[n]arenes<sup>35</sup> are among the major classes of macrocyclic organic host compounds in supramolecular chemistry.<sup>36</sup> The cyclodextrins ( $\alpha$ -,  $\beta$ -,  $\gamma$ -cyclodextrins) and their derivatives (2-O-methyl  $\beta$ -CD hydroxypropyl- $\beta$ -CD, and hydroxypropyl- $\gamma$ -CD) were already proved to complex curcumin,<sup>37-43</sup> improving its solubility by

about 100 times. The improved bio-activity of curcumin-cyclodextrin complexes was confirmed by several studies.<sup>37-40,42</sup> Two recent studies report on the therapeutic effect of curcumin-cyclodextrin formulation *in vivo*, in AD mice models.<sup>43,44</sup> Still, up to now, the possibility to solubilize curcumin with the aid of macromolecules without impeding its ability to target the amyloid peptide and the amyloid deposits, for potential application in the diagnosis of AD was not yet evaluated.

Here we report a new stealth and efficient solubilisation of curcumin using the *para*-sulphonato-calix[4]arene (SC4) and the *para*-sulphonato-calix[6]arene (SC6) and Methyl  $\beta$ -cyclodextrin to form colloidal nanocarriers. Curcumin is available, at least partially, at the surface of the obtained nanocarriers. The potential of using these curcumin nanoparticles as trackers of AD pathology was proved.

## Experimental

### Materials

Curcumin and Methyl  $\beta$ -cyclodextrin were obtained from Sigma Aldrich and were used as received. The *para*-sulphonato-calix[4]arene (SC4) and the *para*-sulphonato-calix[6]arene (SC6) were synthesized according to the method of Jebors, by direct sulphonation of calix[n]arene.<sup>45</sup>

### Curcumin solubilisation

Curcumin was solubilized in ethanol at a concentration of 3 mM. A volume of 5 ml of macromolecules in water was added, drop by drop, to 500  $\mu$ l of curcumin solution, under continuous stirring. The quantity of macromolecules was estimated in order to obtain a final molar ratio of 1:1 between curcumin and the macromolecules. The formation of a colloidal phase is instantaneous. Stirring was allowed for 2 h, without a cap, to completely evaporate ethanol. The so obtained complexes: M $\beta$ CD-curcumin (CD-C), SC4-curcumin (SC4-C) and SC6-curcumin (SC6-C) were kept at 4 °C for 12 h, under a rotatory wheel. The residual curcumin precipitated were eliminated by centrifugation at 10000 rpm for 15 min. The loaded quantity of curcumin was further estimated spectrofluorimetrically and was found to be of 20  $\mu$ g/ml. The colloids were stored at 4 °C until use.

### Molecular docking studies

The 3D molecular structures of curcumin and of the three inclusion complexes were obtained from the Cambridge database. The docking was performed with AutoDock Vina software and analyzed by PYMOL of the Scripps Research Institute. The receptor (CD, SC4 or SC6) and the ligand (curcumin) were built up independently and the inclusion complex model was determined by energy minimization.

### Characterization of the complexes

The size of the particles was estimated by transmission electron microscopy. Volumes of 1  $\mu$ l of each colloid were deposited on formvar-coated copper TEM grids. The morphology of samples was observed using a JEOL-1210 transmission electron microscope (JEOL, Tokyo, Japan) operating at 60 kV.

The monodispersity of the inclusion complexes and the stability in time were evaluated by means of flow cytometry, using a Gallios® cytometer (Beckman Coulter), at room temperature.

### Alzheimer disease cases

AD patients enrolled in a brain donation program of the Brain Bank "GIE NeuroCEB" run by a consortium of Patients Associations (including France Alzheimer Association) were employed for this study. The consent was signed by the patient himself, or the next of kin, in accordance with the French Bioethical Laws. The corpse was transported to the mortuary of a University Hospital belonging to the NeuroCEB network at the time of death. The brain was removed, one hemisphere being fixed in buffered 4% formaldehyde for the neuropathological diagnosis of AD, the other being immediately sliced. Samples from the superior temporal gyrus (Brodmann area 22), were mounted on a cork piece, dipped in isopentane cooled by liquid nitrogen and kept in a deep freezer at -80 °C until use. The present study has been approved by the ad hoc committee of the Brain Bank.

### Diagnosis

Formalin-fixed 5  $\mu$ m thick, from multiple areas of the brain, including hippocampus and isocortical Brodmann area 22, were used for the diagnosis. The diagnosis of AD was confirmed by immunostaining with anti-A $\beta$  (6F/3D clone; Dako, Trappes France) and anti-tau (polyclonal rabbit anti-tau antibody; Dako; Trappes code number A 0024). The diagnosis criteria of the NIA-Reagan Institute were used.<sup>46</sup> Cases with a high number of mature SPs containing an amyloid central core of A $\beta$  peptide were selected.

### Affinity of curcumin complexes for the amyloid deposits

Sections from the temporal isocortex (superior temporal gyrus) of three AD subjects (Braak neurofibrillary stage VI, Thal phase 5), containing numerous amyloid deposits and neurofibrillary tangles were used for the study. *Post-mortem* frozen 10  $\mu$ m thick sections were prepared with the aid of a Leica cryostat. The samples were hydrated for 5 min with Phosphate Buffer Saline and then incubated 2 h with 200  $\mu$ l of the curcumin solution at 1  $\mu$ g/ml. Subsequently, the samples were gently washed in PBS and mounted with a medium minimizing fading due to fluorescence (Dako Fluorescence Mounting Medium). In order to confirm the positive staining of amyloid deposits by curcumin-complex, A $\beta$  immunohistochemistry was also performed before curcumin-staining. After acetone fixation and PBS washing, the sections were incubated for 4 h in 200  $\mu$ l solution of 6F/3D antibody (Dako), at 1/200 dilution. The samples were washed 3 times with PBS and incubated for another 2 h with the secondary antibody bearing the chromogen red Cy3. Following the immunostaining, the samples were further washed in PBS before incubation with curcumin-complexes, as previously described. The colocalization was examined using 488 nm (to detect the staining of curcumin) and 543 nm (for Cy3 detection) excitation wavelengths, the signals being collected between 540-550 nm and 565-580 nm, respectively. Colocalization was indicated by a yellow colour on the "merged" images.

### Cytotoxicity assay

To evaluate the cytotoxicity of curcumin complexes, control SH-SY5Y cells (human neuroblastoma cells), HEK cells (from Human Embryonic Kidney), hAPPsw SH-SY5Y and hAPPsw HEK cells - cells stably overexpressing the human APP gene (hAPP) bearing the Swedish mutation causing familial Alzheimer disease were used. The cells were seeded in 96 multiwell culture plates and grown in DMEM-F12 containing 10% of FCS, for the neuroblastoma, and the embryonic kidney cells) until approximately 80 % confluence. The growth medium was then discarded and the cells were incubated for 24 h in a culture medium enriched in curcumin complexes (final concentration of curcumin 200 ng/ml). The cytotoxicity was assessed by means of MTT, based on the conversion of tetrazolium salt (MTT) into a purple formazan product.<sup>47</sup>

### Rescuing effect

Control SH-SY5Y cells were used for determining the capacity of curcumin-complexes to rescue the toxicity of A $\beta$  42. Cells were seeded in 96 multiwell culture plates and grown until approximately 80% confluence. At this point, the growth medium was replaced by a new medium containing 10% of freshly prepared solution of A $\beta$  42 (purchased from GenicBio) in PBS (100 ng/ml) supplemented or not with curcumin complexes, with a final concentration of curcumin of 200

ng/ml. The cell viability was assessed by an MTT test, the experiments being carried six times in triplicates.

### Aggregation assay

A 5  $\mu$ M solution of A $\beta$  42 in water was freshly prepared and allowed to spontaneously aggregate at 20°C. The effect of curcumin colloids (5  $\mu$ g/ml concentration of curcumin) on the aggregation was measured by Thioflavin T assay,<sup>48</sup> monitoring the fluorescence at 440 nm excitation and 485nm emission wavelengths.

## Results

### Structural characterization of curcumin-macromolecule complexes

The chemical structures of the macromolecules used for the solubilization of curcumin are presented in figure 1a. The M $\beta$ -CD, macromolecule is a 7 membered sugar ring molecule, while SC4 and SC6 are macrocycles composed of respectively 4 and 6 phenolic rings, functionalized at the upper ring with sulphonate groups, favoring numerous electrostatic interaction, besides the hydrophobic aromatic interactions.

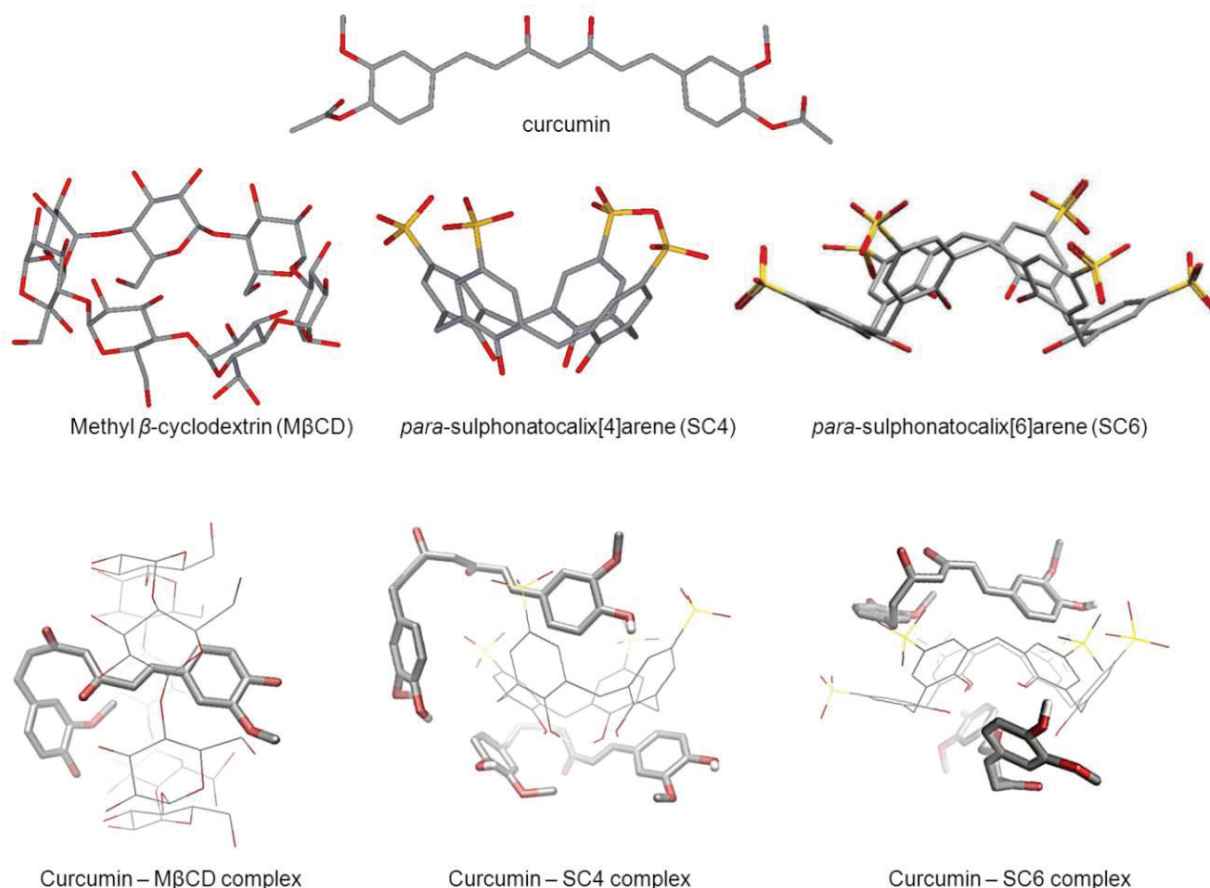


**Fig. 1** Molecular structure of curcumin, of the three macromolecules used for curcumin solubilization and of the inclusion complexes formed by the curcumin with the host-molecule; grey color represents carbon atoms, red color represents the oxygen atoms and the yellow color represents the sulfur atoms.

In the complex with CD, one of the phenolic rings of the curcumin is engaged in the macrocycle, stabilized by hydrogen bonds with the hydroxyl groups. According to the molecular docking, SC4 is able to complex 2 curcumin molecules. One of the molecules, cinctures the macrocycle, the two phenolic rings being involved in  $\pi$ - $\pi$  interactions with the host. Another curcumin is only partly encapsulated by  $\pi$ - $\pi$  stacking of one of the phenols, and by hydrogen bonds with the sulphonate groups of the host; the other moiety of the molecule is free of constraints. In a similar way SC6 is forms a complex with 2 curcumin molecules, one in the upper rim of the calixarene, the other one in the lower rim. Both guest molecules are stabilized by H-bonds interactions with the hydroxyl and sulphonate groups of the guest and implicating the two phenolic rings in  $\pi$ - $\pi$  stacking interactions. Given a 1:1 stoichiometry the complexes involved in the nanocarriers are likely to contain the included molecules for SC4 and SC6. Thus all three complexes will present an amphiphilic supramolecular nature aiding the nanocarrier formation.

#### Characterization of curcumin-macromolecules complexes

The morphology of the curcumin complexes was determined by transmission electron microscopy. Monodispersed nanoparticles of a diameter between 45- 75nm were characteristic for the three complexes (figure 2a). Flow cytometry analysis at different time intervals proved that the size of the nanoparticles reduces slightly in time (several nm), but they remain monodisperse for more than 15 days (figure 2b).

#### Post-mortem AD brain tissue

The affinity of curcumin nanoparticles for the amyloid deposits was tested on post mortem brain samples of three AD patients. The amyloid pathology of the cases chosen for the study was confirmed by immunohistochemistry with an antibody frequently used for the detection of the A $\beta$  deposits, the 6F3D antibody. The cases presented numerous amyloid deposits, from diffuse deposits (an early stage of the senile plaque) to mature senile plaques (Duyckaerts 1990) (figure 3).

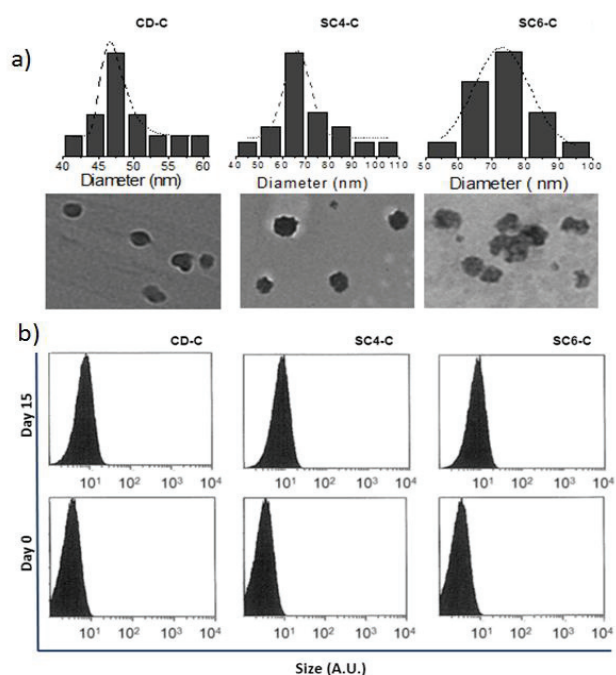


**Fig. 2** Characterization of curcumin complexes: a) Morphological analysis by TEM reveals a monodisperse population of nanoparticles with several tens of nanometers in size; b) stability in time of curcumin-macromolecules complexes, as revealed by flow cytometry.

#### Affinity of curcumin-complexes for amyloid deposits in human AD brains

Numerous amyloid deposits were specifically labeled by the three curcumin complexes. The specificity was confirmed by the double labeling with 6F3D antibody (directed against the A $\beta$  deposits). The senile plaques were strongly labeled by the curcumin nanoparticles (figure 4). The nanoparticles also labeled 65% of the diffuse deposits.

#### Biocompatibility of curcumin-complexes as tracers for the amyloid deposits

The cytotoxicity of CD, SC4 and of SC6 and of the curcumin-complexes with these three macromolecules was evaluated by MTT test on human neuroblastoma SH-SY5Y and embryonic kidney HEK cell, wild type and APP (stably overexpressing hAPP bearing the Swedish mutation). Neither the macromolecules alone (results not shown) nor the curcumin-complexes showed a toxic effect (figure 5).

#### Effect on A $\beta$ toxicity and aggregation

The toxic effect of A $\beta$  42 peptide in the presence of curcumin-nanoparticles was evaluated on SH-SY5Y wild type neuroblastoma cells, over 24h of incubation. The three complexes showed a significant rescuing effect: the viability of cells submitted to A $\beta$ 42 was increased from 76% to 93% by CD-C, 97% by SC4-C and 96% by SC6-C (figure 6a). The link between the rescuing effect of curcumin-complexes and the ability of curcumin to impede peptide aggregation was evaluated with a thioflavin T assay. The three curcumin-complexes showed a strong inhibitory effect on peptide fibrillization, diminishing the fibrillar content to: 62% by CD-C, 39% by SC4-C and 56% by SC6-C (figure 6b).

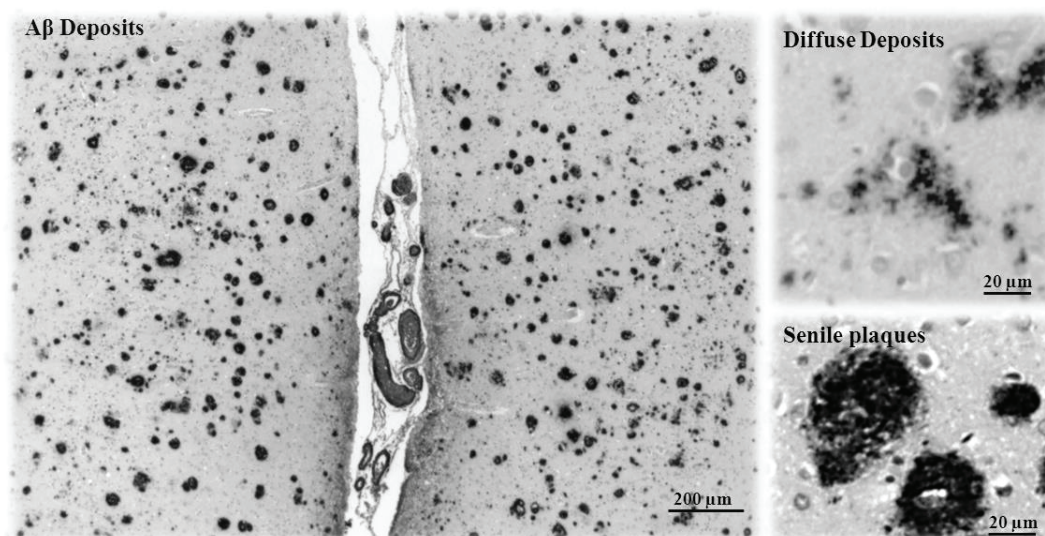


**Fig. 3** Micrographs of a post-mortem superior temporal cortex sample of an AD patient revealed by 6F3D anti A $\beta$  antibody: numerous senile plaques and diffuse deposits are present in the cortical area.

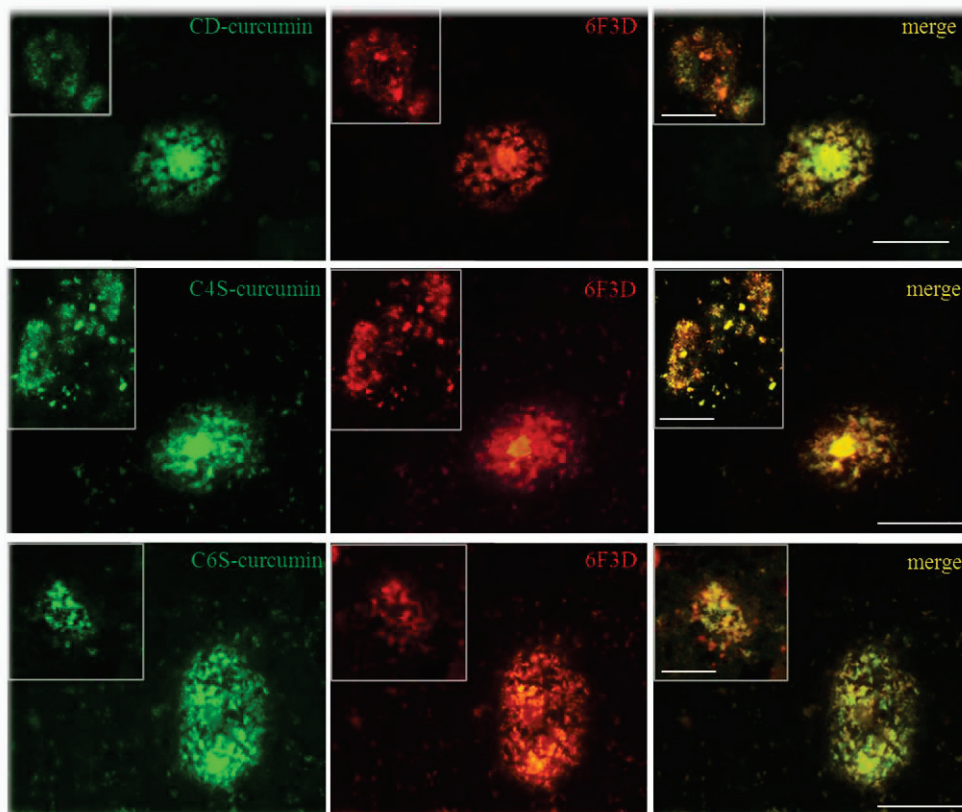


**Fig. 4** Affinity of curcumin-colloids for amyloid deposits; curcumin labeling in green, 6F3D labeling (specific for A $\beta$  deposits) in red and the colocalization of the labeling, on the merged image, in yellow; the insert shows the labeling of the diffuse deposits); scale bar = 50  $\mu$ m.

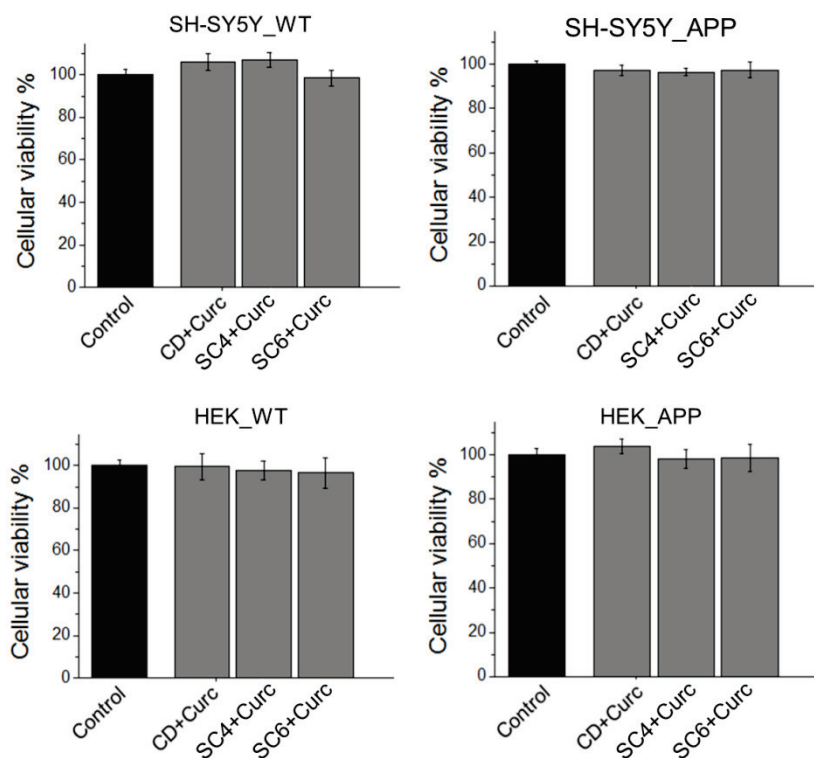


**Fig. 5** Effect of macromolecules and of curcumin-complexes on the cellular viability of several cell lines: Wild Type lines of SH-SY5Y human neuroblastoma and HEK embryonic kidney and their APP mutated lines (stably expressing swap mutation).

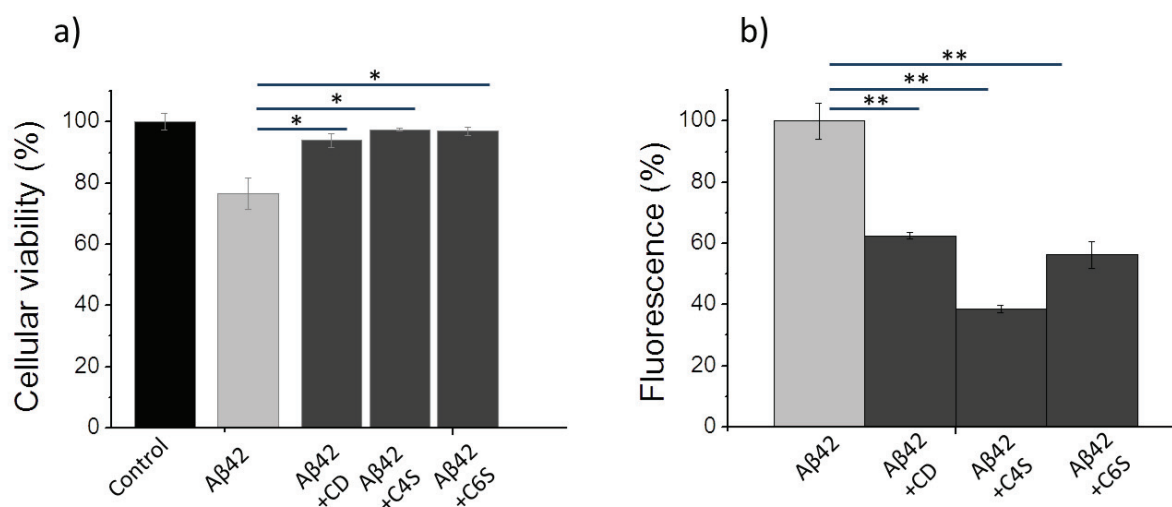


**Fig. 6** Effect of curcumin-complexes on A $\beta$  toxicity and aggregation: a) Rescuing effect of curcumin-complexes on SH-SY5Y human neuroblastoma treated with A $\beta$  42; b) Effect of curcumin complexes on the fibrillization of A $\beta$  peptide.

## Discussion

A new delivery system, based on the use of macromolecules for solubilizing curcumin, is presented in this study. Hydrosoluble calixarenes SC4 and SC6, bearing 4 or 6 aromatic cycles functionalized at the upper rim with sulphonate groups, and M $\beta$ CD efficiently solubilized curcumin.

The curcumin-complexes were organized into nanoparticles of tens of nm diameter, stable in time for at least 15 days. Following the complexation with the macromolecules, the ability of curcumin to interact with the amyloid deposits in post-mortem brain samples of AD patients was conserved. Both mature senile plaques and diffuse deposits – the kinetic precursor of the senile plaques – were labeled by the nanoparticles. This strong affinity for the different types of amyloid deposits may render them new potential radiotracers or MRI markers for early diagnosis in AD. In view of this potential application, several *in vitro* tests proved the biocompatibility of these curcumin nanoparticles: they were shown to be non-toxic on different cells lines, to significantly rescue the toxicity induced by A $\beta$  aggregates and to limit the fibrillization of A $\beta$  peptide.

Alzheimer disease is the most frequent form of dementia, A $\beta$  plaques and NFTs playing a major role in the development of this disease. Significant evidences suggest that progressive accumulation of A $\beta$  in limbic and association cortices precedes the neurodegeneration of tau and the cascade of biochemical and cellular modifications in the brain. The development of strategies to detect A $\beta$  pathological changes *in vivo*, in the early stages of AD is essential. Currently, no imaging techniques capable of early detection of AD are available in clinics. The PET tracer,<sup>11</sup> Pittsburg Coumpound (PIB) is employed for clinical diagnosis since 2004, after the first human study.<sup>49</sup> Other F-amyloid tracers have been developed since, but their

specificity is questioned. Moreover, these tracers have low affinity for the diffuse deposits, the diagnosis indicated being negative in the absence of senile plaques. Magnetic Resonance Imaging (MRI) is also a powerful tool for clinical and biological imaging able to map structure and function with excellent spatial resolution. Numerous amyloid scintillographic and magnetic probes have been or are being developed. Still, not many are the ones fulfilling all the requirements in order to be employed for clinical diagnosis: bioavailable and non-toxic or target specific.

Numerous studies confirm the potential of curcumin in the treatment of AD<sup>7,44,50-54</sup> and lately, in early diagnosis.<sup>5,10,55-58</sup> The lack of complete success of curcumin essays resides in its low bioavailability, related to its insolubility in aqueous solutions. Huge efforts were made to improve its solubility, from chemistry to nanotechnology, either by functionalizing the basic molecule with ionic functions or by conjugation of small molecules (particularly amino acids<sup>59</sup>) or by designing nanoparticles based systems, like liposomes,<sup>30,60-62</sup> solid lipid nanoparticles,<sup>31,33,63-65</sup> or polymeric nanoparticles.<sup>32,44,62,66-70</sup> These types of nano-formulations are generally based on the inner encapsulation of curcumin. Formulations designed to solubilize curcumin by conserving its ability to bind A $\beta$  peptide or to target the amyloid deposits are few<sup>30,60</sup> and they concern liposomes incorporating phosphatidyl serine covalently linked with curcumin through the polar head.

Solubilization of curcumin by means of inclusion complexes represents a convenient alternative for increasing curcumin bioavailability concomitantly with preserving it available for targeting and interaction with the environment. Among the various existing drug carriers,<sup>35,71,72</sup> cyclodextrins have been almost exclusively used for the solubilization of curcumin.<sup>37,41-43</sup> The stoichiometric ratio between cyclodextrins and curcumin was reported to be formation of a 2:1,<sup>37,73</sup> suggesting that each

of the two phenolic rings of curcumin would be sheltered by the lipophilic cavity of two cyclodextrins. By controlling the molar concentration of each component, a complex ratio of 1:1 cyclodextrin/curcumin can be obtained.<sup>38,41,74</sup> Such curcumin-cyclodextrin complexes behave like an amphiphilic supramolecule, being able to self-assemble into vesicular nanostructures in which curcumin is believed to be confined at the interior vesicle.<sup>40</sup> The potential of cyclodextrin-solubilized curcuminoids in the treatment of AD was already evaluated by the group of Quitschke *et al.*: by using 2-hydroxypropyl- $\beta$ -cyclodextrin, they showed that cyclodextrin-solubilized curcuminoids are able to lower the amyloid plaque load in AD transgenic mice.<sup>43</sup> The study focused mainly on the metabolism of curcumin. But can such formulations preserve the targeting ability of curcumin? This question was not examined before, to our knowledge.

In this study, we have proved that curcumin-methyl- $\beta$ -cyclodextrin complex may self-assemble into nanoparticles in a way that retains, at least partially, the curcumin at the surface of the nanoparticles. Likewise curcumin-*para*-sulphonato-calix[4]arene and curcumin-*para*-sulphonato-calix[6]arene complexes self-assemble into nanoparticulate systems, with curcumin at the surface of the particle. Such behaviour is similar to that observed by Liu for both *para*-sulphonato-calix[n]arenes and cyclodextrins.<sup>75</sup>

Several proofs confirm the availability of curcumin at the surface of these nanoparticles: the nanoparticles prevent A $\beta$ 42 induced toxicity; they are able to interact with the A $\beta$  peptide, reducing its aggregation and they showed high affinity for the amyloid deposits, strongly labelling not only the senile plaques but also the diffuse deposits of A $\beta$  on brain tissue of post mortem AD patients.

The potential of such curcumin-macrocyclic host compounds in early diagnosis as well as in the treatment of AD is not to be disregarded as few reports deal with both therapeutic and preventive approach. The use of not only non-toxic, but also pro-active amyloid tracers may offer the possibility of an early diagnosis combined with a subsequent treatment effect, by preventing the toxicity due to A $\beta$  aggregates, limiting A $\beta$  aggregation and reducing the oxidative stress.

## Notes and references

<sup>a</sup>Centre de recherche de l'ICM, (UPMC, INSERM UMR S 975, CNRS UMR 7225), 47 Bd de l'hôpital 75013 Paris, France.

<sup>b</sup>Laboratoire de Neuropathologie Escourrolle, Hôpital de la Salpêtrière, AP-HP, 47 Bd de l'hôpital 75013 Paris, France.

<sup>c</sup>LMI CNRS, UMR 5615, Univ. Lyon 1, Villeurbanne 69622, France.

<sup>d</sup>Département d'Immunologie Cellulaire et Tissulaire, CERVI INSERM U 945, Hôpital Pitié Salpêtrière, 83 Boulevard de l'hôpital, 75 013, Paris, France.

<sup>e</sup>Institut of Physical Chemistry PAN, Polish Academy of Science, Warsaw, Poland.

\* Corresponding author, email: adina\_m31@yahoo.com

† Footnotes should appear here. These might include comments relevant to but not central to the matter under discussion, limited experimental and spectral data, and crystallographic data.

Electronic Supplementary Information (ESI) available: [details of any supplementary information available should be included here]. See DOI: 10.1039/b000000x/

## References

- B.T. Hyman, C.H. Phelps, T.G. Beach, E.H. Bigio, N.J. Cairns, M.C. Carrillo, D.W. Dickson, C. Duyckaerts, M.P. Frosch, E. Masliah, et al. *Alzheimers Dement.*, 2012, **8**, 1-13;
- J. Hardy. *Neurobiol. Aging.*, 1999, **20**, 85;
- J. Hardy. *Neurobiol. Aging.*, 2002, **23**, 1073-1074;
- K. Ono, K. Hasegawa, H. Naiki, M. Yamada. *J. Neurosci. Res.*, 2004, **75**, 742-750;
- F. Yang, G.P. Lim, A.N. Begum, O.J. Ubeda, M.R. Simmons, S.S. Ambegaokar, P.P. Chen, R. Kaye, C.G. Glabe, S.A. Frautschy and G.M. Cole. *J. Biol. Chem.*, 2005, **280**, 5892-5901;
- C. Zhang, A. Browne, D. Child, R.E. Tanzi. *J Biol Chem* 2010, **285**, 28472-28480;
- A.N. Begum, M.R. Jones, G.P. Lim, T. Morihara, P. Kim, D.D. Heath, C.L. Rock, M.A. Pruitt, F. Yang, B. Hudspeth, et al. *J Pharmacol Exp Ther* 2008, **326**, 196-208;
- I. Lee, J. Yang, J.H. Lee, Y.S. Choe. *Bioorg Med. Chem. Lett.*, 2011, **21**, 5765-5769;
- D. Yanagisawa, T. Amatsubo, S. Morikawa, H. Taguchi, M. Urushitani, N. Shirai, K. Hirao, A. Shiino, T. Inubushi, I. Tooyama. *Neuroscience*, **184**, 120-127;
- M. Koronyo-Hamaoui, Y. Koronyo, A.V. Ljubimov, C.A. Miller, M.K. Ko, K.L. Black, M. Schwartz, D.L. Farkas. *Neuroimage*, 2011, **54 Suppl 1**, S204-217;
- B. Ray, D.K. Lahiri. *Curr. Opin. Pharmacol.*, 2009, **9**, 434-444;
- A.L. Cheng, C.H. Hsu, J.K. Lin, M.M. Hsu, Y.F. Ho, T.S. Shen, J.Y. Ko, J.T. Lin, B.R. Lin, W. Ming-Shiang W et al. *Anticancer. Res.*, 2001, **21**, 2895-2900;
- P.R. Holt, S. Katz, R. Kirshoff. *Dig. Dis. Sci.*, 2005, **50**, 2191-2193;
- P. Muthenna, P. Suryanarayana, S.K. Gunda, J.M. Petrash, G.B. Reddy. *FEBS Lett.*, 2009, **583**, 3637-3642;
- J. Lin, S. Zheng, A. Chen. *Lab. Invest.*, 2009, **89**, 1397-1409;
- M. Belviranli, N. Okudan, K.E. Atalik, M. Oz. *Biogerontology*, 2013, **14**, 187-196;
- Y.H. Aldebasi, S.M. Aly, A.H. Rahmani. *Int. J. Physiol. Pathophysiol. Pharmacol.*, 2013, **5**, 194-202;
- N. Kawanishi, K. Kato, M. Takahashi, T. Mizokami, Y. Otsuka, A. Imaizumi, D. Shiva, H. Yano, K. Suzuki. *Biochem. Biophys. Res. Commun.*, 2013, **441**, 573-578;
- B. Meng, J. Li, H. Cao. *Curr. Pharm. Des.*, 2013, **19**, 2101-2113.
- Y. Panahi, A. Sahebkar, S. Parvin, A. Saadat. *Ann Clin Biochem* 2012, **49**, 580-588;
- M. Colitti, B. Gaspardo, A. Della Pria, C. Scaini, B. Stefanon. *Vet. Immunol. Immunopathol.*, 2012, **147**, 136-146;
- A. Shehzad, G. Rehman, Y.S. Lee. *Biofactors*, 2013, **39**, 69-77;

- 23 C.V. Rao, A. Rivenson, B. Simi, B.S. Reddy. *Cancer Res.*, 1995, **55**, 259-266;
- 24 C.Z. Huang, W.Z. Huang, G. Zhang, D.L. Tang. *Mol. Biol. Rep.*, 2014, **40**, 5825-5831;
- 25 A. Shehzad, J.W. Park, J. Lee, Y.S. Lee. *Chem. Biol. Interact.*, 2013, **206**, 394-402;
- 26 Y. Yu, X. Zhang, L. Qiu. *Biomaterials*, 2014, **35**, 3467-3479;
- 27 V. Saxena, M.D. Hussain. *J. Biomed. Nanotechnol.*, 2013, **9**, 1146-1154;
- 28 W.W. Quitschkes. *BMC Biotechnol.*, 2008, **8**.
- 29 P. Basnet, H. Hussain, I. Tho, N. Skalko-Basnet. *J. Pharm. Sci.*, 2012, **101**, 598-609;
- 30 S. Mourtas, M. Canovi, C. Zona, D. Aurilia, A. Niarakis, B. La Ferla, M. Salmona, F. Nicotra, M. Gobbi, S.G. Antimisiaris. *Biomaterials*, 2011, **32**, 1635-1645;
- 31 V. Kakkar, A.K. Mishra, K. Chuttani, I.P. Kaur. *Int. J. Pharm.*, 2013, **448**, 354-359;
- 32 B. Le Droumaguet, J. Nicolas, D. Brambilla, S. Mura, A. Maksimenko, L. De Kimpe, E. Salvati, C. Zona, C. Airoidi, M. Canovi, et al. *ACS Nano.*, 2012, **6**, 5866-5879;
- 33 K. Vandita, B. Shashi, K.G. Santosh, K.I. Pal. *Mol. Pharm.*, 2012, **9**, 3411-3421;
- 34 J. Szejtli. *J. Chem. Rev.*, 1998, **98**, 1743-1754;
- 35 F. Perret, A.N. Lazar, A.W. Coleman. *Chem. Commun.*, 2006, 2425-2438;
- 36 J.W. Steed, J.L. Atwood. *J. Supramol. Chem.* 2009, **46**, 2366-2393;
- 37 P.R. Dandawate, A. Vyas, A. Ahmad, S. Banerjee, J. Deshpande, K.V. Swamy, A. Jamadar, A.C. Dumhe-Klaire, S. Padhye, F.H. Sarkar. *Pharm. Res.*, 2012, **29**, 1775-1786;
- 38 Q. Tan, Y. Li, J. Wu, H. Mei, C. Zhao, J. Zhang. *Int. J. Nanomedicine.*, 2012, **5**, 5385-5393;
- 39 M.A. Tomren, M. Masson, T. Loftsson, H.H. Tonnesen. *Int. J. Pharm.*, 2007, **338**, 27-34;
- 40 M.M. Yallapu, M. Jaggi, S.C. Chauhan. *Colloids Surf. B Biointerfaces.*, 2010, **79**, 113-125;
- 41 K.N. Baglole, P.G. Boland, B.D. Wagne. *Journal of Photochemistry and Photobiology A: Chemistry*, 2005, **173**, 230-237;
- 42 A.B. Hegge, M. Vukicevic, E. Bruzell, S. Kristensen, H.H. Tonnesen. *Eur. J. Pharm. Biopharm.*, 2013, **83**, 95-105;
- 43 W.W. Quitschke, N. Steinhaff, J. Rooney. *Alzheimers Res. Ther.*, 2013, **5**, 16;
- 44 K.K. Cheng, C.F. Yeung, S.W. Ho, S.F. Chow, A.H. Chow, L. Baum. *Aaps J.*, 2013, **15**, 324-336;
- 45 A. W. Coleman, S. Jebors, S. Cecillon, P. Perret, D. Garin, D. Marti-Battle, M. Moulin, *New J Chem*, (2008), **32**, 780-2;
- 46 No authors listed. *Neurobiol. Aging.*, 1997, **18**, S1-2;
- 47 T. Mosmann. *J. Immunol. Methods.*, 1983, **65**, 55-63;
- 48 H. Levin. *Protein Sci.*, 1993, **2**, 76-83;
- 49 W.E. Klunk, H. Engler, A. Nordberg, Y. Wang, G. Blomqvist, D.P. Holt, M. Bergstrom, I. Savitcheva, G.F. Huang, S. Estrada, et al. *Ann. Neurol.*, 2004, **55**, 306-319;
- 50 P. Dkhar, R. Sharma. *Int. J. Dev. Neurosci.*, 2010, **28**, 351-357;
- 51 S.A. Frautschy, W. Hu, P. Kim, S.A. Miller, T. Chu, M.E. Harris-White, G.M. Cole. *Neurobiol. Aging.*, 2001, **22**, 993-1005;
- 52 O.B. Villaflores, Y.J. Chen, C.P. Chen, J.M. Yeh, T.Y. Wu. *Taiwan J. Obstet. Gynecol.*, 2012, **51**, 515-525;
- 53 G.P. Lim, T. Chu, F. Yang, W. Beech, S.A. Frautschy, G.M. Cole. *J. Neurosci.*, 2001, **21**, 8370-8377;
- 54 Y. Wang, H. Yin, J. Li, Y. Zhang, B. Han, Z. Zeng, N. Qiao, X. Cui, J. Lou, J. Li. *Neurosci. Lett.*, 2013, **557 Pt B**, 112-117;
- 55 I. Lee, J. Yang, J.H. Lee, Y.S. Choe. *Bioorg. Med. Chem. Lett.*, 2011, **21**, 5765-5769;
- 56 E.K. Ryu, Y.S. Choe, K.H. Lee, Y. Choi, B.T. Kim. *J. Med. Chem.*, 2006, **49**, 6111-6119;
- 57 M. Sagnou, D. Benaki, C. Triantis, T. Tsotakos, V. Psycharis, C.P. Raptopoulou, I. Pirmettis, M. Papadopoulos, M. Pelecanou. *Inorg. Chem.*, 2011, **50**, 1295-1303;
- 58 D. Yanagisawa, T. Amatsubo, S. Morikawa, H. Taguchi, M. Urushitani, N. Shirai, K. Hirao, A. Shiino, T. Inubushi, I. Tooyama. *Neuroscience*, 2011, **184**, 120-127;
- 59 R.B. Narasingappa, M.R. Javagal, S. Pullabhatla, H.H. Htoo, J.K. Rao, J.F. Hernandez, P. Govitrapong, B. Vincent. *Biochem. Biophys. Res. Commun.*, 2012, **424**, 691-696;
- 60 A.N. Lazar, S. Mourtas, I. Youssef, C. Parizot, A. Dauphin, B. Delatour, S.G. Antimisiaris, C. Duyckaerts. *Nanomedicine*, 2013, **9**, 712-721;
- 61 F. Re, I. Cambianica, C. Zona, S. Sesana, M. Gregori, R. Rigolio, B. La Ferla, F. Nicotra, G. Forloni, A. Cagnotto, et al. *Nanomedicine* 2011, **7**, 551-559;
- 62 S.S. Chiu, E. Lui, M. Majeed, J.K. Vishwanatha, A.P. Ranjan, A. Maitra, D. Pramanik, J.A. Smith, L. Helson. *Anticancer Res.*, 2011, **31**, 907-911;
- 63 C. Puglia, A. Offerta, L. Rizza, G. Zingale, F. Bonina, S. Ronsisvalle. *J. Nanosci. Nanotechnol.*, 2013, **13**, 6888-6893;
- 64 A. Guri, I. Gulseren, M. Corredig. *Food Funct.*, 2013, **4**, 1410-1419;
- 65 W. Wang, R. Zhu, Q. Xie, A. Li, Y. Xiao, K. Li, H. Liu, D. Cui, Y. Chen, S. Wang. *Int. J. Nanomedicine*, 2012, **7**, 3667-3677;
- 66 R. Feng, Z. Song, G. Zhai. *Int. J. Nanomedicine*, 2012, **7**, 4089-4098;
- 67 A. Mathew, T. Fukuda, Y. Nagaoka, T. Hasumura, H. Morimoto, Y. Yoshida, T. Maekawa, K. Venugopal, D.S. Kumar. *PLoS One*, 2012, **7**:e32616;
- 68 S. Doggui, J.K. Sahni, M. Arseneault, L. Dao, C. Ramassamy. *J. Alzheimers Dis.*, 2012, **30**, 377-392;
- 69 B. Ray, S. Bisht, A. Maitra, A. Maitra, D.K. Lahiri. *J Alzheimers Dis* 2011, **23**, 61-77;
- 70 R.S. Mulik, J. Monkkonen, R.O. Juvonen, K.R. Mahadik, A.R. Paradkar. *Mol. Pharm.*, 2010, **7**, 815-825;
- 71 K.T. Al-Jamal, C. Ramaswamy, A.T. Florence. *Adv. Drug Deliv. Rev.*, 2005, **57**, 2238-2270;
- 72 A. Abderrezak, P. Bourassa, J.S. Mandeville, R. Sedaghat-Herati, H.A. Tajmir-Riahi. *PLoS One*, 2012, **7**, e33102;
- 73 B. Tang, L. Ma, H.Y. Wang, G.Y. Zhang. *J. Agric Food Chem.*, 2002, **50**, 1355-1361;
- 74 H.H. Tonnesen, M. Masson, T. Loftsson. *Int. J. Pharm.*, 2002, **244**, 127-135.
- 75 D.S. Guo, Y. Liu. *Acc. Chem Res.*, 2014, **47**, 1925-1934



# Discussion

During the 10 last years, there has been a growing interest in calix[n]arene capped silver nanoparticles for their uses in biosensing and much more recently for their intrinsic therapeutic properties.

The first part of results presented in the present thesis (chapter B-I) describes their use as biosensors for a wide range of molecules. Cost effective, portable and ultra-sensitive analytical tools are one of the major expectations of the applications of silver nanoparticles capped with calix[n]arenes. They have been demonstrated here to detect various types of biomolecules, including nucleobases, surfactants and proteins at a micromolar detection limit. Their advantages and limits compared to others analytical methods are presented in that discussion.

In the second part of results (chapter B-II), the biological activities of calix[n]arene capped silver nanoparticles are presented through three different studies. Evidences for their promising interest potential as antibiotic, anti-oxydants and antiviral or anticancer medications are presented. Collaborative work on several research axes including the relationship between the decrease of ROS level, their antibiotic effect, and protein inhibition *in vitro* appears to have promise, in the long term. Another additional study has investigated the anti-Alzheimer Disease activities of calix[n]arene as nanoparticles.

Because of their future therapeutic applications, their toxicity is major concern that is discussed at the end of this section.

## **I- Biosensing by calix[n]arene capped silver nanoparticles (chapter B-I)**

In this chapter, the molecular recognition of a specific class of bio molecules (nucleic bases, protein and surfactant) by calix[n]arene capped silver nanoparticles has been studied. The physical signal transducing the molecular recognition event of a targeted ligand is based on the change of the optical properties of silver nanoparticles. Indeed, the complexation of ligand onto the surface of the hybrid nanoparticles, changes both the wavelength and the intensity of maximum absorbance of light. The plasmonic absorption band of spherical

shaped silver nanoparticles is typically in the range 390-400 nm, yielding a yellow colour for the colloidal dispersion. Aggregation provoked by the complexation of a ligand to the receptor which can bridge between the nanoparticles, induces a change in the polarity of the local environment and a change in size. At higher size, the resonance of electronic shift from a simple mode to multipolar mode which are characterized optically by a strong red shift and an enlargement of the plasmonic band. This can be readily observed, even by the naked eye (more details are given in the LSPR section in Part A).

A series of anionic calix[n]arenes has been selected for capping silver nanoparticles, because of their high solubility, low toxicity and ability to recognize biomolecules bearing positively charged amine groups (protein, DNA, surfactants). Moreover the argentophilic nature of anionic calix[n]arenes makes possible their attachments over silver nanoparticles. As a consequence, calix[n]arene capped silver nanoparticles have been the most studied among the macrocyclic capped silver nanoparticles in the literature [Tauran *et al.*, 2013a]. The different mode of synthesis and the chemical properties of calix[n]arene capped silver nanoparticles are presented in the review entitled Bio-applications of capped silver nanoparticles in Part A [Tauran *et al.*, 2015].

In the current work, *para*-sulphonato-calix[4]arene capped silver nanoparticles have been demonstrated to discriminate purine and pyrimidine nucleobase molecules [Tauran *et al.*, 2011]. For the pyrimidine nucleotides there is appearance of a new absorption band around 550 nm, and a color change from yellow to orange red and pinks. A new model about the organization of the calix[n]arenes has been proposed for explaining both the molecular recognition by calix[n]arenes and the attachment of calix[n]arenes on silver nanoparticles (Figure 1). This model which the calix[n]arene are organized in a classical bilayer is more consistent than the previous one described in the literature by Xiong, which the calix[n]arene cavity was pointing unto the nanoparticles surface making impossible the molecular recognition [Xiong *et al.*, 2008].

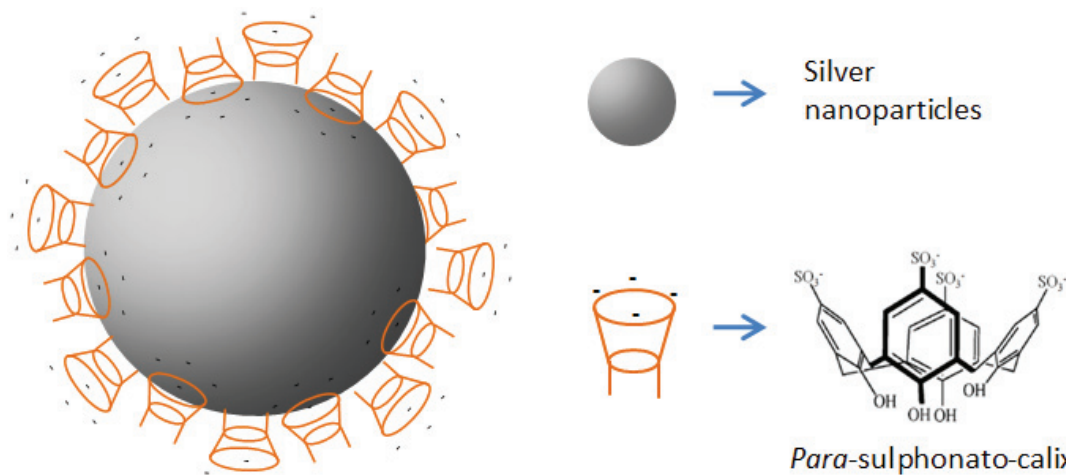


**Figure 1.** Schematic representation of *para-sulphonato-calix[4]arene* capped silver nanoparticles. From [Tauran et al., 2011]

Secondly, a series of silver nanoparticles capped by nine different calix[4,6,8]arenes bearing sulphonate groups at the *para* and/or phenolic faces have investigated for their ability to interact with different charged surfactant (cationic, neutral and anionic) [Tauran *et al.*, 2012]. Only the calix[4]arene derivatives sulphonated at the *para* position have shown optical change in the plasmonic absorption with cationic surfactants. This result shows that the size ring and the conic geometry of the calix[n]arene is main component for complexing surfactants. The interactions follow the CMC values of the surfactants either as simple molecules or mixed micelles. This is of interest in biochemistry for following the micellisation of cationic surfactant and membrane protein complex. An example of application could be to use such hybrid nanoparticles for verifying the assembly complex of membrane protein extracted from cells.

Thirdly, *para-sulphonato-calix[4]arene* and 1,3-di-O-phosphonato-calix[4]arene have been selected for being capped on silver nanoparticles and for discriminating protein species [Tauran *et al.*, 2013b]. These calix[n]arenes possess argentophilic nature and have been characterized for their interaction for serum albumin proteins. The optical discrimination of the hybrid nanoparticle against the different serum albumin (pork, human, goat, sheep) have been followed on UV-Visible spectrometry as a matter of temperature. The denaturation behaviour of the protein induced by the increasing temperature, makes available new amino acid that are assumed to interact with the hybrid nanoparticles. Optical behaviour of hybrid nanoparticles for one specific albumin specie has been shown. The serum albumins represent the most common protein class in animal physiological fluids with concentrations of up to 40 g/L (0.6 mM) in blood. Discrimination between albumins of different species could be a fast,

cost effective and selective method for identifying meat species in food industry, which became recently an important issue in Europe.

Other researchers have investigated calix[n]arene capped silver nanoparticles for detecting optically others compounds such as cationic amino acids, ferric metal ions or organophosphates [Tauran *et al.*, 2015]. This thesis work has extending our knowledge concerning the molecular recognition of these hybrid nanoparticles toward different class of biomolecules. Moreover, if the optical properties changes of silver nanoparticles due to aggregation are well known for years, a little is known about the chemical assembly between the ligand and the macrocyclic molecules capped noble metal nanoparticles, leading to the aggregation process. In this thesis, a particular effort has been done to understand this mechanism.

In this thesis, the complex assembly process has been extensively investigated for the interaction of a model molecule: the nucleobase cytosine and *para*-sulphonato-calix[4]arene capped silver nanoparticles. Multiple physical methods have been used, including DOSY NMR, fluorescence and visible spectroscopies, DLS, Single Crystal Solid State Diffraction and Electron microscopy. Then complexation assembly has been assumed to be in 2 steps. First, there is a binding event between cytosine and hybrid nanoparticles and subsequently cytosine bridges silver nanoparticles in a 1 : 2 complex, the formation of this super complex induces aggregation assembly (Figure 2) and change of the colloidal solution colour from yellow to red orange. Here, the presence of cytosine can be determined at a minimum concentration of 1  $\mu\text{M}$  by the naked eye [Tauran *et al.*, 2013c].

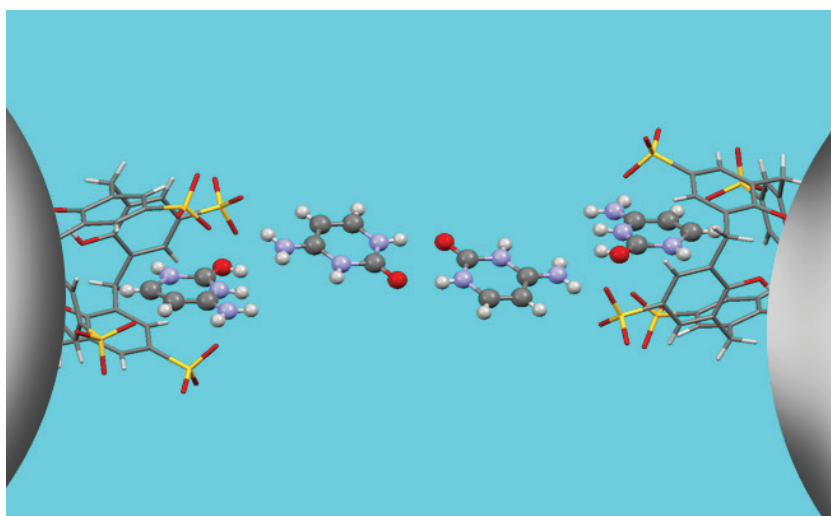


**Figure 2.** Schematic representation of the aggregation mechanism proposed by Coleman *et al.* [Tauran *et al.*, 2013b]. Grey areas represent the surface of silver nanoparticles capped by *para*-sulphonato-calix[4]arene and 4 cytosine nucleic bases bridge the nanoparticles, leading to the aggregation process.

**Table 1** - Advantages and disadvantages of bio-detection method using calix[n]arenes and calix[n]arene capped silver nanoparticles.

Material used	Method of bio detection	Reference	Advantages	Disadvantages
Calix[n]arene capped silver nanoparticles	Optical (naked eye)	[Xiong <i>et al.</i> , 2008]	Cost effective, Fast, Portable	Low detection limit ( $\mu\text{M}$ concentration range )
	Optical (with DLS)	[Pandya <i>et al.</i> , 2013]	Cost effective, Fast, Very sensitive (10 nM )	Not portable
	SERS	[Guerrini <i>et al.</i> , 2009]	Provide structural data, Fast, Ultra sensitive (10 nM)	Not portable, Expensive
	Electrical	[Evtugyn <i>et al.</i> , 2011] [Bian <i>et al.</i> , 2010]	Fast, Portable, Ultra-sensitive (1nM [Evtugyn_2011] and 4nM[Bian_2010])	Expensive
Calix[n]arene	ELISA	[Cecillon <i>et al.</i> , 2005]	Highly specific and very sensitive (10nM concentration range)	Expensive and slow (Need a revelation step of the complex by antibody).
	Mass Spectrometry	[Da Silva <i>et al.</i> , 2006]	Provide structural data. Fast and Sensitive (100nM concentration range)	Not portable and very expensive.
	Western blot	[Cecillon <i>et al.</i> , 2005]	Highly specific, very sensitive (10nM concentration range)	Not portable and slow (Need a revelation step of the complex by antibody).

Because of their unique optical and electrical properties, a various physical approach has been proposed for detecting molecules by calix[n]arene capped silver nanoparticles. Table above summarizes the advantages and disadvantages of each method. Moreover, a comparison is given with conventional methods using calix[n]arenes as the recognition molecule. The table shows that there is not yet a good technique enable to detect biomolecule with all advantages (high specificity, fast, cost effective, ultra-sensitive and portable). Each method possess is own characteristic.

Micro-electronic devices have shown particularly high sensitivity but also many other advantages such fast and portable compared to conventional detection methods (see Table 1). Device coming from micro and nanotechnologies using such hybrid nanoparticles represent probably the future biodetection methods. However, the specificity of the detection is still limited and a pre-treatment of purification appears necessary for analyzing complex mixtures without false positives. The integration and automation of sample treatment step in such electronic device should be one of the main works in future years.

## **II- Biological activities of calix[n]arenes and calix[n]arene capped silver nanoparticles (chapter B-II)**

The biological activities of the calix[n]arenes have been reported on various forms of life from virus, bacteria, fungi and mammalian cells to human beings. These bucket shaped molecules have been characterized as detoxifying agents, antibacterial, antiviral, anticoagulant, anticancer, antifungal, membrane protein modulator / extractor, drug transporters and fluorescent probes. All their biological properties have been reviewed in depth in the review entitled Bio activity of calix[n]arene *in vivo* and at the cellular level (in part A of this thesis). Their combination with silver nanoparticles offers new perspectives for therapeutic applications. In this thesis, their uses as antibacterial, anti-oxydants and antiviral or anticancer through their endonuclease inhibition activity have been investigated.

First, a series of nine different sulphonated calix[n]arenes have been capped on silver nanoparticles and have been tested for their anti-bacterial effects against *B. subtilis* (Gram +) and *E. coli* (Gram -) at a concentration of 100 nM in calix[n]arene [Boudebouze *et al.*, 2012]. The results show that the *para*-sulphonato-calix[n]arenes are active against Gram positive bacteria while the derivatives having sulphonate groups at both *para* and alkyl terminal positions are active against Gram negative bacteria. Calix[n]arene gives to silver

nanoparticles the ability to restrict their antibacterial effect by discriminating Gram positive and negative bacteria. This is a medical interest to target one type of pathogenic bacteria without killing all the other bacteria population important for the well function of human body. Moreover some of these hybrid nanoparticles have shown that they can reduce the bacterial growth at the by 50 % at the lowest concentration of 100nM. Compared to classical antibiotic, hexamidine and chlorhexidine which have antibacterial effect above 1 $\mu$ M, these hybrid nanoparticles have demonstrated to be quite efficient.

Secondly, another study of our group has investigated the ability of anionic calix[n]arene capped silver nanoparticles to complex and to transport antibiotic [Perret *et al.*, 2013]. Calix[4]arene bearing sulphonate, carboxylate or phosphates groups have shown to be highly efficient for complexing positively charged amino antibiotics chlorhexidine and gentamicin sulphate in contrast to neutral antibiotic. The complexes under colloidal suspension characterized by UV-Visible spectrometry have shown stability over 24 hours.

These two studies demonstrate the promising use of these hybrid compounds associated or not with antibiotics for treating or preventing the proliferation of pathogenic multi resistant bacteria. However, the study of synergic effect of the antibiotic associated to the calix[n]arene capped silver nanoparticles needs to be characterized in the future. Their toxicity represents also a major concern that is discussed later.

Another study, concerning the use of calix[n]arene as endonuclease inhibitor has been performed in this thesis work [Tauran *et al.*, 2014]. The endonucleases are a class of enzymes whose biological role is to digest DNA. As such, they play a role in human cell repair but also are key elements in viral infection. They represent a valid target in drug design for anti-cancer or anti-viral. Large negatively charged macrocyclic molecule such as *para*-sulphonato-calix[6]arene, *para*-sulphonato-calix[8]arene and  $\beta$ -cyclodextrin sulphated have shown high inhibition activity against various endonuclease with IC<sub>50</sub> values in the micromolar concentration range, representing a very strong inhibition efficacy compared to standard antiviral drugs. The combination of endonuclease inhibitors to silver nanoparticles represents a great interest in order to allow the cellular uptake of such complex. It has been already reported that cationic nanoparticles are efficient for destabilizing cellular membrane [Hafez *et al.*, 2001]. The inhibition activity has shown to be comparable before or after capping the macrocyclic  $\beta$ -cyclodextrin sulphated to silver nanoparticles. This might be due

to the detachment of the macrocyclic molecules from the silver nanoparticles, to the benefit of the endonuclease protein (even if the complex was previously dialysed).

Finally a last study describes the use of macrocyclic molecules as nanocarriers of the Active Pharmaceutical Ingredient API curcumin for diagnosis and therapeutic uses of Alzheimer's disease [Lazar *et al.*, 2014]. The calix[n]arenes *para*-sulphonato-calix[6]arene, *para*-sulphonato-calix[8]arene, and methyl- $\beta$ -cyclodextrin have shown to solubilize curcumin and to form nanoparticles (15-17 nm of diameter). Curcumin have been shown to be available at the surface of the nanoparticles, and have been reported to have affinity against A $\beta$ 42 peptide and amyloid deposits, which are toxic peptide for normal nerve cells and found in the brains of Alzheimer patients. Previous studies have reported the use of macrocyclic molecules for solubilizing curcumin but it is the first time to our knowledge that these complexes have been reported for diagnosis of Alzheimer's disease.

### III- Toxicity concerns

Calix[n]arene capped silver nanoparticles have shown no cytotoxicity at used concentration (1 mM) on neural PC12 cell lines. They have even been demonstrated by one of our study (not yet published) that they decrease the intra cellular ROS levels [Tauran *et al.*, 2015].

However their toxicity *in vivo* is a concern that should be addressed in the future. Toxicity of hybrid silver nanoparticles in human is still not well understood because of the low number of cases studied. Silver ingestion and topical application can induce the benign condition known as "argyria", a grey-blue discoloration of the skin and liver caused by deposition of silver particles in the basal laminae of such tissues. Although argyria is not a life-threatening condition it is, however, cosmetically undesirable [Fung *et al.*, 1996]. Wong *et al.* [Wong *et al.*, 2010] have reviewed and investigated the effect on health of silver nanoparticles. They injected silver nanoparticles intravenously into experimental mice and did not observe any overt systemic effects, despite the silver nanoparticle solution used being at the relatively high concentration of 100 mmol/L.

Caraglia *et al.* have recently compared the toxicity of various nanoparticle systems. [Lamberti *et al.*, 2014]. Even if these nanosystems offer promising therapeutic effect, they may present unexpected toxic side-effects. Liposome can trigger immune response [Marra *et al.*, 2012] and polymeric micelles can be cytotoxic with regards to their stability, uptake and

release in cell culture media [Ostacolo\_2010], in this context the lack of immune response towards calix[n]arenes is promising [Schrader *et al.*, 2006]. Carbon nanotubes have shown to be carcinogenic for lung, gastrointestinal tract, and blood [Magrini *et al.*, 2006]. Again the calix[n]arenes are promising in view of their anti-cancer properties [Rodik *et al.*, 2009]. Finally, the toxicity of metallic nanoparticles is generally related to the metal toxicity itself because of their release under ionic state after being oxidized. Generation of Reactive Oxygen Species, induced by the metal ion, appears to be one of the main ways leading to genotoxic and cytotoxic effects. Besides, their behavior as free metal ions increases the local ionic concentration and subsequently disturbs the cellular functions. As examples,  $Zn^{2+}$  can inhibit the cellular respiration, and  $Ag^+$  can act as an analog on  $Ca^{2+}$  receptor sites [Frohlich *et al.*, 2013]. However, *in vitro* and *in vivo* studies have shown that hybrid silver nanoparticles possess various levels of toxicity according to their size, shape, functionalization and mode of exposition [Dos Santos *et al.*, 2014].

Such toxicity problems will only be resolved by suitable testing *in vivo* on several animal species and thus will require a lengthy period of waiting.

## Reference

- Bian Y, Li C, Li H. ***para*-Sulfonatocalix[6]arene-modified silver nanoparticles electrodeposited on glassy carbon electrode: Preparation and electrochemical sensing of methyl parathion.** *Talanta*. 81 : 1028–1033 (2010).
- Boudebouze S, Coleman AW, Tauran Y, Mkaouer H, Perret F, Garnier A, Brioude A, Kim B, Maguin E, Rhimi M. **Discriminatory antibacterial effects of calix[n]arene capped silver nanoparticles with regard to Gram positive and Gram negative bacteria.** *Chem. Commun.* 49: 7150-7152 (2013).
- Cecillon S, Coleman AW, Eveno-Nobile A, Perron H, Rodrigue M. **Method for detecting aggregate-forming circulating protein forms using an agent for aggregating said forms and an agent for capturing formed aggregates.** Patent US 8158441 B2 (2005).
- Da Silva E, Rousseau CF, Zanella-Cleon I, Becchi M, Coleman AW. **Mass spectrometric determination of association constants of Bovine Serum Albumin (BSA) with para-sulphonato-calix[n]arene derivatives.** *J. Inc. Phenom. Macro. Chem.* 54: 53–59 (2006).
- Dos Santos CA, Seckler MM, Inle AP, Gupta I, Galdiero S, Galdiero M, Gade A, Rai M. **Silver nanoparticles: therapeutic uses, toxicity, and safety issues.** *J. Pharm. Sci.* 103: 1931–1944 (2014).
- Evtugyn GA, Shamagsumova RV, Sitdikov RR. **Dopamine sensor based on a composite of silver nanoparticles implemented in the electroactive matrix of calixarenes.** *Electroanalysis*, 23(10): 2281 – 2289 (2011).

Fröhlich E. **Cellular targets and mechanisms in the cytotoxic action of non-biodegradable engineered nanoparticles.** *Curr Drug Metab.* 14: 976–988 (2013).

Fung MC, Bowen DL. **Silver products for medical indications: risk-benefit assessment.** *J. Toxicol. Clin. Toxicol.* 34: 119-126 (1996).

Guerrini L, Garcia-Ramos JV, Domingo C, Sanchez-Cortes S. **Sensing polycyclic aromatic hydrocarbons with dithiocarbamate-functionalized Ag nanoparticles by surface-enhanced raman scattering.** *Anal. Chem.* 81: 953–960 (2009).

Hafez IM, Maurer N, Cullis PR. **On the mechanism whereby cationic lipids promote intracellular delivery of polynucleic acids.** *Gene Therapy.* 8: 1188–1196. (2011).

Lamberti M, Zappavigna S, Sannolo N, Porto S, Caraglia M. **Advantages and risks of nanotechnologies in cancer patients and occupationally exposed worker.** *Expert Opin. Drug Deliv.* 11: 1087-1101 (2014)

Lazar AN, Ramdani L, Bourboulou R, Belkouch M, Langui D, Jebors S, Tauran Y, Parizot C, Suwinska K, Coleman AW, Duyckaerts C. **Multifunctional curcumin-nanocarriers based on host-guest interaction for Alzheimer Disease diagnostic.** *RSC Advances.* submitted. (2014).

Magrini A, Bergamaschi A, Bergamaschi E. **Carbon nanotubes (CNT) and nanoparticles (NP): interaction with lung epithelium and other biological systems.** *G. Ital. Med. Lav. Ergon.* 28: 266-269 (2006).

Marra M, Salzano G, Leonetti C, Porru M, Franco R, Zappavigna S, *et al.* **New self-assembly nanoparticles and stealth liposomes for the delivery of zoledronic acid: a comparative study.** *Biotechnology Advances.* 30: 302–309 (2012).

Ostacolo L, Marra M, Ungaro F, Zappavigna S, Maglio G, Quaglia F, *et al.* **In vitro anticancer activity of docetaxel-loaded micelles based on poly(ethylene oxide)-poly(epsilon-caprolactone) block copolymers: Do nanocarrier properties have a role?** *J. Cont. Releas.* 148: 255-263 (2010).

Pandya A, Sutariya PG, Lodha A, Menon SK. **A novel calix[4]arene thiol functionalized silver nanoprobe for selective recognition of ferric ion with nanomolar sensitivity via DLS selectivity in human biological fluid.** *Nanoscale.* 5 : 2364-2371 (2013).

Perret F, Tauran Y, Suwinska K, Kim B, Chassain-Nely C, Boulet M, Coleman AW. **Molecular recognition and transport of Active Pharmaceutical Ingredients on anionic calix[4]arene capped silver nanoparticles.** *Journal of Chemistry,* 2013, 1-9 (2013).

Rodik R.V., Boyko V.I., Kalchenko V.I. **Calixarenes in Bio-Medical Researches.** *Curr. Med. Chem.* 16: 1630-1655 (2009).

Schrader T., Klaerner F.G., Fokkens M., Zadmand R., Polkowska J., Bastkowski F., Less C.J. **Novel active substances for treating, diagnosing and preventing macular degeneration.** WO 2006056182 A1 (2006).

Tauran Y, Grosso M, Brioude A, Kassab R, Coleman AW. **Colourimetric and spectroscopic discrimination between nucleotides and nucleosides using para-sulfonato-calix[4]arene capped silver nanoparticles.** *Chem. Commun.* 47(36); 10013-10015 (2011).

Tauran Y, Brioude A, Shahgaldian P, Cumbo A, Kim B, Perret F, Coleman AW, Montasser I. **Calixarene silver nanoparticles interactions with surfactants are charge, size and critical micellar concentration dependent.** *Chem. Commun.* 48: 9483-9485 (2012).

Tauran Y, Brioude A, Coleman AW, Rhimi M, Kim B. **Molecular recognition by gold, silver and copper nanoparticles.** *World Journal of Biological Chemistry.* 4, 35-63 (2013a).

Tauran Y, Brioude A, Kim B, Perret F, Coleman AW. **Anionic Calixarene-Capped Silver Nanoparticles Show Species-Dependent Binding to Serum Albumins.** *Molecules*. 18, 5993-6007 (2013b).

Tauran Y, Rhimi M, Ueno R, Grosso M, Brioude A, Janneau E, Suwinska K, Kassab R, Shahgaldian P, Cumbo A, Fenet B, Kim B, Coleman AW. **Cytosine: *para*-sulphonato-calix[4]arene assemblies: in solution, in the solid-state and on the surface of hybrid silver nanoparticles.** *J Incl Phenom Macrocycl Chem*. 77, 213-221 (2013c).

Tauran Y, Anjard C, Kim B, Rhimi M, Coleman AW. **Large supramolecular organic macrocycles as inhibitors of endonuclease enzymes.** *Chem. Commun.* 50: 11404-11406 (2014)

Tauran Y, Kim B, Coleman AW. **Biological activities of calixarene at cellular level and in vivo.** *EXCLI Journal*. Submitting (2015).

Wong KKY, Liu X. **Silver nanoparticles-the real "silver bullet" in clinical medicine.** *Med. Chem. Commun.* 1: 125-131 (2010).

Xiong D, Chen M, Li H. **Synthesis of *para*-sulfonatocalix[4]arene-modified silver nanoparticles as colorimetric histidine probes.** *Chem. Commun.* (7), 880-882 (2008).



# General conclusion

The study of supramolecular chemistry makes possible the design of new molecules able to organize themselves and with other molecules by low energy bonds so as to create higher molecular complexes with different chemical and physical properties. These molecular assemblies occur from the nanometric to macroscopic scale. They are involved in major biochemical reactions and biological functions (e.g. DNA replication, immune response). Calix[n]arene represents one of the most studied supramolecular systems for their abilities to interact with a wide range of artificial or biological molecules.

One of the main purposes of this thesis has been to investigate biomolecular detection by calix[n]arenes when they were capped on silver nanoparticles. The unique LSPR properties of silver nanoparticles, combined with the biomolecular recognition properties of the calix[n]arenes have enabled the optical discrimination of various biomolecular classes. Calix[n]arene capped silver nanoparticles have been reported here to discriminate between classes of nucleic acid (pyridine from pyrimidine), different serum albumin species (human, beef, pork, sheep), or the organization of surfactants (monomer to micelle) with regard to the molecular recognition of the calix[n]arene used. This bio discrimination represents interest for the consumer as these bio-sensing methods are cost effective, fast, portable and sensitive (e.g. down to 1  $\mu$ M for cytosine). However the selectivity of the detection is not suitable for a direct molecular detection in complex media. The need of a purification treatment will be required for such analysis.

In a second part, the biological activities of these calix[n]arene capped nanoparticles have been investigated. It has been demonstrated that these hybrid nanoparticles possess anti-oxidant and antibacterial activities, to be able to transport Active Pharmaceutical Ingredients and to reach antiviral and anti-cancer targets. The antibacterial effects are particularly promising with really high efficiency ( $IC_{50} > 100$ nM for Gram - bacteria). Their synergic effects when nanoparticles are transporting antibiotic or other API needs to be evaluated. On the other hand, it has been shown that some calix[n]arene derivatives have an inhibitory activity against endonuclease enzymes with also high efficiency ( $IC_{50} > 100$ nM for restriction enzyme). Their inhibitory activity should be extended to other types of endonucleases such as

those expressed in cancer cells, or viral infections. The purification of viral endonucleases is underway and their antiviral activity will also need to be studied at the cellular level.

However the use of conventional analytical tools such as mass spectrometry and NMR has shown some limitations in some of our molecular assembly studies. The aggregation of some complexes at high levels is not appropriate to the concentrations required by such analyses. The use of micro electro mechanical systems (MEMS) has been performed and has been shown to be a promising alternative as an analytical tool. Silicon Nano Tweezers SNT are devices that can monitor in real time the change of mechanical properties (stiffness and viscous losses) of fibers or polymers trapped between the moving tips of the tweezers.

The change of mechanical properties of DNA induced by calix[n]arene nanoparticles measured by SNTs has been also investigated during this thesis work. The development of such artificial DNA binders is of great interest in biomedical applications like gene therapy, or in material science fields. The understanding of the dependence between the supramolecular interactions and the DNA condensation is crucial in the development of more efficient artificial DNA binders.

The study of certain biological functions induced by the molecular assembly between biomolecules and calix[n]arene has been a major concern to address in that work. More than 10 different anionic calix[n]arenes have been tested against a wide range of biomolecules (nucleotides, nucleic acids, APIs, surfactants, amino acids, metal ions and proteins). The selectivity for biomolecules has been characterized by conventional and more recent analytical technologies. To the end, this work has mainly contributed to extending our knowledge about the molecular mechanisms and functions of these supramolecular systems and paves the way to the development of new molecules with improved biological effect.

# Annex



## *Supporting Information*

### **Colourimetric and Spectroscopic discrimination between nucleotides and nucleosides using para-sulphonato-calix[4]arene capped silver nanoparticles**

Yannick Tauran,<sup>a</sup> Marie Grosso,<sup>a</sup> Arnaud Brioude,<sup>a</sup> Rima Kassab<sup>b</sup> and Anthony W. Coleman<sup>a\*</sup>

<sup>a</sup>LMI, UMR 5615, Université Lyon1 CNRS, Campus La Doua, Villeurbanne, F69622, France

Tel 33 4 72 43 1027, E-mail [antony.coleman@adm.univ-lyon1.fr](mailto:antony.coleman@adm.univ-lyon1.fr)

<sup>b</sup> University of Balamand, Faculty of Sciences- Department of Chemistry P.O Box : 100 –Tripoli-Lebanon, Tel :961 6 930250, email [rima.kassab@balamand.edu.lb](mailto:rима.kassab@balamand.edu.lb)

#### **Contents:**

- **Experimental details**
- **Supporting figures**

## Experimental details:

### Synthesis of p-sulphonatocalix[4]arene

The synthesis of p-sulphonatocalix[4]arene was carried out according to the method described in Parker[1].

### Synthesis of p-sulphonatocalix[4]arene modified silver nanoparticles

The procedure of Li[2] was slightly modified as follows. 10 mL of  $10^{-2}$  M  $\text{AgNO}_3$  solution was added to 80 mL of deionized water. To this solution, 10 mL of  $10^{-2}$  M p-sulphonatocalix[4]arene aqueous solution was added as stabilizer with stirring for 30 min. And then, 44 mg of  $\text{NaBH}_4$  was added to the solution. The silver colloidal suspensions were obtained after 5 minutes.

### p-sulphonatocalix[4]arene analysis

$^1\text{H}$  NMR (600 MHz,  $[\text{D}_6]\text{DMSO}$ , tetramethylsilane):  $\delta=3.72\text{--}3.94$  (-CH<sub>2</sub>-), 7.14–7.36 (Ar-H);

MALDI-TOF-MS:  $m/z$   $[\text{M}+\text{H}]^+$  calced for  $(\text{C}_{28}\text{H}_{24}\text{O}_{16}\text{S}_4+\text{H})$ : 744,8, found: 745,8;

### UV-Visible Absorption assays

The mixture experiments were conducted by monitoring the change in absorbance between 340 nm and 650 nm, using a 96 well titre visible spectrometer, (BioTek Power Wave 340).

### **TEM Imaging:**

The TEM sample was prepared by dropping 6  $\mu$ L of the sample solution on carbon coated grid (50 mesh, Ted Pella). After 30 seconds, the sample was wicked from the grid by touching its edge with a piece of filter paper. TEM studies were conducted by using a Topcon EM 002B, operating with an accelerating voltage of 200 kV.

### **References and Note**

- [1] D. Parker, *Macrocyclic synthesis: a practical approach*, Oxford University Press, Oxford, 1996;
- [2] D. Xiong, M. Chen and H. Li, *Chem. Commun.*, 2008, **7**, 880-882;

## Supporting Figures:

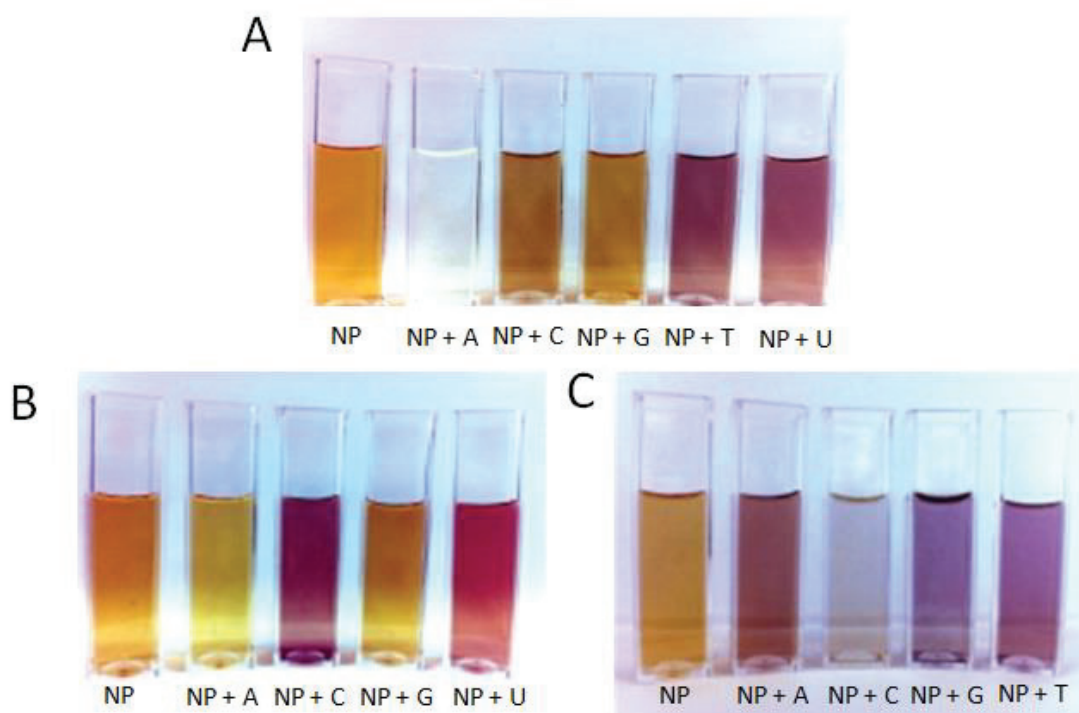


**Fig. S1** Photographs of the complexation of A) nucleotides B) nucleosides and C) deoxy-nucleosides bases with SC4:Ag NPs after 24 hours at a final concentration of  $10^{-3}M$ .

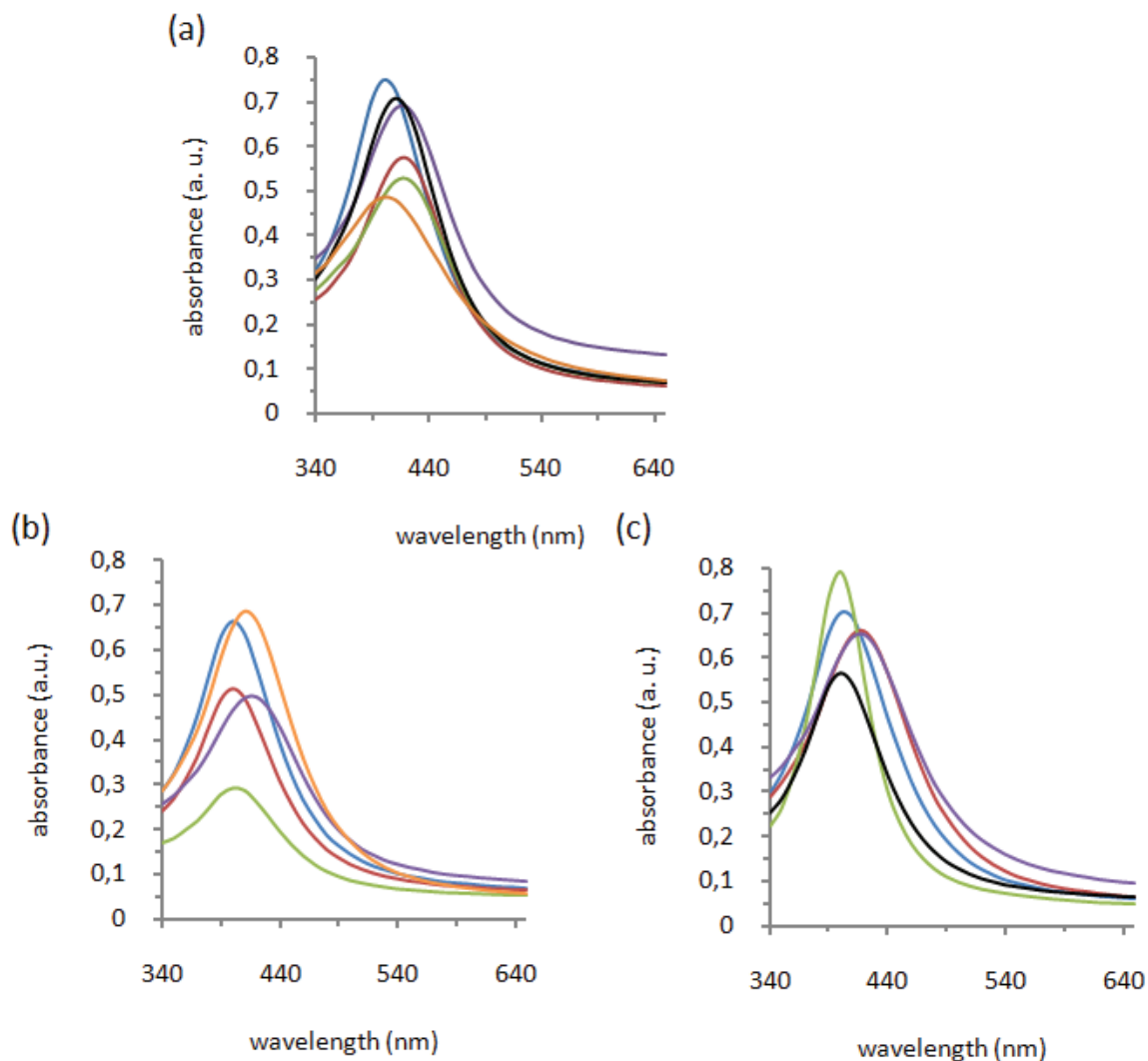


**Fig. S2** Visible spectra of the complexation of a) nucleotides, b) nucleosides and c) deoxy-nucleosides bases with SC6:Ag NPs after one hour at a final concentration of  $10^{-3}$ M. Blue line: pSC6:Ag NP; Red line: pSC6-Ag NP + A; Purple line: pSC6-Ag NP + G; Green line: pSC6-Ag NP + C; Orange line: pSC6-Ag NP + U; Black line: pSC6- Ag NP + T.

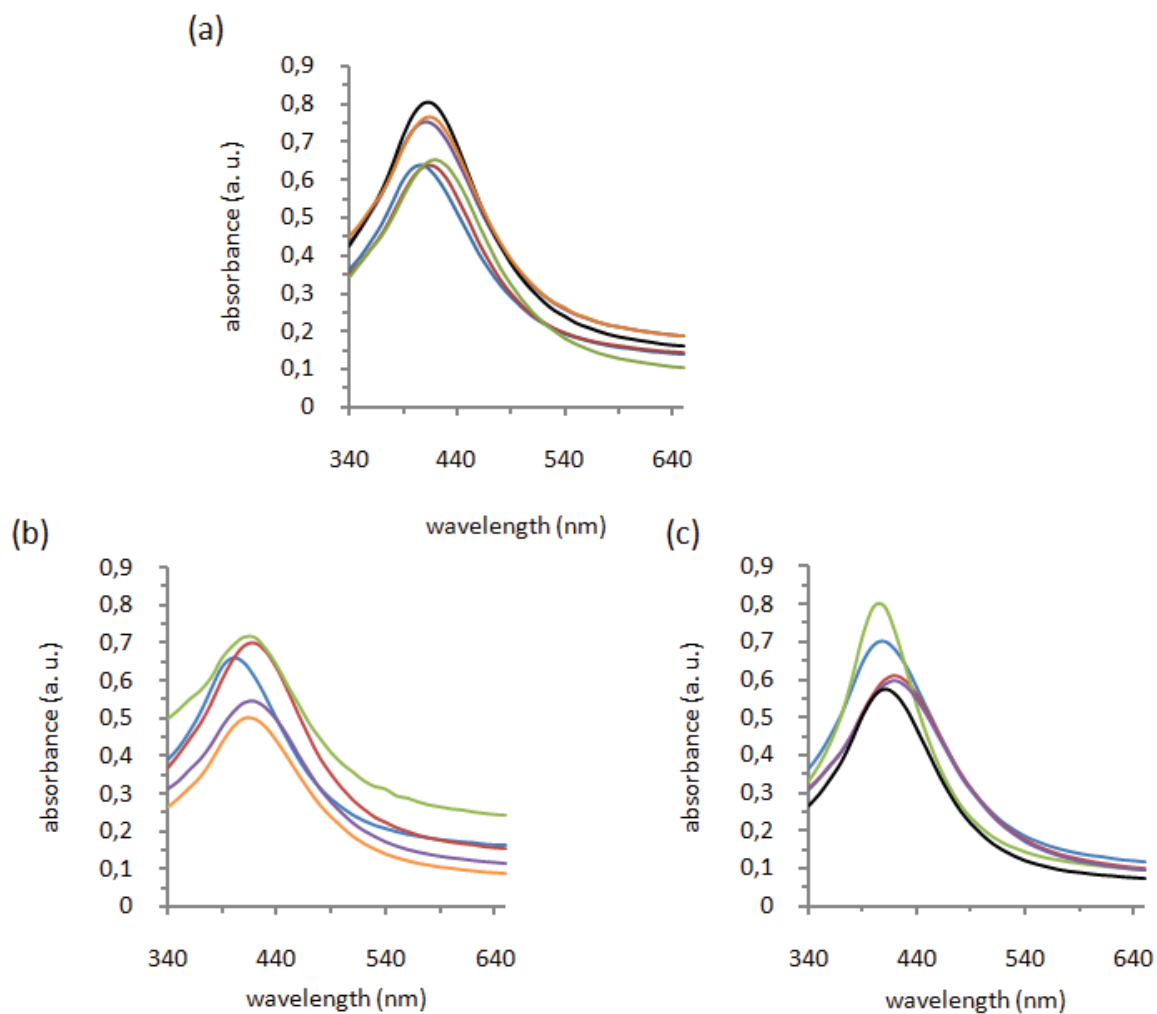


**Fig. S3** Visible spectra of the complexation of a) nucleotides, b) nucleosides and c) deoxy-nucleosides bases with SC8:Ag NPs after one hour at a final concentration of  $10^{-3}$ M. Blue line: pSC8:Ag NP; Red line: pSC8-Ag NP + A; Purple line: pSC8-Ag NP + G; Green line: pSC8-Ag NP + C; Orange line: pSC8-Ag NP + U; Black line: pSC8-Ag NP + T.

**Table S1** Summary of the wavelength absorption of SC4:Ag NPs solution

mixed one hour with each type of base

Entry	$\lambda$ 1 <sup>a</sup> (nm)	$\lambda$ 2 <sup>b</sup> (nm)	$\lambda$ 3 <sup>c</sup> (nm)	Base class
NP alone	---	390	440	
NP + adenosine	360	400	450	Nucleosides
NP + cytidine	360	400	490	
NP + guanosine	360	400	450	
NP + uridine	---	400	450	
NP + adenosine	360	400	460	Deoxy Nucleosides
NP + cytidine	360	400	---	
NP + guanosine	360	400	460	
NP + thymidine	360	400	490	
NP + adenine	360	400	520	Nucleotides
NP + cytosine	360	400	540	
NP + guanine	360	400	---	
NP + thymine	360	400	580	
NP + uracil	360	400	580	

<sup>a</sup> First wavelength absorption. <sup>b</sup> Second plasmon wavelength absorption. <sup>c</sup> Third plasmon wavelength absorption.

**Table S2** Summary of the wavelength absorption of SC4:Ag NPs solution

mixed 24 hours with each type of base

Entry	$\lambda 1^a$ (nm)	$\lambda 2^b$ (nm)	$\lambda 3^c$ (nm)	Base class
NP	---	390	440	
NP + adenosine	360	400	520	Nucleosides
NP + cytidine	360	400	520	
NP + guanosine	360	400	520	
NP + uridine	360	400	470	
NP + adenosine	360	400	470	Deoxy Nucleosides
NP + cytidine	360	400	---	
NP + guanosine	360	400	500	
NP + thymidine	360	400	520	
NP + adenine	---	---	---	Nucleotides
NP + cytosine	360	400	540	
NP + guanine	360	400	540	
NP + thymine	360	400	580	
NP + uracil	360	400	590	

<sup>a</sup> First wavelength absorption. <sup>b</sup> Second Plasmon wavelength absorption. <sup>c</sup> Thirst plasmon wavelength absorption.

## ***Supporting Information***

### **Calix-arene silver nanoparticles interactions with surfactants are charge, size and critical micellar concentration dependent**

Yannick Tauran,<sup>a,b</sup> Arnaud Brioude,<sup>a</sup> Patrick Shahgaldian,<sup>c</sup> Alessandro Cumbo,<sup>c</sup> Beomjoon Kim,<sup>b,d</sup> Florent Perret,<sup>e</sup> Anthony W. Coleman<sup>a,\*</sup> and Imed Montasser<sup>f</sup>

<sup>a</sup> LMI CNRS UMR 5615, Univ. Lyon 1, Villeurbanne, F69622, France.  
Tel: +33 4 4243 1027; E-mail: antony.coleman@adm.univ-lyon 1.fr

<sup>b</sup> LIMMS/CNRS-IIS (UMI 2820), University of Tokyo, Tokyo, Japan.

<sup>c</sup> Fachhochschule Nordwestschweiz, Hochschule für Lifesciences,  
Grüdenstrasse 40, 4132 Muttenz, Switzerland. E-mail:  
patrick.shahgaldian@fhnw.ch

<sup>d</sup> CIRMM, Institute of Industrial Science, University of Tokyo, Tokyo, Japan. E-mail: bjoonkim@iis.u-tokyo.ac.jp

<sup>e</sup> ICBMS, UMR 5246, Univ. Lyon 1, Villeurbanne, F69622, France.  
Tel: +33 4 2623 4404 ; E-mail: florent.perret@univ-lyon1.fr

<sup>f</sup> Institut National de Recherche et d'Analyse physico-chimique Technopôle de Sidi Thabet, Tunisia. E-mail : imed.montasser@inrap.rnrt.tn

**Contents:**

- **Experimental details**
- **Supporting figures**

## Experimental details:

### Synthesis of *para*-sulphonato-calix[n]arene

#### Materials and reagents

All chemicals were purchased from Acros Organics or Sigma Aldrich and used without further purification. The starting materials, calix[n]arenes, were prepared by debutylation of *para*-*t*-butylcalix[n]arenes, using the procedure described by Gutsche. [1] Solvents were of chemical grade and were used without any purification. The structure and purity of the products were verified by <sup>1</sup>H NMR spectroscopy at 300K using a Bruker 300 MHz, D<sub>2</sub>O as solvent. All products were also characterised by electrospray mass spectroscopy, using a Perkin-Elmer Sciex spectrometer.

#### General procedure for the preparation of *para*-sulphonato-calix[n]arenes SC4a, SC6a and SC8a

*para*-sulphonatocalix[n]arenes have been synthesized according to the procedure described by Shinkai *et al.* [2]

Calix[n]arenes (3 mmol) was mixed with concentrated sulfuric acid (10ml) and the solution was heated at 60°C for 24h. The completion of the reaction is followed by withdrawing an aliquot from the reaction mixture into water. When no water insoluble material was detected, the reaction was completed. After cooling, the reaction mixture is added on diethyl

ether solution for precipitating the sulfonato-calix[n]arene. After filtration, the reaction was washed with cold acetone and dried under vacuum.

All the NMR, Mass spectra and I.R. spectra were conform to literature data.

**Calix[4]arene-*para*-tetrasulphonic acid SC4a**

Yield 95% , m.p. > 300 °C, IR.  $\nu$  (cm<sup>-1</sup>): 3430 (OH), 1040 and 1178 ( SO), 1H

NMR ( D<sub>2</sub>O, 300MHz)  $\delta$  (ppm) : 4.12 (8 H, s, ArCH<sub>2</sub>Ar) and 7.74 (8 H, s, ArH),

ES m/z [M+H]<sup>+</sup>: 745,2 (100,0%), [M+Na]<sup>+</sup>: 767,3 (57,0%)

**Calix[6]arene-*para*-hexasulphonic acid SC6a**

Yield 80% , m.p. > 300 °C, IR.  $\nu$  (cm<sup>-1</sup>): 3430 (OH), 1045 and 1190 ( SO), 1H

NMR ( D<sub>2</sub>O, 300MHz)  $\delta$  (ppm) : 4.10 (12 H, bs, ArCH<sub>2</sub>Ar) and 7.65 (12 H, s,

ArH), ES m/z [M+H]<sup>+</sup>: 745,2 (100,0%), [M+Na]<sup>+</sup>: 767,3 (57,0%), ES m/z

[M+H]<sup>+</sup>: 1119,1 (100,0%), [M+Na]<sup>+</sup>: 1131,3 (35,0%)

**Calix[8]arene-*para*-octasulphonic acid SC8a**

Yield 85%, m.p. > 300 °C, IR.  $\nu$  (cm<sup>-1</sup>): 3425 (OH), 1050 and 1190 ( SO), 1H

NMR ( D<sub>2</sub>O, 300MHz)  $\delta$  (ppm) : 4.11 (16 H, bs, ArCH<sub>2</sub>Ar) and 7.61 (16 H, s,

ArH); ES m/z [M+H]<sup>+</sup>: 1489,2 (100,0%), [M+Na]<sup>+</sup>: 1511,4 (51,0%).

**General procedure for the preparation of calix[n]arenes propane-3-sulphonic acid. SC4b, SC6b, SC8b**

Compounds SCnb were synthesized by the reaction of these calix[n]arenes

with propane-1,3-sultone described for t-Bu calix[6]arene by Shinkai et al.

[3]

Calix[n]arene (2 mmol) was dissolved in tetrahydrofuran (THF) (100 ml) at 50°C under a stream of nitrogen. After cooling, sodium hydride (5eq. per hydroxyl group) was added and the mixture was stirred until evolution of hydrogen ceased (ca. 1 h). Propane- 1,3-sultone (3eq. per hydroxyl group) was then added dropwise and the mixture was stirred at room temperature for 24 h. Remaining NaH was decomposed by addition of methanol, after which the solvent was evaporated under reduced pressure, and the residue dissolved in hot water (500 ml). Any insoluble material was removed by centrifugation. Finally, SCnb was precipitated by the salting-out method with sodium acetate: yielding to a precipitate. After drying and purification by preparative HPLC, the desired compound in acidic form is obtained in good yield.

**Calix[4]aryloxy-25,26,27,28-tetrakis(propane-3-sulphonic acid) SC4b**

Yield 45%, m.p. > 300°C; <sup>1</sup>H NMR ( D<sub>2</sub>O, 300MHz) δ (ppm) : 2.22 (8H, m,

CH<sub>2</sub>CH<sub>2</sub>O), 2.96 (8H, t, CH<sub>2</sub>S), 3.25 and 4,36 (8H, 2 x d, ArCH<sub>2</sub>Ar), 4.04(8H, t,

OCH<sub>2</sub>), 6.59 (4H, s, ArH<sub>para</sub>), 6,75 (8H, s, ArH<sub>meta</sub>); <sup>13</sup>C NMR ( D<sub>2</sub>O,

100MHz) δ (ppm) : 25.56 (O-CH<sub>2</sub>-CH<sub>2</sub>), 31.06 (Ar-CH<sub>2</sub>-Ar), 48.28 (CH<sub>2</sub>-S),

73.54 (CH<sub>2</sub>-O-Ar), 128.66 (*para*C-Ar), 135.35 (*meta*C-Ar), 156.26 (*ortho*C-Ar),

181.91 (ArC-O-CH<sub>2</sub>); ES m/z neg [M-H]<sup>-</sup>: 911.3 (100,0%)

**Calix[6]aryloxy-37,38,39,40,41,42-hexakis(propane-3-sulphonic acid)  
SC6b**

Yield 35%, m.p. > 300°C; <sup>1</sup>H NMR (D<sub>2</sub>O, 300MHz) δ (ppm) : 1.80 (12H, m, CH<sub>2</sub>CH<sub>2</sub>O), 2.81 (12H, t, CH<sub>2</sub>S), 3.39 (12H, d, O-CH<sub>2</sub>), 3.81(12H, bs, ArCH<sub>2</sub>Ar), 6.69 (6H, s, ArH<sub>para</sub>), 6.75 (12H, s, ArH<sub>meta</sub>); <sup>13</sup>C NMR ( D<sub>2</sub>O, 100MHz) δ(ppm) : 25.60 (O-CH<sub>2</sub>-CH<sub>2</sub>), 30.77 (Ar-CH<sub>2</sub>-Ar), 48.31 (CH<sub>2</sub>-S), 71.80 (CH<sub>2</sub>-O-Ar), 114.78 (*para*C-Ar), 118.65 (*meta*C-Ar), 134.53 (*ortho*C-Ar), 163.17 (ArC-O-CH<sub>2</sub>); ES m/z neg [M-H]<sup>-</sup> : 1367.2 (100,0%)

**Calix[8]aryloxy-49,50,51,52,53,54,55,56-octakis(propane-3-sulphonic acid) SC8b**

Yield 23%, m.p. > 300°C; <sup>1</sup>H NMR (D<sub>2</sub>O, 300MHz) δ (ppm) : 2.04 (16H, m, CH<sub>2</sub>CH<sub>2</sub>O), 2.84 (16H, t, CH<sub>2</sub>S), 3.60 (16H, d, O-CH<sub>2</sub>), 3.74 (16H, bs, ArCH<sub>2</sub>Ar), 6.79 (8H, s, ArH<sub>para</sub>), 6.92 (16H, s, ArH<sub>meta</sub>); <sup>13</sup>C NMR ( D<sub>2</sub>O, 100MHz) δ(ppm) : 25.63 (O-CH<sub>2</sub>-CH<sub>2</sub>), 32.57 (Ar-CH<sub>2</sub>-Ar), 48.51 (CH<sub>2</sub>-S), 71.80 (CH<sub>2</sub>-O-Ar), 116.70 (*para*C-Ar), 118.80 (*meta*C-Ar), 134.35 (*ortho*C-Ar), 164.07 (ArC-O-CH<sub>2</sub>); ES m/z neg [M-H]<sup>-</sup> : 1823.6(20,0%), [M-2H]<sup>2-</sup> : 911.9 (100,0%).

**General procedure for the preparation of *para*-sulphonatocalix[n]arene propane-3-sulphonic acids. SC4c, SC6c, SC8c.**

*para*-sulphonato-calix[n]arene propane-3-sulphonic acids ( SCnc) have been prepared following the procedure described by Hwang et al. [4] and adapting the procedure of Shinkai et al. [5]

*para*-sulphonato calix[n]arene (SCna) (2 mmol) was mixed with NaOH (10 eq. per OH group) in DMSO (15 mL) . Propane- 1,3-sultone (3eq. per hydroxyl group) was then added dropwise and the mixture was heated at

60°C for 2 days. DMSO is then distilled under reduced pressure. The obtained orange solid is dissolved in a minimum of water and then the product was precipitated from the solution by diluting with ethanol. This operation was repeated 3 times in order to remove inorganic salts. The obtained precipitate is filtered off, dried under vacuum and purified on HPLC.

***para*-sulphonato-calix[4]aryloxy-25,26,27,28-tetrakis-(propane-3-sulphonic acid) SC4c**

Yield 35%, m.p. 20°C; <sup>1</sup>H NMR (D<sub>2</sub>O, 300MHz) δ (ppm) 2.27 (8H, m, CH<sub>2</sub>CH<sub>2</sub>O), 3.32 (8H, t, SCH<sub>2</sub>), 3.75 (8H, bs, ArCH<sub>2</sub>Ar), 3.94 (8H, t, OCH<sub>2</sub>), 7.43 (8H, s, ArH), ES m/z neg [M-H]<sup>-</sup>: 1231.3 (60,0%), [M-2H]<sup>2-</sup>: 615.1 (100,0%).

***para*-sulphonato-calix[6]aryloxy-37,38,39,40,41,42-hexakis-propane-3-sulphonic acid) SC6c**

Yield 20%, m.p. > 290°C; <sup>1</sup>H NMR (D<sub>2</sub>O, 300MHz) δ (ppm) 2.18 (12H, m, CH<sub>2</sub>CH<sub>2</sub>O), 3.36 (12 H, t, SCH<sub>2</sub>), 3.74 (12H, t, OCH<sub>2</sub>), 4.05 (12H, bs, ArCH<sub>2</sub>Ar), 7.53 (12H, s, ArH)  
ES m/z neg [M-H]<sup>-</sup>: 1849.1 (50,0%), [M-2H]<sup>2-</sup>: 924,1 (100,0%).

***para*-sulphonato-calix[8]aryloxy-49,50,51,52,53,54,55,56-octakis-(propane-3-sulphonic acid) SC8c**

Yield 23%, m.p. > 300°C; <sup>1</sup>H NMR (D<sub>2</sub>O, 300MHz) δ (ppm) : 2.14 (16H, m, CH<sub>2</sub>CH<sub>2</sub>O), 3.18 (16H, t, SCH<sub>2</sub>), 3.66 (16H, d, O-CH<sub>2</sub>), 4.04 (16H, bs, ArCH<sub>2</sub>Ar),

7.59 (16H, s, ArH). ES m/z neg  $[M-H]^-$  : 2463.1 (45,0%),  $[M-2H]^{2-}$  : 1231.1 (100,0%).

## **Synthesis of sulphonato-calix[n]arene modified silver nanoparticles**

The procedure of Xiong[6] was slightly modified as follows. 10 mL of  $10^{-2}$  M  $AgNO_3$  solution was added to 80 mL of deionized water. To this solution, 10 mL of  $10^{-2}$  M of the various sulphonato-calix[n]arene aqueous solutions were added as stabilizers with stirring for 30 min. And then, 44 mg of  $NaBH_4$  was added to the solution. The colloidal silver I suspensions were obtained after 5 minutes.

## **UV-Visible Absorption assays**

The mixture experiments were conducted by monitoring the change in absorbance between 340 nm and 650 nm, using a 96 well titre visible spectrometer, (BioTek Power Wave 340).

## **DLS experiments**

Particle size measurements were performed on a Zetasizer Nano ZS (Malvern Instruments, UK) with an angle of detection of  $90^\circ$ . The measurements were done in triplicate. The average hydrodynamic diameter (or Z average) was determined using the cumulant analysis provided by the instrument software with the assumption of spherical particles.

## **SEM experiments**

Samples for SEM acquisitions were prepared by spreading 3  $\mu$ l of the nanoparticle suspensions on freshly cleaved mica surfaces. After drying at room temperature and Au-Pd sputter coating (15s at 15mA), micrographs were acquired using a Supra 40V system (Carl Zeiss, Switzerland) at an accelerating voltage of 20 kV using an in-lens detector. Statistical size measurements were performed measuring the diameter of at least 50 nanoparticles using the analysis<sup>®</sup> (Olympus, Germany) software package.

## References and Note

- [1] I. C. D. Gutsche and L.-G. Lin, *Tetrahedron*, 1986, 42, 1633.
- [2] S. Shinkai, K. Araki, T. Tsubaki, T. Arimura, and O. Manabe, *J. Chem. Soc. Perkin Trans. 1*, 1987, 2297-2299
- [3] S. Shinkai, T. Arimura, K. Araki, and H. Kawabata, *J. Chem. Soc. Perkin Trans. 1*, 1989, 2039-2045
- [4] K.M. Hwang et al., Antithrombotic treatment with calixarene compounds, 1995, US54099959, p.46
- [5] Shinkai, S. Mori, H. Koreishi, T. Tsubaki and O. Manabe, *J. Am. Chem. Soc.*, 1986, 2409-2416
- [6] D. Xiong, M. Chen and H. Li, *Chem. Commun.*, 2008, 7, 880-882;
- [7] T. V. Kharitonova, N. I. Ivanova, B. D. Summ, *Colloid J.*, 2002, 64, 620-630.

## Supporting Figures:

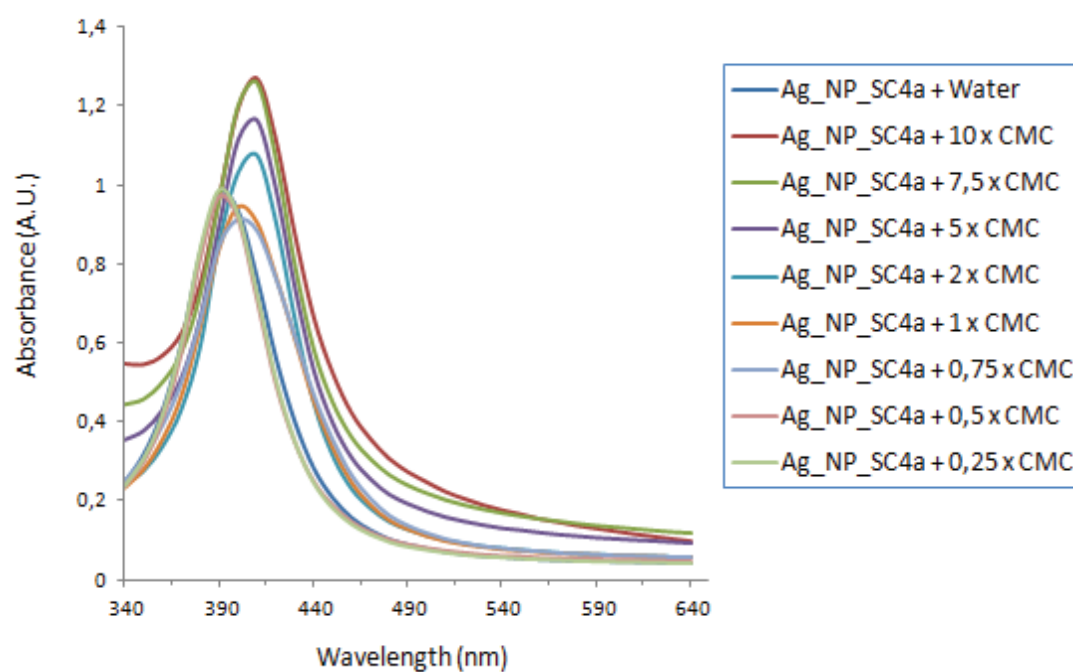


**Fig. S1** UV-Visible spectra of *para*-sulphonato-calix[4]arene capped silver nanoparticles (Ag\_NP\_SC4a) as a function of cetyl pyridinium bromide concentration.

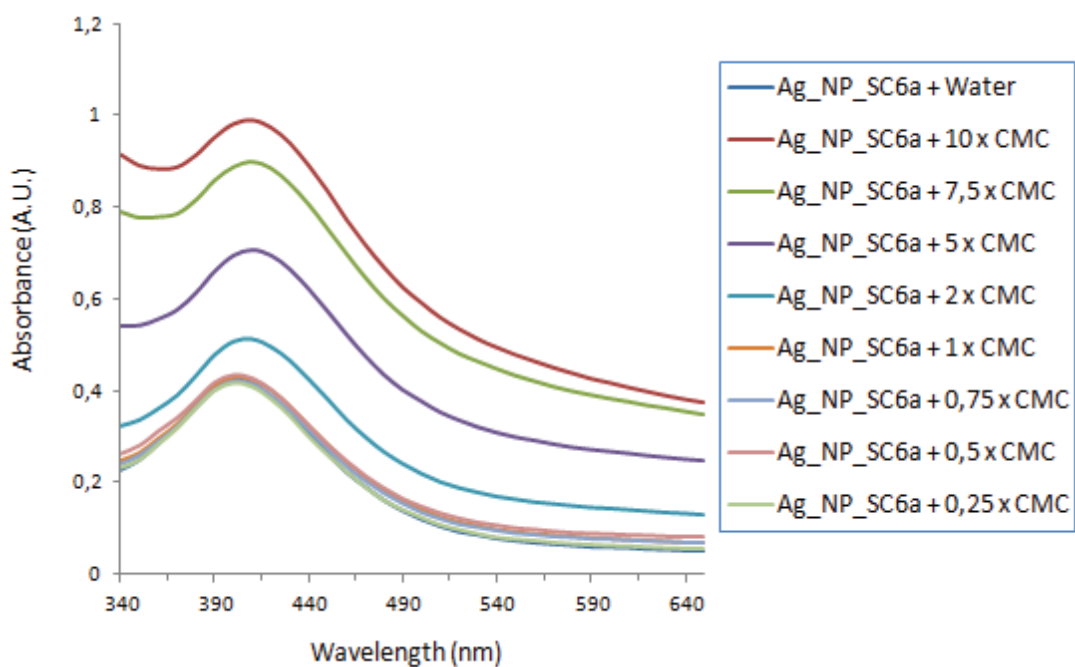


**Fig. S2** UV-Visible spectra of *para*-sulphonato-calix[6]arene capped silver nanoparticles (Ag\_NP\_SC6a) as a function of cetyl pyridinium bromide concentration.

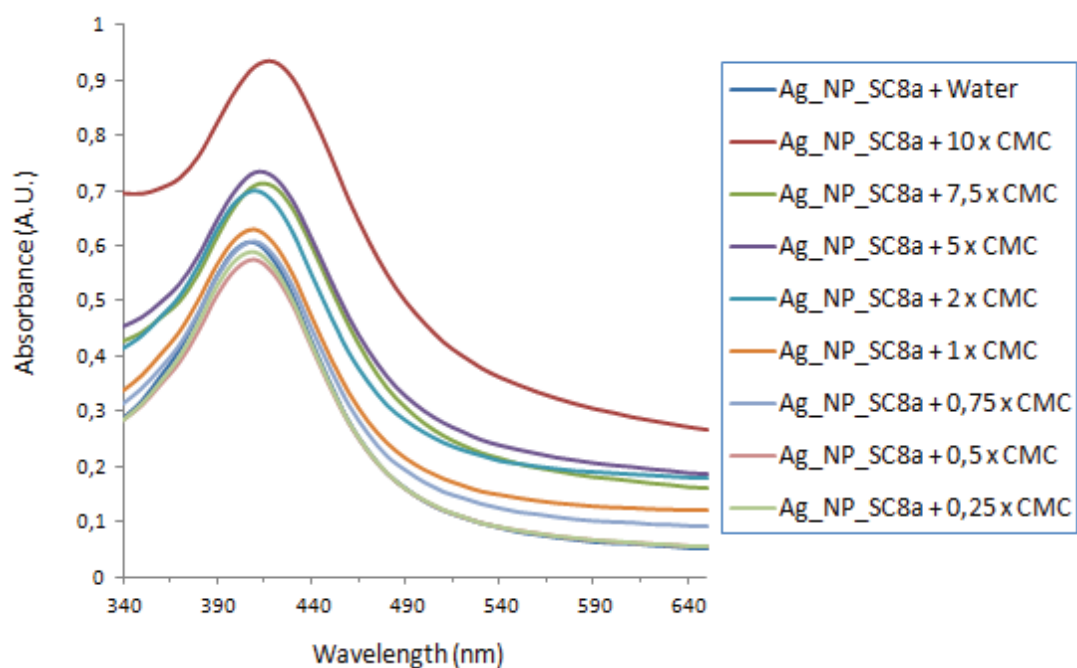


**Fig. S3** UV-Visible spectra of *para*-sulphonato-calix[8]arene capped silver nanoparticles (Ag\_NP\_SC8a) as a function of cetyl pyridinium bromide concentration.

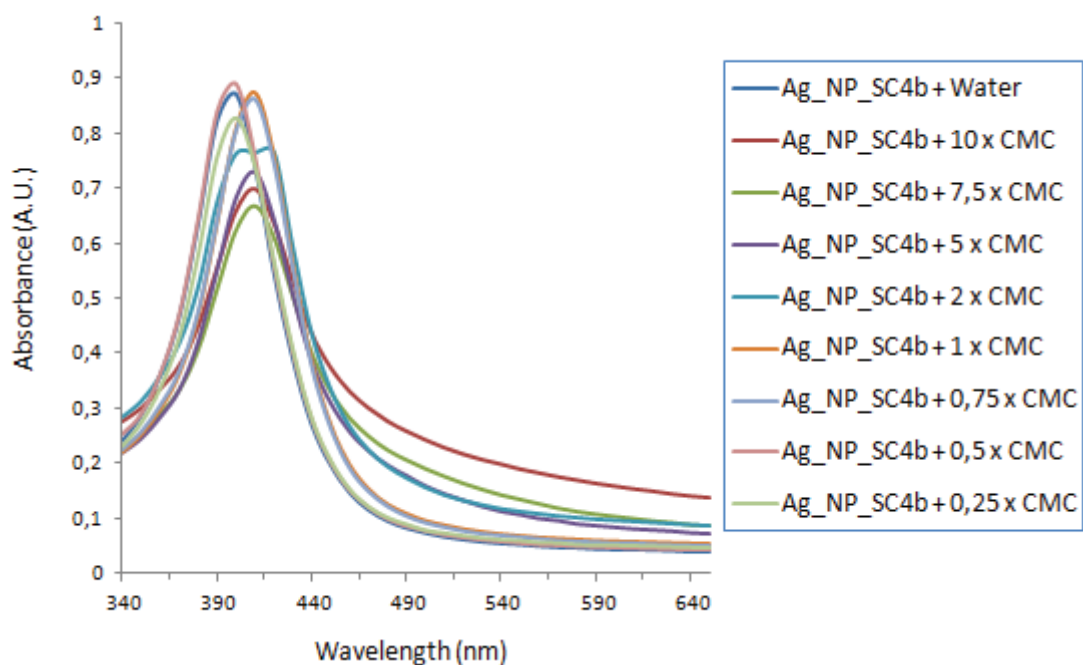


**Fig. S4** UV-Visible spectra O-propoxysulphonate -calix[4]arene capped silver nanoparticles (Ag\_NP\_SC4b) as a function of cetyl pyridinium bromide concentration.

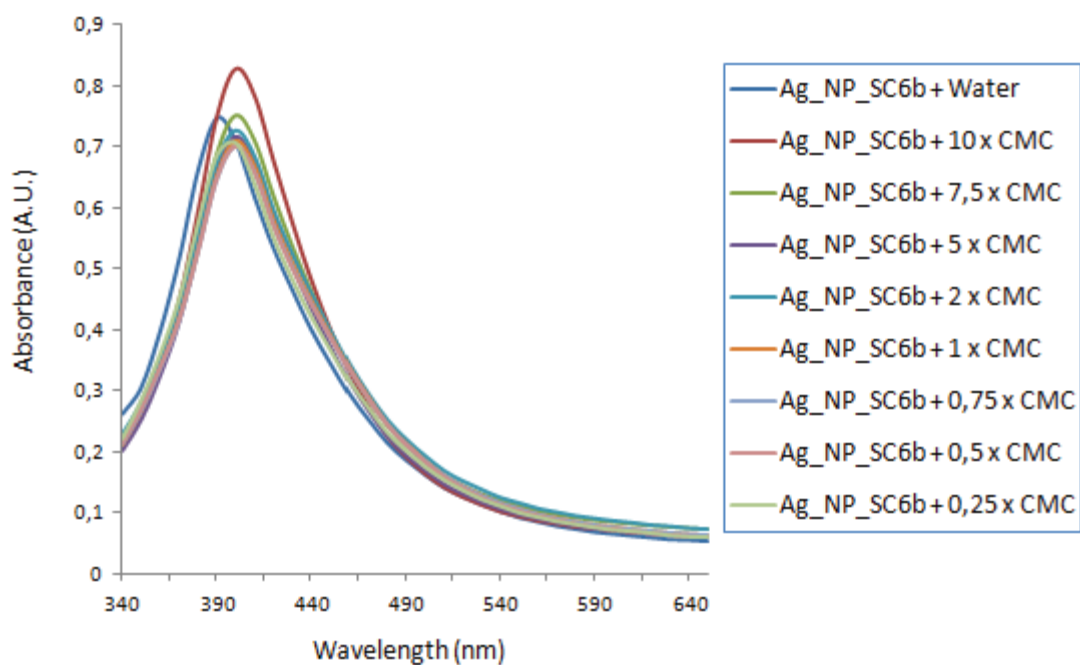


**Fig. S5** UV-Visible spectra of O-propoxysulphonate -calix[6]arene capped silver nanoparticles (Ag\_NP\_SC6b) as a function of cetyl pyridinium bromide concentration.

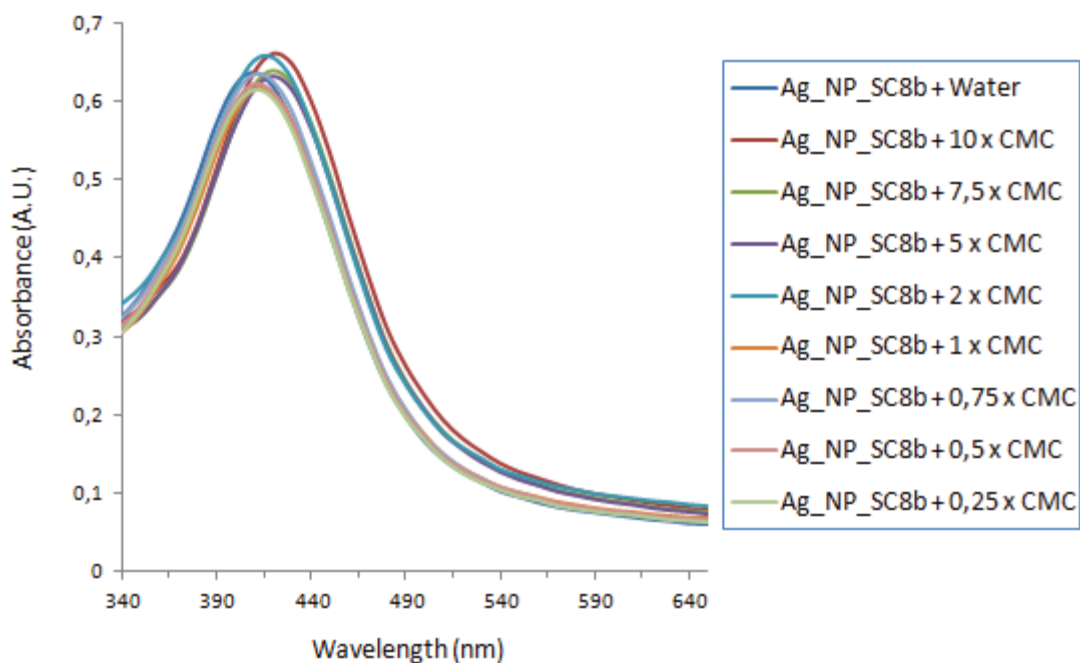


**Fig. S6** UV-Visible spectra of O-propoxysulphonate-calix[8]arene capped silver nanoparticles (Ag\_NP\_SC8b) as a function of cetyl pyridinium bromide concentration.

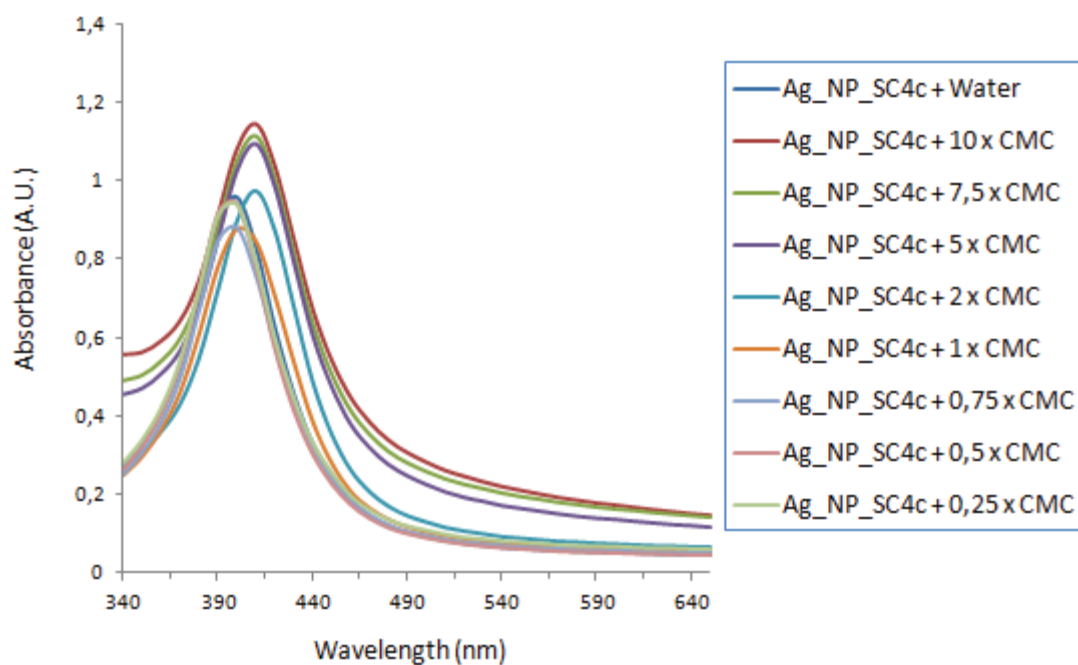


**Fig. S7** UV-Visible spectra of *para*-sulphonato-calix[4]arene O-propoxysulphonate capped silver nanoparticles (Ag\_NP\_SC4c) as a function of cetyl pyridinium bromide concentration.

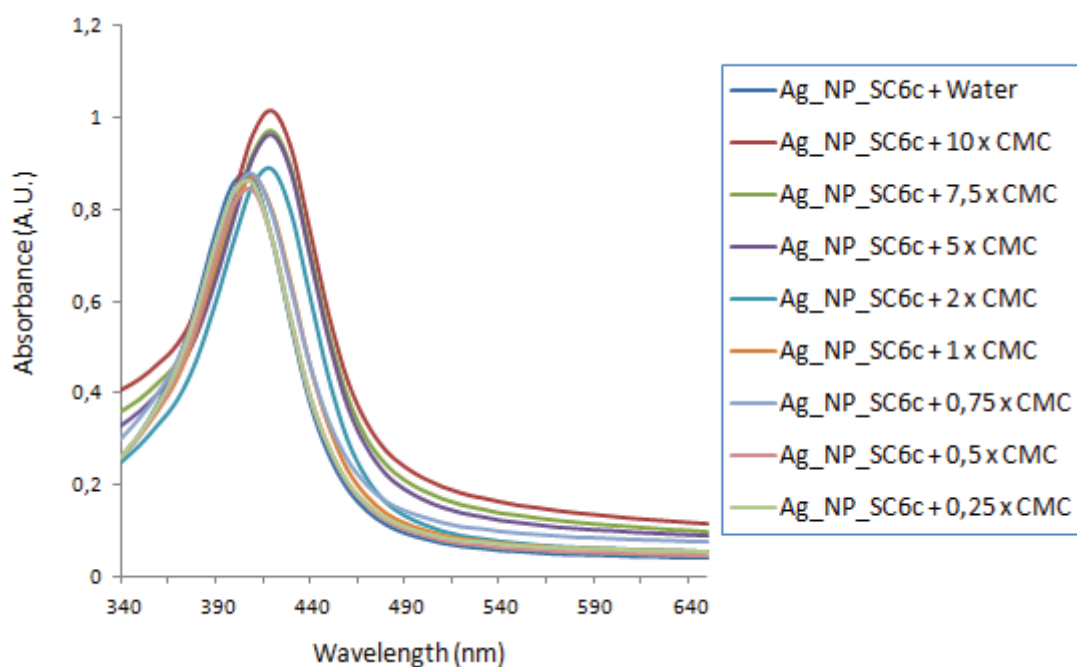


**Fig. S8** UV-Visible spectra of *para*-sulphonato-calix[6]arene O-propoxysulphonate capped silver nanoparticles (Ag\_NP\_SC6c) as a function of cetyl pyridinium bromide concentration.

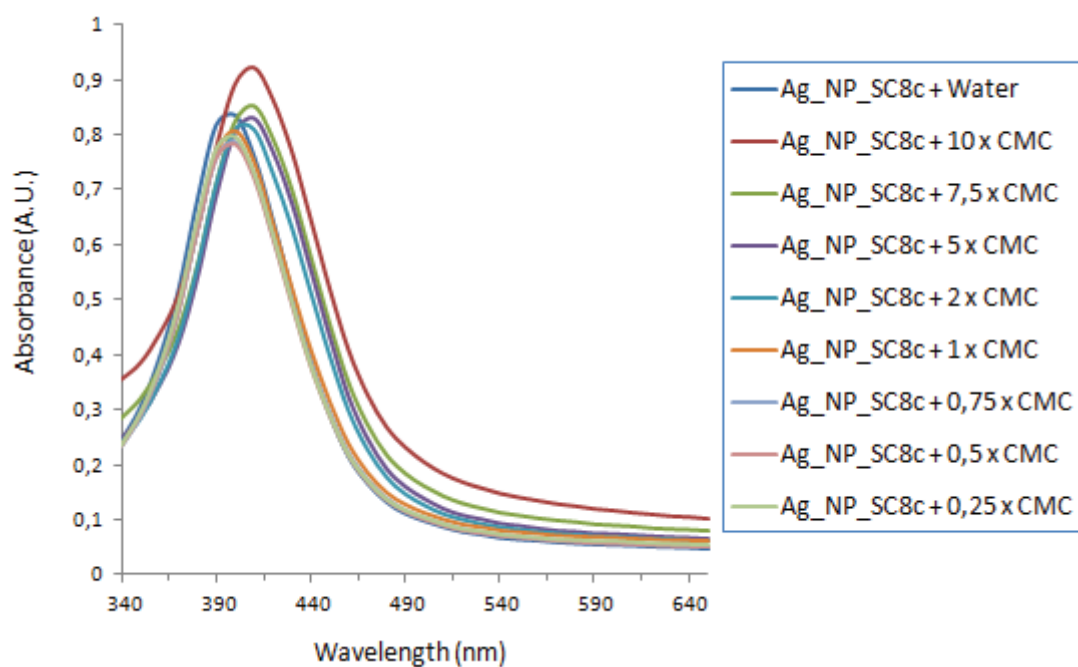


**Fig. S9** UV-Visible spectra of *para*-sulphonato-calix[8]arene O-propoxysulphonate capped silver nanoparticles (Ag\_NP\_SC8c) as function of cetyl pyridinium bromide concentration.

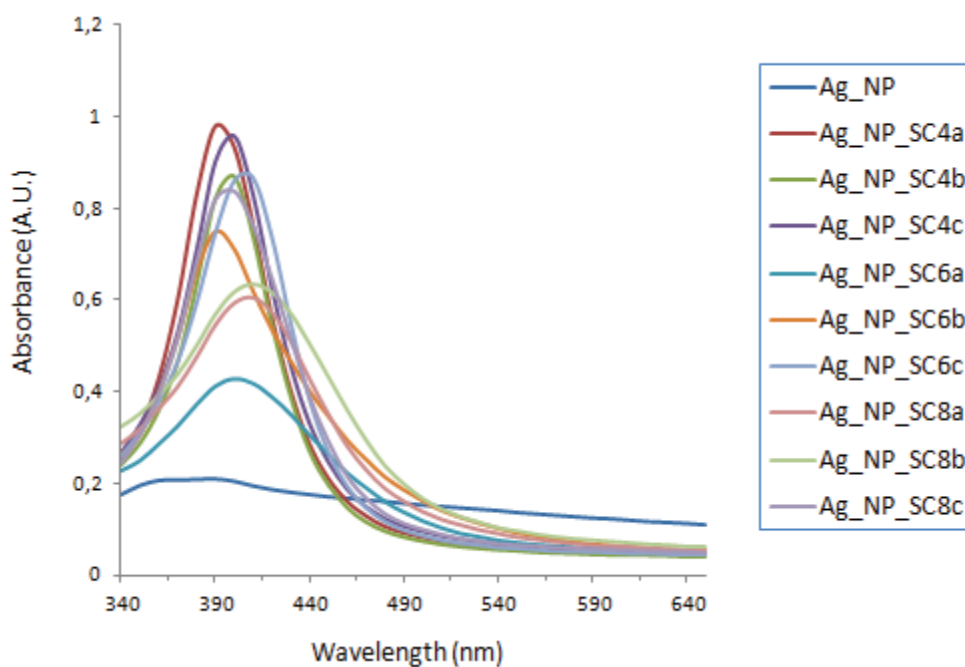


**Fig. S10** UV-Visible spectra of calix[n]arene capped silver nanoparticles after one hour of their preparations. Ag\_NP represents a solution of silver nitrate reduced by  $\text{NaBH}_4$  in the absence of calix[n]arene as stabilizer.

## Electron Microscopy

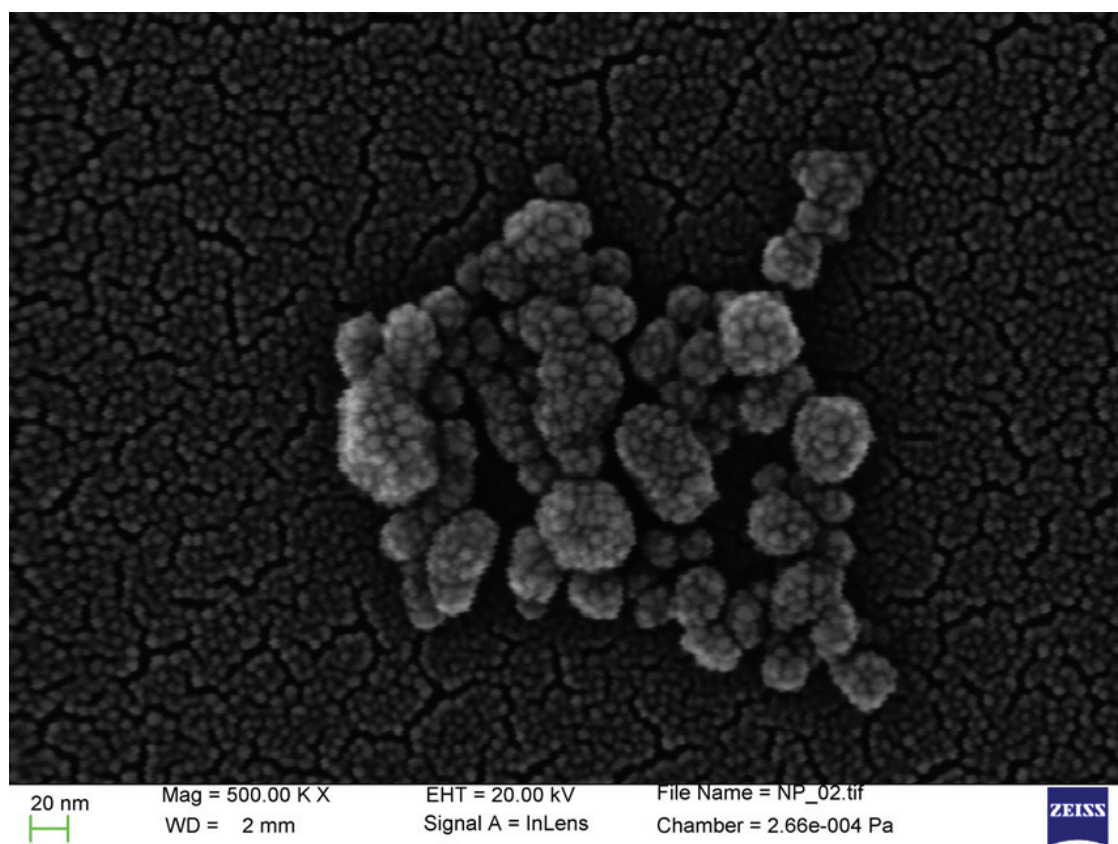


**Fig. S11** SEM image of Ag\_NP\_SC4a

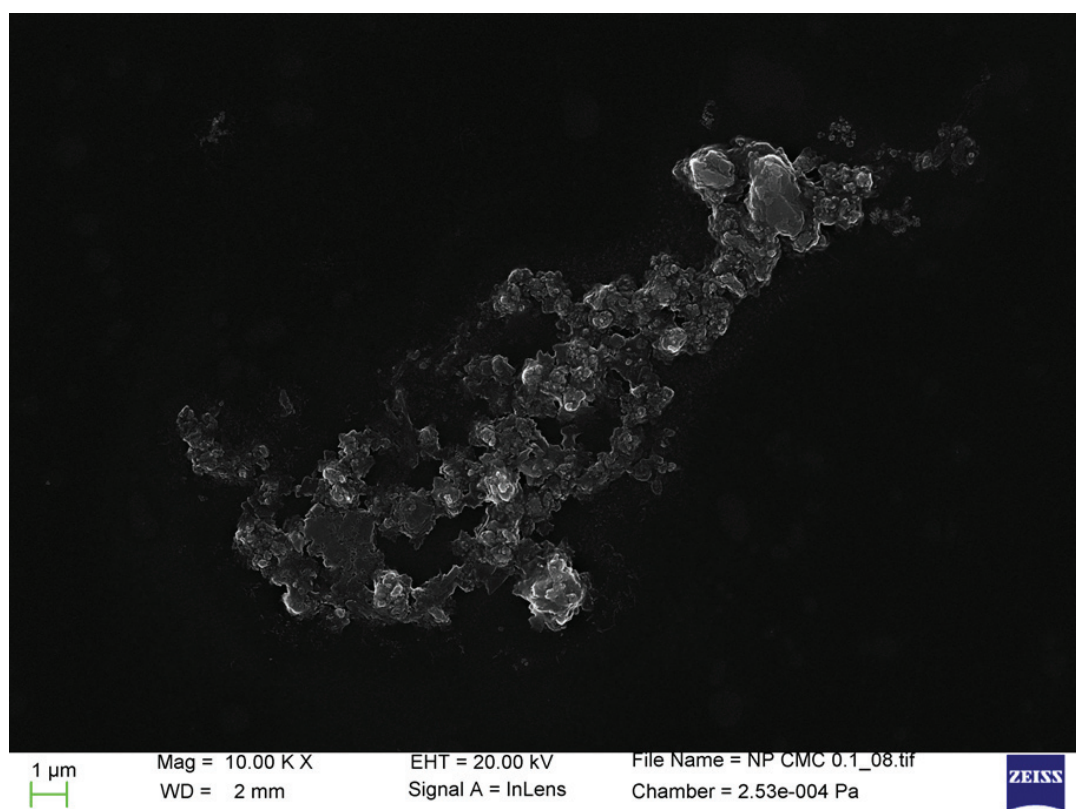


**Fig. S12** SEM image of Ag\_NP\_SC4a mixed with of cetyl pyridinium bromide  
at 0.1 x CMC (ratio surfactant:nanoparticle = 1:1)

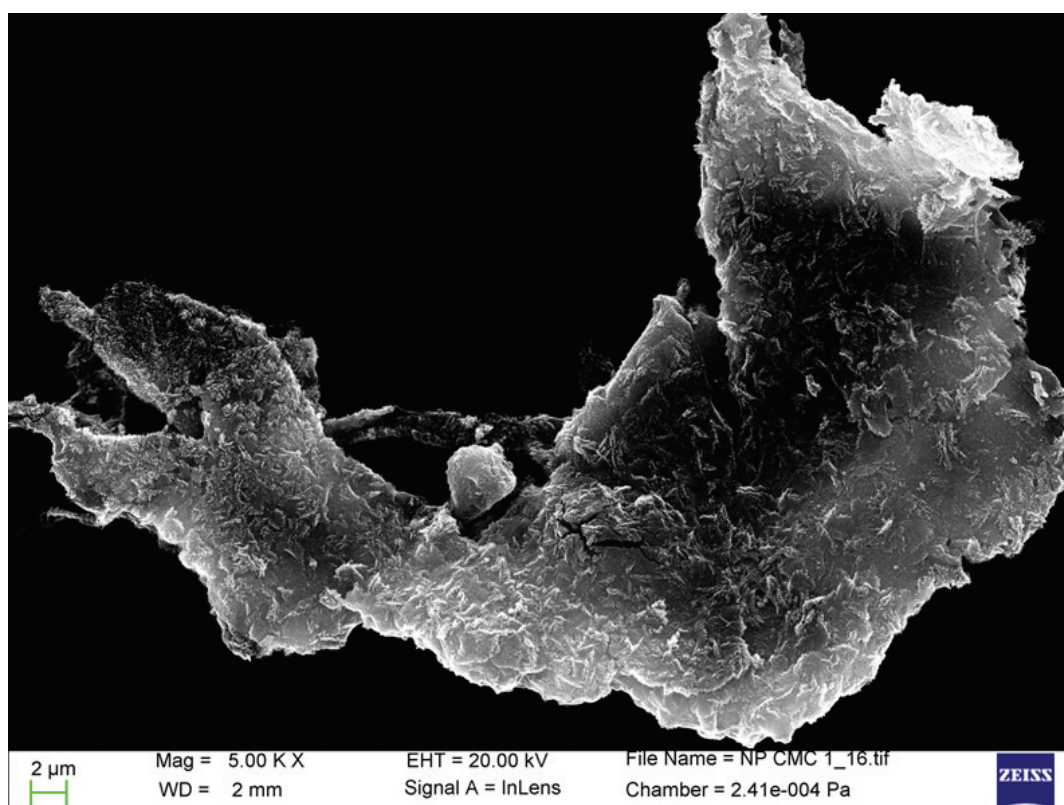


**Fig. S13** SEM image of Ag\_NP\_SC4a mixed with of cetyl pyridinium bromide at 1 x CMC (ratio surfactant:nanoparticle = 10 : 1)

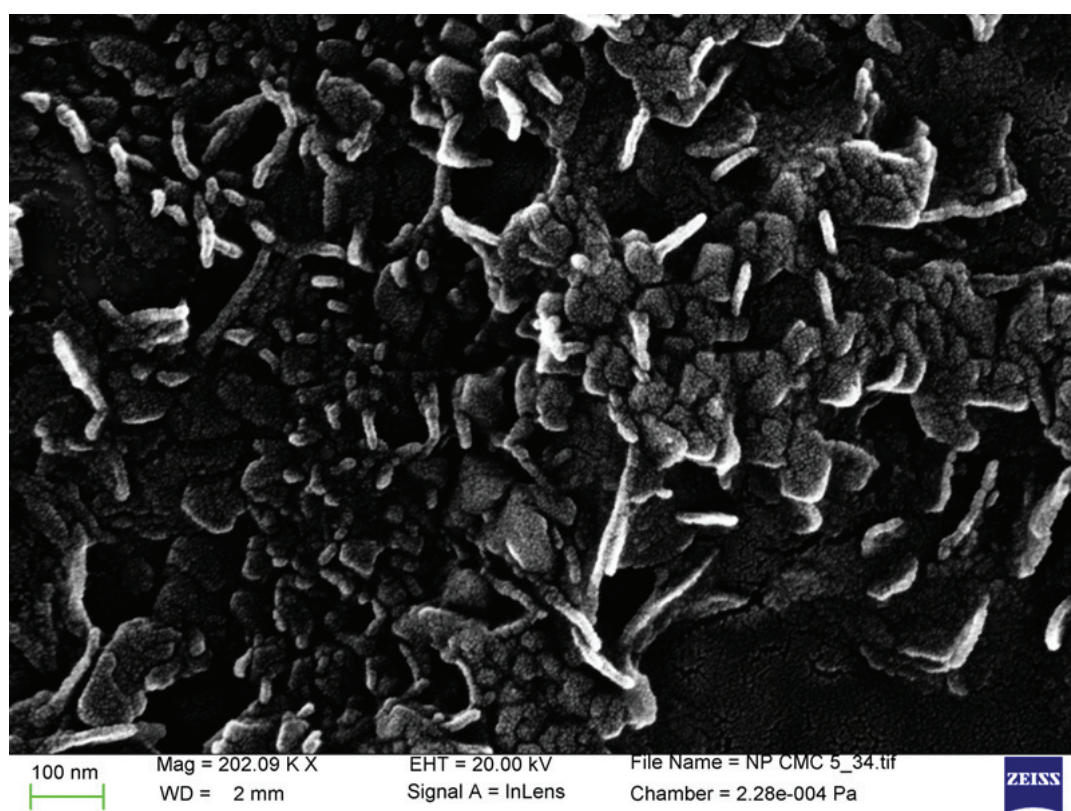


**Fig. S14** SEM image of Ag\_NP\_SC4a mixed with cetyl pyridinium bromide at 5  
x CMC (ratio surfactant:nanoparticle 50 : 1)

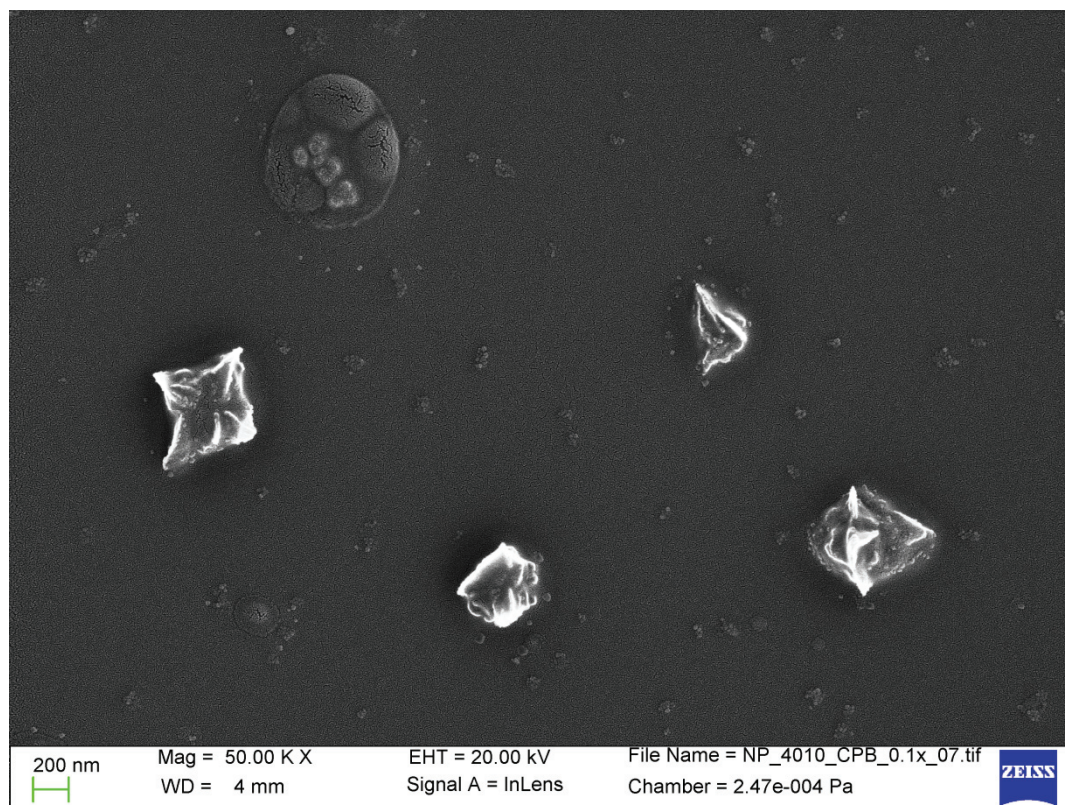


**Fig. S15** SEM images of Ag\_NP\_SC4b mixed with cetyl pyridinium bromide at  
0.1 x CMC (ratio surfactant:nanoparticle 1: 1)

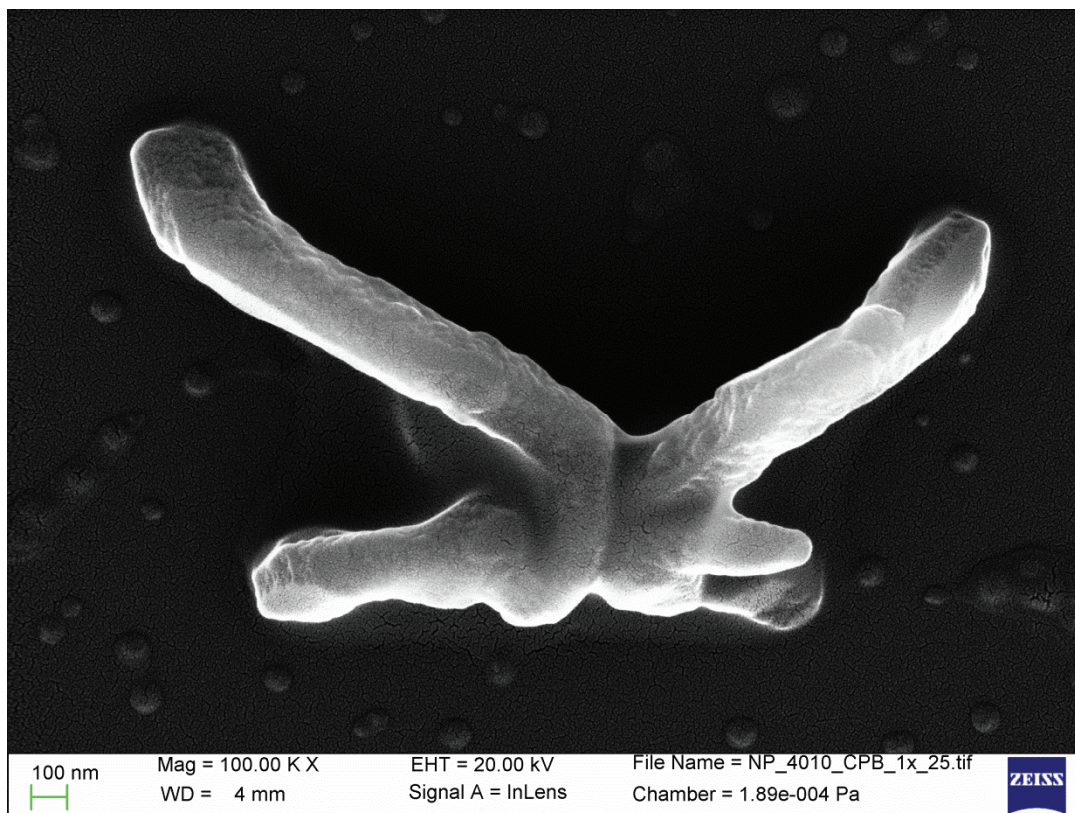


**Fig. S16** SEM images of Ag\_NP\_SC4b mixed with cetyl pyridinium bromide at  
1 x CMC (ratio surfactant:nanoparticle 10 : 1)

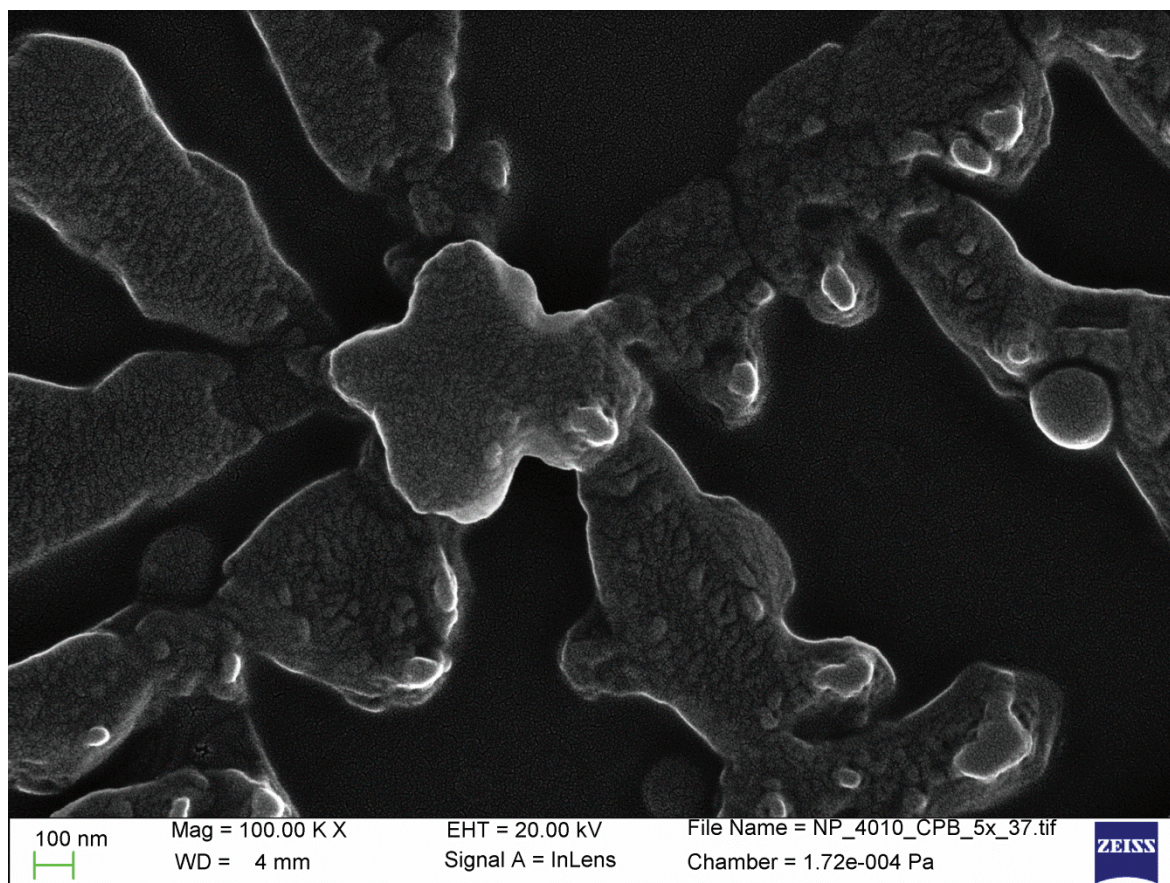


**Fig. S17** SEM images of Ag<sub>NP</sub>\_SC4b mixed with cetyl pyridinium bromide at 5 x CMC (ratio surfactant:nanoparticle 50 : 1)

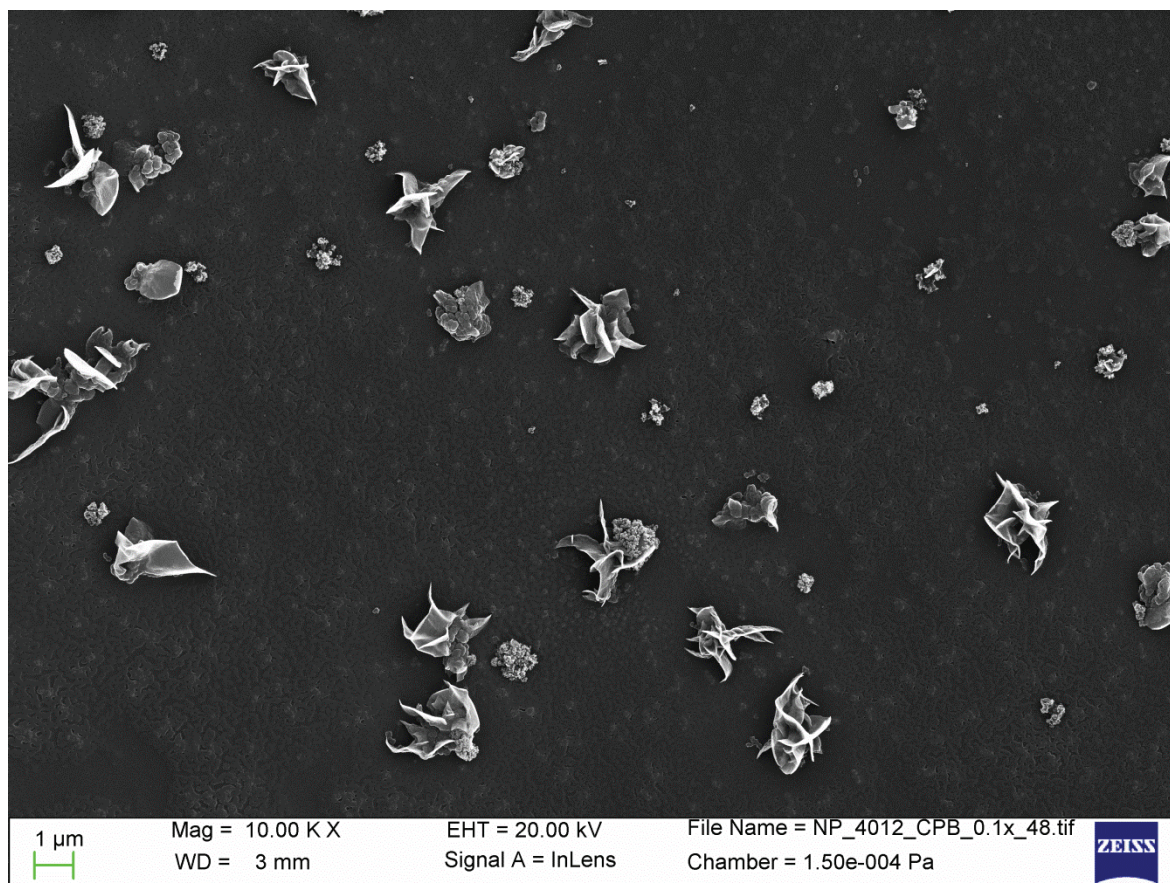


**Fig. S18** SEM images of Ag\_NP\_SC4c mixed with cetyl pyridinium bromide at 0.1 x CMC (ratio surfactant:nanoparticle 1: 1)

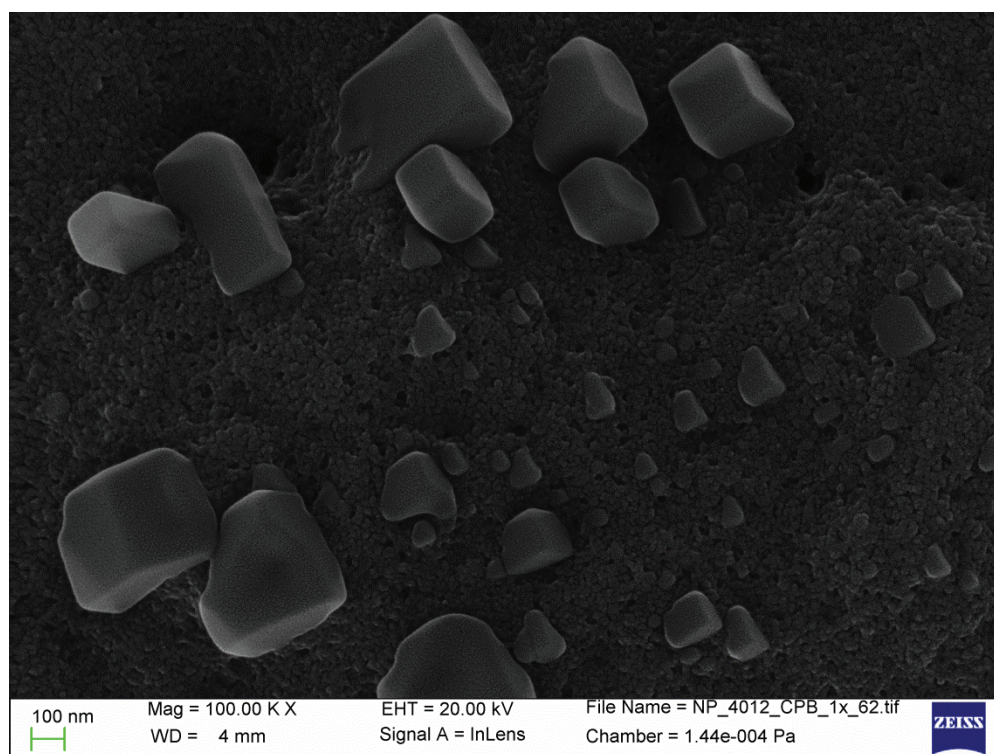


**Fig. S19** SEM images of Ag\_NP\_SC4c mixed with cetyl pyridinium bromide at  
1 x CMC (ratio surfactant:nanoparticle 10 : 1)

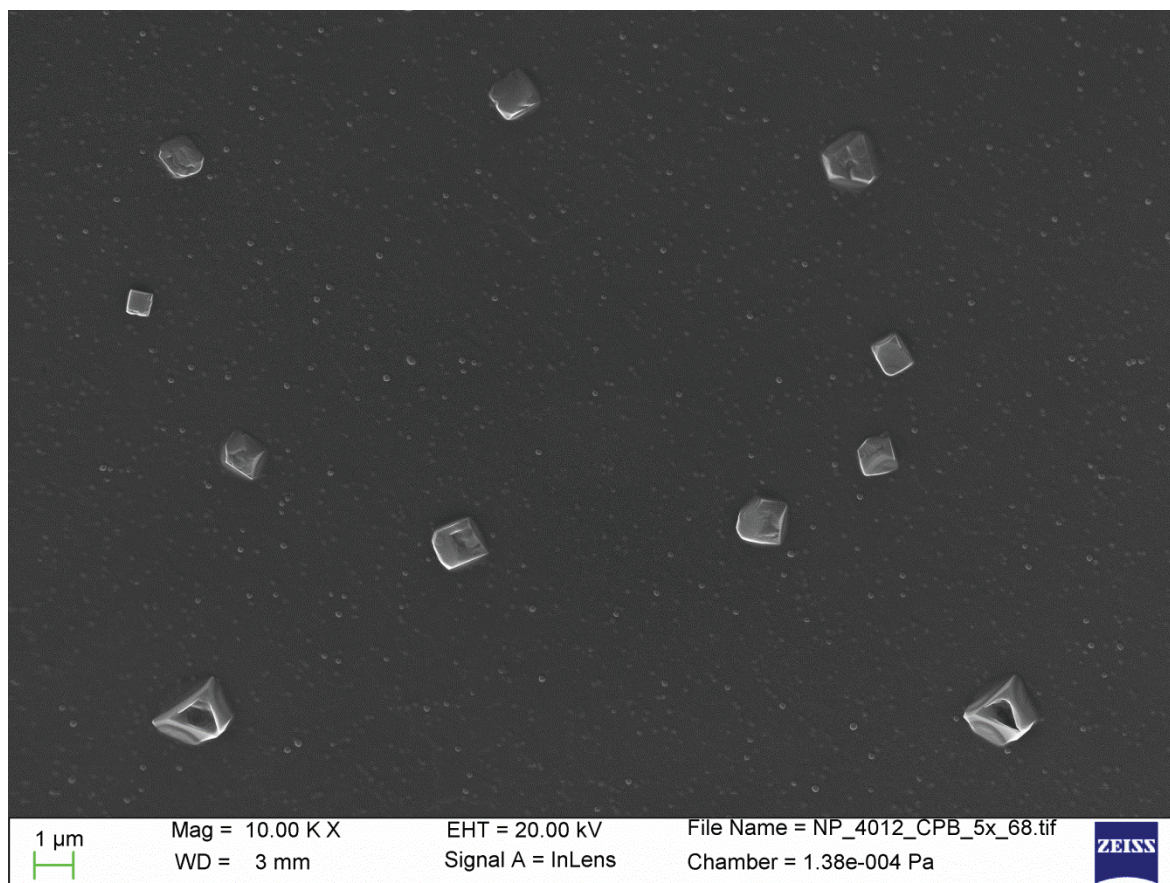


**Fig. S20** SEM images of Ag<sub>NP</sub>SC4c mixed with cetyl pyridinium bromide at  
5 x CMC (ratio surfactant:nanoparticle 50 : 1)

## Dynamic Light Scattering

Sample	Diameter (nm)	PdI
Ag_NP_SC4a	32,99 ± 6,2	0,28
Ag_NP_SC4a + CPB 5x CMC	139,13 ± 0,33	0,16
Ag_NP_SC4a + CPB 1x CMC	60,82 ± 1,2	0,53
Ag_NP_SC4a + CPB 0,1x CMC	31,2 ± 0,96	0,47
Ag_NP_SC4a + CTAB 5x CMC	445,1 ± 9,4	0,26
Ag_NP_SC4a + CTAB 1x CMC	152,2 ± 0,4	0,3
Ag_NP_SC4a + CTAB 0,1x CMC	40,39 ± 5,46	0,28

Sample	Diameter (nm)	PdI
Ag_NP_SC4b	56,98 ± 0,92	0,099
Ag_NP_SC4b + CPB 5x CMC	69,38 ± 6,26	0,717
Ag_NP_SC4b + CPB 1x CMC	41,21 ± 1,59	0,467
Ag_NP_SC4b + CPB 0,1x CMC	596,26 ± 24,96	0,409
Ag_NP_SC4b + CTAB 5x CMC	53,8 ± 17,26	0,381
Ag_NP_SC4b + CTAB 1x CMC	44,07 ± 1,45	0,447
Ag_NP_SC4b + CTAB 0,1x CMC	99,98 ± 2,02	0,572

Sample	Diameter (nm)	PdI
Ag_NP_SC4c	62,25 ± 15,48	0,086
Ag_NP_SC4c + CPB 5x CMC	146,56 ± 0,74	0,099
Ag_NP_SC4c + CPB 1x CMC	105,9 ± 0,2	0,236
Ag_NP_SC4c + CPB 0,1x CMC	42,02 ± 13,98	0,323
Ag_NP_SC4c + CTAB 5x CMC	160,1 ± 2,4	0,176
Ag_NP_SC4c + CTAB 1x CMC	88,89 ± 0,5	0,233
Ag_NP_SC4c + CTAB 0,1x CMC	49,43 ± 36,88	0,34

**Table S1** Z average of calix[4]arene capped silver nanoparticles (Ag\_NP\_SC4a, Ag\_NP\_SC4b and Ag\_NP\_SC4c) mixed with CTAB or CPB at different concentration ratio.

Sample	Diameter (nm)	PdI
Ag_NP_SC4a	32,99 ± 6,2	0,28
Ag_NP_SC4a + CPB / NOG 5x C <sup>M</sup>	140,6 ± 0,5	0,37
Ag_NP_SC4a + CPB / NOG 1x C <sup>M</sup>	77,6 ± 1,25	0,42
Ag_NP_SC4a + CPB / NOG 0,1x C <sup>M</sup>	47,1 ± 1,2	0,08
Ag_NP_SC4a + CTAB / NOG 5x C <sup>M</sup>	200,1 ± 8,2	0,21
Ag_NP_SC4a + CTAB / NOG 1x C <sup>M</sup>	128,2 ± 1,2	0,34
Ag_NP_SC4a + CTAB / NOG 0,1x C <sup>M</sup>	44,45 ± 2,1	0,1

Sample	Diameter (nm)	PdI
Ag_NP_SC4b	56,98 ± 0,92	0,099
Ag_NP_SC4b + CPB / NOG 5x C <sup>M</sup>	80,38 ± 3,05	0,469
Ag_NP_SC4b + CPB / NOG 1x C <sup>M</sup>	55,48 ± 1,53	0,475
Ag_NP_SC4b + CPB / NOG 0,1x C <sup>M</sup>	44,13 ± 0,7	0,339
Ag_NP_SC4b + CTAB / NOG 5x C <sup>M</sup>	74,55 ± 1,24	0,363
Ag_NP_SC4b + CTAB / NOG 1x C <sup>M</sup>	62,1 ± 0,32	0,276
Ag_NP_SC4b + CTAB / NOG 0,1x C <sup>M</sup>	64,43 ± 1,2	0,419

Sample	Diameter (nm)	PdI
Ag_NP_SC4c	62,25 ± 15,48	0,086
Ag_NP_SC4c + CPB / NOG 5x C <sup>M</sup>	215,36 ± 4,83	0,266
Ag_NP_SC4c + CPB / NOG 1x C <sup>M</sup>	142,43 ± 3,66	0,479
Ag_NP_SC4c + CPB / NOG 0,1x C <sup>M</sup>	112,5 ± 0,7	0,312
Ag_NP_SC4c + CTAB / NOG 5x C <sup>M</sup>	1444 ± 55	0,492
Ag_NP_SC4c + CTAB / NOG 1x C <sup>M</sup>	191,26 ± 1,74	0,24
Ag_NP_SC4c + CTAB / NOG 0,1x C <sup>M</sup>	130,23 ± 4,93	0,357

**Table S2** Z average of calix[4]arene capped silver nanoparticles (Ag\_NP\_SC4a, Ag\_NP\_SC4b and Ag\_NP\_SC4c) mixed with NOG and CTAB (or CPB) at different concentration ratio.

Sample	Diameter (nm)	PdI
Ag_NP_SC4a	32,99 ± 6,2	0,28
Ag_NP_SC4a + CPB / Triton 5x C <sup>M</sup>	159,8 ± 1,2	0,25
Ag_NP_SC4a + CPB / Triton 1x C <sup>M</sup>	46,16 ± 0,3	0,43
Ag_NP_SC4a + CPB / Triton 0,1x C <sup>M</sup>	39,22 ± 12,7	0,26
Ag_NP_SC4a + CTAB / Triton 5x C <sup>M</sup>	217,1 ± 2,1	0,24
Ag_NP_SC4a + CTAB / Triton 1x C <sup>M</sup>	140,4 ± 0,6	0,56
Ag_NP_SC4a + CTAB / Triton 0,1x C <sup>M</sup>	30,48 ± 0,8	0,5

Sample	Diameter (nm)	PdI
Ag_NP_SC4b	56,98 ± 0,92	0,099
Ag_NP_SC4b + CPB / Triton 5x C <sup>M</sup>	48,94 ± 3,65	0,46
Ag_NP_SC4b + CPB / Triton 1x C <sup>M</sup>	51,61 ± 16,76	0,34
Ag_NP_SC4b + CPB / Triton 0,1x C <sup>M</sup>	79,5 ± 0,66	0,247
Ag_NP_SC4b + CTAB / Triton 5x C <sup>M</sup>	54,02 ± 8,91	0,436
Ag_NP_SC4b + CTAB / Triton 1x C <sup>M</sup>	41,7 ± 1,95	0,448
Ag_NP_SC4b + CTAB / Triton 0,1x C <sup>M</sup>	69,03 ± 1,41	0,46

Sample	Diameter (nm)	PdI
Ag_NP_SC4c	62,25 ± 15,48	0,086
Ag_NP_SC4c + CPB / Triton 5x C <sup>M</sup>	368,8 ± 9,6	0,446
Ag_NP_SC4c + CPB / Triton 1x C <sup>M</sup>	64,88 ± 0,86	0,274
Ag_NP_SC4c + CPB / Triton 0,1x C <sup>M</sup>	69,21 ± 0,15	0,255
Ag_NP_SC4c + CTAB / Triton 5x C <sup>M</sup>	266,23 ± 0,53	0,499
Ag_NP_SC4c + CTAB / Triton 1x C <sup>M</sup>	90,91 ± 0,55	0,248
Ag_NP_SC4c + CTAB / Triton 0,1x C <sup>M</sup>	81,84 ± 54,86	0,257

**Table S3** Z average of calix[4]arene capped silver nanoparticles (Ag\_NP\_SC4a, Ag\_NP\_SC4b and Ag\_NP\_SC4c) mixed with Triton and CTAB (or CPB) at different concentration ratio.

Sample	Molar fraction Triton	$C^M$ (M)
CTAB	0,19	0,000215
CPB	0,16	0,000258

**Table S4** Exemple of calculation of  $C^M$ . The determination of the Critical Micellar Concentration Mixture (or  $C^M$ ) was done from the molar ration of Triton used in all experiments. To obtain these values, we reported on the results obtained by Kharitonova [7]

Sample	Total concentration of CTAB / Triton (M)	$C^M$ (M)
5x $C^M$	0,00615	28,6
1 x $C^M$	0,00123	5,7
0,1 x $C^M$	0,000123	0,6

Sample	Total concentration of CPB / Triton (M)	$C^M$ (M)
5x $C^M$	0,00735	28,5
1 x $C^M$	0,00147	5,7
0,1 x $C^M$	0,000147	0,6

**Table S5** Exemple of calculation of  $C^M$ . The Critical Micellar Concentration Mixture (or  $C^M$ ) is then calculated proportionally to the  $C^M$  previously

determined according to the total concentration of surfactant mixture used in our experiments.

## ***Supporting Information***

### **Discriminatory antibacterial effects of calix[n]arene capped silver nanoparticles with regard to Gram positive and Gram negative bacteria**

Samira Boudebouze<sup>a</sup>, Anthony W. Coleman<sup>b,\*</sup>, Yannick Tauran<sup>b</sup>, Hela Mkaouar<sup>a</sup>, Florent Perret<sup>c</sup>,  
Alexandrine Garnier<sup>a</sup>, Arnaud Brioude<sup>b</sup>, Beomjoon Kim<sup>d</sup>, Emmanuelle Maguin<sup>a</sup> and Moez Rhimi<sup>a,\*</sup>

<sup>a</sup> INRA, UMR 1319 Micalis, F-78350 Jouy-en-Josas, France.

Tel: +33 1 3465 2294; E-mail: moez.rhimi@jouy.inra.fr

<sup>b</sup> LMI CNRS UMR 5615, Univ. Lyon 1, Villeurbanne, F69622, France.

Tel: +33 4 4243 1027; E-mail: antony.coleman@adm.univ-lyon 1.fr

<sup>c</sup> ICBMS, UMR 5246, Univ. Lyon 1, Villeurbanne, F69622, France.

<sup>d</sup> Institute of Industrial Science, University of Tokyo, Tokyo, Japan.

#### **Contents:**

.

## Experimental details:

### Synthesis of sulphonato-calix[n]arenes

#### Materials and reagents

All chemicals were purchased from ACROS Organics or Sigma Aldrich and used without further purification. Solvents were of chemical grade and were used without any purification. The structure and purity of the products were verified by  $^1\text{H}$  NMR spectroscopy at 300K using a Bruker 500 MHz NMR spectrometer, with  $\text{D}_2\text{O}$  as solvent. All products were characterised by electrospray mass spectroscopy, using a Perkin-Elmer Sciex spectrometer.

The starting materials, calix[n]arenes, were prepared by debutylation of *para*-tert-butylcalix[n]arenes, using the procedure described by Gutsche. [1] All calix[n]arenes used in this work have been previously described [2].

#### Synthesis of sulphonato-calix[n]arene modified silver nanoparticles

The procedure of Xiong [3] was slightly modified as follows. 10 mL of  $10^{-2}$  M  $\text{AgNO}_3$  solution was added to 80 mL of deionized water. To this solution, 10 mL of  $10^{-2}$  M of a sulphonato-calix[n]arene aqueous solution was added as stabilizer with stirring for 30 min. And then, 44 mg of  $\text{NaBH}_4$  was added to the solution. Silver nanoparticle suspensions were obtained after 5 minutes. The silver nanoparticles were then diluted 10 fold for storage at a final concentration of  $1 \times 10^{-4}$  M.

All calix[n]arene capped silver nanoparticles were stable excepted for SC8c capped silver nanoparticles which precipitated after a few hours.

#### Characterisation of the Capped Nanoparticles

##### UV-Visible absorption assays

The mixture experiments were conducted by monitoring the absorbance intensity between 340 nm and 650 nm, using a 96 well titre visible spectrometer, (BioTek Power Wave 340).

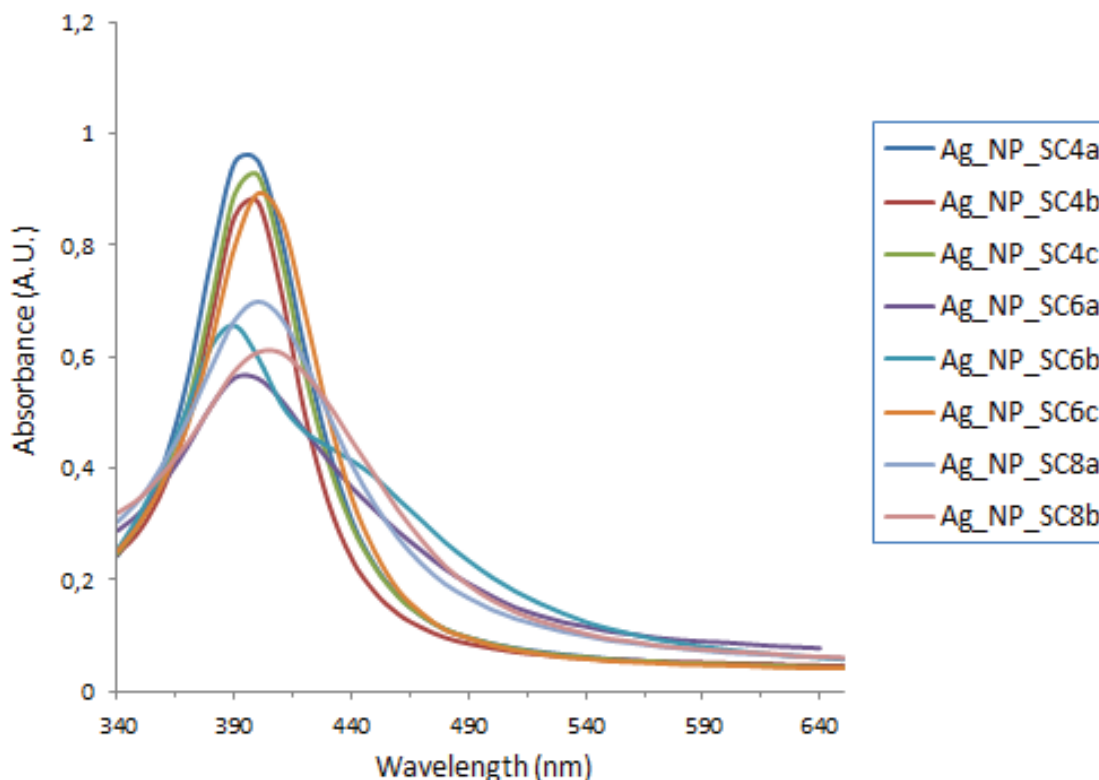


**Fig. S1** UV-Visible spectra of the calix[n]arene capped silver nanoparticles.

### Dynamic Light Scattering

Particle size measurements were performed on a Zetasizer Nano ZS (Malvern Instruments, UK) with a detection angle of 90°. The measurements were carried out in triplicate. The average hydrodynamic diameter (or Z average) was determined using the cumulant analysis provided by the instrument software with the assumption of spherical particles.

**Table S1** Z average of calix[n]arene capped silver nanoparticles

Sample	Diameter (nm)	Polydispersity Index
Ag_NP_SC4a	32.99 ± 6.2	0.28
Ag_NP_SC4b	68.18 ± 2	0.185
Ag_NP_SC4c	45.41 ± 6.7	0.245
Ag_NP_SC6a	51.19 ± 9.8	0.137

Supplementary Material (ESI) for Chemical Communications  
 This journal is (c) The Royal Society of Chemistry 2011

Ag_NP_SC6b	74.47	± 14.47	0.151
Ag_NP_SC6c	42.35	± 1.1	0.515
Ag_NP_SC8a	21.97	± 0.1	0.56
Ag_NP_SC8b	69.15	± 10.1	0.769

### Zeta Potential

The zeta potential of the calix[n]arene capped silver nanoparticles was determined by Laser Doppler Micro electrophoresis on a Zetasizer Nano ZS (Malvern Instruments, UK). From the measurement of the electrophoretic mobility, the zeta potential and its distribution was calculated. The measurements were carried out in triplicate at 25°C.

**Table S2** Zeta potential average of calix[n]arene capped silver nanoparticles.

Sample	Zeta Potential (mV)	Zeta deviation (mV)	Electrophoretic mobility ( $\mu\text{m.cm/Vs}$ )
Ag_NP_SC4a	-27.3	5.72	-2,139
Ag_NP_SC4b	-35.3	10.79	-2,765
Ag_NP_SC4c	-35.4	12.66	-2,775
Ag_NP_SC6a	-42.03	9.54	-3,296
Ag_NP_SC6b	-26.66	13.53	-2,11
Ag_NP_SC6c	-33.53	10.59	-2,414
Ag_NP_SC8a	-44.56	10.5	-3,494
Ag_NP_SC8b	-36.03	12.33	-2,822

### Bacteria growth conditions and kinetics

*B. subtilis* and *E. coli* were cultured in Luria Bertani (LB) medium at 37 °C with agitation (220 rpm, Infors system). From overnight cultures we inoculated cultures at initial OD600

nm of 0.1. Growth kinetic was carried out by measurement of the OD<sub>600</sub> nm each hour using a visible spectrophotometer (BioPhotometer, Eppendorf) [4].

### References and Note

[1] C. D. Gutsche and L.-G. Lin, *Tetrahedron*, 1986, **42**, 1633

[2] Y. Tauran, A. Brioude, P. Shahgaldian, A. Cumbo, B.J. Kim, F. Perret, A.W. Coleman, I. Montasser, *Chem. Commun.*, 2012, **48**, 9483-9485.

[3] D. Xiong, M. Chen and H. Li, *Chem. Commun.*, 2008, **7**, 880-882.

[4] G. Sezonov, D. Joseleau-Petit, R. D'Ari. *J. Bacteriology*, 2012, **189**, 8746-8749.

## *Supporting Information*

### **Large negatively charged organic host molecules as inhibitors of endonuclease enzymes**

Yannick Tauran,<sup>a,b</sup> Christophe Anjard,<sup>c</sup> Beomjoon Kim,<sup>b,d</sup> Moez Rhimi<sup>e</sup> and Anthony W. Coleman<sup>\*,a</sup>

<sup>a</sup> LMI CNRS UMR 5615, Univ. Lyon 1, Villeurbanne, F69622, France.  
Tel: +33 4 4243 1027; E-mail: antony.coleman@adm.univ-lyon 1.fr

<sup>b</sup> LIMMS/CNRS-IIS (UMI 2820), University of Tokyo, Tokyo, Japan.

<sup>c</sup> CGPhiMC UMR5534, Univ. Lyon 1, Villeurbanne, F69622

<sup>d</sup> CIRMM, Institute of Industrial Science, University of Tokyo, Tokyo, Japan. E-mail: bjoonkim@iis.u-tokyo.ac.jp

<sup>e</sup> INRA, UMR 1319 Micalis, F-78350 Jouy-en-Josas, France.

**Contents:**

- **Experimental details**
- **Supporting figure**

## Experimental details:

### Synthesis and characterization of calix[n]arenes

*Para*-sulphonato-calix[n]arenes have been synthesized as per the literature method of Coleman *et al* [1] and Calix[4]arene dihydroxyphosphorous acid as per the method of Markovsky and Kalchenko [2]

All the physical characteristics of the synthesized calixarenes correspond to the literature values.

### Material and reagent

Sulphated  $\beta$ -cyclodextrin has been purchased from Sigma-Aldrich and restriction enzymes and rh DNase I from Takara company.

### Synthesis and characterization of sulphated $\beta$ -cyclodextrin capped silver nanoparticles

10 mL of  $10^{-2}$  M  $\text{AgNO}_3$  solution was added to 80 mL of deionized water. To this solution, 10mL of  $10^{-2}$  M of the sulphated  $\beta$ -cyclodextrin aqueous solutions were added as stabilizers with stirring for 30 min. And then, 44 mg of  $\text{NaBH}_4$  was added to the solution. The colloidal silver suspensions were obtained after 5 minutes.

The sulphated  $\beta$ -cyclodextrin capped silver nanoparticles were then characterized by UV-Visible Absorption assays using a 96 well titre visible spectrometer (BioTek Power Wave 340). The presence of stable silver nanoparticles has been characterized by a maximum absorbance at 400nm.

### Restriction enzymes inhibition assay for organic host molecules

100 $\mu\text{M}$  of each macrocyclic molecule  $\beta$ -CDsul, SC6 and SC8 (figure 1) have been mixed to 0.5 $\mu\text{g}$  of  $\lambda$ -DNA in a buffer at final concentration of 10mM Tris HCl pH 7.5, 50mM NaCl, 10 mM  $\text{MgCl}_2$ , 1mM DTT

The mixture was then mixed with the restriction enzymes and incubated 1 hour at 37°C.

The samples have been deposited on agarose gel 0.6% previously mixed with Ethidium bromide and run over 90 minutes at 75V. The gel was then scanned on ChemiDoc XRS system (Bio-Rad).

The digestion activity is then plotted as a matter of inhibitor concentration by quantifying the intensity of the digested bands with imageJ software.

### **Restriction enzymes inhibition assay for sulphated $\beta$ -cyclodextrin capped silver nanoparticles DNase I inhibition assay**

A part of the  $\beta$ -CDsul capped silver nanoparticles (annotated Ag\_NP\_ $\beta$ -CDsul) solution prepared according to the method described above has been dialysed overnight in DI Water, using a dialysis cassette with a cut off of 10 000 Da (Slide-A-Lyzer Dialysis Cassettes, 10K MWCO, Pierce).

Then a varying concentration (from 100nM to 100 $\mu$ M) of  $\beta$ -CDsul, Ag\_NP\_ $\beta$ -CDsul not dialysed and Ag\_NP\_ $\beta$ -CDsul dialysed have been mixed to 0.5 $\mu$ g of  $\lambda$ -DNA in a buffer at final concentration of 10mM Tris HCl pH 7.5, 50mM NaCl, 10 mM MgCl<sub>2</sub>, 1mM DTT.

The mixture was then mixed with the restriction enzymes NruI and incubated 1 hour at 37°C.

The samples have been deposited on agarose gel 0.8% previously mixed with Ethidium bromide and run over 45 minutes at 75V. The gel was then scanned on ChemiDoc XRS system (Bio-Rad).

The digestion activity is then plotted as a matter of inhibitor concentration by quantifying the intensity of the digested bands with imageJ software.

### **rh DNase I inhibition assay for organic host molecules**

The unit of rh DNase I and restriction enzymes are not equivalent. 1 unit for restriction will completely digest 1  $\mu$ g of substrate DNA in 60 minutes, while 1 unit for rh DNase I corresponds to the amount of the enzyme that increases the absorbance at 260 nm by 0.001 per minute at 25 °C, pH5.0, with calf thymus DNA as the substrate.

IC<sub>50</sub> of rh DNase I for the macrocyclic molecules cannot be determined by agarose gel electrophoresis. Kinetic has been performed to compare the inhibition effect between the molecules.

100 $\mu$ M of each macrocyclic molecules SC4 and SC8 have been mixed to 0.5 $\mu$ g of  $\lambda$ -DNA in a buffer at final concentration of 10mM Tris HCl pH 7.5, 50mM NaCl, 10 mM MgCl<sub>2</sub>, 1mM DTT

The mixture was then mixed with the rh DNase I (diluted 1000 time in the same buffer) at different incubation time of 1, 5, 10, 30 and 60 minutes, at 37°C.

The samples have been deposited on agarose gel 0.8% previously mixed with Ethidium bromide and run over 40 minutes at 75V. The gel was then scanned on ChemiDoc XRS system (Bio-Rad).

## References and Note

- [1] A. W. Coleman, S. Jebors, S. Cecillon, P. Perret, D. Garin, D. Marti-Battle, and M. Moulin, *New J. Chem.*, 2008, **32**(5), 780-782 ;
- [2] V. I. Kalchenko, D. M. Rudkevich, L. N. Markovskii, *Zhurnal Obshchei Khimii*, 1990, **60** (1-2), 2813-2814.

## Supporting Figures:

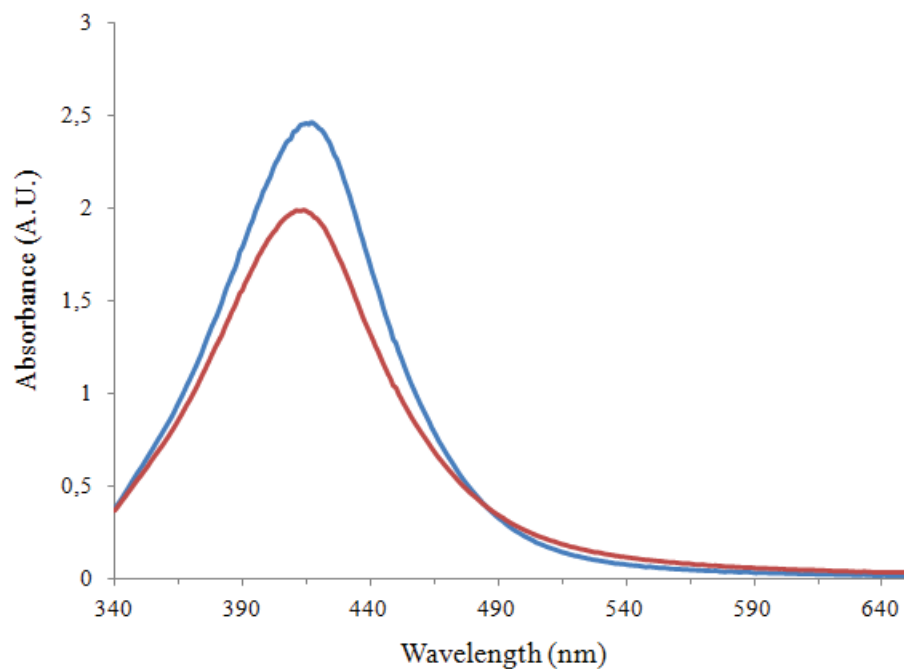


**Fig. S1** UV-Visible spectra of  $\beta$ -cyclodextrin sulphate capped silver nanoparticles. Blue curve corresponds to nanoparticles before dialysis and Red curve represents nanoparticles after dialysis. The dialysis was performed over night with a cut off of 10 000 Da against DI Water.

# The solid-state structures of the ethanol solvated complexes of *para*-sulphonato-calix[4]arene with magnesium and calcium ions

Kinga Suwinska · Erwann Janneau ·  
Yannick Tauran · Anthony W. Coleman

Received: 26 April 2013 / Accepted: 5 June 2013  
© Springer Science+Business Media Dordrecht 2013

**Abstract** The structures ethanol solvated complexes of *para*-sulphonato-calix[4]arene with magnesium and calcium have been determined. Both show the classical bilayer structure of *para*-sulphonato-calix[4]arene. The cations are situated between the bilayers. In the case of the magnesium complex the cation is octahedrally coordinated by six water molecules, however for the calcium complex the cation is coordinated in two different geometries by water molecules, bridging oxygen atoms of the sulphonate anions and an oxygen of an ethanol molecule. Both complexes contain an ethanol molecule embedded in the macrocyclic cavity.

**Keywords** Solid-state structure · *para*-Sulphonato-calix[4]arene · Magnesium · Calcium · Ethanol · Inclusion

## Introduction

The calix[*n*]arenes represent the major class of organic macrocyclic host molecules [1]. This is due to the ease of

their chemical modification [2], and their capacity to complex a vast range of substrates in solution [3], and in the solid-state [4]. Since 1984 with the first synthesis of the *para*-sulphonato-calix[*n*]arenes by Shinkai et al. [5], and more importantly with the first crystallographic determination of a sodium complex of *para*-sulphonato-calix[4]arene by Atwood and coworkers [6], the route to complex molecular architectures [7], and a novel biochemistry of the calix[*n*]arenes both in solution [8–10], and in the solid state [11, 12] has been opened. Both indirect biological activity as drug carriers [13, 14], and also direct biological activity as anti-coagulants, anti-viral agents, and ion-channels modulators has been observed for these molecules [15–17].

The structural chemistry of the *para*-sulphonato-calix[4]arene debuted in 1988 with the analysis of the ammonium methylsulphonic acid complex with *para*-sulphonato-calix[4]arene [18]. However the real structural analysis of the compounds relates to the work of Atwood again in 1988 with the determination of the structure of the sodium salt of *para*-sulphonato-calix[4]arene and the denomination of the system as an organic clay analog in view of the bilayer *para*-sulphonato-calix[4]arene motif [6], this hypothesis was supported by later work on the bilayer structures of other Group 1 metal cations [19]. In a recent paper Steed has carried out an in-depth study of the behavior of water in the sodium salts of *para*-sulphonato-calix[4]arene in the solid state [20].

While the structural chemistry of *para*-sulphonato-calix[4]arene has considerably enlarged to include organic cation structures [21], a large body of work by Raston on sodium-organic co-structures [22], and has expanded to include non-bilayer structures based organic cations [23], lanthanides [24], and recently aluminium [25], strangely there are no published reports of structural studies of

K. Suwinska  
Institute of Physical Chemistry, Polish Academy of Sciences,  
Kasprzaka 44/52, 01-224 Warsaw, Poland  
e-mail: ksuwinska@ichf.edu.pl

E. Janneau  
Centre de diffractométrie Henri Longchambon,  
Université Lyon 1, 69622 Villeurbanne, France

Y. Tauran · A. W. Coleman (✉)  
LMI, CNRS UMR 5615, Université Lyon 1,  
69622 Villeurbanne, France  
e-mail: aw.coleman@ibcp.fr

**Table 1** Crystal data and structure refinement details

Compound	1-Mg <sup>2+</sup>	1-Ca <sup>2+</sup>
Empirical formula	C <sub>28</sub> H <sub>20</sub> O <sub>16</sub> S <sub>4</sub> <sup>4-</sup> ·2[Mg(H <sub>2</sub> O) <sub>6</sub> ] <sup>2+</sup> ·2(C <sub>2</sub> H <sub>5</sub> OH)·3(H <sub>2</sub> O)	C <sub>28</sub> H <sub>20</sub> O <sub>16</sub> S <sub>4</sub> <sup>4-</sup> ·[Ca(H <sub>2</sub> O) <sub>3</sub> (C <sub>2</sub> H <sub>5</sub> OH)] <sup>2+</sup> ·[Ca(H <sub>2</sub> O) <sub>4</sub> (C <sub>2</sub> H <sub>5</sub> OH)] <sup>2+</sup> ·H <sub>2</sub> O
Formula weight	1151.68	1057.10
Temperature (K)	150	150
Diffractometer	Xcalibur, Atlas, Gemini ultra	Xcalibur, Atlas, Gemini ultra
Wavelength (Å)	0.7107	1.5418
Crystal	Prism, colorless	Needle, colorless
Crystal size (mm)	0.64 × 0.62 × 0.29	0.20 × 0.06 × 0.03
Crystal system	Triclinic	Triclinic
Space group	<i>P</i> -1	<i>P</i> -1
<i>a</i> (Å)	12.0527(2)	11.8483(9)
<i>b</i> (Å)	14.3247(3)	13.0167(7)
<i>c</i> (Å)	14.4753(3)	14.6781(9)
$\alpha$ (°)	88.972(2)	107.731(5)
$\beta$ (°)	86.392(2)	95.534(6)
$\gamma$ (°)	83.492(2)	97.069(5)
Volume (Å <sup>3</sup> )	2478.01(8)	2118.2(2)
<i>Z</i>	2	2
Calculated density (mg m <sup>-3</sup> )	1.544	1.657
<i>F</i> (000)	1212	1104
Absorption coefficient (mm <sup>-1</sup> )	0.318	5.032
$\theta$ Range for data collection (°)	4.3–29.6	3.6–66.5
<i>hkl</i> ranges	<i>h</i> = −16 → 15 <i>k</i> = −19 → 19 <i>l</i> = −19 → 19	<i>h</i> = −13 → 14 <i>k</i> = −15 → 15 <i>l</i> = −17 → 17
Reflections collected/unique	67221/12752	25217/7392
Completeness (%) to $\theta$	0.98	0.99
<i>T</i> <sub>min</sub> , <i>T</i> <sub>max</sub>	0.870, 0.936	0.471, 0.875
Refinement method	Least-squares full matrix on <i>F</i> <sup>2</sup>	Least-squares full matrix on <i>F</i> <sup>2</sup>
Data/restraints/parameters	12748/0/715	7392/0/613
Goodness-of-fit on <i>F</i> <sup>2</sup>	1.044	1.038
Final <i>R</i> indices [ <i>I</i> > 2σ( <i>I</i> )]	<i>R</i> = 0.041 <i>wR</i> = 0.103	<i>R</i> = 0.041 <i>wR</i> = 0.099
<i>R</i> indices (all data)	<i>R</i> = 0.051 <i>wR</i> = 0.112	<i>R</i> = 0.057 <i>wR</i> = 0.106

*para*-sulphonato-calix[4]arene with Group 2a divalent cations.

In this paper we report on the structures of ethanol inclusion complexes of *para*-sulphonato-calix[4]arene with magnesium and calcium divalent cations. Both structures show the bilayer structure. In both cases an ethanol molecule floats in the macrocyclic cavity much as wine would fill the calyx crater. For the magnesium cation the expected octahedral coordination [26], is observed. For the calcium structure two types of coordination around the ions are present; one is hepta-coordinated and the other is octa-coordinated [27].

## Experimental

Synthesis and analysis of *para*-sulphonato-calix[4]arene

The synthesis of *para*-sulphonato-calix[4]arene was carried out according to the method described by Coleman et al. [9].

Crystal growth

For the calcium/*para*-sulphonato-calix[4]arene complex—a solution of *para*-sulphonato-calix[4]arene in ethanol at a

final concentration of 33.6 mM was mixed in an aqueous solution of calcium chloride and glutamic acid at a final molar ratio calixarene:calcium:glutamic acid equals to 1:3:1.

For the magnesium/*para*-sulphonato-calix[4]arene complex—a solution of *para*-sulphonato-calix[4]arene in ethanol at a final concentration of 67.1 mM was mixed in an aqueous solution of magnesium chloride and aspartic acid at a final molar ratio calixarene:magnesium:glutamic acid equals to 1:6:1.

#### Experimental crystal data

The experimental crystal data are given in the Table 1 beside.

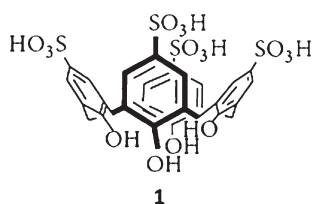
### Results and discussion

The structural formula of *para*-sulphonato-calix[4]arene, **1**, is shown in Scheme 1.

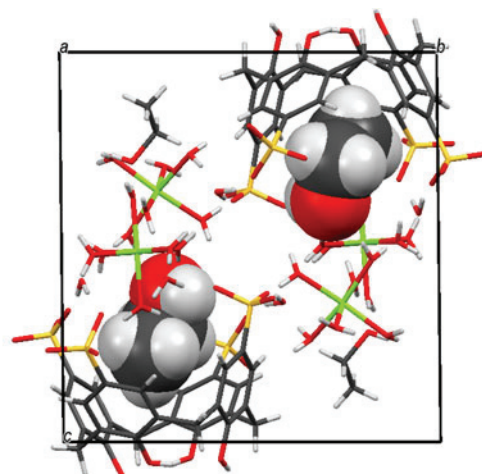
The crystals used in this study resulted from attempts to grow co-crystals of **1** with aspartic acid or glutamic acid in the presence of magnesium or calcium salts, this tentative resulted from the observation of an enhancement of the complexation of these amino-acids with *para*-sulphonato-calix[4]arene capped silver nanoparticles in the presence of these two divalent cations. However, only the cation-ethanol inclusion complexes of **1** were found in the obtained crystals.

The unit cells of **1**-Mg<sup>2+</sup> and **1**-Ca<sup>2+</sup> are given below in Fig. 1a, b, respectively. In cases charge balance is achieved through the presence of two cations for each tetra-anion, with no apparent deprotonation at the phenolic face being observed.

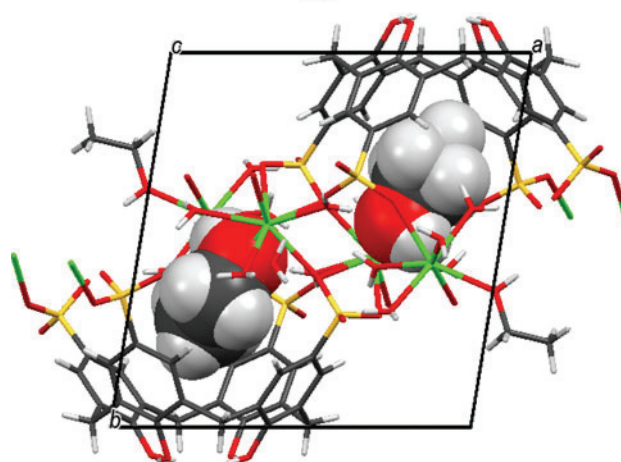
Although both complexes crystallize in the same centrosymmetric triclinic space group and have similar composition, they are not isostructural and the molecular structures are very different. In case of magnesium complex the crystal asymmetric unit consists of isolated *para*-sulphonato-calix[4]arene tetra-anion, two hexa-hydrated Mg<sup>2+</sup> cations, two isolated ethanol molecules, one of them included into macromolecular cavity and three isolated water molecules. The included ethanol molecule is located in such a way that the aliphatic part is sitting inside the cavity and the hydroxyl



**Scheme 1** Structure of *para*-sulphonato-calix[4]arene, **1**



**(a)**



**(b)**

**Fig. 1** Structural unit cell of the complex: **a** *para*-sulphonato-calix[4]arene/magnesium, view along *a* crystallographic axis and **b** *para*-sulphonato-calix[4]arene/calcium, view along *c* crystallographic axis

group is interacting with two SO<sub>3</sub> groups by hydrogen bonds (the OH group is disordered over two positions with s.o.f. 0.8 and 0.2). The *para*-sulphonato-calix[4]arene molecules form a corrugated layer with hydrophilic surfaces on both sides of the layer. Free water molecules and hydrated cations are situated between the layers of *para*-sulphonato-calix[4]arenes. Ethanol molecules, which are not included in the macrocyclic cavity of *para*-sulphonato-calix[4]arene are located in recesses between calixarene molecules in such a way, that aliphatic part of ethanol molecule is directed into the layer and hydroxyl group is pointing to the surface of the layer Fig. 2a.

In case of calcium complex the *para*-sulphonato-calix[4]arene tetra-anions are not isolated. Two, related by the center of symmetry, calixarene tetra-anions form a complex system in which two of calixarene are bound by

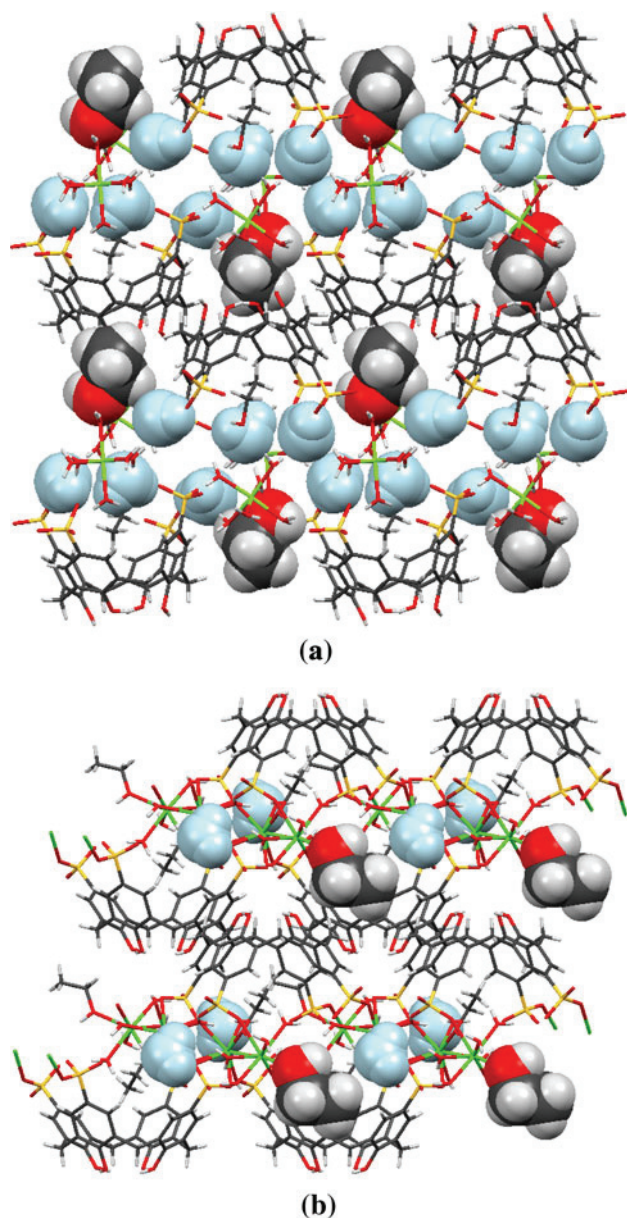


**Fig. 2** Layer-type structure: **a** *para*-sulphonato-calix[4]arene/magnesium and **b** *para*-sulphonato-calix[4]arene/calcium; not coordinated to cation water (blue) and not included in calixarene ethanol molecules showed in space-filling mode. (Color figure online)

four bridges composed by hydrated calcium cations resulting in capsule formation, Fig. 3.

One symmetry related pair of bridges is formed by  $\text{Ca}^{2+}$  cation hepta-coordinated (Ca2), where the ligands are four water molecules, one ethanol molecule and two oxygen atoms from sulphonate groups from centrosymmetrically related calixarene tetra-anions. The second bridge is a cluster composed by two octa-coordinated  $\text{Ca}^{2+}$  cations (Ca1), where the ligands are three water molecules, one ethanol molecule, two oxygen atoms from one sulphonate group (one of these atoms is coordinating also the second

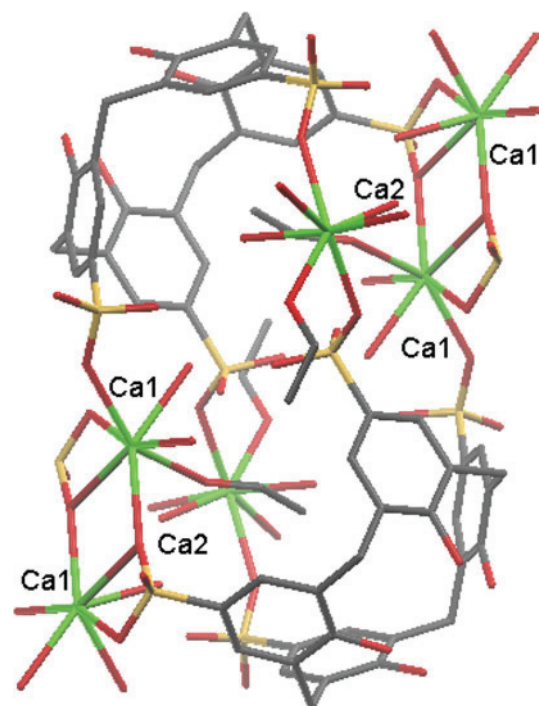


**Fig. 3** Complex capsule formation in  $1\text{-Ca}^{2+}$

Ca1 cation) and an oxygen atom from sulphonate group belonging to neighboring capsule. The ethanol molecule solvating Ca1 cation is pointing inwards the calixarene cavity and forms an inclusion complex with the *para*-sulphonato-calix[4]arene tetra-anion. Figure 4 shows the coordination of the Ca cations and coordination polyhedral around Ca1 and Ca2. In this crystal there is only one water molecule which is neither solvating metal cations nor included within the macrocyclic cavity or capsule (Fig. 2b). As the cluster with two Ca1 cations is shared by two adjacent capsules a 1D coordination polymer is formed (Fig. 5).

In both structures the anions of *para*-sulphonato-calix[4]arene are present in the pinched cone conformation with cone angles of  $39.6^\circ$  and  $86.9^\circ$  for the complex  $1\text{-Mg}^{2+}$ , and  $57.5^\circ$  and  $77.0^\circ$  for the  $1\text{-Ca}^{2+}$ . The cone structures are held in place by the characteristic ring of  $\text{O-H}\cdots\text{O-H}$  hydrogen bonds at the phenolic face, Tables 2 and 3.

For both systems a molecule of ethanol floats in the macrocyclic cavity, with heights of 0.825 and 1.037 Å above the *para*-carbon atom centroids for  $1\text{-Mg}^{2+}$  and  $1\text{-Ca}^{2+}$ , respectively, and here the analogy with the Greek calyx crater is more exact than usual. There are no C-H- $\pi$  short contacts, all distances between the methyl carbon atom and the aromatic centroids are greater than 2.525 Å for the magnesium complex and 3.815 Å for the  $\text{Ca}^{2+}$  complex.

**Fig. 4** Coordination spheres for calcium anions: **a** coordination to the SO<sub>3</sub> group belonging to the same “dimer” is marked with “”, coordination to the SO<sub>3</sub> group belonging to another dimer and extending the coordination polymer is marked with ‘; **b** coordination polyhedra

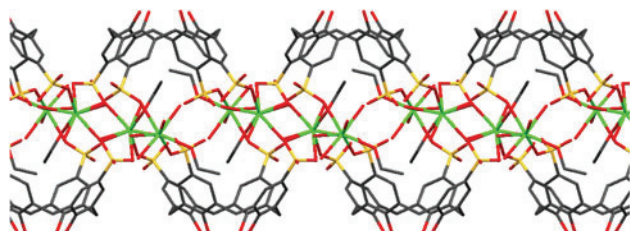
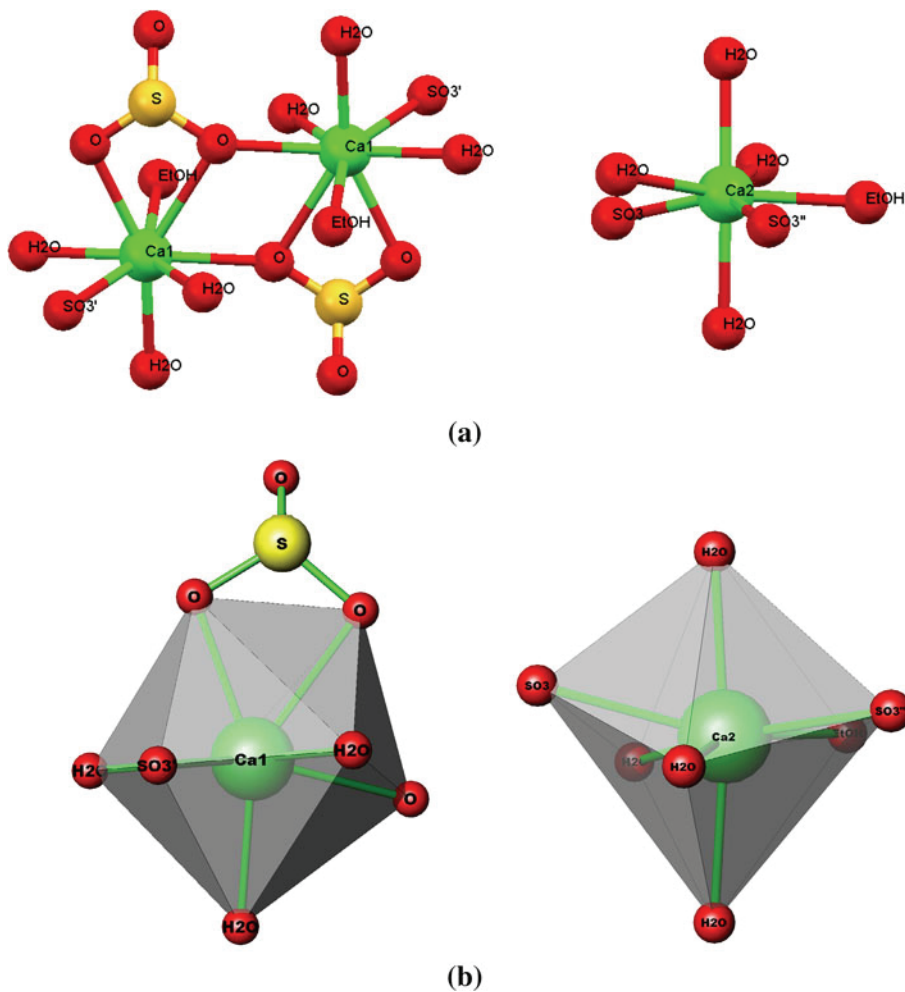


**Fig. 5** 1D coordination polymer in 1-Ca<sup>2+</sup>

The data for the coordination about the metal cations in 1-Mg<sup>2+</sup> and 1-Ca<sup>2+</sup> and is given in Table 4, below.

**Conclusion**

In conclusion we have determined the structures of the first two Group 2a complexes with *para*-sulphonato-calix[4]-arene, those with magnesium and calcium as cations. In contrast to the known structures with Group 1a cations in both structures we found inclusion of one ethanol molecule in calixarene cavity. Work is currently underway to attempt

**Table 2** Geometry of hydrogen bonds for *para*-sulphonato-calix[4]arene/magnesium complex (Å and °)

D–H...A	D–H	H...A	D...A	D–H...A
O11–H11...O40	0.84	1.88	2.710(2)	170
O23–H23...O11	0.84	2.23	2.878(2)	135
O23–H23...O51 <sup>ii</sup>	0.84	2.51	3.034(2)	122
O36–H36...O23	0.84	1.91	2.715(2)	161
O40–H40...O32 <sup>iii</sup>	0.84	2.01	2.711(2)	141
O40–H40...O36	0.84	2.53	2.909(2)	109
O50–H50A...O63	0.90	1.82	2.724(2)	175
O50–H50B...O64	0.88	2.02	2.873(2)	165
O51–H51A...O18 <sup>v</sup>	0.84	1.98	2.816(2)	174
O51–H51B...O46 <sup>vi</sup>	0.84	1.91	2.751(2)	176
O52–H52A...O48 <sup>vi</sup>	0.87	1.90	2.762(2)	169
O52–H52B...O71 <sup>i</sup>	0.89	2.24	3.095(3)	161
O53–H53A...O31 <sup>v</sup>	0.84	1.96	2.755(2)	157
O53–H53B...O30 <sup>i</sup>	0.94	1.88	2.806(2)	165
O54–H54A...O68A <sup>iv</sup>	0.86	2.06	2.911(2)	167
O54–H54A...O68B <sup>iv</sup>	0.86	1.88	2.709(2)	162
O54–H54B...O67	0.85	2.00	2.844(2)	167

**Table 2** continued

D–H...A	D–H	H...A	D...A	D–H...A
O55–H55A...O4	0.90	1.89	2.776(2)	171
O55–H55B...O32 <sup>i</sup>	0.89	1.89	2.769(2)	170
O57–H57A...O48 <sup>v</sup>	0.84	1.94	2.782(2)	176
O57–H57B...O64 <sup>iv</sup>	0.87	1.85	2.706(2)	168
O58–H582...O19 <sup>iv</sup>	0.87	1.90	2.748(2)	164
O58–H58A...O31 <sup>vii</sup>	0.85	1.97	2.808(2)	167
O59–H59A...O63	0.84	1.97	2.783(2)	162
O59–H59B...O2	0.88	1.87	2.747(2)	177
O60–H60A...O68A <sup>vii</sup>	0.85	1.91	2.759(2)	176
O60–H60A...O68B <sup>vii</sup>	0.85	1.95	2.737(3)	154
O60–H60B...O71	0.88	1.88	2.741(3)	166
O61–H61A...O17 <sup>iv</sup>	0.85	1.98	2.823(2)	171
O61–H61B...O67 <sup>viii</sup>	0.87	1.90	2.768(2)	171
O62–H62A...O47 <sup>v</sup>	0.79	2.25	3.017(2)	165
O62–H62B...O46 <sup>vii</sup>	1.01	1.82	2.823(2)	171
O63–H63A...O3 <sup>iv</sup>	0.89	1.91	2.770(2)	163
O63–H63B...O17 <sup>iv</sup>	0.91	2.10	2.865(2)	141
O64–H64...O18 <sup>ix</sup>	0.84	1.92	2.734(2)	163
O67–H67A...O17 <sup>iv</sup>	0.96	1.90	2.839(2)	165
O67–H67B...O47 <sup>iv</sup>	0.88	1.98	2.819(2)	157
O68A–H68A...O3	0.84	2.13	2.946(2)	165
O68B–H68B...O47	0.94	2.07	2.965(3)	160
O71–H71B...O30	0.85	2.00	2.738(3)	145
C15–H151...O31 <sup>i</sup>	0.95	2.52	3.456(2)	170

*Symmetry codes* (i)  $x-1, y, z$ ; (ii)  $-x+1, -y+1, -z+2$ ; (iii)  $-x+2, -y+1, -z+2$ ; (iv)  $-x+1, -y+1, -z+1$ ; (v)  $x, y+1, z$ ; (vi)  $x-1, y+1, z$ ; (vii)  $-x+2, -y+1, -z+1$ ; (viii)  $-x+1, -y+2, -z+1$ ; (ix)  $-x+1, -y, -z+1$

**Table 3** Geometry of hydrogen bonds for *para*-sulphonato-calix[4]arene/calcium complex (Å and °)

D–H...A	D–H	H...A	D...A	D–H...A
O12–H121...O44	0.84	1.93	2.723(3)	157
O30–H301...O49	0.84	1.92	2.690(3)	152
O44–H441...O30	0.84	1.87	2.735(3)	150
O49–H491...O12	0.84	1.97	2.735(3)	150
O51–H51A...O64 <sup>ii</sup>	1.00	1.86	2.773(3)	149
O51–H51B...O39 <sup>ii</sup>	0.93	1.84	2.731(3)	160
O52–H52A...O25	0.96	2.02	2.932(3)	157
O52–H522B...O5 <sup>iii</sup>	0.85	2.00	2.813(3)	160
O53–H53B...O39	0.79	1.94	2.717(3)	167
O54–H54A...O24 <sup>iv</sup>	1.06	1.81	2.860(3)	169
O54–H54B...O40 <sup>ii</sup>	0.95	1.76	2.699(3)	170
O55–H55...O51 <sup>ii</sup>	0.97	1.86	2.800(3)	164
O58–H58A...O25	0.79	2.18	2.907(3)	154
O58–H58B...O59 <sup>v</sup>	0.77	2.01	2.769(3)	167
O59–H59...O19 <sup>vi</sup>	0.94	1.89	2.810(3)	165
O62–H62A...O18 <sup>v</sup>	0.90	1.93	2.783(3)	159

**Table 3** continued

D–H...A	D–H	H...A	D...A	D–H...A
O62–H62B...O64 <sup>vi</sup>	0.88	1.94	2.811(3)	170
O63–H63A...O18 <sup>v</sup>	0.99	1.88	2.822(3)	158
O63–H63B...O19 <sup>vi</sup>	0.90	2.03	2.875(3)	154
O64–H64A...O25 <sup>i</sup>	0.87	1.98	2.845(3)	170
O64–H64B...O24 <sup>vii</sup>	0.85	2.03	2.832(3)	157
C14–H14...O2 <sup>i</sup>	0.95	2.59	3.541(4)	177
C33–H33B...O40 <sup>viii</sup>	0.99	2.37	3.333(3)	165
C56–H56A...O44 <sup>ix</sup>	0.99	2.56	3.378(6)	140

*Symmetry codes* (i)  $x+1, y, z, -z+1$ ; (ii)  $-x, -y+1, -z, -z+1$ ; (iii)  $-x-1, -y+1, -z+1$ ; (iv)  $-x-1, -y+1, -z, -z$ ; (v)  $-x-1, -y+1, -z+1$ ; (vi)  $x-1, y, z$ ; (vii)  $-x, -y+1, -z$ ; (viii)  $-x, -y, -z$ ; (ix)  $x, y+1, z$

**Table 4** Geometry of the divalent cation coordination for **1**-Mg<sup>2+</sup> complex and **1**-Ca<sup>2+</sup> complex

<b>1</b> -Mg <sup>2+</sup>	Distance (Å)	<b>1</b> -Ca <sup>2+</sup>	Distance (Å)
Mg1–H <sub>2</sub> O	2.031	Ca1–H <sub>2</sub> O	2.364
Mg1–H <sub>2</sub> O	2.040	Ca1–H <sub>2</sub> O	2.375
Mg1–H <sub>2</sub> O	2.040	Ca1–H <sub>2</sub> O	2.452
Mg1–H <sub>2</sub> O	2.046	Ca1–H <sub>2</sub> O	2.433
Mg1–H <sub>2</sub> O	2.090	Ca1–EtOH	2.590
Mg1–H <sub>2</sub> O	2.003	Ca1–SO <sub>3</sub>	2.628
Mg2–H <sub>2</sub> O	2.067	Ca1–SO <sub>3</sub>	2.439
Mg2–H <sub>2</sub> O	2.071	Ca1–SO <sub>3</sub>	2.448
Mg2–H <sub>2</sub> O	2.074	Ca2–H <sub>2</sub> O	2.344
Mg2–H <sub>2</sub> O	2.075	Ca2–H <sub>2</sub> O	2.370
Mg2–H <sub>2</sub> O	2.077	Ca2–H <sub>2</sub> O	2.358
Mg2–H <sub>2</sub> O	2.080	Ca2–H <sub>2</sub> O	2.450
		Ca2–EtOH	2.453
		Ca2–SO <sub>3</sub>	2.439
		Ca2–SO <sub>3</sub>	2.366

to extend the solid-state characterization to include the other Group 2a metals.

**Acknowledgments** Y.T. thanks the Université Lyon 1 for financial support.

## References

1. Steed, J.W., Atwood, J.L.: *Supramolecular Chemistry*, 2nd edn. Wiley, UK (2009)
2. Gutsche, C.D.: *Calixarenes Revisited: Monographs in Supramolecular Chemistry*. The Royal Society of Chemistry, Cambridge (1998)
3. Perret, F., Coleman, A.W.: *Biochemistry of anionic calix[n]arenes*. *Chem. Commun.* **47**, 7303–7319 (2011)
4. Hardie, M.J.: *Hydrogen bonded network structures constructed from molecular hosts*. *Struct. Bond.* **111**, 139–174 (2004)

5. Shinkai, S., Mori, S., Tsubaki, T., Sone, T., Manabe, O.: New water soluble host molecules derived from calix[6]arene. *Tetrahedron Lett.* **25**(46), 5315–5318 (1984)
6. Coleman, A.W., Bott, S.G., Morley, S.D., Means, C.M., Robinson, K.D., Zhang, H.M., Atwood, J.L.: Novel layer structure of sodium calix[4]arenesulfonate complexes: a class of organic clay mimics. *Angew. Chem. Int. Ed.* **27**, 1361–1362 (1988)
7. Orr, G.W., Barbour, L.J., Atwood, J.L.: Controlling molecular self-organization: formation of nanometer-scale spheres and tubules. *Science* **285**(5430), 1049–1052 (1999)
8. Perret, F., Lazar, A.N., Coleman, A.W.: Biochemistry of the para-sulphonato-calix[*n*]arenes. *Chem. Commun.* **23**, 2425–2438 (2006)
9. Coleman, A.W., Jebors, S., Cecillon, S., Perret, P., Garin, D., Marti-Battle, D., Moulin, M.: Toxicity and biodistribution of para-sulphonato-calix[4]arene in mice. *New J. Chem.* **32**, 780–782 (2008)
10. Memmi, L., Lazar, A., Brioude, A., Ball, V., Coleman, A. W.: Protein–calixarene interactions: complexation of bovine serum albumin by sulfonatocalix[*n*]arenes. *Chem. Commun.* 2474–2475 (2001)
11. Lazar, A., Da Silva, E., Navaza, A., Barbey, C., Coleman, A.W.: A new packing motif for para-sulfonatocalix[4]arene: the solid state structure of the para-sulfonatocalix[4]arene D-arginine complex. *Chem. Commun.* **19**, 2162–2163 (2004)
12. Danylyuk, O., Suwinska, K.: Solid-state interactions of calixarenes with biorelevant molecules. *Chem. Commun.* **39**, 5799–5813 (2009)
13. Da Silva, E., Lazar, A.N., Coleman, A.W.: Biopharmaceutical applications of calixarenes. *J. drug deliv. sci. technol.* **14**, 3–20 (2004)
14. Perret, F., Tauran, Y., Suwinska, K., Kim, B.J., Chassain-Nely, C., Boulet, M., Coleman, A.W.: Molecular recognition and transport of active pharmaceutical ingredients on anionic calix[4]arene capped silver nanoparticles. *J. Chem.* (2013). doi: 10.1155/2013/191828
15. Da Silva, E., Ficheux, D., Coleman, A.W.: Anti-thrombotic activity of water-soluble calix[*n*] arenes. *J. Inclusion Phenom. Macrocycl. Chem.* **17**(52), 201–206 (2005)
16. Tsou, L.K., Dutschman, G.E., Gullen, E.A., Telpoukhovskaia, M., Cheng, Y.C., Hamilton, A.D.: Discovery of a synthetic dual inhibitor of HIV and HCV infection based on a tetrabutoxycalix[4]arene scaffold. *Bioorg. Med. Chem. Lett.* **20**(7), 2137–2139 (2010)
17. Atwood, J. L., Bridges, R. J., Juneja, R. K., Singh. A. K.: US Patent 5 489 612, 1996
18. Bott, S.G., Coleman, A.W., Atwood, J.L.: Intercalation of cationic, anionic, and molecular species by organic hosts. preparation and crystal structure of [NH<sub>4</sub>][6]calix[4]arenesulfonate][MeOS-O<sub>3</sub>](H<sub>2</sub>O). *J. Am. Chem. Soc.* **110**(2), 610–611 (1988)
19. Atwood, J.L., Coleman, A.W., Zhang, H., Bott, S.G.: Organic clays. Synthesis and structure of Na<sub>5</sub>[calix[4] arene sulfonate]·12H<sub>2</sub>O, K<sub>5</sub>[calix[4]arene sulfonate]·8H<sub>2</sub>O, Rb<sub>5</sub>[calix[4]arene sulfonate]·5H<sub>2</sub>O, and Cs<sub>5</sub>[calix[4] arene sulfonate]·4H<sub>2</sub>O. *J. Inc. Phenom.* **7**, 203–211 (1989)
20. Fucke, K., Anderson, K.M., Filby, M.H., Henry, M., Wright, J., Mason, S.A., Gutmann, M.J., Barbour, L.J., Oliver, C.L., Coleman, A.W., Atwood, J.L., Howard, J.A.K., Steed, J.W.: The structure of water in *p*-sulfonatocalix[4]arene. *Chem. Eur. J.* **17**, 10259–10271 (2011)
21. Da Silva, E., Nouar, F., Nierlich, M., Rather, B., Zaworotko, M.J., Barbey, C., Navaza, A., Coleman, A.W.: A comparative structural study of four para-sulphonato-calix-[4]-arene organic di- and triammonium cation complexes. *Cryst. Eng.* **6**, 123–135 (2003)
22. Atwood, J.L., Barbour, L.J., Hardieb, M.J., Raston, C.L.: Metal sulfonatocalix[4,5]arene complexes: bi-layers, capsules, spheres, tubular arrays and beyond. *Coord. Chem. Rev.* **222**, 3–32 (2001)
23. Nichols, P.J., Makha, M., Raston, C.L.: Confinement of nucleic acid bases and related compounds using tetra-*para*-sulfonatocalix[4] arene. *Cryst. Growth Des.* **6**, 1161–1167 (2006)
24. Atwood, J.L., Barbour, L.J., Dalgarno, S., Raston, C.L., Webb, H.R.: Supramolecular assemblies of *p*-sulfonatocalix[4]arene with aquated trivalent lanthanide ions. *J. Chem. Soc. Dalton Trans.* **23**, 4351–4356 (2002)
25. Lesniewska, B., Danylyuk, O., Suwinska, K., Wojciechowski, T., Coleman, A.W.: Supramolecular versatility in the solid-state complexes of para-sulphonatocalix[4]arene with phenanthroline. *Cryst. Eng. Commun.* **13**, 3265–3272 (2011)
26. Greenwood, N.N., Earnshaw, A.: *Chemistry of the Elements*, 1st edn. Pergamon Press, Oxford (1984)
27. Yang, W.H., Lee, W., Hellinga, H., Yang, J.J.: Structural analysis, identification, and design of calcium-binding sites in proteins. *Proteins Struct. Funct. Genet.* **47**, 344–356 (2002)



# MECHANICAL EFFECT OF CALIX[N]ARENE CAPPED SILVER NANOPARTICLES ON DNA MEASURED WITH SILICON NANO TWEEZERS

Yannick Tauran<sup>1,2</sup>, Momoko Kumera<sup>1,3</sup>, Nicolas Lafitte<sup>1,3</sup>, Ryohei Ueno<sup>3</sup>, Laurent Jalabert<sup>1,3</sup>, Yuki Takayama<sup>3</sup>, Dominique Collard<sup>1,3\*</sup>, Hiroyuki Fujita<sup>1,3</sup>, Anthony W. Coleman<sup>2\*</sup> and Beomjoon Kim<sup>1,3\*</sup>

<sup>1</sup> LIMMS-CNRS/IIS, UMI2820, Japan

<sup>2</sup> LMI, UMR5615, University of Lyon, France

<sup>3</sup> Institute of Industrial Science, The University of Tokyo, Japan

## ABSTRACT

This paper reports the use of a microelectro-mechanical system (MEMS)-based nano-tweezer in order to measure the effects of the interaction of calix[n]arene capped silver nanoparticles on the mechanical properties of DNA molecules.

**KEYWORDS:** Silicon Nano Tweezers, DNA, silver nanoparticles, Calix[n]arene

## INTRODUCTION

The interaction between metallic nanoparticles and DNA offers great potential. A large number of studies have already shown the interest of this complexation for biological uses including diagnostics [1] and medical applications [2]. With regard to electronic and plasmonic applications, the self assembly properties of DNA can be associated with metallic nanoparticles to construct a variety of metallised and nanostructured shapes [3]. Manipulation of DNA at the molecular level is essential for understanding the effects of such interactions between specific functional nanoparticles and DNA molecules. Biophysical information concerning the interaction of DNA with other elements is usually performed using optical tweezers [4], magnetic tweezers [5] or atomic force microscopy [6]. Because of their low cost, ease of sample preparation, and use of biocompatible conditions, Silicon-Nano-Tweezers (SNT) has recently proved its great interest [7]. Here, we will present for the first time the mechanical effect of *para*-sulphonato-calix[4]arene (SC4) capped silver nanoparticles on DNA molecules.

## EXPERIMENTAL

The SC4 capped silver nanoparticles solution (Fig.1-a) were prepared by the method of Xiong [8]. We have recently demonstrated their abilities to interact with nucleotides and nucleosides [9]. DNA  $\lambda$ -phage was purchased from TaKaRa (Japan). DNA and nanoparticles were at a final concentration of 1  $\mu\text{g}/\mu\text{L}$  and  $1.10^{-4}\text{M}$  respectively. DeIonized water was used as blank instead DNA. Their interactions with DNA  $\lambda$ -phage has been observed colorimetrically (Fig. 1-b) and spectrophotometrically with a UV-visible spectrophotometer (Fig.1-c). After adding DNA into the nanoparticles solution, we observed a slight red shift (10 nm) of the plasmon resonance absorption of the hybrid nanoparticles. Moreover, AFM imaging measurements confirmed the attachment of the nanoparticles along the DNA (data not shown).

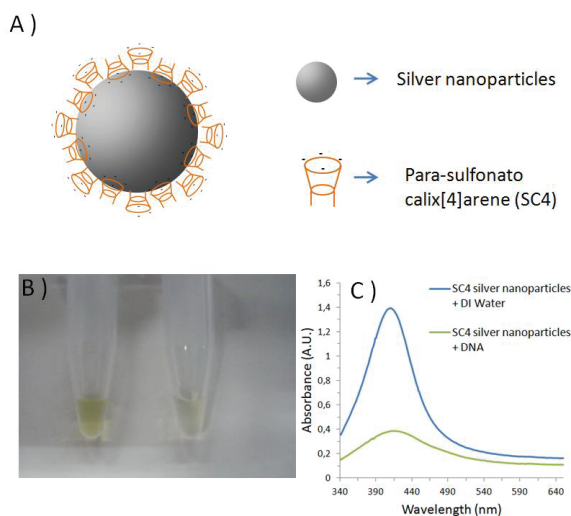


Figure 1: (1-a) Schematic representation of the organization of SC4 on silver nanoparticles (1-b) Pictures of SC4 silver nanoparticles mixed with DI water (on the left) and DNA (on the right). (1-c) UV Visible spectra of SC4 silver nanoparticles mixed with DI water or  $\lambda$  DNA.

SNT (Fig.2-a) are fabricated using standard microfabrication processes [7]. They consist of 1) a pair of opposing nanotips, 2) an electrostatic actuator for nanometer accuracy motion, and 3) a capacitive displacement sensor.

In the first step, the tweezer tips are brought to the surface of the DNA solution (droplet) on a glass slip and an AC voltage is applied between the tips (1 MHz, 16 Vpp) (Fig.2-b). By dielectrophoresis, a DNA bundle is extended and trapped between two tips of the tweezers (Fig.2-c). Next, the probes of SNT with trapped DNA bundle are introduced into the silver nanoparticles solution or DI water as negative control. Resonance characteristics (frequency and amplitude) of the system are continuously recorded every 0.6 seconds following the 90° phase rotation at the resonance frequency.

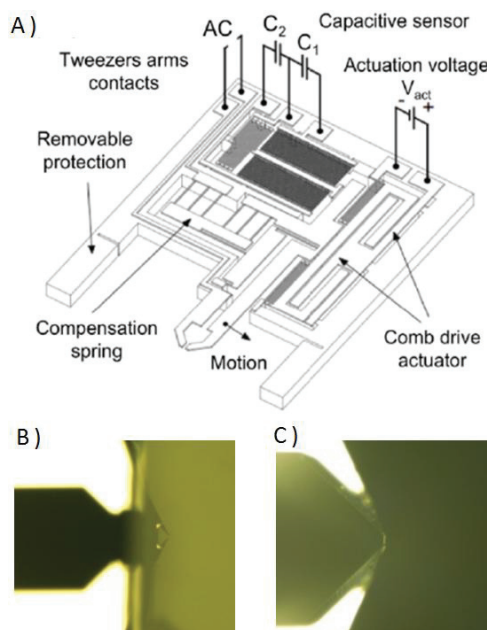


Figure 2: (2-a) Schematic diagram of silicon nano tweezers. (2-b) Tweezers tip immersed in DNA droplet. (2-c) DNA molecule bundle trapped in between tips (in air).

## RESULTS AND DISCUSSION

Figure 3 shows the frequency resonance (black line) and the Q factor (red line) of the tweezers. From the immersion start of the tweezers with the DNA bundle into the nanoparticles solution and as the interaction of the nanoparticles proceeds along the DNA bundle, the resonance frequency increases and the Q factor is stable (Fig.3-b). The stability of the Q factor means that there is no difference in the amplitude of oscillations and as a consequence no energy loss. Interestingly, the increase of the resonance frequency indicates the stiffening of the DNA bundle with the nanoparticles attachment. For the witnesses, the bundle in water has shown no frequency variation in absence of nanoparticles (data not shown). The tweezers without DNA trapping proved to be very stable inside nanoparticles solution (Fig.3-a).

Transmission electronic microscopy has been performed after 5 minutes of immersion. Figure 4a confirms that the bundle of DNA did not break up after removing the tweezer from the nanoparticle solution prior to observation by TEM. Figure 4b is focused on the bundle of DNA, confirming the attachment of the silver nanoparticles along the DNA.

## CONCLUSION

SNT is a powerful tool to monitor in real-time the dynamic of silver nanoparticles attachment. SC4 nanoparticles provided extensive effect on DNA. Other calix[n]arene derivate capped silver nanoparticles will be investigated. We expect other mechanical and electrical properties according to their assemblies with DNA. This is promising for such applications as genotyping, or as news hybrid materials assemblies.

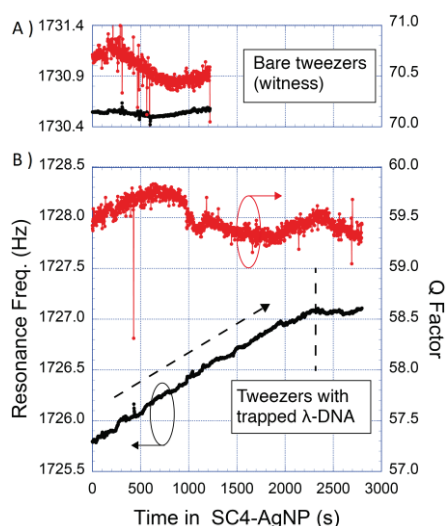


Figure 3: Frequency and factor  $Q$  vs time (3-a) Tweezers inside nanoparticles solution (3-b) Tweezers + DNA inside nanoparticles solution.

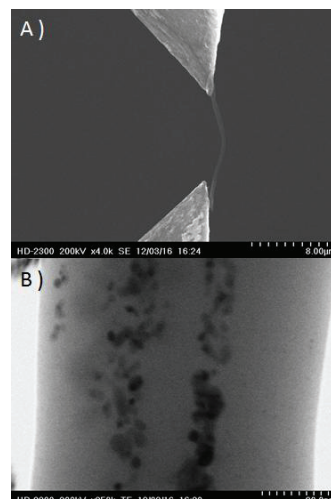


Figure 4: TEM picture of tweezers + DNA immersed inside nanoparticles solution (4-a) shows the bundle of DNA (4-b) shows silver nanoparticles along the DNA.

## REFERENCES

1. "Nanodiagnostics: application of nanotechnology in molecular diagnostics," K. K. Jain, *Expert review of molecular diagnostics*, **3**, 153 (2003).
2. "Binding of functionalized paramagnetic nanoparticles to bacterial lipopolysaccharides and DNA," L. Bromberg, E. P. Chang, C. Alvarez-Lorenzo, B. Magarinos, A. Concheiro and T.A. Hatton, *Langmuir*, **26**, 8829 (2010).
3. "Connecting the nanodots: programmable nanofabrication of fused metal shapes on DNA templates," M. Pilo-Pais, E. Samano, T. H. LaBean and G. Finkelstein, *Nanoletters*, **11**, 3489 (2011).
4. "A general method for manipulating DNA sequences from any organism with optical tweezers," D. N. Fuller, G. J. Gemmen, J. P. Rickgauer, A. Dupont, R. Millin, P. Recouvreux and D. E. Smith, *Nucleic Acids Research*, **34**, 9 (2006).
5. "Single-molecule study of DNA unlinking by eukaryotic and prokaryotic type-II topoisomerases," G. Charvin, and V. Croquette, *Proceedings of the National Academy of Science*, **100**, 9820 (2003).
6. "Reversible unfolding of individual titin immunoglobulin domains by AFM," M. Rief, M. Gautel, F. Oesterhelt, J. M. Fernandez and H. E. Gaub, *Science*, **276**, 1109 (1997).
7. "Single-DNA-molecule trapping with silicon nanotweezers using pulsed dielectrophoresis," M. Kumemura, D. Collard, N. Sakaki, C. Yamahata, M. Hosogi, G. Hashiguchi and H. Fujita, *Journal of MEMS*, **21**, (2011).
8. "Synthesis of p-sulfonatocalix[4]arene modified silver nanoparticles as colorimetric histidine probes," D. Xiong, M. Chen and H. Li, *Chemical Communications*, **7**, 880 (2008).
9. "Colourimetric and spectroscopic discrimination between nucleotides and nucleosides using parasulfonatocalix[4]arene capped silver nanoparticles," Y. Tauran, M. Grosso, A. Brioude, R. Kassab and A. W. Coleman, *Chemical Communications*, **47**, 12307 (2011).

## CONTACT

\* D. Collard, LIMMS-CNRS/IIS, UMI2820, Institute of Industrial Science, The University of Tokyo, 4-6-1 Komaba, Meguroku, 153-8505, Tokyo, JAPAN, Tel: +81-3-5452-6036; Fax: +81-3-5452 -6088; E-mail: collard@iis.u-tokyo.ac.jp

\* A.W. Coleman, LMI, UMR5615, Université de Lyon, Domaine scientifique de la DOUA, Bat. Berthollet, 22, av. Gaston Berger, 69622, Lyon, France, Tel: +33-4-4243-1027 ; E-mail: antony.coleman@adm.univ-lyon 1.fr

\* B.J. Kim, LIMMS-CNRS/IIS, UMI2820, CIRMM, Institute of Industrial Science, The University of Tokyo, 4-6-1 Komaba, Meguroku, 153-8505, Tokyo, JAPAN, E-mail: bjoonkim@iis.u-tokyo.ac.jp